Identification of Genes Associated with the Endocrine Heart under Normal and Pathophysiological Conditions using Genomic and Transcriptional Analysis

Monica Forero McGrath

Thesis submitted to the
Faculty of Graduate and Postdoctoral Studies
In partial fulfillment of the requirements
For the Ph.D. degree in Cellular and Molecular Medicine program

Department of Cellular and Molecular Medicine
Faculty of Medicine
University of Ottawa

© Monica Forero McGrath, Canada, 2011

Authorization and license agreements

Some text, tables and figures in this thesis have been previously published in the following papers with permission from the publishers Elsevier and BioMed Central. Elsevier license agreements can be found in appendices 1, 2, and 3.

McGrath, M.F. and A.J. de Bold, *Determinants of natriuretic peptide gene expression*. Peptides, 2005. 26(6): p. 933-43.

McGrath, M.F., M.L. de Bold, and A.J. de Bold, *The endocrine function of the heart*. Trends Endocrinol Metab, 2005. 16(10): p. 469-77.

Ogawa, T., Forero, M., Burgon, P. G., Kuroski de Bold, M. L., Georgalis, T. and de Bold, A. J., *Role of potassium channels in stretch-promoted atrial natriuretic factor secretion*. J Am Soc Hypertens, 2009. 3(1): p. 9-18.

McGrath, M.F. and A.J. de Bold, *Transcriptional analysis of the mammalian heart with special reference to its endocrine function*. BMC Genomics, 2009. 10: p. 254.

Abstract

The endocrine heart synthesises and secretes two polypeptide hormones: the natriuretic peptides (NP) atrial natriuretic factor (ANF) and B-type natriuretic peptide (BNP). The biological actions of these hormones serve both acutely and chronically to reduce systemic blood pressure and hemodynamic load to the heart, thus contributing to the maintenance of cardiorenal homeostasis. Considerable effort has been focused on the elucidation of the mechanistic underlying ANF and BNP gene expression and secretion but much remains to be determined regarding specific molecular events involved in the cardiocyte secretory function. These hormones are produced by the atrial muscle cells (cardiocytes), which display a dual secretory/muscle phenotype. In contrast, ventricular cardiocytes display mainly a muscle phenotype. Comparatively little information is available regarding the genetic background for this important phenotypic difference with particular reference to the endocrine function of the heart.

We postulated that comparison of gene expression profiles between atrial and ventricular muscles would help identify transcripts that underlie the phenotypic differences associated with the endocrine function of the heart as well as identify signaling pathways involved in its regulation.

The cardiac atrial and ventricular transcriptomes were analyzed using oligonucleotide microarrays under normal or chronically induced aortocaval shunt volume-overload conditions. Transcriptional differences were validated by RT-PCR and transcripts of interest were knocked-down by RNAi. Comparison of gene expression profiles in the rat heart revealed a total of 1415 differentially expressed genes between

normal atrial and ventricular tissues. Functional classification and pathway analysis identified numerous transcripts involved in mechanosensing, vesicle trafficking, hormone secretion, and G protein signaling. Volume-overloaded animals exhibited a progressive increase in cardiac mass over the four-week time course, an increase in expression of known hypertrophic genes, as well as the differential expression of 700 genes within the atria. Volume-overload specifically downregulated the accessory protein for heterotrimeric G protein signaling RASD1 in the atria. *In vitro*, knockdown of RASD1 in the atrial-derived HL-1 cells, significantly increased ANF secretion, demonstrating a previously unknown negative modulator role for RASD1.

The data developed in this investigation provides insight into the expression profiles of genes particularly centered on the secretory function of the heart under normal and chronic hemodynamic overload conditions. Genome-wide expression profile analysis identified RASD1 as being differentially expressed between cardiac tissues as well as being modulated by chronic volume overload. RASD1 emerges as a tonic inhibitor of ANF secretion. The novel function identified herein for RASD1 in the atria is of considerable interest given the fact that secretory impairment of the cardiac natriuretic hormones can negatively impact cardiovascular homeostasis.

Table of contents

AUTHORIZATION AND LICENSE AGREEMENTS ..... **II**
ABSTRACT ..... **III**
TABLE OF CONTENTS ..... **V**
LIST OF TABLES ..... **VIII**
LIST OF FIGURES ..... **IX**
ABBREVIATIONS ..... **XII**
ACKNOWLEDGMENTS ..... **XV**
INTRODUCTION **1**
DISCOVERY OF THE CARDIAC NATRIURETIC PEPTIDES 1
PROPERTIES OF ANF AND BNP 2
Biochemistry of ANF and BNP *2*
Biosynthesis and storage of ANF and BNP *3*
Mechanisms of ANF Secretion *8*
NP receptors and signaling *9*
Metabolism and clearance of ANF *13*
REGULATION OF ANF GENE EXPRESSION AND SECRETION 15
Genetic elements involved in ANF expression *15*
Developmental regulation of ANF expression *17*
Mechanical and neuroendocrine regulation of ANF expression *18*
Acute myocardial stretch 19
Subacute hemodynamic load 20
Chronic hemodynamic overload 21
Neuroendocrine hormones 22
Other secretagogues 24
The role of calcium on ANF secretion 25
Effect of atrial muscle mechanical activity on ANF secretion 25
Differential regulation of NP gene expression *26*
BIOLOGICAL ACTIONS OF ANF AND BNP 27
Actions on the cardiovascular system *27*
Actions on the renal system *29*
Actions on the RAAS *30*
Actions on the central nervous system *31*
IMPORTANCE OF THE FUNCTION OF THE ENDOCRINE HEART 32
MAMMALIAN HEART 33
Heart development *33*
Adult heart *34*
Cardiocyte ultrastructure *35*
Atrial and ventricular cardiocyte phenotypes *36*
Pathophysiological cardiac hypertrophy *37*
AORTOCAVAL SHUNT: A MODEL OF VOLUME-OVERLOAD INDUCED CARDIAC HYPERTROPHY 41
GENE EXPRESSION ANALYSIS 42
Oligonucleotide arrays 43

AIM OF STUDY **46**

HYPOTHESIS **47**

MATERIAL AND METHODS **48**

ANIMALS 48

Normal *48*

Aortocaval shunt *48*

PLASMA SAMPLES 51

RADIOIMMUNOASSAY 51

RNA EXTRACTION 52

Normal animals *52*

Aortocaval shunt animals *53*

Tissue culture *53*

NORTHERN BLOT 53

GENE EXPRESSION ARRAYS 54

Hybridization *54*

Normal animals 55

Aortocaval shunt animals 55

GeneChip Analysis *56*

REVERSE TRANSCRIPTION-POLYMERASE CHAIN REACTION 57

Normal animals *58*

Aortocaval shunt animals *58*

Tissue culture *58*

DIFFERENTIAL CENTRIFUGATION 60

WESTERN BLOT 61

IMMUNOFLUORESCENCE 62

CELL LINE AND CULTURE 64

RNA-INTERFERENCE MEDIATED SILENCING IN HL-1 CELLS 64

RNA QUALITY CONTROL 67

PROTEIN EXTRACTION FROM HL-1 CELLS 68

PHARMACOLOGICAL STIMULATION 68

RESULTS **69**

CHAPTER 1: PILOT STUDY AND GENECHIP QUALITY CONTROL 69

Pilot study *69*

GeneChip quality control of replicate study *74*

CHAPTER 2: GENE EXPRESSION ANALYSIS OF NORMAL TISSUE 85

Background *85*

Differentially expressed genes between normal atrial and ventricular tissues *85*

RT-PCR validation *87*

Functional classification *88*

Biological processes 90

Cellular component 95

Molecular function 96

Pathway analysis *99*

Protein validation *105*

CHAPTER 3: GENE EXPRESSION ANALYSIS OF VOLUME-OVERLOAD TISSUE 125

Background *125*

Development of cardiac hypertrophy *125*

Time course measurements of plasma ANF and BNP secretion and gene expression *127*

Gene Expression Analysis *131*

Differentially expressed genes between volume-overload and sham atrial tissues 131

Differential expression between volume-overloaded atrial and ventricular tissues 135
RT-PCR validation *141*
CHAPTER 4: RNAI SILENCING 145
Background *145*
RNAi knockdown optimization in HL-1 cells *147*
RNAi knockdown in HL-1 cells *158*
RASD1 RNAi knockdown modulates ANF secretion in HL-1 cells 158
RASD1 and Gαo RNAi knockdown modulates ANF secretion in HL-1 cells 165
Mastoparan-7 stimulates ANF secretion in HL-1 cells 168
ANF RNAi knockdown modulates ANF secretion 171
Gβ1 and Gγ2 RNAi knockdown modulates ANF secretion in HL-1 cells 174

DISCUSSION 177
CHAPTER 1: PILOT STUDY AND GENECHIP QUALITY CONTROL 177
CHAPTER 2: GENE EXPRESSION ANALYSIS OF NORMAL TISSUE 179
Conclusions *188*
CHAPTER 3: GENE EXPRESSION ANALYSIS OF VOLUME-OVERLOAD TISSUE 189
Differentially expressed genes between volume-overload and sham atrial tissues *190*
Differential expression between volume-overloaded atrial and ventricular tissues *192*
Conclusions *197*
CHAPTER 4: RASD1 AND ANF SECRETION GLEANED FROM RNAI SILENCING EXPERIMENTS 198
Background *198*
Overview of RNA interference *199*
RNAi mediated knockdown in HL-1 cells *200*
RASD1 RNAi knockdown modulates ANF secretion in HL-1 cells *203*
ANF RNAi knockdown modulates ANF secretion *205*
Mastoparan-7 stimulates ANF secretion in HL-1 cells *207*
Gαo, Gβ1 and Gγ2 RNAi knockdown modulates ANF secretion in HL-1 cells *210*
RASD1 in the secretory pathway *213*

CONCLUSIONS 220

FUTURE DIRECTIONS 225

REFERENCES 228

APPENDICES 275

List of tables

TABLE 1. PRIMER OLIGONUCLEOTIDE SEQUENCES USED FOR REAL-TIME PCR 59

TABLE 2. RNAI OLIGONUCLEOTIDE SEQUENCES DESIGNED BY DHARMACON 66

TABLE 3. DSRNA SEQUENCES DESIGNED BY IDT 67

TABLE 4. NUMBER OF DIFFERENTIALLY EXPRESSED GENES IDENTIFIED BETWEEN VARIOUS TISSUE AND CONDITION COMPARISONS IN THE MICROARRAY PILOT STUDY. 73

TABLE 5. LIST OF DIFFERENTIALLY EXPRESSED GENES CLASSIFIED INTO G PROTEIN DEPENDENT SIGNALING AND RELATED FUNCTIONAL GROUPS 91

TABLE 6. LIST OF DIFFERENTIALLY EXPRESSED GENES POSSESSING HORMONE, HORMONAL ACTIVITY, OR HORMONE RECEPTOR LIGAND GENE ONTOLOGY ANNOTATIONS 97

TABLE 7. LIST OF DIFFERENTIALLY EXPRESSED GENES ENCODING FOR POTASSIUM CHANNELS 98

TABLE 8. FUNCTIONAL ANNOTATION CLUSTERING OF DIFFERENTIALLY EXPRESSED GENES FOUND BETWEEN VO AND SHAM ATRIAL TISSUES. 133

TABLE 9. ATRIAL ABUNDANT GENES FOUND DIFFERENTIALLY EXPRESSED BETWEEN VO ATRIAL AND VENTRICULAR TISSUES, CLASSIFIED INTO THE "SECRETION" FUNCTIONAL GROUPS. 138

List of figures

FIGURE 1. SCHEMATIC REPRESENTATION OF ANF, BNP AND CNP. 5

FIGURE 2. AMINO ACID SEQUENCES AND STRUCTURES OF HUMAN NATRIURETIC PEPTIDE HORMONES ANF, BNP AND CNP. 6

FIGURE 3. AORTOCAVAL SHUNT SURGERY. 50

FIGURE 4. BNP RELATIVE FOLD CHANGE BETWEEN NUMEROUS TISSUE COMPARISONS AS DETERMINED BY MICROARRAY AND NORTHERN BLOT. 71

FIGURE 5. BNP RELATIVE EXPRESSION LEVELS IN RIGHT ATRIAL AND RIGHT VENTRICULAR TISSUES. 72

FIGURE 6. WITHIN-CLASS SCATTER PLOTS. 76

FIGURE 7. BETWEEN-CLASS SCATTER PLOTS. 78

FIGURE 8. SAMPLE HIERARCHICAL CLUSTERING TREES. 80

FIGURE 9. BOX PLOTS DISPLAYING LOG_2 SIGNAL INTENSITIES OF CONTROL ATRIAL AND VENTRICULAR MICROARRAY REPLICATES. 82

FIGURE 10. BOX PLOTS DISPLAYING LOG_2 SIGNAL INTENSITIES OF 28-DAY SHAM AND SHUNT ATRIAL AND VENTRICULAR MICROARRAY REPLICATES 83

FIGURE 11. COMPARISON OF MICROARRAY AND RT-PCR RESULTS IN NORMAL ATRIAL AND VENTRICULAR SAMPLES. 87

FIGURE 12. FUNCTIONAL CLASSIFICATION OF DIFFERENTIALLY EXPRESSED GENES FOUND BETWEEN THE ATRIA AND THE VENTRICLES WITH KNOWN GENE ONTOLOGY ANNOTATIONS. 89

FIGURE 13. NORMALIZED INTENSITY VALUES OF SPECIFIC TRANSCRIPTS IN ALL ATRIAL AND VENTRICULAR MICROARRAY REPLICATES. 93

FIGURE 14. FATTY ACID SYNTHESIS PATHWAY. 100

FIGURE 15. PROSTAGLANDIN SYNTHESIS AND REGULATION PATHWAY 101

FIGURE 16. LONG-CHAIN FATTY-ACID BETA-OXIDATION PATHWAY 102

FIGURE 17. CLASSICAL COMPLEMENT ACTIVATION PATHWAY. 103

FIGURE 18. G PROTEIN SIGNALING PATHWAYS GENERATED BY GENMAPP 104

FIGURE 19. REPRESENTATIVE IMAGES OF WESTERN BLOTS FOR PROANF, $G\alpha o$, RASD1, TREK-1 AND $G\gamma_2$. 107

FIGURE 20. TREK-1 IMMUNOFLUORESCENCE IN THE HEART. 109

FIGURE 21. TREK-1 IMMUNOFLUORESCENCE IN HL-1 CELLS. 111

FIGURE 22. BET1 IMMUNOFLUORESCENCE IN HL-1 CELLS. 112

FIGURE 23. RASD1 IMMUNOFLUORESCENCE IN THE HEART. 114

FIGURE 24. RASD1 IMMUNOFLUORESCENCE IN HL-1 CELLS. 117

FIGURE 25. GαO IMMUNOFLUORESCENCE IN HL-1 CELLS. 119

FIGURE 26. DOUBLE LABELING IMMUNOFLUORESCENCE OF RASD1 AND GαO IN HL-1 CELLS. 120

FIGURE 27. PROANF IMMUNOFLUORESCENCE IN THE HEART 122

FIGURE 28. PROANF IMMUNOFLUORESCENCE IN HL-1 CELLS. 123

FIGURE 29. BODY AND CARDIAC CHAMBER WEIGHTS AT VARIOUS TIME POINTS POST AORTOCAVAL SHUNT (SOLID COLUMNS) AND SHAM (OPEN COLUMNS) SURGERY 126

FIGURE 30. A) ANF AND B) BNP PLASMA LEVELS AT VARIOUS TIME POINTS POST AORTOCAVAL SHUNT (SOLID COLUMNS) AND SHAM (OPEN COLUMNS) SURGERY 128

FIGURE 31. NORTHERN BLOT ANALYSIS OF THE RELATIVE ABUNDANCE OF ANF AND BNP TRANSCRIPTS. 130

FIGURE 32. NUMBER OF ATRIAL ABUNDANT DIFFERENTIALLY EXPRESSED GENES PER GENE ONTOLOGY TERM BASED ON GOSTAT ANALYSIS ($P < 0.001$). 137

FIGURE 33. VENN DIAGRAM OF TWO-WAY ANOVA ANALYSIS. 140

FIGURE 34. COMPARISON OF MICROARRAY AND REAL-TIME PCR RESULTS IN ATRIAL SHUNT VS. SHAM SAMPLES. 142

FIGURE 35. COMPARISON OF MICROARRAY AND REAL-TIME PCR RESULTS IN ATRIAL AND VENTRICULAR SAMPLES UNDER BOTH SHAM AND SHUNT CONDITIONS. 143

FIGURE 36. RASD1 HEAT MAP. 146

FIGURE 37. WESTERN BOT ANALYSIS FOR RASD1 AND GAPDH IN RNAI TRANSFECTED HL-1 CELLS. 149

FIGURE 38. BIOANALYZER RESULTS. 150

FIGURE 39. WESTERN BLOT ANALYSIS OF RASD1 IN RNAI TRANSFECTED HL-1 CELLS. 152

FIGURE 40. RELATIVE EXPRESSION LEVELS OF GAPDH, ANF, BNP AND GαO IN RNAI TRANSFECTED HL-1 CELLS. 153

FIGURE 41. WESTERN BLOT ANALYSIS OF GαO IN RNAI TRANSFECTED HL-1 CELLS. 154

FIGURE 42. TYE™ 563-LABELED TRANSFECTION POSITIVE CONTROL IN HL-1 CELLS....156

FIGURE 43. RELATIVE EXPRESSION LEVELS OF HPRT AND RASD1 IN RNAI TRANSIENTLY TRANSFECTED HL-1 CELLS. 157

FIGURE 44. RELATIVE EXPRESSION LEVELS OF HPRT AND RASD1 IN RNAI TRANSIENTLY TRANSFECTED HL-1 CELLS. 160

FIGURE 45. RNAI KNOCKDOWN OF RASD1 MODULATES ANF SECRETION IN HL-1 CELLS. 161

FIGURE 46. RNAI KNOCKDOWN OF RASD1 INCREASES ANF SECRETION IN HL-1 CELLS....163

FIGURE 47. RNAI KNOCKDOWN OF RASD1 INCREASES ANF SECRETION IN HL-1 CELLS CULTURED IN SERUM STARVED AND SUPPLEMENTED CLAYCOMB MEDIUM. 164

FIGURE 48. RELATIVE EXPRESSION LEVELS OF HPRT, RASD1 AND GαO IN RNAI TRANSFECTED HL-1 CELLS. 166

FIGURE 49. RNAI KNOCKDOWN OF GαO NEGATIVELY MODULATES ANF SECRETION....167

FIGURE 50. MAS-7 STIMULATES ANF SECRETION IN HL-1 CELLS. 169

FIGURE 51. MAS-7 STIMULATES ANF SECRETION IN RNAI TRANSIENTLY TRANSFECTED HL-1 CELLS....170

FIGURE 52. RNAI MEDIATED KNOCKDOWN OF ANF NEGATIVELY MODULATES ANF SECRETION IN HL-1 CELLS. 172

FIGURE 53. MAS-7 STIMULATES ANF SECRETION IN RNAI TARGETED KNOCKDOWN OF ANF TRANSFECTED HL-1 CELLS. 173

FIGURE 54. RELATIVE EXPRESSION LEVELS OF Gβ1 AND Gγ2 IN RNAI TRANSIENTLY TRANSFECTED HL-1 CELLS. 175

FIGURE 55. RNAI KNOCKDOWN OF Gβ1 AND Gγ2 SUBUNITS NEGATIVELY MODULATES ANF SECRETION IN HL-1 CELLS 176

FIGURE 56. RASD1 MRNA SEQUENCE. 202

FIGURE 57. DIAGRAM OF SEVERAL DIFFERENTIALLY EXPRESSED GENES FOUND ABUNDANT IN THE ATRIA. .223

Abbreviations

ACE	angiotensin converting enzyme
Acta1	skeletal a-actin
ACTH	adrenocorticotropin
ANF	atrial natriuretic factor
ANG-II	angiotensin-II
Ankrd1	ankyrin repeat domain 1
ANOVA	analysis of variance
AP-1	adaptor protein-1
AP-1	activator-protein-1
ARF	ADP-ribosylation factor
ATP	adenosine triphosphate
BNP	b-type natriuretic peptide
bp	base pair
cGMP	cyclic guanosine monophosphate
CNP	c-type natriuretic peptide
CVD	cardiovascular disease
DAVID	database for annotation, visualization, and integrated discovery
DOCA	deoxycorticosterone acetate
dsRNA	double-stranded RNA
E	embryonic day
EDTA	ethylene-diamine tetraacetic acid
Egr-1	early growth response 1
ERK	extracellular signal-regulated kinase
ET-1	endothelin-1
ETA	endothelin receptor A
FBS	fetal bovine serum
FDR	false discovery rate
FITC	fluorescein isothiocyanate
G6PD	glucose-6-phosphate dehydrogenase
Gαo	Guanine nucleotide binding protein, alpha o
GAP	GTPase accelerating protein
Gβ1	Guanine nucleotide binding protein, beta 1
GC	guanylyl cyclase
GDP	guanosine diphosphate
GEF	guanine nucleotide exchange factor
GenMAPP	gene map annotator and pathway profiler
GEO	gene expression omnibus
Gγ2	Guanine nucleotide binding protein, gamma 2
GPCR	G-protein coupled receptor

GPCR	G protein coupled receptor
GTP	guanosine triphosphate
L-NAME	N-nitro-L-arginine methyl ester
Ica1	islet cell autoantigen 1
Igfbp3	insulin-like growth factor binding protein 3
IL-1β	interleukin-1β
ILGF-1	insulin-like growth factor-1
IP3R	inositol trisphosphate receptor
Irx4	iroquois homeobox protein 4
kb	kilobase
Kcnj3	potassium inwardly-rectifying channel, subfamily J, member 3
Kcnj5	potassium inwardly-rectifying channel, subfamily J, member 5
LA	left atria
LPA	lysophosphatidic acid
LV	left ventricles
MAPK	mitogen-activated protein kinase
MAS5	microarray analysis suite 5.0
MAS-7	mastoparan-7
MHC	myosin heavy chain
MLC-2a	regulatory myosin light chain 2, atrial isoform
MLC-2v	regulatory myosin light chain 2, ventricular isoform
MLC1A	essential myosin light chain 1, atrial isoform
MLC1V	essential myosin light chain 1, ventricular isoform
NEP	neutral endopeptidase
NO	nitric oxide
NPR-A	natriuretic peptide receptor type-A
NPR-B	natriuretic peptide receptor type-B
NPR-C	natriuretic peptide receptor type-C
Nr2f2	nuclear receptor subfamily 2, group F, member 2
NSF	N-ethylmaleimide-sensitive factor
PBS	phosphate buffered saline
PE	phenylephrine
PFA	paraformaldehyde
PGE2	prostaglandin E2
PGF2a	prostaglandin F2a
Pitx2	paired-like homeodomain transcription factor 2
PKce	protein kinase C epsilon
PKG	phophoglycerate kinase
PLA2	phospholipase A2
PLD1	phospholipase D1
PPT2	palmitoyl-proteinthioesterase 2
PRA1	prenylated Rab acceptor domain family member 1
PTX	pertussis toxin

RA	right atria
RAAS	renin-angiotension-aldosterone system
RGS	regulator of G protein signaling
RIA	radioimmunoassay
RIN	RNA integrity number
RISC	RNA-Induced Silencing Complex
RNAi	RNA inteference
RPL23	Ribosomal protein L23
RT-PCR	reverse-transcription polymerase chain reaction
RV	right ventricles
S1P	sphingosine 1-phosphate
SAM	significance analysis of microarray
SD	standard deviation
SGNE1	secretory granule neuroendocrine protein 1
siRNA	short infering RNA
SNAP	soluble (N-ethylmaleimide-sensitive factor) attachment protein
SNARE	SNAP receptor
T-tubules	transverse tubules
TBST	tris-buffered saline and tween 20
Tbx5	T-box protein 5
TGF	transforming growth factor
TGN	trans Golgi network
TNFα	tumor necrosis factor α
VAMP	vesicle-associated membrane protein
VMAT2	vesicular monoamine transporter 2
VO	volume-overload

Acknowledgments

This work could not have been possible without the support and mentorship of my supervisor, Dr. Adolfo de Bold. Over the years, Dr. de Bold has not only taught me important scientific skills, critical and independent thinking and interpersonal management, but he has also shared with me his enthusiasm for outdoor asados, leisure boating, and his beautiful native country Argentina. I am very thankful to Dr. de Bold for everything he has taught me. I would like to thank my advisory committee members, Dr. Miguel Andrade, Dr. James Van Huysse and Dr. John Copeland for their advice and insightful discussions. I would also like to thank past and present members of the Cardiovascular Endocrinology Laboratory, especially Dr. Mercedes Kuroski-de Bold and Dr. Tsuneo Ogawa for their helpful discussions, scientific knowledge and technical support.

I am extremely grateful to my parents, Victor and Simonne, for their unwavering encouragements throughout my life, which have always helped me to push myself forward and reach my goals. Muchas gracias papi y mami! I would like to acknowledge Fernando and David for their brotherly attention during my graduate studies. Even though they could never explain to their friends what I was doing besides remembering that I worked with hearts and rats, they always demonstrated great admiration towards my dedication and pursuit of knowledge. Et finalement, j'aimerais remercier mon merveilleux mari Jean-François pour son amour inconditionnel, sa compréhension et son support moral pendant toutes ces années d'études. J'aimerais dédier cette oeuvre à mon mari et à ma famille, sans qui je ne serais pas la personne que je suis aujourd'hui.

Introduction

Discovery of the cardiac natriuretic peptides

Early morphological studies of the mammalian heart identified an important phenotypic difference between the atrial and ventricular cardiocytes (Kisch, 1963). The atrial cardiocytes possessed a "large population of spherical, electron-opaque granules", which were not present in the ventricles, and thus termed "specific granules" by Jamieson and Palade (Jamieson and Palade, 1964). Subsequent morphological investigations determined a cause-and-effect relationship between water and sodium load, and the number of specific granules found in the atria (de Bold, 1979; Marie et al., 1976). It was demonstrated in rats that sodium and deoxycorticosterone acetate (DOCA) overloading caused a decrease in granularity, while water and sodium restriction caused an increase in atrial granular content (de Bold, 1979; Marie et al., 1976). The endocrine function of the heart was first established 30 years ago, by de Bold *and colleagues* (de Bold et al., 1981), when the acute renal effects of crude atrial extracts was assessed. The injection of homogenized atrial extracts, but not ventricular extracts, into bioassay rats produced an immediate and strong diuresis and natriuresis as well as hypotension and increase in hematocrit (de Bold et al., 1981). Based on a proteinase treatment, it was determined that the factor contained within the atrial specific granules was of peptide in origin. This peptide hormone was termed atrial natriuretic factor (ANF) or, later, atrial natriuretic peptide (ANP). ANF was the first member of the natriuretic peptide (NP) family to be discovered followed by the

isolation of the brain natriuretic peptide (BNP) (Sudoh et al., 1988), also referred to as B-type natriuretic peptide, and the C-type natriuretic peptide (CNP) (Sudoh et al., 1990). These peptides are produced and secreted by several tissues but their main sites of synthesis are the heart atria (ANF and BNP) and the vascular endothelium (CNP). ANF and BNP participate in cardiovascular homeostasis and modulation of cell growth. These peptides have paved the way for a new specialized field in cardiac research, i.e. cardiovascular endocrinology, and it is not going unnoticed. Pharmaceutical companies are particularly interested in the potential therapeutic use that these hormones possess for treatment of acutely decompensated heart failure and in the treatment of post acute myocardial infarction cardiac remodeling (Rademaker and Richards, 2005).

Properties of ANF and BNP

Biochemistry of ANF and BNP

Two distinct genes, *Nppa* and *Nppb*, encode for the cardiac NPs ANF and BNP, respectively. In humans, both genes are located on the distal short arm of chromosome 1 (1p36.2) whereas in the mouse and in the rat, these genes reside on chromosome 4 and 5, respectively (Szpirer et al., 1990; Yang-Feng et al., 1985). The sequences encoding these peptides are located on the same DNA strand and are organized in tandem (Tamura et al., 1996). In humans, *Nppb* is located approximately 8 kb from *Nppa* (Tamura et al., 1996). The mammalian genome contains only a single copy of the

genomic sequence encoding for preproANF, which facilitates the genetic manipulation of the gene in knockout and transgenic animal models.

The gene structures of ANF and BNP are similar, and are composed of three exons separated by two introns (Ogawa et al., 1994; Seidman et al., 1984a). The signal sequence is located in exon 1 whereas the majority of the protein-coding sequences, which also contain the bioactive portion of the molecule, are found in exon 2. In the rat, exon 3 encodes a Tyr-Arg-Arg sequence. Following translation the Arg–Arg pair is removed (Flynn et al., 1985; Lewicki et al., 1986). In humans, these two C-terminal arginine residues are absent (Oikawa et al., 1984).

ANF has a high degree of homology across mammals (Takei, 2001). Apart from a single nucleotide substitution, at codon position 110, all amino acids are conserved (Flynn et al., 1983; Kangawa et al., 1984; Maki et al., 1984; Oikawa et al., 1985; Seidman et al., 1984a; Vlasuk et al., 1986). In contrast to ANF, BNP is comparatively poorly conserved (Rosenzweig and Seidman, 1991). Mature BNP from sheep, cow, pig and dog share sequence homologies (Aitken et al., 1999).

Biosynthesis and storage of ANF and BNP

Human ANF is synthesized predominantly in the atrial cardiocytes as a 151-amino acid (152-amino acids in rat) preprohormone, while human BNP is synthesized as a 134 amino acid preprohormone (Figure 1). The removal of the N-terminal signal peptide generates proANF ($ANF_{1–126}$) and proBNP ($BNP_{1–108}$) (Azzazy and Christenson, 2003). Additional processing of proANF via phosphorylation has been demonstrated to

occur at the N terminus (Bloch et al., 1987; Wildey et al., 1990) but the functional importance of this posttranslational event has yet to be determined. In atrial cardiocytes, ANF and BNP are stored together in storage organelles referred to as specific atrial granules. ANF is stored as the precursor form $proANF_{1–126}$ and is further processed during secretion at the monobasic cleavage site Arg^{98}-Ser^{99} into the circulating biologically active form $ANF_{99–126}$ and the N-terminal-$ANF_{1–98}$ form (Flynn et al., 1985). BNP, however, is stored as a C-terminal bioactive $BNP_{77–108}$ and an N-terminal-$proBNP_{1–76}$ (Sudoh et al., 1989; Yokota et al., 1995). The C-terminal portion of all NP share a 17-amino acid ring formed by a disulfide linkage between Cys^{105} and Cys^{121} (Misono et al., 1984). This ring structure is essential for biological activity (Hirata et al., 1988) (Figure 2).

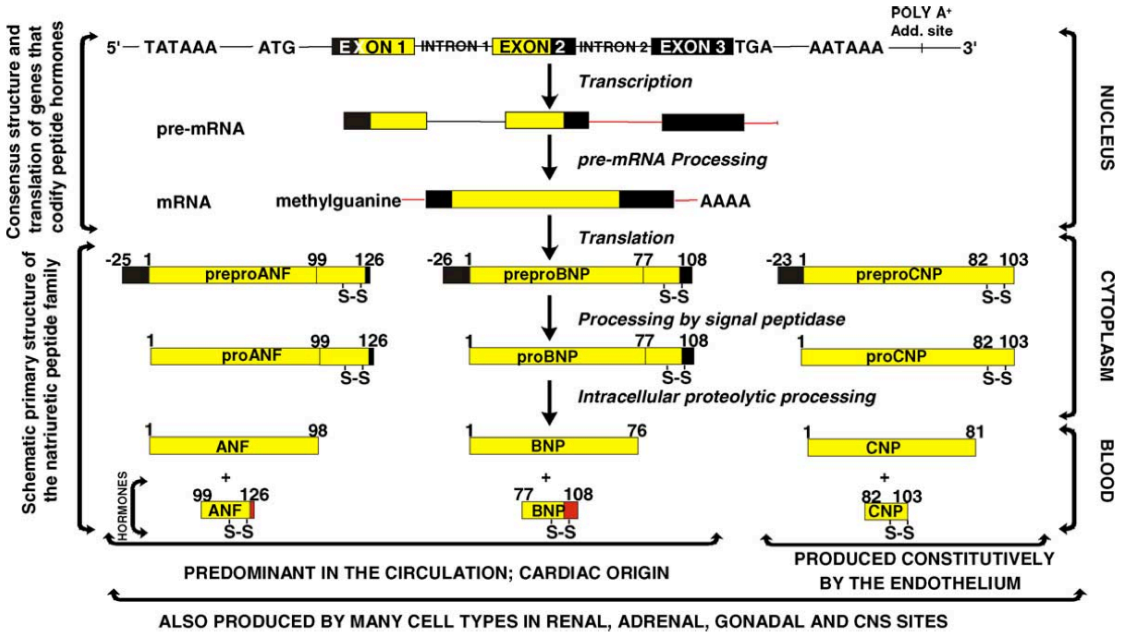


Figure 1. Schematic representation of ANF, BNP and CNP.

Schematic representation of the consensus structure and translational events of genes coding for peptide hormones as well as the processing steps involved in generating the circulating forms of the natriuretic peptide family (ANF, BNP and CNP).

Reprinted with permission (McGrath and de Bold, 2005).

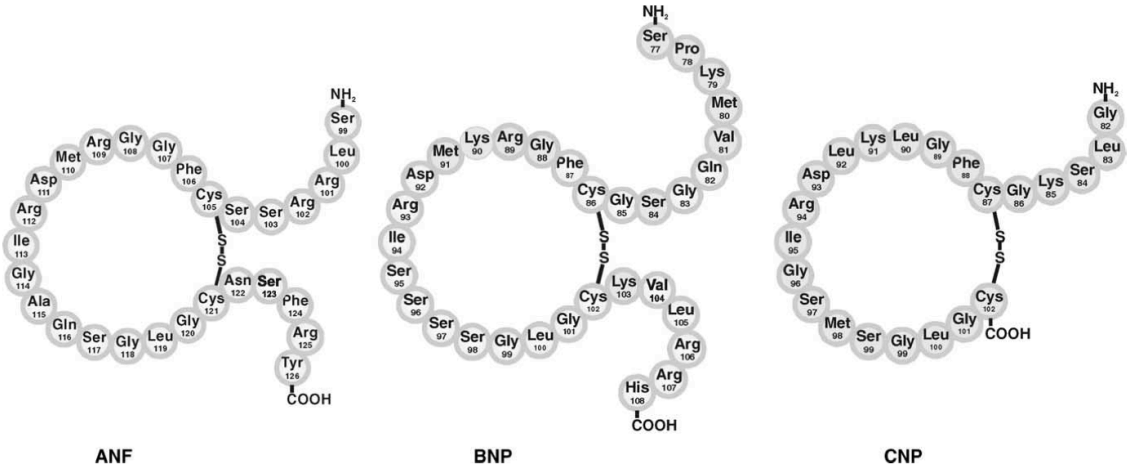


Figure 2. Amino acid sequences and structures of human natriuretic peptide hormones ANF, BNP and CNP.

Reprinted with permission (McGrath and de Bold, 2005).

The specific atrial granules contain ANF predominantly as $proANF_{1–126}$. Several serine protease have been suggested to be involved in the maturation of ANF including a specific peptidase found in bovine atrial microsomal fractions known as atrioactivase (Imada et al., 1988); IRCMSP1, found in the rodent heart (Seidah et al., 1986); as well as kallikren (Currie et al., 1984) and thrombin (Michener et al., 1986). Corin, a type II transmembrane serine protease has been shown to convert recombinant human proANF to $ANF_{99–126}$ in a sequence- specific manner *in vitro* (Wu et al., 2002; Yan et al., 2000). Corin is abundantly expressed in the heart (Hooper et al., 2000). Unlike ANF, BNP is stored in the atrial granules as the processed and mature form $BNP_{77–108}$. Corin appears to play a role in proBNP processing as well (Yan et al., 2000).

ANF expression is mostly restricted to the atria of the heart (1–3% of total mRNA) (Seidman et al., 1985). The ventricles (1% of atrial levels) (Lattion et al., 1986), aortic arch (Gardner et al., 1987a), as well as other extra-cardiac sites such as the pituitary (Gardner et al., 1986a), lungs (Gardner et al., 1986b), hypothalamus (Gardner et al., 1987c), adrenal medulla (Morel et al., 1989), and kidneys (Dagnino et al., 1991) also express ANF, albeit at much lower levels compared with the atria. Cultured cardiac fibroblasts produce BNP (Tsuruda et al., 2002). ANF mRNA expression has been shown in fibroblasts located in infarcted tissue, which corresponds with the transition of these cells to myofibroblasts (Cameron et al., 2000). Transcript and protein levels of ANF, BNP and CNP, as well as their cognate receptors, are highly expressed by myofibroblasts in human coronary atheromas (Casco et al., 2002).

Mechanisms of ANF Secretion

Peptide hormones are secreted via several pathways including regulated secretion, constitutive secretion and constitutive-like secretion. Regulated secretion occurs upon stimulation by agonists whereby the hormone packaged within storage granules is released thus allowing endocrine cells to secrete hormones at a rate that exceeds its biosynthesis. The constitutive-like pathway is independent from both regulated and constitutive secretion and it is insensitive to cycloheximide treatment. This mode of secretion has been characterized in the exocrine and endocrine pancreas where secretion would seem to occur via exocytosis of vesicles budding off from immature granules (Arvan and Castle, 1987; Arvan et al., 1991; Kuliawat and Arvan, 1992).

The constitutive pathway involves the passive diffusion of hormone in the absence of stimuli. The presence of clathrin-coated vesicles in the atrial cardiocytes is indicative of the existence of this constitutive pathway (Burgess and Kelly, 1987; Iida and Shibata, 1994; Page et al., 1986). Further, protein synthesis inhibition by cycloheximide significantly though partially, decreases ANF secretion. This suggests that basal ANF secretion is to a degree, dependent on newly synthesized hormone. However, a component of basal secretion appears to depend on stored hormone (Ogawa et al., 1999). Radiolabeling studies have demonstrated that 60% of the newly synthesized ANF is intended for storage whereas the remaining 40% is secreted under unstimulated conditions (Iida and Shibata, 1994).

Stretch- and endothelin-1- (ET-1) stimulated ANF secretion is based on a newly

synthesized granule pool of hormone. Furthermore, monensin, an ionophore that impairs protein sorting and transport in the trans Golgi network (TGN) and inhibits vesicle formation without directly affecting protein synthesis, completely inhibits stretch- and ET-1-stimulated ANF secretion (Ogawa et al., 1999) but it does not affect baseline release. This occurs despite the fact that the cells have a large storage pool of hormone in the older hormone storage compartment suggesting that a constitutive-like type of release, which entails the regulated secretion of immature secretory granules (Arvan et al., 1991), is the main release mechanism of stimulated hormone secretion operating in atrial cardiocytes.

A mechanism for ANF externalization involving caveolae has been suggested based on immunoelectron microscopy studies. In these studies, ANF was localized in caveolae found adjacent to the specific atrial granules. It seems that these caveolae are contiguous with the atrial granules thus allowing ANF to transit from the atrial granules to the caveolae and into the interstitial space (Page et al., 1986; Page et al., 1994).

NP receptors and signaling

The properties of NP are predominantly mediated through increases in intracellular cyclic guanosine monophosphate (cGMP) produced by activating guanylyl cyclase-coupled receptors. Systemic administration of ANF results in elevation of cGMP concentration in plasma and urine (Gerzer et al., 1985). Both ANF and BNP are agonists of the natriuretic peptide receptor (NPR) type-A (NPR-A) while CNP signals through

the natriuretic peptide receptor type-B (NPR-B). Intracellular cGMP receptors include cGMP-dependent protein kinases, cGMP-gated ion channels and cGMP-regulated cyclic nucleotide phosphodiesterases (Lincoln and Cornwell, 1993). A third receptor type, natriuretic peptide receptor type-C (NPR-C), is considered to be a clearance receptor although G-protein signaling has been associated with this receptor (Anand-Srivastava et al., 1991). NPR-C possesses a comparatively short 37-amino acid cytoplasmic portion. Biological effects mediated by NPR-A activation include the relaxation of vascular smooth muscle through the activation of cGMP-dependent kinases leading to phosphorylation of calcium-activated potassium channels and inositol trisphosphate receptor (IP3R)-associated cGMP kinase substrate and thus resulting in a reduction in cytosolic calcium concentrations (Feil et al., 2003; Sausbier et al., 2000; Schlossmann et al., 2000). It has been demonstrated using the NPR-A deficient mouse model that the hypotensive and diuretic/natriuretic effects of ANF and BNP were mediated exclusively through NPR-A (Lopez et al., 1997; Lopez et al., 1995). The NPR-A gene disruption also induces an increase in plasma aldosterone levels further supporting the role of the ANF/NPR-A system in inhibiting the renin–angiotensin–aldosterone system (RAAS) (Shi et al., 2001).

The purification and cloning of a putative membrane guanylyl cyclase of a sea urchin paved the way to the identification of the ANF receptor (Singh et al., 1988). By probing a human kidney cDNA library with the cDNA probe encoding for the cytoplasmic domain of the sea urchin resact receptor, which at the time was thought to be a membrane guanylyl cyclase, it was possible to isolate homologous sequences that encoded for the NPR-A. Later, segments of the NRP-A cDNA were used in a low

stringency hybridization of rat brain cDNA library to identify the second member of the guanylyl cyclase receptor family: NPR-B (Takayanagi et al., 1985). A fourth member of the guanylyl cyclase receptor family has been cloned, the guanylyl cyclase type C (GC-C) receptor, which should not be confused with the NP clearance receptor C (NPR-C). This receptor binds uroguanylin, guanylin, and *Escherichia coli* heat-stable enterotoxin (Schulz et al., 1990). A novel type of natriuretic peptide receptor, the NPR-D, has been identified in an eel gill cDNA library (Kashiwagi et al., 1995). This receptor, which has also been identified in the pouched lamprey *Geotria australis* (Toop et al., 1998), has 70% sequence identity to the eel NPR-C and possesses a short cytoplasmic tail, which places both NPR-C and NPR-D in a subfamily of the NPR family. Based on the NPR-D predicted sequence, it was possible to identify a crucial motif involved in the binding of natriuretic peptides (Kashiwagi et al., 1995). In the eel, NPR-D is mostly found in the brain with moderate levels in the gill and low levels in the heart (Hirose et al., 2001). NRP-D has not been identified in mammals.

The NPRs are made up of an extracellular ligand-binding domain that can bind natriuretic peptides, a short transmembrane region, and intracellular domains. The extracellular ligand-binding domain contains consensus sites for glycosylated residues at the N-terminus as well as cysteine residues. The glycosylation of the N-terminus residues has been postulated to be important in ligand binding and may play a role in NPRs folding and transport to the cell membrane (Lowe and Fendly, 1992; Miyagi et al., 2000). The NPR-A contains six cysteine residues, which are thought to form two intramolecular disulfide loops. The ligand-binding domain is 43% homologous among natriuretic receptors. This low level of similarity between the extracellular domains

implies that natriuretic peptides might interact with NPRs with different affinities. The binding potency of receptors is ranked as follows: NPR-A=ANF≥BNP≫CNP; NPR-B=CNP≫ANF≥BNP; NPR-C = ANF > CNP ≥ BNP (Suga et al., 1992).

The intracellular domain of NPR is linked to its extracellular domain by a single transmembrane region. The intracellular region contains a protein kinase homology domain as well as a C-terminus cyclase catalytic domain, which are separated by an amphipathic-helical hinge region (Kuhn, 2003). Upon ANF binding, NPR-A cyclase activity is noticeably increased in the presence of ATP (Chang et al., 1990; Sharma et al., 2001). It has been proposed that the binding of ANF and ATP leads to a conformational change of NPR-A, which removes the protein kinase domain inhibition on the catalytic domain. Deletion and point mutation studies have shown that the protein kinase domain is involved in the negative regulation of the cyclase catalytic domain (Chinkers and Garbers, 1989; Koller et al., 1993) as well as acting as a docking site for other proteins such as phosphatase PP5 and HSP90 (Kumar et al., 2001). Under unstimulated conditions, the protein kinase domain is phosphorylated. Upon contact with the ligand, phosphates are removed from the intracellular domain. This dephosphorylation coincides with NPR-A desensitization (Potter and Garbers, 1992).

The hinge region is involved in oligomerization of the NPR and is essential for the activation of the catalytic domain (Wilson and Chinkers, 1995). In human and rat, the intracellular regions of NPR-A and NPR-B have 73% homology (Koller et al., 1992).

The NPR-A is found in several tissues such as the kidney, smooth muscle vasculature, adrenal gland, brain, heart, testis, eye, intestine and olfactory mucosa (Drewett and Garbers, 1994). In addition to its endocrine function, ANF is also thought

to exert local autocrine/paracrine actions. Tissues such as lung, brain, kidney and adrenals express both ANF (although at levels that are 1–2% of those found in the atria) and its receptor (Kuhn, 2003). Furthermore, NPR-A is also expressed within the heart itself suggesting a role for NP in the regulation of cardiac function.

Metabolism and clearance of ANF

ANF is removed from circulation via two mechanisms: NPR-C-mediated internalization and proteolytic cleavage by neutral endopeptidase (NEP) 24.11. The extracellular domain of NPR-C is 30% homologous with NPR-A and NPR-B (van den Akker, 2001). The intracellular domain of NPR-C is composed of a 37 amino acid cytoplasmic tail, which is found in several other proteins involved in peptide and macromolecule clearance. NPR-C is well conserved in mammals: it is 95% homologous in human, rat and bovine species. NPR-C is expressed in several tissues, including kidneys, adrenals, lungs, vascular wall, heart, intestine and brain (Cerra, 1994; Fuller et al., 1988). In the normal heart, NPR-C mRNA is detected in all four cardiac chambers although most abundantly in the atria (Nunez et al., 1992). Upon development of cardiac hypertrophy, there is an increase in ANF expression accompanied by a significant loss of cardiac NPR-C expression as well as an increase in the NPR-A and NPR-B receptors abundance (Brown et al., 1993). In the kidney cortex, 95% of NPR are NPR-C (Maack et al., 1987). In general, glomerular and vascular structures of the kidney that are perfused with a large proportion of the total cardiac output possess NPR-C (Fuller et al., 1988).

The vast and strategic distribution of NPR-C further supports its role in sequestering and clearing the NP. The NPR-C binding potency in humans is ANF > CNP ≥ BNP (Suga et al., 1992), with one order of magnitude separating ANF from BNP. NPR-C recognizes an eight-amino acid linear fragment of the ANF molecule. This structural requirement is much less stringent than the 17-amino acid disulfide-bridged ring necessary for ANF binding to the NPR-A receptor. NPR-C internalization occurs at a rate of 5–7%/min (Cohen et al., 1996). This phenomenon is not stimulated by ligand binding making this a constitutive process. Since receptor internalization occurs much faster than ANF dissociation from its NPR-C receptor, efficient ligand transport and degradation can be achieved. Following ANF/NPR-C internalization, ANF is hydrolyzed by lysosomes and NPR-C is recycled to the cell surface, making the clearance receptors available for removing natriuretic peptides from circulation. Rapid endocytosis of the NPR-C is insured by dimerization, which can be twice the rate of the monomer form (Cohen et al., 1996). The circulation half-life of ANF is between 3 and 5 min, depending on the species, whereas BNP possesses a half-life significantly longer of 22.6 min. This divergence can be explained by the reduced binding affinity of BNP to NPR-C as well as its slower rate of hydrolysis by NEP 24.11 (Holmes et al., 1993).

Through NEP 24.11 ANF is inactivated by cleavage of its hydrophilic residues (Erdos and Skidgel, 1989). This zinc metalloprotease is found mainly in the proximal renal tubules of the kidney as well as throughout the vascular endothelium, lung and heart. NEP 24.11 is non-saturable and is found co-localized with angiotensin-converting enzyme (ACE) (Skidgel et al., 1984). Under pathophysiological conditions, when NPR-C is thought to be saturated, NEP 24.11 contributes significantly to ANF

removal (Erdos and Skidgel, 1989). NEP 24.11 binding affinity to natriuretic peptides is: CNP > ANF > BNP (Suga et al., 1992).

Regulation of ANF gene expression and secretion

Genetic elements involved in ANF expression

Earliest experiments that led to the discovery of ANF, assessed ANF gene expression in the atria of rats using morphological techniques specially developed to assess changes in the number of granules after different experimental maneuvers, including those known to affect water and electrolyte balance (de Bold, 1979). Similar experiments were carried out later, once the ability to measure ANF transcript abundance by Northern blot was developed. A sodium-free diet and water deprivation were shown to cause a reduction in ANF mRNA levels (Takayanagi et al., 1985). DOCA-salt treatment (Takayanagi et al., 1985), endothelin-1 (ET-1) (Fukuda et al., 1989), and hemodynamic overload (Day et al., 1987; Rozich et al., 1995), on the other hand, increased ANF transcript levels, implying the presence of regulatory elements on the ANF promoter.

Located at approximately 30 bp upstream of the transcription initiation site, a TATAA box drives the expression of the rat ANF gene (Seidman et al., 1984a). Additional sequences have been found several kilobases from the start codon, which are involved in ANF gene expression. These include an enhancer-like element at position −137 to −693 bp (Rosenzweig et al., 1991), tissue-specific expression *cis*-

acting elements at positions −3003 to −638 bp as well as a 315 bp *cis*-regulatory sequence involved in α-adrenergic inducibility (Knowlton et al., 1991). Sequence analysis of the latter ANF promoter sequence revealed putative serum-responsive element (SRE)/CArG, Egr-1, activator protein-1 (AP-1), AP-2, and a cAMP-responsive element (CRE) motifs at position −638 to −323 bp (Knowlton et al., 1991).

ANF gene promoter studies have made it evident that *cis*-acting consensus sequences differ among species and that these regulatory sequences may be found at different locations between species (Rosenzweig and Seidman, 1991). The rat ANF gene, for example, possesses putative glucocorticoid-binding sequences (Seidman et al., 1988) that are not present in the mouse gene counterpart (Seidman et al., 1984b). A 2.4 kilobase (kb) 5′ flanking sequence of the rat ANF gene is enough to direct atrial specific transcription of a reporter gene, but the gene activity is significantly reduced when the flanking region is decreased to 700 bp (Seidman et al., 1988). Studies undertaken with the human ANF gene reveal that a sequence located between −409 and −333 bp (corresponding to the positions -389 to -191 bp in the rat gene) is sufficient to drive tissue-specific expression in primary cultures of neonatal rat atrial cardiocytes (LaPointe et al., 1988; Wu et al., 1989). It is worth noting that even though species-specific differences are found in the position of *cis*-acting sequences, ANF expression remains tissue specific in these different species (Wu et al., 1989).

The ANF gene contains two important GATA binding sites, at -120 and -280 bp (Durocher and Nemer, 1998; McBride and Nemer, 2001). These sites, which are conserved across species, bind GATA-4 at the WGATAR motif and regulate cardiac specific expression of the ANF gene (Grepin et al., 1994; McBride and Nemer, 2001).

Nkx-2.5, one of the earliest developmental regulators of cardiac-specific gene expression, binds the NKE response element of the ANF promoter at -78 bp (Durocher et al., 1996; McBride and Nemer, 2001). The essential cardiac-specific elements, NKE, WGATAR (Grepin et al., 1994), and CArG (Argentin et al., 1994) confer spatial- and temporal-specific transcription of ANF.

Developmental regulation of ANF expression

In the atria, ANF levels rise continuously during embryonic and postnatal development, while ventricular ANF levels decrease rapidly after birth (Zeller et al., 1987). By *in situ* hybridization, ANF transcripts are first detectable in mouse myocardial cells, at embryonic day 8 (E8) (Zeller et al., 1987). By E9, ANF mRNA levels are detectable in both the atrium and the primitive ventricle. This stage corresponds with the initiation of regular beating of the primitive heart (Cameron and Ellmers, 2003). After septal formation (E12), which leads to the creation of the four heart chambers, strong ANF expression is detected in both atria and the trabeculated regions of the left ventricle (Zeller et al., 1987). After birth, ANF is significantly higher in the atria than in the ventricles. A negative modulator might cause ventricular downregulation of ANF expression. A study by Bruneau *et al.* (Bruneau et al., 2001), demonstrated that Irx4-deficient mice expressed inappropriate levels of ANF, α-skeletal actin, and β-myosin heavy chain (MHC) in the postnatal ventricles. In fact, 10 days after birth, ANF and α-skeletal actin mRNA levels were increased by a factor of 5.2 and 5.8, respectively, when compared to controls. β-MHC mRNA levels were increased

as well at 6 weeks. This upregulation is maintained even at 24 weeks of age, when ANF mRNA levels reached a factor of 6.7, α-skeletal actin a factor of 5.4, and β-MHC a factor of 2.7 compared to wild-type animals (Bruneau et al., 2001). These observations indicate that Irx4 is probably involved in the ventricular repression of ANF after birth.

Mechanical and neuroendocrine regulation of ANF expression

ANF is continuously secreted from the heart into the circulation thus providing for a baseline level of the hormone in blood. In humans, ANF and BNP plasma levels are significantly correlated with age and gender (Cowie et al., 2003). In subjects without known cardiovascular, renal or pulmonary disease, BNP levels are higher in women than in men, and these levels increase with age within each gender (Redfield et al., 2002). The importance of baseline secretion is reflected by the fact that blockade or genetic disruption of ANF or NP receptors results in impairment of cardiorenal homeostasis (John et al., 1995; Kishimoto et al., 1996; Sano et al., 1992a; Sano et al., 1992c; Yokota et al., 1994) (see section: Importance of the function of the endocrine heart). The infusion of the NPR-A antagonist A71915 (Delporte et al., 1992) has demonstrated that large artery distensibility, vascular volume and vascular tone are influenced by baseline ANF secretion (Schmitt et al., 2004). ANF baseline levels are modified by changes in pressure or volume load and by the neuroendocrine environment. The response of the heart to pressure or volume load varies in relation to whether the challenge is acute, subacute or chronic (de Bold et al., 1996).

Acute myocardial stretch

The increased secretion of ANF following acute mechanical atrial stretch is based on a phenomenon referred to as "stretch–secretion coupling" (Kuroski-de Bold and de Bold, 1991). This event is dependent upon a depletable ANF pool and is characterized by a phasic, short-term (i.e. minutes) burst of NP secretion with no apparent effect on synthesis (de Bold et al., 2001). This phenomenon underlies the increase in ANF secretion seen during head-out water immersion (Miki et al., 1986; Miki et al., 1988). In humans with cardiac tamponade, the increased atrial pressure does not result in increased ANF circulating levels but pericardiocentesis intervention leads to increased ANF circulating levels thus demonstrating that increased atrial stretch rather than atrial pressure is the key stimulus for acute ANF secretion (de Bold et al., 1996; Koller et al., 1987; Northridge et al., 1989).

In a recently published study, using an isolated adult rat atria model (Bensimon et al., 2004) to investigate the effect of agents known to affect G protein function on ANF secretion, it was shown that Gαi/o protein inhibition by pertussis toxin (PTX) abolished stretch–secretion coupling without affecting baseline secretion through a mechanism that is independent of Gαq signaling agonists. Mastoparan-7 (MAS-7), a Gi/o agonist, significantly increased ANF secretion even in the absence of muscle stretch through a PTX-sensitive mechanism. By confocal microscopy and by electron immunocytochemistry, ANF and Gαo partially co-localized while ultracentrifugation analysis suggested the presence of two populations of granules, one of which was partially associated with Gαo. PTX did not affect ET-1- or phenylephrine (PE)-

stimulated ANF secretion, in line with the view that these agonists signal mainly through Gαq (Bensimon et al., 2004).

Subacute hemodynamic load

While the acute stimulation of ANF secretion by atrial muscle stretch does not appear to affect ANF stores and is not dependent on ANF synthesis whereas chronic stimulated ANF secretion (see below) results in increased synthesis and secretion in both atria and the ventricles, there is an intermediate level stimulation of the endocrine heart whereby increased synthesis and secretion of NP is evident only in the atria. This may be observed during mineralocorticoid escape. Mineralocorticoid escape is a phenomenon characterized by a transient period of positive sodium balance resulting from chronic exposure to mineralocorticoid excess, such as aldosterone or DOCA followed by a vigorous natriuresis leading to a new steady state of sodium balance. The rise in intravascular volume and central venous pressure leads to increased NP production by the atria. The hypothesized mechanisms by which the kidney "escapes" from the sustained sodium retaining effects of mineralocorticoid excess are many (Hall et al., 1984; Higgins, 1970; Schnermann et al., 1975). ANF plasma levels rise in both animals (Grekin et al., 1986) and in humans (Cappuccio et al., 1987) during mineralocorticoid escape as well as in patients with primary hyperaldosteronism (Tunny et al., 1986). Yokota *et al.* (Yokota et al., 1994) clearly demonstrated that *in vivo* blockade of the NP receptors by the compound HS-142-1 significantly reduces that ability of the kidney to affect a mineralocorticoid escape.

Chronic hemodynamic overload

Under chronic hemodynamic overload conditions, as seen in long-standing hypertension and in chronic congestive heart failure, the cardiocytes undergo dramatic phenotypical alterations such as hypertrophy in order to normalize wall stress. The activation of the immediate early genes c-myc, c-fos and c-jun is a characteristic early response to mechanical or neurohumoral hypertrophic stimuli. These proto-oncogenes code for DNA binding proteins that activate other genes, such as contractile protein-coding genes and ANF. This event is then followed by a significant modification in the spatiotemporal expression of several genes, such as the re-expression of the cardiac fetal gene program (Olson and Srivastava, 1996) (see section: Pathological cardiac hypertrophy).

The increase in atrial NP gene expression and secretion observed during hemodynamic overload (de Bold et al., 2001; van Bilsen and Chien, 1993) is viewed as a cardioprotective mechanism based on the capacity of ANF and BNP to reduce load through their effects on renal function, vascular tone and growth. The level of ANF expression in the ventricles is usually correlated with the degree of hypertrophy (Lee et al., 1988; Ogawa et al., 1996). However, the amount secreted from the ventricles remains lower than that from the atria. In isolated perfused hearts from spontaneously hypertensive rats, only 38% of BNP and 16% of ANF originated from the ventricles (Ruskoaho, 2003). Pressure overload alone is not sufficient to upregulate ANF gene expression. In the *N*-Ω-nitro-l-arginine methyl ester (L-NAME) hypertensive rat model, it was found that left ventricular ANF gene expression increased in relation to cardiac

hypertrophy and was independently related to pressure overload (de Bold et al., 2001; Zhang et al., 2003). In fact, it was observed that left ventricular overload, in the absence of anatomical hypertrophy, was not associated with a rise in natriuretic peptide expression, while significant correlations were found between ANF mRNA levels and left ventricle weight/body weight in animals exhibiting left ventricular hypertrophy.

Neuroendocrine hormones

Numerous biological and pharmacological agents have been investigated in their ability to modify NP gene expression and secretion both *in vivo* and *in vitro* (de Bold et al., 1996). Some of these agents act directly on cardiocytes to promote ANF and BNP synthesis or secretion while others produce hemodynamic changes that lead indirectly to modifications on NP synthesis and secretion. Many of the agonists of NP secretion signal through G-protein coupled receptors and stimulate the Ras/c-Raf-1 signaling pathway and the phosphoinositide pathway leading to the recruitment and activation of effector molecules such as those found in mitogen-activated protein kinase (MAPK) cascades (de Bold et al., 2001; Kyosseva, 2004). There exist three major groups of MAPK in mammalian cells: extracellular signal-regulated kinase (ERK e.g. P44/42 also known as ERK-1/ERK-2), c-jun N-terminal kinase, and p38 MAP kinase. These kinases can activate transacting factors such as those from the Fos and Jun families that make up the activator protein-1 (AP-1), among many others. The AP-1 protein is a transcription factor that binds to specific recognition sequences of the 5′ flanking region of the ANF promoter thus modulating gene expression (Adcock, 1997).

Among promoters of NP gene expression and secretion, ET-1, has been extensively studied and has emerged as one of the most powerful agonists of NP gene expression. ET-1 is a powerful vasoconstrictor synthesized and released by endothelial (Yanagisawa and Masaki, 1989) and mesothelial cells (Eid et al., 1994). ET-1 has been shown to increase ANF gene expression in cultured neonatal rat cardiocytes as well as to induce the expression of early response genes, c-fos and Egr-1 (Shubeita et al., 1990), and the β-MHC isoform in ventricular cardiocytes. This process is reminiscent of molecular changes associated with the onset of cardiac hypertrophy. It has been proposed that ET-1 may act as a paracrine agent and thus play a role in the mechanism of cardiac hypertrophy (Ito et al., 1994) as well as modulating ANF secretion. Stretch-induced ANF secretion is reportedly inhibited by endothelin receptor A (ETA) antagonists (Skvorak et al., 1995). However, the kinetics of ANF secretion following stretch is different from that obtained following stimulation by ET-1 suggesting that mechanically-induced ANF secretion is independent of a paracrine mechanism in which ET-1 may be involved. Increases in ANF secretion after ET-1 stimulation is transient and might possibly be due to the ETA desensitization as well as the downregulation of its effector molecule, phospholipase C (PLC) (Leite et al., 1994). In order to better understand the role of ET-1 in the upregulation of cardiac ANF gene expression, chronic blockade of ETA was performed in DOCA-salt hypertensive rats (Bianciotti and De Bold, 2000). Chronic administration of a selective ETA receptor antagonist (ABT-627) prevented the rise in blood pressure along with circulating ANF levels in DOCA-salt treated rats. ANF gene expression was reduced in the ventricles in both control and DOCA-salt treated rats while no changes were observed in the atria upon ABT-627

treatment. In a similar fashion, atrial ANF production was not affected by treatment of aortic-banded hypertensive rats with the ACE inhibitor ramipril (Ogawa et al., 1996) suggesting that there are differences between atrial and ventricular NP gene expression in terms of their sensitivity to the endocrine environment.

Other secretagogues

Other neuroendocrine agents can act on cardiocytes to modulate ANF and BNP secretion. These include glucocorticoids (Shields et al., 1988), thyroid hormone (Kohno et al., 1993), acetylcholine (Ruskoaho et al., 1985; Toth et al., 1986), vasopressin (Inoue et al., 1988; Katsube et al., 1985), angiotensin II (ANG-II) (Edwards et al., 1986; Uehlinger et al., 1986), prostaglandins (Gardner and Schultz, 1990), α1-adrenergic agonists (Currie and Newman, 1986), hypoxia (Lawrence et al., 1990; McKenzie et al., 1986), myocardial ischemia (Lang et al., 1986), and opiates (Chen et al., 1989; Yamada et al., 1991). Some of these substances actively contribute to the modulation of ANF and BNP synthesis and secretion in both the normal and pathophysiological states (Bianciotti and de Bold, 2002; Bianciotti et al., 2001). Negative modulators of ANF and BNP secretion include hydroxyvitamin D3 (Li and Gardner, 1994), retinoids (Zhou et al., 1995) and nitric oxide (NO) (Leskinen et al., 1995; Melo and Sonnenberg, 1996). Several of these molecules also affect ANF gene expression levels. These include ET-1 (Fukuda et al., 1989; Gardner et al., 1991; Shubeita et al., 1990), glucocorticoids (Gardner et al., 1988), thyroid hormone (Gardner et al., 1987b), growth factors (transforming growth factor (TGF) type β1) (Parker et al., 1990; Takahashi et al.,

1994), α1-adrenergic agonists, such as PE (Knowlton et al., 1991), ANG-II (Sadoshima and Izumo, 1993), thrombin (Yokota et al., 1993) and prostaglandins, such as PGF2α, PGE2, (Gardner and Schultz, 1990).

The role of calcium on ANF secretion

It has been reported that Ca^{+2} tonically inhibits ANF secretion (de Bold and de Bold, 1989; Greenwald et al., 1989; Wen et al., 2000). These results place ANF secretion from atrial cardiocytes in a similar relationship to calcium as the secretion of renin by renal juxtaglomerular cell, which, unlike most other hormones, is also tonically inhibited by Ca^{+2} (Yao et al., 2003; Yatsu et al., 2003).

Effect of atrial muscle mechanical activity on ANF secretion

Atrial muscle stretch induces an increase in ANF secretion in both, spontaneously beating and quiescent atria thus showing that stretch–secretion coupling is independent of atrial beating. Electrical pacing of the perfused, quiescent rat left atrium induces an increase in basal ANF secretion, but this effect is only observed upon development of muscle tension. Stepwise increase in pacing frequency results in a significant decrease in ANF secretion (Cho et al., 1991) (McGrath and de Bold, 2005). Similar observations have been made using perfused rat hearts (Katoh et al., 1990) and rabbit atria (Cho et al., 1991). *In vivo*, cardiac pacing induces profound

changes in ANF plasma levels (Armstrong et al., 1986) but these changes are not only related to heart rate but also to atrial pressure and volume (Moe et al., 1990). Chemical depolarization of atrial muscle by high potassium (49 mM) arrests beating and abolishes developed tension without affecting ANF secretion (Kuroski-de Bold and de Bold, 1991).

Differential regulation of NP gene expression

Although in general ANF and BNP respond at the transcriptional, translational and secretory levels to a variety of agonists in a similar manner, there are some instances in which a discoordinated regulation of these peptides is observed. In acute myocardial infarction, a rapid ventricular induction of BNP gene expression is observed in early phases while only minor changes in ANF gene expression are detected (Hama et al., 1995). Prior to and during cardiac allograph rejection episodes, BNP secretion is selectively upregulated (Masters et al., 1999). In neonatal rat ventricular cardiocytes the pro-inflammatory cytokines tumor necrosis factor-α (TNF-α) and interleukin-1β (IL-1β) significantly increase BNP gene expression and secretion while ANF mRNA and secretion are not altered (Ma et al., 2004). As yet unidentified pro-inflammatory cytokines may also be involved. Conditioned medium from alloactivated T-lymphocytes cultures, which do not contain detectable amounts of TNF-α or IL-1β have the same effect than these cytokines on BNP expression. The p38 MAP kinase inhibitor SB203580 blunts the cytokine-stimulated upregulation of BNP gene expression and secretion as well as the increased BNP promoter activity (Ma et al., 2004).

Biological actions of ANF and BNP

ANF and BNP mediate their broad biological effects through their cognate guanylyl cyclase-coupled receptor, NPR-A, which are expressed in numerous tissues (see section: NP receptors and signaling). Hence, the modulation of cardiovascular function by ANF and BNP takes place at a number of different levels. Largely, the biological actions of these hormones serve both acutely and chronically to reduce systemic blood pressure and hemodynamic load to the heart (McGrath et al., 2005), thus contributing to the maintenance of cardiorenal homeostasis.

Actions on the cardiovascular system

Early investigations demonstrated that crude atrial extracts as well as ANF infusions generate a significant increase in hematocrit (Almeida et al., 1986; de Bold et al., 1981; Fluckiger et al., 1986; Trippodo and Barbee, 1987). ANF and BNP directly affect blood vessel function by decreasing vascular smooth muscle tone, peripheral vascular resistance, and by increasing capillary permeability (Chen et al., 2000; Januszewicz et al., 1987; Lainchbury et al., 1997; Nakamura et al., 1998; Sabrane et al., 2005).

The direct effect of the cardiac natriuretic peptides on regulating blood pressure has been well established based on transgenic mice studies where the NP/NPR-A system has been disrupted (see section: Importance of the function of the endocrine heart). Mice deficient in either ANF or its receptor exhibit higher blood pressure than

their control littermates (John et al., 1995; Lopez et al., 1995; Oliver et al., 1997), while mice over-expressing ANF or BNP had significantly lower blood pressure (Ogawa et al., 1994; Steinhelper et al., 1990).

Recently, tissue-specific knockout studies have confirmed the important contribution of the NP/NPR-A vascular system on regulating arterial blood pressure (Sabrane et al., 2005; Skryabin et al., 2004). NPR-A is highly expressed in both smooth muscle cells and endothelia of blood vessels. Isolated arteries deficient in NPR-A, specifically in smooth muscle cells, did not produce vasorelaxation in response to ANF infusion, as compared to control littermates (Holtwick et al., 2002). In contrast, the vasorelaxing response to ANF was preserved in mice with endothelium-targeted knockout of NPR-A (Sabrane et al., 2005). These mice exhibit hypervolemia, with an increase in plasma volume by 10-13%, cardiac hypertrophy (20% increase in weight), and chronic hypertension. The increase in systolic and diastolic blood pressure, by 12-15 mmHg and 5-10 mmHg, respectively, observed in these animals, represents about one third of the increase in systolic and diastolic blood pressure (27.4 mmHg and 15.3 mmHg, respectively) observed in global NPR-A genetic disruption (Lopez et al., 1995). Hence, ANF/NPR-A in the vascular system accounts for a significant portion of the hypotensive effects of ANF.

ANF and BNP possess growth-suppressing and antiproliferative properties. ANF has been shown to inhibit vascular smooth muscle cell proliferation in culture and angiotensin-induced hypertrophy (Abell et al., 1989; Itoh et al., 1991). Growth promoting effects generated by norepinephrine were inhibited by ANF treatment in both cardiocytes and fibroblasts (Calderone et al., 1998). Other cell types, such as

cultured endothelial cells respond similarly to NP treatment (Pedram et al., 2001). *In vivo*, ANF or NPR-A deficient mice have pronounced cardiac hypertrophy (John et al., 1995) (Lopez et al., 1995; Skryabin et al., 2004), presumably caused by the chronic increase in blood pressure. However, NPR-A deficient mice treated with anti-hypertensive agents still progressed to cardiac hypertrophy (Knowles et al., 2001), thus suggesting an anti-hypertrophic role of the NP/NPR-A system. Alternatively, mice overexpressing ANF have a 27% reduction in total heart weight as compared to their control littermates (Barbee et al., 1994).

BNP appears to inhibit cardiac interstitium remodeling through its antifibrotic effects (Tamura et al., 2000). BNP inhibition of TGF-β induced fibrosis was shown to be associated with cGMP-dependent protein kinase G and MEK/ERK pathways (Kapoun et al., 2004). Furthermore, *in vitro* studies demonstrated that BNP was produced in cardiac fibroblasts and that it significantly decreased *de novo* collagen synthesis and specifically increased protein expression of the metalloproteinases MMP-1,-2, and -3 (Tsuruda et al., 2002).

Actions on the renal system

The powerful natriuretic and diuretic effects of ANF and BNP are mainly related to an increase in glomerular filtration rate and filtration fraction as well as the inhibition of Na^+ reabsorption at the level of the collecting duct (Melo et al., 2000; Vanderheyden et al., 2004). The increase in glomerular filtration rate and filtration fraction results from dilatation of afferent arterioles and constriction of efferent

arterioles, which leads to an increase in glomerular capillary hydraulic pressure (Marin-Grez et al., 1986). These actions enhance the driving force for ultrafiltration and also contribute to an unfavorable gradient for Na^+ and water reabsorption (Maack, 1996). At the proximal tubule, ANF inhibits angiotensin-stimulated Na^+ and water reabsorption (Harris et al., 1987), while in the inner-medullary collecting duct ANF increases Na^+ urinary excretion by inhibiting its absorption through the cGMP-mediated inhibition of an amiloride-sensitive cation channel (Light et al., 1990; Light et al., 1989).

Intrarenal administration of ANF produces a significant inhibition of renin release (Burnett et al., 1984). Under low-output heart failure conditions, intrarenal infusion of ANF maintains renin release inhibition despite a sustained decrease in arterial pressure (Scriven and Burnett, 1985). ANF potent inhibitory action on renin release from the juxtaglomerular cells is mediated by cGMP-dependent protein kinases (Gambaryan et al., 1998; Kurtz et al., 1986).

Actions on the RAAS

Both ANF and BNP have powerful inhibitory effects on the RAAS. In the adrenal glands, ANF directly inhibits basal aldosterone secretion and regulates the adrenocortical response to adrenocorticotropin (ACTH) and ANG-II (Kudo and Baird, 1984). *In vivo*, intravenous administration of ANF in dogs reduced blood pressure, plasma renin levels, and plasma aldosterone levels (Maack et al., 1984). Disruption of NPR-A significantly increased renin and ANG-II levels shortly after birth, which

demonstrates a direct inhibitory effect of the NP/NPR-A system on renin and ANG-II (Shi et al., 2001). In heart failure, activation of the RAAS system is suppressed by ANF and BNP through direct inhibition of aldosterone synthesis and secretion (Franco-Saenz et al., 1989) and by suppression of renin release (Brenner et al., 1990; Burger et al., 2005).

Actions on the central nervous system

ANF and BNP have multiple actions on nerve activity. ANF reduces cardiac baroreceptor activity, which leads to the suppression of sympathetic outflow to the heart (Jin et al., 1992; Schultz et al., 1988). A diminished sympathetic activity together with an increase in vagal afferent activity leads to a reduction in heart rate and cardiac output (Schultz et al., 1988). Salt and water appetite is negatively influenced by ANF and BNP, thus leading to a reduction in extracellular fluid volume (Tarjan et al., 1988). Also, ANF suppresses water reabsorption by inhibiting vasopressin secretion from the posterior pituitary. This inhibitory action is sustained even in acute hemorrhage or prolonged dehydration (Samson, 1985). Furthermore, blunting of renal sympathetic nerve activity by ANF and BNP results in a reduction in Na^+ reabsorption (Thoren et al., 1986).

Importance of the function of the endocrine heart

To highlight the importance of the natriuretic peptide system in both physiological and pathophysiological states, investigators have disrupted the ANF gene, defined as *Nppa*, as well as its cognate receptor NPR-A, encoded by *Npr1* (Hill et al., 1995; John et al., 1995; Ogawa et al., 2001; Oliver et al., 1997; Sano et al., 1992b; Sano et al., 1992c; Yokota et al., 1994). John and colleagues (John et al., 1995) successfully reduced the circulating levels of ANF in homozygous *Nppa* null mice. These mice exhibited salt-sensitive hypertension, whereby the increase in blood pressure observed under standard diet is further increased under high salt diet (John et al., 1995). Since both ANF and BNP mediate their biological effects through the NPR-A receptor, knocking-out the gene encoding for the receptor would negate both ANF and BNP actions. Lopez *et al*. genetically disrupted the *Npr1* gene and observed an impairment of the cardiorenal system of mice fed on a normal salt diet which resulted in chronic elevation of blood pressure (Lopez et al., 1995), as similarly seen in the *Nppa* knockout mice (John et al., 1995). To further drive the point that the NPR-A receptor is crucial in the regulation of blood pressure, Oliver *et al.* generated mice with either a deficiency or an above normal copy number of the *Npr1* gene. Mice deficient in the *Npr1* gene displayed salt-sensitive hypertension, whereas those overexpressing the *Npr1* gene had lower blood pressure (Oliver et al., 1998). In another *Npr1* knockout model, deficiency of NPR-A caused significant hypertension leading to marked cardiac hypertrophy and interstitial fibrosis (Oliver et al., 1997). To demonstrate the local cardioprotective effects of the NP system *in vivo*, Holtwick *et al.* generated mice with

cardiocyte specific deletion of the *Npr1* gene (Holtwick et al., 2003). Under physiological conditions, these mice exhibited cardiac hypertrophy, while mice subjected to pressure overload displayed enhanced cardiac hypertrophy and marked diminishment of cardiac function (Holtwick et al., 2003). Consequently, impairment of the cardiorenal homeostasis and myocardial structure due to the genetic alterations in the *Nppa* or *Npr1* genes highlight the importance of the NP system in both physiological and pathophysiological conditions.

Mammalian heart

Heart development

Organ development, in embryogenesis involves the proper orchestration of morphogenetic events. The heart is the first organ to form and its development is highly conserved across species, from flies to humans (Srivastava and Olson, 2000). Progenitor cells within the anterior lateral plate mesoderm become committed to a cardiogenic fate after gastrulation (Schultheiss et al., 1995). The transcription factor, Mesp1, is the earliest marker identified of cardiovascular development (Saga et al., 2000). Mesp1 is required for the migration of cardiac precursors out of the primitive streak and is a key regulator of a number of cardiac specification transcription factors including Nkx2-5, GATA4, Mef2c, Hand2, and myocardin (Bondue and Blanpain, 2010; Evans et al., 2010). The transcription factor Nkx2.5 is the earliest specific molecular marker of cardiac lineage (Srivastava and Olson, 2000), while ANF, Chisel, connexins 40

and 43 are the earliest molecular markers of the four-chambered working myocardium (Christoffels et al., 2000; Delorme et al., 1997; Habets et al., 2002; Hiroi et al., 2001).

Lineage tracing experiments demonstrated that in the developing heart, the atrial and ventricular myogenic lineages are specified before the cardiac chambers become morphologically distinguishable, after cardiac looping (Meilhac et al., 2004; Meilhac et al., 2003). The specification of the atrial and ventricular precursors is dependant on their position along the anterior-posterior axis of the embryo. The ventricles derive from the anterior cardiac precursor cells, while the atria derive from the posterior regions of the primitive heart tube (Yutzey and Bader, 1995). The precise molecular events involved in chamber identity/specification are not completely known but to confer atrial or ventricular chamber specific identity, selective transcriptional activation and repression or restriction is required. COUP-TFII, for instance, is required for atrial growth and is specifically expressed in atrial precursors (Pereira et al., 1999). The transcription factor T-box protein 5 (Tbx5) confers atrial identity, while Irx4 and Hey2 confers ventricular identity by activating ventricular-specific genes and repressing atrial-specific genes (Evans et al., 2010).

Adult heart

The fully developed heart has important circulatory and endocrine functions. The structural and functional characteristics of the cardiac muscle lies somewhere between the skeletal and visceral muscles. In fact, like the skeletal muscle, the heart needs a large amount of energy in order to produce contractions. Similarly to visceral

muscles, the cardiac muscle undergoes continuous contractions which are rhythmic and are controlled by intrinsic mechanisms and modulated by external autonomic and hormonal stimuli.

The heart is a heterogeneous tissue primarily composed, based on mass, of rod-shaped cardiocytes that form myofibers, the contractile machinery of the heart. Modified cardiocytes, originating from the right atrial pacemaker tissue, form a conduction system that propagates action potential impulses throughout the heart (Moorman and Christoffels, 2003). The atrial cardiocytes secrete the polypeptide hormones ANF and BNP, which mediates the endocrine function of the heart (de Bold et al., 1981) and thus defines the heart as a contractile and endocrine organ. The heart is also made-up of various other cell types, such as vascular smooth muscle cells, endothelial cells, mast cells, and blood vessels (Moorman and Christoffels, 2003).

Cardiocyte ultrastructure

Cardiocytes are primarily composed of contractile proteins and mitochondria, which comprise 50% and 35% of the myocardial cell volume, respectively (Katz, 2001; Sommer and Waugh, 1978). Intercalated discs, which connect individual cardiocytes with each other, as well as a centrally located nucleus that can undergo division without partitioning the cytoplasm, distinguishes the cardiocytes from other cell types. The cardiocyte sarcoplasmic reticulum is less developed than the skeletal muscle because of the lack of large terminal cisternae, thus reducing the intracellular reserves of calcium. The mitochondria are arranged in rows within the myofibrillar interspace

and the transverse tubules (T-tubules), which carry the muscle action potentials down into the cells via invaginations of the sarcolemma, are transversely orientated and extend into the sarcomere Z line of the myofibrils (Sperelakis, 2001).

Atrial and ventricular cardiocyte phenotypes

The atrial cardiocytes are phenotypically distinct from the ventricle cardiocytes. In fact, the atrium is made up of cardiocytes that contain specific atrial granules (de Bold et al., 2001; Jamieson and Palade, 1964), that co-store the polypeptide hormones ANF and BNP. Other defining characteristic of the atrial cardiocytes is the presence of a rough-sarcoplasmic reticulum and a highly developed Golgi apparatus (Hibbs and Ferrans, 1969). These organelles are important in synthesizing and packaging ANF and BNP into the specific atrial granules. The T-tubules are poorly developed or absent in the atrial cardiocytes, while extensively present in the ventricular cardiocytes (Bootman et al., 2006). The thin wall atria, which are subjected to relative low pressure, have a lower density of myofibrils in the cardiocytes than the ventricles, which have a thicker muscular wall due to the higher pressure (Narolska et al., 2005). In contrast to the atrial cardiocytes, the ribbon-shaped contracting cells of the ventricles are larger and contain more densely packed mitochondria (Sperelakis, 2001).

The atria are further distinct from the ventricles with respect to their contractile proteins. The molecular motor of the heart is composed of two myosin heavy chains (MHC) and two pairs of myosin light chains (MLC). In the mammalian heart, MHC is

expressed by two distinct isoforms: α and β. These isoforms differ from one another in their intrinsic ATPase activity, i.e. the α isoform has a higher ATPase activity than the β isoform (Weiss and Leinwand, 1996). In the human, the atria express predominantly the α-MHC isoform, while the ventricles express predominantly the β-MHC isoform (Schaub et al., 1997; Swynghedauw, 1986), at 90% of the total MHC content (LeWinter, 2005; Miyata et al., 2000; Nagueh et al., 2004). In rodents, however, the atria and ventricles are mainly composed of the α-MHC isoform (Lompre et al., 1984). During fetal life, the β-MHC is the predominant isoform in the ventricles. The essential or alkali myosin light chains have two chamber specific isoforms, the atrial (ALC-1 or MLC1A) and ventricular (VLC-1 or MLC1V) isoforms (Hernandez et al., 2007). The atria and ventricles also express chamber specific regulatory MLC isoforms, MLC-2a (Kubalak et al., 1994) and MLC-2v (O'Brien et al., 1993), respectively.

Pathophysiological cardiac hypertrophy

Cardiovascular disease (CVD) is the number one cause of death in Canada, accounting for 31% of all deaths in 2005 (Statistics_Canada, 2005). Globally, CVD is responsible for more deaths than any other disease, with an estimated 17.1 million deaths in 2004 (WHO, 2004). CVD encompasses a wide range of cardiac and circulatory pathologies, including the debilitating disease of heart failure. Pathological cardiac hypertrophy, resulting from prolonged mechanical and/or neurohumoral stimuli, is the single most powerful predictor of the clinical course of heart failure, and it is an important risk factor for cardiovascular mortality in humans (Adams, 2001). Cardiac

hypertrophy is associated with the chronic increase in circulating levels of both vasoconstrictive and vasodilatory hormones (Nicholls et al., 1996), including those associated with the RAAS and sympathetic nervous system, as well as the cardiac hormones, ANF and BNP, respectively. In contrast to the adverse hemodynamic consequences generated by the vasoconstrictive systems, the NPs ANF and BNP are involved in the maintenance of the cardiorenal homeostasis (de Bold et al., 1996). In addition to the aforementioned cardiovascular regulation properties, ANF regulates myocardial structure through its growth-suppressing properties, which is attributable to its inhibitory regulation of cardiocyte hypertrophy (Horio et al., 2000), thus protecting the heart from excessive cardiac remodeling (Tokudome et al., 2005) (see section: Biological actions of ANF and BNP).

The cardiocytes, which are terminally differentiated and non-proliferating cells, increase their protein content and energy requirement to compensate for the increased workload produced by prolonged mechanical and/or neurohumoral stimuli. During the first phase of hypertrophy, the cardiocyte nuclei increase in size, the poorly developed ventricular Golgi complex hypertrophies, the ribosomes increase in number and the growing myofibrils are arranged perpendicularly to the cell's axis (Ferrans, 1982). Compensated and degenerated hypertrophy, which defines the second phase of cardiac hypertrophy, is characterized by an increase in cardiocyte size, cellular and myofibrillar disorganization, sarcoplasmic reticulum proliferation, Z-band abnormalities, sarcomeric disruption and an increase in collagen and interstitial fibrosis (Ferrans, 1982; Jones and Ferrans, 1979; Maron and Ferrans, 1978; Maron et al., 1975).

At the molecular level, there is a significant modification in the spatiotemporal expression of several genes, some of which are hallmarks of cardiac hypertrophy. These include genes coding for contractile proteins that are typically expressed during embryonic development. There is an increase expression in sarcomeric proteins, such as the β-MHC isoform. During increasing cardiac overload, the atrial and ventricle cardiocytes lose the α-MHC isoform gradually, whereas the selective expression of genes encoding the slow β-isoform increase, further replacing the α-isoform (LeWinter, 2005). Muscles that contain low myosin ATPase activity and slow intrinsic shortening velocity seem to work more efficiently when chronically overloaded and thus the increase in the β-isoform can play an important role in the long-term adaptation of cardiac performance to chronic overload (Katz and Katz, 1989). Furthermore, in overloaded ventricles, the reversion to the fetal phenotype is accompanied by an increase in skeletal α-actin expression (Chien et al., 1991), re-expression of the alpha smooth muscle actin (Black et al., 1991), and by the reappearance of atrial MLC isoforms, which replace the ventricular isoforms (Dorn et al., 2003; Schaub et al., 1998). The induction of the non-contractile proteins ANF and BNP is also observed in cardiac hypertrophy. During embryogenesis, ANF is expressed in both atrial and ventricular chambers, but its expression is specifically restricted to the atria shortly after birth. The activation of the cardiac fetal gene program during cardiac hypertrophy is also characterized by the ventricular re-expression of ANF and BNP. The increase atrial secretion of both ANF and BNP as well as their ventricular re-expression is a biological response highly conserved among a wide variety of species and across

various hypertrophic stimuli, e.g. pressure overload, volume overload, genetic mutation, hypertension, and neurohumoral stimulation (Chien et al., 1991).

The morphogenic changes occurring during cardiac hypertrophy is dependent on the type of hemodynamic stress. In volume overload, as seen in mitral or aortic valve regurgitation, atrial or ventricular septal defects, anemia, heart block, and aortocaval fistula, a chronic increase in preload or diastolic pressure produces eccentric cardiac hypertrophy due to serial replication of sarcomeres, which increases cardiocytes length (Grossman et al., 1975). This in turn increases chamber volume with ventricular wall thickness increased in proportion to chamber dimensions (Carabello, 1996; Dorn et al., 2003). In contrast, pressure-overload conditions (increase afterload or systolic pressure), such as hypertension, mitral valve stenosis and aortic valve stenosis lead to concentric hypertrophy (Abassi et al., 2011) due to parallel replication of sarcomeres, which in turn increases cardiocytes cross-sectional area and leads to an increase in ventricular wall thickness with no change in chamber volume (Dorn et al., 2003; Grossman et al., 1975). Eccentric hypertrophy appears to be mediated by growth factors, such as insulin-like growth factor 1 (ILGF-1), and at a lesser extent by ANG-II (Haddad et al., 2003; Ruzicka et al., 1993), while concentric hypertrophy is predominantly mediated by neurohumoral activation of Gαq protein signaling pathway (Wettschureck et al., 2001).

Aortocaval shunt: a model of volume-overload induced cardiac hypertrophy

Experimental animal models of cardiac hypertrophy and heart failure have been developed based on the etiology of the corresponding clinical outcome under investigation. These included: transgenic or knockout mice, aortic banding, coronary ligation, salt-sensitive and spontaneous hypertension, and aortocaval shunt. The aortocaval shunt is the most frequently used animal model for inducing volume-overload (VO) hypertrophy in rats (Bader, 2010; Patten and Hall-Porter, 2009). This model produces a chronic increase in preload or diastolic pressure as a consequence of the diversion of a portion of the arterial blood flow to the venous circulation and generates a progressive and substantial increase in cardiac hypertrophy and dilatation accompanied with myocardial remodeling (Abassi et al., 1990; Abassi et al., 2001; Abassi et al., 1997; Brodsky et al., 1998; Hoffman et al., 1991; Karram et al., 2005; Winaver et al., 1988). As a consequence to the increase venous blood flow to the right atria, aortocaval shunt produces a decrease in mean arterial pressure and subsequent activation of vasoconstricive neurohumoral systems, through the baroreceptors in the arterial circulation. As a compensatory mechanism, vasodilatory and natriuretic systems, mediated by ANF, BNP, NO and PGE2, are activated (Abassi et al., 2011; Flaim et al., 1980; Liu et al., 1991). During volume-overload, the cardiac tissue stretches to accommodate the extra blood volume, similar to the levels observed in the pathophysiological conditions described above, with the greatest and earliest effect being seen in the atria (Haddad et al., 2003; Haddad et al., 2005; Wahlander et al., 1993). Intra-atrial volume expansion produces atrial cardiocytes stretch, which is the

main stimulus for the secretion of ANF and BNP hormones into the circulation (Kuroski-de Bold and de Bold, 1991). The induction of ANF and BNP secretion is a hallmark feature observed in pathological cardiac hypertrophy and is markedly elevated in the volume-overload model (Hoffman et al., 1988; Hoffman et al., 1991; Villarreal and Freeman, 1991; Villarreal et al., 1991, 1992; Willenbrock et al., 1999; Winaver et al., 1988) as well as other animal models of congestive heart failure (Burnett et al., 1986; Lee et al., 1989; Riegger et al., 1988; Villarreal and Freeman, 1991; Villarreal et al., 1993). The reversal of the hemodynamic overload to the heart is coupled with a significant reduction in plasma ANF levels (Alexander and Imbembo, 1989; Hoffman et al., 1990). Hence, aortocaval shunt is an ideal model for the analysis of the molecular changes involved in the stimulation of the endocrine heart.

Gene expression analysis

Traditionally, gene expression has been defined as the process by which cells convert DNA sequence information derived from protein-coding genes to mRNA and then decode the mRNA information to functional products, i.e. amino acid sequences of polypeptides (Brown, 2002). These series of events are known as transcription and translation, respectively. The complete collection of RNA molecules transcribed from the genome makeup the transcriptome of a given cell, cell population, or organism, while the proteome is comprised of the expressed proteins. Changes in cellular responses to environmental and biological perturbations resulting in both morphological and phenotypic changes are indicative of alterations in gene expression

(Morozova et al., 2009). Determining when, where and to what extent a gene is being differentially expressed under specific conditions is crucial for the understanding of the biological function of the encoded protein (Lockhart and Winzeler, 2000).

The low throughput techniques used to study mRNA transcript levels, such as Northern blot and RT-PCR, are base on a candidate gene approach. This approach necessitates previous knowledge and understanding of the mechanisms underlying the disease under investigation and thus limits the potential discovery of new genes implicated in the disease process. Genome-wide analysis, on the other hand, is a method that measures expression levels of thousands of known or putative transcripts simultaneously, allowing for large-scale gene expression profiling of the cell population or tissue under investigation. Microarrays, a method based on the principals behind Northern and Southern blots (Heller, 2002), are used to assess the presence, absence and abundance of thousands of transcripts, thus providing important insight into global cellular processes and responses, previously not achievable by the classical candidate gene approach (Heller, 2002).

Oligonucleotide arrays

Oligonucleotide microarrays, such as those manufactured by Affymetrix (Lockhart et al., 1996), are made using both photolithography and combinatorial chemistry technology (Fodor et al., 1991; Lockhart et al., 1996). Over a million different oligonucleotide probes are synthesized *in situ*, in specific locations, onto a glass surface, i.e. array. The array is coated with chemical linkers containing light-sensitive

protecting groups. A series of masks are applied to protect or deprotect the photolabile groups upon ultraviolet light exposure, according to a specific grid pattern. When light shines through the mask windows, the protecting groups are selectively removed and thus able to couple to a protected nucleotide (Dalma-Weiszhausz et al., 2006; Heller, 2002). The array is then bathed with either adenine, cytosine, thymine or guanine photolabile protected nucleotides. *In situ* oligonucleotide synthesis is achieved by successive cycles of masking, light deprotection, and chemical coupling of selective protected nucleotide (Dalma-Weiszhausz et al., 2006; Heller, 2002). Each synthesized oligonucleotide probe is 25-bp in length and can be represented over a million times in its specific location (Lipshutz et al., 1999). Each protein-coding gene is represented by eleven distinct oligonucleotide probe sets on the array. This allows for multiple independent measurements of each target transcript, thus increasing the reliability and reproducibility of each data point (Ness, 2007).

To determine gene expression levels within a biological sample, high quality total RNA is isolated and reversed transcribed into double stranded cDNA. An *in vitro* transcription step then incorporates a biotin-labeled uracil base to the cRNA. The labeled cRNA is fragmented and added to the microarray (Affymetrix, 2009). Hybridization occurs when specific complimentary sequences of both the labeled cRNA and oligonucleotide probes interact. The microarray is washed to remove unbound cRNA, stained with streptavidin phycoerythrin conjugate and finally scanned to excite the fluorescent labeled cRNA (Affymetrix, 2009). The light emitted at 570 nm is proportional to the bound target at each oligonucleotide position on the probe array

(Affymetrix, 2009). Each probe set intensity is summarized into an expression measure using model-based summary statistics (Irizarry et al., 2003a).

Aim of study

The endocrine heart synthesises and secretes two polypeptide hormones: the natriuretic peptides ANF (de Bold et al., 1981) and BNP (Maekawa et al., 1988). The biological actions of these hormones serve both acutely and chronically to reduce systemic blood pressure and hemodynamic load to the heart (McGrath et al., 2005), thus contributing to the maintenance of cardiorenal homeostasis. Considerable effort has been focused on the elucidation of the mechanistic underlying ANF and BNP gene expression and secretion by the atrial cardiocytes, but much remains to be determined regarding specific molecular events involved in the cardiocyte secretory function.

The focus of this work was to identify genes involved in the transcriptional response of the endocrine heart under normal and stimulated states with the ultimate purpose of characterizing targets to manipulate synthesis or secretion of the cardiac natriuretic peptides and to eventually identify targets for molecular therapy. The results acquired from this work will provide insight into the mechanism of natriuretic peptide secretion, which is of considerable importance given their beneficial effects in cardiovascular diseases.

Hypothesis

Gene expression profiling of the atrial and ventricular muscles under normal conditions and under conditions known to stimulate the endocrine heart will identify specific genes in defined functional clusters that participate in the regulation of the endocrine function of the heart.

Material and methods

Animals

Normal

Normal male Sprague Dawley rats (225–275 g; Charles River Laboratories, Wilmington, MA) were used as control animals. The hearts were excised from thirteen rats, weighed and dissected in cold saline. The tissues (left atrium appendage (LA), right atrium appendage (RA), left ventricular free wall (LV) and right ventricle (RV)) were wrapped in aluminum foil and snap-frozen in liquid nitrogen and stored at -80 ˚C. The experimental protocol was carried out according to the Canadian Council on Animal Care Guide to the Care and use of Experimental Animals following approval by the University of Ottawa Animal Care Committee.

Aortocaval shunt

The aortocaval shunt was produced in rats by a method previously described (Garcia and Diebold, 1990). A laparotomy, under isoflurane anesthesia was performed in Sprague-Dawley rats (225-275 g; Charles River Laboratories, Wilmington, MA) in order to isolate the inferior vena cava and abdominal aorta. The abdominal aorta and inferior vena cava were clamped and an 18-gauge needle was used to puncture the abdominal aorta below the left renal artery. The needle was pushed within the vessel

and redirected towards the adjacent inferior vena cava until puncturing of the vena cava (Figure 3). After removal of the needle, cyanoacrylate glue (Krazy glue ®) was applied to the puncture in order to seal the wound. The clamp was removed allowing blood to flow back into the vessels. The sham-operated rats underwent the same surgical procedure with the exclusion of the vessel puncture. The rats were sacrificed by decapitation 1, 2, 7, and 28 days post surgery. The hearts were excised, weighed and dissected according to the 4 chambers in cold saline. The tissues were wrapped in aluminum foil and snap-frozen in liquid nitrogen and stored at -80˚C. Each shunt (volume-overload; VO) and sham groups was comprised of 6 rats. As I was a junior trainee, Dr. Tsuneo Ogawa carried out the aortocaval shunt surgeries while he trained me in this technique. The experimental protocol was carried out according to the Canadian Council on Animal Care Guide to the Care and use of Experimental Animals following approval by the University of Ottawa Animal Care Committee.

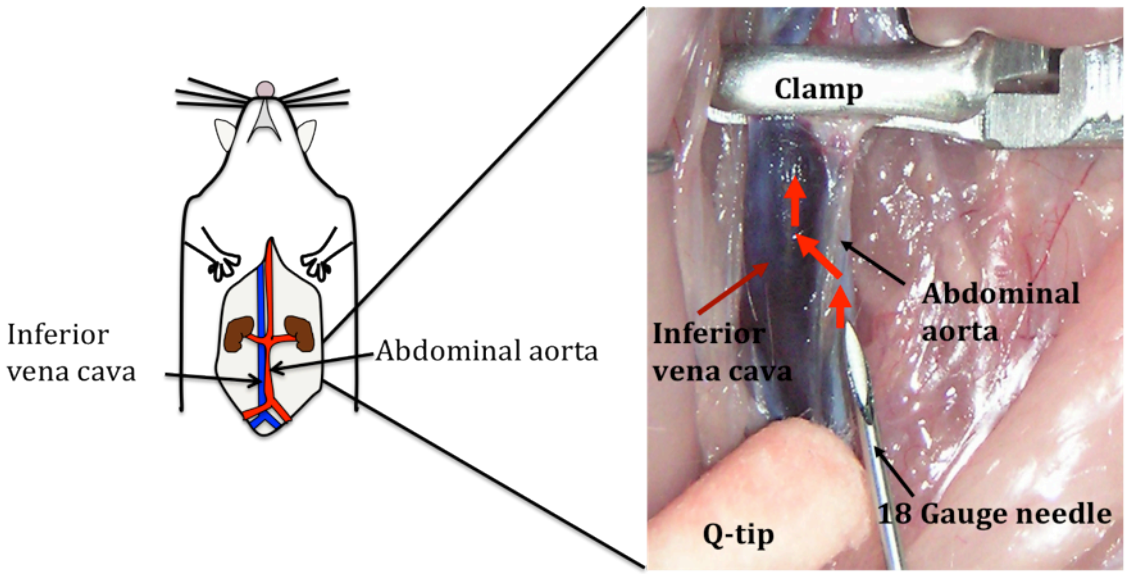


Figure 3. Aortocaval shunt surgery.

An 18-gauge needle is used to puncture the abdominal aorta below the left renal artery. The needle is pushed within the vessel and redirected towards the adjacent inferior vena cava until puncturing of the vena cava and by consequence creating a shunt. The wound is sealed with cyanoacrylate glue and the clamp removed. Slight pulsation of the inferior vena-cava as well as incorporation of arterial blood with venous blood in the vena-cava confirmed the success of the shunt.

Plasma samples

Trunk blood samples were collected in chilled Vacutainer tubes containing ethylene-diamine tetraacetic acid (EDTA) (VWR International Ltd., Mississauga, Ontario, Canada). Plasma was immediately separated by centrifugation at 2000 *x g* for 20 min at 4˚C and then stored in cryovials at –80˚C until assayed. Upon thawing, plasma samples were acidified by adding 100 µl 1.0 N HCl/ml plasma and extracted with Sep-Pak C_{18} cartridges (Millipore-Waters Corp., Milford, MA).

Radioimmunoassay

Radioimmunoassay (RIA) was performed using the double antibody technique as previously described by Sarda *et al*. (Sarda et al., 1989). Briefly, standard curves were made in RIA buffer (0.1 M potassium phosphate, 0.9% NaCl, 0.01% sodium azide, 0.1% triton X-100, and 0.1% heat-treated BSA) with the following concentrations (pg/0.1 ml) of $ANF_{99\text{-}126}$ peptide (Peninsula laboratories, Belmont, CA): 3.125, 6.25, 12.5, 25, 50, and 100. Quality control samples were prepared with 12.5 and 25.0 pg/0.1ml of $ANF_{99\text{-}126}$ peptide. One hundred µL of standard solution, quality control or sample (in duplicate) were incubated with 100 µL of antiserum (dilution: 1:12000) obtained from rabbits immunized against $ANF_{99\text{-}126}$ (Phoenix Pharmaceuticals, Burlingame, CA; RAB 005-24, lot # 505903) for 4h at 4˚C. One hundred µL of iodinated

$ANF_{99\text{-}126}$ (9000 to 10000 cpm) was added to the standard solution, quality control, samples, blank (without antiserum) and empty tube (represents the total cpm count) for 18h at 4˚C. To separate free and bound fractions of ANF, 100 μL 5% normal rabbit serum and 100 μL of goat anti-rabbit IgG serum (Phoenix Pharmaceuticals, Burlingame, CA; GAR-500) were added to each tube and incubated for 2h at room temperature. Prior to centrifugation, 1.5 ml of 6.25% polyethylene glycol (Sigma-Aldrich) was added to each tube. Following centrifugation at 2700 rpm (Beckman J-6) for 45 min at 4˚C, supernatant was removed by decantation and the radioactive pellet was counted in a gamma counter. Values are means ± standard deviation (SD). To determine pairwise statistical differences, Student's *t*-tests were performed. $P < 0.05$ was considered significant.

RNA extraction

Normal animals

The left atrial appendages as well as the left ventricular free wall of thirteen normal male Sprague Dawley rats were pooled in order to create 4 biological replicates per tissue type. Total RNA was extracted using Trizol® (Invitrogen, Carlsbad, CA) following the manufacturer's instructions. The quality of the extracted RNA was assessed using an Agilent Bioanalyzer (Agilent Technologies, Palo Alto, CA).

Aortocaval shunt animals

Total RNA was extracted from the 1, 2, 7 and 28 day post surgery left and right atria appendages as well as left ventricular free wall and right ventricle of sham and aortocaval shunt operated rats using Qiagen RNeasy Mini columns (Mississauga, Ontario), following the manufacturer's instructions. Since the cardiac muscle contains substantial amount of contractile proteins, the adapted "RNeasy Mini protocol for isolation of total RNA from heart, muscle and skin tissue" was use, which contains a proteinase K digestion step. For GeneChip hybridization, RNA extracted from the 28-day time point was pooled in order to create three biological replicate per group.

Tissue culture

Total RNA was extracted from HL-1 cells using 1 ml of Trizol® (Invitrogen, Carlsbad, CA) per tissue culture well (24 well plate), following the manufacturer's instructions. The quality of the extracted total RNA was assessed by the Agilent 2100 Bioanalyzer, using the Agilent RNA 6000 Nano kit (Agilent Technologies, Palo Alto, CA).

Northern Blot

Total RNA from atrial appendages (7 μg) and ventricles (7 μg) were electrophoretically separated in an agarose-formaldehyde gel and blotted onto a nylon membrane (Hybond N+, Amersham Corp., Arlington Heights, IL) overnight. Four cDNA probes were used. The cDNA probes used: 1) a 900-bp EcoRI/HindIII fragment

containing the full-length rat ANF cDNA, 2) a 595-bp SalI fragment containing full-length rat BNP cDNA, 3) a 5-kb EcoRI/SalI fragment of the mouse 28S rRNA cDNA probe, and, 4) a 2-kb BamHI/BglII fragment of the mouse phosphoglycerate kinase (PGK) gene cDNA (Bruneau and de Bold, 1994). The housekeeping probes PGK and 28S ribosome were used as internal control for normalization to correct for loading conditions and mRNA transfer onto the membranes. The bands were scanned and quantified using Molecular Imager Fx (BIO-RAD, Mississauga, ON) and Quantity One version 4.1.1 software (BIO-RAD, Mississauga, ON). Values are means ± SD. To determine pairwise statistical differences, Student's *t*-tests were performed. $P < 0.05$ was considered significant.

Gene expression arrays

Hybridization

Ten µg of total RNA was used to generate the first strand cDNA using the one cycle target labeling protocol. The biotin-labeled cRNA was prepared according to the manufacturer's protocol and hybridized to the GeneChip® Rat Genome 230 2.0 Array (Affymetrix, Santa Clara, CA) which contains 31042 probe sets and analyses over 30000 transcripts from 28000 genes. Detailed description of the hybridization protocol is available at https://genomequebec.mcgill.ca/nanuqAdministration/nanuq-administration/protocols.go. These steps were carried out by the Genome Québec Innovation Centre (Montreal, QC).

A pilot study was undertaken to determine the efficacy of the GeneChip technology. The Rat Expression set 230 (RAE 230A and RAE 230B) GeneChips were hybridized with the cRNA generated from the LA and the LV tissue from normal, sham and aortocaval shunt animals (1, 2, 7 and 28 day post surgery). A single GeneChip replicate per group was generated. The Genome Centre at the Ottawa Hospital Research Institute carried out the pilot study.

Normal animals

Four biological replicates per tissue type, i.e. LA and LV, were generated for the normal animals. These replicates are assigned as:

-Control LA 1, Control LA 2, Control LA 3, Control LA 4
-Control LV 1, Control LV 2, Control LV 3, Control LV 4

Aortocaval shunt animals

Three biological replicates per tissue type, i.e LA, RA and LV, were generated for the 28-day post surgery sham (replicates 1 to 3) and aortocaval shunt (replicates 4 to 6) animals. These replicates are assigned as:

- 28d shunt LA 1, 28d shunt LA 2, 28d shunt LA 3
- 28d shunt RA 1, 28d shunt RA 2, 28d shunt RA 3
- 28d shunt LV 1, 28d shunt LV 2, 28d shunt LV 3
- 28d sham LA 4, 28d sham LA 5, 28d sham LA 6
- 28d sham RA 4, 28d sham RA 5, 28d sham RA 6
- 28d sham LV 4, 28d sham LV 5, 28d sham LV 6

GeneChip Analysis

Following microarray hybridization, the average background and noise values of each array were assessed. All arrays that were subsequently compared had similar background values. Poly-A controls, generated from *B. subtilis* genes (*dap, lys, phe, thr,* and *trp*), as well as biotin-labeled *E. coli* genes (*bioB, bioC, bioD,* and *cre*) were used as spike controls to serve as internal controls and evaluate sample hybridization efficiency to the arrays.

The files containing cell intensities (.CEL) were visually inspected with the dChip (www.dchip.org) and Flexarray (http://genomequebec.mcgill.ca/FlexArray/) softwares as a quality control measure in order to identify local image artifact prior to normalization. Preliminary expression summaries produced by Microarray Analysis Suite 5.0 (MAS5) software (Affymetrix, Santa Clara, CA) were used to generate scatter plots and detection calls. The expression level summary files were computed by Robust Multiple-Array Averaging (RMA), which is implemented in Bioconductor (www.bioconductor.org).

For the two group comparisons, differential expression of genes was considered to be significant based Significance Analysis of Microarrays (SAM) (www-stat.stanford.edu/~tibs/SAM) with a False Discovery Rate (FDR) of 0.1 %, followed by a Welch *t*-test with a standard Bonferroni p-value < 0.01 correction. Genes were considered biologically differentially expressed based on an up- or down-regulation of expression levels by at least 1.8 fold (log base 2 = 0.848).

For multiple group comparisons, differential expression of genes was considered to be significant based on a two-way analysis of variance (ANOVA) with a $p < 0.001$ and a FDR adjusted $p< 0.045$ (factor 1: tissue, factor 2: condition).

Sample hierarchical clustering was performed with TIGR MeV software (http://www.tm4.org/) using the Pearson uncentered correlation with complete linkage. Pathway analysis, which identifies biologically relevant networks that exist among differentially expressed genes, was done by Gene Map Annotator and Pathway Profiler (GenMAPP) software (www.genmapp.org). Functional annotation clustering and gene functional classification was carried out using Database for Annotation, Visualization, and Integrated Discovery (DAVID) (http://david.abcc.ncifcrf.gov/). Statistically over-represented Gene Ontology terms were assessed with the GOstat program (www.gostat.wehi.edu.au/).

The microarray data has been deposited in the National Center for Biotechnology Information's Gene Expression Omnibus (GEO) and complies with MIAME standards (accession numbers: GSE5266 and GSE12758).

Reverse transcription-polymerase chain reaction

Real-time reverse transcription-polymerase chain reaction (RT-PCR) was used to validate expression profiles of selected genes. One microgram of total RNA was used for reverse-transcription, using the Transcriptor First-Strand cDNA Synthesis kit, (Roche Applied Science, Laval). Quantitative PCR was performed using the LightCycler 480 SYBR green 1 Master, according to the manufacturer's protocol (Roche Applied

Science, Laval). The analysis was performed using the Roche LightCycler 480 relative quantification software.

Normal animals

Primer nucleotide sequences were obtained from the literature and validated by Primer3 software (http://frodo.wi.mit.edu/primer3/input.htm). Primer nucleotide sequences are listed in Table 1. Standard curves were performed in triplicate for each primer pair. Glucose-6-phosphate dehydrogenase (G6PD) was used as the reference gene. RT-PCR was performed in quadruplet for each gene. Concentration ratios were subjected to calibrator normalization and efficiency correction.

Aortocaval shunt animals

Primer nucleotide sequences were designed using Primer3 software (http://frodo.wi.mit.edu/primer3/input.htm) (Table 1). Standard curves were constructed in triplicate for each primer pair. G6PD was used as the reference gene. RT-PCR was performed in triplicate for each gene. Concentration ratios were subjected to calibrator normalization and efficiency correction.

Tissue culture

Primer nucleotide sequences were designed using Primer3 software (http://frodo.wi.mit.edu/primer3/input.htm) or designed by Integrated DNA Technologies (IDT, Iowa, USA) (Table 1). Standard curves were constructed in triplicate for each primer pair. Ribosomal protein L23 (RPL23) was used as the reference gene. RT-PCR was performed in triplicate for each gene. Concentration ratios were subjected to calibrator normalization and efficiency correction.

Table 1. Primer oligonucleotide sequences used for real-time PCR

Name	Forward Primer	Reverse Primer
1368987_at	CTTTTCTCATCCCCTCACCA	GGGAAGAAAGGGAGATCCTG
1373628_at	GTGGTGTGAAAGCAGGTGAA	CAGACATTTTTCCCCCTGTG
Acta1	CTCTCTCTCCTCAGGACGACAATC	CAGAATGGCTGGCTTTAATGCTTC
ANF	GCCGGTAGAAGATGAGGTCA	GGGCTCCAATCCTGTCAATC
Bet1	AAGCAAGTGGGAGAGCAGAA	GAGGAAAGAAACGGCCCTAC
BNP	TCTGCTCCTGCTTTTCCTTA	GAACTATGTGCCATCTTGGA
Cxcr4	CTCCAAGCTGTCACACTCCA	TCCCCACGTAATACGGTAGC
Ebp4.1l3	GCTGGCTCAGGCAATTAAAG	ACATAGGCTCCGGTTTTCCT
EDG2	GCCAGAGGAGACGAAGACAC	GGCTTAGGCCAAACCACATA
Fgg	GGCCACCTCAATGGAGTTTA	CTGTTTGGATCCTCCCATGT
FZD2	ATCGTCATCGCCTGCTACTT	TGGTGAGACGCGTGTAGAAC
G6PD	CCAGCCTTCTACAAGCACCTCAA	AATAGCCCCCACAACCCTCAGTA
Gαo	GTCACCGACATCATCATTGC	AGGTTAGACAGGGGCTTGGT
GAPDH	ACCCAGAAGACTGTGGATGG	ACACATTGGGGGTAGGAACA
Gja4	TGATCACAGGTGGTTCTGGA	AGCCAGCAGCCTACATCAGT
HPRT	GGCTATAAGTTCTTTGCTGACCTGC	GCTTGCAACCTTAACCATTTTGGG
ICA1	GAACCTGAAAGTGGGGACAA	GTGAAGGAAGGAACGCAGAG
Kcna5	CCCAGCAGAGGGATAATCAA	GTGTCCCAGGAAATGGTGAC
Kcnj5	TCCTTCTAGTGCAGGCCATC	TTTTCCAAGGTGAGGACTGG
Kir6.1	CACAAGAACATCCGAGAGCA	CAGACTCCAGGCCACTCTTC
Nr2f2	AAAGTCCCAGTGTGCTTTGG	ATATCCCGGATGAGGGTTTC
Pitx2	GTACCCCGGCTACTCGTACA	CACCATGCTGGACGACATAC
Rab15	GTCTCCGAGCAACCTCTGTC	GCTTTGACTCCAGCCTTGAC
RASD1	GCGGCGAAGTCTACCAGTTG	TGTCTAAGCTGAACACCAGAATGA
RGS2	ATTGGAAGACCCGTTTGAGCTA	TTCCTCAGGAGAAGGCTTGATAA
RGS4	CCCAGACTGCTGTCTCACAA	CGCTGAGGCCTATAAAGCAC
RGS6	ATGTCGGCGTTTGAAGAATC	AAGCTTTCAGCCACTTTGGA
RPL23	CTGTGAAGGGAATCAAGGGA	TGTCGAATTACCACTGCTGG
Sec22	GCAAGATGTGCAGAGGATCA	ATCTCACAGCCACCAAAACC
SGNE1	TCCAAATCCCTGTCCTCTTG	TGTCCAGCCTCTTTCCTTGT
Snca1	TCCTAAGATCTGCCCAGGTG	CAGCACACAAGAGCCTGCTA
Thbs4	CATTCCGTGCAGTAGCAGAA	AAAACCGCACCCTGATGTAG
TREK-1	GTGTCCTCTTCGTGGCTCTC	ACGAGGATCCAGAACCACAC
Wisp2	GTAGAGCCACTGAGCGATCC	TTCAGGCAATCTGCTGTCTG

Differential centrifugation

Differential centrifugation was used to isolate the microsomal fraction from homogenized tissue. The left and right atria appendages and the left ventricular free wall were obtained from normal male Sprague Dawley rats (225-275 g; Charles River Laboratories, Wilmington, MA), sacrificed by decapitation. Atrial and ventricular tissues were respectively homogenized with a polytron in ice-cold buffer (50 mM Tris-HCl pH 7.4, 1 mM EDTA pH 8.0, 100 mM NaCl, 10 mM DTT, 1 mM phenylmethylsulfonyl fluoride (PMSF) and proteinase inhibitor cocktail). The samples were further processed with a glass homogenizer. The final homogenate was centrifuged at 1900 x g_{max} for 10 min at 4°C with JA-20 rotor (J-21 series centrifuge). The post-nuclear supernatant was collected. The pellet was re-homogenized and centrifuged at 1900 x g_{max} for 10 min at 4°C. The supernatants from both centrifugations were pooled. The pooled supernatants were centrifuged at 1900 x g_{max} for 10 min at 4°C. The supernatant was collected and centrifuged at 32000 x g_{max} for 10 min at 4°C. Supernatant was aliquoted into polycarbonate tubes and ultracentrifuged at 144880 x g_{av} for 90 min at 4°C with 50.2 Ti rotor Ultracentrifuge. The post-ultracentrifugation supernatant fraction was stored in -80°C and the membrane protein pellet was homogenized with a glass Potter Elvehjem and solubilized overnight at 4°C in RIPA buffer (150 mM NaCl, 50 mM Tris, 1 mM EDTA, 1% Nonidet P-40, 0.5 % sodium deoxycholate, 1 mM PMSF, 5 ug/ml proteinase inhibitor cocktail). Protein concentration was determined by BCA protein assay kit (Pierce, Thermo Scientific).

Western blot

Prior to electrophoresis, protein samples taken up in 10 µl 5X sample buffer and 5 µl 1M DTT were heated for 5 min at 95°C. Samples were loaded on a 10-20% precast linear gradient polyacrylamide Tris-HCl Ready Gel (Bio-Rad, Mississauga, Ontario), run at room temperature for 45 min at 200 V and transferred onto a PVDF membrane either at 100 V for one hour or overnight at 4°C at 67 V. Membranes were blocked (blocking buffer: Tris-buffered saline Tween-20 (TBST), 5% w/v non fat milk) for 1 hour at room temperature. Blots were washed 3 times with TBST for 5 minutes and incubated overnight at 4°C in primary antibody dilution buffer (TBST, 5% w/v non fat milk). Primary antibody dilutions: proANF 1:1000 (rabbit 5, bleed 8 (R5B8)), Gαo 1:1000 (551, MBL, Japan), Gγ2 1:700 (sc-374, Santa Cruz Biotechnology, CA), TREK-1 1:200 (sc-11556, Santa Cruz Biotechnology, CA), RASD1 1:1000 (AB15794, Millipore, Temecula, CA), GAPDH 1: 500 (sc-32233, Santa Cruz Biotechnology, CA), and α-tubulin 1:400 (sc-8035, Santa Cruz Biotechnology, CA). Membranes were washed 3 times with TBST for 5 minutes. The immune complex was detected by using secondary antibodies conjugated to horseradish peroxidase enzyme (goat anti-rabbit (sc-2004, Santa Cruz Biotechnology, CA), donkey anti-goat (sc-2020, Santa Cruz Biotechnology, CA), goat anti-mouse (sc-2005, Santa Cruz Biotechnology, CA) and anti-biotin (Cell Signaling Technology, MA)) followed by enhanced chemiluminescence, Supersignal west Femto (Pierce, Fisher Scientific). Images were taken with the FluroChem Imaging System (Alpha Innotech). The biotinylated protein ladder (77275, Cell Signaling Technology, MA), kaleidoscope protein ladder (161-0375, Bio-Rad Life Science, CA) and positive

control rat brain extract (sc-2392, Santa Cruz Biotechnology, CA) were also loaded on the gels.

Immunofluorescence

Paraffin-embedded, paraformaldehyde (PFA)-fixed rat atrial tissue sections were deparaffinized in toluene and hydrated in a graded alcohol series. The sections were incubated for 30 minutes in 3% H_2O_2/methanol and washed for 5 minutes in phosphate buffered saline (PBS).

HL-1 cells were culture on pre-coated gelatin/fibronectin microscope slides for 48h and fixed in 2 % PFA for 30 minutes at room temperature. For TYE™ 563-labeled transfection control, cover slips were placed at the bottom of each well (from 24 well plate) and pre-coated with gelatin/fibronectin. HL-1 cells were plated (20000 cells per well) and the following day, transfected with TYE™ 563-labeled transfection control. Cells were fixed the next day in 2% PFA for 30 min.

The tissue sections as well as the fixed cells sections were then blocked with 5% normal goat serum in PBS for 30 min followed by a single wash in PBS. The sections were then incubated with primary antibody in 2 % normal goat serum, 2 % BSA in PBS overnight at 4°C. Primary antibody dilutions: ANF 1:800 (R5B8), TREK-1 1:100 (sc-11556, Santa Cruz Biotechnology, CA), and RASD1 1:1000 (AB15794, Millipore, Temecula, CA), Gαo 1:200 (551, MBL, Japan), Bet1 1:50 (sc-28084, Santa Cruz Biotechnology, CA). Sections were rinsed in PBS for 5 min and incubated for 30 min with diluted biotinylated goat anti-rabbit IgG (H+L) (BA-1000, Vector Laboratories, CA)

or donkey anti-goat-FITC (sc-2024, Santa Cruz Biotechnology, CA) secondary antibody. Sections were rinsed in PBS for 5 min then incubated for 30 min with either Vectastain ABC Texas Red-Avidin D (A-2006, Vector Laboratories, CA) or Fluorescein Avidin DCS (A-1100, Vector Laboratories, CA). Sections were mounted with Vectashield mounting medium with DAPI (H-1200, Vector Laboratories, CA). Images were obtained with Leica fluorescence confocal microscope. Unless otherwise stated, all images were taken while sections were under oil immersion.

For double immunofluorescence labeling, sections were incubated overnight with primary antibody against the first antigen, RASD1, as above. Following 30 min incubation with biotinylated secondary antibody, sections were incubated with Avidin conjugate Fluorescein Avidin DCS (A-1100, Vector Laboratories, CA). Sections were rinsed in PBS and re-incubated with an excess of biotinylated secondary antibody to mask all free primary antibody IgG sites that may not have been targeted earlier. Sections were rinsed in PBS and incubated with Avidin D blocking solution for 15 min followed by incubation with Biotin blocking solution for 15 min (Avidin/Biotin blocking kit, SP-2001, Vector Laboratories, CA). Sections were incubated in citric phosphate buffer, pH 2.2 for 1 hour. Sections were then incubated with second primary antibody, against Gαo, overnight. The remainder of the immunofluorescence procedure is carried as above. Note Avidin conjugate Texas Red-Avidin D (A-2006, Vector Laboratories, CA) was used instead of Fluorescein Avidin DCS. Sections were mounted with Vectashield mounting medium with DAPI (H-1200, Vector Laboratories, CA). Images were obtained with Leica fluorescence confocal microscope.

Cell line and culture

The immortalized cell line, HL-1, derived from AT-1 mouse atrial cardiocytes, was a generous gift from Dr. W. C. Claycomb (Louisiana State University, New Orleans, LA) (Claycomb et al., 1998). In a 24 well plate, HL-1 cells were seeded at an initial density of 50000 cells/well. HL-1 cells were cultured at 37°C under 5% CO_2 on pre-coated gelatin/fibronectin wells in Claycomb medium supplemented with 10% fetal bovine serum (FBS), 0.1 mM norepinephrine, 2 mM $_L$-glutamine and 100 U/ml:10 μg/ml penicillin/streptomycin (White et al., 2004).

RNA-interference mediated silencing in HL-1 cells

For the HL-1 cell line, transfection optimization was required in order to determine the appropriate cell plating density, identify the optimal DharmaFECT transfection reagent as well as the ideal DharmaFECT reagent volume per tissue culture well. In a 24 well plate, HL-1 cells were seeded, at an initial density of 50000 cells/well. HL-1 cells were cultured as described above with the exclusion of 100 U/ml:10 μg/ml penicillin/streptomycin. For starved experiments, HL-1 cells were incubated in antibiotic free Dulbeccos's Modified Eagle's Medium nutrient mixture F-12 HAM (DMEM F-12) (D6421, Sigma Aldrich) supplemented with insulin-transferrin-sodium selenite (I1884, Sigma Aldrich).

For RNA interference (RNAi), 27-mer double stranded RNA (dsRNA) duplexes targeting RASD1, Gαo, Gβ1, Gγ2, as well as the controls (scrambled universal negative control (NC), HPRT-S1-DS positive control and TYE™ 563-labeled transfection controls) were designed and synthesized by Integrated DNA Technologies (Integrated DNA Technologies (IDT), Coralville, IA), as part of the TriFECTa™ kit. ANF and GAPDH (positive control) targeted short interference RNA (siRNA) oligonucleotides were designed and synthesized by Dharmacon (Thermo-Scientific, Lafayette, CO). RNAi sequences are listed in Table 2 and Table 3.

Twenty-four hours after plating HL-1 cells, 10 nM of dsRNA (IDT) or 100 nM siRNA (Dharmacon), was transfected into HL-1 cells using DharmaFECT1 (Thermo-Scientific, Lafayette, CO) transfection reagent, according to the manufacturer's instructions. Media was collected and replaced with fresh antibiotic-free Claycomb media every 24hs. HL-1 cells were harvested at 48 hours or 72 hours post-transfection for total RNA or protein extraction.

Table 2. RNAi oligonucleotide sequences designed by Dharmacon

Name/ product number	Sense target sequence
Mouse RASD1, NM_009026 ON-TARGETplus set of 4 LQ-040275-00-0002 J-040275-05,06,07,08	CAACCGCGACUCAUUCGAA CAAGGUAUCUGUGCAGUAC GAUGUUCCGUGCGCUCUUU GCGGCGAAGUCUACCAGUU
Mouse RASD1, NM_009026 siGENOME set of 4 MU-040275-01-0002 D-040275-01,02,03,04	GACACAUUCCGGCAAUCAU GAUGUUCCGUGCGCUCUUU GCGACGUACUGCACAAGAA CAACCGCGACUCAUUCGAA
Mouse RASD1, NM_009026 ON-TARGETplus set of 4 LQ-040275-01-0002 J-040275-09,10,11,12	CCAAGAGAAUGUGGACGU CCUCAUGUACAUUCGUGAA CGGCAUUGUGUCGCGCUU GGGAAGUAGAGCAGCGGGA
Mouse Nppa, NM_008725 ON-TARGETplus SMARTpool L-051029-01-0005	CCUCGGAGCCUACGAAGAU CUAUCACGAUCGAUGUUAA ACACAGAUCUGAUGGAUUU AUAUUAAGGUAGAUCCUCA
Mouse GAPDH, NM_008084 ON-TARGETplus control pool D-001830-20-05	GUGUGAACCACGAGAAAUA GGAGAAACCUGCCAAGUAU UCAAGAAGGUGGUGAAGCA UGGUGAAGCAGGCAUCUGA

Table 3. dsRNA sequences designed by IDT

Name/ product number	Sense	Antisense
TYE563 DS transfection control	T*CCUUCCUCUCUUUCUC UCCUUGUG*A	T*CACAAGGGAGAGAAAG AGAGGAAGG*A
HPRT-S1 DS positive control	GCCAGACUUUGUUGGAUU UGAAATT	AAUUUCAAAUCCAACAAA GUCUGGCUU
NC1 DS Negative control	CGUUAAUCGCGUAUAAUA CGCGUAT	AUACGCGUAUUAUACGCG AUUAACGAC
RASD1 NM_009026 duplex 1 MMC.RNAI.009026.10.1	GGACUAAUAAUAGGGCAU UAUCUTG	CAAGAUAAUGCCCUAUUA UUAGUCCUG
RASD1 NM_009026 duplex 2 MMC.RNAI.009026.10.2	GCGACGUACUGCACAAGA AGGCUCT	AGAGCCUUCUUGUGCAGU ACGUCGCAG
RASD1 NM_009026 duplex 3 MMC.RNAI.009026.10.3	CCUGUGACUUAAAGUAAC UGUCC	GGACAGUUACUUUAAGUC UCACAGGCU
RASD1 NM_009026 duplex 4 MMC.RNAI.009026.10.4	GAAAGAGAACUAGCUAAG ACAGGAG	CUCCUGUCUUAGCUAGUU CUCUUUCCU
Gnao1 NM_010308 duplex 4 MMC.RNAI.01030812.4	GGUGCUCCACGAGGACGA AACCACG	CGUGGUUUCGUCCUCGUG GAGACCUG
Gnb1 NM_001160016 duplex 1 MMC.RNAI.001160016.12.1	AGAGCACAAUUCCCAUUA AGAGAAG	CUUCUCUUAAUGGGAAUU GUGCUCUUG
Gnb1 NM_001160016 duplex 2 MMC.RNAI.001160016.12.2	AGCACUGAGACGUGAAGA UGAGUGA	UCACUCAUCUUCACGUCU CAGUGCUUU
Gnb1 NM_001160016 duplex 3 MMC.RNAI.001160016.12.3	AGAAUCGCAUGCUGUAGA AAUGCTC	GAGCAUUUCUACAGCAUG CGAUUCUAA
Gng2 NM_0010238637 duplex 1 MMC.RNAI.0010238637.12.1	GGAGUUAACUAUGUCCAA UUAAAGT	ACUUUAAUUGGACAUAGU UAACUCCUU
Gng2 NM_0010238637 duplex 2 MMC.RNAI.0010238637.12.2	GGACGCUCAUGAAGAUUU AAUGGTA	UACCAUUAAAUCUUCAUG AGCGUCCCG
Gng2 NM_0010238637 duplex 3 MMC.RNAI.0010238637.12.3	GGGACAUACAUGUAGAGU UCCUAGC	GCUAGGAACUCUACAUGU AUGUCCCAG

RNA quality control

Prior to RT-PCR, total RNA quality was assessed. RNA sample aliquots were heat denatured (70°C, 2 min) and 1 μl of each aliquot was pipetted into the corresponding wells of the RNA Nano Chip, according to the manufacture's instructions (Agilent RNA 6000 Nano kit, Agilent Technologies, Palo Alto, CA). The 2100 Bioanalyzer Expert Software calculated the RNA concentration, RIN value, and ribosomal ratio for each RNA sample.

Protein extraction from HL-1 cells

HL-1 cells were washed once in ice cold PBS and scraped with ice-cold RIPA buffer (150 mM NaCl, 50 mM Tris-HCl, pH 7.4, 1 mM EDTA, 1% Nonidet P-40, 0.5% sodium deoxycholate, 5 μg/ml Protease inhibitor cocktail and 1 mM PMSF). Lysate was incubated for 1 hour at 4°C with orbital shaker and stored at -80°C overnight. Samples were then centrifuged at 10000 rpm for 10 min at 4°C. The pellet was discarded and protein concentration of the supernatant was determined using the bicinchoninic acid (BCA) protein assay kit (Pierce, Thermo Scientific). Western blots were carried out as described above.

For ANF content determination, HL-1 cells were grown in a 24 well plate in the conditions described above. At 90% confluency, cells were rinsed twice in DMEM F-12 medium and scraped into 500 μl of DMEM F-12 medium. Cells were lysed be repeated freeze/thaw cycles, and centrifuged (500 *x g* for 5 min) prior to RIA.

Pharmacological stimulation

MAS-7 (Sigma Aldrich) effect on ANF secretion was determined in HL-1 cells, 72 hours post-RNAi-transfection, for concentrations ranging from 5 to 40 μM. Media was collected at various time points to determine ANF secretion levels.

Results

Chapter 1: Pilot study and GeneChip quality control

Pilot study

To determine the efficacy of the microarray technology, a pilot study was undertaken whereby the labeled cRNA generated from the left atrial (LA) and the left ventricular (LV) tissues from normal, sham and aortocaval shunt rats, at 1, 2, 7 and 28 days post-surgery, was hybridized to the Rat Expression set 230 (RAE 230A and RAE 230B) GeneChips. The expression levels of the cardiac natriuretic peptides, ANF and BNP, in normal and diseased states, in both atrial and ventricular tissues, are well documented. For this reason, the differential expression levels of ANF and BNP were evaluated in various microarray comparisons to determine the reliability of this technology. The gene expression profiles of both ANF and BNP were then validated by Northern blot. In general, ANF and BNP gene expression patterns were similar between the microarray and Northern blot techniques, with the exception of the LV control vs. LA control comparison (see Figure 4 for BNP expression levels). In this comparison, BNP was not differentially expressed between the normal atrial and ventricular tissues according to the microarray data (Figure 4), while Northern blot analysis demonstrated a 2-fold difference. The microarray data was not consistent with the expected fold change difference of BNP in normal heart tissue. Hence relative BNP expression levels were also assessed in the right atria and right ventricles by Northern

blot and real-time RT-PCR, in seven normal Sprague-Dawley rats. Both Northern blot (not shown) and real-time RT-PCR (Figure 5) confirmed higher atrial abundance of BNP expression levels, as compared to the ventricles. This demonstrated that reliable microarray data could only be achieved by increasing the number of animals per group (replicates).

Several hundreds of genes were differentially expressed, based on a 2-fold change cut-off, in various comparisons (Table 4), thus demonstrating that the microarrays were sensitive enough to detect global gene expression differences in the heart, between different conditions and tissues. However, since the microarray pilot study did not contain biological replicates, significance in differential gene expression levels could not be determined. Furthermore, chamber specific genes, such as the atrial abundant genes ANF, BNP, MLC1A, and MLC-2a, as well as the ventricular abundant genes MLC1V and MLC-2v, were found differentially expressed between LA sham vs. LV sham samples which supports the strength of the GeneChip technology and demonstrates that the differences in gene expression profiles observed between the tissues are not due to chance.

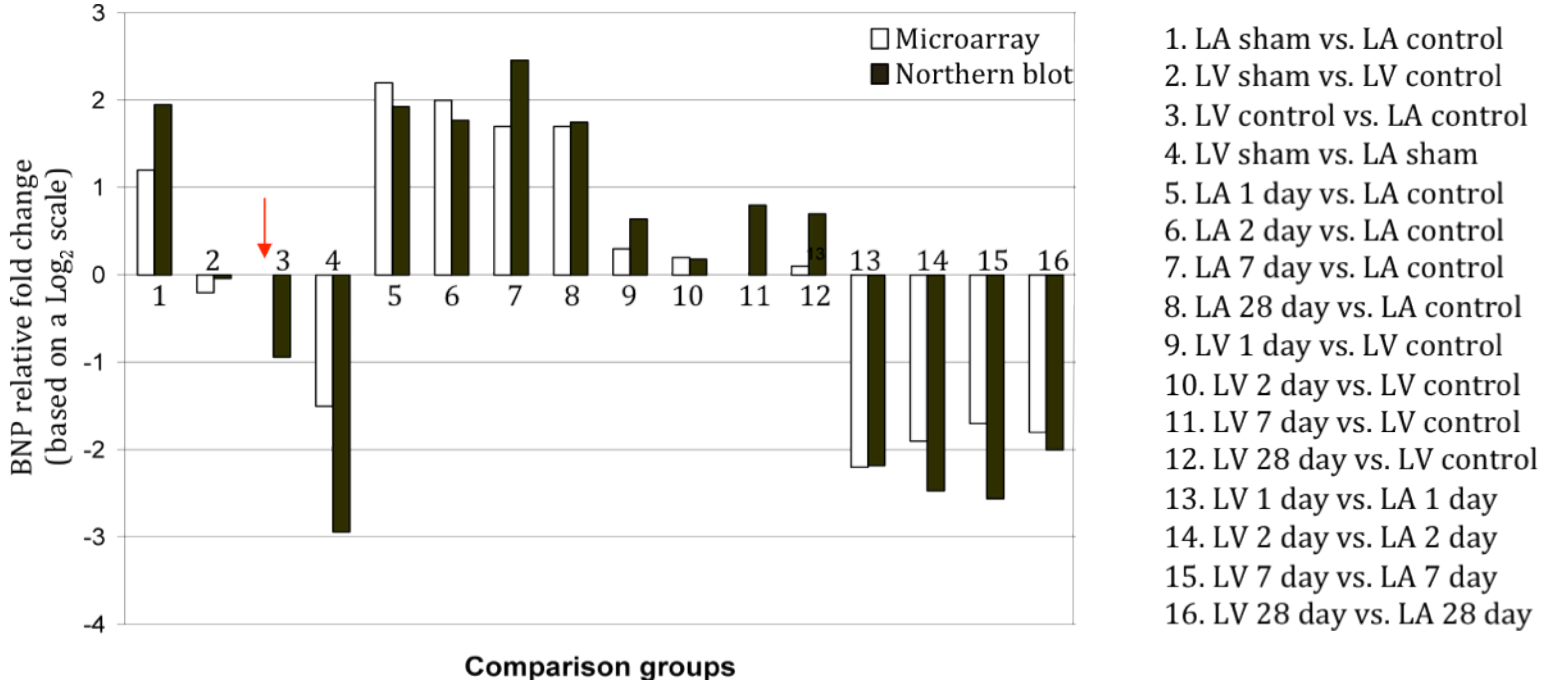


Figure 4. BNP relative fold change between numerous tissue comparisons as determined by microarray and Northern blot.

Each tissue comparison is listed on the right of the figure. Open columns represent BNP relative fold change obtained by microarray, while solid columns represent BNP relative fold change obtained by Northern blot. The arrow points to the comparison that did not show differential expression of BNP between control atrial and ventricular tissues.

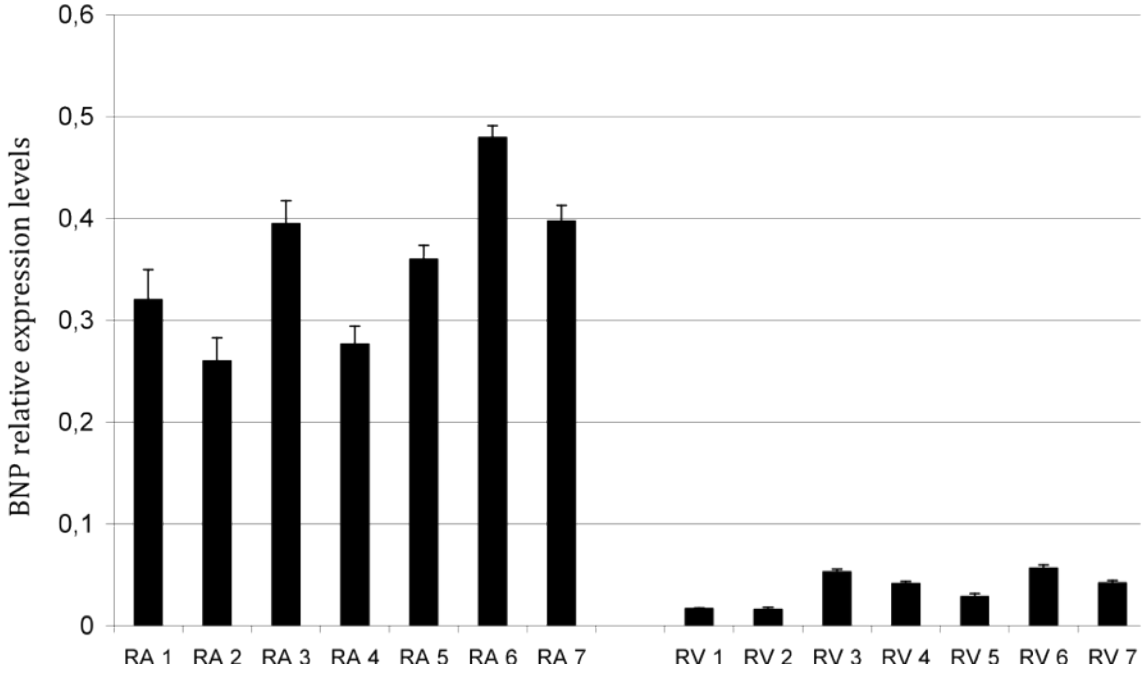


Figure 5. BNP relative expression levels in right atrial and right ventricular tissues.

Expression levels obtained by real-time RT-PCR, n= 5.

Table 4. Number of differentially expressed genes identified between various tissue and condition comparisons in the microarray pilot study.

Comparisons	Number of genes differentially expressed	
	A chip	B chip
LA sham vs. LA control	22	8
LV sham vs. LV control	101	128
LA control vs. LV control	203	36
LA sham vs. LV sham	423	116
LA 1 day shunt vs. LA control	163	67
LA 2 day shunt vs. LA control	264	104
LA 7 day shunt vs. LA control	173	74
LA 28 day shunt vs. LA control	78	39
LA 1 day shunt vs. LV 1 day shunt	452	66
LA 2 day shunt vs. LV 2 day shunt	281	151
LA 7 day shunt vs. LV 7 day shunt	255	54
LA 28 day shunt vs. LV 28 day shunt	233	133

The RAE 230 GeneChip set is composed of two chips: A and B. Differentially expressed genes were determined based on a 2-fold cut-off. Only probe sets having a "present" call were included in the data set.

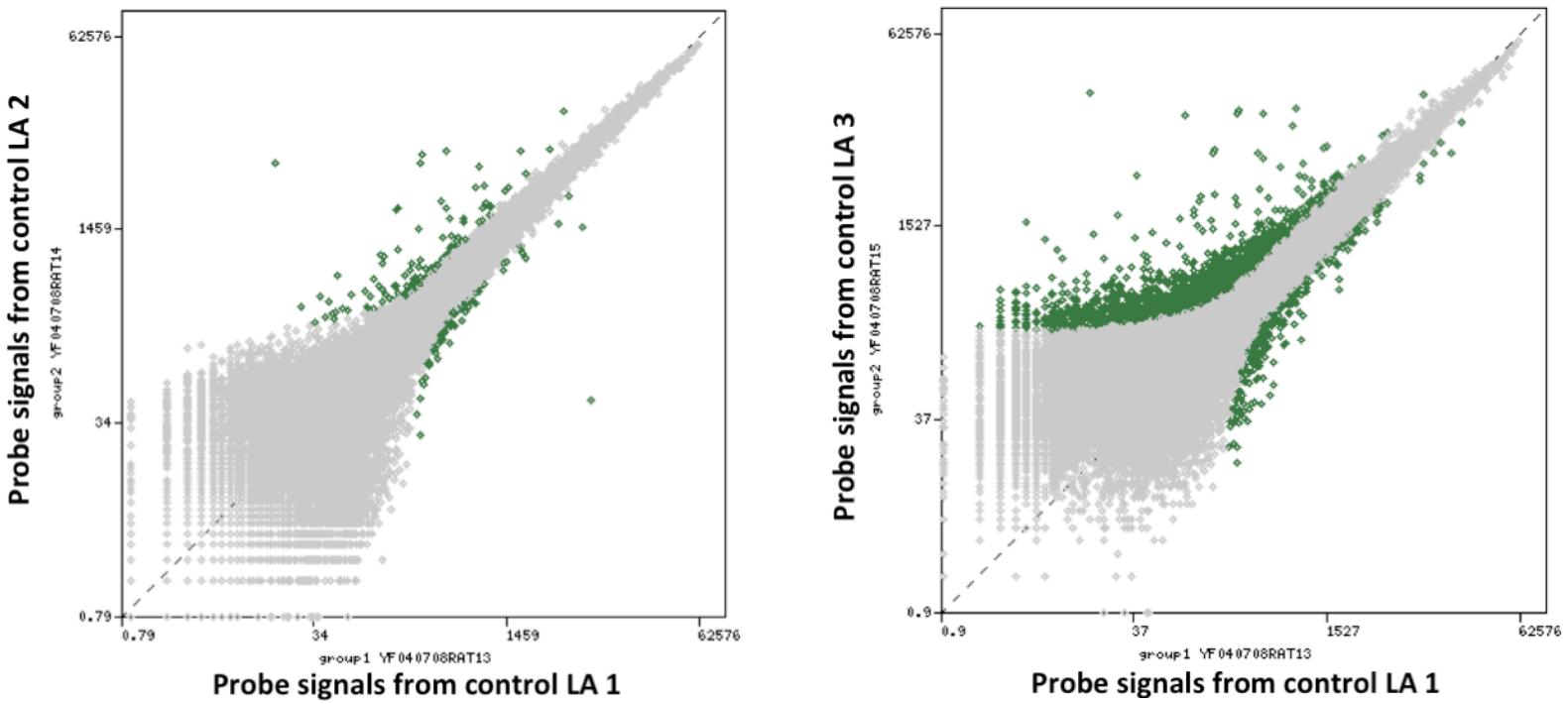
GeneChip quality control of replicate study

The quality of the RNA samples was analyzed prior to GeneChip hybridization. The RNA integrity numbers (RIN) obtained from the Agilent Bioanalyzer electropherograms were all above 9.0, out of a possible 10.

The cell intensity files, which contain the signal intensity data, were visually inspected as a quality control measure in order to identify local image contamination. Among all GeneChips analyzed, only one array had a hybridization problem (YF040708RAT15), which represented the normal LA 3 replicate. This GeneChip was discarded and a new array was hybridized with the remainder of the labeled cRNA obtained from the normal LA 3 sample (YF040722RAT01).

Preliminary expression summaries produced by MAS5 software were used to generate scatter plots, to assess microarray reproducibility, and detection calls. The signal intensities from all GeneChips were visualized by pairwise scatter plots, where individual chips within the same group were plotted against each other. Under the same conditions, a within-class scatter plot (intra-experimental scatter plot) will generate a graph with data points tightly grouped along the dashed y=x line. Within-class plots were created for all control LA replicate combinations, control LV replicate combinations as well as for 28d shunt LA, 28d shunt RA, 28d shunt LV, 28d sham LA, 28d sham RA, and 28d sham LV replicate combinations in order to detect large differences between probe intensities (outliers). A typical within-class scatter plot is shown in Figure 6A, where the signal intensities from the control LA 1 GeneChip was

plotted against those from the control LA 2 GeneChip. All but one within-class scatter plot showed a minimal degree of variation. The scatter plot generated from the control LA 1 vs. control LA 3 GeneChip signal intensities showed poor agreement between both biological replicates, as demonstrated by the looser groupings along the dashed y=x line at the lower probe intensity range (Figure 6B). This result corroborated the cell intensity data analysis, as well as the poor percentage of "present" calls of the control LA 3 GeneChip, which indicated poor hybridization. None of the GeneChips had to undergo manual correction for localized background errors.

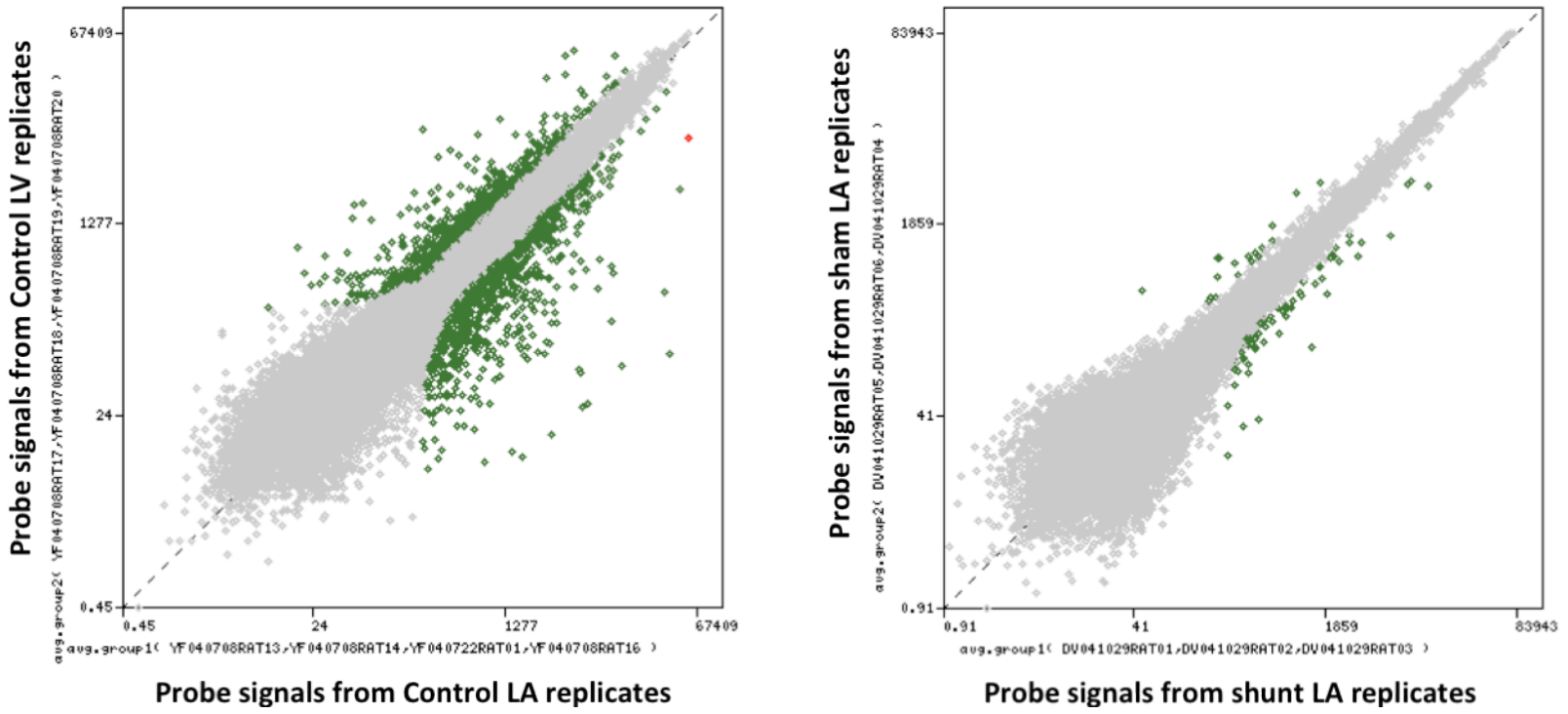


A) B)

Figure 6. Within-class scatter plots.

A) Control LA 1 (YF040708RAT13) vs. control LA 2 (YF040708RAT14) signal intensities. B) Control LA 1 (YF040708RAT13) vs. control LA 3 (YF040708RAT15) signal intensities. Selected probes are differentially expressed by > 2 fold. Note, control LA 3 (YF040708RAT15) array was discarded and replaced due to poor hybridization.

Between-class scatter plots represent the average expression level of each probe set between two groups. It is possible to evaluate, at a glance, the extent of the differential expression in a given comparison. When comparing two different tissues, such as the left atria and the left ventricle, one would expect to obtain a large number of differentially expressed genes (Figure 7A). Conversely, comparing samples from the same tissue origin, such as 28-day shunt LA vs. 28-day sham LA, but under different conditions might yield a smaller number of differentially expressed genes (Figure 7B). The between-class scatter plots confirm the expected differential gene expression results.



A) B)

Figure 7. Between-class scatter plots.

A) Between-class scatter plots representing the average of differentially expressed genes between group 1 (X=control LA replicates) and group 2 (Y=control LV replicates). B) Between-class scatter plot representing the average of differentially expressed genes between group 1 (X=28 day shunt LA replicates) and group 2 (Y=28 day sham LA replicates). Highlighted spots represent probe sets differentially expressed >1.8 fold.

Hierarchical clustering of all microarray replicate samples was performed in order to validate the quality of the biological replicates. Sample clustering consist in identifying and joining together the pair of samples that is most similar, followed by the identification of the next most similar pair of samples. These steps are repeated until all samples are integrated into a single larger cluster. Hence, samples within the same biological replicate are likely to cluster together since their gene expression profiles should be very similar. As expected, all control LA replicates clustered together as well as all control LV replicates (Figure 8A). Replicates from 28-day shunt and sham LA chips clustered together as did the 28-day shunt and sham LV samples (Figure 8A). However, within the 28-day shunt and sham LV cluster, the 28-day shunt LV 2 sample appeared to be more similar to the 28-day sham LV replicates. This inconsistency disappeared once the sample hierarchical clustering tree was generated with the data obtained from only the statistically differentially expressed genes found between the 28-day sham LV replicates and 28-day shunt LV replicates (Figure 8B). Subsequent analysis of the right and left atrial tissues from 28-day sham and shunt conditions demonstrated that the biological replicate clustered together (Figure 8C).

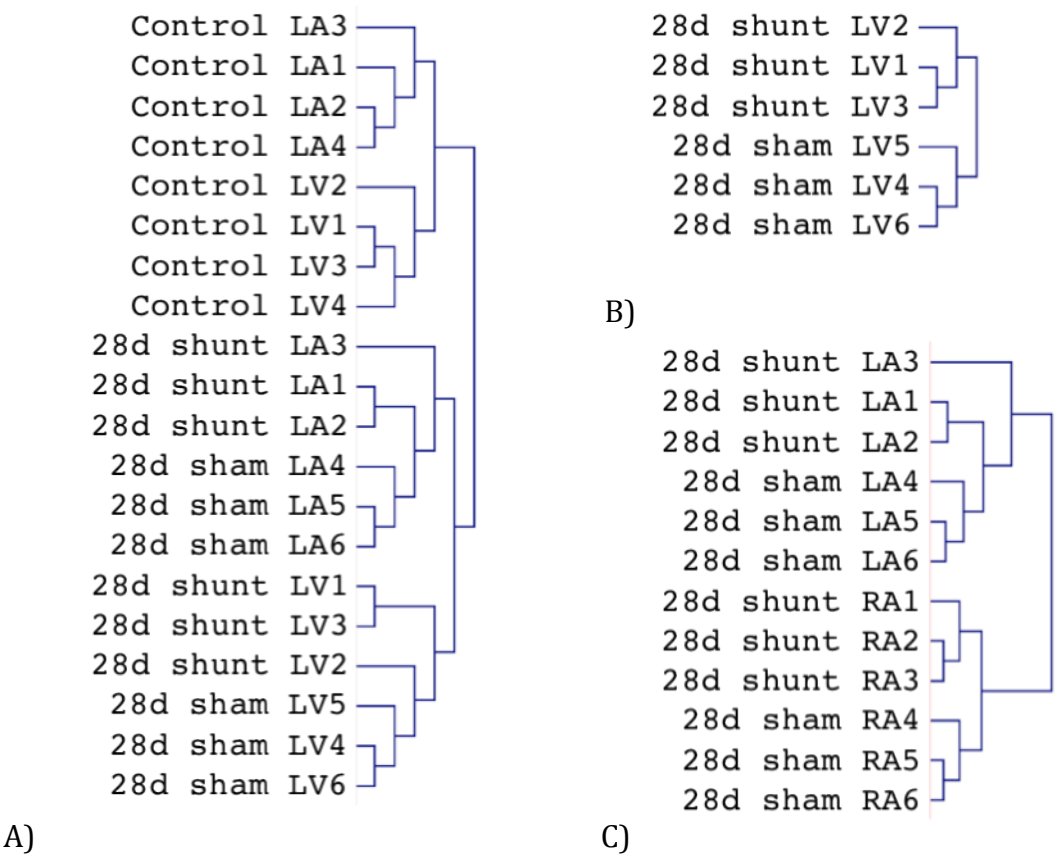
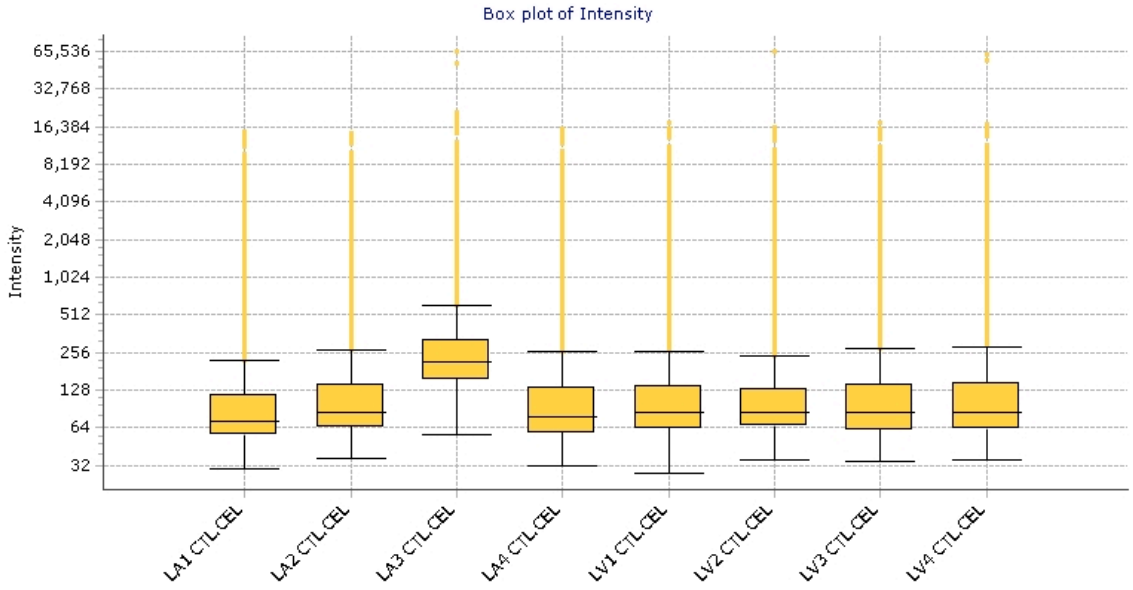


Figure 8. Sample hierarchical clustering trees.

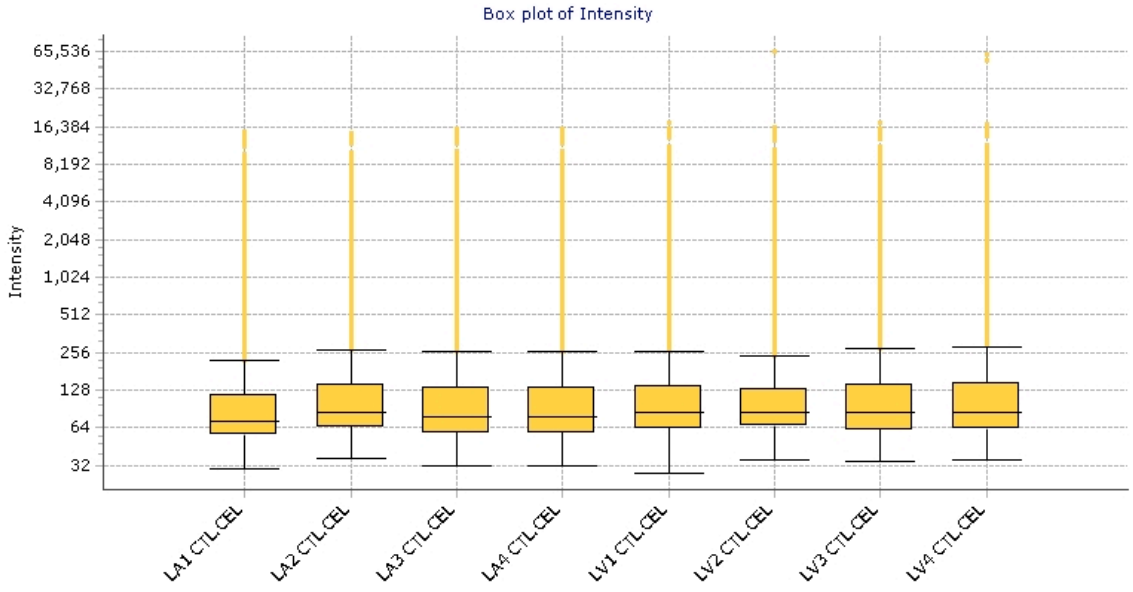
A) Sample hierarchical clustering tree of 20 microarray gene expression profile samples obtained prior to statistical analysis. B) Sample hierarchical clustering tree of 28-day shunt and sham LV replicates based on statistically differentially expressed gene list. C) Sample hierarchical clustering tree of right and left atrial 28-day shunt and sham replicates obtained prior to statistical analysis. Distance: Pearson uncentered with complete linkage.

Box plots were generated in order to visualize the amount of variation found in the raw microarray data within an array and between arrays. Each box plot is composed of a central line that represents the signal intensity median of the array, a box, which represents the 75th percentile (top edge of box) and 25th percentile (bottom edge of box) of the signal intensities, and vertical lines which represent the 95th percentile (top edge of the vertical line) and the 5th percentile (bottom edge of the vertical line) of signal intensities. All other signal intensity values are found below or above the vertical lines.

The box plots generated from the microarray data of the control LA and control LV samples are shown in Figures 9A and B. All samples had similar signal intensity variation and median values with the exception of the control LA3 array (LA3 CTL.CEL) (Figure 9A). As mentioned previously, this array was subsequently discarded and replaced with a new array. The new control LA3 array displayed similar box plot properties as the other replicates (Figure 9B). Box plots obtained from the LA and LV 28-day sham and shunt samples had similar signal intensity variations (Figure 10A). Right atrial sham and shunt samples had higher median and signal intensity variations than those from the left atrial sham and shunt samples (Figure 10B). The variation in the raw microarray data is explained by differences in system noise. The samples obtained from the right atria were hybridized to the arrays on a different date and by a different technician than those from the left atria. The signal intensity variations were corrected following quantile normalization.



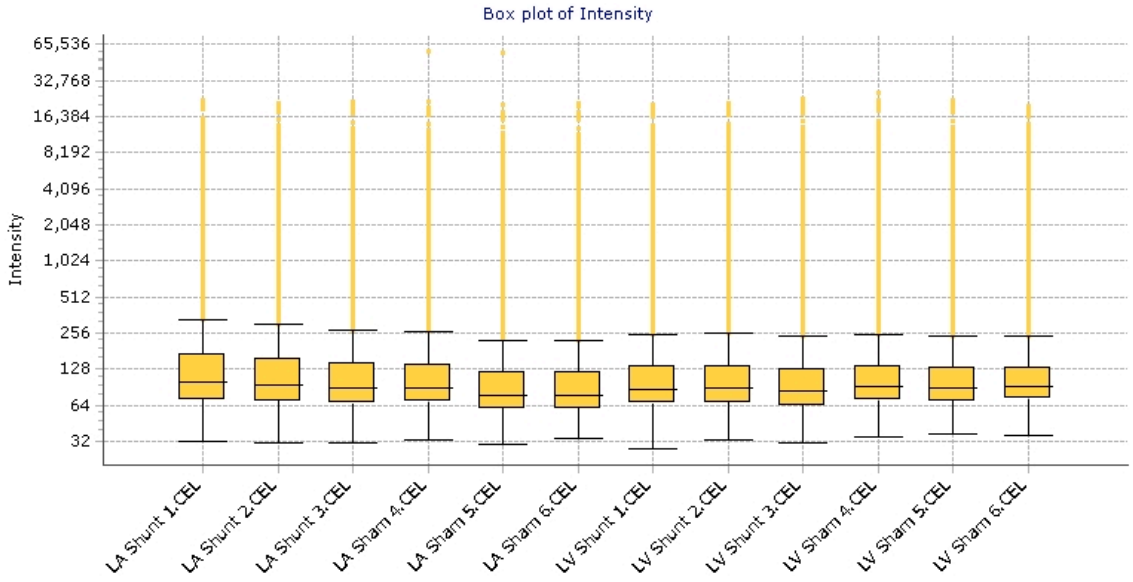
A)



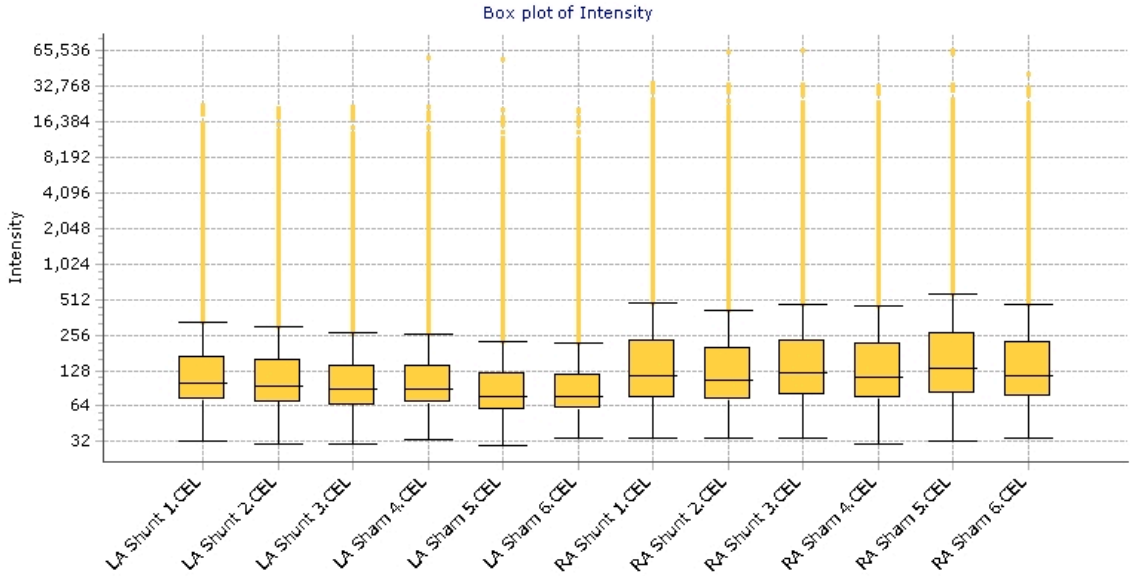
B)

Figure 9. Box plots displaying log_2 signal intensities of control atrial and ventricular microarray replicates.

A) Box plots of atrial (left atria (LA) (n) control (CTL)) and ventricular (left ventricles (LV)(n) control (CTL)) samples. Note the higher median of LA3 CTL.CEL sample. B) Box plots of LA n CTL and LV n CTL samples, with the substituted LA3 CTL array.



A)



B)

Figure 10. Box plots displaying log_2 signal intensities of 28-day sham and shunt atrial and ventricular microarray replicates.

A) Box plots of left atrial (LA) shunt replicates (n), LA sham replicates (n), left ventricular (LV) shunt replicates (n) and LV sham replicates (n). B) Box plots of left

atrial (LA) shunt replicates (n), LA sham replicates (n), right atrial (RA) shunt replicates (n) and RA sham replicates (n).

Chapter 2: Gene expression analysis of normal tissue

Background

Following the pilot study, presented in chapter 1 of the results section, it was determined that the Affymetrix GeneChips were able to detect changes in gene expression levels of several hundreds of genes across numerous sample comparisons. This demonstrated that microarrays were sensitive enough to detect global gene expression differences in the heart. To identify statistically significant differentially expressed genes, a replicate study under normal conditions was undertaken whereby four biological replicates per tissue type (i.e. atrium vs. ventricle) were used, for a total of 8 microarrays. In chapter 1, scatter plots, hierarchical sample clustering and box plots were generated to assess sample quality prior to gene expression analysis.

Differentially expressed genes between normal atrial and ventricular tissues

From the 31042 probe sets found on the Rat genome 230 2.0 microarray, an average of 59% and 56% of probes had present calls in the atria and ventricles, respectively. Based on a 1.8 fold change ratio criterion, 1415 probe sets were statistically differentially expressed between the atria and ventricles. Of these, 859 probe sets showed higher expression levels in the atrial samples and 556 probe sets showed higher expression levels in the ventricles. The degree of change of the differentially expressed probes ranged between the 1.8 fold minimum set cut-off and

245 fold (see Appendix 4, p, 284). Chamber specific genes were found differentially expressed in our dataset. Sarcolipin, an atrial-specific Ca^{+2} binding protein was expressed 245.97 fold higher in the atria than the ventricles. Other atrial specific genes include dickkopf homolog 3 (3.32 fold), ANF (12.88 fold), and MLC2a (26.19 fold). In the ventricles, four-and-a-half LIM domain 2 (8.63 fold), myosin light chain polypeptide 3 (14.78 fold) and Iroquois homeobox protein 4 (Irx4) (18.44 fold) were identified. Differential expression of 14 candidate genes was confirmed by real time-PCR. The results show excellent agreement between the microarray and PCR data (Figure 11). Several genes exhibited a higher fold change ratio when analyzed by PCR as compared to microarray.

RT-PCR validation

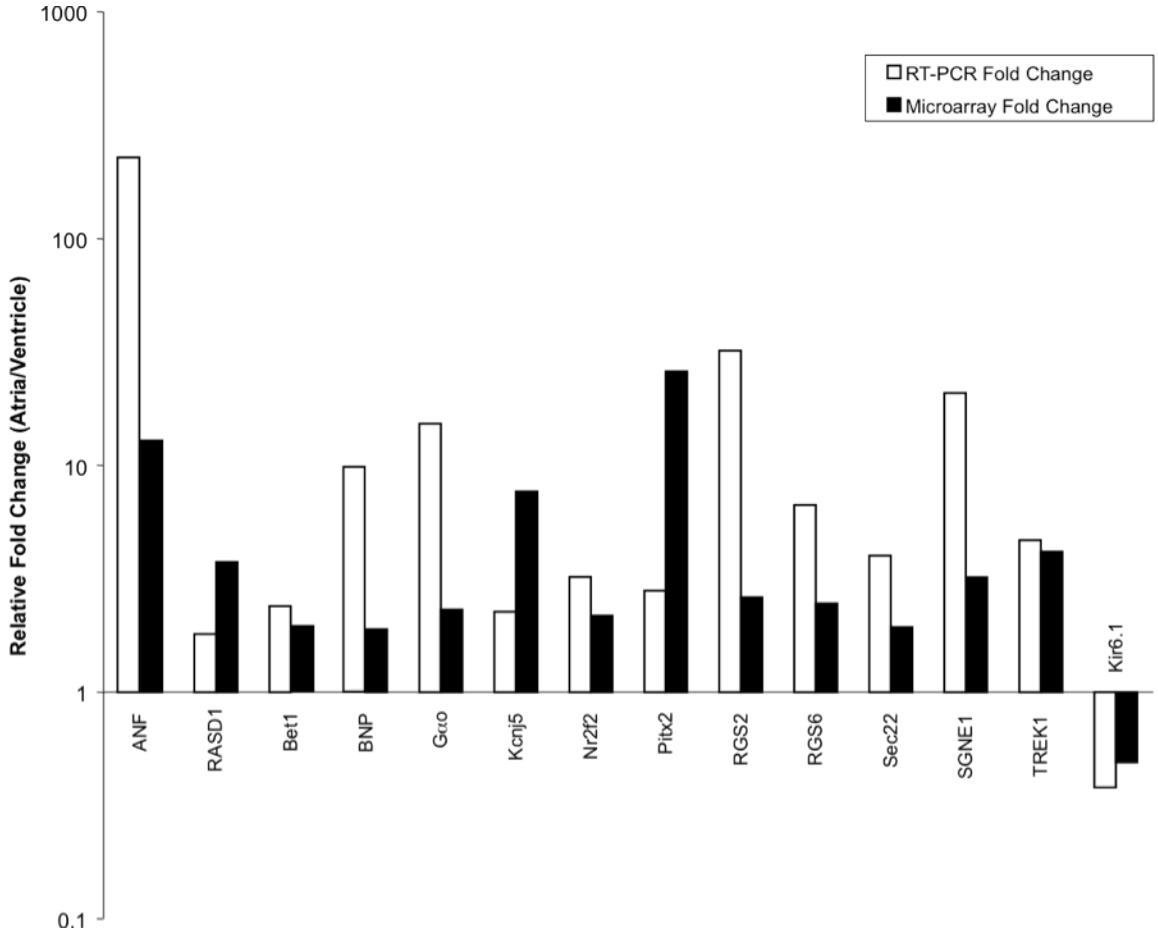


Figure 11. Comparison of microarray and RT-PCR results in normal atrial and ventricular samples.

Relative fold change of 14 candidate genes is shown. The results demonstrate agreement between the microarray and RT-PCR data, although the degree of fold change can vary. Open columns represent relative fold changes obtained by RT-PCR, while solid columns represent relative fold changes obtained by microarray. Figure obtained and modified with permission (McGrath and de Bold, 2009).

Functional classification

Differentially expressed genes between the atria and the ventricles were functionally classified into four major Gene Ontology categories: biological process, cellular component, molecular function and unclassified. An individual transcript was included in several categories or subcategories because of its relevance to more than one category or subcategory. Out of the 1415 significantly differentially expressed probes, 837 were grouped as unclassified, i.e. had unknown annotations at the time of the study. Figure 12 illustrates the extent in gene expression differences found between the two heart tissues across functional classes.

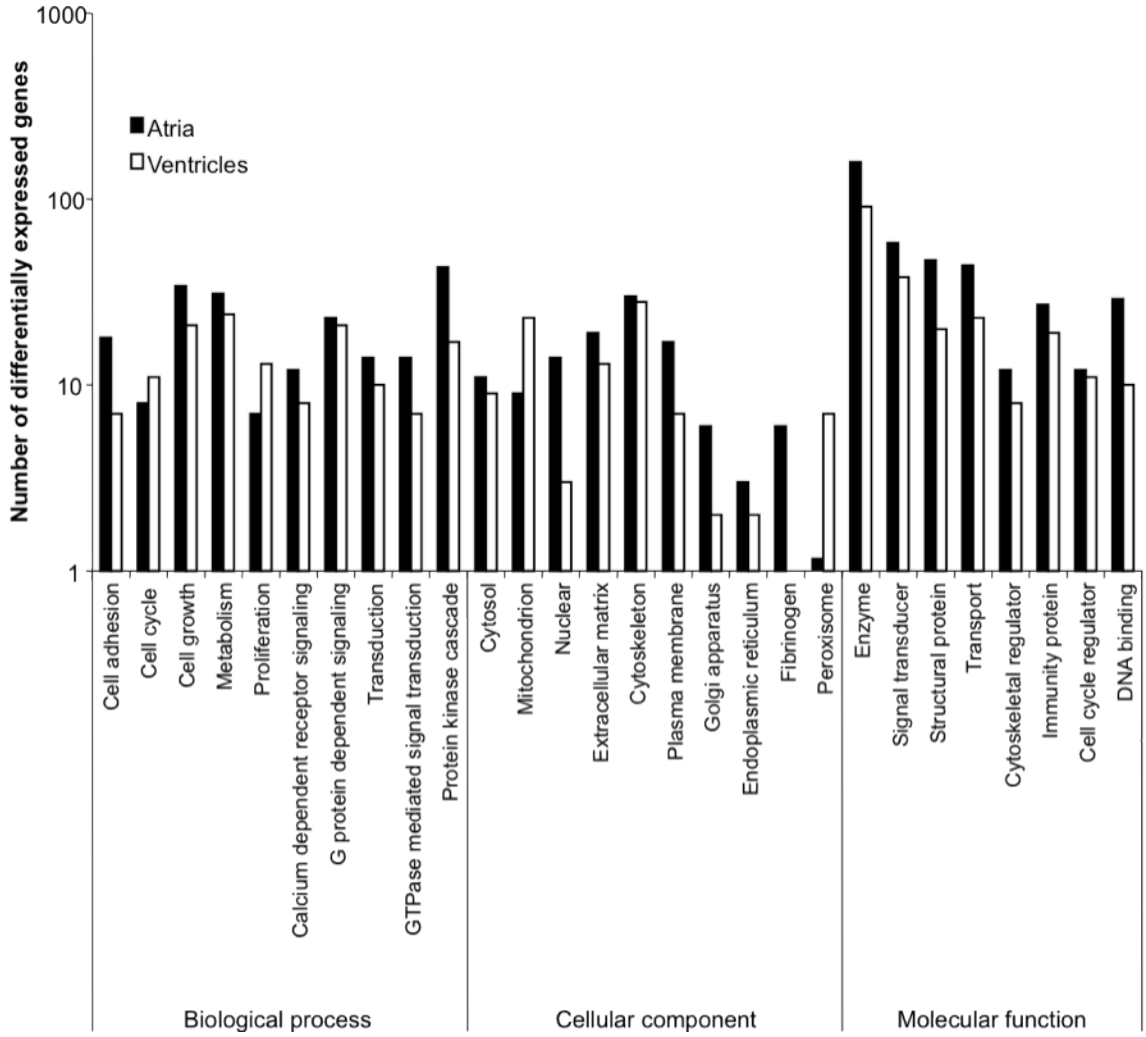


Figure 12. Functional classification of differentially expressed genes found between the atria and the ventricles with known Gene Ontology annotations.

Note, the number of differentially expressed genes is plotted according to muscle type, i.e. atrium or ventricle. Reprinted with permission (McGrath and de Bold, 2009).

Biological processes

Differentially expressed genes were similarly abundant in cell communication and signal transduction processes and they were mainly found involved in cell growth, metabolism, transport, G protein-dependent signaling, and protein kinase cascade (Figure 12). Differentially expressed G protein-dependent signaling transcripts include those grouped in subcategories such as glutamate signaling, G protein signaling, neuropeptide signaling pathway, and serotonin receptor signaling (Table 5). Regulators of G-protein signaling (RGS) RGS2 and RGS6 were more abundant in the atria (2.61 and 2.47 fold, respectively) while RGS5 was prevalent in the ventricles (2.33 fold) (see Figure 13). Other accessory proteins for G proteins that were found differentially expressed include periplakin (4.23 fold), RASD1 (3.75 fold) and β-site APP cleaving enzyme 2 (3.54 fold). These genes were more abundant in the atria while Rasd2 (3.32 fold) and AGS3-like (11.43) were more abundant in the ventricles. All these accessory proteins, including the RGS proteins interact with Gαi/o (Sato et al., 2006). Small GTPase-mediated signal transduction transcripts found differentially expressed include regulators of membrane trafficking Rab15 (24.53 fold), Rab34 (1.90 fold) and Rab40b (3.27 fold). The Rab escort protein choroidermia, known to interact with Rab3a and Rab27a, as well as the Rab27a effector protein synaptotagmin-like 2 were abundantly expressed in the atria by 1.86 and 32.25 fold, respectively. The latter is known to bind and regulate the GTP-bound form of Ras-related protein Rab27a, which has been shown to positively regulate the exocytosis of secretory granules in pancreatic beta cells and pituitary tissue (Yi et al., 2002).

Table 5. List of differentially expressed genes classified into G protein dependent signaling and related functional groups

Functional Group/ Probe set ID	Gene Description	Fold change
G Protein signaling		
1369740_at	Potassium inwardly-rectifying channel, subfamily J, member 3	7.76
1368560_at	Potassium inwardly-rectifying channel, subfamily J, member 5	7.68
1369741_at	Potassium inwardly-rectifying channel, subfamily J, member 3	6.35
1369273_a_at	Natriuretic peptide receptor 3	6.02
1396249_at	Natriuretic peptide receptor 3	4.06
1387803_at	Protein phosphatase 2, regulatory subunit B, beta isoform	3.94
1367920_at	Endothelial differentiation, sphingolipid G-protein-coupled receptor, 5	3.27
1367791_at	Receptor (calcitonin) activity modifying protein 1	3.05
1392905_at	Guanine nucleotide binding protein, gamma 2	2.74
1368879_a_at	Guanine nucleotide binding protein, alpha o	2.31
1369377_at	Hypocretin receptor 2	2.00
1373202_at	Guanine nucleotide binding protein, gamma 3	1.96
1369647_at	Calcitonin receptor-like	-1.82
1369115_at	Adrenergic receptor, beta 2	-1.83
1368660_at	cAMP-regulated guanine nucleotide exchange factor I	-1.93
1388109_at	G protein-coupled hepta-helical receptor Ig-Hepta	-1.95
1370449_at	G protein-coupled receptor 105	-2.20
1368534_at	Adrenergic receptor, alpha 1d	-2.34
1398530_at	guanine nucleotide binding protein (G protein), gamma 11	-2.34
1368300_at	Adenosine A2a receptor	-2.46
1370522_at	Glucagon receptor	-3.07
1395473_at	Guanine nucleotide binding protein, beta 3	-3.65
1387671_at	Secretin receptor	-4.31
Accessory proteins for G proteins		
1391187_at	Periplakin (predicted)	4.23
1387908_at	RAS, dexamethasone-induced 1 RASD1	3.75
1377390_at	Beta-site APP-cleaving enzyme 2	3.54
1387074_at	Regulator of G-protein signaling 2	2.61
1379517_at	Regulator of G-protein signaling 6	2.47
1369957_at	Regulator of G-protein signaling 5	-2.33
1370372_at	RASD family, member 2	-3.32
1372383_at	G-protein signaling modulator 1 (AGS3-like, C. elegans)	-11.43
Neuropeptide signaling pathway		
1367992_at	Secretory granule neuroendocrine protein 1	3.20
1382967_at	G protein-coupled receptor 64	2.50
1369377_at	Hypocretin receptor 2	2.00
1368428_at	X-prolyl aminopeptidase (aminopeptidase P) 2, membrane-	-1.99

	bound	
1371696_at	G protein-coupled receptor 56	-2.16
1367949_at	Preproenkephalin	-13.55
Serotonin receptor signaling		
1369125_at	5-hydroxytryptamine (serotonin) receptor 2A	7.84
1369124_at	5-hydroxytryptamine (serotonin) receptor 2A	1.88

Positive fold change values indicate a higher abundance in the atria as compared to the ventricles, while negative fold change values demonstrate a higher ventricular abundance in comparison to the atria. From McGrath *et al.,* 2009. Reprinted with permission.

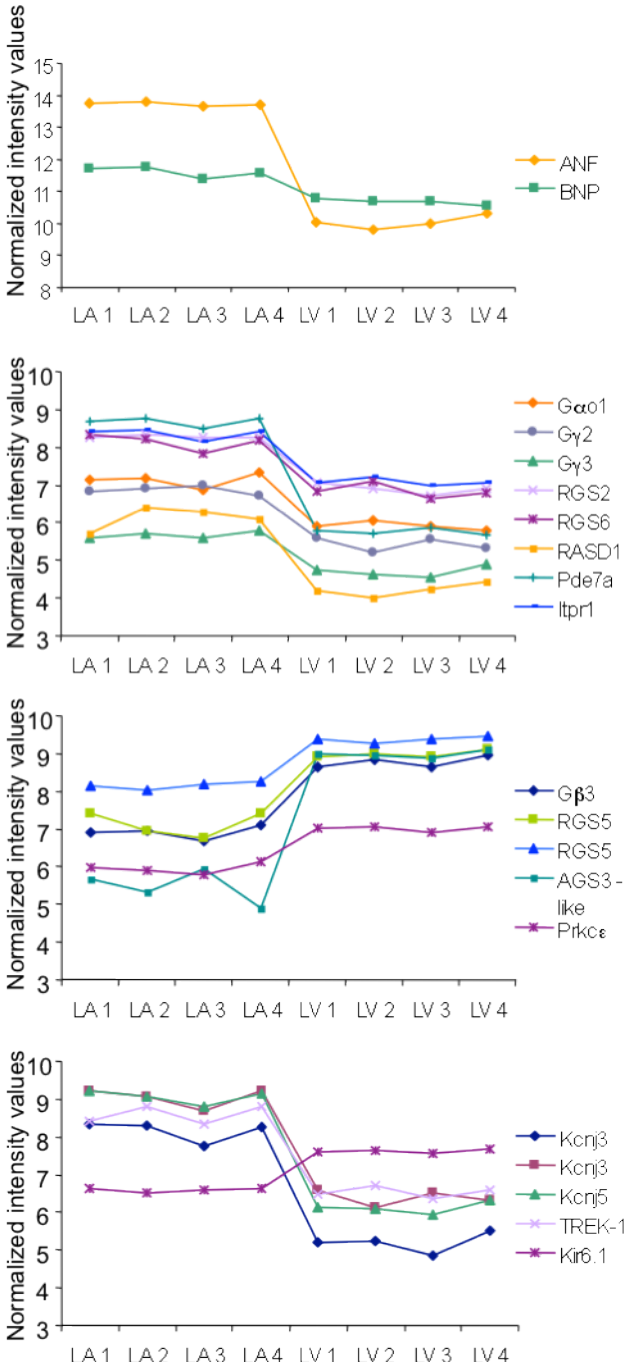


Figure 13. Normalized intensity values of specific transcripts in all atrial and ventricular microarray replicates.

The data is displayed in four different panels for visual simplicity. Note that atrial and ventricular microarrays are labelled as LA(n) and LV(n), and the scale of the ordinate

axis is different for the upper panel due to high signal intensity values for ANF and BNP. Also note that RGS5 and Kcnj3 are represented by two distinct probe sets. From McGrath *et al.,* 2009. Reprinted with permission.

Genes involved in secretion included signal sequence receptor gamma (SSR3) (1.82 fold), blocked early in transport 1 homolog (*S.cerevisiae*) (Bet1) (1.93 fold), vesicle trafficking protein like 1 (Sec22) (1.93 fold), synapsin III (1.93 fold) and annexin A1 (2.04 fold). These genes were found more abundant in the atria when compared to the ventricles.

Cellular component

Within the Gene Ontology category of cellular components, the intracellular components subcategory contained the largest amount of differentially expressed genes (n = 156) in comparison to the extracellular (n = 37) and the membrane components (n = 37). Cellular components that had prominent atrial abundant transcripts included those associated with the plasma membrane, the endoplasmic reticulum (ER), the Golgi apparatus, and the nucleus, while the ventricles were associated with abundant transcripts found within the mitochondrion and peroxisome components (Figure 12). ER and Golgi-associated genes that were abundantly expressed in the atria include stearoyl-CoA desaturase 1 (20.81 fold) and 2 (2.21 fold), IP3R (2.44 fold), ribosome associated membrane protein 4 (2.22 fold), Sec11 like 3 (2.05 fold), as well as SSR3. Transcripts involved in ER to Golgi vesicle-mediated transport include the previously mentioned genes Sec22 and Bet1. Other atrial abundant Golgi resident proteins include islet cell autoantigen-1 (Ica1) (4.63 fold), TGF-β2 (3.89 fold), nucleobindin 2 (2.35 fold) and Golgi transport 1 homolog B (Golt1b) (2.60 fold).

Molecular function

The molecular function subcategories that were most notably differentially expressed between atrial and ventricular muscles included enzyme, signal transducer, structural protein, and transport (see Figure 12). The signal transducer subcategory is composed of ligands and receptors (see Appendices 5 and 6 for complete list of genes, p. 309 and p.311, respectively). The cytokines, frizzled receptor ligands, growth factor receptor ligands as well as hormone receptor ligands subcategories were also significantly differentiated. Differentially expressed genes involved in hormone, hormonal activity, and hormone receptor ligand subcategories, including ANF (12.88 fold) and BNP (1.89 fold), as well as secretory granule neuroendocrine protein 1 (SGNE1) (3.20 fold) are listed in Table 6. Differentially expressed transcription factors/DNA binding proteins were more abundant in the atria than in the ventricles (see Appendix 7 for complete list, p. 313).

In general, genes coding for transport proteins were more abundant in the atria than in the ventricles. Potassium channels, which were most abundant in the atria, included potassium channel subfamily K member 2 (Kcnk2 or TREK-1), as well as potassium inwardly-rectifying channel, subfamily J, member 3 (Kcnj3) and 5 (Kcnj5) (Table 7). The ventricles were most abundant in the potassium inwardly-rectifying channel, subfamily J, member 8 (Kcnj8 also known as Kir6.1) channel subunit.

Table 6. List of differentially expressed genes possessing hormone, hormonal activity, or hormone receptor ligand Gene Ontology annotations

Probe Set ID	Gene Description	Fold change
1367564_at	Natriuretic peptide precursor type A (ANF)	12.88
1367616_at	Natriuretic peptide precursor type B (BNP)	1.89
1371400_at	Thyroid hormone responsive protein	38.59
1387396_at	Hepcidin antimicrobial peptide	11.24
1369484_at	WNT1 inducible signaling pathway protein 2	4.79
1387625_at	Insulin-like growth factor binding protein 6	3.61
1368883_at	Nephroblastoma overexpressed gene	3.51
1367992_at	Secretory granule neuroendocrine protein 1 (SGNE1)	3.20
1368367_at	CUB and zona pellucida-like domains 1	3,17
1368367_at	Integral membrane-associated protein 1	3.16
1376734_at	Nephroblastoma overexpressed gene	2.79
1372168_s_at	Insulin-like growth factor binding protein 6	2.25
1367631_at	Connective tissue growth factor	2.20
1389651_at	Apelin, AGTRL1 ligand	2.00
1387219_at	Adrenomedullin	1.87
1367894_at	Growth response protein (CL-6)	1.82
1370563_at	3-alpha-hydroxysteroid dehydrogenase	-1.92
1368428_at	X-prolyl aminopeptidase (aminopeptidase P) 2, membrane-bound	-1.99
1396101_at	Stanniocalcin 1	-2.14
1368468_at	Cytochrome P450, subfamily 11A	-3.97
1367949_at	Preproenkephalin, related sequence	-13.55

Positive fold change values indicate a higher abundance in the atria as compared to the ventricles, while negative values demonstrate a higher ventricular abundance in comparison to the atria.

Table 7. List of differentially expressed genes encoding for potassium channels

Probe Set ID	Gene Description	Symbols	Fold Change
1369740_at	Potassium inwardly-rectifying channel, subfamily J, member 3	Kcnj3 or GIRK1	7.78
1368560_at	Potassium inwardly-rectifying channel, subfamily J, member 5	Kcnj5 or GIRK4	7.67
1369741_at	Potassium inwardly-rectifying channel, subfamily J, member 3	Kcnj3 or GIRK1	6.36
1370342_at	Potassium channel, subfamily K, member 2	Kcnk2 or TREK-1	4.17
1368911_at	Potassium inwardly-rectifying channel, subfamily J, member 8	Kcnj8 or Kir6.1	-2.03

Positive fold change values indicate a higher abundance in the atria as compared to the ventricles, while negative values demonstrate a higher ventricular abundance in comparison to the atria.

Pathway analysis

Pathway analysis using the GenMapp software identified clusters of differentially expressed genes found within the same biological pathway. Visual representation of specific known pathways, referred as Mapps, revealed several Mapps in which atrial gene expression was predominant. These Mapps included pathways of fatty acid synthesis (Figure 14), eicosanoid and prostaglandin synthesis (Figure 15), which shows a higher abundance of phospholipase A2 (PLA2) (3.28 fold) and several prostaglandin synthase enzymes. In contrast, mitochondrial long-chain fatty acid β-oxidation (Figure 16) and glucocorticoid metabolism pathways (not shown) were dominant in ventricular samples. Mapps other than those from metabolic processes, revealed atrial regional specialization in regards to the classical component activation pathway (Figure 17) and G-protein signaling pathway (Figure 18). The latter demonstrated a higher abundance of the $G\alpha o_1$ subunit (Gnao), Kcnj3 (also known as GIRK1) and Kcnj5 (also known as GIRK4) in the atria compared to the ventricles by 2.3, 6.35 (second probe set = 7.76 fold) and 7.68 fold, respectively. Also, $G\gamma_2$ (Gng2), $G\gamma_3$ (Gng3) (2.74 and 1.96 fold, respectively) and phosphodiesterase 7a (Pde7a) (7.52 fold) as well as IP3R (2.44 fold) were highly expressed in the atria while protein kinase C epsilon (Pkcε) was more abundant in the ventricles by 2.09 fold. Gβ subunits 1, 2, and 5 were present in both atria and ventricles at roughly similar levels while $G\beta_3$ (Gnb3) was expressed at higher levels in the ventricles (3.66 fold). Several accessory proteins for G protein signaling were also differentially expressed.

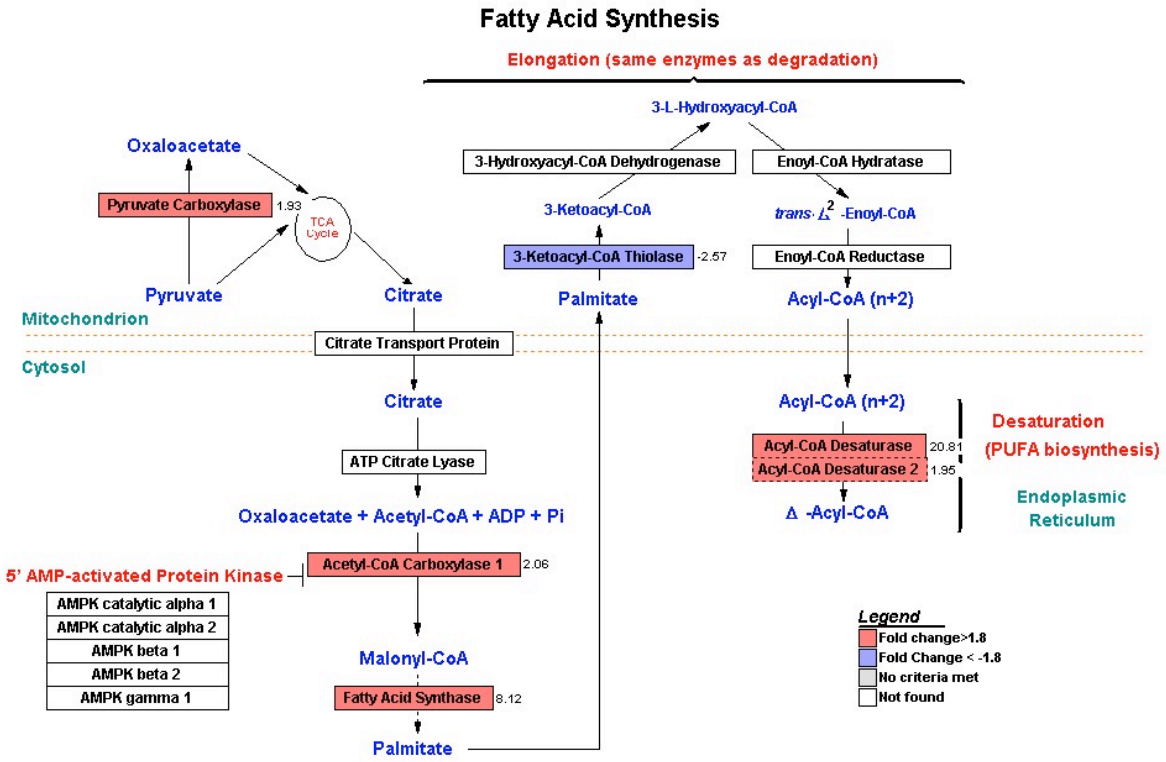


Figure 14. Fatty acid synthesis pathway.

Genes labeled in red indicate a higher expression level in the atria as compared to the ventricles based on statistical significance and a 1.8 fold threshold cut-off. Genes labeled in blue indicate a higher expression level in the ventricles as compared to the atria based on statistical significance and a -1.8 fold threshold cut-off. Genes labeled in white were not found in the list of statistically significant differentially expressed genes that was uploaded in GenMapp program. The fold is shown on the right of the gene symbol.

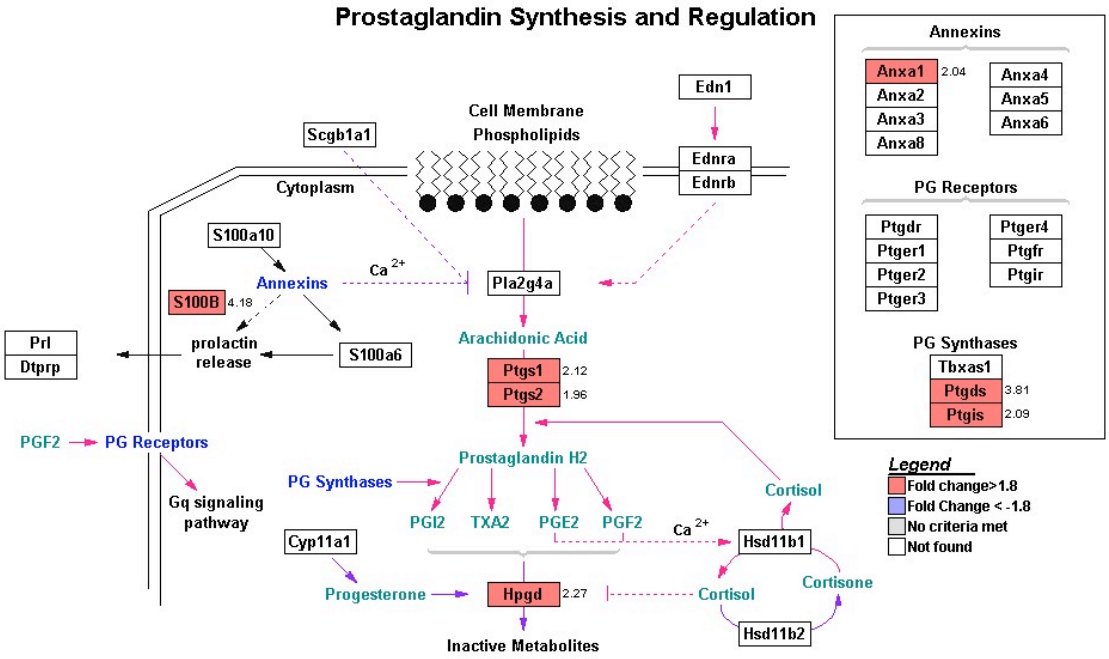


Figure 15. Prostaglandin synthesis and regulation pathway.

Genes labeled in red indicate a higher expression level in the atria as compared to the ventricles based on statistical significance and a 1.8 fold threshold cut-off. Genes labeled in white were not found in the list of statistically significant differentially expressed genes that was uploaded in GenMapp program. The fold is shown on the right of the gene symbol.

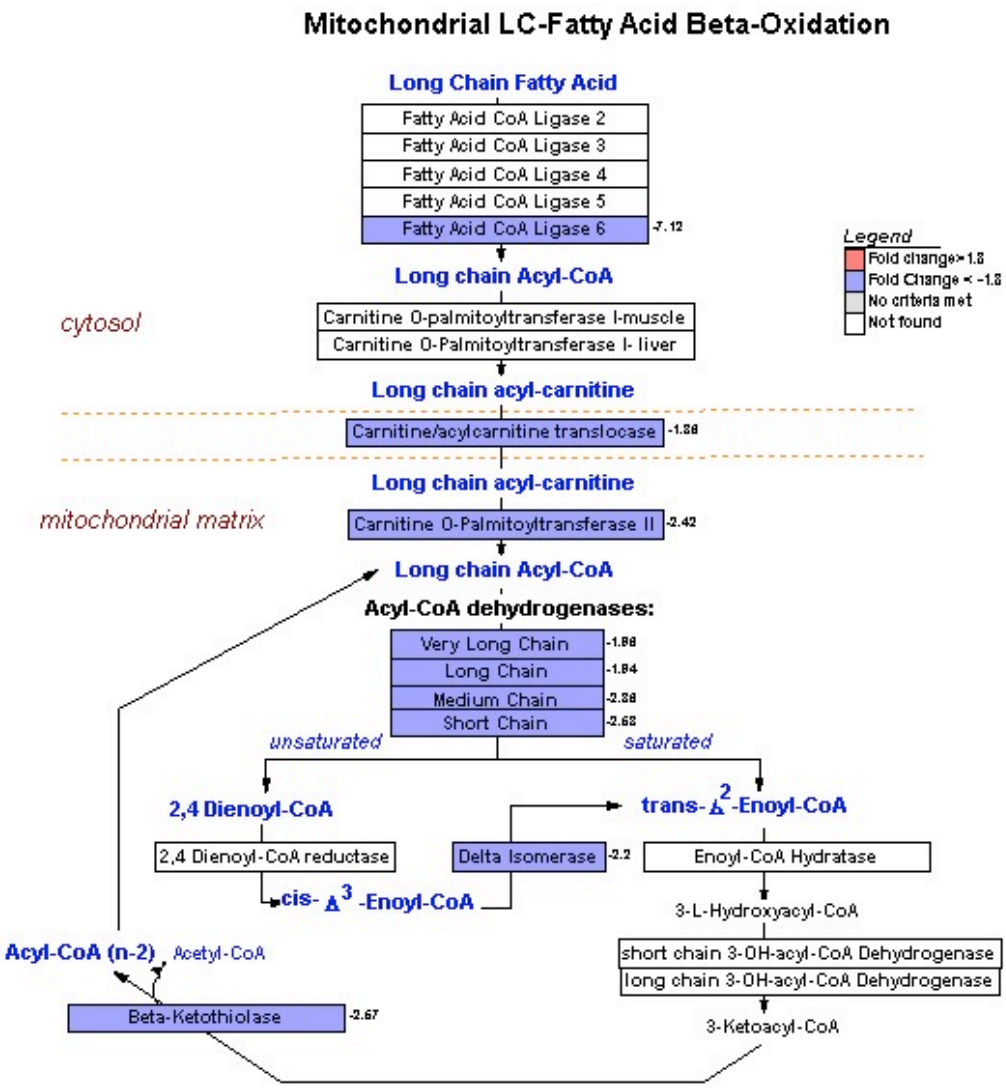


Figure 16. Long-chain fatty-acid beta-oxidation pathway.

Genes labeled in blue indicate a higher expression level in the ventricles as compared to the atria based on statistical significance and a -1.8 fold threshold cut-off. Genes labeled in white were not found in the list of statistically significant differentially expressed genes that was uploaded in GenMapp program. The fold is shown on the right of the gene symbol.

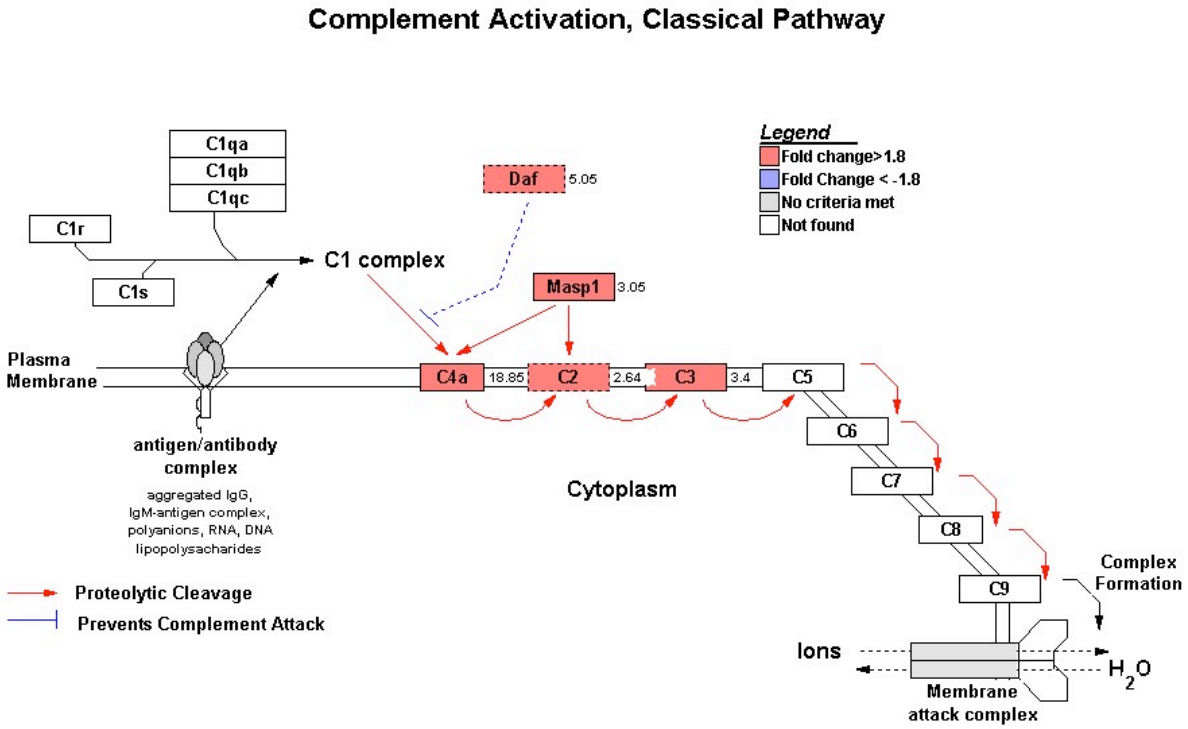


Figure 17. Classical complement activation pathway.

Genes labeled in red indicate a higher expression level in the atria as compared to the ventricles based on statistical significance and a 1.8 fold threshold cut-off. Genes labeled in white were not found in the list of statistically significant differentially expressed genes that was uploaded in GenMapp program. The fold is shown on the right of the gene symbol.

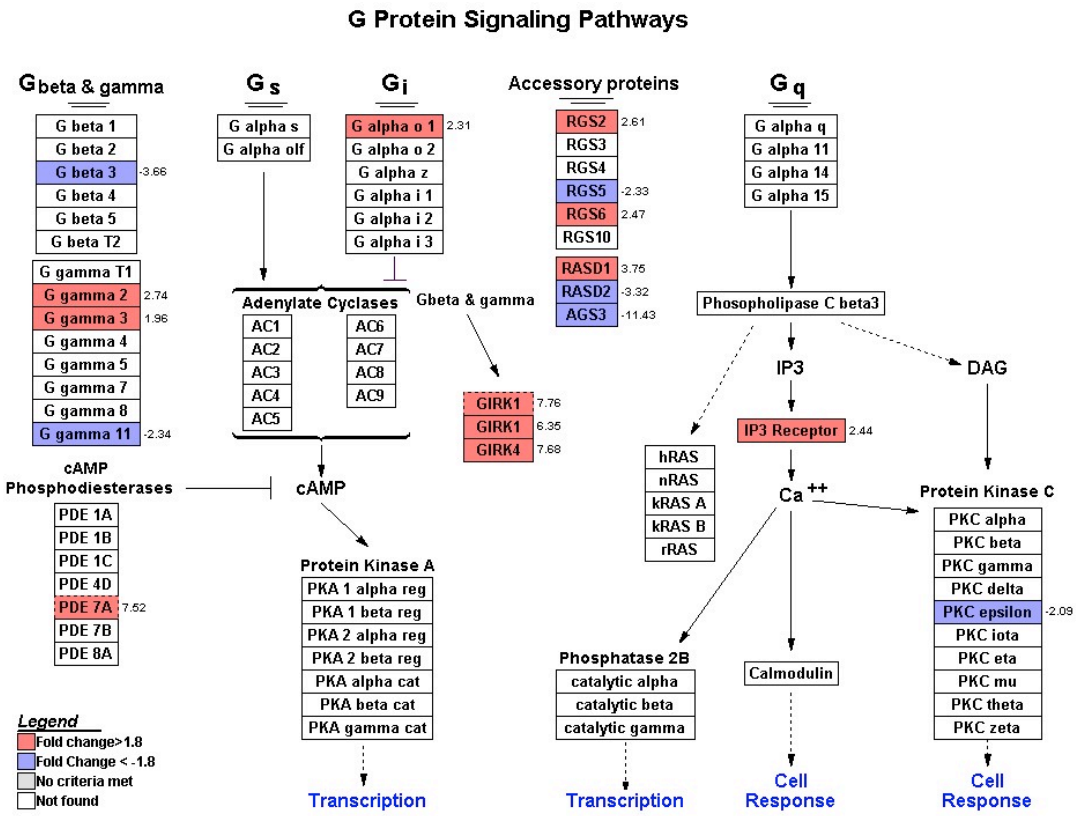


Figure 18. G protein signaling pathways generated by GenMapp.

Genes labeled in red indicate a higher expression level in the atria as compared to the ventricles based on statistical significance and a 1.8 fold threshold cut-off. Genes labeled in blue indicate a higher expression level in the ventricles as compared to the atria based on statistical significance and a -1.8 fold threshold cut-off. Genes labeled in white were not found in the list of statistically significant differentially expressed genes that was uploaded in GenMapp program. The fold is shown on the right of the gene symbol. From McGrath *et al.,* 2009. Reprinted with permission.

Protein validation

Several atrial abundant genes that were found differentially expressed between the normal atrial and ventricular tissues in the microarray analysis were also validated by western blot and immunofluorescence. Figure 19 shows western blot analysis in atrial and ventricular tissues, as well as in some cases in the atrial derived HL-1 cells for proANF, Gαo, RASD1, TREK-1 and $G\gamma_2$. All these proteins were expressed in both atrial and ventricular tissues, with the exception of proANF and $G\gamma_2$, which were not detected in the ventricle.

Immunofluorescence analyses of candidate genes are shown in Figures 20-28. Plasmalemmal and nuclear localization of the mechanosensitive two-pore potassium channel TREK-1 was evident in atrial tissue sections (Figure 20A). No staining was observed in ventricular sections (Figure 20C). TREK-1 had a predominant nuclear localization in the atrial derived HL-1 cells (Figure 21). Bet1, a vesicular transport protein, was localized in the perinuclear region of the atrial derived HL-1 cells (Figure 22), but was not specifically detected in the heart tissue sections due to high background fluorescence (not shown). In rat heart tissue sections, RASD1 exhibited strong punctate staining in the atrium section and a light punctate staining in the ventricle section (Figures 23A, C and E). Immunofluorescence analysis of the atrial derived HL-1 cells, demonstrated that RASD1 was localized in the perinuclear region, an area known to contain atrial specific granules and Golgi apparatus, as well as in the cytoplasm, as evidenced by punctate staining, indicative of vesicular distribution (Figure 24A and C). The perinuclear expression pattern of RASD1 in these HL-1 cells

was similar to the pattern observed for Gαo (Figure 25A and C). Colocalization of both RASD1 and Gαo is shown in Figure 26. Immunofluorescence analysis of proANF was used as a positive control. Figures 27A and E show proANF perinuclear staining, texas-red and fluorescein, respectively, in atrial tissue sections while Figure 27C and G show negligible proANF staining in the ventricular sections. Perinuclear and Golgi staining of proANF were also present in HL-1 cells (Figure 28A).

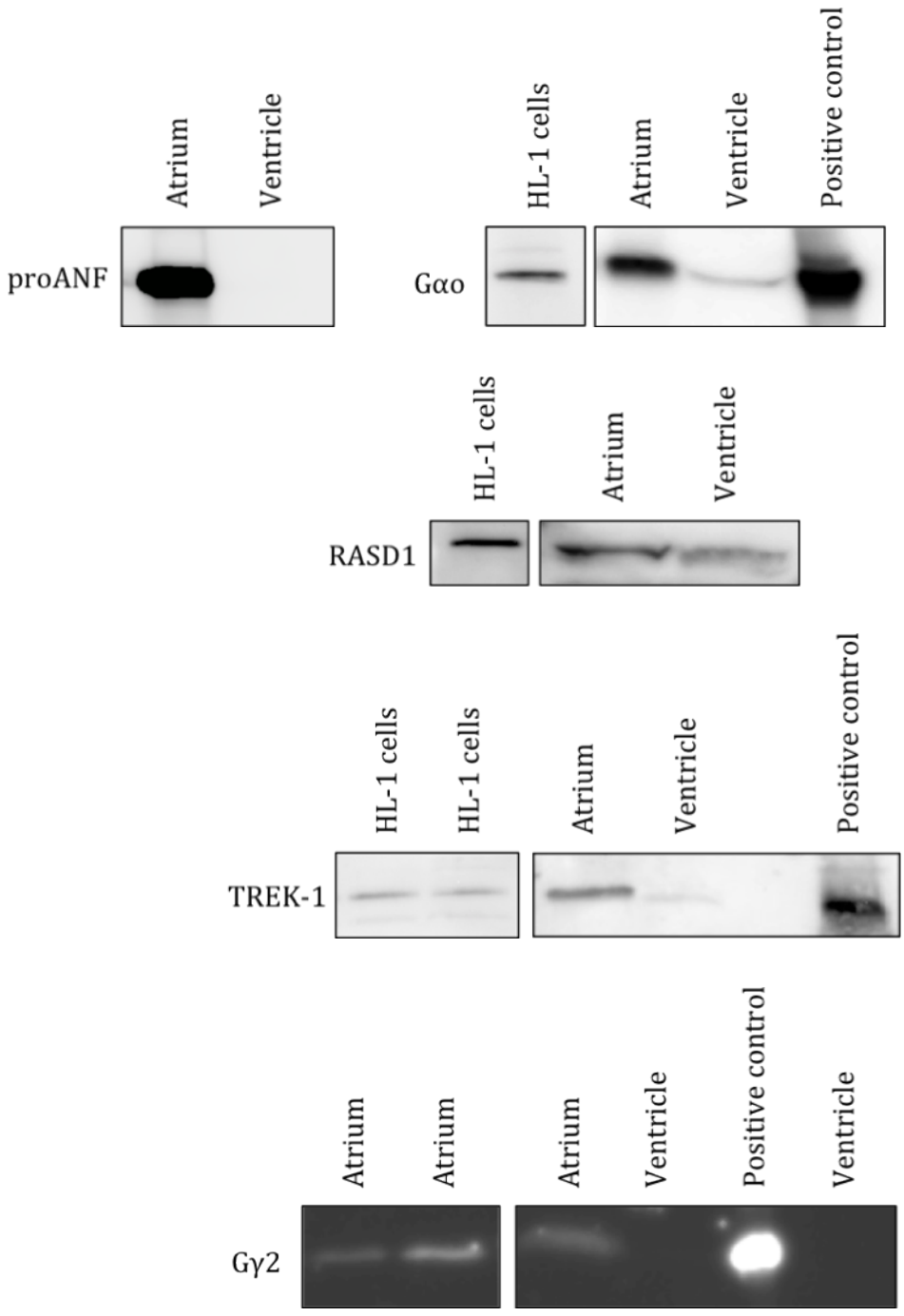


Figure 19. Representative images of Western blots for proANF, Gαo, RASD1, TREK-1 and $G\gamma_2$.

To detect membrane bound proteins, 30 μg of the microsomal fraction obtained from atrial and ventricular tissues, as well as HL-1 cells were loaded onto a 10-20% precast

linear gradient polyacrylamide Tris-HCl Ready Gel and then transferred onto a PVDF membrane. Rat brain extract was used as positive control for Gαo, TREK-1 and $G\gamma_2$. Primary antibody dilutions: proANF 1:1000 (rabbit 5, bleed 8 (R5B8)), Gαo 1:1000 (551, MBL, Japan), RASD1 1:1000 (AB15794, Millipore, Temecula, CA), TREK-1 1:200 (sc-11556, Santa Cruz Biotechnology, CA), and Gγ2 1:700 (sc-374, Santa Cruz Biotechnology, CA).

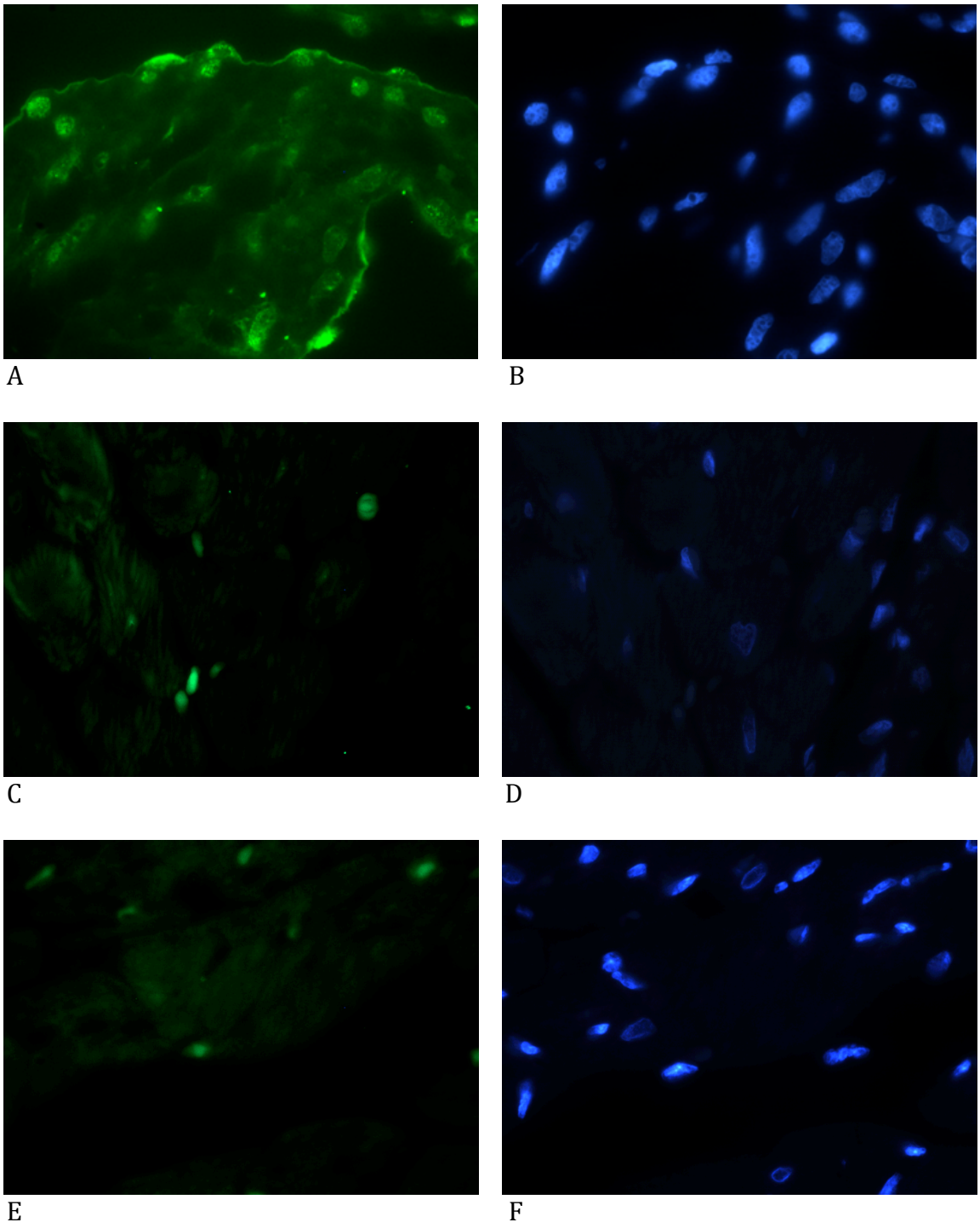


Figure 20. TREK-1 immunofluorescence in the heart.

(A) Immunofluorescence staining of TREK-1 (green) in rat atrial appendage. (B) DAPI nuclear staining of section shown in panel (A). (C) Absence of TREK-1 staining in the

rat ventricle section. (D) DAPI nuclear staining of section shown in panel (C). (E) Negative control in atrial appendage section: absorbed TREK-1 antibody with excess of TREK-1 peptide. (F) DAPI nuclear staining of section shown in panel (E).

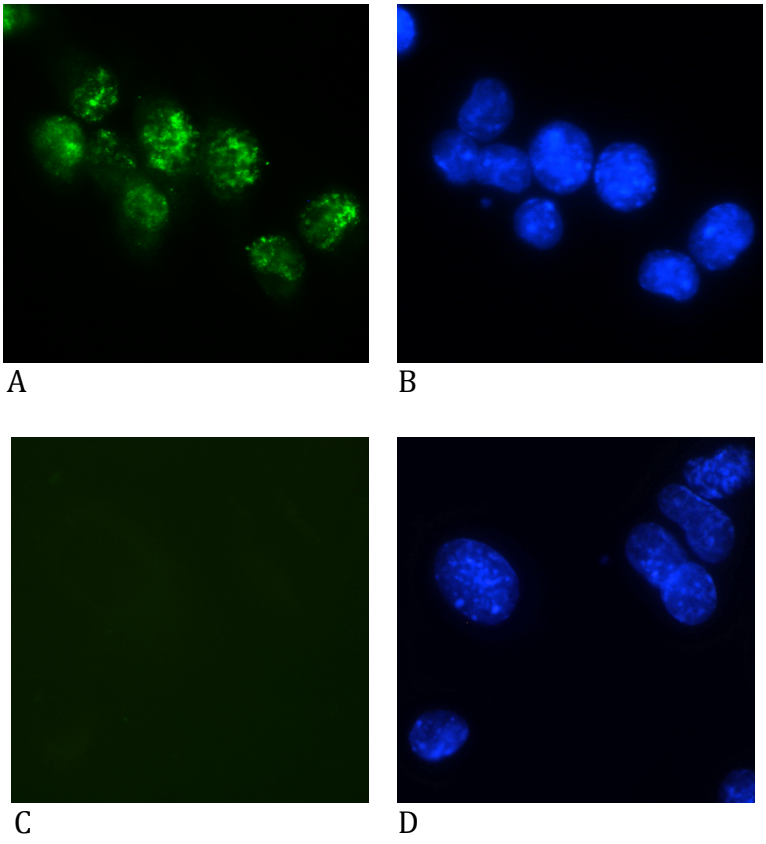
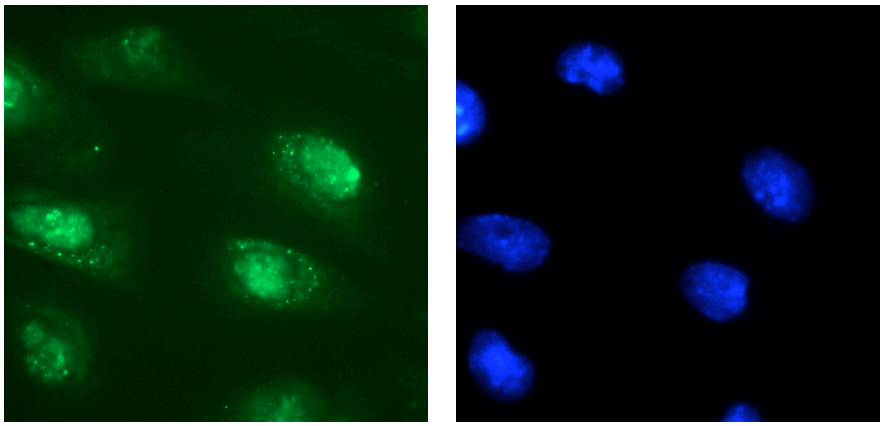


Figure 21. TREK-1 immunofluorescence in HL-1 cells.

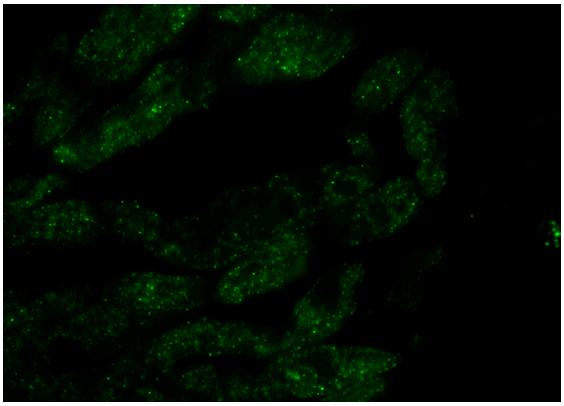
(A) Predominant nuclear staining of TREK-1 in HL-1 cells. (C) Negative control: absorbed TREK-1 antibody with excess of TREK-1 peptide. (B and D) DAPI nuclear staining of sections shown in panels A) and C).



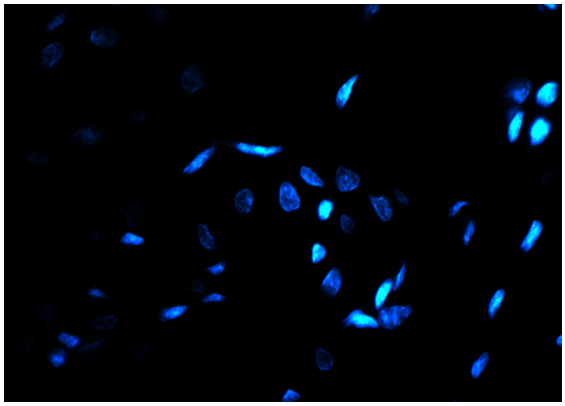
A B

Figure 22. Bet1 immunofluorescence in HL-1 cells.

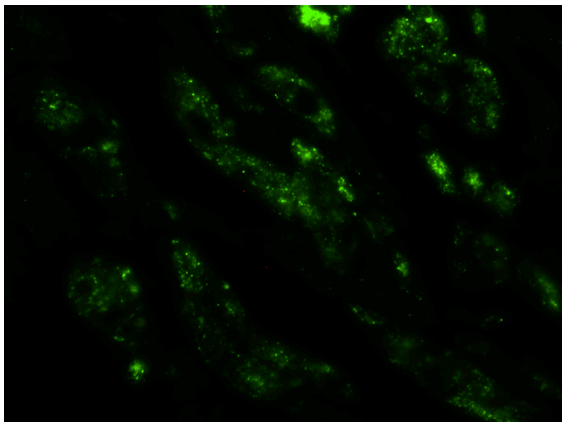
(A) Perinuclear staining of Bet1 in HL-1 cells. (B) DAPI nuclear staining of section shown in panel (A).



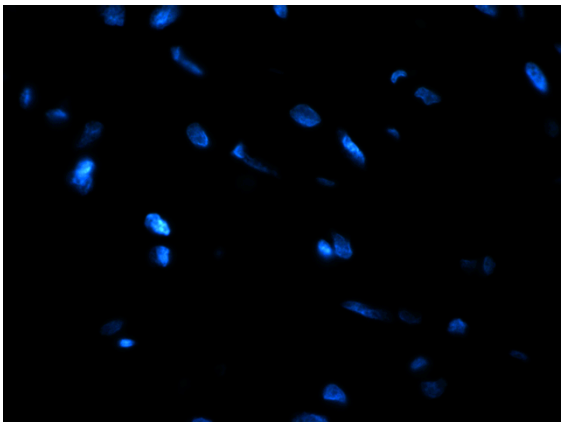
A



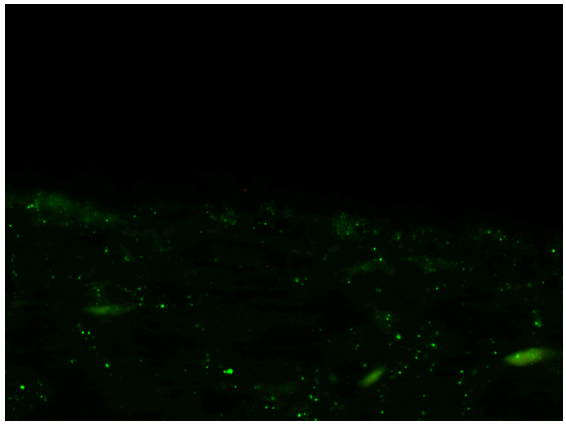
B



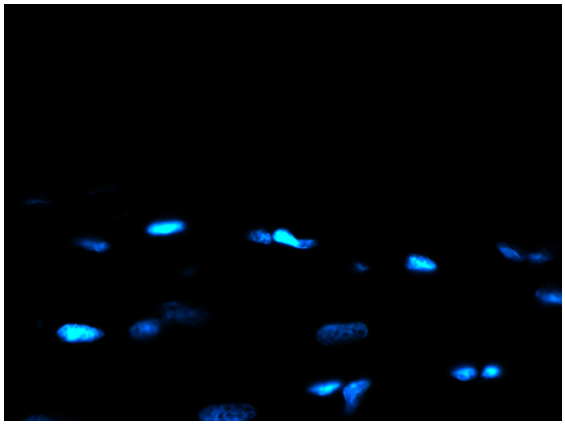
C



D



E



F

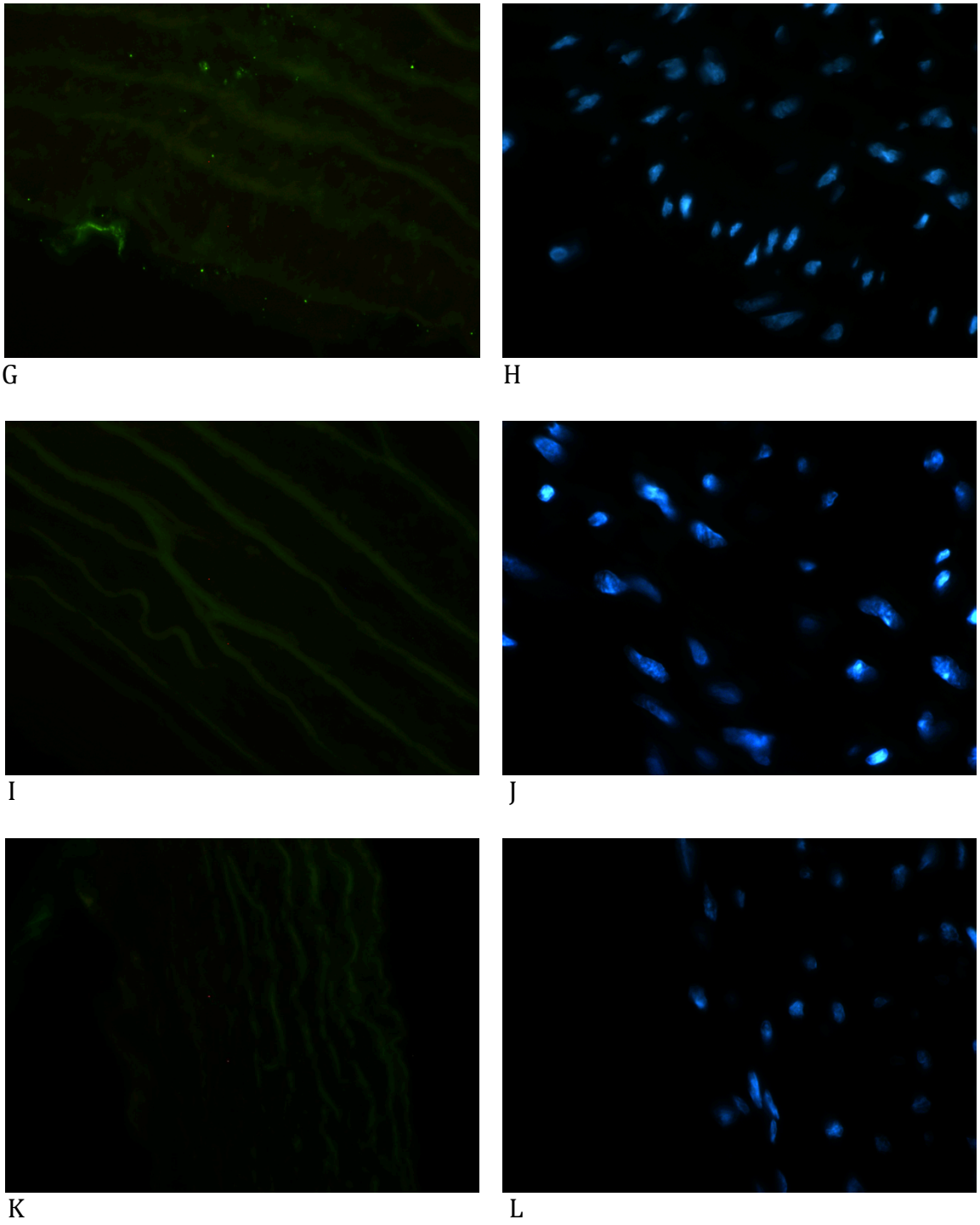
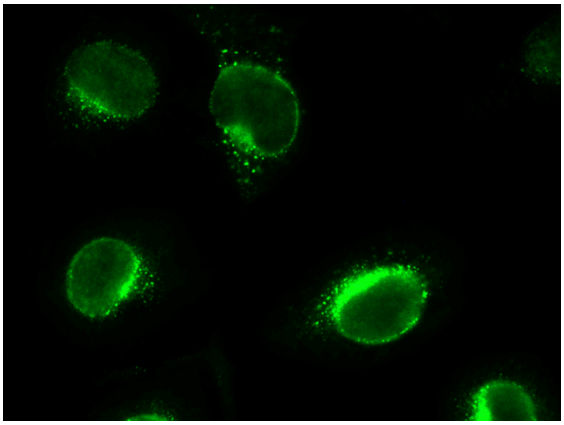


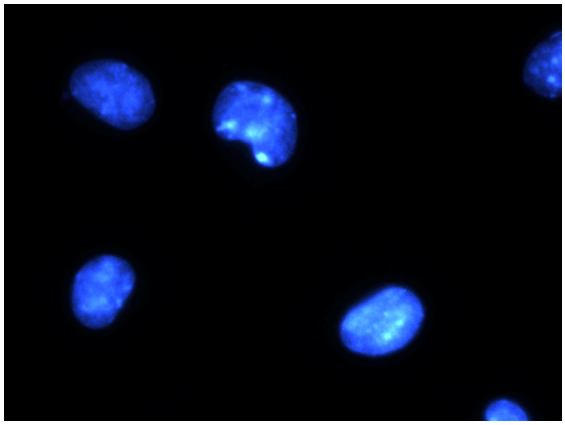
Figure 23. RASD1 immunofluorescence in the heart.

(A and C) Immunofluorescence staining of RASD1 in rat atrial appendage. (E) RASD1 staining in the rat ventricle section. (G) Negative control: primary antibody was not

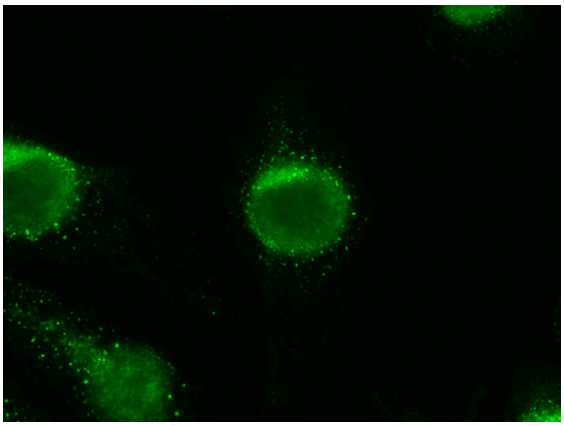
added to atrial section. (I) Negative control: secondary antibody was omitted from atrial section. (K) Negative control: fluorescein-avidin DCS was omitted from atrial section. (B, D, F, H, J and L) DAPI nuclear staining of sections shown in panels A, C, E, G, I and K.



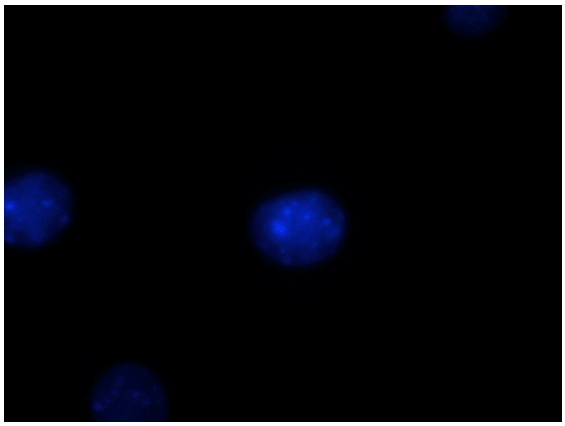
A



B



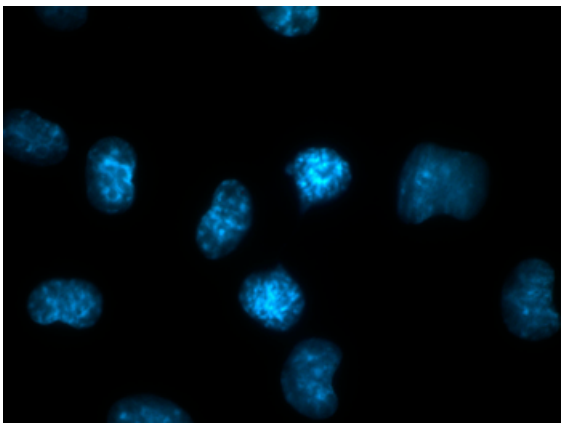
C



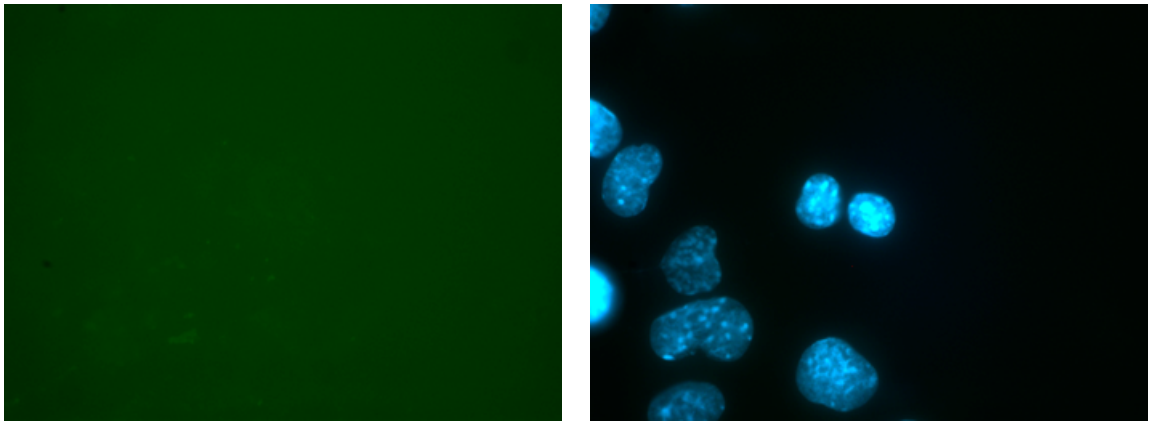
D



E



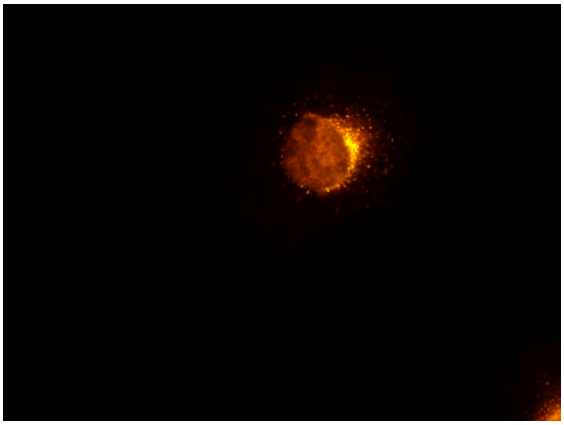
F



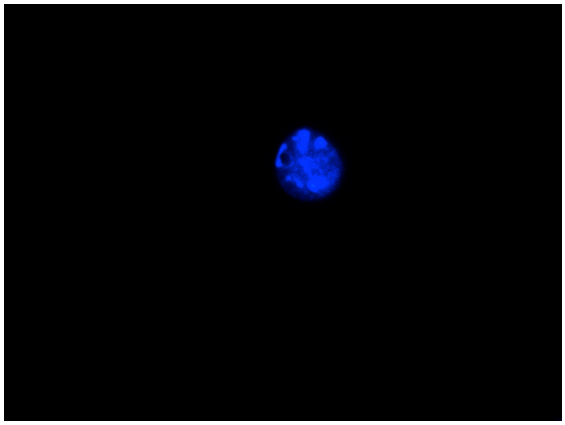
G H

Figure 24. RASD1 immunofluorescence in HL-1 cells.

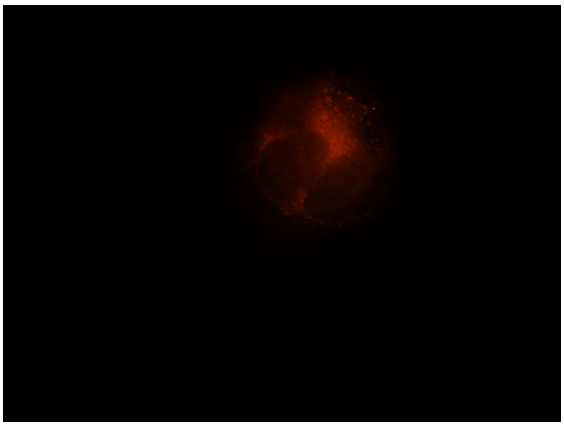
(A and C) Perinuclear and cytoplasmic staining of RASD1 in HL-1 cells. (E) Negative control: primary antibody was not added. (G) Negative control: secondary antibody was absent. (B, D, F, and H) DAPI nuclear staining of sections shown in panels A, C, E and G.



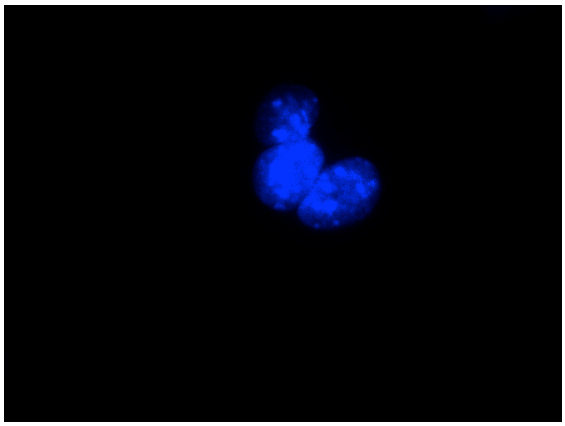
A



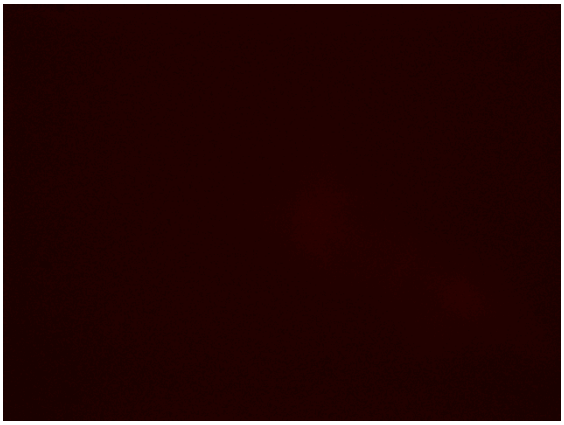
B



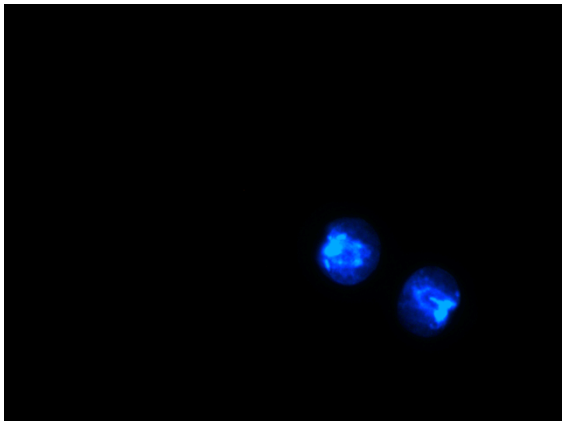
C



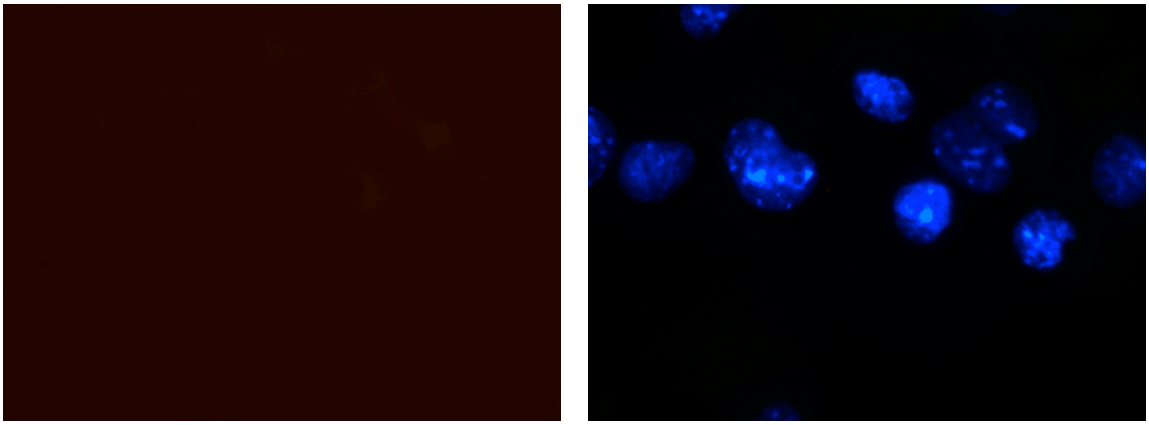
D



E



F



H I

Figure 25. Gαo immunofluorescence in HL-1 cells.

(A and C) Perinuclear and cytoplasmic staining of Gαo in HL-1 cells (Texas red staining). (E) Negative control: primary antibody was not added. (G) Negative control: secondary antibody was absent. (B, D, F, and H) DAPI nuclear staining of sections shown in panels A, C, E and G.

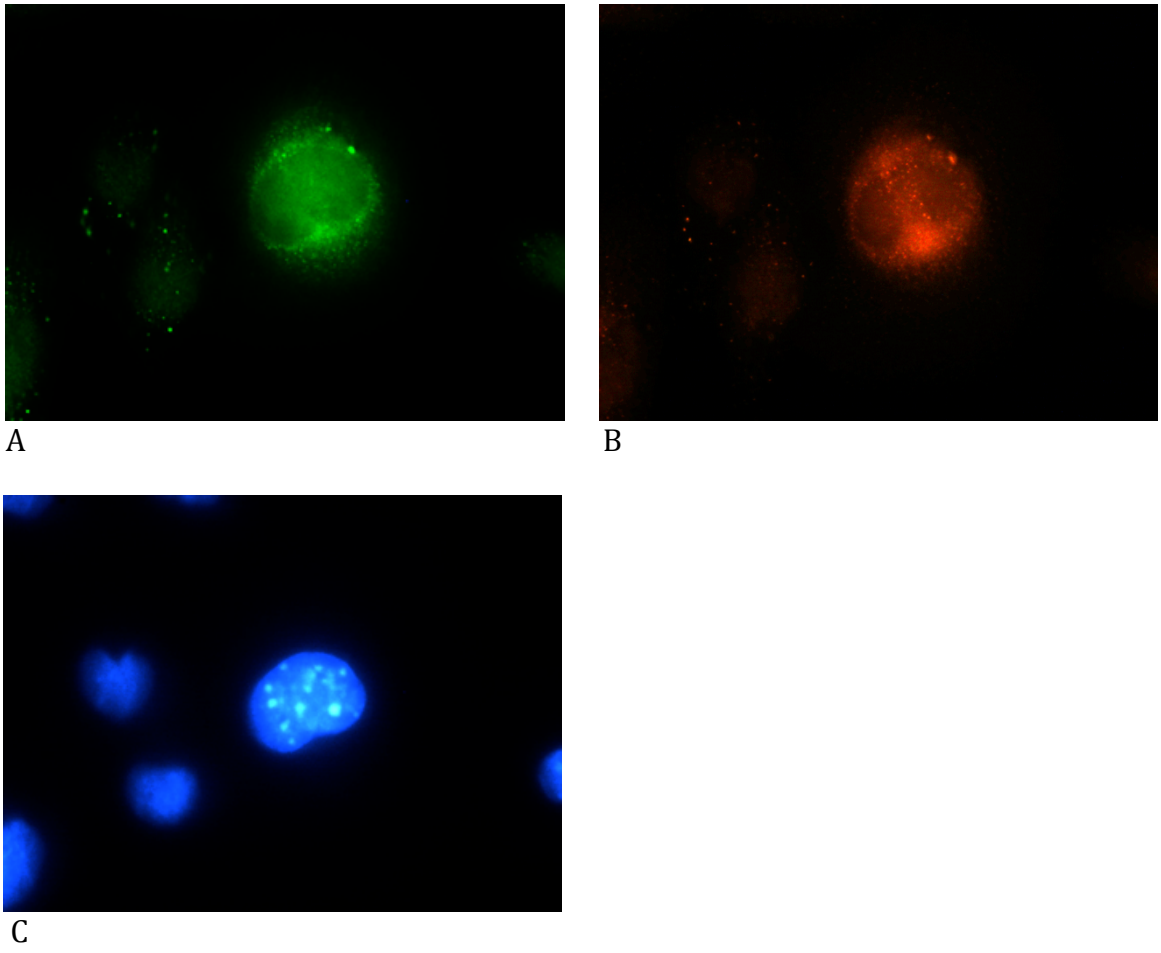
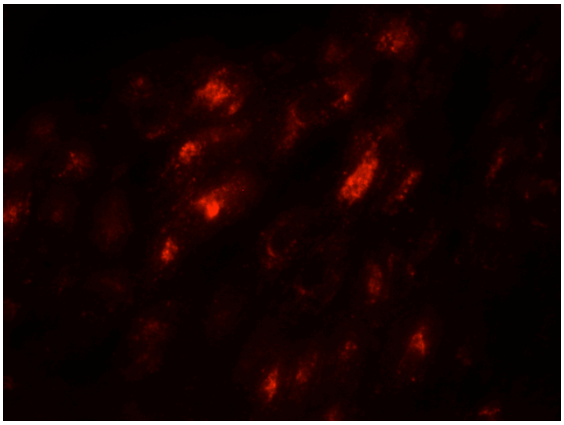
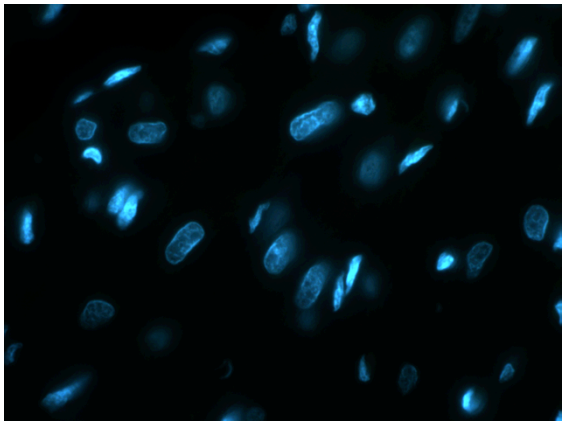


Figure 26. Double labeling immunofluorescence of RASD1 and Gαo in HL-1 cells.

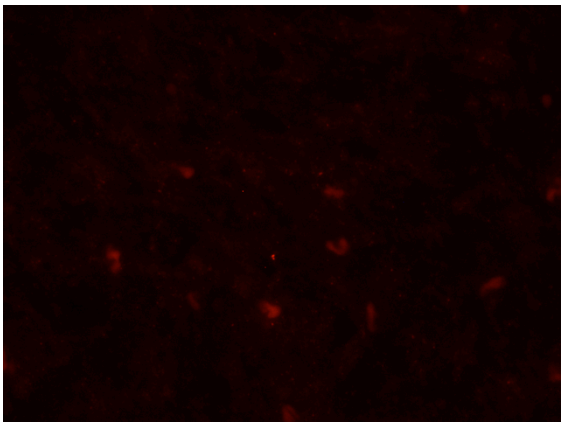
(A) Perinuclear staining of RASD1 (fluorescein staining) in HL-1 cells. (B) Perinuclear staining of Gαo (texas-red staining) in HL-1 cells. (C) DAPI nuclear staining of sections shown in panels A and B.



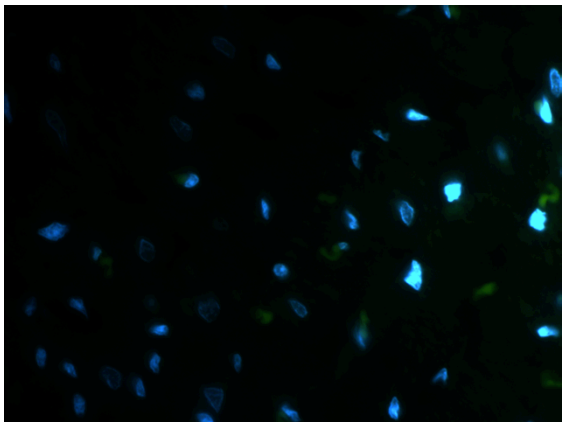
A



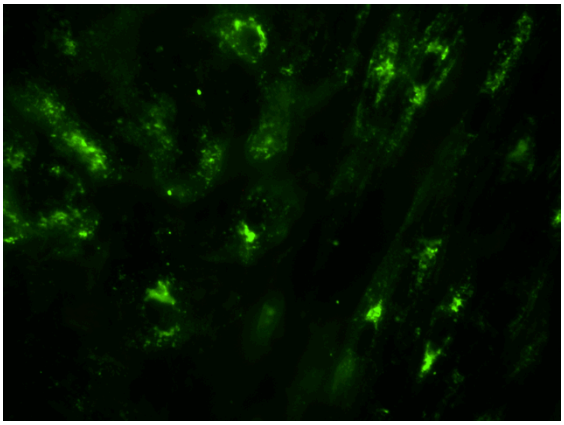
B



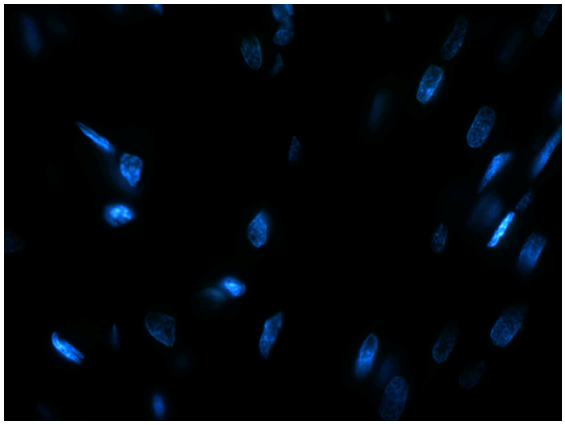
C



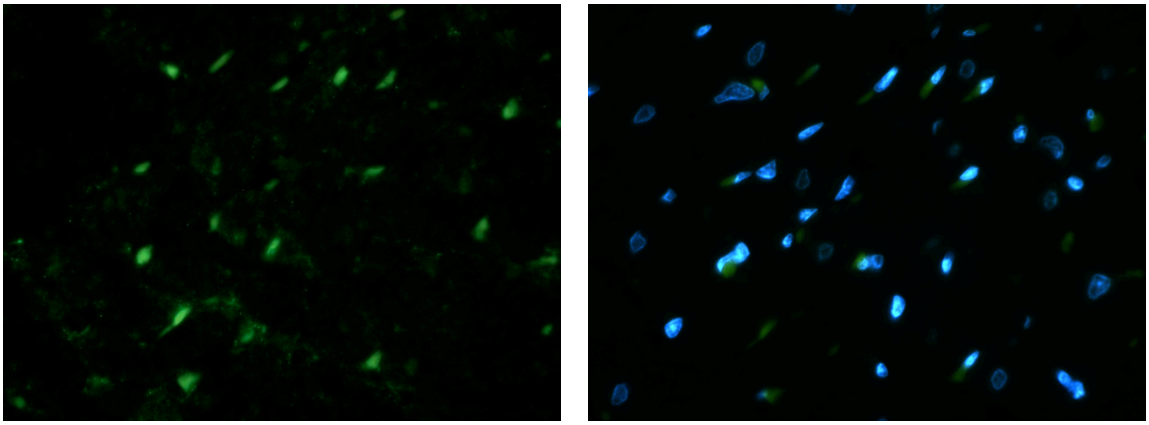
D



E



F



G H

Figure 27. ProANF immunofluorescence in the heart.

(A) Perinuclear staining of proANF in rat atrial appendage (texas red staining). (C) Absence of proANF staining in rat ventricle section. (E) Perinuclear staining of proANF in rat atrial appendage (fluorescein staining). (G) Absence of proANF staining in rat ventricle section. (B, D, F and H) DAPI nuclear staining of sections shown in panels A, C, E and G.

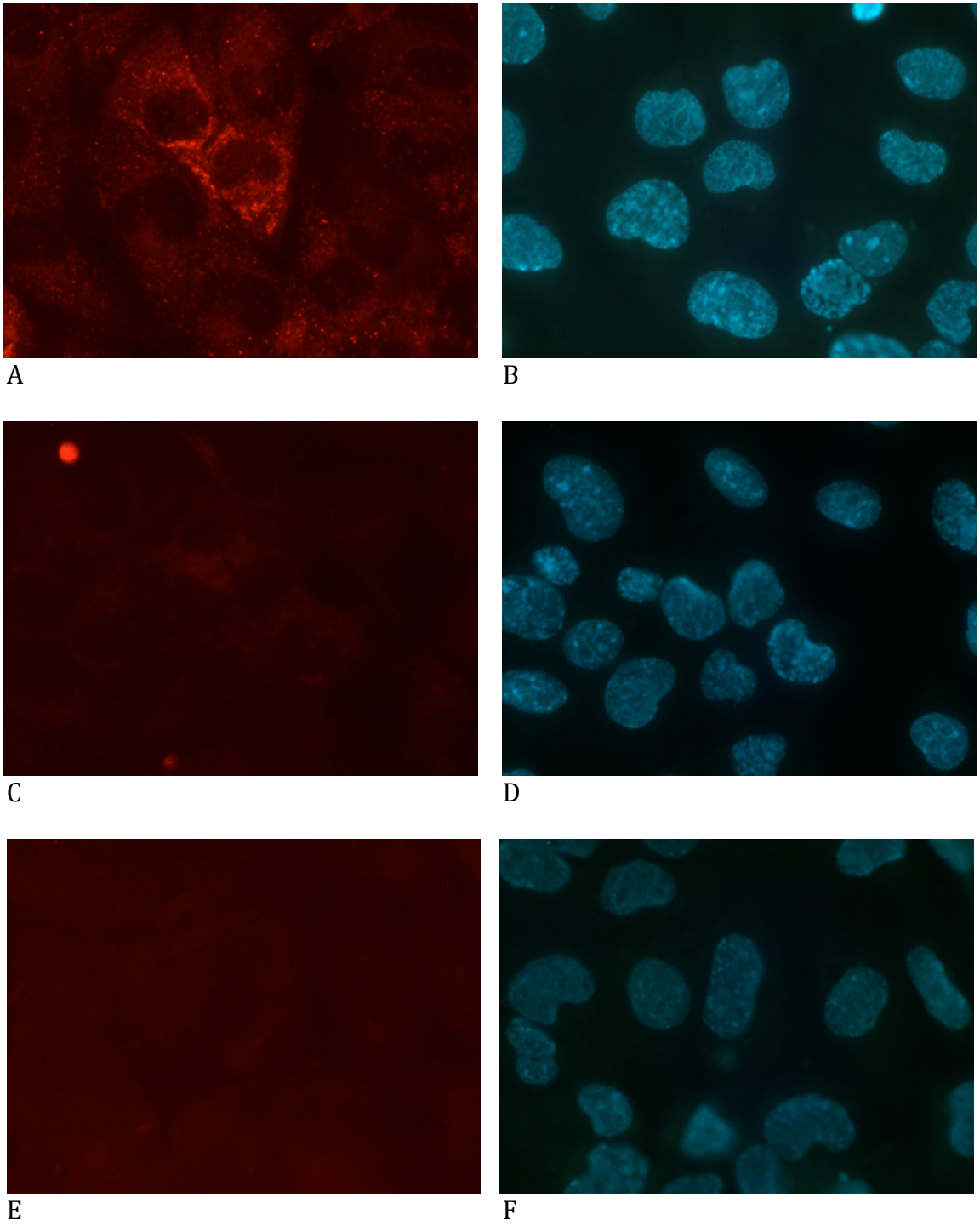


Figure 28. ProANF immunofluorescence in HL-1 cells.

(A) Perinuclear and cytoplasmic staining of proANF in HL-1 cells (texas red staining). (E) Negative control: primary antibody was not added. (G) Negative control: secondary

antibody was omitted. (B, D, and F) DAPI nuclear staining of sections shown in panels A, C, and E.

Chapter 3: Gene expression analysis of volume-overload tissue

Background

Gene expression profiles of normal atrial and ventricular tissues were analyzed in chapter 2 of the results section. The results obtained from that investigation described for the first time data on gene expression profiles particularly centered on the secretory function of the heart.

Next, an *in vivo* time course investigation was carried out to define the overall gene expression profile associated with the activation of the endocrine heart following aortocaval shunt surgery. Affymetrix GeneChip quality was assessed in chapter 1 of the results section.

Development of cardiac hypertrophy

Body weight did not differ between the aortocaval shunt- and sham-operated rats over the 4 week period (Figure 29). The progression of cardiac hypertrophy of the VO animals is shown in Figure 29B-E. All four cardiac chambers exhibited significant hypertrophy in shunt-operated rats as compared to sham-operated rats at 28 days post surgery.

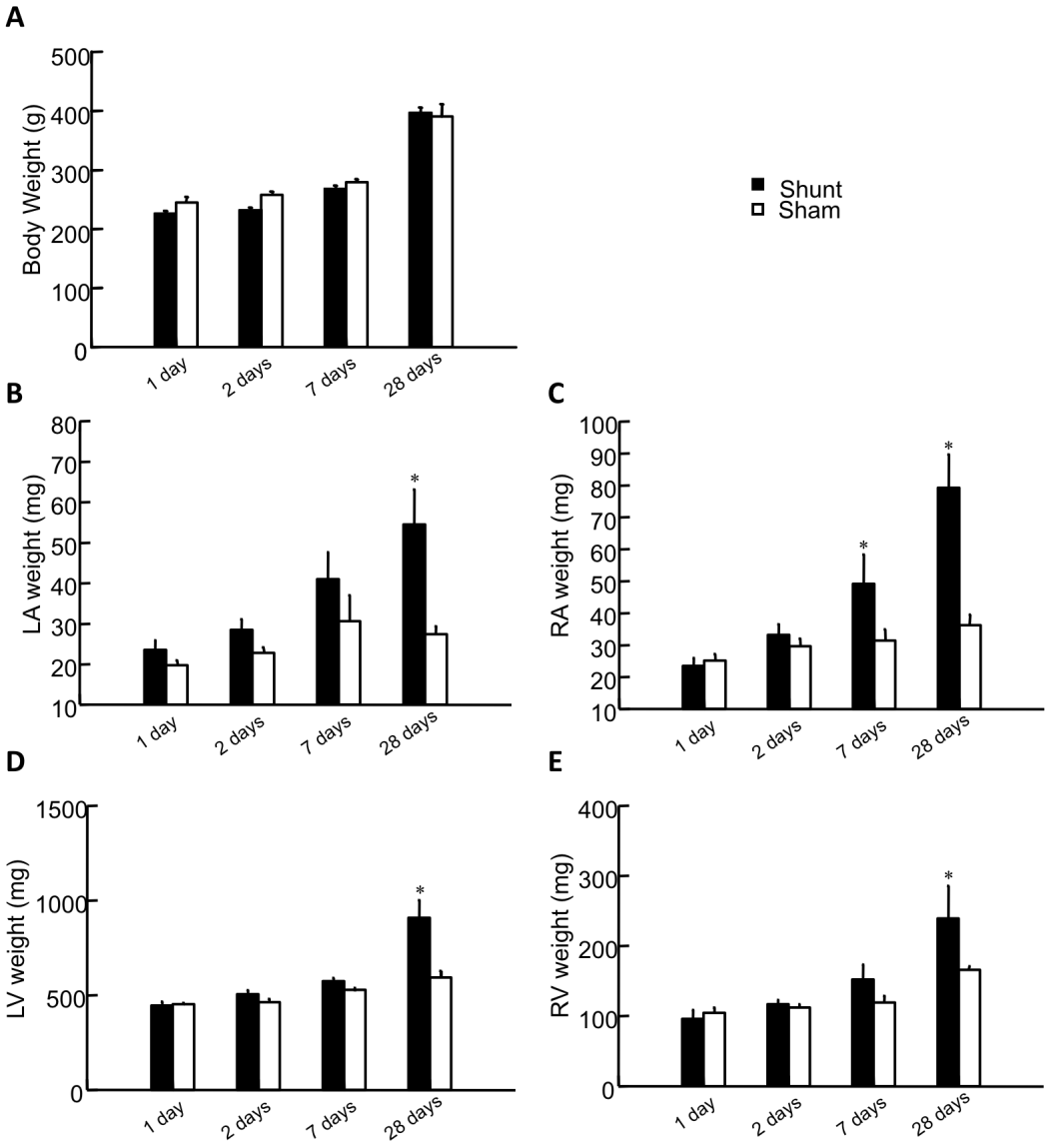


Figure 29. Body and cardiac chamber weights at various time points post aortocaval shunt (solid columns) and sham (open columns) surgery.

Atrial hypertrophy is evident at 7 and 28 days post-surgery, while ventricular hypertrophy was evident at 28 days post-surgery. n= 5; $P< 0.05$.

Time course measurements of plasma ANF and BNP secretion and gene expression

The aortocaval shunt procedure significantly increased plasma ANF and BNP levels by over two fold at days 2, 7 and 28 compared to the sham-operated rats (Figure 30). Across all time points, ANF plasma levels were on average 10 fold higher than BNP plasma levels. In the sham-operated rats, ANF and BNP plasma levels were constant across all time points.

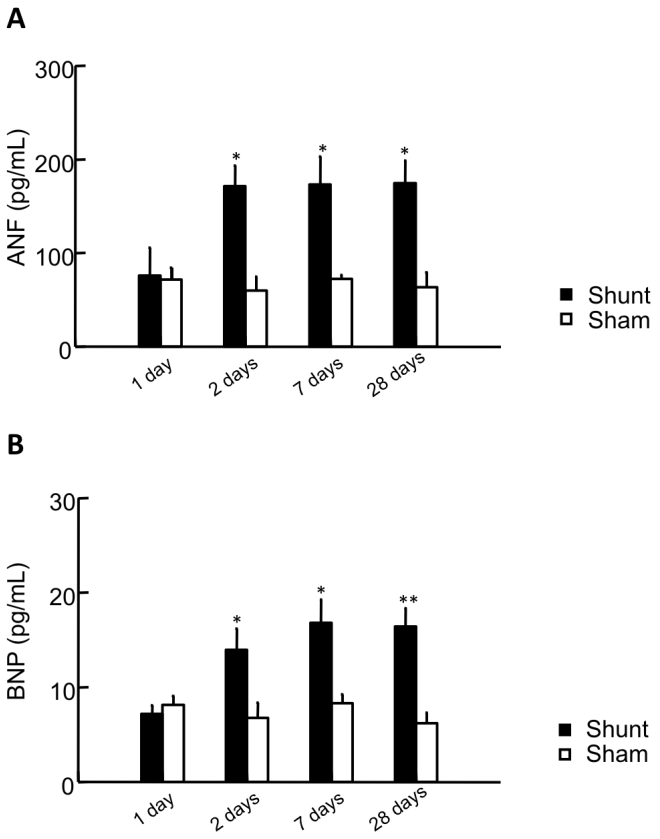


Figure 30. A) ANF and B) BNP plasma levels at various time points post aortocaval shunt (solid columns) and sham (open columns) surgery.

The aortocaval shunt procedure significantly increased plasma ANF and BNP levels by over two fold at days 2, 7 and 28 compared to the sham-operated rats. Across all time points, ANF plasma levels were on average 10 fold higher than BNP plasma levels. n = 5; *, $P<0.05$; **, $P<0.01$.

ANF and BNP gene expression levels significantly increased as VO induced cardiac hypertrophy progressed (Figure 31). On day 2, the right ventricles exhibited the first signs of increased ANF gene expression levels, while an increase in BNP levels was observed in the left atria. ANF gene expression in the VO rats increased significantly in all cardiac chambers on days 7 and 28. Elevated BNP mRNA levels were observed in all cardiac chambers by day 7 and were maintained elevated at the four week time point in the VO animals.

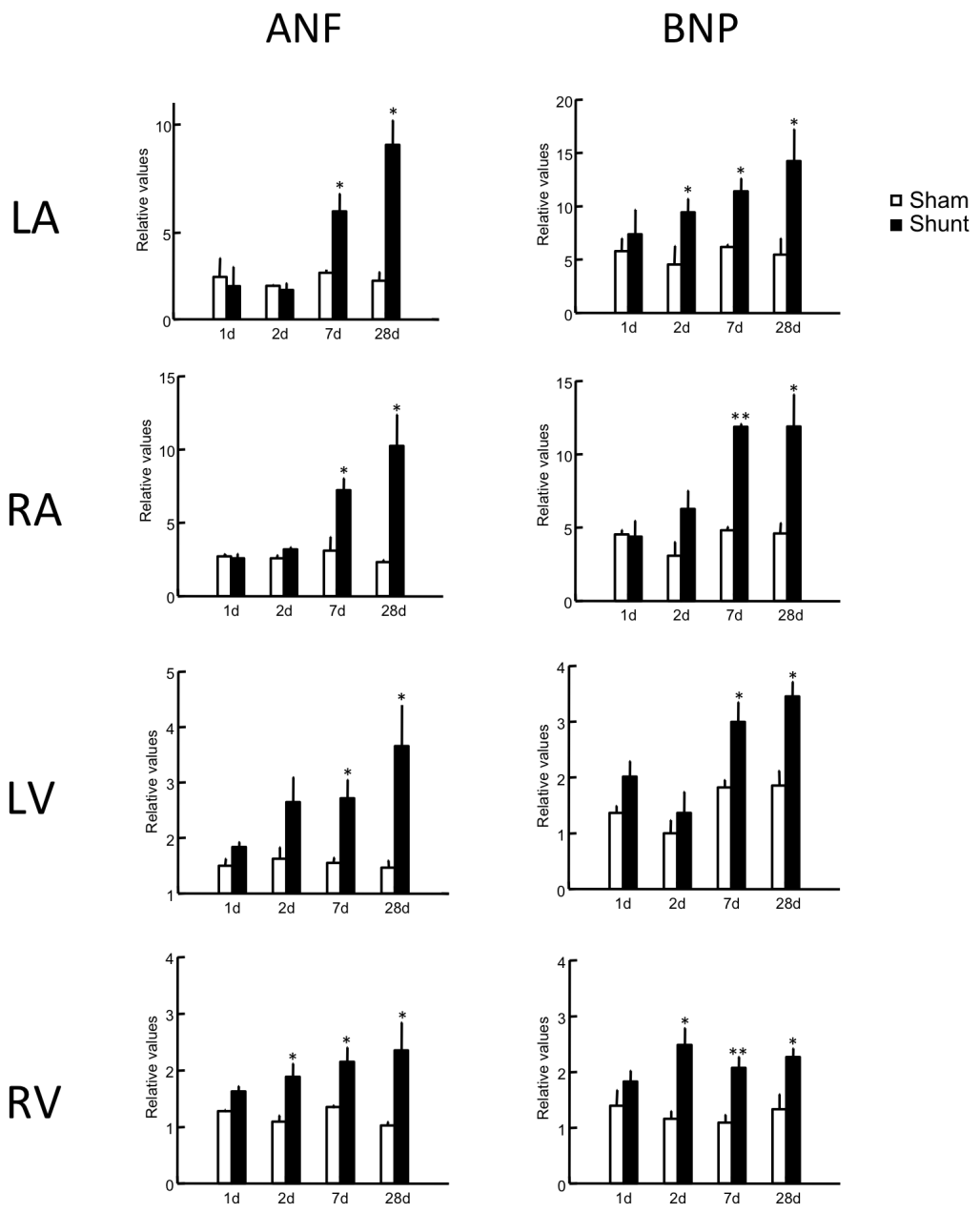


Figure 31. Northern Blot analysis of the relative abundance of ANF and BNP transcripts.

Relative abundance of ANF and BNP transcripts at various time points in left atria (LA), right atria (RA), left ventricles (LV) and right ventricles (RV) in aortocaval shunt (solid columns) and sham (open columns) operated rats. n = 5; *, $P<0.05$; **, $P<0.01$.

Gene Expression Analysis

Differentially expressed genes between volume-overload and sham atrial tissues

In order to assess the transcriptional response of the endocrine heart under chronic hemodynamic overload conditions, gene expression arrays were used to evaluate differential gene expression profiles between sham and VO atrial tissue, at 28-days post-surgery, at which time ANF and BNP expression levels were the greatest. An average of 54 % and 56 % of probes had present calls in the sham and VO arrays, respectively. Seven hundred probe sets exhibited a significant experimental condition effect based on a two-way ANOVA analysis (p-value < 0.001, FDR 0.045) between hemodynamically overloaded atria and their sham counterpart. Four hundred and eight probe sets were induced in the VO atrial samples whereas 292 probe sets exhibited a downregulation in these same samples (see Appendix 8, p. 314).

Ranking in the top 25 significantly differentially expressed probe sets (p-value < 1.3×10^{-7}, FDR < 0.0032) is the insulin-like growth factor binding protein 3 (Igfbp3), which is downregulated in VO conditions. Other significantly repressed genes include the second probe set for Igfbp3, fibrinogen gamma polypeptide, sodium/potassium/calcium exchanger (Slc24a3), Hsdl2, as well as the Ras-related protein RASD1. Volume-overload significantly induced skeletal α-actin (Acta1), ankyrin repeat domain 1 (Ankrd1), SCHIP-1, intersectin 2, ADP-ribosyltransferase 3, Bnip3, Wisp2, Ppp1r3c, and Psme4. Ten unknown genes were listed within these top 25 probes sets.

Due to the redundant nature of GO annotations, functional annotation clustering was performed on the 700 differentially expressed genes data set, in order to identify clusters of meaningful annotation terms and to infer biological significance. The functional clustering groups, including biological regulation, cell morphogenesis, actin binding, GTPase regulator activity and focal adhesion are listed in Table 8, with their corresponding score. Because of space allowance, a single annotation term is listed per functional clustering group. Pathway analysis identified several signaling cascades differentially expressed between the VO and sham atria, namely in cell communication, focal adhesion and MAPK pathway.

Table 8. Functional annotation clustering of differentially expressed genes found between VO and sham atrial tissues.

Each functional group represents a cluster of similar GO annotation terms. For clarity, a single representative GO annotation term is listed. Functional groups are listed based on their enrichment score, which is derived from the terms p-value obtained from the Fisher Exact statistic. Classification stringency was based on a similarity score of 0.5.

Functional annotation cluster	Representative GO term	Enrichment score
1	GO:0065007~biological regulation	10.04
2	GO:0009653~anatomical structure morphogenesis	4.94
3	GO:0000902~cell morphogenesis	4.73
4	GO:0048514~blood vessel morphogenesis	3.22
5	GO:0003779~actin binding	3.11
6	GO:0007399~nervous system development	2.92
7	GO:0030695~GTPase regulator activity	2.88
8	GO:0043067~regulation of programmed cell death	2.71
9	GO:0005539~glycosaminoglycan binding	2.69
10	GO:0005925~focal adhesion	2.6
11	GO:0006928~cell motility	2.36
12	GO:0007517~muscle development	2.23
13	GO:0005886~plasma membrane	2.19
14	GO:0031012~extracellular matrix	2.07
15	GO:0005737~cytoplasm	2.07
16	GO:0006810~transport	1.97
17	GO:0016787~hydrolase activity	1.95
18	GO:0005509~calcium ion binding	1.92
19	GO:0006936~muscle contraction	1.89
20	GO:0016192~vesicle-mediated transport	1.89

Hallmark genes that are known to be associated with cardiac hypertrophy, such as ANF, BNP, α-actin 1 and β-MHC were upregulated in the VO animals. Numerous transcription factors were also differentially expressed (Appendix 9, p. 337, under functional group 4) including Hey2, JunD, and Ankrd1, which are involved in the stimulation or repression of known hypertrophic regulated genes, as well as novel nucleic acid binding proteins that might be involved in the progression of cardiac hypertrophy.

Numerous signal transduction transcripts were differentially expressed between the sham and VO operated animals. These include G protein coupled receptor (GPCR) signaling pathway proteins (Angtrl1, Cxcr4, Fzd2, Eltd1, Gprk6, Igf2, RGS3 and CD97, as well as Smo, Edg2, RhoGEF17 and RASD1 (3.85 fold), upregulated and downregulated, respectively), growth factors, cytokines and hormones. Upregulated transcripts involved in cell surface mechanosensing included osteoglycin (1.41 fold), α5-integrin (1.38 fold), as well as the previously mentioned Ankrd1. Four potassium channels were downregulated in the VO atria (Kcna5, Kcnj12, Kcne2 and Kcnj9) while the L-type calcium channel, Cacna1d, was upregulated. The calcium binding proteins S100A4, S100A6 and S100A10 were all upregulated in the VO atria. The S100A10 binding partner, Annexin-A2, was also up regulated in the VO atria, by 1.38 fold. This is of interest since it was demonstrated that Annexin-A2 cross-links secretory granules to their docking sites (Burgoyne and Morgan, 1993) and recently it was shown that S100A10 mediates Annexin-A2 translocation to the plasma membrane, at specific soluble N-ethylmaleimide- sensitive factor attachment protein receptors (SNAREs)-containing exocytotic sites, upon secretagogue stimulation (Umbrecht-Jenck et al.,

2010). Other members of the SNARE complex that were upregulated in the VO atria included VAMP1, VAMP3 and Syntaxin 11.

Differential expression between volume-overloaded atrial and ventricular tissues

Atrial and ventricular gene expression profiles from the VO animals were determined based on a SAM statistical analysis test with a fold change cut-off of 1.5. A total of 2347 genes were found differentially expressed between the two groups (not listed in Appendix, refer to GEO accession number GSE12758 for the raw data (GEO)). One thousand three hundred seventy two genes were more abundant in the atria, while 975 genes were more abundant in the ventricles. Atrial abundant genes (greater than 20 fold change) included the calcium binding proteins sarcolipin and visinin-like 1, Myosin-binding protein H, paired-like homeodomain transcription factor 2 (Pitx2), α-synuclein, the sodium or proton exchanger Atp1b4, as well as palmitoyl-protein thioesterase 2 (PPT2).

Statistically overrepresented GO terms based on $p < 0.001$ were determined using GOstat software. Nine GO terms were found overrepresented in the VO atria (Figure 32, and Appendix 10, p.340) and 30 GO terms were found overrepresented in the VO ventricles (not shown). Atrial abundant transcripts that had GO annotations related to secretion are listed in Table 9. This list included the intra-Golgi trafficking proteins ARF1, ARF4, KDELR1, ARFGAP1, as well as phospholipase D1 (PLD1). The atrial abundant PLD1, which is activated by ARF1 (Kim et al., 1998) promotes

exocytosis of large dense-core granules (Zeniou-Meyer et al., 2007) and was recently shown to be an essential regulator of insulin secretion (Hughes et al., 2004).

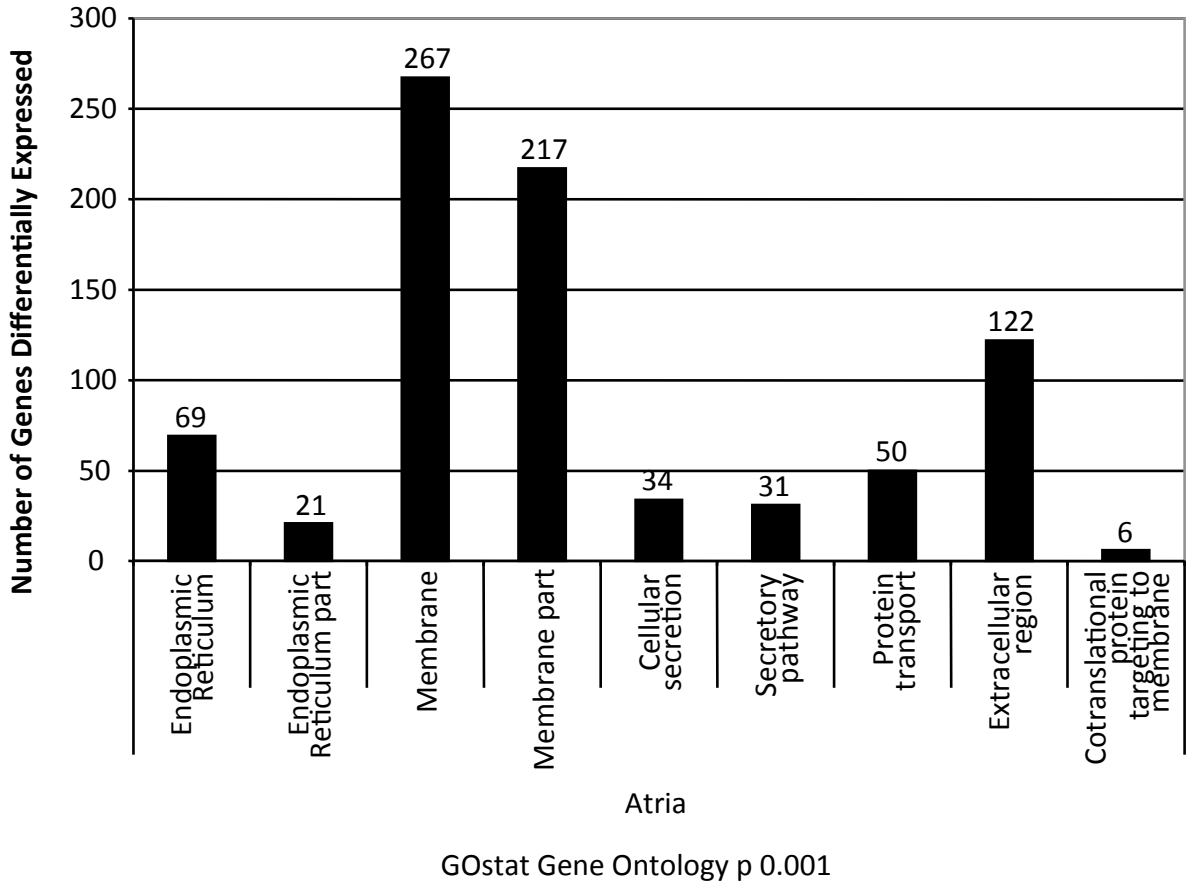


Figure 32. Number of atrial abundant differentially expressed genes per Gene Ontology term based on GOstat analysis (p< 0.001).

Input gene list was from the 1372 differentially expressed genes found more abundant in the hypertrophic atria as compared to the hypertrophic ventricles. For the complete list of gene symbols and associated p-values found in each column, refer to Appendix 10.

Table 9. Atrial abundant genes found differentially expressed between VO atrial and ventricular tissues, classified into the "Secretion" functional groups.

Gene Ontology annotation	GO	Gene Symbols
GO:0032940	cellular secretion	ARFGAP1; SEC22L1; ZWINT; LYN; ARF1; EXOC4; SEC23A; LPHN1; SNCAIP; SRPR; YWHAQ; SSR1; KDELR1; CSPG2; RAB2; SAR1A; SNCA; RAB15;MYH10; TRAPPC1; SCAMP1; SSR2;SEPT5; TLOC1; TRAM1; VDP; OSBPL5; ICA1;BACE2; SEC61A1; YIPF5; KDELR2; SEC13L1
GO:0051046	regulation of secretion	SGNE1; ICA1; SNCA; GCK; SNCAIP
GO:0045055	regulated secretory pathway	ICA1; SNCA; LPHN1; RAB15; SNCAIP
GO:0045047	protein targeting to ER	SRPR; SSR1; CSPG2; SSR2; TLOC1
GO:0006888	ER to Golgi vesicle-mediated transport	ARFGAP1; RAB2; VDP; SEC23A; SAR1A; SEC22L1; PLD1; ARF1; ARF4 ; YIPF5; TRAPPC1; KDELR1; SEC13L1; KDELR2
GO:0006892	post-Golgi vesicle-mediated transport	OSBPL5; SCAMP1

Gene symbols are listed as opposed to gene names.

Figure 33 depicts a Venn diagram illustrating the number of differentially expressed genes obtained following a two-way ANOVA analysis ($p<0.001$) for each factor (i.e. tissue (atria vs. ventricles) or condition (sham vs. shunt)) and their interaction, i.e. genes that are differentially expressed due to the experimental condition as well as their tissue origin. An upregulation of the stretch sensitive Trpm7 channel, as well as a downregulation of the cholinergic receptor, muscarinic 2 Kcnj3 channel was observed in both atrial and ventricular tissues under VO (condition effect $p<0.001$). At a lesser p-value, Kcnj5 ($p=0.0051$) and the stretch sensitive potassium channel TREK-1 ($p= 0.008$) were downregulated in both tissues under VO conditions. These transcripts were also more abundant in the atria than in the ventricles under both sham and VO conditions. Fifty-two transcripts were found to exhibit an interaction effect between the two factors. These included transcripts involved in the regulation of G protein signaling, such as RASD1, RGS3 and RGS4, as well as genes involved in signal transduction, transcription and transport (Appendix 11, p. 343). RASD1 was significantly downregulated only in the VO atria, by 3.85 fold (as mentioned in the above section), while RGS3 was upregulated in the VO atria and RGS4 was uniquely upregulated in the VO ventricles (1.63 fold). Other regulators of G protein signaling or heterotrimeric G proteins transcripts were differentially expressed between the VO atria and ventricles, which included ventricular abundant Gγ5, as well as the atrial abundant Gαo1, Gβ5, Gγ2, RGS3. A probe set with high similarity to human RGS6 was 2.57 fold more abundant in the VO atria as compared to the ventricles.

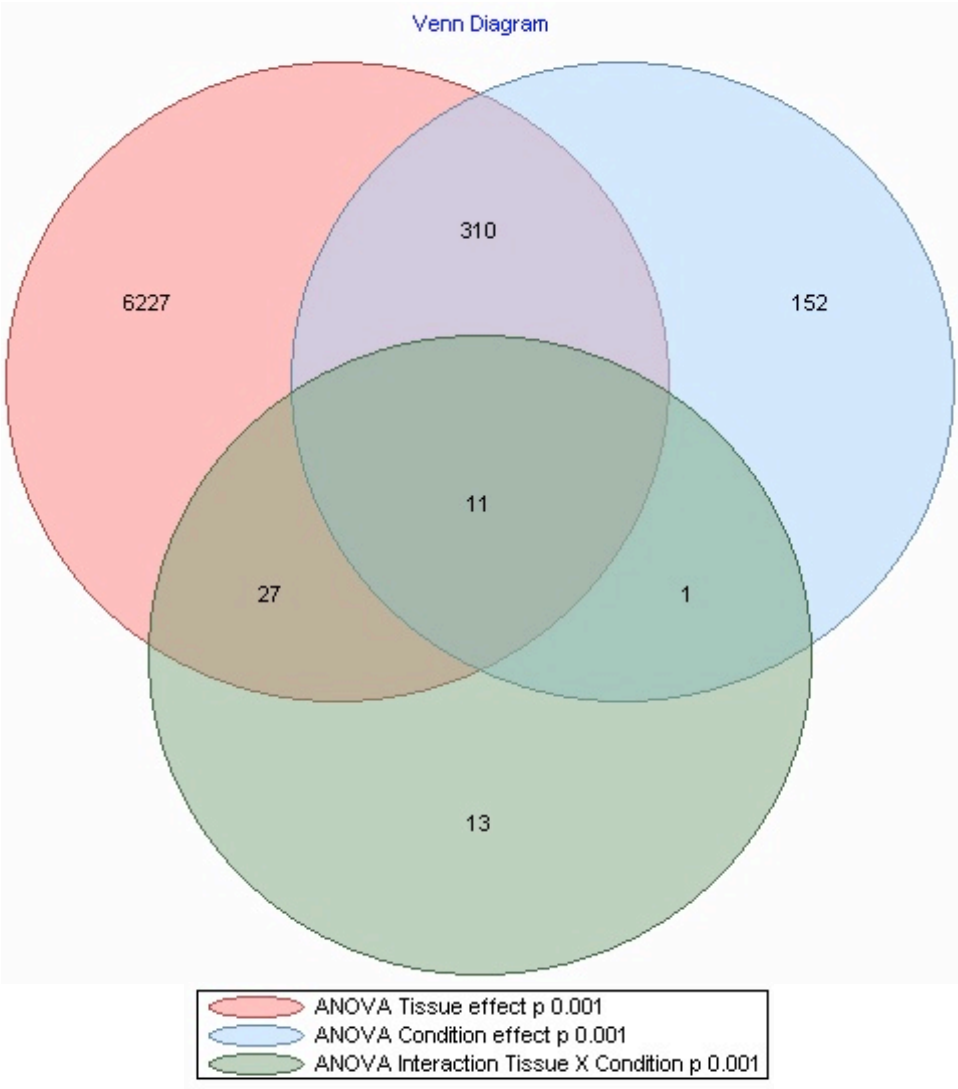


Figure 33. Venn diagram of two-way ANOVA analysis.

Venn diagram illustrating the number of genes grouped within each category obtained from two-way ANOVA analysis of the following four groups: atria sham, atria shunt, ventricles sham and ventricles shunt ($p<0.001$).

RT-PCR validation

Gene expression profile analysis identified numerous candidate genes involved in the regulation of the endocrine function of the heart. A subset of these genes was validated by RT-PCR. Figure 34 shows the relative fold change of 13 genes found differentially expressed between the atria of 28 day VO vs. sham-operated animals. In order to validate the microarray data in an unbiased manner, two probe sets with unknown annotations were also validated by RT-PCR (1373628_at and 1368987_at). RASD1 temporal regulation across the four week VO experiment was determined in LA and LV tissues following 1, 2, and 7 days post aortocaval shunt and sham surgery. In the shunt LA tissue, RASD1 expression levels decreased on days 2 and 7 by 6 and 6.4 fold, respectively, as compared to LA sham. RASD1 expression levels did not change in the shunt LV on those days. RASD1 differential expression levels for the 28-day time point is shown in Figures 33 and 34A. The RT-PCR validation of several differentially expressed genes found between the atria and ventricular tissues of VO animals are depicted in Figure 35. The fold changes derived by RT-PCR were in agreement with the data obtained by the microarray experiment with the exception of 1368987_at and Rab15, which had opposing fold changes in the left ventricles shunt vs. sham comparison. This discrepancy is likely due to the very low abundance of these transcripts in the ventricles, as assessed by the MAS5 detection calls, which identifies these transcripts as absent in the ventricles. Several genes exhibited a higher fold change ratio when analyzed by RT-PCR as compared to microarray.

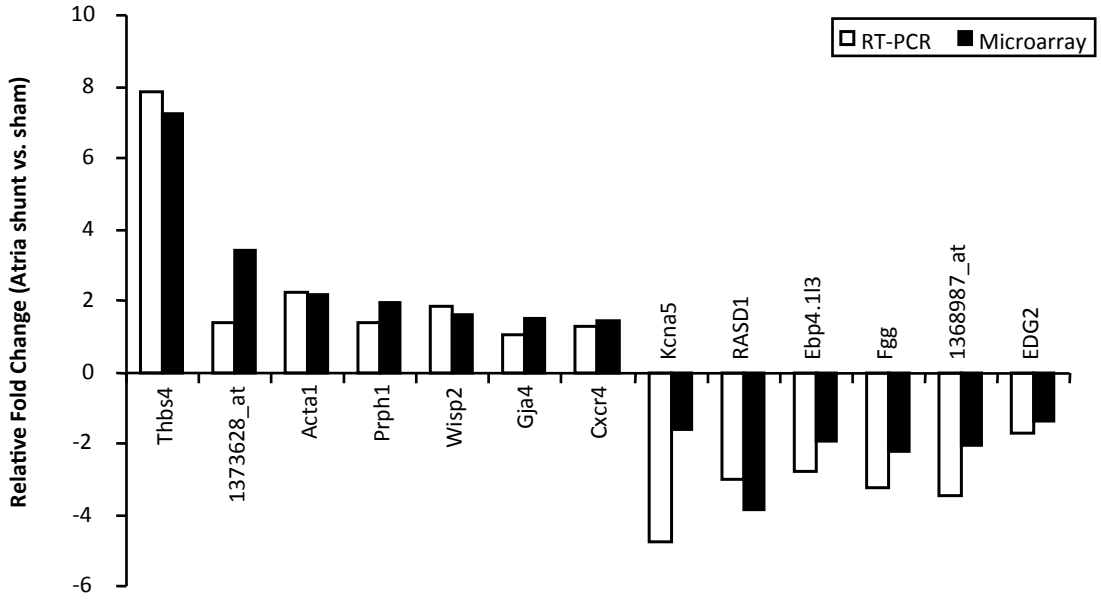


Figure 34. Comparison of microarray and real-time PCR results in atrial shunt vs. sham samples.

Relative fold change of 13 transcripts found between atria shunt vs. atria sham samples is depicted. Open columns represent relative fold changes obtained by RT-PCR, while solid columns represent relative fold changes obtained by microarray. Negative fold changes indicate lower expression of the atria shunt samples as compared to the sham.

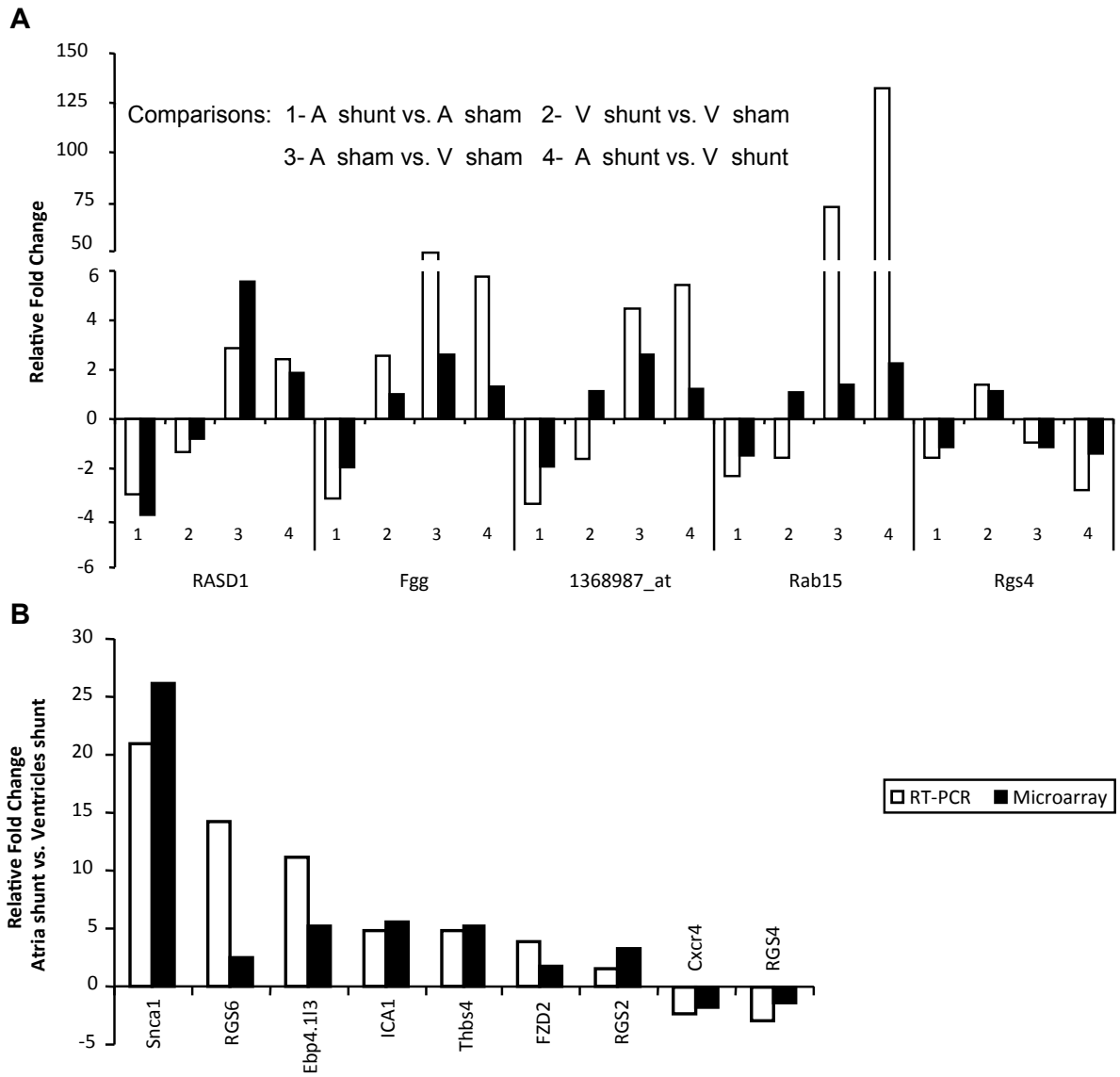


Figure 35. Comparison of microarray and real-time PCR results in atrial and ventricular samples under both sham and shunt conditions.

A) Relative fold change of 5 transcripts that were identified as having a tissue x condition interaction effect based on a two-way ANOVA analysis ($p < 0.001$) in various comparisons (1-4). Note the break in the ordinate axis. B) Relative fold change of 9 transcripts found between atria shunt vs. ventricles shunt expression levels. Open

columns represent relative fold changes obtained by RT-PCR, while solid columns represent relative fold changes obtained by microarray.

Chapter 4: RNAi silencing

Background

In chapters 2 and 3 of the results section, gene expression profiling experiments was performed on atrial and ventricular tissues under normal and under chronic VO, respectively, to define the overall gene expression profile associated with hemodynamic activation of the ANF and BNP genes. Several modulators of G protein signaling were identified, such as RASD1, which were differentially expressed between the various groups. RASD1 was highly expressed in the heart, with higher expression in the atria as compared to the ventricles. Under chronic VO (28 days post surgery), RASD1 was significantly downregulated in the atria by 3.85 fold, but no significant change in expression levels was observed in the ventricles, i.e. RASD1 gene expression levels remained low in the ventricles. The differential expression of RASD1 in atrial and ventricular tissues can be readily visualized by a heat map (Figure 36). While not determined by microarray, RT-PCR analysis demonstrated that RASD1 expression levels were also specifically decreased in the VO atria on days 2 and 7 following aortocaval shunt surgery. To further investigate the role of RASD1, RNAi knockdown experiments in HL-1 cells were performed.

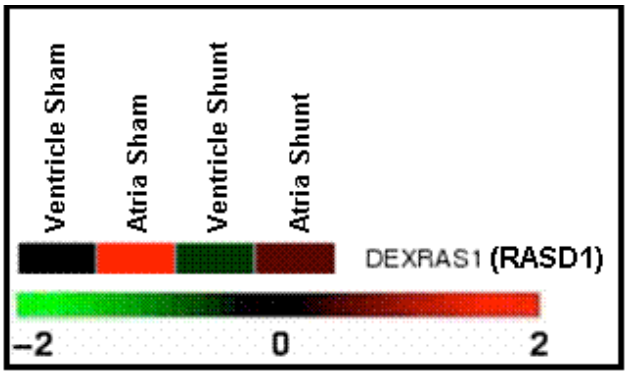


Figure 36. RASD1 heat map.

Heat map illustrating RASD1 gene expression levels across different tissues (ventricles and atria) and conditions (sham and shunt). Note, expression levels are colored green for lower signal intensities as compared to the reference GeneChip array, i.e. Ventricle sham, and red for higher signal intensities as compared to the reference GeneChip. The scale is base $\log_2$.

RNAi knockdown optimization in HL-1 cells

Transient transfections of siRNA oligonucleotides targeting GAPDH (positive control) were carried out in HL-1 cells to determine optimal cell plating density, the suitable cationic lipid transfection reagent (either DharmaFECT1, DharmaFECT2, DharmaFECT3 or DharmaFECT4), as well as the appropriate amount of transfection reagent per tissue culture well (for a 24 well plate). It was determined that the ideal cell plating density ranged between 20k to 25k cells per well, and that one μl/well of either DharmaFECT1 and DharmaFECT2 transfection reagents reduced GAPDH mRNA expression levels by at least 75% as compared to the scrambled siRNA negative control (not shown).

Knockdown of RASD1 was unsuccessful with the ON-TARGETplus set of four siRNA oligonucleotide sequences, from Dharmacon (LQ-040275-00-0002), in three independent transfection experiments. RASD1 mRNA expression levels was on average reduced by 6%, as compared to the siNegative control. Western blot analysis of RASD1 protein levels further confirmed the RT-PCR results (Figure 37). Knockdown of RASD1 was also attempted with several different concentrations of siRNA as well as with a different transfection reagent, i.e. Fugene (Roche Applied Science, Laval), unsuccessfully (not shown). RNA quality of each transfection samples was assessed with the Agilent Bioanalyzer. In general, all samples had high RNA quality, as determined by high RIN values and distinct 18S and 28S ribosomal RNA peaks with low noise between peaks (see Figure 38 for a representative Electrophoresis Gel-Like image and electropherograms). The derivative melting curves of the real-time PCR

reactions showed a single amplicon peak while electrophoresis analysis of the PCR amplicon product of RASD1 revealed a single band (not shown), hence excluding any problems with the RT-PCR reaction or template samples, such as genomic DNA contamination and primer-dimer amplicons.

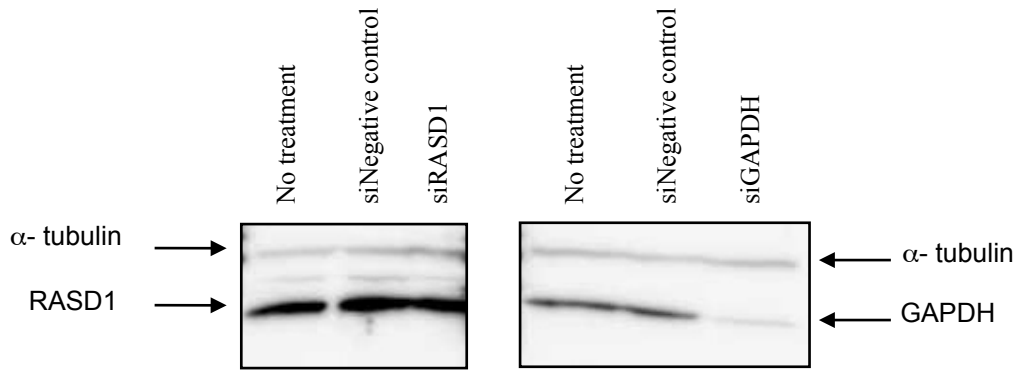


Figure 37. Western bot analysis for RASD1 and GAPDH in RNAi transfected HL-1 cells.

RASD1 or GAPDH protein expression in HL-1 cells transfected with negative control siRNA (siNegative control) and RNAi targeting RASD1 (siRASD1) or GAPDH (siGAPDH). Fifteen μg of total protein was loaded. α-tubulin was used as loading control. Proteins of interest were probed simultaneously with corresponding antibodies.

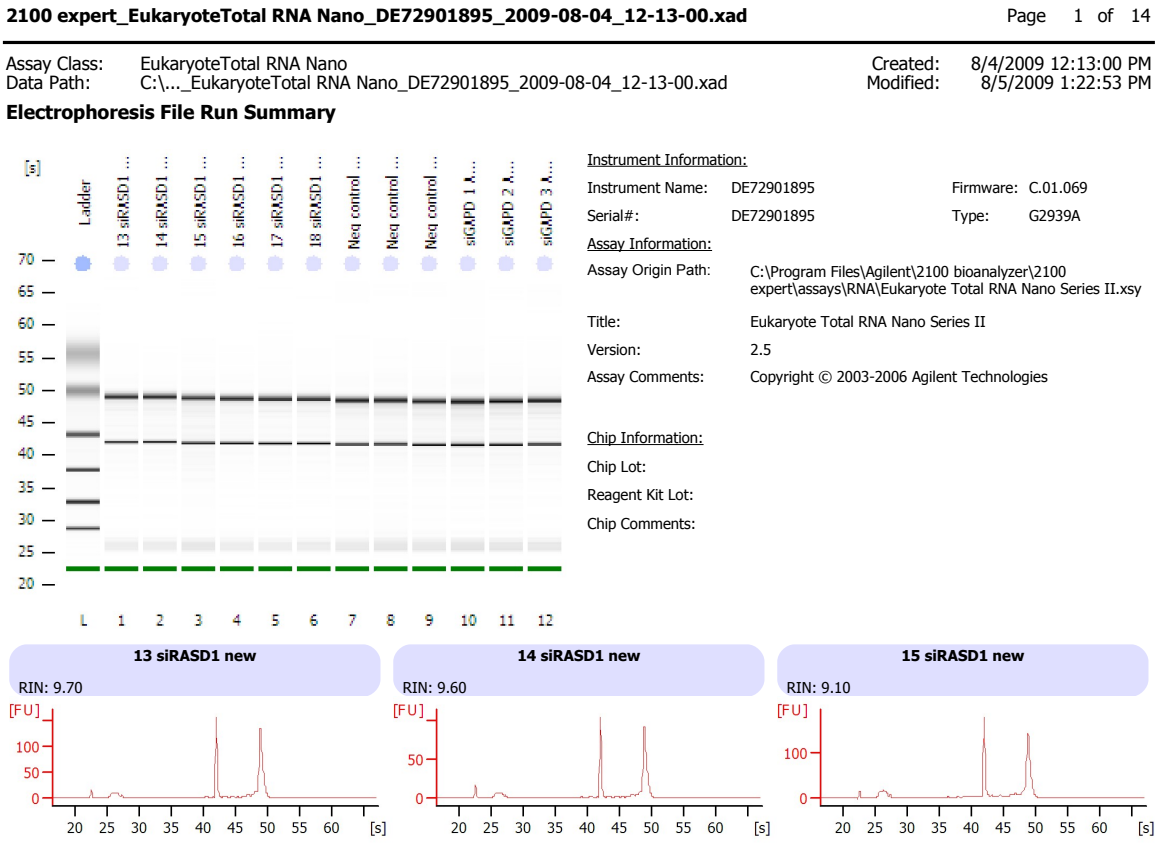


Figure 38. Bioanalyzer results.

Electrophoresis Gel-Like image and the corresponding first three (out of 12) electropherograms showing high quality of total RNA samples, i.e. distinct 18S and 28S ribosomal RNA peaks, low noise between the peaks and a minimum low molecular weight contamination (between 30 and 40 seconds).

Knockdown of RASD1 in HL-1 cells was attempted again with a second set of four pooled siRNA oligonucleotides (MU-040275-01-0002, Dharmacon). Total RNA was extracted from transfected HL-1 cells at various time points (24h, 36h, 48h, 72h, and 96h) in order to find the window in which RASD1 was effectively knockdown (not shown). These transfection experiments were unable to reduce RASD1 expression levels. At length, a third set of four pooled siRNA oligonucleotides (LQ-040275-01-0002) targeting RASD1 was tested. RASD1 was knockdown by 34%, as compared to the negative control, but this reduction was not paralleled at the protein level (Figure 39). Even though silencing of RASD1 was not successful with Dharmacon's RNAi oligonucleotide sequences, ANF, BNP and Gαo were successfully knocked-down with the optimized transfection protocol (Figures 40 and 41).

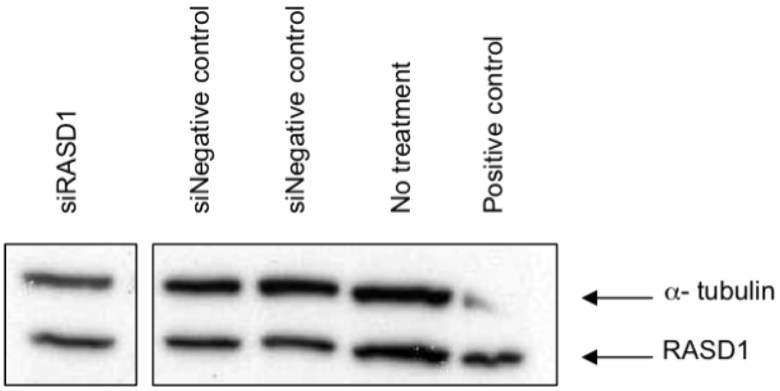


Figure 39. Western blot analysis of RASD1 in RNAi transfected HL-1 cells.

RASD1 protein expression in HL-1 cells transfected with negative control siRNA (siNegative control) and RNAi targeting RASD1 (siRASD1). Thirty μg of total protein was loaded. α-tubulin was used as loading control. Rat brain extract was used as positive control for RASD1.

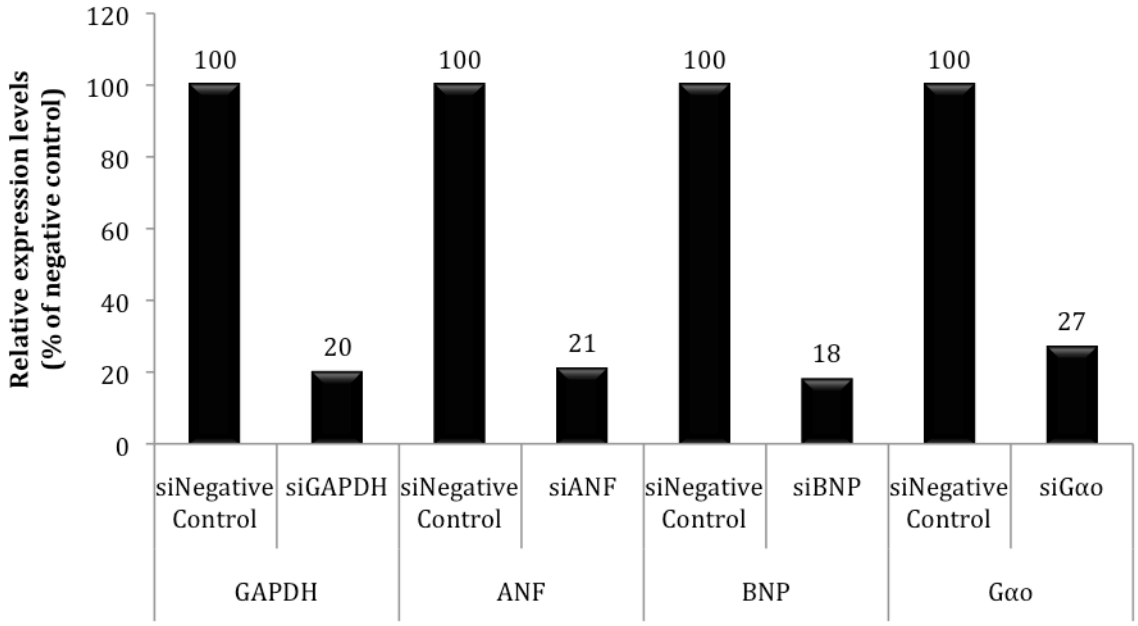


Figure 40. Relative expression levels of GAPDH, ANF, BNP and Gαo in RNAi transfected HL-1 cells.

Relative expression levels of GAPDH, ANF, BNP or Gαo in HL-1 cells transfected with negative control siRNA (siNegative control) and RNAi targeting the positive control GAPDH (siGAPDH), ANF (siANF), BNP (siBNP) or Gαo (siGαo).

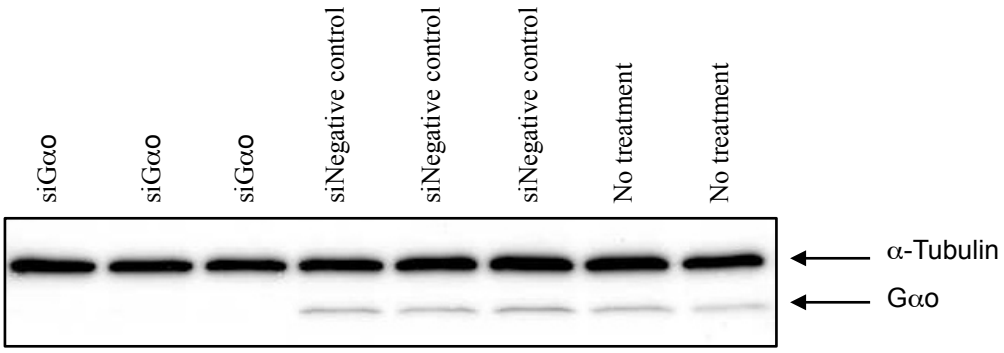


Figure 41. Western blot analysis of Gαo in RNAi transfected HL-1 cells.

Gαo protein expression in HL-1 cells transfected with siRNA negative control (siNegative control) and RNAi targeting Gαo (siGαo). Thirty μg of total protein was loaded. α-tubulin was used as loading control.

A different molecular strategy was sought out to knockdown of RASD1 in HL-1 cells. As an alternative to the RNAi mediated knockdown by 21-mer sequences (as provided by Dharmacon), 27-mer double-stranded RNA (dsRNA) (from IDT) were used in the attempt to silence RASD1. The dsRNA is theorized to be a substrate of the endoribonuclease Dicer, while the 21-mer sequence is the product of Dicer and thus dsRNA may be more efficient in entering the RNA Induced Silencing Complex (RISC) by Dicer for sequence-specific degradation of complementary mRNA species (Kim et al., 2005; Lee et al., 2004; Pham et al., 2004).

Transfection efficiency of dsRNA was assessed by TYE™ 563-labeled transfection control in HL-1 cells (Figure 42). Immunofluorescence analysis demonstrated that HL-1 cells were positively stained for TYE™ 563 regardless of the amount of DharmaFECT1 transfection reagent used (1.5, 1.0 or 0.75 μl/well, in a 24 well plate). In all subsequent transfections, 1.0 μl/well, DharmaFECT1 transfection reagent was used. Knockdown of RASD1 by three independent dsRNA (duplexes 1, 2 or 3) was assessed in HL-1 cells. Both duplexes 1 and 3 reduced RASD1 expression by 62% and 44% as compared to the negative control, respectively, while duplex 2 did not change RASD1 mRNA levels (Figure 43A). In combination, duplexes 1 and 3 knockdown RASD1 levels by 78% (Figure 43B). dsRNA duplex 2 was subsequently replaced by a different dsRNA (duplex 4). Succeeding transfection experiments were carried out with dsRNA duplexes 1, 3 or 4, or in combination, designated as siRASD1(n), where n= duplex number.

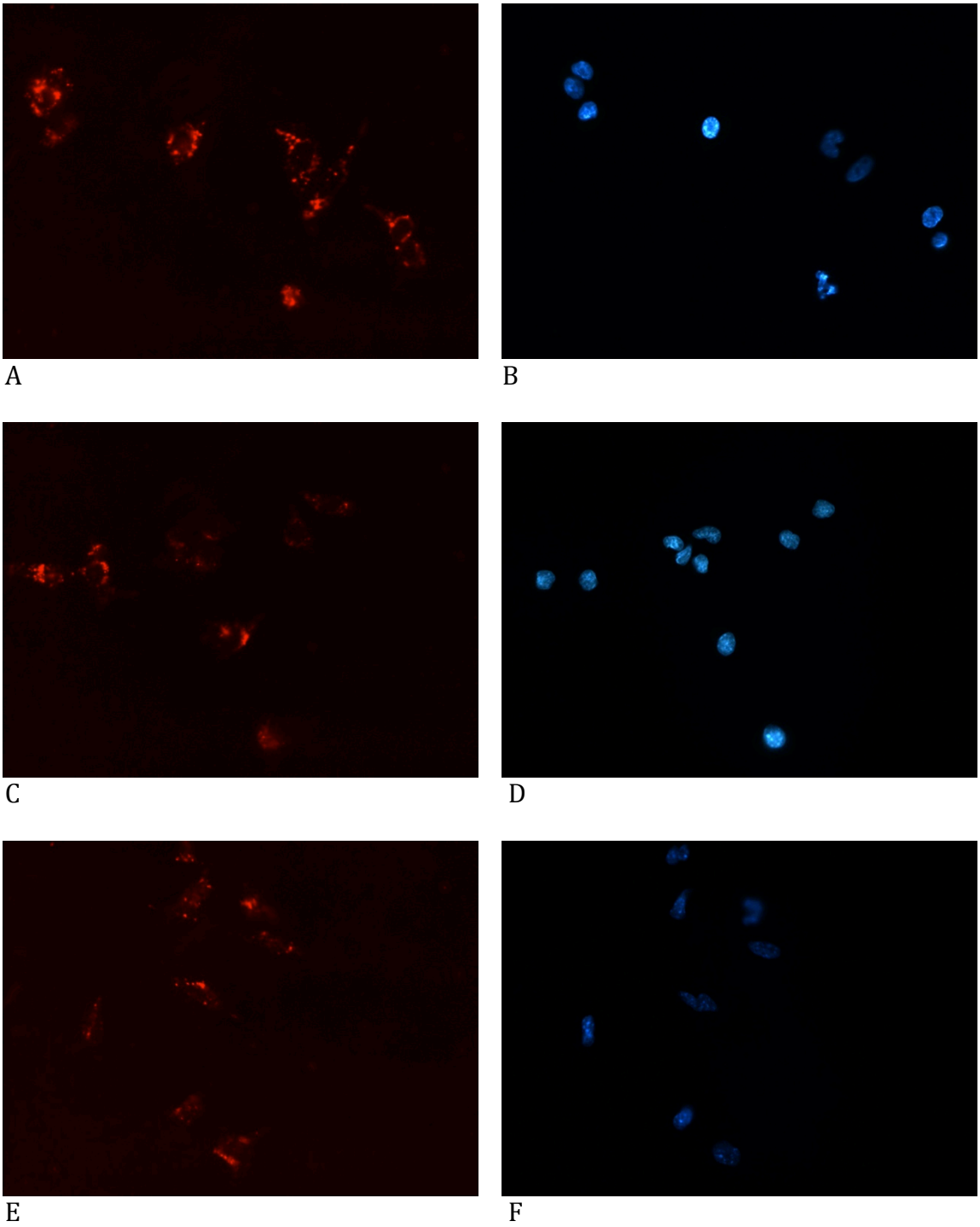
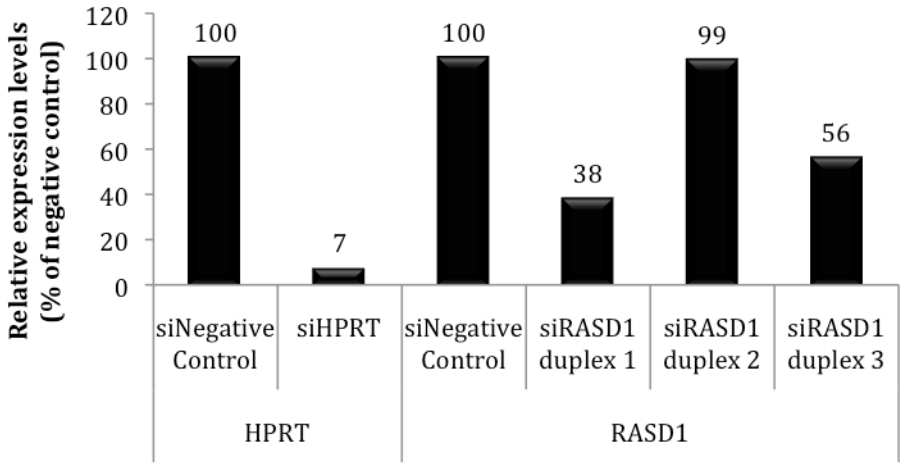


Figure 42. TYE™ 563-labeled transfection positive control in HL-1 cells

TYE™ 563-labeled dsRNA transfected in HL-1 cells with 1.5 μl/well (A), 1.0 μl/well (C), or 0.75 μl/well (E) of DharmaFECT1 transfection reagent. (B, D and F) DAPI nuclear stains of sections found in panels (A, C and E).

A



B

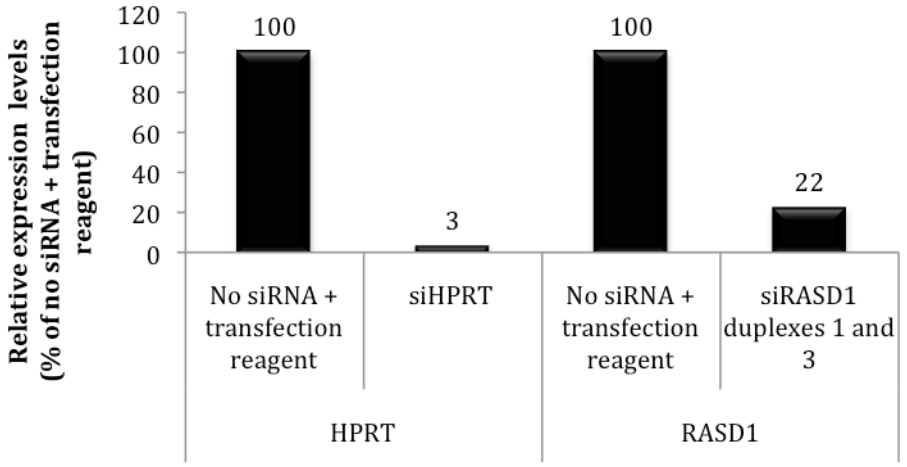


Figure 43. Relative expression levels of HPRT and RASD1 in RNAi transiently transfected HL-1 cells.

A) Relative expression levels of either HPRT or RASD1 in HL-1 cells transfected with negative control siRNA (siNegative control) and RNAi targeting the positive control HPRT (siHPRT), RASD1 (siRASD1 duplex 1, 2 or 3) or B) a combination of RNAi targeting RASD1 (siRASD1 duplexes 1 and 3).

RNAi knockdown in HL-1 cells

RASD1 RNAi knockdown modulates ANF secretion in HL-1 cells

RNAi mediated knockdown decreased RASD1 expression levels from 68% to 88% (Figure 44). Physiologically, the reduction of RASD1 by RNAi duplexes 1, 4 or 1 and 4 significantly increased ANF secretion at 48h and 72h post-transfection by 4.34, 3.05 and 6.88 fold, respectively, as compared to siNegative control, at 72h post-transfection (Figure 45). Interestingly, siRASD1(3) had no effect on ANF secretion, as compared to the control groups, even though it significantly reduced RASD1 mRNA to comparable levels of siRASD1(4). When transfected in combination with other siRASD1 duplexes, siRASD1(3) reduced ANF secretion levels as compared to HL-1 cells transfected with a single siRASD1 duplex. This effect can be explained by the fact that when siRNA duplexes targeting the same gene are transfected in combination, the total amount of RNAi remains the same, while the proportion of each individual RNAi duplex is reduced. The RNAi transfection control groups were as follows: HL-1 cells incubated in either non-targeting scrambled RNAi duplex (siNegative control), media containing DharmaFECT1 transfection reagent without any RNAi duplexes (No RNAi + transfection reagent), antibiotic free media (No treatment), RNAi duplex targeting the transfection positive control HPRT (siHPRT) and fibronectin coated wells containing media without any adherent cells (media). The latter does not modulate ANF expression and secretion levels and thus serves as another control. These other controls are useful since on occasion it would appear that the siNegative control

stimulates ANF secretion (Figure 45), an effect that is usually lost once the transfection media is replaced by fresh antibiotic-free media.

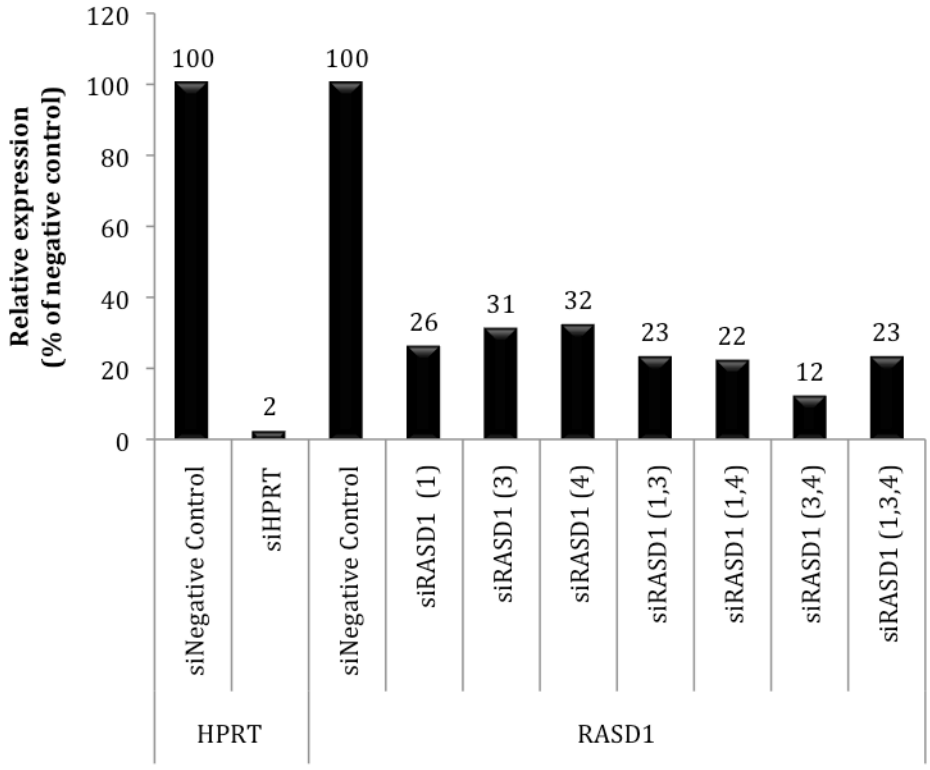


Figure 44. Relative expression levels of HPRT and RASD1 in RNAi transiently transfected HL-1 cells.

Relative expression levels of either HPRT or RASD1 in HL-1 cells transfected with negative control siRNA (siNegative control) and RNAi targeting the positive control HPRT (siHPRT), RASD1 (siRASD1 duplexes 1, 3 or 4) or a combination of RNAi duplexes targeting RASD1.

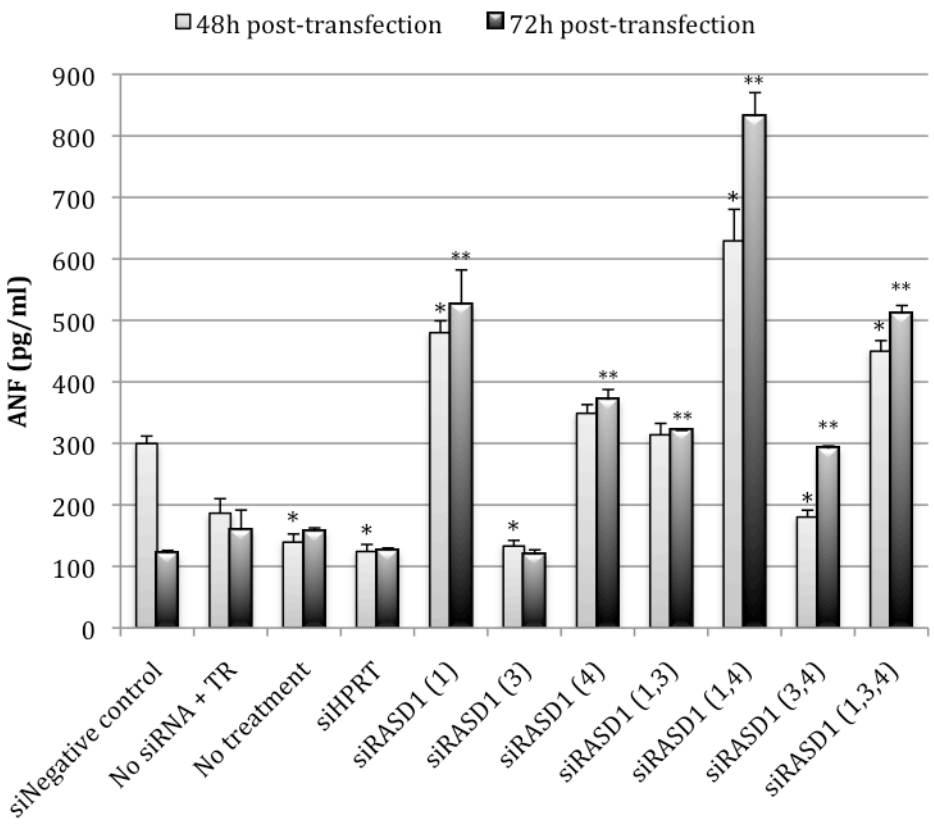


Figure 45. RNAi knockdown of RASD1 modulates ANF secretion in HL-1 cells.

ANF secretion levels at 48h (light shaded column) or 72h (dark shaded column) post RNAi transfection. siRASD1 (1) and (4) increase ANF secretion while siRASD1 (3) has no effect on ANF secretion. Media was collected and replaced every 24h. Values are mean ± standard deviation (48h n = 6/group; 72h n = 3/group). *, $P<0.01$ *vs.* 48h siNegative control; *, $P<0.01$ *vs.* 72h siNegative control. Representative graph of three independent experiments. Abbreviation: TR, Transfection Reagent.

Based on the results obtained in Figure 45, subsequent RNAi knockdown of RASD1 was performed with duplexes 1, 4 or in combination. RNAi duplexes 1, 4 or 1 and 4 reduced RASD1 expression levels by 53%, 50% and 62%, respectively, while the positive control HPRT was reduced by 97%, as compared to the siNegative control. Even though RASD1 was not as efficiently knocked down as previous transfection experiments (Figure 44), the physiological effect was the same at 72h post-transfection (Figure 46). ANF levels were similar between groups 24h post-transfection, while at 72h post-transfection ANF levels were significantly increased in the RASD1 targeted knockdown groups. The increase in ANF secretion by siRASD1 is also apparent when HL-1 cells are cultured in serum-starved conditions (Figure 47).

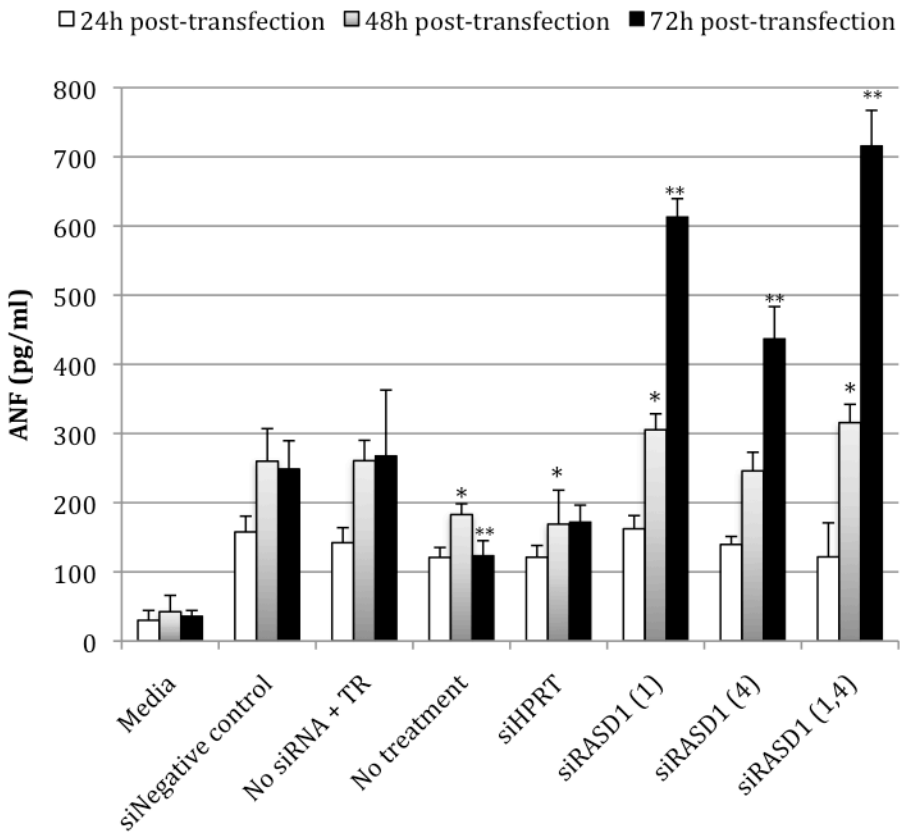


Figure 46. RNAi knockdown of RASD1 increases ANF secretion in HL-1 cells.

ANF secretion levels at 24h (white columns), 48h (light shaded columns) or 72h (dark shaded columns) post RNAi transfection. Media was collected and replaced every 24h. Values are mean ± standard deviation (24h n= 6/group; 48h n = 6/group; 72h n = 6/group). *, $P<0.05$ *vs.* 48h siNegative control; **, $P<0.01$ *vs.* 72h siNegative control. Abbreviation: TR, Transfection Reagent.

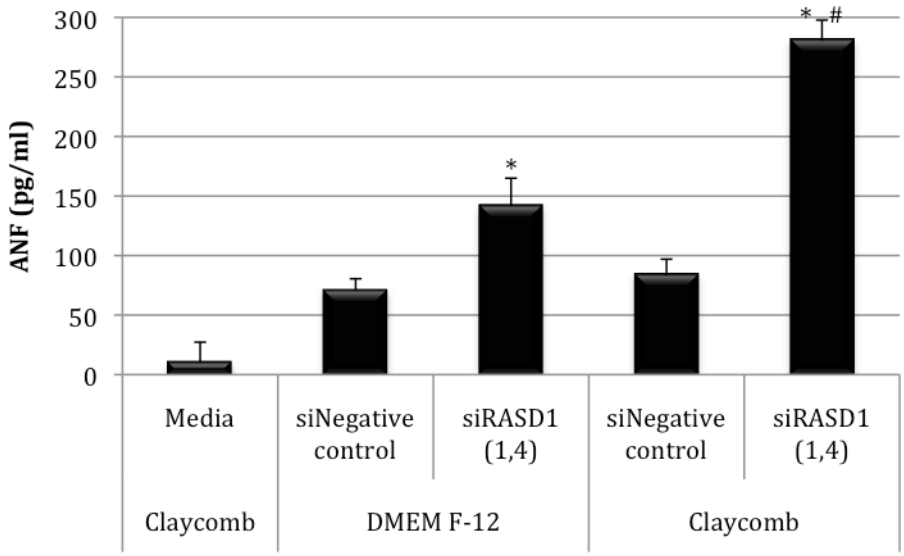


Figure 47. RNAi knockdown of RASD1 increases ANF secretion in HL-1 cells cultured in serum starved and supplemented Claycomb medium.

ANF secretion levels at 48h post RNAi transfection. For the last 24h, HL1-cells were incubated with either DMEM F-12 medium or supplemented FBS Claycomb medium. RNAi knockdown of RASD1 reduced RASD1 mRNA expression levels by 62%, as compared to siNegative control. Values are mean ± standard deviation (n= 3/group). *, $P<0.01$ *vs.* siNegative control; #, $P<0.01$ *vs.* DMEM F-12 siRASD1(1,4).

RASD1 and Gαo RNAi knockdown modulates ANF secretion in HL-1 cells

Since RASD1 has been demonstrated to modulate heterotrimeric Gαi/oβγ protein signaling (Blumer et al., 2005; Lanier, 2004; Takesono et al., 2002) RNAi knockdown of Gαo (siGαo) in combination with siRASD1 was done in HL-1 cells. Gαo expression levels were reduced by at least 66% in siGαo transfected HL-1 cells. Relative expression levels of HPRT, RASD1 and Gαo are found in Figure 48. RASD1 mediated knockdown increased ANF secretion levels by 2.83 and 3.59 fold, as compared to siNegative control, for siRASD1(1) and siRASD1(1,4), respectively. Knockdown of Gαo reduced ANF secretion levels by 1.58 fold ($p = 0.025$), as compared to siNegative control. The positive effect of siRASD1(1) on ANF secretion was blunted when HL-1 cells were co-transfected with siGαo (Figure 49, compare siRASD1(1) vs. siRASD1(1) + siGαo). However, ANF secretion levels were still significantly higher (1.8 fold, $p = 0.07$) than cells transfected with only siGαo (Figure 49, compare siRASD1(1) + siGαo vs. siGαo). Similarly, HL-1 cells co-transfected with siRASD1(1,4) and siGαo reduced ANF secretion levels by 1.44 fold, as compared to cells transfected with only siRASD1(1,4). The amount of ANF secreted by HL-1 cells transfected with siRASD1(1,4) + siGαo remain significantly higher than control groups (2.49 fold), probably due to the significant effect of siRASD1(1,4) on ANF secretion.

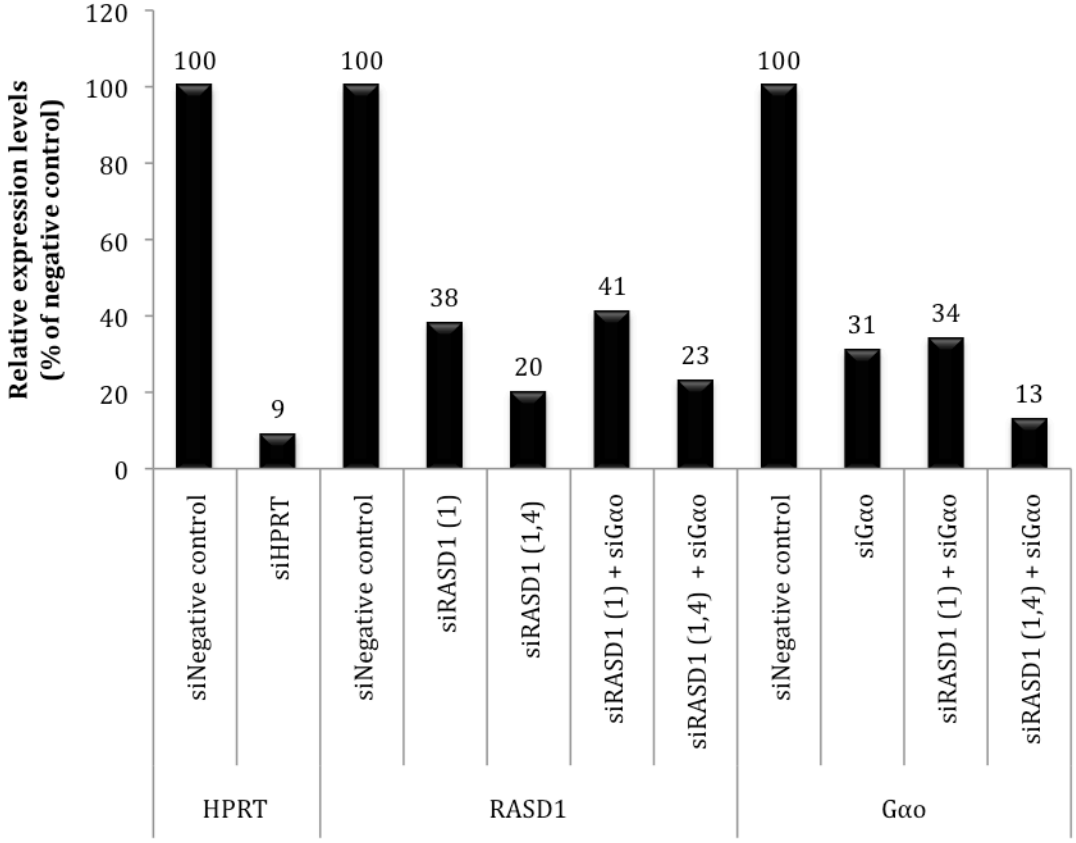


Figure 48. Relative expression levels of HPRT, RASD1 and Gαo in RNAi transfected HL-1 cells.

Relative expression levels of HPRT, RASD1 and Gαo in HL-1 cells transfected with negative control siRNA (siNegative control) and RNAi targeting the positive control HPRT (siHPRT), RASD1 (siRASD1 (1) or (4)), Gαo (siGαo) or a combination of RNAi duplexes targeting RASD1 and Gαo.

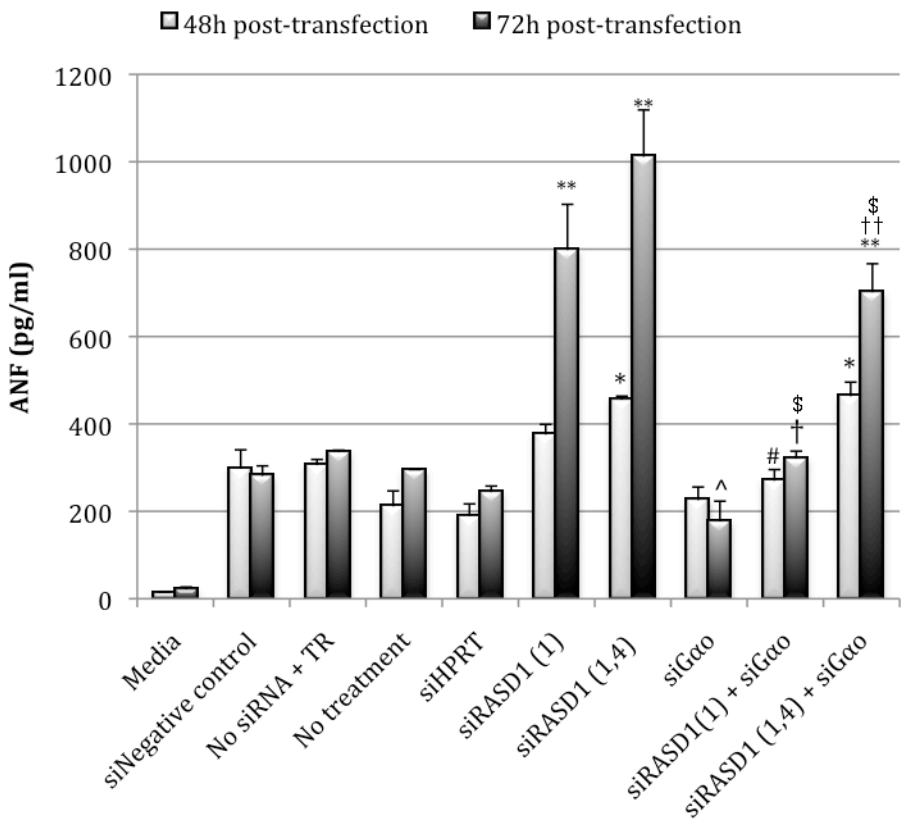


Figure 49. RNAi knockdown of Gαo negatively modulates ANF secretion.

ANF secretion levels at 48h (light shaded column) or 72h (dark shaded column) post RNAi transfection. siRASD1 (1) and (4) increased ANF secretion while siGαo significantly reduced ANF secretion, as compared to the siNegative control. Media was collected and replaced every 24h. Values are mean ± standard deviation (48h n = 3/group; 72h n = 3/group). *, $P<0.01$ *vs.* 48h siNegative control; #, $P<0.01$ *vs.* 48h siRASD1(1); ^, $P<0.05$ *vs.* 72h siNegative control; **, $P<0.01$ *vs.* 72h siNegative control; †, $P<0.01$ *vs.* 72h siRASD1 (1); ††, $P<0.01$ *vs.* 72h siRASD1 (1-4); $, $P<0.01$ *vs.* 72h siGαo. Representative graph of three independent experiments. Abbreviation: TR, Transfection Reagent.

Mastoparan-7 stimulates ANF secretion in HL-1 cells

Pharmacological stimulation of ANF secretion by the Gi/o agonist MAS-7 was dose and time dependent (Figure 50). At the highest concentration, MAS-7 seem to have an adverse effect on the HL-1 cells since a third of the cells were no longer adherent. The media was centrifuged briefly (500 x *g*) to pellet any cells present in the media that could skew the radioimmunoassay results. Total ANF content of HL-1 cells was measured for 6 independent wells. On average, HL-1 cells contained 2652 pg/ml ± 252.96 of ANF.

RNAi transfected HL-1 cells from a previous experiment (Figures 48 and 49) were treated with 5 μM MAS-7. The 5 μM MAS-7 concentration was chosen since it was the lowest dose in which a physiological response was seen (Figure 50). MAS-7 treatment significantly increased ANF secretion in all RNAi transfected cells, as compared to the No siRNA + transfection reagent control, at 72 hours post-transfection (Figure 51). HL-1 cells transfected with siGαo had a significant lower response to MAS-7 as compared to the cells transfected with siNegative control. HL-1 cells transfected with siRASD1 (1,4) had a higher response to MAS-7 treatment than did siNegative control.

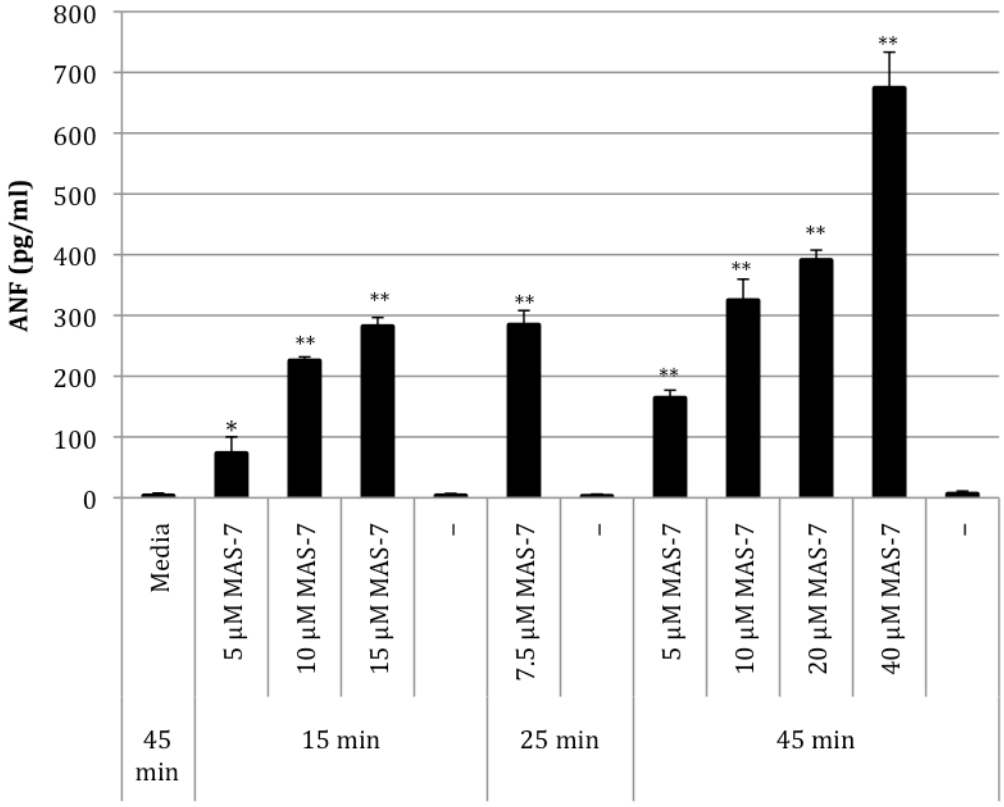


Figure 50. MAS-7 stimulates ANF secretion in HL-1 cells.

MAS-7 stimulates ANF secretion in a dose and time dependent manner. Values are mean ± standard deviation (n = 3/group); *, $P<0.01$ *vs.* No treatment (-); **, $P<0.001$ *vs.* No treatment (-).

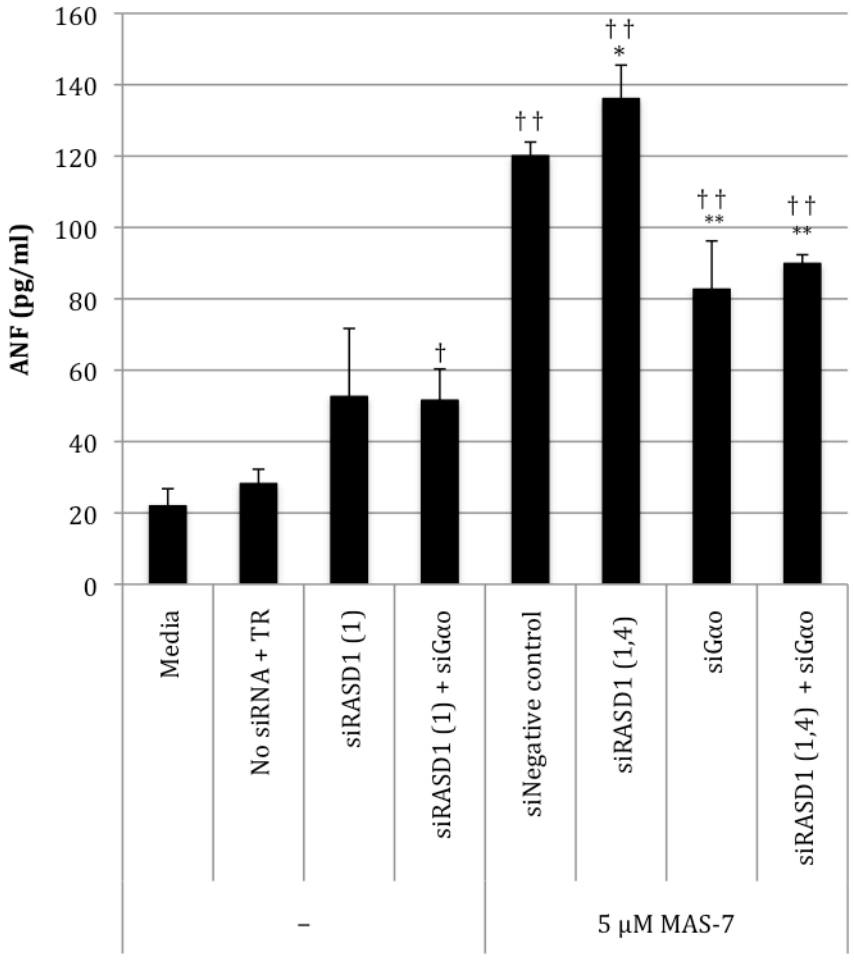


Figure 51. MAS-7 stimulates ANF secretion in RNAi transiently transfected HL-1 cells

ANF secretion levels in the absence (-) or presence of 5 μM MAS-7. Media was collected following 45 min incubation period. Even though MAS-7 stimulated ANF secretion in all RNAi transfected cells, those transfected with siGαo did not secrete as much ANF as did the siNegative control cells. Values are mean ± standard deviation (n = 3/group). *, $P<0.05$ *vs.* MAS-7 siNegative control; **, $P<0.01$ *vs.* MAS-7 siNegative control; †, $P<0.05$ *vs.* (-) No siRNA + TR; ††, $P<0.01$ *vs.* (-) No siRNA + TR. Abbreviation: TR, Transfection Reagent.

ANF RNAi knockdown modulates ANF secretion

HL-1 cells were transiently transfected with RNAi targeting HPRT (siHPRT), RASD1 (siRASD1 (1, 4), ANF (siANF) or both RASD1 and ANF (siRASD1 (1, 4) + siANF). The positive control HPRT was knockdown by 85%, RASD1 by 55%, and ANF by 87%, as compared to the siNegative control. As shown in previous sections, secretion of ANF was significantly increased by siRASD1 at 48h and 72h post-transfection (2.07 and 4.77 fold vs. siNegative control, respectively), while siANF completely abolished ANF secretion (Figure 52). The amount of ANF measured in the media from the siANF group was not significantly different than that obtained from the media itself (background levels). The inhibition of ANF secretion was also observed in the double knockdown of RASD1 and ANF.

MAS-7 treatment, at a dose of 7.5 μM, stimulated ANF secretion in all knockdown conditions, 72 hours post-transfection (Figure 53). Following MAS-7 stimulation, HL-1 cells were incubated in fresh DMEM F-12 medium for another 25 minutes. MAS-7 stimulatory effect on ANF secretion was still evident, albeit at reduced levels.

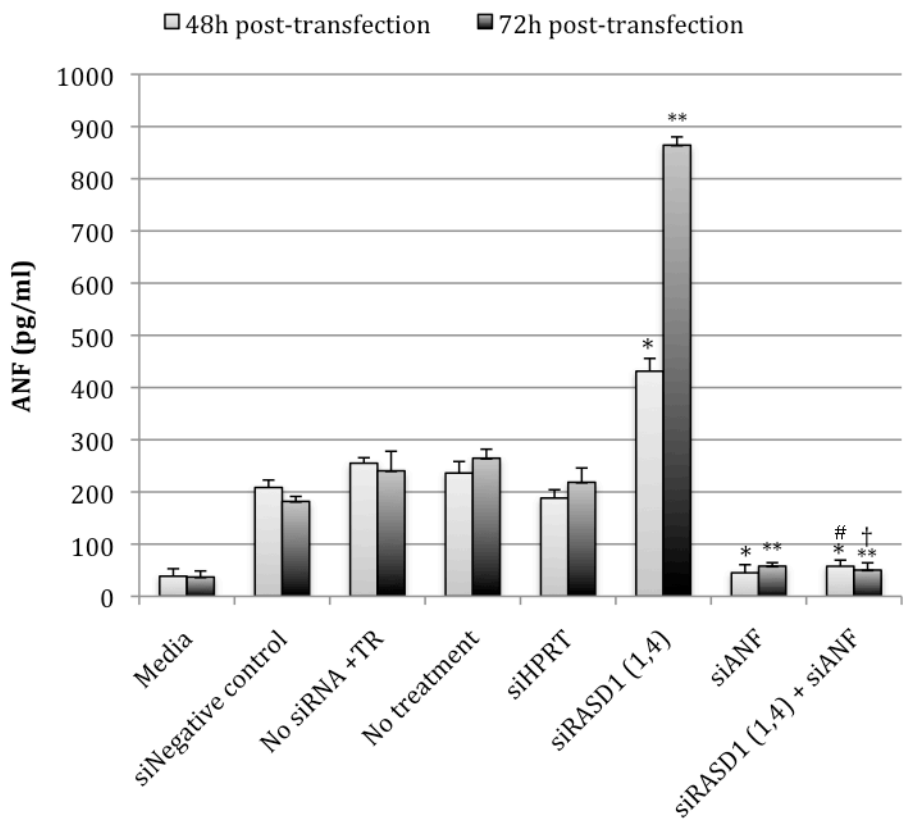


Figure 52. RNAi mediated knockdown of ANF negatively modulates ANF secretion in HL-1 cells.

ANF secretion levels at 48h (light shaded column) or 72h (dark shaded column) post RNAi transfection. siRASD1(1,4) increased ANF secretion while siANF significantly blunted ANF secretion, as compared to siNegative control. Media was collected and replaced every 24h. Values are mean ± standard deviation (48h n = 3/group; 72h n = 3/group). *, $P<0.001$ *vs.* 48h siNegative control; #, $P<0.00001$ *vs.* 48h siRASD1(1,4); **, $P<0.001$ *vs.* 72h siNegative control; †, $P<10^{-7}$ *vs.* 72h siRASD1(1,4). Representative graph of three independent experiments. Abbreviation: TR, Transfection Reagent.

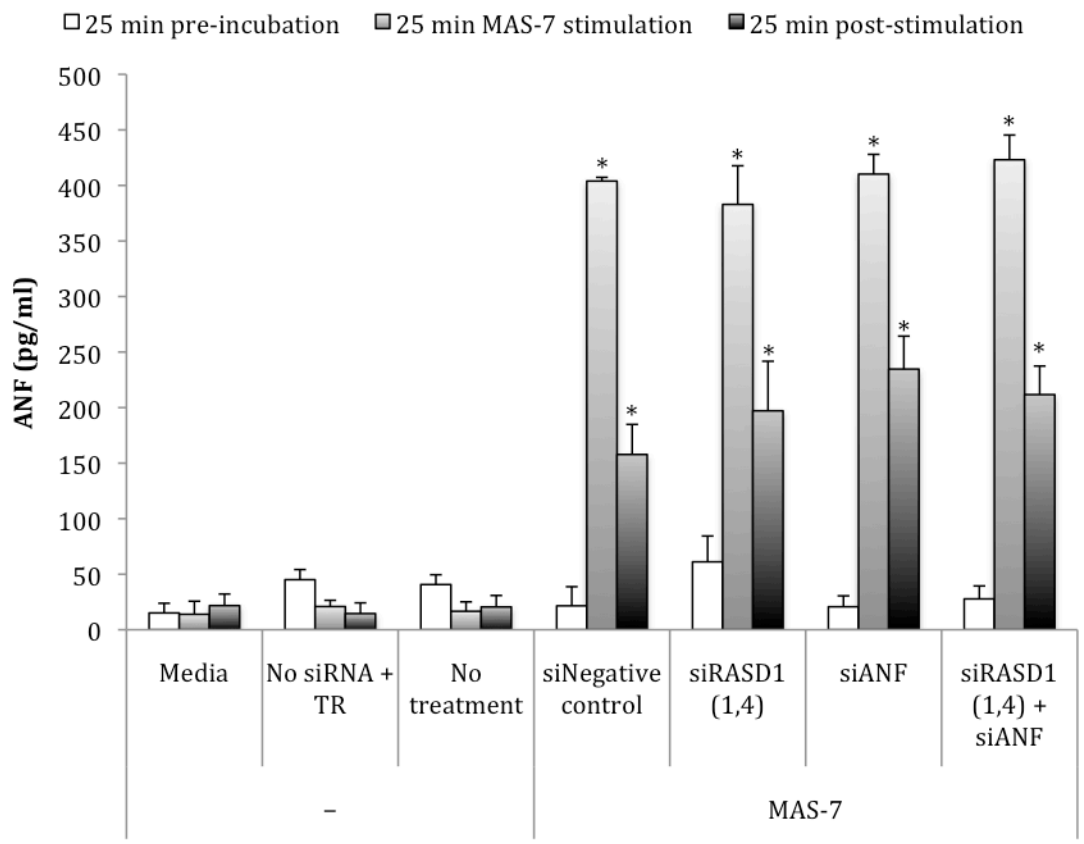


Figure 53. MAS-7 stimulates ANF secretion in RNAi targeted knockdown of ANF transfected HL-1 cells.

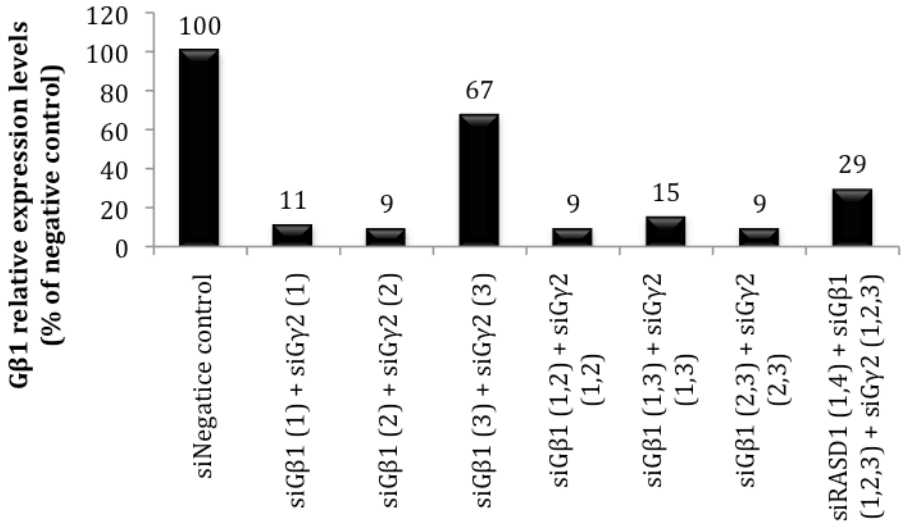
ANF secretion levels in the absence (-) or presence of 7.5 μM MAS-7. Media was collected following 25 min pre-incubation in DMEM F-12 medium (white columns), following 25 min incubation period in the absence or presence of 7.5 μM MAS-7 (light grey columns), and finally after 25 min post-incubation in DMEM F-12 medium (dark grey columns). Values are mean ± standard deviation (n = 3/group); *, $P<0.0001$ *vs.* no siRNA + TR. Abbreviations: TR, Transfection Reagent.

Gβ1 and Gγ2 RNAi knockdown modulates ANF secretion in HL-1 cells

It was demonstrated in a previous section entitled: RASD1 and Gαo RNAi knockdown modulates ANF secretion in HL-1 cells; that siGαo reduced ANF secretion levels, as compared to the siNegative control, and significantly diminished siRASD1 positive effect on ANF secretion (Figure 49). Since RASD1 modulates both Gαi/o and Gβγ protein signaling, RNAi silencing of Gβ1 and Gγ2 proteins was done in HL-1 cells. These cells were co-transfected with RNAi duplexes in various combinations targeting both Gβ1 (siGβ1(n), where n= duplex number) and Gγ2 (siGγ2(n), where n= duplex number) subunits, as well as HPRT (siHPRT) and RASD1 (siRASD1(n), where n= duplex number). HPRT and RASD1 were knockdown by 95% and 93%, respectively. Relative expression levels of Gβ1 and Gγ2 in various RNAi co-transfected cells are depicted in Figure 54. Gβ1 knockdown by siGβ1 duplexes 1 and 2 was more efficient than duplex 3, while siGγ2 duplexes 1 and 3 reduced Gγ2 expression levels to a greater extant than did duplex 2.

RNAi targeted knockdown of Gβ1 and Gγ2 subunits by siGβ1 (1) + siGγ2 (1), siGβ1 (3) + siGγ2 (3), and siGβ1 (1,3) + siGγ2 (1,3) significantly reduced ANF secretion by 2.12, 1.89, and 1.73 fold, respectively, as compared to siNegative control (Figure 55). Co-transfection of siRASD1 (1,4) and siGβ1 (1,2,3) + siGγ2 (1,2,3) significantly reduced ANF secretion levels by 2.3 fold, as compared to siRASD1 (1,4). However, ANF secretion levels were still significantly higher (1.62 fold, $p = 0.002$) than cells transfected with siGβ1 (1,2,3) + siGγ2 (1,2,3).

A



B

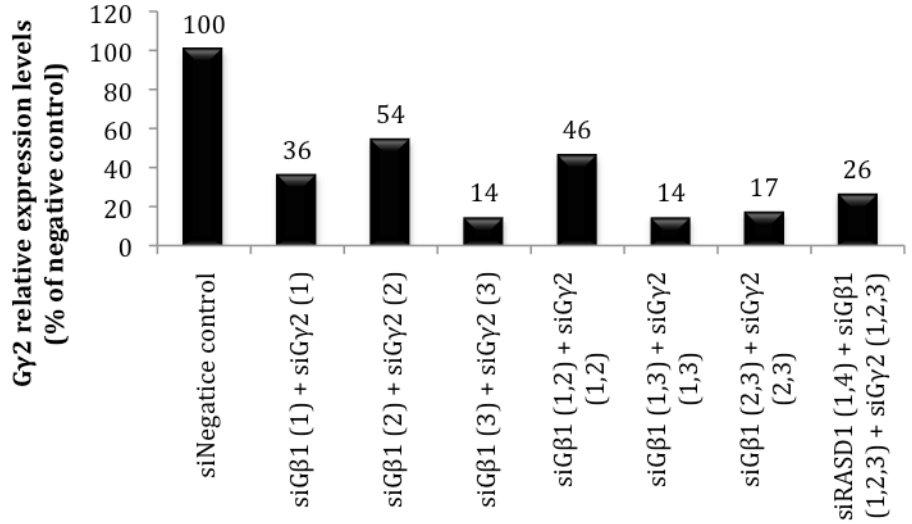


Figure 54. Relative expression levels of Gβ1 and Gγ2 in RNAi transiently transfected HL-1 cells.

Relative expression levels of Gβ1 (A) and Gγ2 (B) in HL-1 cells transfected with negative control siRNA (siNegative control) and various combinations of RNAi targeting Gβ1 (siGβ1(n), where n= duplex number), Gγ2 (siGγ2(n), where n = duplex number) and RASD1 (siRASD1(1, 4)).

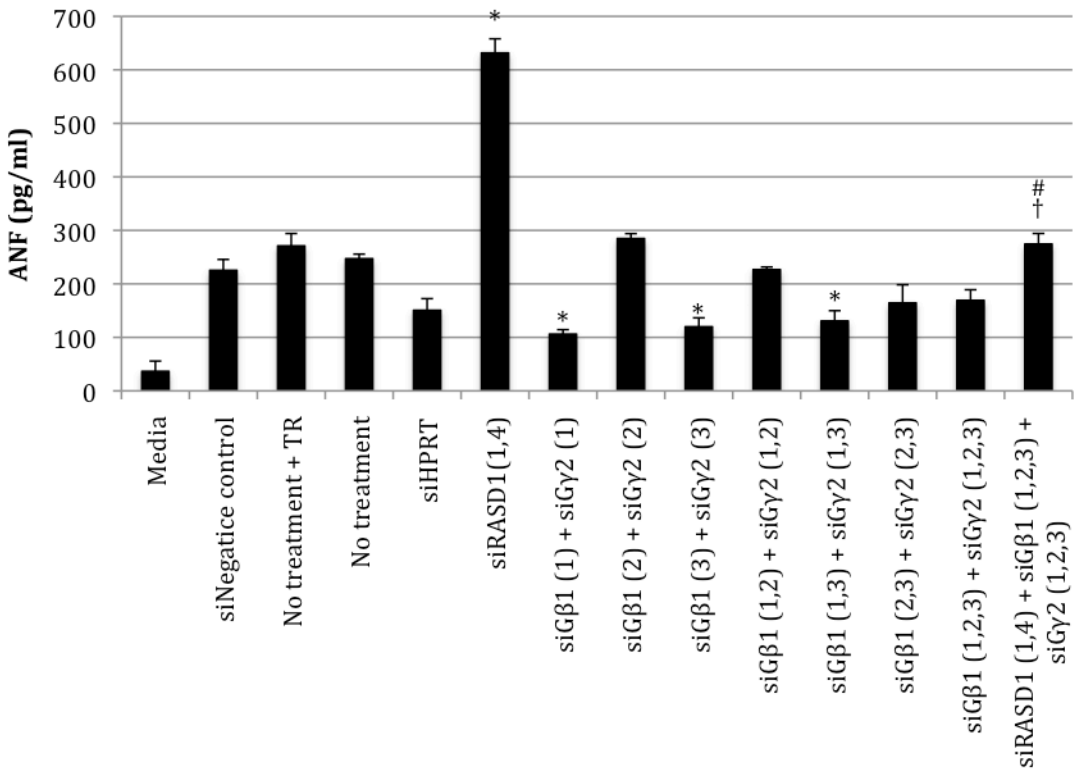


Figure 55. RNAi knockdown of Gβ1 and Gγ2 subunits negatively modulates ANF secretion in HL-1 cells

ANF secretion levels following 72h post RNAi transfection. siRASD1 (1,4) increased ANF secretion while siGβ1 (1) + siGγ2 (1), siGβ1 (3) + siGγ2 (3), and siGβ1 (1,3) + siGγ2 (1,3) significantly reduced ANF secretion, as compared to the siNegative control. Co-transfection of siRASD1 (1,4) and siGβ1 (1,2,3) + siGγ2 (1,2,3) significantly blunted siRASD1 (1,4) positive effect on ANF secretion. Media was collected and replaced every 24h. Values are mean ± standard deviation (72h n = 3/group); *, $P<0.01$ *vs.* siNegative control; †, $P<0.01$ *vs.* siRASD1; #, $P<0.01$ *vs* siGβ1 (1,2,3) + siGγ2 (1,2,3). Abbreviation: TR, Transfection Reagent.

Discussion

Chapter 1: Pilot study and GeneChip quality control

From this investigation it is evident that the phenotypic differences between atrial and ventricular muscle types results from differences in degree or presence of genes that number in the thousands. Since these muscles contain a mixture of cell types present in different proportions, the observed differences in genetic expression of various atrial and ventricular genes go beyond those differences that arise from the differences in cardiocyte type. Moreover, regional differences in cardiocyte phenotype exist in the heart related to the different degrees in which basic cellular functions, including excitability, contraction and secretion, are expressed by cardiocytes.

In spite of the complex background of expression mentioned above, the reproducibility observed in the present studies was excellent. The RMA summary method was used, which generates background adjustments, quantile normalizations and summarizations of the raw scanned data in order to produce a measure of mRNA expression levels. It has been shown that RMA has superior precision, better estimation of fold change and provides higher specificity and sensitivity when analyzing fold changes to detect differentially expressed genes (Irizarry et al., 2003a; Irizarry et al., 2003b). Microarray reproducibility was assessed prior to statistical bioinformatics analysis, whereby within-class pairwise scatter plots and sample hierarchical clustering confirmed the homogeneity of the biological replicates (Figures 6 and 8). Stringent statistical analysis including a Welch t-test with a standard Bonferroni (p-

value <0.01) correction, as well as a Significance Analysis of Microarrays (SAM) (Tusher et al., 2001) analysis with a False Discovery Rate (FDR) of 0.1 % was performed on the microarray data. The cut-off p-value of 0.01 for the Welch t-test was preferred over 0.05 in order to limit the number of genes that could be called differentially expressed only by chance (e.g. 300 vs. 1500 for 30 000 probes). Nevertheless, several publications used a higher p-value cut-off causing a larger output of genes while others only look at fold change in expression (Fiarresga et al., 2005; Fischer et al., 2005; Ma et al., 2005). Although a p-value <0.01 may be considered significant, in a microarray experiment hundreds of genes could still be differentially expressed by chance. For this reason, a statistical method adapted specifically for microarrays was used (SAM) in addition to the previously mentioned t-test.

Chapter 2: Gene expression analysis of normal tissue

Mammalian atrial and ventricular cardiocytes display striking differences in phenotype. The bulk of atrial cardiocytes have, in addition to features commonly associated with striated cardiac muscle cell cytology, organelles that are normally found in cells engaged in the synthesis, vectorial transport and secretion of polypeptide hormones. These include an abundance of rough endoplasmic reticulum, a highly developed Golgi complex and storage granules containing hormonal products. These cytological features led to a series of past investigations that culminated in the discovery of the endocrine function of the heart (de Bold et al., 1981), which is largely mediated by the polypeptide hormones ANF and BNP.

From the data presented here it is evident that the phenotypic differences between the atria and the ventricles results from underlying differences in degree or presence/absence of several specific genes. Despite this complex background of differential expression, the microarray data reproducibility observed in different biological replicates was excellent.

The proportion of probes that were called present, as well as the number of differentially expressed genes was higher in the atria than in the ventricles. This observation could be related to a higher functional complexity of the atrial tissue, which includes contraction, excitation, conduction, secretion and the presence of profuse innervations (Barth et al., 2005; Ellinghaus et al., 2005). The detection of numerous known chamber specific transcripts (Ellinghaus et al., 2005; Small and Krieg,

2004; Tabibiazar et al., 2003; Zhao et al., 2002) supports the robustness of the GeneChip data and demonstrates that the differences in gene expression profiles observed between the atrial and ventricular tissues are not spurious in nature.

Based on atrial and ventricular phenotypical differences, the strategy used in the data mining process was to identify genes that had Gene Ontology annotations relating to hormone secretion, hormone activity, vesicle/granule packaging and transport. Screening for Gene Ontology terms classified as Golgi apparatus and ER cellular components was also undertaken in an effort to identify genes involved in the regulation of NP packaging. Differentially expressed transcription factors as well as transcripts coding for proteins involved in signal transduction such as ligands and receptors were also of great interest. Differentially expressed genes coding for proteins involved in metabolic processes as well as contractile proteins were not specifically looked at since these differences are expected to be found between the atrial and ventricular tissues, but are not thought to be involved in the endocrine function of the heart. In general, functional classification of the differentially expressed genes according to their cellular components, identified in our study, parallels the results obtained by Barth *et al*. (Barth et al., 2005), which include ventricular abundance of mitochondrial genes as well as the identification of numerous atrial abundant ER and Golgi apparatus transcripts, such as Sec22 and Rab34. The larger number of probes hybridizing to cellular components involved in secretory function agrees with the phenotypic and functional differences between atrial and ventricular muscle. For example, atrial tissue was more abundant in the transcripts coding for ANF, BNP and adrenomedullin than the ventricles. Correspondingly, ANF transcript abundance, which

constitutes one to three percent of total atrial mRNA (Seidman et al., 1984a) was found to provide for the top one percent of the GeneChip® signal intensities. Saturation of the fluorescent signal is thought to have occurred for ANF probe sets, which explains the plateau level of 12 fold difference between atrial vs. ventricular tissues as compared to 163 fold with RT-PCR (Figure 11). Oligonucleotide probe saturation can occur when the labeled cRNA is at high enough levels to result in an almost 100% probe/cRNA hybridization complex. Any other increase in expression would not be measurable due to the oligonucleotide hybridization saturation. It is difficult to estimate the amount of cRNA needed to saturate the oligonucleotide probes since the specific number of oligonucleotide probes tiled onto the 11^2 micron surface area of the GeneChip® is proprietary information.

Storage granule-associated proteins identified in this study include Ica1 (Spitzenberger et al., 2003) and SGNE1. The evolutionary conserved gene Ica1, was shown to be abundant in human pancreas and heart, and moderately expressed in brain (Pietropaolo et al., 1993). Variable expression of 5'-untranslated region exons from the Ica1 gene was shown to be tissue specific, where cardiac tissue distinctively expressed the exon B2 transcript variant (Friday et al., 2003). The original observation that Ica1 expression levels were high in the heart, but null in skeletal muscle, lead Pietropaolo *et al*. (Pietropaolo et al., 1993) to postulate that Ica1 was present in selective cells. It was demonstrated in this investigation that Ica1 is expressed specifically in the atria given that all four ventricular replicates exhibited an absent detection call for this transcript (an absent call indicates that the microarray expression level for a particular transcript was below the threshold of detection).

Several studies have been able to co-localize SGNE1, a member of the secretogranin family, with neuropeptides and hormones in various tissues that are primarily composed of neuronal or endocrine cells, as well as tissues known to contain a sub-population of neuroendocrine cells (Mbikay et al., 2001). RT-PCR analysis further confirmed atrial abundance of SGNE1 (Figure 11). SGNE1 has not been previously associated with the atria or the heart.

Differentially expressed transcription factors/DNA binding proteins that were more abundant in the atria than in the ventricles included numerous orphan nuclear receptors. Two out of the three Affymetrix probe sets assaying for nuclear receptor subfamily 2, group F, member 2 (Nr2f2) transcripts were identified in the atrial abundant gene list. Nr2f2 expression pattern is in agreement with previously published data (Tabibiazar et al., 2003) and real-time PCR analysis further validated its atrial abundance (Figure 11). Other atrial abundant transcription factors include paired-like homeodomain transcription factor 2 (Pitx2), which is involved in atrial septation; Tbx5, a known activator of the ANF promoter; and early growth response 1 (Egr-1), which is upregulated in the atria during PE, ET-1, and stretch treatments (Bruneau et al., 1996, 1997) and in neonatal rat cardiocytes by ANG-II and norepinephrine (Shamim et al., 1999). The mechanosensitivity of Egr-1 has been established both *in vitro* (i.e. isolated vascular smooth muscle cells (Grote et al., 2004), fetal lung epithelial cells (Copland and Post, 2007), osteoblastic cells, (Romanello et al., 2005), and endothelial cells (Stula et al., 2000)) and *in vivo,* in vein grafts isolated from Egr-1 knockout mice (Wu et al., 2010). Hairy/enhancer-of-split related with YRPW motif 1 (Hey1), as well as its activator Notch1 were more abundant in the ventricles than in the atria. Hey1 is

thought to repress ANF expression in the ventricles (Fischer et al., 2005). The known tissue specificity of several of these transcription factors further illustrates the soundness of the dataset.

Of special importance to the understanding of the regulation of hormone secretion by the atria are genes that encode for molecular species involved in mechanical aspect of atrial activity given that a major stimulus for ANF and BNP secretion is atrial muscle stretch. This phenomenon is referred to as "stretch-secretion-coupling" (Kuroski-de Bold and de Bold, 1991). Questions still remain regarding the exact stimulus perceived by the atrial cardiocytes as well as the precise signal transduction cascade that leads to an increase in ANF and BNP secretion following stretch. Therefore, the finding that mechanoreceptors (i.e. mechanically gated ion channels, such as TREK-1), mechanosensors (i.e. PLA2) as well as mechanosensitive transcription factors (i.e Egr-1) are most abundant in the atria is central to the generation and the testing of hypothesis. Because some prostaglandins are known to be potent stimulators of ANF synthesis and secretion (Froldi et al., 2005), it is of interest that the mechanosensor PLA2 is abundantly expressed in the atria. Activation of PLA2 following plasma membrane stretch could cause the release of arachidonic acid, a substrate for prostaglandin synthase.

The rapid secretory response following stretch of atrial cardiocytes, as compared to the response to other ANF secretion agonists such as ET-1 (Ogawa et al., 1999), has long suggested that the phenomenon of stretch-secretion coupling was related to mechanosensitive ion channels. It has been suggested that K_{ATP} channels are involved in stretch-secretion coupling (Jiao et al., 2000; Kim et al., 1997; Saegusa et al.,

2005; Xu et al., 1996). These channels are stretch-sensitive (Van Wagoner, 1993), are known to couple to G proteins, including Gαo (Sanchez et al., 1998; Zaugg and Schaub, 2003), and have been associated with other secretory processes (Betsholtz et al., 1990; Minami et al., 2004; Straub and Sharp, 2002). The results and conclusions reached from investigations on the involvement of K_{ATP} channels on ANF secretion have often been contradictory. An inspection of the literature suggests that a likely reason for these discrepancies may lie on differences in experimental systems (*in vivo* or *in vitro,* perfused or non perfused tissues, etc.) (Jiao et al., 2000; Kim et al., 1997; Saegusa et al., 2005; Xu et al., 1996). Most importantly, pharmacological studies have been made with little reference to the several candidate ion channels that may be present in the atria. The present investigation shows that Kir6.1 is significantly expressed in the ventricles. The ATP binding cassette SUR2, whose expression level (1.79 fold) didn't meet the fold change cut-off criteria was more abundant in the ventricles, and, while not significant, Kir6.2 and SUR1 had marginally higher expression in atria. Subsequent pharmacological experiments in the isolated atrial perfusion by our group (Ogawa et al., 2009) demonstrated that the K_{ATP} channel ligands repaglinide and tobutamine, which close the channel, significantly increased basal and stretch-stimulated ANF secretion, while the K_{ATP} channel openers pinacidil, diazoxid and cromakalim decreased basal and stretch-induced ANF secretion. Of note, repaglinide and pinacidil effects on ANF secretion were inhibited by PTX. The modulation of ANF secretion by K_{ATP} channel ligands may result from the decrease in potassium outward currents, provoking membrane depolarization and leading to the activation of voltage-gated Ca^{2+}

channels (Ashcroft, 2005; Cook et al., 1988). The increase calcium influx would then potentially promote ANF secretion (Ogawa et al., 2009).

Three other channels had significantly higher levels of expression in the atria over the ventricles. These included the inward rectifiers Kcnj3, Kcnj5 and background channel TREK-1. Kcnj3, 5 channels, which are activated by GPCR coupled to PTX sensitive Gαi/o proteins, exhibit mechanosensitive properties and might participate in a mechanoelectrical feedback pathway regulating ANF and BNP secretion (Ji et al., 1998; Kubo et al., 2005). This view is in line with the finding that PTX can abolish stretch-secretion coupling (Bensimon et al., 2004). The background channel TREK-1 produces an outwardly rectifying current and is a member of the two-pore domain potassium (K_{2P}) channel family. TREK-1 has been characterized as a stretch-activated membrane channel. It is primarily expressed in the central nervous system but has been found in cardiac tissues (Liu and Saint, 2004) as well as in specific endocrine cells, such as adrenocortical cells (Enyeart et al., 2004). Atrial abundance of TREK-1 was further validated by RT-PCR, western blot and immunofluorescence (Figures 11, 19 and 20). Immunofluorescence analysis localized TREK-1 protein in the atrial derived HL-1 cells as well as in isolated adult rat atrial cardiocytes and it is suggested that TREK-1 may act as a regulator of ANF secretion (Terrenoire et al., 2001). TREK-1 was localized at the plasma membrane as well as in the nucleus of rat atrial cardiocytes (Figure 20). Several reports have also described a nuclear localization of TREK-1, but the significance of this distribution is not clear since this localization is not expected to contribute to the regulation of plasma membrane potential or cell volume (Bai et al., 2005a; Bai et al., 2005b; Voloshyna et al., 2008). To further characterize the role of

TREK-1 in the atria, our group (Ogawa et al., 2009) inhibited TREK-1 currents in the isolated rat atrial preparation with the non-specific inhibitor oleylamine. At low doses, oleylamine significantly increased ANF basal secretion, as compared to the control experiments, while higher doses significantly increased ANF secretion under both basal and stretch-stimulated conditions (Ogawa et al., 2009). It is not clear however if stretch-mediated opening of TREK-1 channel can oppose ANF secretion in a negative feedback manner.

The complex signal transduction pathways resulting from the activation of GPCRs is in part orchestrated by an assorted population of G proteins, assembled from a various combinations of 20 Gα, 5 Gβ and 12 Gγ isoforms (Sato et al., 2006). Ligand binding to GPCRs activates heterotrimeric G proteins by promoting a conformational change and subsequent exchange of GDP for GTP on the Gα subunit (Levitzki, 1988). Activated GTP-bound Gα and Gβγ subunits dissociate and modulate their effectors. Termination of the signal is mediated by the intrinsic GTPase activity of the Gα subunit. Pathway analysis of the microarray data revealed differential expression of genes involved in G protein signaling pathways between atrial and ventricular tissues. The G protein Gαo isoform 1 was found more abundant in the atria by microarray, RT-PCR and western blot analyses (Figures 11, 18 and 19) and was demonstrated by immunofluorescence to co-localize with ANF in atrial granules and in the sarcolemma (Bensimon et al., 2004), as well as with the accessory protein RASD1 in HL-1 cells (Figure 26). Differential expression of the Gβ and Gγ subunit isoforms was also observed between the atria and ventricles, but the functional significance of the differential G protein subunit diversity is not well known.

The identification of accessory proteins involved in the modulation of G protein signal transduction has helped to gain insight into the mechanisms involved in the specificity of a cellular response from an assortment of external stimuli. RGS proteins are capable of inhibiting signaling by acting as a GTPase Accelerating/Activating Protein (GAP), which accelerate the intrinsic rate of GTP hydrolysis of the Gαi/o subunit (Wieland and Mittmann, 2003). The preponderance of genes encoding for RGS proteins appears to be tissue specific. RGS2 and RGS6 (Figure 11) were abundantly expressed in the atria while RGS5 was found at higher levels in the ventricles. These findings are confirmed by other studies in which RGS mRNA and protein levels were measured within atrial and ventricular cardiocytes (Doupnik et al., 2001; Kardestuncer et al., 1998; Wieland and Mittmann, 2003).

In addition to the previously mentioned accessory proteins, in this work we identified the atrial specific transcript RASD1. RASD1, which was previously detected in the heart (Kemppainen and Behrend, 1998; Tu and Wu, 1999), was found more abundant in the atria than in the ventricles by microarray, RT-PCR, western blot and immunofluorescence analyses (Figures 11, 18, 19, and 23). In the absence of receptor stimulation, RASD1, a member of the Ras subgroup of small G proteins, specifically activates Gi/o heterotrimeric signaling pathways by promoting nucleotide GDP/GTP exchange on Gαi/o proteins and enhancing Gβγ uncoupling from Gαi/o (Cismowski et al., 2000). However, in the presence of GPCR agonists, RASD1 has been shown to inhibit heterotrimeric Gi/o protein signaling (Takesono et al., 2002).

Since stretch secretion coupling of ANF and BNP is mediated by PTX-sensitive Gαi/o, the differential expression of RASD1, as well as the other accessory proteins for

G proteins identified in this investigation, is of particular interest. Due to RASD1 opposing effects on Gi/o mediated signaling following agonist dependent or independent GPCR activation (Graham et al., 2001; Graham et al., 2002; Graham et al., 2004; Takesono et al., 2002), RASD1 may help orchestrate the complex diversity and specificity of G protein signaling under different conditions.

Conclusions

The data developed in this part of the investigation describes for the first time gene expression profiles particularly centered on the secretory function of the heart. Based on our data mining strategy, we narrowed down the list of the 1415 differentially expressed genes to a subset, described herein, that are likely involved in the endocrine function of the heart. Of special interest is the relationship between G proteins of the inhibitory type, as well as their accessory proteins, and members of the inward rectifiers and the two-pore domain K^+ channel superfamily.

Chapter 3: Gene expression analysis of volume-overload tissue

Pathological cardiac hypertrophy, resulting from prolonged mechanical and/or neurohumoral stimuli, is the single most powerful predictor of the clinical course of heart failure, and it is an important risk factor for cardiovascular mortality in humans (Adams, 2001). Cardiac hypertrophy is associated with a chronic increase in plasma levels of the cardiac hormones ANF and BNP. These hormones are involved in the maintenance of the cardiorenal homeostasis (de Bold et al., 1996) and regulation of myocardial structure through ANF growth-suppressing properties (Horio et al., 2000) and BNP antifibrotic properties (Tamura et al., 2000), thus protecting the heart from excessive cardiac remodeling (Tokudome et al., 2005). The phenotypical and molecular changes associated with pathological cardiac hypertrophy encountered in pressure or volume-overload states are initially beneficial and compensatory but eventually lead to heart failure.

The aortocaval shunt procedure used in the present work is an *in vivo* experimental hemodynamic overload model that generates a volume or diastolic overload. VO leads to stimulation of the endocrine heart and to increased expression and secretion of NP (Garcia and Diebold, 1990). The VO rats exhibited a progressive increase in cardiac mass over the four-week time course, as compared to the sham operated animals. The extent of cardiac hypertrophy is in agreement with other investigations (Di Fusco et al., 2000; Hirano et al., 2000; Nishikimi et al., 2005). The

plasma and mRNA expression levels of the known cardiac hypertrophic markers ANF and BNP significantly increased as VO induced hypertrophy progressed.

Differentially expressed genes between volume-overload and sham atrial tissues

The aortocaval shunt operated animals exhibited an increase in the number of probe sets that had present calls in the atria (56% vs. 54%), which represents over 700 probes sets when compared to the sham operated counterpart. Various cellular reactions such as cell surface receptor activation, intracellular transduction and cytosolic/nuclear events, all contribute in mediating cardiac hypertrophy. At 28 days post surgery, in response to an increase in hemodynamic workload, an induction in the fetal cardiac gene program was observed in the atria. ANF, BNP, α-actin 1 and β-MHC transcripts were upregulated in the VO animals.

Numerous genes other than those from the cardiac fetal genes program were differentially expressed in the hypertrophic atria. These include genes encoding for transcription factors and other DNA binding proteins. The cardiac specific transcription factors Hey2, JunD, YY1, and Ankrd1 were modulated during cardiac hypertrophy. Hey2, JunD and YY1 have been hypothesized to act as anti-hypertrophic factors (Hilfiker-Kleiner et al., 2006; Sucharov et al., 2008; Xiang et al., 2006) and have been demonstrated to modulate ANF and/or BNP promoter activity in the presence and/or absence of hypertrophic stimuli (Glenn et al., 2009; Hilfiker-Kleiner et al., 2006; Xiang et al., 2006).

A two-way ANOVA analysis ranked the atrial VO differentially expressed genes based on their p-value significance (p-value < 1.3×10^{-7}, FDR < 0.0032). Several genes listed within the top 25 differentially expressed genes are either involved in linking the cytoplasmic membrane to the cytoskeleton (skeletal α-actin, Ankrd1, SCHIP-1 (Goutebroze et al., 2000; McClatchey and Giovannini, 2005), and intersectin-2 (Okamoto et al., 1999; Pucharcos et al., 2000) or have previously been identified in cardiac hypertrophy (Bnip3 (Weng et al., 2010) and WISP2 (Chen et al., 2004; Yoon et al., 2010)). These genes were all induced in the VO atria as compared to the atria sham control. Ankrd1 is consistently upregulated during cardiac hypertrophy, as demonstrated herein and by others (Aihara et al., 2000; Kuo et al., 1999). Aihara *et al.* demonstrated a strong correlation between Ankrd1 and BNP mRNA levels during cardiac hypertrophy (Aihara et al., 2000). Of note, Ankrd1, which interacts with titin in the myofibrillar I band region of the sarcomere, translocates to the nucleus in response to stretch, thus acting as both a mechanosensor and transcription factor (Kojic et al., 2010). In fact, Ankrd1 was shown to respond to cardiocyte stretch by increasing its protein expression in both the nucleus and on the myofibrils (Miller et al., 2003). Therefore, Ankrd1 appears to be strategically localized for sensing stretch, produced by VO, at the plasma membrane-cytoskeletal interface, and transducing the stretch-response to the nucleus.

VO upregulated transcripts involved in cell surface mechanosensing, such as osteoglycin and α5-integrin. Osteoglycin, which is known to be involved in bone homeostasis, was previously identified as a mechanosensitive gene (Patel et al., 2007) and was found up regulated in mechanical tibia loading experiments (Xing et al., 2005).

Osteoglycin is uniquely distributed in numerous organs where tension and elastic forces play an important role (Fernandez et al., 2003) and hence could act as a mechanosensor in the heart. The role of α5-integrin as a mechanoreceptor has been well established in chondrocytes (Lee et al., 2000; Millward-Sadler et al., 2000; Millward-Sadler et al., 1999; Wright et al., 1997). Of interest, α5-intergrin has been shown to form a complex with CD47, a receptor for thrombospondin, and seems to act similarly to GPCR and activate heterotrimeric Gi/o proteins (Brown, 2001; Brown and Frazier, 2001). In fact, heterotrimeric Gi/o proteins have been shown to functionally couple to CD47 (Frazier et al., 1999; Green et al., 1999). Furthermore, CD47-α5-integrin complex was shown to be important in coupling the P2Y2 receptor to Gαo since anti-α5-integrin antibody partially inhibited P2Y2 agonist induced signaling events (Erb et al., 2001). Hence, mediation of α5-integrin mechanotransduction activity in chondrocytes could involve the heterotrimeric Gαi/o proteins (Orazizadeh et al., 2008). This is of particular interest since stretch-secretion coupling of ANF is mediated by Gαi/o proteins (Bensimon et al., 2004).

Differential expression between volume-overloaded atrial and ventricular tissues

Sixteen transcripts were more than 20 fold more abundant in the VO atria as compared to the ventricles. At 367-fold difference, sarcolipin was the most differentiated. Atrial specific expression of sarcolipin has been previously described (McGrath and de Bold, 2009; Minamisawa et al., 2003) as well as its altered expression

during cardiac pathologies (Minamisawa et al., 2003; Shimura et al., 2005). In our hands, sarcolipin was slightly downregulated in the right atria of VO animals, but it did not meet statistical significance. The calcium binding protein visinin like-1 is another highly abundant atrial gene. This gene was shown to modulate insulin secretion in pancreatic β-cells (Dai et al., 2006) as well as modulate the activity of the natriuretic receptor type-A and –B (NPR-A,-B) in neuronal cells (Buttgereit et al., 2010), the cognate receptors of ANF/BNP and CNP, respectively. Visinin like-1 regulatory effect on NPR-B was recently described in cardiocytes, whereby it is postulated that visinin like-1 modulates the amount of NPR-B receptor at the plasma membrane directly or by influencing clathrin-dependent receptor recycling (Brackmann et al., 2005; Buttgereit et al., 2010). Alpha-synuclein, which was 26 fold more abundant in the VO atria, had unknown physiological functions until recently. Burré *et al.* (Burre et al., 2010), demonstrated that in neuronal cells α-synuclein directly interacts with synaptobrevin-2 and enhances SNARE protein function by promoting SNARE complex assembly and thus maintaining continuous SNARE-cycling. Triple knockout mice of the synuclein isoforms did not have any obvious phenotype, but it later became apparent that α-synuclein was important during increased synaptic activity (Burre et al., 2010). In the context of the heart, α-synuclein may be necessary for proper cardiac autonomic nervous system function as well as hormonal secretion under high demand, such as in VO.

Numerous transcripts were found differentially expressed between the atria and ventricles based on innate tissue differences themselves as well as a result of VO. Several G-protein signaling transcripts as well as their accessory proteins were found

differentially expressed between the atria and ventricles (e.g. Gαo1, Gβ5 and Gγ2), but a subset of them displayed an interaction effect, i.e. they were differentially expressed due to the experimental condition as well as their tissue of origin (e.g. RGS4 and RASD1).

In an earlier investigation Bensimon *et al*. (Bensimon et al., 2004) demonstrated the involvement of Gαi/o proteins in the stretch-secretion coupling events. PTX inhibition of Gαi/o abolished this event but did not affect baseline secretion. Pathway analysis of the microarray data revealed differential expression of genes involved in G protein signaling pathways between the normal atrial and ventricular tissues (as presented in chapter 2 of the results). The G protein $G\alpha_o$ isoform 1 was found more abundant in the normal atria by microarray, RT-PCR, western blot analyses and was demonstrated by immunohistochemistry to co-localize with ANF in atrial granules (in the perinuclear zone of atrial cardiocytes) and is present in the sarcolemma (Bensimon et al., 2004; McGrath and de Bold, 2009). The increased activation of the endocrine heart under hemodynamic overload, i.e. increased synthesis and secretion of the natriuretic peptides, was not paralleled with increased expression levels of Gαi/o proteins, as assessed by our microarray data. This data is in accordance with Wang *et al*. (Wang et al., 2004) and Di Fusco *et al.* (Di Fusco et al., 2000) who demonstrated that aortocaval shunt induced hypertrophy did not alter Gαi expression levels, as compared to sham operated rats. In the heart, multiple accessory proteins can regulate Gαi/o proteins, as discussed in chapter 2. Under chronic hemodynamic overload, RGS3 as well as RGS4 were differentially expressed in the atria as well as in the ventricles. RGS4 was downregulated in the VO atria whereas in the VO ventricles, RGS4 was

upregulated. RGS4 may regulate distinct processes within these two tissues, which might explain the opposite direction in gene regulation. In fact, it was demonstrated that RGS4 negatively modulates Gαq signaling in the ventricles and inhibits cardiac hypertrophy through a NPR-A mediated pathway (Tokudome et al., 2008).

As presented above, a number of G-protein signaling transcripts as well as their accessory proteins were found differentially expressed between the atria and ventricles, but a subset of them displayed an interaction effect, i.e. they were differentially expressed due to the experimental condition as well as their tissue of origin. This notably included RASD1. In fact, RASD1 had higher expression in the atria as compared to the ventricles (as demonstrated in chapter 2 of the results), while under chronic hemodynamic overload, RASD1 was significantly downregulated in the atria but not in the ventricles.

In the context of hormonal secretion, constitutively active RASD1 has been found to regulate spontaneous and, at a greater extent cAMP-stimulated secretion of human growth hormone in AtT-20 corticotroph cells (Graham et al., 2001); indicating that RASD1 may act at the level of the dense core secretory granule pathway. In the absence of receptor stimulation, RASD1 specifically activates Gi/o heterotrimeric signaling pathways by promoting nucleotide exchange on Gαi/o proteins and enhancing Gβγ uncoupling from Gαi/o (Cismowski et al., 2000). The Gβγ mediated activation of ERK1/2 pathway by RASD1 is sensitive to PTX treatment as well as β-adrenergic receptor kinase carboxyl terminus (scavenger of free Gβγ) (Graham et al., 2002). Furthermore, RASD1 expression has been shown to inhibit adenylyl cyclase activity and downstream signaling by cAMP-responsive nuclear transcription factor

(CREB) (Graham et al., 2004). Hence, RASD1 acts on both Gαi/o and Gβγ through ligand receptor independent activation of Gi/o protein signaling. However, Graham *et al*. demonstrated that RASD1 acts as an inhibitor of ligand-dependent ERK1/2 signaling cascade by the Gi-coupled N-formyl peptide receptor (Graham et al., 2002). Similarly, Takesono and colleagues (Takesono et al., 2002), showed RASD1 inhibitor activity of G protein-coupled inwardly-rectifying potassium channel (Kcnj3,5) activated by GPCR cholinergic receptor, muscarinic 2, and suggested that RASD1 may antagonize GPCR signaling by modifying the pool of heterotrimeric G proteins available for receptor coupling. Furthermore, RASD1 was shown to attenuate agonist-dependent $Ca_v2.2$ channel inhibition through Gi-coupled receptors, an effect that was blocked by PTX (Thapliyal et al., 2008). Hence, RASD1 appears to modulate ion influx in a GPCR ligand-dependent manner, thereby potentially influencing Ca^{2+}-dependent events such as hormone secretion.

Since stretch-secretion coupling of ANF and BNP secretion is mediated by PTX sensitive Gαi/o (Bensimon et al., 2004) the differential expression of RASD1 in the heart is of particular interest. The temporal down regulation of RASD1 in the VO atria, starting on day 2-post aortocaval shunt surgery, corresponds to the time point in which the initial increase in ANF secretion is observed (Figure 30). The selective downregulation of RASD1 in the VO atria may be a process that insures successful coupling of Gαi/o proteins to the GPCR, since the interaction of RASD1 with the heterotrimeric G proteins would diminish their availability to the activated GPCR and thus partially blunt GiPCR-mediated signaling. Further, since RASD1 modulates both Gαi/o and Gβγ signaling (Cismowski et al., 2001; Graham et al., 2002; Graham et al.,

2004) it is possible that RASD1 tonically inhibits ANF secretion by modulating these heterotrimeric G proteins.

Conclusions

The data developed in this part of the investigation provides insight into the expression profiles of genes particularly centered in the secretory function of the heart under chronic hemodynamic overload. As expected, chronic hemodynamic overload produced a potent hypertrophic response, including increased heart weight and the re-expression of the cardiac fetal gene program. In addition, a differential regulation of signaling molecules was apparent, including mechanosensors and accessory proteins to G-protein signaling. The specific downregulation of RASD1 in the VO atria indicates a role for this accessory protein as a critical molecular regulator of Gαi/o, which, in turn, is known to participate in stretch-secretion coupling in the atria. The putative novel function identified herein for RASD1 in the atria is of considerable interest given the fact that secretory impairment of the cardiac natriuretic hormones can negatively impact on cardiovascular homeostasis.

Chapter 4: RASD1 and ANF secretion gleaned from RNAi silencing experiments

Background

An investigation was carried out to define the overall gene expression profile associated with hemodynamic activation of the ANF and BNP genes, using the Affymetrix Rat Genome 230 2.0 array. To this purpose we performed gene expression profiling experiments of the atria and ventricles under normal and under chronic volume-overload, induced by aortocaval shunt.

As described in chapter 2 of the results section, hundreds of genes were found more abundant in the normal atria as compared to the normal ventricles. Among others, RASD1 was significantly more abundant in the normal atria by 3.75 fold as compared to the ventricles (Figure 18). Immunofluorescence analysis localized RASD1 predominantly in the perinuclear region of the atrial derived cardiocyte HL-1 cells (Figure 24), a region known to contain atrial specific granules.

In chapter 3 of the results section, RASD1 was identified among the top 25 significantly differentially expressed genes found between atrial shunt vs. sham tissues, based on its p-value. Furthermore, following a two-way ANOVA analysis with a FDR correction, RASD1 was listed in a small subset of genes that exhibited an interaction effect between tissue (atria vs. ventricles) and condition (VO shunt vs. sham) factors. Under chronic hemodynamic overload, RASD1 was significantly downregulated in the

both left and right atria by 3.85 and 2.87 fold, respectively, but no significant change in expression levels was observed in the ventricles.

To further characterize RASD1, RNAi mediated knockdown of RASD1 was carried out in the atrial derived HL-1 cells. HL-1 cells are derived from AT-1 mouse atrial cardiocytes, which express the SV40 large T antigen under the control of the ANF promoter (Claycomb et al., 1998; Field, 1988). HL-1 cardiocytes have been shown to continuously divide and maintain a differentiated adult cardiac phenotype through multiple passages in tissue culture (Claycomb et al., 1998). Most importantly, in immunohistochemical studies, HL-1 cells have been shown to contain atrial specific granules (White et al., 2004).

Overview of RNA interference

RNAi is defined as "a gene-silencing mechanism induced by double stranded RNA (dsRNA)" (Martin and Caplen, 2007). Fire and Mello, who received the Nobel Prize in 2006 for the discovery of RNAi, were the first to describe a sequence-specific reduction of mRNA expression following the administration of long dsRNA in *C. elegans* (Fire et al., 1998). Mechanistically, the post-transcriptional silencing of a gene begins in the cytoplasm by the recognition and cleavage of long dsRNA, into short RNA duplexes of about 21 nucleotides in length with 2 nucleotides 3'-overhands, by the RNAse III-like enzyme Dicer (Bernstein et al., 2001; Lee et al., 2004). These short dsRNAs (siRNA) interact with the RNA-induced silencing complex (RISC), which unwinds the dsRNA and cleaves the passenger strand (mediated by Argonaute 2 (Hammond et al., 2001)),

and associates with the guide strand (Martinez et al., 2002). The guide strand, which is complementary to the target mRNA, directs RISC to the mRNA, in a sequence-specific manner (Dykxhoorn et al., 2003). The targeted mRNA is cleaved and degraded, preventing translation from occurring and thus silencing the expression of the gene from which the RNA was transcribed (Martin and Caplen, 2007). Synthetic siRNAs as well as long dsRNA, can be designed to associate with the RISC complex or Dicer, respectively, and target complementary mRNAs for degradation.

RNAi mediated knockdown in HL-1 cells

Standard 21-mer sequences (designed by Dharmacon) were unable to knockdown RASD1, while the Dicer-substrate 27-mer duplexes (designed by IDT) significantly reduced RASD1 expression levels. One possible explanation for this difference in knockdown efficiency is that the 27-mer dsRNA is theorized to be a substrate of the endoribonuclease Dicer while the 21-mer sequence is the product of Dicer and thus dsRNA may be more efficient in entering the RISC by Dicer for sequence-specific degradation of complementary mRNA species (Kim et al., 2005; Lee et al., 2004; Pham et al., 2004). This does not hold true in the case of RNAi duplex 2 (designed by IDT), since it was inactive in reducing RASD1 expression levels. Upon closer examination of the target sequence of RNAi duplex 2, as well as the other RNAi target sequence tested, it was apparent that the target of RNAi duplex 2 lies within the same region as several inefficient siRNA, designed by Dharmacon (Figure 56). RNAi target secondary structure and accessibility was determined by measuring RASD1

mRNA Minimum Free Energy structure by RNAfold (Gruber et al., 2008). According to a loop-based energy model high-energy bonds are colored in red, medium energy in green and low energy blue. RNAi duplexes 1, 3 and 4 target regions color-coded in green, while RNAi duplex 2 targets a region color-coded in red (Figure 56). It would thus appear that the inefficiency of RNAi duplex 2 and other siRNAs could be due to poor accessibility of the RNAi guide strand to the target sequence. The importance of the target secondary structure and accessibility for efficient siRNA silencing has been well documented (Bohula et al., 2003; Overhoff et al., 2005; Schubert et al., 2005; Shao et al., 2007; Vickers et al., 2003; Westerhout et al., 2005). Even though several siRNA designed by Dharmacon did not target the same region, as did those in the proximity of RNAi duplex 2, they were still inactive. This could be explained by the observation of Holen *et al.,* who demonstrated that co-transfection of an active and inactive siRNA reduced the efficiency of the most effective siRNA, by a sequence-independent competition manner (Holen et al., 2002).

A

B

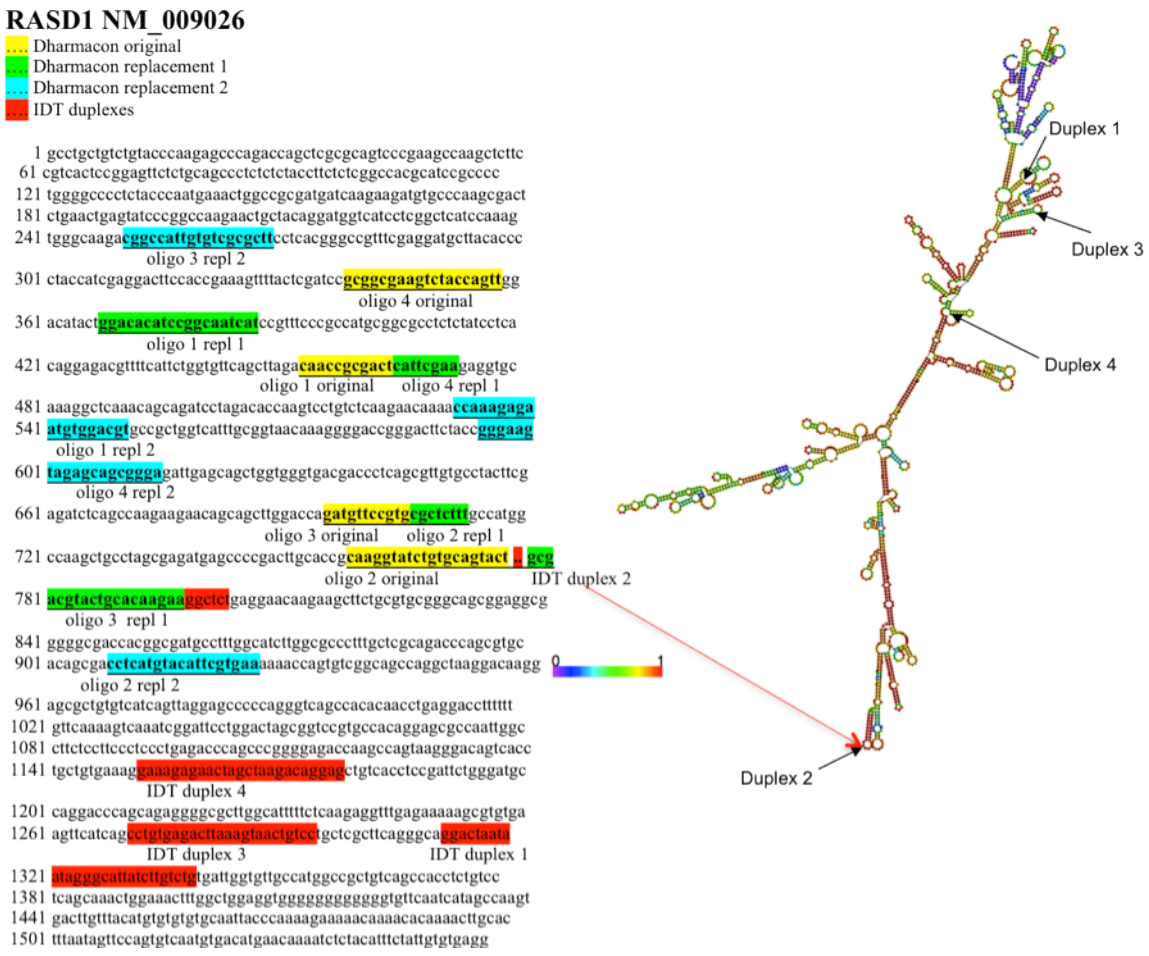


Figure 56. RASD1 mRNA sequence.

A) Target sequences of various RNAi are highlighted in yellow, green, and blue (siRNA oligonucleotide sequences designed by Dharmacon), as well as in red (dsRNA designed by IDT). Note, some sequences overlap with each other and thus only a partial sequence is highlighted. B) RASD1 mRNA secondary structure, as computed by RNAfold. Arrows indicate target regions of RNAi duplexes 1, 2, 3, and 4. According to a loop-based energy model, high-energy bonds are colored in red, medium energy in green and low energy blue. Abbreviations: oligo, oligonucleotide; repl, replacement.

RASD1 RNAi knockdown modulates ANF secretion in HL-1 cells

It demonstrated, in chapter 4 of the results section, that RNAi mediated knockdown of RASD1 significantly increased ANF secretion, thus suggesting a negative modulator role for RASD1 in ANF secretion. It would appear that co-transfection of RNAi duplexes 1 and 4 increases ANF secretion through synergism or addition, since transfection of either duplex alone produced a smaller response in ANF secretion (Figures 45 and 46) Interestingly, the degree of RNAi efficiency, i.e. the percent of reduction of RASD1 expression, is not indicative or predictive of the extent of ANF secretion. In fact, knockdown of RASD1 by duplexes 1 and 4 produced similar increases in ANF secretion despite residual levels of RASD1 of 7% to 45% (see Figures 45, 46, 52 and 55 for ANF secretion levels), thus suggesting that the secretory mechanism of ANF is very sensitive to small changes in RASD1 abundance.

RASD1 mediated knockdown significantly increased ANF secretion in both serum-starved and complete medium conditions. Serum starvation is commonly used to increase the cellular response to, among others, pharmacological agents and enzymes, since FBS can contain a mixture of defined and undefined components such as growth-promoters and growth-inhibitors, lipids and minerals that may interact with the product under investigation and interfere with the response. In the presence of serum, RASD1 targeted knockdown increased ANF secretion levels by two fold, as compared to serum-starved conditions (Figure 47), indicating that a portion of ANF secretory response is modulated by undefined components present in the serum that are sensitive to RASD1. Since RASD1 has been demonstrated to modulate G protein

signaling pathways (Blumer et al., 2005; Cismowski et al., 2001; Lanier, 2004; Nguyen and Watts, 2005, 2006; Thapliyal et al., 2008) it would be expected that the undefined components present in FBS are GPCR agonists. In fact, knockdown experiments demonstrated that 10% FBS stimulated phosphoinositide hydrolysis by coupling to PLC-β3 and PLCε, presumably through Gαq and Gβγ subunits (Kelley et al., 2006). In a human breast cell line, 10% FBS increased oxytocin receptor (OTR) expression, while serum-starvation resulted in a loss of OTR expression (Copland et al., 1999). Similarly, in human myometrial cells FBS was found to upregulate OTR ligand binding and increase OTR mRNA half-life (Jeng et al., 2003). The active components found in FBS were sensitive to PTX treatment, thus implying the participation of GPCR coupled to Gi/o proteins. The lysophospholipids lysophosphatidic acid (LPA) and sphingosine 1-phosphate (S1P), which activate Edg2 and Edg1, 3, 5 receptors, respectively, could mimic the effects of FBS and were PTX sensitive. The authors concluded that the agents present in FBS that mediate OTR mRNA stability through Gi/o stimulation are likely LPA and S1P (Jeng et al., 2003).

Furthermore, ANF secretion levels were two fold greater in RASD1 targeted knockdown cells, as compared to the siNegative control, in serum-starved conditions (Figure 47), thus demonstrating that RASD1 also negatively modulates ANF secretion in unstimulated conditions.

ANF RNAi knockdown modulates ANF secretion

ANF targeted knockdown blunted ANF secretion to background levels (Figure 52) indicating that the basal ANF secretion levels observed under control conditions originate entirely from newly synthesized ANF. This is consistent with constitutive secretion, whereby "newly" synthesized proteins are delivered to the cell surface for exocytosis in the absence of stimulation. Double knockdown of RASD1 and ANF completely abolished the increased secretory response observed in the RASD1 knockdown alone. This indicates that the increased ANF secretion resulting from RASD1 knockdown also originates from a "newly" synthesized ANF pool. This pool is expected to be less than 24h old since the modulation of ANF secretion was not observed within the first 24h post RNAi transfection, probably due to the lag time necessary for the RNAi mediated knockdown of RASD1, but rather was first seen 48h post RNAi transfection (Figure 52).

It has been previously demonstrated in cultured atrial cardiocytes as well as in isolated rat atrial preparations that the unstimulated release of ANF contributes to a significant portion of total ANF secreted from the cells (Iida et al., 1988; Iida and Page, 1989; Suzuki et al., 1992). Iida *et al.* showed by radioimmunoassay that isolated atrial cardiocytes secreted ANF at a constant rate in the absence of secretagogue stimulation and that 40% of the newly synthesized radiolabeled ANF is secreted into the media under this condition, while the remaining 60% of ANF is targeted for storage (Iida and Shibata, 1994). This is in contrast with the pancreatic beta cells which secrete only 1%

of insulin by the constitutive pathway (Rhodes and Halban, 1987). Prorenin, on the other hand, is predominantly secreted from the juxtaglomerular cells by the constitutive pathway, while only 25% of newly synthesized peptide is destined for storage (Pratt et al., 1987). Analysis of atrial cardiocytes determined that newly synthesized protein was incorporated into atrial specific granules one hour following tritiated leucine exposure (de Bold and Bencosme, 1975). Hence, newly synthesized hormone can be defined as being synthesized within a period of one hour, while products synthesized within 5 hours or more are destined for long-term storage (Mangat and de Bold, 1993; Ogawa et al., 1999). It was shown in the perfused isolated atrium preparation that protein synthesis inhibition, by cycloheximide, significantly decreased, but not completely, total ANF release under basal conditions. This demonstrates that a portion of ANF basal release is dependent on newly synthesized hormone, while the other portion is dependent on stored hormone (Ogawa et al., 1999).

It would appear that basal release of ANF is not only dependent on newly synthesized hormone, but also on a 24-48h-storage pool, since RNAi mediated knockdown of ANF blunted basal ANF secretion 48h and 72h post-transfection, thus inhibiting the production of newly synthesized hormone and by consequence its storage. Hence the long term storage pool of ANF, i.e. greater than 48h, does not contribute to basal secretion. Pancreatic beta granule half-life is estimated to be between 3-5 days, time after which granules undergo degradation by autophagy and crinophagy (Halban and Wollheim, 1980; Marsh et al., 2007). Hence, by extrapolation,

inhibition of ANF secretion under unstimulated conditions following RNAi knockdown is well within the granule turnover rate.

Mastoparan-7 stimulates ANF secretion in HL-1 cells

MAS-7 is a mastoparan derivate that activates Gi/o proteins in a manner analogous to GPCR by stimulating the exchange of GDP for GTP on the Gα subunit, and thus permitting the dissociation of the Gα from the Gβγ (Higashijima et al., 1990). Mastoparan, which also competes with the GPCR for binding to Gαi/o subunits, has been found to interact with the carboxyl-terminal region of the Gαo subunit (Higashijima et al., 1990; Mousli et al., 1990; Weingarten et al., 1990). This interaction is catalytically enhanced by the presence of the Gβγ (Higashijima and Ross, 1991). Mastoparan stimulates secretion from various cells such as mast cells (Mousli et al., 1989), platelets (Ozaki et al., 1990; Wheeler-Jones et al., 1992), anterior pituitary (Kurihara et al., 1986), adrenal chromaffin cells (Vitale et al., 1994), pancreatic β-cells (Jones et al., 1993; Yokokawa et al., 1989) and atrial cardiocytes (Bensimon et al., 2004).

ANF secretion was significantly stimulated from HL-1 cells in a dose dependent manner by MAS-7 (Figure 50). The stimulatory effect of MAS-7 was maintained, at lesser degree, 25 min post-stimulation (Figure 53). The time dependent effect of MAS-7 on ANF secretion is consistent with the results obtained from the isolated right atria whereby both MAS-7 and mechanical stretch immediately stimulated ANF secretion from the atria, peaked within 20 min and then started to decrease (Bensimon et al.,

2004), thus demonstrating the physiological similarities between the two systems. MAS-7 significantly stimulated ANF secretion from HL-1 cells transfected with RNAi targeting ANF, indicating that MAS-7 stimulatory action modulates older ANF pools. This is in agreement with perfusion studies that demonstrated that protein synthesis inhibition by cycloheximide did not significantly modulate ANF secretion levels upon secretagogue stimulation with stretch, ET-1 or PE (Ogawa et al., 1999; Page et al., 1991). Based on double-isotope-labeling pulse-chase and the previously mentioned cycloheximide studies, Ogawa *et al.,* concluded that stretch promoted the secretion of ANF from a pool synthesized more than 5 hours before stretch (Ogawa et al., 1999). Based on the present RNAi experiments, MAS-7 elicited robust ANF secretion from a storage pool at least 48h old. No difference was observed in the magnitude of secretion between control cells and those transfected with RNAi targeting ANF knockdown, thus indicating that younger storage pool of ANF (less than 48h) is not regulated by MAS-7 treatment. Alternatively, if a portion of the younger pool (less than 48h) had been secreted by control cells, it may have been diluted by the overwhelming amount of ANF secreted by the older stored pool upon the addition of the secretagogue. However, if this would be the case, then the secretion of ANF would not be additive since the magnitude of ANF secretion is equal between treatments.

MAS-7-induced ANF secretion was partly inhibited by RNAi targeted knockdown of Gαo, suggesting the involvement of heterotrimeric G proteins in the secretory response of HL-1 cells to MAS-7. ANF stimulated secretion by MAS-7 was not completely inhibited by the absence of Gαo which may indicate that other G proteins of the inhibitory class could still mediate the effect of MAS-7 or that the residual mRNA

levels of Gαo (13-34%) following RNAi knockdown were able to mediate ANF secretion. Alternatively, MAS-7 could also influence ANF secretory process by modulating signaling pathways independently of the heterotrimeric G proteins, such as by the low molecular weight G proteins (Amin et al., 2003; Koch et al., 1991) (Daniel et al., 2002) or PLC (Choi et al., 1992; Garcia-Sainz et al., 1991; Mousli et al., 1989; Schnabel et al., 1997). Several members of the large superfamily of small GTPase proteins, which include the Ras, Rho, Rab, Ran and Arf subfamilies (Wennerberg et al., 2005) and their effectors, have been implicated in numerous essential steps in granule/vesicle membrane trafficking, including Golgi budding, transport delivery, tethering, and finally fusion with the plasma membrane (Gillingham and Munro, 2007; Grosshans et al., 2006; Novick and Guo, 2002). Several studies have demonstrated the involvement of Rho and Cdc42 in mastoparan-induced insulin secretion (Amin et al., 2003; Koch et al., 1991) (Daniel et al., 2002). Therefore, it would be possible that mastoparan-induced secretion could involve more than one G protein, i.e. heterotrimeric Gi/o proteins and small GTPase proteins, which could have different roles in the regulated secretory pathway. On the other hand, MAS-7 could partially stimulate ANF secretion by activating PLC. Endothelin-1, one of the most potent neuroendocrine agonist of ANF secretion (Bruneau and de Bold, 1994; de Bold et al., 1996; Mantymaa et al., 1990; Schiebinger and Gomez-Sanchez, 1990; Stasch et al., 1989) activates the PLC-coupled ETA receptor, and therefore the activation of PLC by mastoparan, independently of GPCR activation, could potentially stimulate ANF secretion. The activation of PLC by mastoparan has been demonstrated in human myocardial tissue (Schnabel et al., 1997) as well as in several cell types (Garcia-Sainz et

al., 1991; Mousli et al., 1989; Tohkin et al., 1990). Activation of PLC or other small G proteins, by mastoparan, could explain the partial inhibition of MAS-7-stimulated increase of ANF in the isolated atria preparation by PTX, as observed by Bensimon *et al.* (Bensimon et al., 2004).

Gαo, Gβ1 and Gγ2 RNAi knockdown modulates ANF secretion in HL-1 cells

RNAi mediated knockdown of heterotrimeric G proteins was attempted in HL-1 cells in order to identify RASD1 effector proteins. Gαo protein was knocked down since it was previously demonstrated that stretch-secretion coupling of ANF was mediated by heterotrimeric Gαi/o proteins (Bensimon et al., 2004) (see Discussion chapters 2 and 3) and, as demonstrated in chapter 2 of the results section, Gαo is highly abundant in atrial tissue. Since RASD1 modulates both branches of the G protein-signaling cascade, i.e. Gαi/o and Gβγ (Cismowski et al., 2001; Graham et al., 2002; Graham et al., 2004), Gβγ subunits were also knockdown. Given that RASD1 has been shown, by yeast-two-hybrid and co-immunoprecipitation studies, to interact with the Gβ1 subunit (Hiskens et al., 2005; Tan et al., 2011), and that Gβ1 can interact with most Gγ subunits (Iniguez-Lluhi et al., 1992), this subunit was selected for targeted knocked down. The rational employed in the choice of the Gγ2 subunit was based on the observation that Gγ2 was significantly more abundant in the normal atria as compared to the ventricles (as demonstrated in chapter 2 of the results section). In addition, Gγ2 subunits have a geranylgeranyl modification, a form of prenylation that enables these subunits to bind

more efficiently to their effectors, as compared to Gγ1, which possesses a farnesyl modification (Blackmer et al., 2005). The covalent prenylation modification on the Gγ2 subunit enables efficient targeting of the Gβγ subunits to the plasma membrane as well as stabilizes the heterotrimeric G protein complex (Higgins and Casey, 1996; Muntz et al., 1992; Nusse and Neer, 1996).

RNAi targeted knockdown of the heterotrimeric G proteins αo1 and β1γ2 significantly reduced ANF secretion, under basal conditions albeit in the presence of FBS, indicating that both branches of the G protein-signaling cascade, i.e. Gαo and Gβγ, influence ANF secretion. Alternatively, knockdown of the Gβ1γ2 subunits may have disrupted Gαo targeting to endomembranes and plasma membrane resulting in a mis-localization of Gαo and thus impairing its function. In fact, purified Gαo proteins are unable to interact with phospholipid vesicles in the absence of Gβγ subunits (Sternweis, 1986).

Since the subcellular localization of G proteins is directly related to their functional role, it is not surprising to observe a modulation in ANF secretion upon their targeted knockdown, given that Gαo proteins have been found along the secretory pathway, from the TGN (Leyte et al., 1992), the secretory granules (Bensimon et al., 2004; Konrad et al., 1995; Muller et al., 1994; Padfield and Panesar, 1997; Vitale et al., 1997; Wolf et al., 1998), and up to the plasma membrane (Gudermann et al., 1997; Morris and Malbon, 1999; Toutant et al., 1987).

Interestingly, RNAi mediated double knockdown of the G protein subunits αo1 or β1γ2 and RASD1 considerably reduced ANF secretion levels, as compared to unique RASD1 targeted knockdown (Figures 49 and 55). The data obtained from these

transient-transfection studies indicate that RASD1 may negatively modulate the heterotrimeric G proteins and by consequence ANF secretion, since in the absence of these G proteins the stimulatory effect of RASD1 knockdown on ANF secretion is partially eliminated. The intermediate effect observed under double knockdown of RASD1 and Gαo1 or Gβ1γ2, i.e. ANF levels are lower than under unique RASD1 RNAi knockdown conditions yet higher than under Gαo1 or Gβ1γ2 RNAi knockdown conditions, indicates that the G proteins are not a rate limiting step for RASD1 and that perhaps RASD1 may be modulating other G proteins or effectors.

The signal transduction cascade leading to the activation of the heterotrimeric Gαoβγ proteins, upon stretch-secretion coupling remains elusive. The same holds true for the identity of the Gαo effectors. Gαo has been shown to regulate secretory granule transport in chromaffin cells by modulating Rho and phosphatidylinositol 4-kinase (PI4-kinase) activity to control actin cytoskeletal reorganization (Gasman et al., 1998; Vitale et al., 1996). More distally, Gαoβγ proteins can directly modulate potassium and calcium channels. In fact, inwardly rectifying potassium channels were shown to be activated by acetylcholine in a PTX-sensitive manner (Wickman et al., 1994). Purified bovine heterotrimeric G proteins confirmed the preferential activation of the cardiac potassium channel by Gβγ subunits (Logothetis et al., 1987). Recently, Gαi/o proteins have been shown to bind and activate the neuronal G-protein-gated inwardly rectifying potassium channels (Clancy et al., 2005). The involvement of Gαi/o proteins in the modulation of calcium current was demonstrated by PTX abrogation of the inhibition of voltage-gated calcium channel by noradrenaline (Holz et al., 1986). Other Gi/o protein coupled receptors, such as NPY, somatostatin, prostaglandin, opioid, adrenergic

and adenosine receptors, have been shown to inhibit calcium currents upon agonist activation (Hille, 1994). Other than ion channels, Gαi negatively modulate adenylyl cyclase (Kobayashi et al., 1990) while Gαo directly binds and impairs cAMP-dependent protein kinase A translocation (Ghil et al., 2006). In C. *elegans*, Gαo1 antagonizes the Gq-PLC-β-diacylglycerol (DAG) signaling pathway (Matsuki et al., 2006). Effectors directly modulated by Gαo are scarce in contrast to the Gβγ subunits or other Gα subunits. The isolation of Gαo/effector complexes from both atrial tissue and atrial derived HL-1 cells was attempted for several months. Cross-linking experiments with either 1% paraformaldehyde or DSP (dithiobis[succinimidylpropionate]) and in the presence or absence of aluminum-fluoride, a known activator of heterotrimeric G proteins (Bigay et al., 1987), followed by immunoprecipitaion were unsuccessful in isolating Gαo/effector complexes (as assessed by immunoblots and 2-dimensional electrophoresis followed by mass spectrometry (not shown)).

RASD1 in the secretory pathway

How is RASD1 modulating ANF secretion in the absence of secretagogue? Since the targeted knockdown of RASD1 produced a robust increase in the release of ANF, even in the absence of FBS, it would appear that ANF is released through a constitutive pathway. The constitutive secretory pathway, which is present in all eukaryotic cells, shuttles newly synthesized proteins to the cell surface in a secretagogue independent manner (Kelly, 1985; Ponnambalam and Baldwin, 2003). This pathway is mainly driven

by the rate of synthesis of the secretory protein at the endoplasmic reticulum and thus an increase in the constitutive pathway results from an increase in protein synthesis (Blazquez and Shennan, 2000; Wieland et al., 1987). Cycloheximide treatment, as well as RNAi knockdown of ANF, reduced and abolished ANF release under un-stimulated conditions, respectively (Ogawa et al., 1999) (Figure 52), demonstrating the participation of the constitutive pathway in basal secretion. Conversely, RNAi knockdown of RASD1 did not increase ANF transcription levels (not shown) indicating that the enhanced release of ANF is not correlated with an increase in gene expression and by consequence protein synthesis. RASD1 may thus have a role in sorting secretory proteins into regulated granules and that in its absence the secretory proteins are diverted to the constitutive pathway. This could explain why RASD1 levels are low in the ventricles as compared to the atria, since ventricular cardiocytes are thought to secrete the natriuretic peptides ANF and BNP through a constitutive secretory pathway. RASD1 role in targeting or sorting the secretory proteins to granules for long-term storage would not be necessary in ventricular cardiocytes, since under pathophysiological conditions, the ventricles continuously synthesis and immediately secrete the NPs, without any evidence of secretory granule storage (Bloch et al., 1986; Irons et al., 1993).

The TGN is considered the central protein sorting station, whereby constitutively secreted proteins and proteins targeted for storage granules are sorted within the late Golgi (Arvan and Castle, 1998). Constitutive secretion has been considered a default pathway for protein secretion, whereby in the absence of a sorting signal or receptor, proteins are transported to the plasma membrane (Wieland et al.,

1987). Two non-mutually exclusive modes of sorting peptide hormones into the regulated secretory pathway have been observed, i.e. sorting at entry and sorting by retention. Sorting at entry requires a mildly acidic environment and Ca^{2+} to drive protein aggregation, which excludes constitutive proteins, as well as sorting receptors that interact with the protein aggregates at the TGN membrane (Bauerfeind and Huttner, 1993; Canaff et al., 1996; Chanat and Huttner, 1991; Chung et al., 1989). Sorting by retention implies that regulated secretory proteins and constitutive secretory proteins are packaged into nascent secretory granules, which bud off the TGN, and that the constitutive proteins are subsequently transferred to constitutive-like vesicles while the regulated secretory proteins are retained in the maturing granule by receptor protein-protein interactions (Arvan and Castle, 1998; Park and Loh, 2008). Constitutive-like secretion therefore releases newly synthesized proteins independently from constitutive and regulated secretion (Kuliawat and Arvan, 1992).

Downregulation of sorting receptors have been shown to misroute regulated secretory proteins to the constitutive pathway. Knockdown of carboxypeptidase E (CPE) in Neuro-2a cells increased proenkephalin basal release by 3.5 fold, as compared to wild type cells (Normant and Loh, 1998). Depletion of CPE also missorted proinsulin into the constitutive pathway but not chromogranin A (Normant and Loh, 1998). It was later determined that chromogranin A secretion could be enhanced by cooperation of CPE and secretogranin III (Hosaka et al., 2005). In a subsequent study, Han *et al.* demonstrated that depletion of secretogranin III by RNAi impaired chromogranin A and adrenomedullin retention in PC12 cells and redirected these peptides to the constitutive secretory pathway (Han et al., 2008). Therefore, impairment of sorting

proteins or their adaptors diverts regulated proteins to the constitutive pathway. In the atrial cardiocytes, RASD1 could be modulating the activity of an unidentified sorting protein or acting as an adaptor or chaperon for other regulatory proteins from either the lumen or the cytoplasmic milieu. In fact, the sorting into large dense core vesicles of the vesicular monoamine transporter 2 (VMAT2) depends on a C-terminal cytoplasmic dileucine-like motif (Erickson et al., 1995; Liu et al., 1994) and hence its interaction with cytosolic sorting machinery (Asensio et al., 2010). Asensio *et al.* identified the adaptor protein AP-3 in an RNAi screen and demonstrated its importance in promoting sorting of VMAT2 to the regulated secretory pathway (Asensio et al., 2010). In addition, Lui-Roberts *et al.* demonstrated the essential role of an external scaffold containing AP-1 and clathrin in the formation of Weibel-Palade bodies and in vesicle protein content selection (Lui-Roberts et al., 2005). RNAi knockdown of AP-1 increased the constitutive release of von Willebrand factor (Lui-Roberts et al., 2005).

Alternatively, RASD1 could modulate signaling molecules, such as the heterotrimeric G proteins, at the site of granule exocytosis on the plasma membrane. Both Gαo and Gβ1γ2 subunits have been shown to regulate granule docking/priming and exocytosis, respectively (Blackmer et al., 2005; Zhao et al., 2010). Gβ1γ2 binds to SNAP-25 of the SNARE complex and inhibits synaptotagmin/SNAP-25 interaction, in a calcium dependent manner (Blackmer et al., 2005). The SNARE (SNAP (soluble N-ethylmaleimide-sensitive factor (NSF)) Attachment protein) receptor) complex mediates fusion by linking proteins from the opposing membranes of the vesicle/granule (v-SNARE, also known as R-SNARE) and the target plasma membrane (t-SNARE, also known as Q-SNARE) (Hu et al., 2003; Sollner et al., 1993). v-SNARE

members include, among others, the syntaxin family and SNAP-25, while t-SNARE members include the VAMP (vesicle-associated membrane protein) family (Hong, 2005). The v-SNAREs are inserted into vesicle membranes concomitantly with the packaging of other cargo/secretory proteins at the TGN and are transported to the plasma membrane where tethering factors enable proper positioning of the vesicle to enable accurate pairing of the v-SNARE with the cognate t-SNARE (Gillingham and Munro, 2003; Whyte and Munro, 2002). Rab GTPases are important in regulating membrane requirement of tethering factors (Christoforidis et al., 1999; Grosshans et al., 2006). SNARE protein complex function is positively and negatively regulated by various proteins as well as by post-translational modifications (Hinners et al., 2003; Hong, 2005; Sorensen, 2004; Veit et al., 1996). Known SNARE regulators include NSF (Hohl et al., 1998), α-SNAP (Marz et al., 2003), Munc18 (Scott et al., 2004), complexins (McMahon et al., 1995), synaptophysin (Valtorta et al., 2004), synaptotagmin I (Bai and Chapman, 2004), as well as the small GTP-binding protein of the Rab superfamily (Stroupe et al., 2009). *In vitro* and *in vivo* studies demonstrated that the Gβγ subunits are able to interact with syntaxin-1A, synaptobrevin, and SNAP-25 (Gerachshenko et al., 2005; Jarvis et al., 2002; Yoon et al., 2007) and modulate SNARE complex function and thus vesicle exocytosis (Blackmer et al., 2005). RASD1 could potentially sequester the Gαβγ subunits and decrease the available heterotrimeric G protein pool for subsequent GPCR-dependent or independent signaling events and hence modulate vesicle exocytosis. Knockdown of RASD1 could thus result in an increase in available heterotrimeric G proteins and perhaps other effectors at the plasma membrane. However, RASD1 knockdown did not change the secretory response of HL-1 cells in the

presence of the secretagogue MAS-7. Over-expressing RASD1 in HL-1 cells could help evaluate its functional role in stimulation-secretion coupling.

It has recently been demonstrated by yeast-two-hybrid assay and co-immunoprecipitation that RASD1 interacts with prenylated Rab acceptor domain family member 1 (PRAF1 or PRA1) (Compton et al., 2009). PRA1 was initially identified as a binding partner for both Rab3a and the v-SNARE VAMP2, and was suggested to control vesicle docking and fusion (Martincic et al., 1997). PRA1 is highly expressed in the heart (Martincic et al., 1997) and is more abundant in the atria than the ventricles (our own observation, but it did not meet the fold change cut off). PRA1 dissociates inactive Rabs bound to GDI (guanine nucleotide dissociation inhibitor) and delivers them onto membranes (Ohya et al., 2009; Sivars et al., 2003). VAMP2 interaction with t-SNAREs is blocked by PRA1 until Rab3a is recruited to the vesicle membrane and interacts with PRA1. PRA1-Rab3a interaction is thought to disrupt PRA1-VAMP2 interaction, which allows VAMP2 to associate with the t-SNARE synthaxin and promote vesicle fusion. RASD1 is thought to inhibit ACTH secretion by blocking PRA1-Rab3a-VAMP2 interaction, presumably by inducing a conformational change in PRA1, since RASD1 does not bind PRA1 in the same sites, as do Rab3a and VAMP2 (Compton et al., 2009). In addition, PRA1 mutations, which impair Rab3a interaction, diverted ACTH containing granules to the constitutive pathway (Compton et al., 2009), thus implying that PRA1 may act as a sorting receptor for Rab GTPases at the TGN (Figueroa et al., 2001). Of note, PRA1 not only binds Rab proteins in a prenylation-dependent manner but also H-Ras, RhoA, and Rap1a (Figueroa et al., 2001). PRA1 could potentially bind

other prenylated proteins such as Gγ2 subunits. The subcellular location of RASD1 and PRA1 interaction was unfortunately not determined in that study.

Taken together, RASD1 could potentially modulate ANF secretion at various stages, i.e. from protein sorting at the TGN or nascent granule to the docking site for vesicle exocytosis. These regulatory events most likely involve the participation of the heterotrimeric Gαoβγ proteins, given their undeniable relationship with RASD1.

Conclusions

The importance of the cardiac hormones ANF and BNP in maintaining cardiorenal homeostasis by acutely and chronically reducing systemic blood pressure and hemodynamic load to the heart has been well established. Significant effort has been focused on the elucidation of the mechanistic underlying ANF and BNP gene expression and secretion by the atrial cardiocytes, but much remains to be determined regarding specific molecular events involved in the cardiocyte secretory function. The focus of this thesis was to determine and investigate the differential gene expression profiles of atrial and ventricular tissues, under normal and chronic hemodynamic overload conditions, with the purpose of identifying targets that could regulate NP synthesis or secretion.

The data developed in this investigation provides, for the first time, insight into the expression profiles of genes particularly centered in the secretory function of the heart. In particular, pathway analysis of the differentially expressed genes between the normal atria and ventricles revealed unique expression profiles in the atria for G protein signaling that included Gαo1, Gγ2 and Gγ3, RASD1, RGS2, and RGS6 and the related K+ channels Kcnj3 and Kcnj5 (see summary diagram, Figure 57). Transcripts involved in vesicle trafficking, such as Rab GTPases, hormone secretion, such as the SNARE adaptor proteins Bet1 and synaptotagmin-like-2, as well as mechanosensors, such as TREK-1, were among others identified.

Following the transcriptional analysis of normal atrial tissue, an *in vivo* investigation was carried out to define the overall gene expression profile associated with stretch activation of the endocrine heart following an increase in venous return to the heart obtained by aortocaval shunt. As expected, chronic hemodynamic overload produced a potent hypertrophic response, including increased heart weight and the re-expression of the cardiac fetal gene program. Gene expression profiling of the pathological tissues added new insight into the transcriptional regulation of the endocrine heart under chronic stimulation. Hundreds of genes were differentially expressed between the VO atria and ventricles, but a subset of them displayed an interaction effect, i.e. they were differentially expressed due to the experimental condition as well as their tissue of origin. One such gene was RASD1. VO specifically downregulated the accessory protein for heterotrimeric G protein signaling RASD1 in the atria. *In vitro*, knockdown of RASD1 in the atrial-derived HL-1 cells, significantly increased ANF secretion, demonstrating a previously unknown negative modulator role for RASD1.

Since stretch-secretion coupling of ANF is mediated by PTX sensitive Gαi/o, the differential gene expression of RASD1 observed in our oligonucleotide study is of particular interest. The modulation of Gi/o signaling by RASD1, in the context of ANF secretion is consistent with the RNAi knockdown studies presented herein. Due to RASD1 opposing effects on Gi/o mediated signaling following agonist dependent or independent GPCR activation, RASD1 may help orchestrate the complex diversity and specificity of G protein signaling under different conditions and hence deserves further investigation. The novel function identified herein for RASD1 in the atria is of

considerable interest given the fact that secretory impairment of the cardiac natriuretic hormones can negatively impact on cardiovascular homeostasis, a fact evidenced by the results of genetic disruption of the natriuretic peptide system (Holtwick et al., 2003; John et al., 1995; Lopez et al., 1995). The results acquired from this work advance our knowledge on the mechanism of NP secretion, which is of great importance given their beneficial effects in cardiovascular diseases.

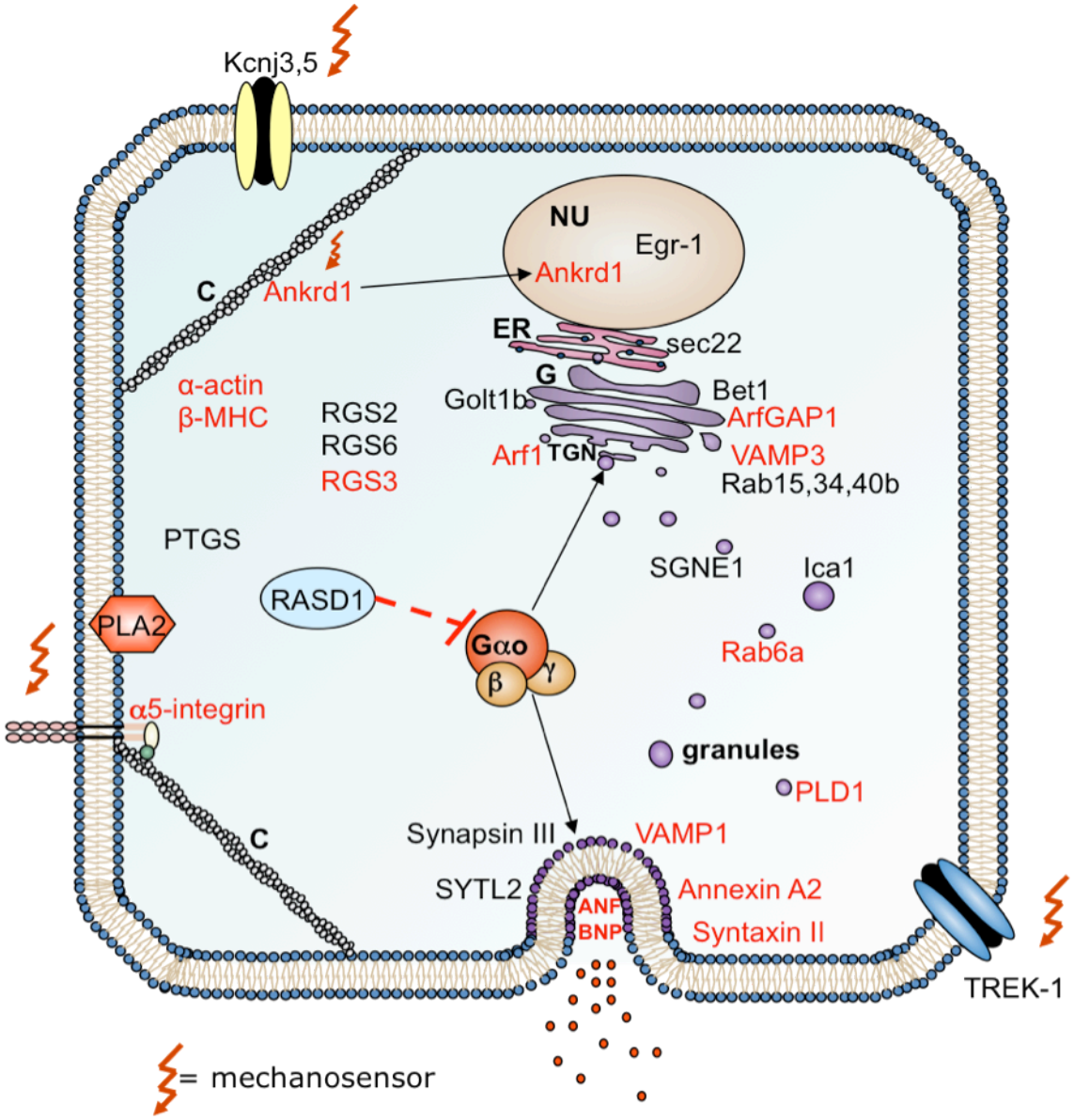


Figure 57. Diagram of several differentially expressed genes found abundant in the atria

Secretory proteins are synthesized in the rough ER and then transported in vesicles to the Golgi (G) for further processing, modification and sorting. Secretory proteins are then packaged into vesicles or granules, which bud off the TGN. Vesicles containing proteins destined for constitutive secretion are targeted to the plasma membrane for the immediate release of their contents while regulated granules wait in the cytoplasm

until the secretagogue signal is received. All these steps are tightly regulated by various proteins, some of which were found differentially expressed in the atria and are depicted in the diagram. Note that in the diagram ANF and BNP secretion is shown independently of the mode of secretion. Atrial abundant genes, as compared to the ventricles, are listed in black while genes upregulated in the atria during VO are listed in red. Mechanosensing molecules, indicated by a lighting bolt, include Kcnj3,5 channels, α5-integrin, TREK-1 and PLA2. Note that Gαo can be located on the Golgi, granules and plasma membrane. RASD1 can potentially moduate Gαo activity at various sites in the secretory pathway. Abbreviations: Ankrd1, ankyrin repeat domain 1; C, cytoskeleton; Egr-1, early growth response 1; ER, endoplasmic reticulum; G, Golgi; Ica1, islet cell autoantigen 1, NU, nucleus; PLA2, phospholipase A2; PLD1, phospholipase D1; PTGS, prostaglandin synthase; RGS, Regulator of G protein Signaling; SGNE1, secretory granule neuroendocrine protein 1; SYTL2, synaptotagmin like 2; TGN, trans- Golgi network; VAMP, vesicle-associated membrane protein.

Future directions

In order to better understand the Gi/o signaling events leading up to ANF secretion, a series of experiments could be designed to address the question of how RASD1 is modulating ANF secretion. Additional *in vitro* experiments whereby RASD1 expression levels would be overexpressed by adenoviral transfection in HL-1 cells and treatment of these cells with MAS-7, which is known to enhance ANF release, as demonstrated herein, could further ascertain RASD1 importance in ANF regulated secretion. RNAi targeted knockdown of Gαo and Gβγ subunits, as previously performed for RASD1 downregulated experiments, could be done to further determine their modulator effect on ANF regulated secretion. In combination with these experiments, other signaling molecules could also be knocked-down in order to identify upstream mediators and downstream effectors of RASD1-Gαo.

Furthermore, these *in vitro* experiments could be carried out in conjunction with pharmacological studies in order to determine the location within the secretory pathway where RASD1 is acting. Monensin, which inhibits protein sorting and vesicle formation in the TGN (Mollenhauer et al., 1990) could be used to ascertain the hypothesis that in the absence of RASD1, such as demonstrated herein, secretory proteins are diverted to the constitutive secretory pathway. In the isolated atria, monensin treatment decreased basal and stimulated ANF secretion, while in conjunction with cycloheximide, which inhibits protein synthesis, ANF secretion was enhanced (Ogawa et al., 1999). It was then hypothesized that cycloheximide inhibited

the synthesis of a protein regulator that negatively modulated ANF secretion somewhere along the basal secretory pathway (Ogawa et al., 1999).

Finally, experiments could be carried out *in vivo* by generating heart specific RASD1 knockout mice in order to examine the physiological role of RASD1 in ANF basal and stimulated secretion. ANF plasma levels would be measured (by RIA) in order to assess the susceptibility of RASD1 knockout mice to an acute volume expansion challenge, by isotonic saline injection. Saline infusions, which increase plasma volume, have been shown to stimulate ANF release in both humans and rodents (Deloof and Chatelain, 1994; Kishimoto et al., 1996; Lang et al., 1993; Schreier et al., 2008). Since the *in vitro* data presented herein demonstrated a negative modulator role of RASD1 on ANF basal secretion, it would be expected that under normal conditions, ANF plasma levels from RASD1 knockout mice would be increased as compared to wild-type mice. Under volume-expansion conditions, ANF plasma levels would be expected to be significantly higher in RASD1 knockout mice than wild-type controls, since RASD1 modulator actions on the heterotrimeric Gαi/o proteins would be alleviated. Furthermore, ANF atrial tissue content could also be assessed (by RIA) to determine if, in the absence of RASD1, there is a defect in ANF storage. In addition, microscopic and immunofluorescence analysis of the atrial appendages of both wild-type and knockout mice could further give insight in the effects of RASD1. In fact, if mice deficient in RASD1 exhibit altered ANF storage, it would be expected to observe phenotypical changes, such as reduced size or quantity of atrial specific granules, as well as reduced ANF immunofluorescent staining.

These investigations could further define the functional role of RASD1 in the context of atrial hormone secretion and ascertain its role as a critical molecular regulator of various intracellular signaling pathways, specifically in the modulation of the responsiveness of Gi/o proteins in the endocrine heart under physiological and pathophysiological conditions. This appears a worthwhile pursuit given the importance of ANF and BNP in the maintenance of cardiovascular homeostasis and myocardial remodeling in both healthy and diseased states.

References

Abassi, Z., Goltsman, I., Karram, T., Winaver, J., and Hoffman, A. (2011). Aortocaval fistula in rat: a unique model of volume-overload congestive heart failure and cardiac hypertrophy. J Biomed Biotechnol *2011*, 729497.

Abassi, Z., Haramati, A., Hoffman, A., Burnett, J.C., Jr., and Winaver, J. (1990). Effect of converting-enzyme inhibition on renal response to ANF in rats with experimental heart failure. Am J Physiol *259*, R84-89.

Abassi, Z.A., Brodsky, S., Karram, T., Dobkin, I., Winaver, J., and Hoffman, A. (2001). Temporal changes in natriuretic and antinatriuretic systems after closure of a large arteriovenous fistula. Cardiovasc Res *51*, 567-576.

Abassi, Z.A., Gurbanov, K., Mulroney, S.E., Potlog, C., Opgenorth, T.J., Hoffman, A., Haramati, A., and Winaver, J. (1997). Impaired nitric oxide-mediated renal vasodilation in rats with experimental heart failure: role of angiotensin II. Circulation *96*, 3655-3664.

Abell, T.J., Richards, A.M., Ikram, H., Espiner, E.A., and Yandle, T. (1989). Atrial natriuretic factor inhibits proliferation of vascular smooth muscle cells stimulated by platelet-derived growth factor. Biochem Biophys Res Commun *160*, 1392-1396.

Adams, K.F., Jr. (2001). New epidemiologic perspectives concerning mild-to-moderate heart failure. Am J Med *110 Suppl 7A*, 6S-13S.

Adcock, I.M. (1997). Transcription factors as activators of gene transcription: AP-1 and NF-kappa B. Monaldi Arch Chest Dis *52*, 178-186.

Affymetrix (2009). GeneChip® Expression Analysis Technical Manual. With Specific Protocols for Using the GeneChip® Hybridization, Wash, and Stain Kit.

Aihara, Y., Kurabayashi, M., Saito, Y., Ohyama, Y., Tanaka, T., Takeda, S., Tomaru, K., Sekiguchi, K., Arai, M., Nakamura, T.*, et al.* (2000). Cardiac ankyrin repeat protein is a novel marker of cardiac hypertrophy: role of M-CAT element within the promoter. Hypertension *36*, 48-53.

Aitken, G.D., Raizis, A.M., Yandle, T.G., George, P.M., Espiner, E.A., and Cameron, V.A. (1999). The characterization of ovine genes for atrial, brain, and C-type natriuretic peptides. Domest Anim Endocrinol *16*, 115-121.

Alexander, J.J., and Imbembo, A.L. (1989). Aorta-vena cava fistula. Surgery *105*, 1-12.

Almeida, F.A., Suzuki, M., and Maack, T. (1986). Atrial natriuretic factor increases hematocrit and decreases plasma volume in nephrectomized rats. Life Sci *39*, 1193-1199.

Amin, R.H., Chen, H.Q., Veluthakal, R., Silver, R.B., Li, J., Li, G., and Kowluru, A. (2003). Mastoparan-induced insulin secretion from insulin-secreting betaTC3 and INS-1 cells: evidence for its regulation by Rho subfamily of G proteins. Endocrinology *144*, 4508-4518.

Anand-Srivastava, M.B., Gutkowska, J., and Cantin, M. (1991). The presence of atrial-natriuretic-factor receptors of ANF-R2 subtype in rat platelets. Coupling to adenylate cyclase/cyclic AMP signal-transduction system. Biochem J *278 (Pt 1)*, 211-217.

Argentin, S., Ardati, A., Tremblay, S., Lihrmann, I., Robitaille, L., Drouin, J., and Nemer, M. (1994). Developmental stage-specific regulation of atrial natriuretic factor gene transcription in cardiac cells. Mol Cell Biol *14*, 777-790.

Armstrong, P.W., Stopps, T.P., Ford, S.E., and de Bold, A.J. (1986). Rapid ventricular pacing in the dog: pathophysiologic studies of heart failure. Circulation *74*, 1075-1084.

Arvan, P., and Castle, D. (1998). Sorting and storage during secretory granule biogenesis: looking backward and looking forward. Biochem J *332 (Pt 3)*, 593-610.

Arvan, P., and Castle, J.D. (1987). Phasic release of newly synthesized secretory proteins in the unstimulated rat exocrine pancreas. J Cell Biol *104*, 243-252.

Arvan, P., Kuliawat, R., Prabakaran, D., Zavacki, A.M., Elahi, D., Wang, S., and Pilkey, D. (1991). Protein discharge from immature secretory granules displays both regulated and constitutive characteristics. J Biol Chem *266*, 14171-14174.

Asensio, C.S., Sirkis, D.W., and Edwards, R.H. (2010). RNAi screen identifies a role for adaptor protein AP-3 in sorting to the regulated secretory pathway. J Cell Biol *191*, 1173-1187.

Ashcroft, F.M. (2005). ATP-sensitive potassium channelopathies: focus on insulin secretion. J Clin Invest *115*, 2047-2058.

Azzazy, H.M., and Christenson, R.H. (2003). B-type natriuretic peptide: physiologic role and assay characteristics. Heart Fail Rev *8*, 315-320.

Bader, M. (2010). Rat models of cardiovascular diseases. Methods Mol Biol *597*, 403-414.

Bai, J., and Chapman, E.R. (2004). The C2 domains of synaptotagmin--partners in exocytosis. Trends Biochem Sci *29*, 143-151.

Bai, X., Bugg, G.J., Greenwood, S.L., Glazier, J.D., Sibley, C.P., Baker, P.N., Taggart, M.J., and Fyfe, G.K. (2005a). Expression of TASK and TREK, two-pore domain K+ channels, in human myometrium. Reproduction *129*, 525-530.

Bai, X., Greenwood, S.L., Glazier, J.D., Baker, P.N., Sibley, C.P., Taggart, M.J., and Fyfe, G.K. (2005b). Localization of TASK and TREK, two-pore domain K+ channels, in human cytotrophoblast cells. J Soc Gynecol Investig *12*, 77-83.

Barbee, R.W., Perry, B.D., Re, R.N., Murgo, J.P., and Field, L.J. (1994). Hemodynamics in transgenic mice with overexpression of atrial natriuretic factor. Circ Res *74*, 747-751.

Barth, A.S., Merk, S., Arnoldi, E., Zwermann, L., Kloos, P., Gebauer, M., Steinmeyer, K., Bleich, M., Kaab, S., Pfeufer, A.*, et al.* (2005). Functional profiling of human atrial and ventricular gene expression. Pflugers Arch *450*, 201-208.

Bauerfeind, R., and Huttner, W.B. (1993). Biogenesis of constitutive secretory vesicles, secretory granules and synaptic vesicles. Curr Opin Cell Biol *5*, 628-635.

Bensimon, M., Chang, A.I., de Bold, M.L., Ponce, A., Carreras, D., and De Bold, A.J. (2004). Participation of G proteins in natriuretic peptide hormone secretion from heart atria. Endocrinology *145*, 5313-5321.

Bernstein, E., Caudy, A.A., Hammond, S.M., and Hannon, G.J. (2001). Role for a bidentate ribonuclease in the initiation step of RNA interference. Nature *409*, 363-366.

Betsholtz, C., Baumann, A., Kenna, S., Ashcroft, F.M., Ashcroft, S.J., Berggren, P.O., Grupe, A., Pongs, O., Rorsman, P., Sandblom, J.*, et al.* (1990). Expression of voltage-gated K+ channels in insulin-producing cells. Analysis by polymerase chain reaction. FEBS Lett *263*, 121-126.

Bianciotti, L.G., and De Bold, A.J. (2000). Effect of selective ET(A) receptor blockade on natriuretic peptide gene expression in DOCA-salt hypertension. Am J Physiol Heart Circ Physiol *279*, H93-H101.

Bianciotti, L.G., and de Bold, A.J. (2002). Natriuretic peptide gene expression in DOCA-salt hypertension after blockade of type B endothelin receptor. Am J Physiol Heart Circ Physiol *282*, H1127-1134.

Bianciotti, L.G., Vatta, M.S., Vescina, C., Trippodi, V., Sabbatini, M.E., and Fernandez, B.E. (2001). Centrally applied atrial natriuretic factor diminishes bile secretion in the rat. Regul Pept *102*, 127-133.

Bigay, J., Deterre, P., Pfister, C., and Chabre, M. (1987). Fluoride complexes of aluminium or beryllium act on G-proteins as reversibly bound analogues of the gamma phosphate of GTP. EMBO J *6*, 2907-2913.

Black, F.M., Packer, S.E., Parker, T.G., Michael, L.H., Roberts, R., Schwartz, R.J., and Schneider, M.D. (1991). The vascular smooth muscle alpha-actin gene is reactivated during cardiac hypertrophy provoked by load. J Clin Invest *88*, 1581-1588.

Blackmer, T., Larsen, E.C., Bartleson, C., Kowalchyk, J.A., Yoon, E.J., Preininger, A.M., Alford, S., Hamm, H.E., and Martin, T.F. (2005). G protein betagamma directly regulates SNARE protein fusion machinery for secretory granule exocytosis. Nat Neurosci *8*, 421-425.

Blazquez, M., and Shennan, K.I. (2000). Basic mechanisms of secretion: sorting into the regulated secretory pathway. Biochem Cell Biol *78*, 181-191.

Bloch, K.D., Jones, S.W., Preibisch, G., Seipke, G., Seidman, C.E., and Seidman, J.G. (1987). Proatrial natriuretic factor is phosphorylated by rat cardiocytes in culture. J Biol Chem *262*, 9956-9961.

Bloch, K.D., Seidman, J.G., Naftilan, J.D., Fallon, J.T., and Seidman, C.E. (1986). Neonatal atria and ventricles secrete atrial natriuretic factor via tissue-specific secretory pathways. Cell *47*, 695-702.

Blumer, J.B., Cismowski, M.J., Sato, M., and Lanier, S.M. (2005). AGS proteins: receptor-independent activators of G-protein signaling. Trends Pharmacol Sci *26*, 470-476.

Bohula, E.A., Salisbury, A.J., Sohail, M., Playford, M.P., Riedemann, J., Southern, E.M., and Macaulay, V.M. (2003). The efficacy of small interfering RNAs targeted to the type 1 insulin-like growth factor receptor (IGF1R) is influenced by secondary structure in the IGF1R transcript. J Biol Chem *278*, 15991-15997.

Bondue, A., and Blanpain, C. (2010). Mesp1: a key regulator of cardiovascular lineage commitment. Circ Res *107*, 1414-1427.

Bootman, M.D., Higazi, D.R., Coombes, S., and Roderick, H.L. (2006). Calcium signalling during excitation-contraction coupling in mammalian atrial myocytes. J Cell Sci *119*, 3915-3925.

Brackmann, M., Schuchmann, S., Anand, R., and Braunewell, K.H. (2005). Neuronal Ca2+ sensor protein VILIP-1 affects cGMP signalling of guanylyl cyclase B by regulating clathrin-dependent receptor recycling in hippocampal neurons. J Cell Sci *118*, 2495-2505.

Brenner, B.M., Ballermann, B.J., Gunning, M.E., and Zeidel, M.L. (1990). Diverse biological actions of atrial natriuretic peptide. Physiol Rev *70*, 665-699.

Brodsky, S., Gurbanov, K., Abassi, Z., Hoffman, A., Ruffolo, R.R., Jr., Feuerstein, G.Z., and Winaver, J. (1998). Effects of eprosartan on renal function and cardiac hypertrophy in rats with experimental heart failure. Hypertension *32*, 746-752.

Brown, E. (2001). Integrin-associated protein (CD47): an unusual activator of G protein signaling. J Clin Invest *107*, 1499-1500.

Brown, E.J., and Frazier, W.A. (2001). Integrin-associated protein (CD47) and its ligands. Trends Cell Biol *11*, 130-135.

Brown, L.A., Nunez, D.J., and Wilkins, M.R. (1993). Differential regulation of natriuretic peptide receptor messenger RNAs during the development of cardiac hypertrophy in the rat. J Clin Invest *92*, 2702-2712.

Brown, T.A. (2002). Genomes, 2010/09/08 edn.

Bruneau, B.G., Bao, Z.Z., Fatkin, D., Xavier-Neto, J., Georgakopoulos, D., Maguire, C.T., Berul, C.I., Kass, D.A., Kuroski-de Bold, M.L., de Bold, A.J.*, et al.* (2001). Cardiomyopathy in Irx4-deficient mice is preceded by abnormal ventricular gene expression. Mol Cell Biol *21*, 1730-1736.

Bruneau, B.G., and de Bold, A.J. (1994). Selective changes in natriuretic peptide and early response gene expression in isolated rat atria following stimulation by stretch or endothelin-1. Cardiovasc Res *28*, 1519-1525.

Bruneau, B.G., Piazza, L.A., and de Bold, A.J. (1996). Alpha 1-adrenergic stimulation of isolated rat atria results in discoordinate increases in natriuretic peptide secretion and gene expression and enhances Egr-1 and c-Myc expression. Endocrinology *137*, 137-143.

Bruneau, B.G., Piazza, L.A., and de Bold, A.J. (1997). BNP gene expression is specifically modulated by stretch and ET-1 in a new model of isolated rat atria. Am J Physiol *273*, H2678-2686.

Burger, M., Denzinger, S., Filbeck, T., Hartmann, A., Rossler, W., and Hammerschmied, C. (2005). A metachronous, atypical, multifocal renal oncocytoma with a concomitant renal cell carcinoma of the contralateral side and bilateral multifocal oncocytomas: two case reports and review of literature. ScientificWorldJournal *5*, 545-549.

Burgess, T.L., and Kelly, R.B. (1987). Constitutive and regulated secretion of proteins. Annu Rev Cell Biol *3*, 243-293.

Burgoyne, R.D., and Morgan, A. (1993). Regulated exocytosis. Biochem J *293 (Pt 2)*, 305-316.

Burnett, J.C., Jr., Granger, J.P., and Opgenorth, T.J. (1984). Effects of synthetic atrial natriuretic factor on renal function and renin release. Am J Physiol *247*, F863-866.

Burnett, J.C., Jr., Kao, P.C., Hu, D.C., Heser, D.W., Heublein, D., Granger, J.P., Opgenorth, T.J., and Reeder, G.S. (1986). Atrial natriuretic peptide elevation in congestive heart failure in the human. Science *231*, 1145-1147.

Burre, J., Sharma, M., Tsetsenis, T., Buchman, V., Etherton, M.R., and Sudhof, T.C. (2010). Alpha-synuclein promotes SNARE-complex assembly in vivo and in vitro. Science *329*, 1663-1667.

Buttgereit, J., Qadri, F., Monti, J., Langenickel, T.H., Dietz, R., Braunewell, K.H., and Bader, M. (2010). Visinin-like protein 1 regulates natriuretic peptide receptor B in the heart. Regul Pept *161*, 51-57.

Calderone, A., Thaik, C.M., Takahashi, N., Chang, D.L., and Colucci, W.S. (1998). Nitric oxide, atrial natriuretic peptide, and cyclic GMP inhibit the growth-promoting effects of norepinephrine in cardiac myocytes and fibroblasts. J Clin Invest *101*, 812-818.

Cameron, V.A., and Ellmers, L.J. (2003). Minireview: natriuretic peptides during development of the fetal heart and circulation. Endocrinology *144*, 2191-2194.

Cameron, V.A., Rademaker, M.T., Ellmers, L.J., Espiner, E.A., Nicholls, M.G., and Richards, A.M. (2000). Atrial (ANP) and brain natriuretic peptide (BNP) expression after myocardial infarction in sheep: ANP is synthesized by fibroblasts infiltrating the infarct. Endocrinology *141*, 4690-4697.

Canaff, L., Brechler, V., Reudelhuber, T.L., and Thibault, G. (1996). Secretory granule targeting of atrial natriuretic peptide correlates with its calcium-mediated aggregation. Proc Natl Acad Sci U S A *93*, 9483-9487.

Cappuccio, F.P., Markandu, N.D., Buckley, M.G., Sagnella, G.A., Shore, A.C., and MacGregor, G.A. (1987). Changes in the plasma levels of atrial natriuretic peptides during mineralocorticoid escape in man. Clin Sci (Lond) *72*, 531-539.

Carabello, B.A. (1996). Models of volume overload hypertrophy. J Card Fail *2*, 55-64.

Casco, V.H., Veinot, J.P., Kuroski de Bold, M.L., Masters, R.G., Stevenson, M.M., and de Bold, A.J. (2002). Natriuretic peptide system gene expression in human coronary arteries. J Histochem Cytochem *50*, 799-809.

Cerra, M.C. (1994). Cardiac distribution of the binding sites for natriuretic peptides in vertebrates. Cardioscience *5*, 215-224.

Chanat, E., and Huttner, W.B. (1991). Milieu-induced, selective aggregation of regulated secretory proteins in the trans-Golgi network. J Cell Biol *115*, 1505-1519.

Chang, C.H., Kohse, K.P., Chang, B., Hirata, M., Jiang, B., Douglas, J.E., and Murad, F. (1990). Characterization of ATP-stimulated guanylate cyclase activation in rat lung membranes. Biochim Biophys Acta *1052*, 159-165.

Chen, H., Huang, X.N., Stewart, A.F., and Sepulveda, J.L. (2004). Gene expression changes associated with fibronectin-induced cardiac myocyte hypertrophy. Physiol Genomics *18*, 273-283.

Chen, H.H., Grantham, J.A., Schirger, J.A., Jougasaki, M., Redfield, M.M., and Burnett, J.C., Jr. (2000). Subcutaneous administration of brain natriuretic peptide in experimental heart failure. J Am Coll Cardiol *36*, 1706-1712.

Chen, M., Lee, J., Huang, B.S., Grekin, R.J., and Malvin, R.L. (1989). Clonidine and morphine increase atrial natriuretic peptide secretion in anesthetized rats. Proc Soc Exp Biol Med *191*, 299-303.

Chien, K.R., Knowlton, K.U., Zhu, H., and Chien, S. (1991). Regulation of cardiac gene expression during myocardial growth and hypertrophy: molecular studies of an adaptive physiologic response. FASEB J *5*, 3037-3046.

Chinkers, M., and Garbers, D.L. (1989). The protein kinase domain of the ANP receptor is required for signaling. Science *245*, 1392-1394.

Cho, K.W., Seul, K.H., Kim, S.H., Seul, K.M., and Koh, G.Y. (1991). Atrial pressure, distension, and pacing frequency in ANP secretion in isolated perfused rabbit atria. Am J Physiol *260*, R39-46.

Choi, O.H., Padgett, W.L., and Daly, J.W. (1992). Effects of the amphiphilic peptides melittin and mastoparan on calcium influx, phosphoinositide breakdown and arachidonic acid release in rat pheochromocytoma PC12 cells. J Pharmacol Exp Ther *260*, 369-375.

Christoffels, V.M., Habets, P.E., Franco, D., Campione, M., de Jong, F., Lamers, W.H., Bao, Z.Z., Palmer, S., Biben, C., Harvey, R.P., *et al.* (2000). Chamber formation and morphogenesis in the developing mammalian heart. Dev Biol *223*, 266-278.

Christoforidis, S., McBride, H.M., Burgoyne, R.D., and Zerial, M. (1999). The Rab5 effector EEA1 is a core component of endosome docking. Nature *397*, 621-625.

Chung, K.N., Walter, P., Aponte, G.W., and Moore, H.P. (1989). Molecular sorting in the secretory pathway. Science *243*, 192-197.

Cismowski, M.J., Ma, C., Ribas, C., Xie, X., Spruyt, M., Lizano, J.S., Lanier, S.M., and Duzic, E. (2000). Activation of heterotrimeric G-protein signaling by a ras-related protein. Implications for signal integration. J Biol Chem *275*, 23421-23424.

Cismowski, M.J., Takesono, A., Bernard, M.L., Duzic, E., and Lanier, S.M. (2001). Receptor-independent activators of heterotrimeric G-proteins. Life Sci *68*, 2301-2308.

Clancy, S.M., Fowler, C.E., Finley, M., Suen, K.F., Arrabit, C., Berton, F., Kosaza, T., Casey, P.J., and Slesinger, P.A. (2005). Pertussis-toxin-sensitive Galpha subunits selectively bind to C-terminal domain of neuronal GIRK channels: evidence for a heterotrimeric G-protein-channel complex. Mol Cell Neurosci *28*, 375-389.

Claycomb, W.C., Lanson, N.A., Jr., Stallworth, B.S., Egeland, D.B., Delcarpio, J.B., Bahinski, A., and Izzo, N.J., Jr. (1998). HL-1 cells: a cardiac muscle cell line that contracts and retains phenotypic characteristics of the adult cardiomyocyte. Proc Natl Acad Sci U S A *95*, 2979-2984.

Cohen, D., Koh, G.Y., Nikonova, L.N., Porter, J.G., and Maack, T. (1996). Molecular determinants of the clearance function of type C receptors of natriuretic peptides. J Biol Chem *271*, 9863-9869.

Compton, S.L., Kemppainen, R.J., and Behrend, E.N. (2009). Prenylated Rab acceptor domain family member 1 is involved in stimulated ACTH secretion and inhibition. Cell Signal *21*, 1901-1909.

Cook, D.L., Satin, L.S., Ashford, M.L., and Hales, C.N. (1988). ATP-sensitive K+ channels in pancreatic beta-cells. Spare-channel hypothesis. Diabetes *37*, 495-498.

Copland, I.B., and Post, M. (2007). Stretch-activated signaling pathways responsible for early response gene expression in fetal lung epithelial cells. J Cell Physiol *210*, 133-143.

Copland, J.A., Jeng, Y.J., Strakova, Z., Ives, K.L., Hellmich, M.R., and Soloff, M.S. (1999). Demonstration of functional oxytocin receptors in human breast Hs578T cells and their up-regulation through a protein kinase C-dependent pathway. Endocrinology *140*, 2258-2267.

Cowie, M.R., Jourdain, P., Maisel, A., Dahlstrom, U., Follath, F., Isnard, R., Luchner, A., McDonagh, T., Mair, J., Nieminen, M.*, et al.* (2003). Clinical applications of B-type natriuretic peptide (BNP) testing. Eur Heart J *24*, 1710-1718.

Currie, M.G., Geller, D.M., Chao, J., Margolius, H.S., and Needleman, P. (1984). Kallikrein activation of a high molecular weight atrial peptide. Biochem Biophys Res Commun *120*, 461-466.

Currie, M.G., and Newman, W.H. (1986). Evidence for alpha-1 adrenergic receptor regulation of atriopeptin release from the isolated rat heart. Biochem Biophys Res Commun *137*, 94-100.

Dagnino, L., Drouin, J., and Nemer, M. (1991). Differential expression of natriuretic peptide genes in cardiac and extracardiac tissues. Mol Endocrinol *5*, 1292-1300.

Dai, F.F., Zhang, Y., Kang, Y., Wang, Q., Gaisano, H.Y., Braunewell, K.H., Chan, C.B., and Wheeler, M.B. (2006). The neuronal Ca2+ sensor protein visinin-like protein-1 is expressed in pancreatic islets and regulates insulin secretion. J Biol Chem *281*, 21942-21953.

Dalma-Weiszhausz, D.D., Warrington, J., Tanimoto, E.Y., and Miyada, C.G. (2006). The affymetrix GeneChip platform: an overview. Methods Enzymol *410*, 3-28.

Daniel, S., Noda, M., Cerione, R.A., and Sharp, G.W. (2002). A link between Cdc42 and syntaxin is involved in mastoparan-stimulated insulin release. Biochemistry *41*, 9663-9671.

Day, M.L., Schwartz, D., Wiegand, R.C., Stockman, P.T., Brunnert, S.R., Tolunay, H.E., Currie, M.G., Standaert, D.G., and Needleman, P. (1987). Ventricular atriopeptin. Unmasking of messenger RNA and peptide synthesis by hypertrophy or dexamethasone. Hypertension *9*, 485-491.

de Bold, A.J. (1979). Heart atria granularity effects of changes in water-electrolyte balance. Proc Soc Exp Biol Med *161*, 508-511.

de Bold, A.J., and Bencosme, S.A. (1975). Autoradiographic analysis of label distribution in mammalian atrial and ventricular cardiocytes after exposure to tritiated leucine. Recent Adv Stud Cardiac Struct Metab *8*, 129-138.

de Bold, A.J., Borenstein, H.B., Veress, A.T., and Sonnenberg, H. (1981). A rapid and potent natriuretic response to intravenous injection of atrial myocardial extract in rats. Life Sci *28*, 89-94.

de Bold, A.J., Bruneau, B.G., and Kuroski de Bold, M.L. (1996). Mechanical and neuroendocrine regulation of the endocrine heart. Cardiovasc Res *31*, 7-18.

de Bold, A.J., Ma, K.K., Zhang, Y., de Bold, M.L., Bensimon, M., and Khoshbaten, A. (2001). The physiological and pathophysiological modulation of the endocrine function of the heart. Can J Physiol Pharmacol *79*, 705-714.

de Bold, M.L., and de Bold, A.J. (1989). Effect of manipulations of Ca2+ environment on atrial natriuretic factor release. Am J Physiol *256*, H1588-1594.

Deloof, S., and Chatelain, A. (1994). Effect of blood volume expansion on basal plasma atrial natriuretic factor and adrenocorticotropic hormone secretions in the fetal rat at term. Biol Neonate *65*, 390-395.

Delorme, B., Dahl, E., Jarry-Guichard, T., Briand, J.P., Willecke, K., Gros, D., and Theveniau-Ruissy, M. (1997). Expression pattern of connexin gene products at the early developmental stages of the mouse cardiovascular system. Circ Res *81*, 423-437.

Delporte, C., Winand, J., Poloczek, P., Von Geldern, T., and Christophe, J. (1992). Discovery of a potent atrial natriuretic peptide antagonist for ANPA receptors in the human neuroblastoma NB-OK-1 cell line. Eur J Pharmacol *224*, 183-188.

Di Fusco, F., Hashim, S., and Anand-Srivastava, M.B. (2000). Volume overload cardiac hypertrophy exhibits decreased expression of g(s)alpha and not of g(i)alpha in heart. Am J Physiol Cell Physiol *279*, C990-998.

Dorn, G.W., 2nd, Robbins, J., and Sugden, P.H. (2003). Phenotyping hypertrophy: eschew obfuscation. Circ Res *92*, 1171-1175.

Doupnik, C.A., Xu, T., and Shinaman, J.M. (2001). Profile of RGS expression in single rat atrial myocytes. Biochim Biophys Acta *1522*, 97-107.

Drewett, J.G., and Garbers, D.L. (1994). The family of guanylyl cyclase receptors and their ligands. Endocr Rev *15*, 135-162.

Durocher, D., Chen, C.Y., Ardati, A., Schwartz, R.J., and Nemer, M. (1996). The atrial natriuretic factor promoter is a downstream target for Nkx-2.5 in the myocardium. Mol Cell Biol *16*, 4648-4655.

Durocher, D., and Nemer, M. (1998). Combinatorial interactions regulating cardiac transcription. Dev Genet *22*, 250-262.

Dykxhoorn, D.M., Novina, C.D., and Sharp, P.A. (2003). Killing the messenger: short RNAs that silence gene expression. Nat Rev Mol Cell Biol *4*, 457-467.

Edwards, B.S., Schwab, T.R., Zimmerman, R.S., Heublein, D.M., Jiang, N.S., and Burnett, J.C., Jr. (1986). Cardiovascular, renal, and endocrine response to atrial natriuretic peptide in angiotensin II mediated hypertension. Circ Res *59*, 663-667.

Eid, H., de Bold, M.L., Chen, J.H., and de Bold, A.J. (1994). Epicardial mesothelial cells synthesize and release endothelin. J Cardiovasc Pharmacol *24*, 715-720.

Ellinghaus, P., Scheubel, R.J., Dobrev, D., Ravens, U., Holtz, J., Huetter, J., Nielsch, U., and Morawietz, H. (2005). Comparing the global mRNA expression profile of human atrial and ventricular myocardium with high-density oligonucleotide arrays. J Thorac Cardiovasc Surg *129*, 1383-1390.

Enyeart, J.A., Danthi, S.J., and Enyeart, J.J. (2004). TREK-1 K+ channels couple angiotensin II receptors to membrane depolarization and aldosterone secretion in bovine adrenal glomerulosa cells. Am J Physiol Endocrinol Metab *287*, E1154-1165.

Erb, L., Liu, J., Ockerhausen, J., Kong, Q., Garrad, R.C., Griffin, K., Neal, C., Krugh, B., Santiago-Perez, L.I., Gonzalez, F.A., *et al.* (2001). An RGD sequence in the P2Y(2) receptor interacts with alpha(V)beta(3) integrins and is required for G(o)-mediated signal transduction. J Cell Biol *153*, 491-501.

Erdos, E.G., and Skidgel, R.A. (1989). Neutral endopeptidase 24.11 (enkephalinase) and related regulators of peptide hormones. FASEB J *3*, 145-151.

Erickson, J.D., Eiden, L.E., Schafer, M.K., and Weihe, E. (1995). Reserpine- and tetrabenazine-sensitive transport of (3)H-histamine by the neuronal isoform of the vesicular monoamine transporter. J Mol Neurosci *6*, 277-287.

Evans, S.M., Yelon, D., Conlon, F.L., and Kirby, M.L. (2010). Myocardial lineage development. Circ Res *107*, 1428-1444.

Feil, R., Lohmann, S.M., de Jonge, H., Walter, U., and Hofmann, F. (2003). Cyclic GMP-dependent protein kinases and the cardiovascular system: insights from genetically modified mice. Circ Res *93*, 907-916.

Fernandez, B., Kampmann, A., Pipp, F., Zimmermann, R., and Schaper, W. (2003). Osteoglycin expression and localization in rabbit tissues and atherosclerotic plaques. Mol Cell Biochem *246*, 3-11.

Ferrans, V.J. (1982). Human cardiac hypertrophy: structural aspects. Eur Heart J *3 Suppl A*, 15-27.

Fiarresga, A., Galrinho, A., Sousa, L., Cunha, J., Andrade, J., da Cruz, A.G., and Quininha, J. (2005). Cardiac extension of renal cell carcinoma. Rev Port Cardiol *24*, 997-1003.

Field, L.J. (1988). Atrial natriuretic factor-SV40 T antigen transgenes produce tumors and cardiac arrhythmias in mice. Science *239*, 1029-1033.

Figueroa, C., Taylor, J., and Vojtek, A.B. (2001). Prenylated Rab acceptor protein is a receptor for prenylated small GTPases. J Biol Chem *276*, 28219-28225.

Fire, A., Xu, S., Montgomery, M.K., Kostas, S.A., Driver, S.E., and Mello, C.C. (1998). Potent and specific genetic interference by double-stranded RNA in Caenorhabditis elegans. Nature *391*, 806-811.

Fischer, A., Klattig, J., Kneitz, B., Diez, H., Maier, M., Holtmann, B., Englert, C., and Gessler, M. (2005). Hey basic helix-loop-helix transcription factors are repressors of GATA4 and GATA6 and restrict expression of the GATA target gene ANF in fetal hearts. Mol Cell Biol *25*, 8960-8970.

Flaim, S.F., Minteer, W.J., and Zelis, R. (1980). Acute effects of arterio-venous shunt on cardiovascular hemodynamics in rat. Pflugers Arch *385*, 203-209.

Fluckiger, J.P., Waeber, B., Matsueda, G., Delaloye, B., Nussberger, J., and Brunner, H.R. (1986). Effect of atriopeptin III on hematocrit and volemia of nephrectomized rats. Am J Physiol *251*, H880-883.

Flynn, T.G., Davies, P.L., Kennedy, B.P., de Bold, M.L., and de Bold, A.J. (1985). Alignment of rat cardionatrin sequences with the preprocardionatrin sequence from complementary DNA. Science *228*, 323-325.

Flynn, T.G., de Bold, M.L., and de Bold, A.J. (1983). The amino acid sequence of an atrial peptide with potent diuretic and natriuretic properties. Biochem Biophys Res Commun *117*, 859-865.

Fodor, S.P., Read, J.L., Pirrung, M.C., Stryer, L., Lu, A.T., and Solas, D. (1991). Light-directed, spatially addressable parallel chemical synthesis. Science *251*, 767-773.

Franco-Saenz, R., Atarashi, K., Takagi, M., and Mulrow, P.J. (1989). Effect of atrial natriuretic factor on renin and aldosterone. J Cardiovasc Pharmacol *13 Suppl 6*, S31-35.

Frazier, W.A., Gao, A.G., Dimitry, J., Chung, J., Brown, E.J., Lindberg, F.P., and Linder, M.E. (1999). The thrombospondin receptor integrin-associated protein (CD47) functionally couples to heterotrimeric Gi. J Biol Chem *274*, 8554-8560.

Friday, R.P., Pietropaolo, S.L., Profozich, J., Trucco, M., and Pietropaolo, M. (2003). Alternative core promoters regulate tissue-specific transcription from the autoimmune diabetes-related ICA1 (ICA69) gene locus. J Biol Chem *278*, 853-863.

Froldi, G., Galzignato, G., Zanetti, M., Montopoli, M., Dorigo, P., and Caparrotta, L. (2005). Are prostanoids related to positive inotropism by UTP and ATP? Pharmacology *73*, 140-145.

Fukuda, Y., Hirata, Y., Taketani, S., Kojima, T., Oikawa, S., Nakazato, H., and Kobayashi, Y. (1989). Endothelin stimulates accumulations of cellular atrial natriuretic peptide and its messenger RNA in rat cardiocytes. Biochem Biophys Res Commun *164*, 1431-1436.

Fuller, F., Porter, J.G., Arfsten, A.E., Miller, J., Schilling, J.W., Scarborough, R.M., Lewicki, J.A., and Schenk, D.B. (1988). Atrial natriuretic peptide clearance receptor. Complete sequence and functional expression of cDNA clones. J Biol Chem *263*, 9395-9401.

Gambaryan, S., Wagner, C., Smolenski, A., Walter, U., Poller, W., Haase, W., Kurtz, A., and Lohmann, S.M. (1998). Endogenous or overexpressed cGMP-dependent protein kinases inhibit cAMP-dependent renin release from rat isolated perfused kidney, microdissected glomeruli, and isolated juxtaglomerular cells. Proc Natl Acad Sci U S A *95*, 9003-9008.

Garcia, R., and Diebold, S. (1990). Simple, rapid, and effective method of producing aortocaval shunts in the rat. Cardiovasc Res *24*, 430-432.

Garcia-Sainz, J.A., Macias-Silva, M., and Romero-Avila, M.T. (1991). Effect of okadaic acid on hormone- and mastoparan-stimulated phosphoinositide turnover in isolated rat hepatocytes. Biochem Biophys Res Commun *179*, 852-858.

Gardner, D.G., Deschepper, C.F., and Baxter, J.D. (1987a). The gene for the atrial natriuretic factor is expressed in the aortic arch. Hypertension *9*, 103-106.

Gardner, D.G., Deschepper, C.F., Ganong, W.F., Hane, S., Fiddes, J., Baxter, J.D., and Lewicki, J. (1986a). Extra-atrial expression of the gene for atrial natriuretic factor. Proc Natl Acad Sci U S A *83*, 6697-6701.

Gardner, D.G., Gertz, B.J., Deschepper, C.F., and Kim, D.Y. (1988). Gene for the rat atrial natriuretic peptide is regulated by glucocorticoids in vitro. J Clin Invest *82*, 1275-1281.

Gardner, D.G., Gertz, B.J., and Hane, S. (1987b). Thyroid hormone increases rat atrial natriuretic peptide messenger ribonucleic acid accumulation in vivo and in vitro. Mol Endocrinol *1*, 260-265.

Gardner, D.G., Hane, S., Trachewsky, D., Schenk, D., and Baxter, J.D. (1986b). Atrial natriuretic peptide mRNA is regulated by glucocorticoids in vivo. Biochem Biophys Res Commun *139*, 1047-1054.

Gardner, D.G., Newman, E.D., Nakamura, K.K., and Nguyen, K.P. (1991). Endothelin increases the synthesis and secretion of atrial natriuretic peptide in neonatal rat cardiocytes. Am J Physiol *261*, E177-182.

Gardner, D.G., and Schultz, H.D. (1990). Prostaglandins regulate the synthesis and secretion of the atrial natriuretic peptide. J Clin Invest *86*, 52-59.

Gardner, D.G., Vlasuk, G.P., Baxter, J.D., Fiddes, J.C., and Lewicki, J.A. (1987c). Identification of atrial natriuretic factor gene transcripts in the central nervous system of the rat. Proc Natl Acad Sci U S A *84*, 2175-2179.

Gasman, S., Chasserot-Golaz, S., Hubert, P., Aunis, D., and Bader, M.F. (1998). Identification of a potential effector pathway for the trimeric Go protein associated with secretory granules. Go stimulates a granule-bound phosphatidylinositol 4-kinase by activating RhoA in chromaffin cells. J Biol Chem *273*, 16913-16920.

GEO. Gene Expression Omnibus.

Gerachshenko, T., Blackmer, T., Yoon, E.J., Bartleson, C., Hamm, H.E., and Alford, S. (2005). Gbetagamma acts at the C terminus of SNAP-25 to mediate presynaptic inhibition. Nat Neurosci *8*, 597-605.

Gerzer, R., Witzgall, H., Tremblay, J., Gutkowska, J., and Hamet, P. (1985). Rapid increase in plasma and urinary cyclic GMP after bolus injection of atrial natriuretic factor in man. J Clin Endocrinol Metab *61*, 1217-1219.

Ghil, S., Choi, J.M., Kim, S.S., Lee, Y.D., Liao, Y., Birnbaumer, L., and Suh-Kim, H. (2006). Compartmentalization of protein kinase A signaling by the heterotrimeric G protein Go. Proc Natl Acad Sci U S A *103*, 19158-19163.

Gillingham, A.K., and Munro, S. (2003). Long coiled-coil proteins and membrane traffic. Biochim Biophys Acta *1641*, 71-85.

Gillingham, A.K., and Munro, S. (2007). The small G proteins of the Arf family and their regulators. Annu Rev Cell Dev Biol *23*, 579-611.

Glenn, D.J., Wang, F., Chen, S., Nishimoto, M., and Gardner, D.G. (2009). Endothelin-stimulated human B-type natriuretic peptide gene expression is mediated by Yin Yang 1 in association with histone deacetylase 2. Hypertension *53*, 549-555.

Goutebroze, L., Brault, E., Muchardt, C., Camonis, J., and Thomas, G. (2000). Cloning and characterization of SCHIP-1, a novel protein interacting specifically with spliced isoforms and naturally occurring mutant NF2 proteins. Mol Cell Biol *20*, 1699-1712.

Graham, T.E., Key, T.A., Kilpatrick, K., and Dorin, R.I. (2001). Dexras1/AGS-1, a steroid hormone-induced guanosine triphosphate-binding protein, inhibits 3',5'-cyclic adenosine monophosphate-stimulated secretion in AtT-20 corticotroph cells. Endocrinology *142*, 2631-2640.

Graham, T.E., Prossnitz, E.R., and Dorin, R.I. (2002). Dexras1/AGS-1 inhibits signal transduction from the Gi-coupled formyl peptide receptor to Erk-1/2 MAP kinases. J Biol Chem *277*, 10876-10882.

Graham, T.E., Qiao, Z., and Dorin, R.I. (2004). Dexras1 inhibits adenylyl cyclase. Biochem Biophys Res Commun *316*, 307-312.

Green, J.M., Zhelesnyak, A., Chung, J., Lindberg, F.P., Sarfati, M., Frazier, W.A., and Brown, E.J. (1999). Role of cholesterol in formation and function of a signaling complex involving alphavbeta3, integrin-associated protein (CD47), and heterotrimeric G proteins. J Cell Biol *146*, 673-682.

Greenwald, J.E., Apkon, M., Hruska, K.A., and Needleman, P. (1989). Stretch-induced atriopeptin secretion in the isolated rat myocyte and its negative modulation by calcium. J Clin Invest *83*, 1061-1065.

Grekin, R.J., Ling, W.D., Shenker, Y., and Bohr, D.F. (1986). Immunoreactive atrial natriuretic hormone levels increase in deoxycorticosterone acetate-treated pigs. Hypertension *8*, II16-20.

Grepin, C., Dagnino, L., Robitaille, L., Haberstroh, L., Antakly, T., and Nemer, M. (1994). A hormone-encoding gene identifies a pathway for cardiac but not skeletal muscle gene transcription. Mol Cell Biol *14*, 3115-3129.

Grosshans, B.L., Ortiz, D., and Novick, P. (2006). Rabs and their effectors: achieving specificity in membrane traffic. Proc Natl Acad Sci U S A *103*, 11821-11827.

Grossman, W., Jones, D., and McLaurin, L.P. (1975). Wall stress and patterns of hypertrophy in the human left ventricle. J Clin Invest *56*, 56-64.

Grote, K., Bavendiek, U., Grothusen, C., Flach, I., Hilfiker-Kleiner, D., Drexler, H., and Schieffer, B. (2004). Stretch-inducible expression of the angiogenic factor CCN1 in vascular smooth muscle cells is mediated by Egr-1. J Biol Chem *279*, 55675-55681.

Gruber, A.R., Lorenz, R., Bernhart, S.H., Neubock, R., and Hofacker, I.L. (2008). The Vienna RNA websuite. Nucleic Acids Res *36*, W70-74.

Gudermann, T., Schoneberg, T., and Schultz, G. (1997). Functional and structural complexity of signal transduction via G-protein-coupled receptors. Annu Rev Neurosci *20*, 399-427.

Habets, P.E., Moorman, A.F., Clout, D.E., van Roon, M.A., Lingbeek, M., van Lohuizen, M., Campione, M., and Christoffels, V.M. (2002). Cooperative action of Tbx2 and Nkx2.5 inhibits ANF expression in the atrioventricular canal: implications for cardiac chamber formation. Genes Dev *16*, 1234-1246.

Haddad, G.E., Blackwell, K., and Bikhazi, A. (2003). Regulation of insulin-like growth factor-1 by the renin-angiotensin system during regression of cardiac eccentric hypertrophy through angiotensin-converting enzyme inhibitor and AT1 antagonist. Can J Physiol Pharmacol *81*, 142-149.

Haddad, G.E., Coleman, B.R., Zhao, A., and Blackwell, K.N. (2005). Regulation of atrial contraction by PKA and PKC during development and regression of eccentric cardiac hypertrophy. Am J Physiol Heart Circ Physiol *288*, H695-704.

Halban, P.A., and Wollheim, C.B. (1980). Intracellular degradation of insulin stores by rat pancreatic islets in vitro. An alternative pathway for homeostasis of pancreatic insulin content. J Biol Chem *255*, 6003-6006.

Hall, J.E., Granger, J.P., Smith, M.J., Jr., and Premen, A.J. (1984). Role of renal hemodynamics and arterial pressure in aldosterone "escape". Hypertension *6*, I183-192.

Hama, N., Itoh, H., Shirakami, G., Nakagawa, O., Suga, S., Ogawa, Y., Masuda, I., Nakanishi, K., Yoshimasa, T., Hashimoto, Y.*, et al.* (1995). Rapid ventricular induction of brain natriuretic peptide gene expression in experimental acute myocardial infarction. Circulation *92*, 1558-1564.

Hammond, S.M., Boettcher, S., Caudy, A.A., Kobayashi, R., and Hannon, G.J. (2001). Argonaute2, a link between genetic and biochemical analyses of RNAi. Science *293*, 1146-1150.

Han, L., Suda, M., Tsuzuki, K., Wang, R., Ohe, Y., Hirai, H., Watanabe, T., Takeuchi, T., and Hosaka, M. (2008). A large form of secretogranin III functions as a sorting receptor for chromogranin A aggregates in PC12 cells. Mol Endocrinol *22*, 1935-1949.

Harris, P.J., Thomas, D., and Morgan, T.O. (1987). Atrial natriuretic peptide inhibits angiotensin-stimulated proximal tubular sodium and water reabsorption. Nature *326*, 697-698.

Heller, M.J. (2002). DNA microarray technology: devices, systems, and applications. Annu Rev Biomed Eng *4*, 129-153.

Hernandez, O.M., Jones, M., Guzman, G., and Szczesna-Cordary, D. (2007). Myosin essential light chain in health and disease. Am J Physiol Heart Circ Physiol *292*, H1643-1654.

Hibbs, R.G., and Ferrans, V.J. (1969). An ultrastructural and histochemical study of rat atrial myocardium. Am J Anat *124*, 251-270.

Higashijima, T., Burnier, J., and Ross, E.M. (1990). Regulation of Gi and Go by mastoparan, related amphiphilic peptides, and hydrophobic amines. Mechanism and structural determinants of activity. J Biol Chem *265*, 14176-14186.

Higashijima, T., and Ross, E.M. (1991). Mapping of the mastoparan-binding site on G proteins. Cross-linking of [125I-Tyr3,Cys11]mastoparan to Go. J Biol Chem *266*, 12655-12661.

Higgins, J.B., and Casey, P.J. (1996). The role of prenylation in G-protein assembly and function. Cell Signal *8*, 433-437.

Higgins, J.T., Jr. (1970). Escape from sodium-retaining effects of deoxycorticosterone in hypotensive and hypertensive dogs. Proc Soc Exp Biol Med *134*, 768-772.

Hilfiker-Kleiner, D., Hilfiker, A., Castellazzi, M., Wollert, K.C., Trautwein, C., Schunkert, H., and Drexler, H. (2006). JunD attenuates phenylephrine-mediated cardiomyocyte hypertrophy by negatively regulating AP-1 transcriptional activity. Cardiovasc Res *71*, 108-117.

Hill, O., Kuhn, M., Zucht, H.D., Cetin, Y., Kulaksiz, H., Adermann, K., Klock, G., Rechkemmer, G., Forssmann, W.G., and Magert, H.J. (1995). Analysis of the human guanylin gene and the processing and cellular localization of the peptide. Proc Natl Acad Sci U S A *92*, 2046-2050.

Hille, B. (1994). Modulation of ion-channel function by G-protein-coupled receptors. Trends Neurosci *17*, 531-536.

Hinners, I., Wendler, F., Fei, H., Thomas, L., Thomas, G., and Tooze, S.A. (2003). AP-1 recruitment to VAMP4 is modulated by phosphorylation-dependent binding of PACS-1. EMBO Rep *4*, 1182-1189.

Hirano, S., Imamura, T., Matsuo, T., Ishiyama, Y., Kato, J., Kitamura, K., Koiwaya, Y., and Eto, T. (2000). Differential responses of circulating and tissue adrenomedullin and gene expression to volume overload. J Card Fail *6*, 120-129.

Hirata, Y., Takata, S., Kawahara, Y., Takai, Y., Chino, N., Kimura, T., and Sakakibara, S. (1988). Molecular mechanism of action by atrial natriuretic peptide in rat vascular smooth muscle cells. Jpn Circ J *52*, 1430-1435.

Hiroi, Y., Kudoh, S., Monzen, K., Ikeda, Y., Yazaki, Y., Nagai, R., and Komuro, I. (2001). Tbx5 associates with Nkx2-5 and synergistically promotes cardiomyocyte differentiation. Nat Genet *28*, 276-280.

Hirose, S., Hagiwara, H., and Takei, Y. (2001). Comparative molecular biology of natriuretic peptide receptors. Can J Physiol Pharmacol *79*, 665-672.

Hiskens, R., Vatish, M., Hill, C., Davey, J., and Ladds, G. (2005). Specific in vivo binding of activator of G protein signalling 1 to the Gbeta1 subunit. Biochem Biophys Res Commun *337*, 1038-1046.

Hoffman, A., Burnett, J.C., Jr., Haramati, A., and Winaver, J. (1988). Effects of atrial natriuretic factor in rats with experimental high-output heart failure. Kidney Int *33*, 656-661.

Hoffman, A., Grossman, E., and Keiser, H.R. (1991). Increased plasma levels and blunted effects of brain natriuretic peptide in rats with congestive heart failure. Am J Hypertens *4*, 597-601.

Hoffman, A., Winaver, J., and Haramati, A. (1990). Atrial natriuretic peptide in the recovery from high-output congestive heart failure. Am J Med *88*, 547.

Hohl, T.M., Parlati, F., Wimmer, C., Rothman, J.E., Sollner, T.H., and Engelhardt, H. (1998). Arrangement of subunits in 20 S particles consisting of NSF, SNAPs, and SNARE complexes. Mol Cell *2*, 539-548.

Holen, T., Amarzguioui, M., Wiiger, M.T., Babaie, E., and Prydz, H. (2002). Positional effects of short interfering RNAs targeting the human coagulation trigger Tissue Factor. Nucleic Acids Res *30*, 1757-1766.

Holmes, S.J., Espiner, E.A., Richards, A.M., Yandle, T.G., and Frampton, C. (1993). Renal, endocrine, and hemodynamic effects of human brain natriuretic peptide in normal man. J Clin Endocrinol Metab *76*, 91-96.

Holtwick, R., Gotthardt, M., Skryabin, B., Steinmetz, M., Potthast, R., Zetsche, B., Hammer, R.E., Herz, J., and Kuhn, M. (2002). Smooth muscle-selective deletion of guanylyl cyclase-A prevents the acute but not chronic effects of ANP on blood pressure. Proc Natl Acad Sci U S A *99*, 7142-7147.

Holtwick, R., van Eickels, M., Skryabin, B.V., Baba, H.A., Bubikat, A., Begrow, F., Schneider, M.D., Garbers, D.L., and Kuhn, M. (2003). Pressure-independent cardiac hypertrophy in mice with cardiomyocyte-restricted inactivation of the atrial natriuretic peptide receptor guanylyl cyclase-A. J Clin Invest *111*, 1399-1407.

Holz, G.G.t., Rane, S.G., and Dunlap, K. (1986). GTP-binding proteins mediate transmitter inhibition of voltage-dependent calcium channels. Nature *319*, 670-672.

Hong, W. (2005). SNAREs and traffic. Biochim Biophys Acta *1744*, 493-517.

Hooper, J.D., Scarman, A.L., Clarke, B.E., Normyle, J.F., and Antalis, T.M. (2000). Localization of the mosaic transmembrane serine protease corin to heart myocytes. Eur J Biochem *267*, 6931-6937.

Horio, T., Nishikimi, T., Yoshihara, F., Matsuo, H., Takishita, S., and Kangawa, K. (2000). Inhibitory regulation of hypertrophy by endogenous atrial natriuretic peptide in cultured cardiac myocytes. Hypertension *35*, 19-24.

Hosaka, M., Watanabe, T., Sakai, Y., Kato, T., and Takeuchi, T. (2005). Interaction between secretogranin III and carboxypeptidase E facilitates prohormone sorting within secretory granules. J Cell Sci *118*, 4785-4795.

Hu, C., Ahmed, M., Melia, T.J., Sollner, T.H., Mayer, T., and Rothman, J.E. (2003). Fusion of cells by flipped SNAREs. Science *300*, 1745-1749.

Hughes, W.E., Elgundi, Z., Huang, P., Frohman, M.A., and Biden, T.J. (2004). Phospholipase D1 regulates secretagogue-stimulated insulin release in pancreatic beta-cells. J Biol Chem *279*, 27534-27541.

Iida, H., Barron, W.M., and Page, E. (1988). Monensin turns on microtubule-associated translocation of secretory granules in cultured rat atrial myocytes. Circ Res *62*, 1159-1170.

Iida, H., and Page, E. (1989). Determinants of atrial natriuretic peptide secretion in cultured atrial myocytes. Am J Physiol *256*, C608-613.

Iida, H., and Shibata, Y. (1994). Phasic secretion of newly synthesized atrial natriuretic factor from unstimulated atrial myocytes in culture. Circ Res *74*, 659-668.

Imada, T., Takayanagi, R., and Inagami, T. (1988). Atrioactivase, a specific peptidase in bovine atria for the processing of pro-atrial natriuretic factor. Purification and characterization. J Biol Chem *263*, 9515-9519.

Iniguez-Lluhi, J.A., Simon, M.I., Robishaw, J.D., and Gilman, A.G. (1992). G protein beta gamma subunits synthesized in Sf9 cells. Functional characterization and the significance of prenylation of gamma. J Biol Chem *267*, 23409-23417.

Inoue, M., Kimura, T., Ota, K., Iitake, K., Shoji, M., Sato, K., Ota, M., and Yoshinaga, K. (1988). Effect of vasopressin on atrial natriuretic peptide release and renal function in dogs. Am J Physiol *255*, E449-455.

Irizarry, R.A., Bolstad, B.M., Collin, F., Cope, L.M., Hobbs, B., and Speed, T.P. (2003a). Summaries of Affymetrix GeneChip probe level data. Nucleic Acids Res *31*, e15.

Irizarry, R.A., Hobbs, B., Collin, F., Beazer-Barclay, Y.D., Antonellis, K.J., Scherf, U., and Speed, T.P. (2003b). Exploration, normalization, and summaries of high density oligonucleotide array probe level data. Biostatistics *4*, 249-264.

Irons, C.E., Sei, C.A., and Glembotski, C.C. (1993). Regulated secretion of atrial natriuretic factor from cultured ventricular myocytes. Am J Physiol *264*, H282-285.

Ito, H., Hiroe, M., Hirata, Y., Fujisaki, H., Adachi, S., Akimoto, H., Ohta, Y., and Marumo, F. (1994). Endothelin ETA receptor antagonist blocks cardiac hypertrophy provoked by hemodynamic overload. Circulation *89*, 2198-2203.

Itoh, H., Pratt, R.E., and Dzau, V.J. (1991). Interaction of atrial natriuretic polypeptide and angiotensin II on protooncogene expression and vascular cell growth. Biochem Biophys Res Commun *176*, 1601-1609.

Jamieson, J.D., and Palade, G.E. (1964). Specific Granules in Atrial Muscle Cells. J Cell Biol *23*, 151-172.

Januszewicz, A., Pegram, B.L., Macphee, A.A., Cole, F.E., Kardon, M.B., and Trippodo, N.C. (1987). Vasorelaxant and natriuretic activities of synthetic atrial peptides. Acta Physiol Pol *38*, 467-476.

Jarvis, S.E., Barr, W., Feng, Z.P., Hamid, J., and Zamponi, G.W. (2002). Molecular determinants of syntaxin 1 modulation of N-type calcium channels. J Biol Chem *277*, 44399-44407.

Jeng, Y.J., Soloff, S.L., Anderson, G.D., and Soloff, M.S. (2003). Regulation of oxytocin receptor expression in cultured human myometrial cells by fetal bovine serum and lysophospholipids. Endocrinology *144*, 61-68.

Ji, S., John, S.A., Lu, Y., and Weiss, J.N. (1998). Mechanosensitivity of the cardiac muscarinic potassium channel. A novel property conferred by Kir3.4 subunit. J Biol Chem *273*, 1324-1328.

Jiao, J.H., Baumann, P., Baron, A., Roatti, A., Pence, R.A., and Baertschi, A.J. (2000). Sulfonylurea receptor ligands modulate stretch-induced ANF secretion in rat atrial myocyte culture. Am J Physiol Heart Circ Physiol *278*, H2028-2038.

Jin, H., Yang, R.H., Calhoun, D.A., Wyss, J.M., and Oparil, S. (1992). Atrial natriuretic peptide modulates baroreceptor reflex in spontaneously hypertensive rat. Hypertension *20*, 374-379.

John, S.W., Krege, J.H., Oliver, P.M., Hagaman, J.R., Hodgin, J.B., Pang, S.C., Flynn, T.G., and Smithies, O. (1995). Genetic decreases in atrial natriuretic peptide and salt-sensitive hypertension. Science *267*, 679-681.

Jones, M., and Ferrans, V.J. (1979). Myocardial ultrastructure in children and adults with congenital heart disease. Cardiovasc Clin *10*, 501-530.

Jones, P.M., Mann, F.M., Persaud, S.J., and Wheeler-Jones, C.P. (1993). Mastoparan stimulates insulin secretion from pancreatic beta-cells by effects at a late stage in the secretory pathway. Mol Cell Endocrinol *94*, 97-103.

Kangawa, K., Tawaragi, Y., Oikawa, S., Mizuno, A., Sakuragawa, Y., Nakazato, H., Fukuda, A., Minamino, N., and Matsuo, H. (1984). Identification of rat gamma atrial natriuretic polypeptide and characterization of the cDNA encoding its precursor. Nature *312*, 152-155.

Kapoun, A.M., Liang, F., O'Young, G., Damm, D.L., Quon, D., White, R.T., Munson, K., Lam, A., Schreiner, G.F., and Protter, A.A. (2004). B-type natriuretic peptide exerts broad functional opposition to transforming growth factor-beta in primary human cardiac fibroblasts: fibrosis, myofibroblast conversion, proliferation, and inflammation. Circ Res *94*, 453-461.

Kardestuncer, T., Wu, H., Lim, A.L., and Neer, E.J. (1998). Cardiac myocytes express mRNA for ten RGS proteins: changes in RGS mRNA expression in ventricular myocytes and cultured atria. FEBS Lett *438*, 285-288.

Karram, T., Abbasi, A., Keidar, S., Golomb, E., Hochberg, I., Winaver, J., Hoffman, A., and Abassi, Z. (2005). Effects of spironolactone and eprosartan on cardiac remodeling and angiotensin-converting enzyme isoforms in rats with experimental heart failure. Am J Physiol Heart Circ Physiol *289*, H1351-1358.

Kashiwagi, M., Katafuchi, T., Kato, A., Inuyama, H., Ito, T., Hagiwara, H., Takei, Y., and Hirose, S. (1995). Cloning and properties of a novel natriuretic peptide receptor, NPR-D. Eur J Biochem *233*, 102-109.

Katoh, S., Toyama, J., Aoyama, M., Miyamoto, N., Seo, H., Matsui, N., Kodama, I., and Yamada, K. (1990). Mechanisms of atrial natriuretic peptide (ANP) secretion by rat hearts perfused in vitro--Ca2(+)-dependent signal transduction for ANP release by mechanical stretch. Jpn Circ J *54*, 1283-1294.

Katsube, N., Schwartz, D., and Needleman, P. (1985). Release of atriopeptin in the rat by vasoconstrictors or water immersion correlates with changes in right atrial pressure. Biochem Biophys Res Commun *133*, 937-944.

Katz, A.M. (2001). Physiology of the heart. 3rd edition (Philadelphia, PA, Lippincott Williams & Wilkins).

Katz, A.M., and Katz, P.B. (1989). Homogeneity out of heterogeneity. Circulation *79*, 712-717.

Kelley, G.G., Kaproth-Joslin, K.A., Reks, S.E., Smrcka, A.V., and Wojcikiewicz, R.J. (2006). G-protein-coupled receptor agonists activate endogenous phospholipase Cepsilon and phospholipase Cbeta3 in a temporally distinct manner. J Biol Chem *281*, 2639-2648.

Kelly, R.B. (1985). Pathways of protein secretion in eukaryotes. Science *230*, 25-32.

Kemppainen, R.J., and Behrend, E.N. (1998). Dexamethasone rapidly induces a novel ras superfamily member-related gene in AtT-20 cells. J Biol Chem *273*, 3129-3131.

Kim, D.H., Behlke, M.A., Rose, S.D., Chang, M.S., Choi, S., and Rossi, J.J. (2005). Synthetic dsRNA Dicer substrates enhance RNAi potency and efficacy. Nat Biotechnol *23*, 222-226.

Kim, J.H., Lee, S.D., Han, J.M., Lee, T.G., Kim, Y., Park, J.B., Lambeth, J.D., Suh, P.G., and Ryu, S.H. (1998). Activation of phospholipase D1 by direct interaction with ADP-ribosylation factor 1 and RalA. FEBS Lett *430*, 231-235.

Kim, S.H., Cho, K.W., Chang, S.H., Kim, S.Z., and Chae, S.W. (1997). Glibenclamide suppresses stretch-activated ANP secretion: involvements of K+ATP channels and L-type Ca2+ channel modulation. Pflugers Arch *434*, 362-372.

Kisch, B. (1963). A Sginificant Electron Microscopic Difference between the Atria and the Ventricles of the Mammalian Heart. Exp Med Surg *21*, 193-221.

Kishimoto, I., Dubois, S.K., and Garbers, D.L. (1996). The heart communicates with the kidney exclusively through the guanylyl cyclase-A receptor: acute handling of sodium and water in response to volume expansion. Proc Natl Acad Sci U S A *93*, 6215-6219.

Knowles, J.W., Esposito, G., Mao, L., Hagaman, J.R., Fox, J.E., Smithies, O., Rockman, H.A., and Maeda, N. (2001). Pressure-independent enhancement of cardiac hypertrophy in natriuretic peptide receptor A-deficient mice. J Clin Invest *107*, 975-984.

Knowlton, K.U., Baracchini, E., Ross, R.S., Harris, A.N., Henderson, S.A., Evans, S.M., Glembotski, C.C., and Chien, K.R. (1991). Co-regulation of the atrial natriuretic factor and cardiac myosin light chain-2 genes during alpha-adrenergic stimulation of neonatal rat ventricular cells. Identification of cis sequences within an embryonic and a constitutive contractile protein gene which mediate inducible expression. J Biol Chem *266*, 7759-7768.

Kobayashi, I., Shibasaki, H., Takahashi, K., Tohyama, K., Kurachi, Y., Ito, H., Ui, M., and Katada, T. (1990). Purification and characterization of five different alpha subunits of guanine-nucleotide-binding proteins in bovine brain membranes. Their physiological properties concerning the activities of adenylate cyclase and atrial muscarinic K+ channels. Eur J Biochem *191*, 499-506.

Koch, G., Haberman, B., Mohr, C., Just, I., and Aktories, K. (1991). Interaction of mastoparan with the low molecular mass GTP-binding proteins rho/rac. FEBS Lett *291*, 336-340.

Kohno, M., Horio, T., Yasunari, K., Yokokawa, K., Ikeda, M., Kurihara, N., Nishizawa, Y., Morii, H., and Takeda, T. (1993). Stimulation of brain natriuretic peptide release from the heart by thyroid hormone. Metabolism *42*, 1059-1064.

Kojic, S., Nestorovic, A., Rakicevic, L., Belgrano, A., Stankovic, M., Divac, A., and Faulkner, G. (2010). A novel role for cardiac ankyrin repeat protein Ankrd1/CARP as a co-activator of the p53 tumor suppressor protein. Arch Biochem Biophys *502*, 60-67.

Koller, K.J., de Sauvage, F.J., Lowe, D.G., and Goeddel, D.V. (1992). Conservation of the kinaselike regulatory domain is essential for activation of the natriuretic peptide receptor guanylyl cyclases. Mol Cell Biol *12*, 2581-2590.

Koller, K.J., Lipari, M.T., and Goeddel, D.V. (1993). Proper glycosylation and phosphorylation of the type A natriuretic peptide receptor are required for hormone-stimulated guanylyl cyclase activity. J Biol Chem *268*, 5997-6003.

Koller, P.T., Grekin, R.J., and Nicklas, J.M. (1987). Paradoxical response of plasma atrial natriuretic hormone to pericardiocentesis in cardiac tamponade. Am J Cardiol *59*, 491-492.

Konrad, R.J., Young, R.A., Record, R.D., Smith, R.M., Butkerait, P., Manning, D., Jarett, L., and Wolf, B.A. (1995). The heterotrimeric G-protein Gi is localized to the insulin secretory granules of beta-cells and is involved in insulin exocytosis. J Biol Chem *270*, 12869-12876.

Kubalak, S.W., Miller-Hance, W.C., O'Brien, T.X., Dyson, E., and Chien, K.R. (1994). Chamber specification of atrial myosin light chain-2 expression precedes septation during murine cardiogenesis. J Biol Chem *269*, 16961-16970.

Kubo, Y., Adelman, J.P., Clapham, D.E., Jan, L.Y., Karschin, A., Kurachi, Y., Lazdunski, M., Nichols, C.G., Seino, S., and Vandenberg, C.A. (2005). International Union of Pharmacology. LIV. Nomenclature and molecular relationships of inwardly rectifying potassium channels. Pharmacol Rev *57*, 509-526.

Kudo, T., and Baird, A. (1984). Inhibition of aldosterone production in the adrenal glomerulosa by atrial natriuretic factor. Nature *312*, 756-757.

Kuhn, M. (2003). Structure, regulation, and function of mammalian membrane guanylyl cyclase receptors, with a focus on guanylyl cyclase-A. Circ Res *93*, 700-709.

Kuliawat, R., and Arvan, P. (1992). Protein targeting via the "constitutive-like" secretory pathway in isolated pancreatic islets: passive sorting in the immature granule compartment. J Cell Biol *118*, 521-529.

Kumar, R., Grammatikakis, N., and Chinkers, M. (2001). Regulation of the atrial natriuretic peptide receptor by heat shock protein 90 complexes. J Biol Chem *276*, 11371-11375.

Kuo, H., Chen, J., Ruiz-Lozano, P., Zou, Y., Nemer, M., and Chien, K.R. (1999). Control of segmental expression of the cardiac-restricted ankyrin repeat protein gene by distinct regulatory pathways in murine cardiogenesis. Development *126*, 4223-4234.

Kurihara, H., Kitajima, K., Senda, T., Fujita, H., and Nakajima, T. (1986). Multigranular exocytosis induced by phospholipase A2-activators, melittin and mastoparan, in rat anterior pituitary cells. Cell Tissue Res *243*, 311-316.

Kuroski-de Bold, M.L., and de Bold, A.J. (1991). Stretch-secretion coupling in atrial cardiocytes. Dissociation between atrial natriuretic factor release and mechanical activity. Hypertension *18*, III169-178.

Kurtz, A., Della Bruna, R., Pfeilschifter, J., Taugner, R., and Bauer, C. (1986). Atrial natriuretic peptide inhibits renin release from juxtaglomerular cells by a cGMP-mediated process. Proc Natl Acad Sci U S A *83*, 4769-4773.

Kyosseva, S.V. (2004). Mitogen-activated protein kinase signaling. Int Rev Neurobiol *59*, 201-220.

Lainchbury, J.G., Richards, A.M., Nicholls, M.G., Hunt, P.J., Ikram, H., Espiner, E.A., Yandle, T.G., and Begg, E. (1997). The effects of pathophysiological increments in brain natriuretic peptide in left ventricular systolic dysfunction. Hypertension *30*, 398-404.

Lang, C.C., Choy, A.M., Turner, K., Tobin, R., Coutie, W., and Struthers, A.D. (1993). The effect of intravenous saline loading on plasma levels of brain natriuretic peptide in man. J Hypertens *11*, 737-741.

Lang, R.E., Dietz, R., Merkel, A., Unger, T., Ruskoaho, H., and Ganten, D. (1986). Plasma atrial natriuretic peptide values in cardiac disease. J Hypertens Suppl *4*, S119-123.

Lanier, S.M. (2004). AGS proteins, GPR motifs and the signals processed by heterotrimeric G proteins. Biol Cell *96*, 369-372.

LaPointe, M.C., Wu, J.P., Greenberg, B., and Gardner, D.G. (1988). Upstream sequences confer atrial-specific expression on the human atrial natriuretic factor gene. J Biol Chem *263*, 9075-9078.

Lattion, A.L., Michel, J.B., Arnauld, E., Corvol, P., and Soubrier, F. (1986). Myocardial recruitment during ANF mRNA increase with volume overload in the rat. Am J Physiol *251*, H890-896.

Lawrence, D.L., Skatrud, J.B., and Shenker, Y. (1990). Effect of hypoxia on atrial natriuretic factor and aldosterone regulation in humans. Am J Physiol *258*, E243-248.

Lee, H.S., Millward-Sadler, S.J., Wright, M.O., Nuki, G., and Salter, D.M. (2000). Integrin and mechanosensitive ion channel-dependent tyrosine phosphorylation of focal adhesion proteins and beta-catenin in human articular chondrocytes after mechanical stimulation. J Bone Miner Res *15*, 1501-1509.

Lee, M.E., Miller, W.L., Edwards, B.S., and Burnett, J.C., Jr. (1989). Role of endogenous atrial natriuretic factor in acute congestive heart failure. J Clin Invest *84*, 1962-1966.

Lee, R.T., Bloch, K.D., Pfeffer, J.M., Pfeffer, M.A., Neer, E.J., and Seidman, C.E. (1988). Atrial natriuretic factor gene expression in ventricles of rats with spontaneous biventricular hypertrophy. J Clin Invest *81*, 431-434.

Lee, Y.S., Nakahara, K., Pham, J.W., Kim, K., He, Z., Sontheimer, E.J., and Carthew, R.W. (2004). Distinct roles for Drosophila Dicer-1 and Dicer-2 in the siRNA/miRNA silencing pathways. Cell *117*, 69-81.

Leite, M.F., Page, E., and Ambler, S.K. (1994). Regulation of ANP secretion by endothelin-1 in cultured atrial myocytes: desensitization and receptor subtype. Am J Physiol *267*, H2193-2203.

Leskinen, H., Vuolteenaho, O., Leppaluoto, J., and Ruskoaho, H. (1995). Role of nitric oxide on cardiac hormone secretion: effect of NG-nitro-L-arginine methyl ester on atrial natriuretic peptide and brain natriuretic peptide release. Endocrinology *136*, 1241-1249.

Levitzki, A. (1988). From epinephrine to cyclic AMP. Science *241*, 800-806.

Lewicki, J.A., Greenberg, B., Yamanaka, M., Vlasuk, G., Brewer, M., Gardner, D., Baxter, J., Johnson, L.K., and Fiddes, J.C. (1986). Cloning, sequence analysis, and processing of the rat and human atrial natriuretic peptide precursors. Fed Proc *45*, 2086-2090.

LeWinter, M.M. (2005). Functional consequences of sarcomeric protein abnormalities in failing myocardium. Heart Fail Rev *10*, 249-257.

Leyte, A., Barr, F.A., Kehlenbach, R.H., and Huttner, W.B. (1992). Multiple trimeric G-proteins on the trans-Golgi network exert stimulatory and inhibitory effects on secretory vesicle formation. EMBO J *11*, 4795-4804.

Li, Q., and Gardner, D.G. (1994). Negative regulation of the human atrial natriuretic peptide gene by 1,25-dihydroxyvitamin D3. J Biol Chem *269*, 4934-4939.

Light, D.B., Corbin, J.D., and Stanton, B.A. (1990). Dual ion-channel regulation by cyclic GMP and cyclic GMP-dependent protein kinase. Nature *344*, 336-339.

Light, D.B., Schwiebert, E.M., Karlson, K.H., and Stanton, B.A. (1989). Atrial natriuretic peptide inhibits a cation channel in renal inner medullary collecting duct cells. Science *243*, 383-385.

Lincoln, T.M., and Cornwell, T.L. (1993). Intracellular cyclic GMP receptor proteins. FASEB J *7*, 328-338.

Lipshutz, R.J., Fodor, S.P., Gingeras, T.R., and Lockhart, D.J. (1999). High density synthetic oligonucleotide arrays. Nat Genet *21*, 20-24.

Liu, W., and Saint, D.A. (2004). Heterogeneous expression of tandem-pore K+ channel genes in adult and embryonic rat heart quantified by real-time polymerase chain reaction. Clin Exp Pharmacol Physiol *31*, 174-178.

Liu, Y., Schweitzer, E.S., Nirenberg, M.J., Pickel, V.M., Evans, C.J., and Edwards, R.H. (1994). Preferential localization of a vesicular monoamine transporter to dense core vesicles in PC12 cells. J Cell Biol *127*, 1419-1433.

Liu, Z., Hilbelink, D.R., and Gerdes, A.M. (1991). Regional changes in hemodynamics and cardiac myocyte size in rats with aortocaval fistulas. 2. Long-term effects. Circ Res *69*, 59-65.

Lockhart, D.J., Dong, H., Byrne, M.C., Follettie, M.T., Gallo, M.V., Chee, M.S., Mittmann, M., Wang, C., Kobayashi, M., Horton, H.*, et al.* (1996). Expression monitoring by hybridization to high-density oligonucleotide arrays. Nat Biotechnol *14*, 1675-1680.

Lockhart, D.J., and Winzeler, E.A. (2000). Genomics, gene expression and DNA arrays. Nature *405*, 827-836.

Logothetis, D.E., Kurachi, Y., Galper, J., Neer, E.J., and Clapham, D.E. (1987). The beta gamma subunits of GTP-binding proteins activate the muscarinic K+ channel in heart. Nature *325*, 321-326.

Lompre, A.M., Nadal-Ginard, B., and Mahdavi, V. (1984). Expression of the cardiac ventricular alpha- and beta-myosin heavy chain genes is developmentally and hormonally regulated. J Biol Chem *259*, 6437-6446.

Lopez, M.J., Garbers, D.L., and Kuhn, M. (1997). The guanylyl cyclase-deficient mouse defines differential pathways of natriuretic peptide signaling. J Biol Chem *272*, 23064-23068.

Lopez, M.J., Wong, S.K., Kishimoto, I., Dubois, S., Mach, V., Friesen, J., Garbers, D.L., and Beuve, A. (1995). Salt-resistant hypertension in mice lacking the guanylyl cyclase-A receptor for atrial natriuretic peptide. Nature *378*, 65-68.

Lowe, D.G., and Fendly, B.M. (1992). Human natriuretic peptide receptor-A guanylyl cyclase. Hormone cross-linking and antibody reactivity distinguish receptor glycoforms. J Biol Chem *267*, 21691-21697.

Lui-Roberts, W.W., Collinson, L.M., Hewlett, L.J., Michaux, G., and Cutler, D.F. (2005). An AP-1/clathrin coat plays a novel and essential role in forming the Weibel-Palade bodies of endothelial cells. J Cell Biol *170*, 627-636.

Ma, K.K., Ogawa, T., and de Bold, A.J. (2004). Selective upregulation of cardiac brain natriuretic peptide at the transcriptional and translational levels by pro-inflammatory cytokines and by conditioned medium derived from mixed lymphocyte reactions via p38 MAP kinase. J Mol Cell Cardiol *36*, 505-513.

Ma, Y.Y., Qi, X.F., Song, S.J., Zhao, Z.Y., Zhu, Z.D., Qi, J., Zhang, X., Xiao, H.S., Teng, Y., and Han, Z.G. (2005). cDNA microarray reveals signaling pathways involved in hormones expression of human pituitary. Gen Comp Endocrinol *143*, 184-192.

Maack, T. (1996). Role of atrial natriuretic factor in volume control. Kidney Int *49*, 1732-1737.

Maack, T., Marion, D.N., Camargo, M.J., Kleinert, H.D., Laragh, J.H., Vaughan, E.D., Jr., and Atlas, S.A. (1984). Effects of auriculin (atrial natriuretic factor) on blood pressure, renal function, and the renin-aldosterone system in dogs. Am J Med *77*, 1069-1075.

Maack, T., Suzuki, M., Almeida, F.A., Nussenzveig, D., Scarborough, R.M., McEnroe, G.A., and Lewicki, J.A. (1987). Physiological role of silent receptors of atrial natriuretic factor. Science *238*, 675-678.

Maekawa, K., Sudoh, T., Furusawa, M., Minamino, N., Kangawa, K., Ohkubo, H., Nakanishi, S., and Matsuo, H. (1988). Cloning and sequence analysis of cDNA encoding a precursor for porcine brain natriuretic peptide. Biochem Biophys Res Commun *157*, 410-416.

Maki, M., Takayanagi, R., Misono, K.S., Pandey, K.N., Tibbetts, C., and Inagami, T. (1984). Structure of rat atrial natriuretic factor precursor deduced from cDNA sequence. Nature *309*, 722-724.

Mangat, H., and de Bold, A.J. (1993). Stretch-induced atrial natriuretic factor release utilizes a rapidly depleting pool of newly synthesized hormone. Endocrinology *133*, 1398-1403.

Mantymaa, P., Leppaluoto, J., and Ruskoaho, H. (1990). Endothelin stimulates basal and stretch-induced atrial natriuretic peptide secretion from the perfused rat heart. Endocrinology *126*, 587-595.

Marie, J.P., Guillemot, H., and Hatt, P.Y. (1976). [Degree of granularity of the atrial cardiocytes. Morphometric study in rats subjected to different types of water and sodium load (author's transl)]. Pathol Biol (Paris) *24*, 549-554.

Marin-Grez, M., Fleming, J.T., and Steinhausen, M. (1986). Atrial natriuretic peptide causes pre-glomerular vasodilatation and post-glomerular vasoconstriction in rat kidney. Nature *324*, 473-476.

Maron, B.J., and Ferrans, V.J. (1978). Ultrastructural features of hypertrophied human ventricular myocardium. Prog Cardiovasc Dis *21*, 207-238.

Maron, B.J., Ferrans, V.J., and Roberts, W.C. (1975). Ultrastructural features of degenerated cardiac muscle cells in patients with cardiac hypertrophy. Am J Pathol *79*, 387-434.

Marsh, B.J., Soden, C., Alarcon, C., Wicksteed, B.L., Yaekura, K., Costin, A.J., Morgan, G.P., and Rhodes, C.J. (2007). Regulated autophagy controls hormone content in secretory-deficient pancreatic endocrine beta-cells. Mol Endocrinol *21*, 2255-2269.

Martin, S.E., and Caplen, N.J. (2007). Applications of RNA interference in mammalian systems. Annu Rev Genomics Hum Genet *8*, 81-108.

Martincic, I., Peralta, M.E., and Ngsee, J.K. (1997). Isolation and characterization of a dual prenylated Rab and VAMP2 receptor. J Biol Chem *272*, 26991-26998.

Martinez, J., Patkaniowska, A., Urlaub, H., Luhrmann, R., and Tuschl, T. (2002). Single-stranded antisense siRNAs guide target RNA cleavage in RNAi. Cell *110*, 563-574.

Marz, K.E., Lauer, J.M., and Hanson, P.I. (2003). Defining the SNARE complex binding surface of alpha-SNAP: implications for SNARE complex disassembly. J Biol Chem *278*, 27000-27008.

Masters, R.G., Davies, R.A., Veinot, J.P., Hendry, P.J., Smith, S.J., and de Bold, A.J. (1999). Discoordinate modulation of natriuretic peptides during acute cardiac allograft rejection in humans. Circulation *100*, 287-291.

Matsuki, M., Kunitomo, H., and Iino, Y. (2006). Goalpha regulates olfactory adaptation by antagonizing Gqalpha-DAG signaling in Caenorhabditis elegans. Proc Natl Acad Sci U S A *103*, 1112-1117.

Mbikay, M., Seidah, N.G., and Chretien, M. (2001). Neuroendocrine secretory protein 7B2: structure, expression and functions. Biochem J *357*, 329-342.

McBride, K., and Nemer, M. (2001). Regulation of the ANF and BNP promoters by GATA factors: lessons learned for cardiac transcription. Can J Physiol Pharmacol *79*, 673-681.

McClatchey, A.I., and Giovannini, M. (2005). Membrane organization and tumorigenesis--the NF2 tumor suppressor, Merlin. Genes Dev *19*, 2265-2277.

McGrath, M.F., and de Bold, A.J. (2005). Determinants of natriuretic peptide gene expression. Peptides *26*, 933-943.

McGrath, M.F., and de Bold, A.J. (2009). Transcriptional analysis of the mammalian heart with special reference to its endocrine function. BMC Genomics *10*, 254.

McGrath, M.F., de Bold, M.L., and de Bold, A.J. (2005). The endocrine function of the heart. Trends Endocrinol Metab *16*, 469-477.

McKenzie, J.C., Tanaka, I., Inagami, T., Misono, K.S., and Klein, R.M. (1986). Alterations in atrial and plasma atrial natriuretic factor (ANF) content during development of hypoxia-induced pulmonary hypertension in the rat. Proc Soc Exp Biol Med *181*, 459-463.

McMahon, H.T., Missler, M., Li, C., and Sudhof, T.C. (1995). Complexins: cytosolic proteins that regulate SNAP receptor function. Cell *83*, 111-119.

Meilhac, S.M., Esner, M., Kelly, R.G., Nicolas, J.F., and Buckingham, M.E. (2004). The clonal origin of myocardial cells in different regions of the embryonic mouse heart. Dev Cell *6*, 685-698.

Meilhac, S.M., Kelly, R.G., Rocancourt, D., Eloy-Trinquet, S., Nicolas, J.F., and Buckingham, M.E. (2003). A retrospective clonal analysis of the myocardium reveals two phases of clonal growth in the developing mouse heart. Development *130*, 3877-3889.

Melo, L.G., and Sonnenberg, H. (1996). Effect of nitric oxide inhibition on secretion of atrial natriuretic factor in isolated rat heart. Am J Physiol *270*, H306-311.

Melo, L.G., Steinhelper, M.E., Pang, S.C., Tse, Y., and Ackermann, U. (2000). ANP in regulation of arterial pressure and fluid-electrolyte balance: lessons from genetic mouse models. Physiol Genomics *3*, 45-58.

Michener, M.L., Gierse, J.K., Seetharam, R., Fok, K.F., Olins, P.O., Mai, M.S., and Needleman, P. (1986). Proteolytic processing of atriopeptin prohormone. Mol Pharmacol *30*, 552-557.

Miki, K., Hajduczok, G., Klocke, M.R., Krasney, J.A., Hong, S.K., and de Bold, A.J. (1986). Atrial natriuretic factor and renal function during head-out water immersion in conscious dogs. Am J Physiol *251*, R1000-1004.

Miki, K., Shiraki, K., Sagawa, S., de Bold, A.J., and Hong, S.K. (1988). Atrial natriuretic factor during head-out immersion at night. Am J Physiol *254*, R235-241.

Miller, M.K., Bang, M.L., Witt, C.C., Labeit, D., Trombitas, C., Watanabe, K., Granzier, H., McElhinny, A.S., Gregorio, C.C., and Labeit, S. (2003). The muscle ankyrin repeat proteins: CARP, ankrd2/Arpp and DARP as a family of titin filament-based stress response molecules. J Mol Biol *333*, 951-964.

Millward-Sadler, S.J., Wright, M.O., Davies, L.W., Nuki, G., and Salter, D.M. (2000). Mechanotransduction via integrins and interleukin-4 results in altered aggrecan and matrix metalloproteinase 3 gene expression in normal, but not osteoarthritic, human articular chondrocytes. Arthritis Rheum *43*, 2091-2099.

Millward-Sadler, S.J., Wright, M.O., Lee, H., Nishida, K., Caldwell, H., Nuki, G., and Salter, D.M. (1999). Integrin-regulated secretion of interleukin 4: A novel pathway of mechanotransduction in human articular chondrocytes. J Cell Biol *145*, 183-189.

Minami, K., Miki, T., Kadowaki, T., and Seino, S. (2004). Roles of ATP-sensitive K+ channels as metabolic sensors: studies of Kir6.x null mice. Diabetes *53 Suppl 3*, S176-180.

Minamisawa, S., Wang, Y., Chen, J., Ishikawa, Y., Chien, K.R., and Matsuoka, R. (2003). Atrial chamber-specific expression of sarcolipin is regulated during development and hypertrophic remodeling. J Biol Chem *278*, 9570-9575.

Misono, K.S., Grammer, R.T., Fukumi, H., and Inagami, T. (1984). Rat atrial natriuretic factor: isolation, structure and biological activities of four major peptides. Biochem Biophys Res Commun *123*, 444-451.

Miyagi, M., Zhang, X., and Misono, K.S. (2000). Glycosylation sites in the atrial natriuretic peptide receptor: oligosaccharide structures are not required for hormone binding. Eur J Biochem *267*, 5758-5768.

Miyata, S., Minobe, W., Bristow, M.R., and Leinwand, L.A. (2000). Myosin heavy chain isoform expression in the failing and nonfailing human heart. Circ Res *86*, 386-390.

Moe, G.W., Angus, C., Howard, R.J., De Bold, A.J., and Armstrong, P.W. (1990). Pathophysiological role of changing atrial size and pressure in modulation of atrial natriuretic factor during evolving experimental heart failure. Cardiovasc Res *24*, 570-577.

Mollenhauer, H.H., Morre, D.J., and Rowe, L.D. (1990). Alteration of intracellular traffic by monensin; mechanism, specificity and relationship to toxicity. Biochim Biophys Acta *1031*, 225-246.

Moorman, A.F., and Christoffels, V.M. (2003). Cardiac chamber formation: development, genes, and evolution. Physiol Rev *83*, 1223-1267.

Morel, G., Chabot, J.G., Gossard, F., and Heisler, S. (1989). Is atrial natriuretic peptide synthesized and internalized by gonadotrophs? Endocrinology *124*, 1703-1710.

Morozova, O., Hirst, M., and Marra, M.A. (2009). Applications of new sequencing technologies for transcriptome analysis. Annu Rev Genomics Hum Genet *10*, 135-151.

Morris, A.J., and Malbon, C.C. (1999). Physiological regulation of G protein-linked signaling. Physiol Rev *79*, 1373-1430.

Mousli, M., Bronner, C., Bockaert, J., Rouot, B., and Landry, Y. (1990). Interaction of substance P, compound 48/80 and mastoparan with the alpha-subunit C-terminus of G protein. Immunol Lett *25*, 355-357.

Mousli, M., Bronner, C., Bueb, J.L., Tschirhart, E., Gies, J.P., and Landry, Y. (1989). Activation of rat peritoneal mast cells by substance P and mastoparan. J Pharmacol Exp Ther *250*, 329-335.

Muller, L., Picart, R., Barret, A., Bockaert, J., Homburger, V., and Tougard, C. (1994). Identification of multiple subunits of heterotrimeric G proteins on the membrane of secretory granules in rat prolactin anterior pituitary cells. Mol Cell Neurosci *5*, 556-566.

Muntz, K.H., Sternweis, P.C., Gilman, A.G., and Mumby, S.M. (1992). Influence of gamma subunit prenylation on association of guanine nucleotide-binding regulatory proteins with membranes. Mol Biol Cell *3*, 49-61.

Nagueh, S.F., Shah, G., Wu, Y., Torre-Amione, G., King, N.M., Lahmers, S., Witt, C.C., Becker, K., Labeit, S., and Granzier, H.L. (2004). Altered titin expression, myocardial stiffness, and left ventricular function in patients with dilated cardiomyopathy. Circulation *110*, 155-162.

Nakamura, M., Arakawa, N., Yoshida, H., Makita, S., Niinuma, H., and Hiramori, K. (1998). Vasodilatory effects of B-type natriuretic peptide are impaired in patients with chronic heart failure. Am Heart J *135*, 414-420.

Narolska, N.A., van Loon, R.B., Boontje, N.M., Zaremba, R., Penas, S.E., Russell, J., Spiegelenberg, S.R., Huybregts, M.A., Visser, F.C., de Jong, J.W.*, et al.* (2005). Myocardial contraction is 5-fold more economical in ventricular than in atrial human tissue. Cardiovasc Res *65*, 221-229.

Ness, S.A. (2007). Microarray analysis: basic strategies for successful experiments. Mol Biotechnol *36*, 205-219.

Nguyen, C.H., and Watts, V.J. (2005). Dexras1 blocks receptor-mediated heterologous sensitization of adenylyl cyclase 1. Biochem Biophys Res Commun *332*, 913-920.

Nguyen, C.H., and Watts, V.J. (2006). Dexamethasone-induced Ras protein 1 negatively regulates protein kinase C delta: implications for adenylyl cyclase 2 signaling. Mol Pharmacol *69*, 1763-1771.

Nicholls, D.P., Onuoha, G.N., McDowell, G., Elborn, J.S., Riley, M.S., Nugent, A.M., Steele, I.C., Shaw, C., and Buchanan, K.D. (1996). Neuroendocrine changes in chronic cardiac failure. Basic Res Cardiol *91 Suppl 1*, 13-20.

Nishikimi, T., Hagaman, J.R., Takahashi, N., Kim, H.S., Matsuoka, H., Smithies, O., and Maeda, N. (2005). Increased susceptibility to heart failure in response to volume overload in mice lacking natriuretic peptide receptor-A gene. Cardiovasc Res *66*, 94-103.

Normant, E., and Loh, Y.P. (1998). Depletion of carboxypeptidase E, a regulated secretory pathway sorting receptor, causes misrouting and constitutive secretion of proinsulin and proenkephalin, but not chromogranin A. Endocrinology *139*, 2137-2145.

Northridge, D.B., McMurray, J., Ray, S., Jardine, A., and Dargie, H.J. (1989). Release of atrial natriuretic factor after pericardiocentesis for malignant pericardial effusion. BMJ *299*, 603-604.

Novick, P., and Guo, W. (2002). Ras family therapy: Rab, Rho and Ral talk to the exocyst. Trends Cell Biol *12*, 247-249.

Nunez, D.J., Dickson, M.C., and Brown, M.J. (1992). Natriuretic peptide receptor mRNAs in the rat and human heart. J Clin Invest *90*, 1966-1971.

Nusse, O., and Neer, E.J. (1996). Localization of G alpha 0 to growth cones in PC12 cells: role of G alpha 0 association with receptors and G beta gamma. J Cell Sci *109 (Pt 1)*, 221-228.

O'Brien, T.X., Lee, K.J., and Chien, K.R. (1993). Positional specification of ventricular myosin light chain 2 expression in the primitive murine heart tube. Proc Natl Acad Sci U S A *90*, 5157-5161.

Ogawa, T., Forero, M., Burgon, P.G., Kuroski de Bold, M.L., Georgalis, T., and de Bold, A.J. (2009). Role of potassium channels in stretch-promoted atrial natriuretic factor secretion. J Am Soc Hypertens *3*, 9-18.

Ogawa, T., Linz, W., Stevenson, M., Bruneau, B.G., Kuroski de Bold, M.L., Chen, J.H., Eid, H., Scholkens, B.A., and de Bold, A.J. (1996). Evidence for load-dependent and load-independent determinants of cardiac natriuretic peptide production. Circulation *93*, 2059-2067.

Ogawa, T., Vatta, M., Bruneau, B.G., and de Bold, A.J. (1999). Characterization of natriuretic peptide production by adult heart atria. Am J Physiol *276*, H1977-1986.

Ogawa, Y., Itoh, H., Tamura, N., Suga, S., Yoshimasa, T., Uehira, M., Matsuda, S., Shiono, S., Nishimoto, H., and Nakao, K. (1994). Molecular cloning of the complementary DNA and gene that encode mouse brain natriuretic peptide and generation of transgenic mice that overexpress the brain natriuretic peptide gene. J Clin Invest *93*, 1911-1921.

Ogawa, Y., Tamura, N., Chusho, H., and Nakao, K. (2001). Brain natriuretic peptide appears to act locally as an antifibrotic factor in the heart. Can J Physiol Pharmacol *79*, 723-729.

Ohya, T., Miaczynska, M., Coskun, U., Lommer, B., Runge, A., Drechsel, D., Kalaidzidis, Y., and Zerial, M. (2009). Reconstitution of Rab- and SNARE-dependent membrane fusion by synthetic endosomes. Nature *459*, 1091-1097.

Oikawa, S., Imai, M., Inuzuka, C., Tawaragi, Y., Nakazato, H., and Matsuo, H. (1985). Structure of dog and rabbit precursors of atrial natriuretic polypeptides deduced from nucleotide sequence of cloned cDNA. Biochem Biophys Res Commun *132*, 892-899.

Oikawa, S., Imai, M., Ueno, A., Tanaka, S., Noguchi, T., Nakazato, H., Kangawa, K., Fukuda, A., and Matsuo, H. (1984). Cloning and sequence analysis of cDNA encoding a precursor for human atrial natriuretic polypeptide. Nature *309*, 724-726.

Okamoto, M., Schoch, S., and Sudhof, T.C. (1999). EHSH1/intersectin, a protein that contains EH and SH3 domains and binds to dynamin and SNAP-25. A protein connection between exocytosis and endocytosis? J Biol Chem *274*, 18446-18454.

Oliver, P.M., Fox, J.E., Kim, R., Rockman, H.A., Kim, H.S., Reddick, R.L., Pandey, K.N., Milgram, S.L., Smithies, O., and Maeda, N. (1997). Hypertension, cardiac hypertrophy, and sudden death in mice lacking natriuretic peptide receptor A. Proc Natl Acad Sci U S A *94*, 14730-14735.

Oliver, P.M., John, S.W., Purdy, K.E., Kim, R., Maeda, N., Goy, M.F., and Smithies, O. (1998). Natriuretic peptide receptor 1 expression influences blood pressures of mice in a dose-dependent manner. Proc Natl Acad Sci U S A *95*, 2547-2551.

Olson, E.N., and Srivastava, D. (1996). Molecular pathways controlling heart development. Science *272*, 671-676.

Orazizadeh, M., Lee, H.S., Groenendijk, B., Sadler, S.J., Wright, M.O., Lindberg, F.P., and Salter, D.M. (2008). CD47 associates with alpha 5 integrin and regulates responses of human articular chondrocytes to mechanical stimulation in an in vitro model. Arthritis Res Ther *10*, R4.

Overhoff, M., Alken, M., Far, R.K., Lemaitre, M., Lebleu, B., Sczakiel, G., and Robbins, I. (2005). Local RNA target structure influences siRNA efficacy: a systematic global analysis. J Mol Biol *348*, 871-881.

Ozaki, Y., Matsumoto, Y., Yatomi, Y., Higashihara, M., Kariya, T., and Kume, S. (1990). Mastoparan, a wasp venom, activates platelets via pertussis toxin-sensitive GTP-binding proteins. Biochem Biophys Res Commun *170*, 779-785.

Padfield, P.J., and Panesar, N. (1997). Identification of Goalpha, Gqalpha, and Gsalpha immunoreactivity associated with the rat pancreatic zymogen granule membrane. Biochem Biophys Res Commun *237*, 235-238.

Page, E., Goings, G.E., Power, B., and Upshaw-Earley, J. (1986). Ultrastructural features of atrial peptide secretion. Am J Physiol *251*, H340-348.

Page, E., Upshaw-Earley, J., and Goings, G.E. (1994). Localization of atrial natriuretic peptide in caveolae of in situ atrial myocytes. Circ Res *75*, 949-954.

Page, E., Upshaw-Earley, J., Goings, G.E., and Hanck, D.A. (1991). Inhibition of atrial peptide secretion at different stages of the secretory process: Ca2+ dependence. Am J Physiol *261*, C1162-1172.

Park, J.J., and Loh, Y.P. (2008). How peptide hormone vesicles are transported to the secretion site for exocytosis. Mol Endocrinol *22*, 2583-2595.

Parker, T.G., Chow, K.L., Schwartz, R.J., and Schneider, M.D. (1990). Differential regulation of skeletal alpha-actin transcription in cardiac muscle by two fibroblast growth factors. Proc Natl Acad Sci U S A *87*, 7066-7070.

Patel, M.J., Liu, W., Sykes, M.C., Ward, N.E., Risin, S.A., Risin, D., and Jo, H. (2007). Identification of mechanosensitive genes in osteoblasts by comparative microarray studies using the rotating wall vessel and the random positioning machine. J Cell Biochem *101*, 587-599.

Patten, R.D., and Hall-Porter, M.R. (2009). Small animal models of heart failure: development of novel therapies, past and present. Circ Heart Fail *2*, 138-144.

Pedram, A., Razandi, M., and Levin, E.R. (2001). Natriuretic peptides suppress vascular endothelial cell growth factor signaling to angiogenesis. Endocrinology *142*, 1578-1586.

Pereira, F.A., Qiu, Y., Zhou, G., Tsai, M.J., and Tsai, S.Y. (1999). The orphan nuclear receptor COUP-TFII is required for angiogenesis and heart development. Genes Dev *13*, 1037-1049.

Pham, J.W., Pellino, J.L., Lee, Y.S., Carthew, R.W., and Sontheimer, E.J. (2004). A Dicer-2-dependent 80s complex cleaves targeted mRNAs during RNAi in Drosophila. Cell *117*, 83-94.

Pietropaolo, M., Castano, L., Babu, S., Buelow, R., Kuo, Y.L., Martin, S., Martin, A., Powers, A.C., Prochazka, M., Naggert, J.*, et al.* (1993). Islet cell autoantigen 69 kD (ICA69). Molecular cloning and characterization of a novel diabetes-associated autoantigen. J Clin Invest *92*, 359-371.

Ponnambalam, S., and Baldwin, S.A. (2003). Constitutive protein secretion from the trans-Golgi network to the plasma membrane. Mol Membr Biol *20*, 129-139.

Potter, L.R., and Garbers, D.L. (1992). Dephosphorylation of the guanylyl cyclase-A receptor causes desensitization. J Biol Chem *267*, 14531-14534.

Pratt, R.E., Carleton, J.E., Richie, J.P., Heusser, C., and Dzau, V.J. (1987). Human renin biosynthesis and secretion in normal and ischemic kidneys. Proc Natl Acad Sci U S A *84*, 7837-7840.

Pucharcos, C., Estivill, X., and de la Luna, S. (2000). Intersectin 2, a new multimodular protein involved in clathrin-mediated endocytosis. FEBS Lett *478*, 43-51.

Rademaker, M.T., and Richards, A.M. (2005). Cardiac natriuretic peptides for cardiac health. Clin Sci (Lond) *108*, 23-36.

Redfield, M.M., Rodeheffer, R.J., Jacobsen, S.J., Mahoney, D.W., Bailey, K.R., and Burnett, J.C., Jr. (2002). Plasma brain natriuretic peptide concentration: impact of age and gender. J Am Coll Cardiol *40*, 976-982.

Rhodes, C.J., and Halban, P.A. (1987). Newly synthesized proinsulin/insulin and stored insulin are released from pancreatic B cells predominantly via a regulated, rather than a constitutive, pathway. J Cell Biol *105*, 145-153.

Riegger, G.A., Elsner, D., Kromer, E.P., Daffner, C., Forssmann, W.G., Muders, F., Pascher, E.W., and Kochsiek, K. (1988). Atrial natriuretic peptide in congestive heart failure in the dog: plasma levels, cyclic guanosine monophosphate, ultrastructure of atrial myoendocrine cells, and hemodynamic, hormonal, and renal effects. Circulation *77*, 398-406.

Romanello, M., Codognotto, A., Bicego, M., Pines, A., Tell, G., and D'Andrea, P. (2005). Autocrine/paracrine stimulation of purinergic receptors in osteoblasts: contribution of vesicular ATP release. Biochem Biophys Res Commun *331*, 1429-1438.

Rosenzweig, A., Halazonetis, T.D., Seidman, J.G., and Seidman, C.E. (1991). Proximal regulatory domains of rat atrial natriuretic factor gene. Circulation *84*, 1256-1265.

Rosenzweig, A., and Seidman, C.E. (1991). Atrial natriuretic factor and related peptide hormones. Annu Rev Biochem *60*, 229-255.

Rozich, J.D., Barnes, M.A., Schmid, P.G., Zile, M.R., McDermott, P.J., and Cooper, G.t. (1995). Load effects on gene expression during cardiac hypertrophy. J Mol Cell Cardiol *27*, 485-499.

Ruskoaho, H. (2003). Cardiac hormones as diagnostic tools in heart failure. Endocr Rev *24*, 341-356.

Ruskoaho, H., Toth, M., and Lang, R.E. (1985). Atrial natriuretic peptide secretion: synergistic effect of phorbol ester and A23187. Biochem Biophys Res Commun *133*, 581-588.

Ruzicka, M., Yuan, B., Harmsen, E., and Leenen, F.H. (1993). The renin-angiotensin system and volume overload-induced cardiac hypertrophy in rats. Effects of

angiotensin converting enzyme inhibitor versus angiotensin II receptor blocker. Circulation *87*, 921-930.

Sabrane, K., Kruse, M.N., Fabritz, L., Zetsche, B., Mitko, D., Skryabin, B.V., Zwiener, M., Baba, H.A., Yanagisawa, M., and Kuhn, M. (2005). Vascular endothelium is critically involved in the hypotensive and hypovolemic actions of atrial natriuretic peptide. J Clin Invest *115*, 1666-1674.

Sadoshima, J., and Izumo, S. (1993). Molecular characterization of angiotensin II--induced hypertrophy of cardiac myocytes and hyperplasia of cardiac fibroblasts. Critical role of the AT1 receptor subtype. Circ Res *73*, 413-423.

Saegusa, N., Sato, T., Saito, T., Tamagawa, M., Komuro, I., and Nakaya, H. (2005). Kir6.2-deficient mice are susceptible to stimulated ANP secretion: K(ATP) channel acts as a negative feedback mechanism? Cardiovasc Res *67*, 60-68.

Saga, Y., Kitajima, S., and Miyagawa-Tomita, S. (2000). Mesp1 expression is the earliest sign of cardiovascular development. Trends Cardiovasc Med *10*, 345-352.

Samson, W.K. (1985). Atrial natriuretic factor inhibits dehydration and hemorrhage-induced vasopressin release. Neuroendocrinology *40*, 277-279.

Sanchez, J.A., Gonoi, T., Inagaki, N., Katada, T., and Seino, S. (1998). Modulation of reconstituted ATP-sensitive K(+)-channels by GTP-binding proteins in a mammalian cell line. J Physiol *507 (Pt 2)*, 315-324.

Sano, T., Imura, R., Morishita, Y., Matsuda, Y., and Yamada, K. (1992a). HS-142-1, a novel polysaccharide of microbial origin, specifically recognizes guanylyl cyclase-linked ANP receptor in rat glomeruli. Life Sci *51*, 1445-1451.

Sano, T., Morishita, Y., Matsuda, Y., and Yamada, K. (1992b). Pharmacological profile of HS-142-1, a novel nonpeptide atrial natriuretic peptide antagonist of microbial origin. I. Selective inhibition of the actions of natriuretic peptides in anesthetized rats. J Pharmacol Exp Ther *260*, 825-831.

Sano, T., Morishita, Y., Yamada, K., and Matsuda, Y. (1992c). Effects of HS-142-1, a novel non-peptide ANP antagonist, on diuresis and natriuresis induced by acute volume expansion in anesthetized rats. Biochem Biophys Res Commun *182*, 824-829.

Sarda, I.R., de Bold, M.L., and de Bold, A.J. (1989). Optimization of atrial natriuretic factor radioimmunoassay. Clin Biochem *22*, 11-15.

Sato, M., Blumer, J.B., Simon, V., and Lanier, S.M. (2006). Accessory proteins for G proteins: partners in signaling. Annu Rev Pharmacol Toxicol *46*, 151-187.

Sausbier, M., Schubert, R., Voigt, V., Hirneiss, C., Pfeifer, A., Korth, M., Kleppisch, T., Ruth, P., and Hofmann, F. (2000). Mechanisms of NO/cGMP-dependent vasorelaxation. Circ Res *87*, 825-830.

Schaub, M.C., Hefti, M.A., Harder, B.A., and Eppenberger, H.M. (1997). Various hypertrophic stimuli induce distinct phenotypes in cardiomyocytes. J Mol Med *75*, 901-920.

Schaub, M.C., Hefti, M.A., Zuellig, R.A., and Morano, I. (1998). Modulation of contractility in human cardiac hypertrophy by myosin essential light chain isoforms. Cardiovasc Res *37*, 381-404.

Schiebinger, R.J., and Gomez-Sanchez, C.E. (1990). Endothelin: a potent stimulus of atrial natriuretic peptide secretion by superfused rat atria and its dependency on calcium. Endocrinology *127*, 119-125.

Schlossmann, J., Ammendola, A., Ashman, K., Zong, X., Huber, A., Neubauer, G., Wang, G.X., Allescher, H.D., Korth, M., Wilm, M.*, et al.* (2000). Regulation of intracellular calcium by a signalling complex of IRAG, IP3 receptor and cGMP kinase Ibeta. Nature *404*, 197-201.

Schmitt, M., Qasem, A., McEniery, C., Wilkinson, I.B., Tatarinoff, V., Noble, K., Klemes, J., Payne, N., Frenneaux, M.P., Cockcroft, J.*, et al.* (2004). Role of natriuretic peptides in regulation of conduit artery distensibility. Am J Physiol Heart Circ Physiol *287*, H1167-1171.

Schnabel, P., Gas, H., Nohr, T., and Bohm, M. (1997). G protein-independent stimulation of human myocardial phospholipase C by mastoparan. Br J Pharmacol *122*, 31-36.

Schnermann, J., Hermle, M., Schmidmeier, E., and Dahlheim, H. (1975). Impaired potency for feedback regulation of glomerular filtration rate in DOCA escaped rats. Pflugers Arch *358*, 325-338.

Schreier, B., Borner, S., Volker, K., Gambaryan, S., Schafer, S.C., Kuhlencordt, P., Gassner, B., and Kuhn, M. (2008). The heart communicates with the endothelium through the guanylyl cyclase-A receptor: acute handling of intravascular volume in response to volume expansion. Endocrinology *149*, 4193-4199.

Schubert, S., Grunweller, A., Erdmann, V.A., and Kurreck, J. (2005). Local RNA target structure influences siRNA efficacy: systematic analysis of intentionally designed binding regions. J Mol Biol *348*, 883-893.

Schultheiss, T.M., Xydas, S., and Lassar, A.B. (1995). Induction of avian cardiac myogenesis by anterior endoderm. Development *121*, 4203-4214.

Schultz, H.D., Gardner, D.G., Deschepper, C.F., Coleridge, H.M., and Coleridge, J.C. (1988). Vagal C-fiber blockade abolishes sympathetic inhibition by atrial natriuretic factor. Am J Physiol *255*, R6-13.

Schulz, S., Green, C.K., Yuen, P.S., and Garbers, D.L. (1990). Guanylyl cyclase is a heat-stable enterotoxin receptor. Cell *63*, 941-948.

Scott, B.L., Van Komen, J.S., Irshad, H., Liu, S., Wilson, K.A., and McNew, J.A. (2004). Sec1p directly stimulates SNARE-mediated membrane fusion in vitro. J Cell Biol *167*, 75-85.

Scriven, T.A., and Burnett, J.C., Jr. (1985). Effects of synthetic atrial natriuretic peptide on renal function and renin release in acute experimental heart failure. Circulation *72*, 892-897.

Seidah, N.G., Cromlish, J.A., Hamelin, J., Thibault, G., and Chretien, M. (1986). Homologous IRCM-serine protease 1 from pituitary, heart atrium and ventricle: a common pro-hormone maturation enzyme? Biosci Rep *6*, 835-844.

Seidman, C.E., Bloch, K.D., Klein, K.A., Smith, J.A., and Seidman, J.G. (1984a). Nucleotide sequences of the human and mouse atrial natriuretic factor genes. Science *226*, 1206-1209.

Seidman, C.E., Bloch, K.D., Zisfein, J., Smith, J.A., Haber, E., Homcy, C., Duby, A.D., Choi, E., Graham, R.M., and Seidman, J.G. (1985). Molecular studies of the atrial natriuretic factor gene. Hypertension *7*, I31-34.

Seidman, C.E., Duby, A.D., Choi, E., Graham, R.M., Haber, E., Homcy, C., Smith, J.A., and Seidman, J.G. (1984b). The structure of rat preproatrial natriuretic factor as defined by a complementary DNA clone. Science *225*, 324-326.

Seidman, C.E., Wong, D.W., Jarcho, J.A., Bloch, K.D., and Seidman, J.G. (1988). Cis-acting sequences that modulate atrial natriuretic factor gene expression. Proc Natl Acad Sci U S A *85*, 4104-4108.

Shamim, A., Pelzer, T., Grohe, C., and Neyses, L. (1999). Induction of Egr-1 mRNA and protein by endothelin 1, angiotensin II and norepinephrine in neonatal cardiac myocytes. Mol Cell Biochem *195*, 11-17.

Shao, Y., Chan, C.Y., Maliyekkel, A., Lawrence, C.E., Roninson, I.B., and Ding, Y. (2007). Effect of target secondary structure on RNAi efficiency. RNA *13*, 1631-1640.

Sharma, R.K., Yadav, P., and Duda, T. (2001). Allosteric regulatory step and configuration of the ATP-binding pocket in atrial natriuretic factor receptor guanylate cyclase transduction mechanism. Can J Physiol Pharmacol *79*, 682-691.

Shi, S.J., Nguyen, H.T., Sharma, G.D., Navar, L.G., and Pandey, K.N. (2001). Genetic disruption of atrial natriuretic peptide receptor-A alters renin and angiotensin II levels. Am J Physiol Renal Physiol *281*, F665-673.

Shields, P.P., Dixon, J.E., and Glembotski, C.C. (1988). The secretion of atrial natriuretic factor-(99-126) by cultured cardiac myocytes is regulated by glucocorticoids. J Biol Chem *263*, 12619-12628.

Shimura, M., Minamisawa, S., Yokoyama, U., Umemura, S., and Ishikawa, Y. (2005). Mechanical stress-dependent transcriptional regulation of sarcolipin gene in the rodent atrium. Biochem Biophys Res Commun *334*, 861-866.

Shubeita, H.E., McDonough, P.M., Harris, A.N., Knowlton, K.U., Glembotski, C.C., Brown, J.H., and Chien, K.R. (1990). Endothelin induction of inositol phospholipid hydrolysis, sarcomere assembly, and cardiac gene expression in ventricular myocytes. A paracrine mechanism for myocardial cell hypertrophy. J Biol Chem *265*, 20555-20562.

Singh, S., Lowe, D.G., Thorpe, D.S., Rodriguez, H., Kuang, W.J., Dangott, L.J., Chinkers, M., Goeddel, D.V., and Garbers, D.L. (1988). Membrane guanylate cyclase is a cell-surface receptor with homology to protein kinases. Nature *334*, 708-712.

Sivars, U., Aivazian, D., and Pfeffer, S.R. (2003). Yip3 catalyses the dissociation of endosomal Rab-GDI complexes. Nature *425*, 856-859.

Skidgel, R.A., Engelbrecht, S., Johnson, A.R., and Erdos, E.G. (1984). Hydrolysis of substance p and neurotensin by converting enzyme and neutral endopeptidase. Peptides *5*, 769-776.

Skryabin, B.V., Holtwick, R., Fabritz, L., Kruse, M.N., Veltrup, I., Stypmann, J., Kirchhof, P., Sabrane, K., Bubikat, A., Voss, M.*, et al.* (2004). Hypervolemic hypertension in mice with systemic inactivation of the (floxed) guanylyl cyclase-A gene by alphaMHC-Cre-mediated recombination. Genesis *39*, 288-298.

Skvorak, J.P., Nazian, S.J., and Dietz, J.R. (1995). Endothelin acts as a paracrine regulator of stretch-induced atrial natriuretic peptide release. Am J Physiol *269*, R1093-1098.

Small, E.M., and Krieg, P.A. (2004). Molecular regulation of cardiac chamber-specific gene expression. Trends Cardiovasc Med *14*, 13-18.

Sollner, T., Whiteheart, S.W., Brunner, M., Erdjument-Bromage, H., Geromanos, S., Tempst, P., and Rothman, J.E. (1993). SNAP receptors implicated in vesicle targeting and fusion. Nature *362*, 318-324.

Sommer, J.R., and Waugh, R.A. (1978). Ultrastructure of heart muscle. Environ Health Perspect *26*, 159-167.

Sorensen, J.B. (2004). Formation, stabilisation and fusion of the readily releasable pool of secretory vesicles. Pflugers Arch *448*, 347-362.

Sperelakis, N. (2001). Heart Physiology and Pathophysiology. 4th edition, 4th edn (San Diego, CA, Academic Press).

Spitzenberger, F., Pietropaolo, S., Verkade, P., Habermann, B., Lacas-Gervais, S., Mziaut, H., Pietropaolo, M., and Solimena, M. (2003). Islet cell autoantigen of 69 kDa is an arfaptin-related protein associated with the Golgi complex of insulinoma INS-1 cells. J Biol Chem *278*, 26166-26173.

Srivastava, D., and Olson, E.N. (2000). A genetic blueprint for cardiac development. Nature *407*, 221-226.

Stasch, J.P., Hirth-Dietrich, C., Kazda, S., and Neuser, D. (1989). Endothelin stimulates release of atrial natriuretic peptides in vitro and in vivo. Life Sci *45*, 869-875.

Statistics_Canada (2005). http://www.statcan.gc.ca.

Steinhelper, M.E., Cochrane, K.L., and Field, L.J. (1990). Hypotension in transgenic mice expressing atrial natriuretic factor fusion genes. Hypertension *16*, 301-307.

Sternweis, P.C. (1986). The purified alpha subunits of Go and Gi from bovine brain require beta gamma for association with phospholipid vesicles. J Biol Chem *261*, 631-637.

Straub, S.G., and Sharp, G.W. (2002). Glucose-stimulated signaling pathways in biphasic insulin secretion. Diabetes Metab Res Rev *18*, 451-463.

Stroupe, C., Hickey, C.M., Mima, J., Burfeind, A.S., and Wickner, W. (2009). Minimal membrane docking requirements revealed by reconstitution of Rab GTPase-dependent membrane fusion from purified components. Proc Natl Acad Sci U S A *106*, 17626-17633.

Stula, M., Orzechowski, H.D., Gschwend, S., Vetter, R., von Harsdorf, R., Dietz, R., and Paul, M. (2000). Influence of sustained mechanical stress on Egr-1 mRNA expression in cultured human endothelial cells. Mol Cell Biochem *210*, 101-108.

Sucharov, C.C., Dockstader, K., and McKinsey, T.A. (2008). YY1 protects cardiac myocytes from pathologic hypertrophy by interacting with HDAC5. Mol Biol Cell *19*, 4141-4153.

Sudoh, T., Kangawa, K., Minamino, N., and Matsuo, H. (1988). A new natriuretic peptide in porcine brain. Nature *332*, 78-81.

Sudoh, T., Maekawa, K., Kojima, M., Minamino, N., Kangawa, K., and Matsuo, H. (1989). Cloning and sequence analysis of cDNA encoding a precursor for human brain natriuretic peptide. Biochem Biophys Res Commun *159*, 1427-1434.

Sudoh, T., Minamino, N., Kangawa, K., and Matsuo, H. (1990). C-type natriuretic peptide (CNP): a new member of natriuretic peptide family identified in porcine brain. Biochem Biophys Res Commun *168*, 863-870.

Suga, S., Nakao, K., Hosoda, K., Mukoyama, M., Ogawa, Y., Shirakami, G., Arai, H., Saito, Y., Kambayashi, Y., Inouye, K., *et al.* (1992). Receptor selectivity of natriuretic peptide family, atrial natriuretic peptide, brain natriuretic peptide, and C-type natriuretic peptide. Endocrinology *130*, 229-239.

Suzuki, E., Hirata, Y., Kohmoto, O., Sugimoto, T., Hayakawa, H., Matsuoka, H., Kojima, M., Kangawa, K., Minamino, N., and et al. (1992). Cellular mechanisms for synthesis and secretion of atrial natriuretic peptide and brain natriuretic peptide in cultured rat atrial cells. Circ Res *71*, 1039-1048.

Swynghedauw, B. (1986). Developmental and functional adaptation of contractile proteins in cardiac and skeletal muscles. Physiol Rev *66*, 710-771.

Szpirer, C., Riviere, M., Szpirer, J., Genet, M., Dreze, P., Islam, M.Q., and Levan, G. (1990). Assignment of 12 loci to rat chromosome 5: evidence that this chromosome is homologous to mouse chromosome 4 and to human chromosomes 9 and 1 (1p arm). Genomics *6*, 679-684.

Tabibiazar, R., Wagner, R.A., Liao, A., and Quertermous, T. (2003). Transcriptional profiling of the heart reveals chamber-specific gene expression patterns. Circ Res *93*, 1193-1201.

Takahashi, N., Calderone, A., Izzo, N.J., Jr., Maki, T.M., Marsh, J.D., and Colucci, W.S. (1994). Hypertrophic stimuli induce transforming growth factor-beta 1 expression in rat ventricular myocytes. J Clin Invest *94*, 1470-1476.

Takayanagi, R., Tanaka, I., Maki, M., and Inagami, T. (1985). Effects of changes in water-sodium balance on levels of atrial natriuretic factor messenger RNA and peptide in rats. Life Sci *36*, 1843-1848.

Takei, Y. (2001). Does the natriuretic peptide system exist throughout the animal and plant kingdom? Comp Biochem Physiol B Biochem Mol Biol *129*, 559-573.

Takesono, A., Nowak, M.W., Cismowski, M., Duzic, E., and Lanier, S.M. (2002). Activator of G-protein signaling 1 blocks GIRK channel activation by a G-protein-coupled receptor: apparent disruption of receptor signaling complexes. J Biol Chem *277*, 13827-13830.

Tamura, N., Ogawa, Y., Chusho, H., Nakamura, K., Nakao, K., Suda, M., Kasahara, M., Hashimoto, R., Katsuura, G., Mukoyama, M., *et al.* (2000). Cardiac fibrosis in mice lacking brain natriuretic peptide. Proc Natl Acad Sci U S A *97*, 4239-4244.

Tamura, N., Ogawa, Y., Yasoda, A., Itoh, H., Saito, Y., and Nakao, K. (1996). Two cardiac natriuretic peptide genes (atrial natriuretic peptide and brain natriuretic peptide) are organized in tandem in the mouse and human genomes. J Mol Cell Cardiol *28*, 1811-1815.

Tan, J.J., Ong, S.A., and Chen, K.S. (2011). Rasd1 interacts with Ear2 (Nr2f6) to regulate renin transcription. BMC Mol Biol *12*, 4.

Tarjan, E., Denton, D.A., and Weisinger, R.S. (1988). Atrial natriuretic peptide inhibits water and sodium intake in rabbits. Regul Pept *23*, 63-75.

Terrenoire, C., Lauritzen, I., Lesage, F., Romey, G., and Lazdunski, M. (2001). A TREK-1-like potassium channel in atrial cells inhibited by beta-adrenergic stimulation and activated by volatile anesthetics. Circ Res *89*, 336-342.

Thapliyal, A., Bannister, R.A., Hanks, C., and Adams, B.A. (2008). The monomeric G proteins AGS1 and Rhes selectively influence Galphai-dependent signaling to modulate N-type (CaV2.2) calcium channels. Am J Physiol Cell Physiol *295*, C1417-1426.

Thoren, P., Mark, A.L., Morgan, D.A., O'Neill, T.P., Needleman, P., and Brody, M.J. (1986). Activation of vagal depressor reflexes by atriopeptins inhibits renal sympathetic nerve activity. Am J Physiol *251*, H1252-1259.

Tohkin, M., Yagami, T., and Matsubara, T. (1990). Mastoparan, a peptide toxin from wasp venom, stimulates glycogenolysis mediated by an increase of the cytosolic free Ca2+ concentration but not by an increase of cAMP in rat hepatocytes. FEBS Lett *260*, 179-182.

Tokudome, T., Horio, T., Kishimoto, I., Soeki, T., Mori, K., Kawano, Y., Kohno, M., Garbers, D.L., Nakao, K., and Kangawa, K. (2005). Calcineurin-nuclear factor of activated T cells pathway-dependent cardiac remodeling in mice deficient in guanylyl cyclase A, a receptor for atrial and brain natriuretic peptides. Circulation *111*, 3095-3104.

Tokudome, T., Kishimoto, I., Horio, T., Arai, Y., Schwenke, D.O., Hino, J., Okano, I., Kawano, Y., Kohno, M., Miyazato, M., *et al.* (2008). Regulator of G-protein signaling subtype 4 mediates antihypertrophic effect of locally secreted natriuretic peptides in the heart. Circulation *117*, 2329-2339.

Toop, T., Grozdanovski, D., and Potter, I.C. (1998). Natriuretic peptide binding sites in the gills of the pouched lamprey Geotria australis. J Exp Biol *201*, 1799-1808.

Toth, M., Ruskoaho, H., and Lang, R.E. (1986). Regulation of atrial natriuretic peptide secretion. J Hypertens Suppl *4*, S538-541.

Toutant, M., Aunis, D., Bockaert, J., Homburger, V., and Rouot, B. (1987). Presence of three pertussis toxin substrates and Go alpha immunoreactivity in both plasma and granule membranes of chromaffin cells. FEBS Lett *215*, 339-344.

Trippodo, N.C., and Barbee, R.W. (1987). Atrial natriuretic factor decreases whole-body capillary absorption in rats. Am J Physiol *252*, R915-920.

Tsuruda, T., Boerrigter, G., Huntley, B.K., Noser, J.A., Cataliotti, A., Costello-Boerrigter, L.C., Chen, H.H., and Burnett, J.C., Jr. (2002). Brain natriuretic Peptide is produced in cardiac fibroblasts and induces matrix metalloproteinases. Circ Res *91*, 1127-1134.

Tu, Y., and Wu, C. (1999). Cloning, expression and characterization of a novel human Ras-related protein that is regulated by glucocorticoid hormone. Biochim Biophys Acta *1489*, 452-456.

Tunny, T.J., Higgins, B.A., and Gordon, R.D. (1986). Plasma levels of atrial natriuretic peptide in man in primary aldosteronism, in Gordon's syndrome and in Bartter's syndrome. Clin Exp Pharmacol Physiol *13*, 341-345.

Tusher, V.G., Tibshirani, R., and Chu, G. (2001). Significance analysis of microarrays applied to the ionizing radiation response. Proc Natl Acad Sci U S A *98*, 5116-5121.

Uehlinger, D.E., Weidmann, P., Gnaedinger, M.P., Shaw, S., and Lang, R.E. (1986). Depressor effects and release of atrial natriuretic peptide during norepinephrine or angiotensin II infusion in man. J Clin Endocrinol Metab *63*, 669-674.

Umbrecht-Jenck, E., Demais, V., Calco, V., Bailly, Y., Bader, M.F., and Chasserot-Golaz, S. (2010). S100A10-mediated translocation of annexin-A2 to SNARE proteins in adrenergic chromaffin cells undergoing exocytosis. Traffic *11*, 958-971.

Valtorta, F., Pennuto, M., Bonanomi, D., and Benfenati, F. (2004). Synaptophysin: leading actor or walk-on role in synaptic vesicle exocytosis? Bioessays *26*, 445-453.

van Bilsen, M., and Chien, K.R. (1993). Growth and hypertrophy of the heart: towards an understanding of cardiac specific and inducible gene expression. Cardiovasc Res *27*, 1140-1149.

van den Akker, F. (2001). Structural insights into the ligand binding domains of membrane bound guanylyl cyclases and natriuretic peptide receptors. J Mol Biol *311*, 923-937.

Van Wagoner, D.R. (1993). Mechanosensitive gating of atrial ATP-sensitive potassium channels. Circ Res *72*, 973-983.

Vanderheyden, M., Bartunek, J., and Goethals, M. (2004). Brain and other natriuretic peptides: molecular aspects. Eur J Heart Fail *6*, 261-268.

Veit, M., Sollner, T.H., and Rothman, J.E. (1996). Multiple palmitoylation of synaptotagmin and the t-SNARE SNAP-25. FEBS Lett *385*, 119-123.

Vickers, T.A., Koo, S., Bennett, C.F., Crooke, S.T., Dean, N.M., and Baker, B.F. (2003). Efficient reduction of target RNAs by small interfering RNA and RNase H-dependent antisense agents. A comparative analysis. J Biol Chem *278*, 7108-7118.

Villarreal, D., and Freeman, R.H. (1991). ANF and the renin-angiotensin system in the regulation of sodium balance: longitudinal studies in experimental heart failure. J Lab Clin Med *118*, 515-522.

Villarreal, D., Freeman, R.H., and Johnson, R.A. (1991). Renal effects of ANF (95-126), a new atrial peptide analogue, in dogs with experimental heart failure. Am J Hypertens *4*, 508-515.

Villarreal, D., Freeman, R.H., and Johnson, R.A. (1992). Captopril enhances renal responsiveness to ANF in dogs with compensated high-output heart failure. Am J Physiol *262*, R509-516.

Villarreal, D., Freeman, R.H., and Johnson, R.A. (1993). Neurohumoral modulators and sodium balance in experimental heart failure. Am J Physiol *264*, H1187-1193.

Vitale, N., Gensse, M., Chasserot-Golaz, S., Aunis, D., and Bader, M.F. (1996). Trimeric G proteins control regulated exocytosis in bovine chromaffin cells: sequential involvement of Go associated with secretory granules and Gi3 bound to the plasma membrane. Eur J Neurosci *8*, 1275-1285.

Vitale, N., Gonon, F., Thierse, D., Aunis, D., and Bader, M.F. (1997). Exocytosis in single chromaffin cells: regulation by a secretory granule-associated Go protein. Cell Mol Neurobiol *17*, 71-87.

Vitale, N., Thierse, D., Aunis, D., and Bader, M.F. (1994). Exocytosis in chromaffin cells: evidence for a MgATP-independent step that requires a pertussis toxin-sensitive GTP-binding protein. Biochem J *300 (Pt 1)*, 217-227.

Vlasuk, G.P., Miller, J., Bencen, G.H., and Lewicki, J.A. (1986). Structure and analysis of the bovine atrial natriuretic peptide precursor gene. Biochem Biophys Res Commun *136*, 396-403.

Voloshyna, I., Besana, A., Castillo, M., Matos, T., Weinstein, I.B., Mansukhani, M., Robinson, R.B., Cordon-Cardo, C., and Feinmark, S.J. (2008). TREK-1 is a novel molecular target in prostate cancer. Cancer Res *68*, 1197-1203.

Wahlander, H., Haraldsson, B., and Friberg, P. (1993). Myocardial capillary diffusion capacity in rat hearts with cardiac hypertrophy due to pressure and volume overload. Am J Physiol *265*, H61-68.

Wang, X., Sentex, E., Chapman, D., and Dhalla, N.S. (2004). Alterations of adenylyl cyclase and G proteins in aortocaval shunt-induced heart failure. Am J Physiol Heart Circ Physiol *287*, H118-125.

Weingarten, R., Ransnas, L., Mueller, H., Sklar, L.A., and Bokoch, G.M. (1990). Mastoparan interacts with the carboxyl terminus of the alpha subunit of Gi. J Biol Chem *265*, 11044-11049.

Weiss, A., and Leinwand, L.A. (1996). The mammalian myosin heavy chain gene family. Annu Rev Cell Dev Biol *12*, 417-439.

Wen, J.F., Cui, X., Ahn, J.S., Kim, S.H., Seul, K.H., Kim, S.Z., Park, Y.K., Lee, H.S., and Cho, K.W. (2000). Distinct roles for L- and T-type Ca(2+) channels in regulation of atrial ANP release. Am J Physiol Heart Circ Physiol *279*, H2879-2888.

Weng, Y.J., Kuo, W.W., Kuo, C.H., Tung, K.C., Tsai, C.H., Lin, J.A., Tsai, F.J., Hsieh, D.J., Huang, C.Y., and Hwang, J.M. (2010). BNIP3 induces IL6 and calcineurin/NFAT3 hypertrophic-related pathways in H9c2 cardiomyoblast cells. Mol Cell Biochem *345*, 241-247.

Wennerberg, K., Rossman, K.L., and Der, C.J. (2005). The Ras superfamily at a glance. J Cell Sci *118*, 843-846.

Westerhout, E.M., Ooms, M., Vink, M., Das, A.T., and Berkhout, B. (2005). HIV-1 can escape from RNA interference by evolving an alternative structure in its RNA genome. Nucleic Acids Res *33*, 796-804.

Wettschureck, N., Rutten, H., Zywietz, A., Gehring, D., Wilkie, T.M., Chen, J., Chien, K.R., and Offermanns, S. (2001). Absence of pressure overload induced myocardial hypertrophy after conditional inactivation of Galphaq/Galpha11 in cardiomyocytes. Nat Med *7*, 1236-1240.

Wheeler-Jones, C.P., Saermark, T., Kakkar, V.V., and Authi, K.S. (1992). Mastoparan promotes exocytosis and increases intracellular cyclic AMP in human platelets. Evidence for the existence of a Ge-like mechanism of secretion. Biochem J *281 (Pt 2)*, 465-472.

White, S.M., Constantin, P.E., and Claycomb, W.C. (2004). Cardiac physiology at the cellular level: use of cultured HL-1 cardiomyocytes for studies of cardiac muscle cell structure and function. Am J Physiol Heart Circ Physiol *286*, H823-829.

WHO (2004). http://www.who.int/mediacentre/factsheets/fs317/en/index.html.

Whyte, J.R., and Munro, S. (2002). Vesicle tethering complexes in membrane traffic. J Cell Sci *115*, 2627-2637.

Wickman, K.D., Iniguez-Lluhl, J.A., Davenport, P.A., Taussig, R., Krapivinsky, G.B., Linder, M.E., Gilman, A.G., and Clapham, D.E. (1994). Recombinant G-protein beta gamma-subunits activate the muscarinic-gated atrial potassium channel. Nature *368*, 255-257.

Wieland, F.T., Gleason, M.L., Serafini, T.A., and Rothman, J.E. (1987). The rate of bulk flow from the endoplasmic reticulum to the cell surface. Cell *50*, 289-300.

Wieland, T., and Mittmann, C. (2003). Regulators of G-protein signalling: multifunctional proteins with impact on signalling in the cardiovascular system. Pharmacol Ther *97*, 95-115.

Wildey, G.M., Fischman, A.J., Margolies, M.N., Graham, R.M., and Homcy, C.J. (1990). Phosphorylation state of pro-atrial natriuretic factor in rat atrial secretory granules. Endocrinology *127*, 2839-2848.

Willenbrock, R., Pagel, I., Scheuermann, M., Hohnel, K., Mackenzie, H.S., Brenner, B.M., and Dietz, R. (1999). Renal function in high-output heart failure in rats: role of endogenous natriuretic peptides. J Am Soc Nephrol *10*, 572-580.

Wilson, E.M., and Chinkers, M. (1995). Identification of sequences mediating guanylyl cyclase dimerization. Biochemistry *34*, 4696-4701.

Winaver, J., Hoffman, A., Burnett, J.C., Jr., and Haramati, A. (1988). Hormonal determinants of sodium excretion in rats with experimental high-output heart failure. Am J Physiol *254*, R776-784.

Wolf, W.P., Spicher, K., Haase, H., and Schulze, W. (1998). Immunocytochemical localization of the G-protein sub-unit, G(o) alpha, in rat heart. Implications for a role of G(o) alpha in secretion of cardiac hormones. J Mol Cell Cardiol *30*, 1149-1162.

Wright, M.O., Nishida, K., Bavington, C., Godolphin, J.L., Dunne, E., Walmsley, S., Jobanputra, P., Nuki, G., and Salter, D.M. (1997). Hyperpolarisation of cultured human chondrocytes following cyclical pressure-induced strain: evidence of a role for alpha 5 beta 1 integrin as a chondrocyte mechanoreceptor. J Orthop Res *15*, 742-747.

Wu, F., Yan, W., Pan, J., Morser, J., and Wu, Q. (2002). Processing of pro-atrial natriuretic peptide by corin in cardiac myocytes. J Biol Chem *277*, 16900-16905.

Wu, J., LaPointe, M.C., West, B.L., and Gardner, D.G. (1989). Tissue-specific determinants of human atrial natriuretic factor gene expression in cardiac tissue. J Biol Chem *264*, 6472-6479.

Wu, X., Cheng, J., Li, P., Yang, M., Qiu, S., Liu, P., and Du, J. (2010). Mechano-sensitive transcriptional factor Egr-1 regulates insulin-like growth factor-1 receptor expression and contributes to neointima formation in vein grafts. Arterioscler Thromb Vasc Biol *30*, 471-476.

Xiang, F., Sakata, Y., Cui, L., Youngblood, J.M., Nakagami, H., Liao, J.K., Liao, R., and Chin, M.T. (2006). Transcription factor CHF1/Hey2 suppresses cardiac hypertrophy through an inhibitory interaction with GATA4. Am J Physiol Heart Circ Physiol *290*, H1997-2006.

Xing, W., Baylink, D., Kesavan, C., Hu, Y., Kapoor, S., Chadwick, R.B., and Mohan, S. (2005). Global gene expression analysis in the bones reveals involvement of several novel genes and pathways in mediating an anabolic response of mechanical loading in mice. J Cell Biochem *96*, 1049-1060.

Xu, T., Jiao, J.H., Pence, R.A., and Baertschi, A.J. (1996). ATP-sensitive potassium channels regulate stimulated ANF secretion in isolated rat heart. Am J Physiol *271*, H2339-2345.

Yamada, K., Yoshida, S., and Shimada, Y. (1991). Atrial natriuretic polypeptide secretion via selective activation of kappa-opioid receptor: role of dynorphin. Am J Physiol *261*, E293-297.

Yan, W., Wu, F., Morser, J., and Wu, Q. (2000). Corin, a transmembrane cardiac serine protease, acts as a pro-atrial natriuretic peptide-converting enzyme. Proc Natl Acad Sci U S A *97*, 8525-8529.

Yanagisawa, M., and Masaki, T. (1989). Endothelin, a novel endothelium-derived peptide. Pharmacological activities, regulation and possible roles in cardiovascular control. Biochem Pharmacol *38*, 1877-1883.

Yang-Feng, T.L., Floyd-Smith, G., Nemer, M., Drouin, J., and Francke, U. (1985). The pronatriodilatin gene is located on the distal short arm of human chromosome 1 and on mouse chromosome 4. Am J Hum Genet *37*, 1117-1128.

Yao, J., Suwa, M., Li, B., Kawamura, K., Morioka, T., and Oite, T. (2003). ATP-dependent mechanism for coordination of intercellular Ca2+ signaling and renin secretion in rat juxtaglomerular cells. Circ Res *93*, 338-345.

Yatsu, T., Kurosawa, H., Hayashi, M., and Satoh, S. (2003). The role of Ca2+ in the control of renin release from dog renal cortical slices. Eur J Pharmacol *458*, 191-196.

Yi, Z., Yokota, H., Torii, S., Aoki, T., Hosaka, M., Zhao, S., Takata, K., Takeuchi, T., and Izumi, T. (2002). The Rab27a/granuphilin complex regulates the exocytosis of insulin-containing dense-core granules. Mol Cell Biol *22*, 1858-1867.

Yokokawa, N., Komatsu, M., Takeda, T., Aizawa, T., and Yamada, T. (1989). Mastoparan, a wasp venom, stimulates insulin release by pancreatic islets through pertussis toxin sensitive GTP-binding protein. Biochem Biophys Res Commun *158*, 712-716.

Yokota, N., Bruneau, B.G., Fernandez, B.E., de Bold, M.L., Piazza, L.A., Eid, H., and de Bold, A.J. (1995). Dissociation of cardiac hypertrophy, myosin heavy chain isoform expression, and natriuretic peptide production in DOCA-salt rats. Am J Hypertens *8*, 301-310.

Yokota, N., Bruneau, B.G., Kuroski de Bold, M.L., and de Bold, A.J. (1994). Atrial natriuretic factor significantly contributes to the mineralocorticoid escape

phenomenon. Evidence for a guanylate cyclase-mediated pathway. J Clin Invest *94*, 1938-1946.

Yokota, N., Yamamoto, Y., Kitamura, K., Kangawa, K., Minamino, N., Matsuo, H., and Eto, T. (1993). Alterations in circulating and cardiac tissue concentrations of brain natriuretic peptide in spontaneously hypertensive rats. Cardiovasc Res *27*, 1312-1315.

Yoon, E.J., Gerachshenko, T., Spiegelberg, B.D., Alford, S., and Hamm, H.E. (2007). Gbetagamma interferes with Ca2+-dependent binding of synaptotagmin to the soluble N-ethylmaleimide-sensitive factor attachment protein receptor (SNARE) complex. Mol Pharmacol *72*, 1210-1219.

Yoon, P.O., Lee, M.A., Cha, H., Jeong, M.H., Kim, J., Jang, S.P., Choi, B.Y., Jeong, D., Yang, D.K., Hajjar, R.J.*, et al.* (2010). The opposing effects of CCN2 and CCN5 on the development of cardiac hypertrophy and fibrosis. J Mol Cell Cardiol *49*, 294-303.

Yutzey, K.E., and Bader, D. (1995). Diversification of cardiomyogenic cell lineages during early heart development. Circ Res *77*, 216-219.

Zaugg, M., and Schaub, M.C. (2003). Signaling and cellular mechanisms in cardiac protection by ischemic and pharmacological preconditioning. J Muscle Res Cell Motil *24*, 219-249.

Zeller, R., Bloch, K.D., Williams, B.S., Arceci, R.J., and Seidman, C.E. (1987). Localized expression of the atrial natriuretic factor gene during cardiac embryogenesis. Genes Dev *1*, 693-698.

Zeniou-Meyer, M., Zabari, N., Ashery, U., Chasserot-Golaz, S., Haeberle, A.M., Demais, V., Bailly, Y., Gottfried, I., Nakanishi, H., Neiman, A.M.*, et al.* (2007). Phospholipase D1 production of phosphatidic acid at the plasma membrane promotes exocytosis of large dense-core granules at a late stage. J Biol Chem *282*, 21746-21757.

Zhang, Y., Carreras, D., and de Bold, A.J. (2003). Discoordinate re-expression of cardiac fetal genes in N(omega)-nitro-L-arginine methyl ester (L-NAME) hypertension. Cardiovasc Res *57*, 158-167.

Zhao, A., Ohara-Imaizumi, M., Brissova, M., Benninger, R.K., Xu, Y., Hao, Y., Abramowitz, J., Boulay, G., Powers, A.C., Piston, D.*, et al.* (2010). Galphao represses insulin secretion by reducing vesicular docking in pancreatic beta-cells. Diabetes *59*, 2522-2529.

Zhao, X.S., Gallardo, T.D., Lin, L., Schageman, J.J., and Shohet, R.V. (2002). Transcriptional mapping and genomic analysis of the cardiac atria and ventricles. Physiol Genomics *12*, 53-60.

Zhou, M.D., Sucov, H.M., Evans, R.M., and Chien, K.R. (1995). Retinoid-dependent pathways suppress myocardial cell hypertrophy. Proc Natl Acad Sci U S A *92*, 7391-7395.

Appendices

Appendix 1. License agreement (McGrath, M.F. and A.J. de Bold, *Determinants of natriuretic peptide gene expression*. Peptides, 2005. 26(6): p. 933-43). See p. 278.

Appendix 2. License agreement (McGrath, M.F., M.L. de Bold, and A.J. de Bold, *The endocrine function of the heart*. Trends Endocrinol Metab, 2005. 16(10): p. 469-77). See p. 280.

Appendix 3. License agreement (Ogawa, T., Forero, M., Burgon, P. G., Kuroski de Bold, M. L., Georgalis, T. and de Bold, A. J., *Role of potassium channels in stretch-promoted atrial natriuretic factor secretion*. J Am Soc Hypertens, 2009. 3(1): p. 9-18). See p. 282.

Appendix 4. Filtered signal intensities data of atrial and ventricular biological replicates. List of 1415 differentially expressed genes. Table includes: Affymetrix Probe Set ID, RefSeq Transcript ID, UniGene Symbol, Gene Title and Fold Change. The average signal intensities of each probe set within the atrial and ventricular replicate groups were calculated and the difference between the two averages was determined (log2 ratio). The anti-log2 was then calculated to determine the fold change ratio. Note, positive fold changes indicate a higher gene expression in the atrial samples while negative fold changes indicate a higher gene expression in the ventricle samples. See p. 284.

Appendix 5. Differentially expressed genes between normal left atrial and left ventricular tissues classified into the "ligand" related functional groups. Positive fold change values indicate a higher abundance in the atria compared to the ventricles, whereas negative fold change values demonstrate a higher ventricular abundance in comparison to the atria. See p. 309.

Appendix 6. Differentially expressed genes between normal left atrial and left ventricular tissues classified into the "receptor" related functional groups. Positive fold change values indicate a higher abundance in the atria compared to the ventricles, whereas negative fold change values demonstrate a higher ventricular abundance in comparison to the atria. See p. 311.

Appendix 7. Differentially expressed genes between normal left atrial and left ventricular tissues classified into the DNA binding protein functional group. Positive fold change values indicate a higher abundance in the atria as compared to the ventricles, while negative fold change values demonstrate a higher ventricular abundance in comparison to the atria. See p. 313.

Appendix 8. Filtered signal intensities data of left and right atria 28-day shunt vs. sham biological replicates. List of 700 genes exhibiting an experimental condition effect based on a two-way ANOVA analysis (p-value < 0.001, FDR 0.045). The average signal intensities of each probe set within each replicate group were calculated and the

difference between the two averages, i.e. right atria 28d shunt minus sham, and left atria 28d shunt minus sham, was determined (log2 ratio). See p. 314.

Appendix 9. Gene functional classification clustering based on functional similarities of the differentially expressed genes found between 28-day volume overload and sham atrial tissues. Genes were grouped according to a high classification stringency setting based on the Kappa statistic implemented in the DAVID program. See p. 337.

Appendix 10. GoStat analysis output identifying highly represented Gene Ontology annotations in the atrial abundant gene list obtained from the VO atria vs. ventricles comparison. The output is sorted by the p-value obtained from the Fisher's Exact Test, which indicates how specific the GO terms are for this list of genes. See p. 340.

Appendix 11. Differentially expressed gene list generated by two-way ANOVA ($p < 0.001$) analysis for the interaction Tissue x Condition effect obtained by comparing the following four groups: LA sham, LA shunt, LV sham and LV shunt. See p. 343.

Appendix 1. License agreement (McGrath, M.F. and A.J. de Bold, *Determinants of natriuretic peptide gene expression*. Peptides, 2005. 26(6): p. 933-43).

ELSEVIER LICENSE
TERMS AND CONDITIONS

Mar 03, 2011

This is a License Agreement between Monica Forero McGrath ("You") and Elsevier ("Elsevier") provided by Copyright Clearance Center ("CCC"). The license consists of your order details, the terms and conditions provided by Elsevier, and the payment terms and conditions.

All payments must be made in full to CCC. For payment instructions, please see information listed at the bottom of this form.

Supplier	Elsevier Limited The Boulevard,Langford Lane Kidlington,Oxford,OX5 1GB,UK
Registered Company Number	1982084
Customer name	Monica Forero McGrath
Customer address	40 Ruskin street
	Ottawa, ON K1Y 4W7
License number	2560480619951
License date	Dec 01, 2010
Licensed content publisher	Elsevier
Licensed content publication	Peptides
Licensed content title	Determinants of natriuretic peptide gene expression
Licensed content author	Monica Forero McGrath, Adolfo J. de Bold
Licensed content date	June 2005
Licensed content volume number	26
Licensed content issue number	6
Number of pages	11
Start Page	933
End Page	943
Type of Use	reuse in a thesis/dissertation
Portion	full article
Format	both print and electronic
Are you the author of this Elsevier article?	Yes

Appendix 1 continued.

Will you be translating?	No
Order reference number	
Title of your thesis/dissertation	Identification of genes associated with the endocrine heart under normal and pathophysiological conditions using genomic and transcriptional analysis
Expected completion date	Feb 2011
Estimated size (number of pages)	250
Elsevier VAT number	GB 494 6272 12
Permissions price	0.00 USD
Value added tax 0.0%	0.0 USD / 0.0 GBP
Total	0.00 USD
Terms and Conditions	

Appendix 2. License agreement (McGrath, M.F., M.L. de Bold, and A.J. de Bold, *The endocrine function of the heart*. Trends Endocrinol Metab, 2005. 16(10): p. 469-77).

ELSEVIER LICENSE
TERMS AND CONDITIONS

Mar 03, 2011

This is a License Agreement between Monica Forero McGrath ("You") and Elsevier ("Elsevier") provided by Copyright Clearance Center ("CCC"). The license consists of your order details, the terms and conditions provided by Elsevier, and the payment terms and conditions.

All payments must be made in full to CCC. For payment instructions, please see information listed at the bottom of this form.

Supplier	Elsevier Limited The Boulevard,Langford Lane Kidlington,Oxford,OX5 1GB,UK
Registered Company Number	1982084
Customer name	Monica Forero McGrath
Customer address	40 Ruskin street Ottawa, ON K1Y 4W7
License number	2561471149587
License date	Dec 03, 2010
Licensed content publisher	Elsevier
Licensed content publication	Trends in Endocrinology & Metabolism
Licensed content title	The endocrine function of the heart
Licensed content author	Monica Forero McGrath, Mercedes L. Kuroski de Bold, Adolfo J. de Bold
Licensed content date	December 2005
Licensed content volume number	16
Licensed content issue number	10
Number of pages	9
Start Page	469
End Page	477
Type of Use	reuse in a thesis/dissertation
Intended publisher of new work	other
Portion	full article
Format	both print and electronic

Appendix 2 continued.

Are you the author of this Elsevier article?	Yes
Will you be translating?	No
Order reference number	
Title of your thesis/dissertation	Identification of genes associated with the endocrine heart under normal and pathophysiological conditions using genomic and transcriptional analysis
Expected completion date	Feb 2011
Estimated size (number of pages)	250
Elsevier VAT number	GB 494 6272 12
Permissions price	0.00 USD
Value added tax 0.0%	0.0 USD / 0.0 GBP
Total	0.00 USD
Terms and Conditions	

Appendix 3. License agreement (Ogawa, T., Forero, M., Burgon, P. G., Kuroski de Bold, M. L., Georgalis, T. and de Bold, A. J., *Role of potassium channels in stretch-promoted atrial natriuretic factor secretion*. J Am Soc Hypertens, 2009. 3(1): p. 9-18).

ELSEVIER LICENSE
TERMS AND CONDITIONS

Mar 03, 2011

This is a License Agreement between Monica Forero McGrath ("You") and Elsevier ("Elsevier") provided by Copyright Clearance Center ("CCC"). The license consists of your order details, the terms and conditions provided by Elsevier, and the payment terms and conditions.

All payments must be made in full to CCC. For payment instructions, please see information listed at the bottom of this form.

Supplier	Elsevier Limited The Boulevard,Langford Lane Kidlington,Oxford,OX5 1GB,UK
Registered Company Number	1982084
Customer name	Monica Forero McGrath
Customer address	40 Ruskin street Ottawa, ON K1Y 4W7
License number	2564190678535
License date	Dec 08, 2010
Licensed content publisher	Elsevier
Licensed content publication	Journal of the American Society of Hypertension
Licensed content title	Role of potassium channels in stretch-promoted atrial natriuretic factor secretion
Licensed content author	Tsuneo Ogawa, Monica Forero, Patrick G. Burgon, Mercedes L. Kuroski de Bold, Tina Georgalis, Adolfo J. de Bold
Licensed content date	January-February 2009
Licensed content volume number	3
Licensed content issue number	1
Number of pages	10
Start Page	9
End Page	18
Type of Use	reuse in a thesis/dissertation
Intended publisher of new	other

Appendix 3 continued.

work	
Portion	full article
Format	both print and electronic
Are you the author of this Elsevier article?	Yes
Will you be translating?	No
Order reference number	
Title of your thesis/dissertation	Identification of genes associated with the endocrine heart under normal and pathophysiological conditions using genomic and transcriptional analysis
Expected completion date	Feb 2011
Estimated size (number of pages)	250
Elsevier VAT number	GB 494 6272 12
Permissions price	0.00 USD
Value added tax 0.0%	0.00 USD / GBP
Total	0.00 USD
Terms and Conditions	

Appendix 4- Fold change ratios of differentially expressed genes between normal atrial and ventricular biological replicates

Probe Set ID	RefSeq Transcript ID	UniGene Symbol	Gene Title	Fold Change Atria vs. Ventricles
1374391_at	NM_001013247	Sln	sarcolipin	245.967
1371293_at	NM_001109495	LOC688228	similar to Myosin light polypeptide 4 (Myosin light chain 1, atrial isoform)	160.422
1389236_at	NM_001014042	RGD1310511	similar to Myosin-binding protein H (MyBP-H) (H-protein)	113.063
1387321_at	NM_053381	Atp1b4	ATPase, (Na+)/K+ transporting, beta 4 polypeptide	68.549
1371400_at	NM_012703	Thrsp	thyroid hormone responsive protein	38.704
1387985_a_at	NM_001033958 /// NM_001033959 /// NM_147215	Obp3	alpha-2u globulin PGCL4	35.173
1367896_at	NM_019292	Ca3	carbonic anhydrase 3	34.873
1390107_at	NM_001108492	Sytl2_predicted	synaptotagmin-like 2 (predicted)	32.253
1367977_at	NM_019169	Snca	synuclein, alpha	31.783
1384035_at	XM_001063122 /// XM_002724859	LOC685277 /// LOC686794	similar to liver-specific bHLH-Zip transcription factor	30.994
1371315_at	NM_001106017	Myl7_predicted	myosin, light polypeptide 7, regulatory (predicted)	26.192
1368785_a_at	NM_001042505 /// NM_019334	Pitx2	paired-like homeodomain transcription factor 2	25.916
1373646_at	NM_198749	Rab15	RAB15, member RAS onocogene family	24.531
1378374_at	XR_008828 /// XR_086030	RGD1560137_predicted	similar to expressed sequence AU021034 (predicted)	22.021
1368441_at	NM_031658	Msln	mesothelin	21.134
1393260_at	NM_001003706	LOC360228	WDNM1 homolog	20.867
1370355_at	NM_139192	Scd1	stearoyl-Coenzyme A desaturase 1	20.81
1388433_at	NM_199498	Krt1-19	keratin complex 1, acidic, gene 19	20.579
1368854_at	NM_012686	Vsnl1	visinin-like 1	19.993
1370892_at	NM_001002805 /// NM_031504	C4-2 /// C4a	complement component 4a /// complement component 4, gene 2	18.847
1379526_at	---	---	Transcribed locus	17.662
1383460_at	---	---	---	17.509
1390638_at	NM_001162411	RGD1560587_predicted	similar to Eph receptor A4 (predicted)	17.506
1368470_at	NM_012960	Ggh	gamma-glutamyl hydrolase	15.66
1375729_at	NM_001162411	RGD1560587_predicted	similar to Eph receptor A4 (predicted)	15.562
1374089_at	---	---	Transcribed locus	13.927
1370198_at	NM_021666	Trdn	triadin	13.382
1367564_at	NM_012612	Nppa	natriuretic peptide precursor type A	12.883
1372935_at	NM_001107155	Tmem119_predicted	transmembrane protein 119 homolog (predicted)	12.882
1375861_at	NM_001044293	MGC105733	similar to nucleosome assembly protein 1-like 5	12.774
1368853_at	NM_012686	Vsnl1	visinin-like 1	12.721
1381575_at	---	Neb_predicted	nebulin (predicted)	12.307
1377275_at	NM_001107541	Art1_predicted	ADP-ribosyltransferase 1 (predicted)	12.274
1384454_at	NM_001107900	Cpa6_predicted	carboxypeptidase A6 (predicted)	11.984
1396206_at	NM_001109344	RGD1562846_predicted	similar to Docking protein 5 (Downstream of tyrosine kinase 5) (Protein dok-5) (predicted)	11.504
1378970_at	NM_001014042	RGD1310511	Similar to Myosin-binding protein H (MyBP-H) (H-protein)	11.425
1387396_at	NM_053469	Hamp	hepcidin antimicrobial peptide	11.265
1374276_at	---	---	Transcribed locus	11.119
1391139_at	---	Adamtsl1_predicted	ADAMTS-like 1 (predicted)	10.593
1368706_at	NM_053785	Tm4sf4	transmembrane 4 superfamily member 4	9.919
1391264_at	---	---	Transcribed locus	9.766
1397610_at	---	---	Transcribed locus	9.748
1372264_at	NM_198780	Pck1	phosphoenolpyruvate carboxykinase 1	9.687
1379970_at	NM_001162411	RGD1560587_predicted	similar to Eph receptor A4 (predicted)	9.646
1371762_at	NM_013162	Rbp4	retinol binding protein 4, plasma	9.633
1371530_at	NM_199370	Krt2-8	keratin complex 2, basic, gene 8	9.599
1381997_at	NM_144744	Adipoq	adiponectin, C1Q and collagen domain containing	9.41
1379022_at	NM_001106811	Adamts8_predicted	a disintegrin-like and metallopeptidase (reprolysin type) with thrombospondin type 1 motif, 8 (predicted)	9.39
1389470_at	NM_212466	Cfb	complement factor B	9.316

	NM_001033958 NM_001033959			
1370479_x_at	NM_147215	Obp3	alpha-2u globulin PGCL4	9.17
1394855_at	---	---	Transcribed locus	8.656
1367755_at	NM_052809	Cdo1	cysteine dioxygenase 1, cytosolic	8.519
1368395_at	NM_012774	Gpc3	glypican 3	8.442
1367707_at	NM_017332	Fasn	fatty acid synthase	8.124
1375983_at	XM_001078660 /// XM_219905	Mamdc2	MAM domain containing 2	8.093
1371447_at	NM_001108353	Plac8_predicted	placenta-specific 8 (predicted)	8.045
1369125_at	NM_017254	Htr2a	5-hydroxytryptamine (serotonin) receptor 2A	7.861
1369740_at	NM_031610	Kcnj3	potassium inwardly-rectifying channel, subfamily J, member 3	7.765
1368560_at	NM_017297	Kcnj5	potassium inwardly-rectifying channel, subfamily J, member 5	7.683
1392583_at	---	---	Transcribed locus	7.619
1383479_at	---	---	Transcribed locus	7.591
1371044_at	NM_031080	Pde7a	phosphodiesterase 7A	7.523
1374630_at	NM_001013080	Clic3	chloride intracellular channel 3	7.461
1372809_at	NM_001106063	LOC290595	hypothetical gene supported by AF152002	7.306
1373110_at	---	---	Transcribed locus	7.154
1368515_at	NM_053927	Epb4.1l3	erythrocyte protein band 4.1-like 3	7.083
1382222_at	NM_001110763	RGD1306212_predicted	similar to hypothetical protein DKFZp566N034 (predicted)	7.048
1378001_at	---	---	Transcribed locus	7.025
1368474_at	NM_012889	Vcam1	vascular cell adhesion molecule 1	6.97
1377139_at	NM_001009964	Tbx5	T-box 5	6.963
1370805_at	NM_172055	Cited1	Cbp/p300-interacting transactivator with Glu/Asp-rich carboxy-terminal domain 1	6.854
1383542_at	---	---	Transcribed locus	6.714
1373773_at	NM_178105	Gpm6a	glycoprotein m6a	6.39
1369741_at	NM_031610	Kcnj3	potassium inwardly-rectifying channel, subfamily J, member 3	6.347
1379625_at	NM_001107661	---	Transcribed locus	6.24
1386598_at	NM_001107541	Art1_predicted	ADP-ribosyltransferase 1 (predicted)	6.203
1390112_at	NM_001012039	Efemp1	epidermal growth factor-containing fibulin-like extracellular matrix protein 1	6.196
1367700_at	NM_080698	Fmod	fibromodulin	6.181
1383846_at	NM_001109344	RGD1562846_predicted	similar to Docking protein 5 (Downstream of tyrosine kinase 5) (Protein dok-5) (predicted)	6.159
1391241_at	NM_001108709 NM_001163156	---	Transcribed locus	6.153
1383757_at	---	---	Transcribed locus	6.098
1369273_a_at	NM_012868	Npr3	natriuretic peptide receptor 3	6.037
1397015_at	NM_001108709 NM_001163156	---	Transcribed locus	6.03
1370503_s_at	NM_053927	Epb4.1l3	erythrocyte protein band 4.1-like 3	6.007
1371861_at	---	---	Transcribed locus	5.996
1369999_a_at	NM_053601 /// NM_181687	Nnat	neuronatin	5.991
1380458_at	---	---	Transcribed locus	5.961
1382878_at	XM_001072532 /// XM_224987	Sfrp1	secreted frizzled-related protein 1	5.904
1385099_at	NM_001108388	Scel_predicted	sciellin (predicted)	5.842
1384468_at	---	---	Transcribed locus	5.786
1368284_at	NM_020086	Plvap	plasmalemma vesicle associated protein	5.765
1385859_at	---	---	Transcribed locus	5.713
1385486_at	NM_001106666	Bnc2_predicted	basonuclin 2 (predicted)	5.706
1383516_at	NM_053455	Fgl2	fibrinogen-like 2	5.668
1382593_at	NM_001108709 NM_001163156	Etv1_predicted	ets variant gene 1 (predicted)	5.634
1367787_at	NM_030844	Ica1	islet cell autoantigen 1	5.626
1378653_at	---	---	Transcribed locus	5.565
1376344_at	---	---	Transcribed locus	5.476
1382931_at	---	---	Transcribed locus	5.391
1388602_at	NM_001077642	Cfd	complement factor D (adipsin)	5.372
1392228_at	---	---	Transcribed locus	5.317
1378305_at	NM_001106434	Tm4sf1_predicted	transmembrane 4 superfamily member 1 (predicted)	5.29
1372398_at	NM_001109141	LOC499129	similar to potassium channel tetramerisation domain containing 15	5.212
1384437_at	XM_002727681 /// XM_229124	Smarca1_predicted	SWI/SNF related, matrix associated, actin dependent regulator of chromatin, subfamily a, member 1 (predicted)	5.13
1386637_at	NM_053455	Fgl2	fibrinogen-like 2	5.055
1370406_a_at	NM_022269	Daf1	decay accelarating factor 1	5.053
1376946_at	---	---	Transcribed locus	5.004

1373781_a_at	NM_001044231	RGD1562305_predicted	similar to suprabasal-specific protein suprabasin (predicted)	4.993
1370410_at	NM_175763	Igsf1	immunoglobulin superfamily, member 1	4.984
1398365_at	NM_001009639	RGD1305061	similar to RIKEN cDNA 2700055K07	4.92
1385014_at	XM_001056321 /// XM_002727533	LOC680248 /// LOC683238	similar to Diphosphoinositol polyphosphate phosphohydrolase 3 alpha (DIPP-3 alpha) (DIPP3 alpha) (Diadenosine 5,5-P1,P6-hexaphosphate hydrolase 3 alpha) (Nucleoside diphosphate-linked moiety X motif 10) (Nudix motif 10)	4.913
1385127_at	NM_001108168	Bmp5_predicted	bone morphogenetic protein 5 (predicted)	4.872
1369484_at	NM_031590	Wisp2	WNT1 inducible signaling pathway protein 2	4.801
1386913_at	NM_019358	Pdpn	podoplanin	4.799
1367852_s_at	NM_053930 /// NM_053931	Gp1bb /// Sept5	glycoprotein Ib, beta polypeptide /// septin 5	4.797
1390459_at	---	---	Transcribed locus	4.791
1383266_at	XM_001072532 /// XM_224987	Sfrp1	secreted frizzled-related protein 1	4.772
1384036_s_at	XM_001063122 XM_002724859	---	---	4.765
1387470_at	NM_031699	Cldn1	claudin 1	4.752
1379275_at	NM_001013085	Snx10	sorting nexin 10	4.729
1384544_at	NM_001004086	Pon3	paraoxonase 3	4.684
1395471_at	---	---	Transcribed locus	4.676
1369953_a_at	NM_012752	Cd24	CD24 antigen	4.607
1388545_at	NM_001002835	Smoc1	SPARC-related modular calcium binding protein 1	4.596
1377773_at	---	---	Transcribed locus, weakly similar to NP_766020.1 RIKEN cDNA C030002O17 [Mus musculus]	4.582
1368194_at	NM_133406	Agpat4	1-acylglycerol-3-phosphate O-acyltransferase 4 (lysophosphatidic acid acyltransferase, delta)	4.515
1390530_at	---	---	Transcribed locus	4.503
1391630_at	NM_001108173	Tbx18_predicted	T-box18 (predicted)	4.486
1378699_at	NM_001034931	Pkhd1l1	polycystic kidney and hepatic disease 1-like 1	4.482
1396152_s_at	NM_012817	Igfbp5	insulin-like growth factor binding protein 5	4.48
1367960_at	NM_019186	Arl4a	ADP-ribosylation factor-like 4A	4.432
1390421_at	NM_001106355	RGD1310475_predicted	Similar to RIKEN cDNA 0610010D20 (predicted)	4.421
1389107_at	NM_001108164	RGD1304623_predicted	similar to KIAA1749 protein (predicted)	4.414
1384737_at	---	---	Transcribed locus	4.4
1392976_at	NM_001024345	MGC109519	similar to tropomyosin 1, embryonic fibroblast - rat	4.33
1372382_at	---	---	Transcribed locus	4.316
1396150_at	NM_031699	Cldn1	claudin 1	4.299
1385638_at	---	---	Transcribed locus	4.261
1381079_at	NM_001108916	Bnc1_predicted	basonuclin 1 (predicted)	4.251
1387029_at	NM_130409	Cfh	complement component factor H	4.245
1393516_at	---	---	Transcribed locus	4.226
1375961_at	NM_001100527	Frzb	frizzled-related protein	4.225
1391187_at	NM_001106976	Ppl_predicted	periplakin (predicted)	4.225
1389803_at	---	---	Transcribed locus	4.216
1388209_at	NM_001030022	Tsga10	testis specific 10	4.213
1369067_at	NM_017352 /// NM_031628	Nr4a3	nuclear receptor subfamily 4, group A, member 3	4.19
1370033_at	NM_001077656 /// NM_020104	Myl1	myosin, light polypeptide 1	4.19
1370342_at	NM_172041 /// NM_172042	Kcnk2	potassium channel, subfamily K, member 2	4.19
1387209_at	NM_053571	Lztr2	leucine zipper transcription regulator 2	4.186
1387951_at	NM_022269	Daf1	decay accelarating factor 1	4.183
1386903_at	NM_013191	S100b	S100 protein, beta polypeptide	4.176
1383903_at	NM_213628	St8sia5	ST8 alpha-N-acetyl-neuraminide alpha-2,8-sialyltransferase 5	4.148
1389500_at	---	LOC678766	similar to ras homolog gene family, member U	4.133
1368368_a_at	NM_032616	Lsr	lipolysis stimulated lipoprotein receptor	4.099
1375056_at	XM_002724958	---	---	4.075
1374432_at	---	---	---	4.071
1394747_at	NM_013220	Ankrd1	Ankyrin repeat domain 1 (cardiac muscle)	4.07
1396249_at	---	---	Transcribed locus	4.055
1389554_at	---	---	Transcribed locus	4.029
1374244_at	---	---	---	4.011
1380477_at	---	---	Transcribed locus	3.987
1377904_at	---	---	Transcribed locus	3.984
1394972_at	NM_001107183	Trove2_predicted	TROVE domain family, member 2 (predicted)	3.952
1383015_at	NM_001081980	RGD1311490_predicted	similar to DKFZP434P1750 protein (predicted)	3.945
1387803_at	NM_022209	Ppp2r2b	protein phosphatase 2 (formerly 2A), regulatory subunit B (PR 52), beta isoform	3.94
1387365_at	NM_031627	Nr1h3	nuclear receptor subfamily 1, group H, member 3	3.938

1376165_at	NM_053505	Slc24a3	solute carrier family 24 (sodium/potassium/calcium exchanger), member 3	3.91
1373970_at	NM_001014166	RGD1311155	similar to RIKEN cDNA 9230117N10	3.894
1394655_at	---	---	Transcribed locus	3.892
1376425_at	NM_031131	Tgfb2	Transforming growth factor, beta 2	3.886
1375936_at	NM_001033688 /// NM_001025289 /// NM_001025291 /// NM_001025292 /// NM_001025293 /// NM_001025294	Dsc2	desmocollin 2	3.867
1368810_a_at	NM_017026	Mbp	myelin basic protein	3.846
1390856_at	---	---	Transcribed locus	3.831
1373335_at	NM_001039016	Zdhhc9	zinc finger, DHHC domain containing 9	3.827
1383062_at	---	---	Transcribed locus	3.823
1367851_at	NM_013015	Ptgds	prostaglandin D2 synthase	3.813
1393159_at	---	---	Transcribed locus	3.789
1393997_at	NM_001163723	RGD1564257_predicted	similar to hypothetical protein FLJ32825 (predicted)	3.789
1370862_at	NM_138828	Apoe	apolipoprotein E	3.778
1369729_at	NM_053979	Arl5a	ADP-ribosylation factor-like 5A	3.761
1375001_at	NM_001134604 /// XM_001077321 ///	---	Transcribed locus	3.761
1387908_at	XM_340809	Rasd1	RAS, dexamethasone-induced 1	3.751
1368702_at	NM_033485	Pawr	PRKC, apoptosis, WT1, regulator	3.744
1395586_at	---	---	Transcribed locus	3.743
1371138_at	NM_021666	Trdn	triadin	3.685
1386660_at	---	---	---	3.678
1384834_at	NM_001107236	Cobl_predicted	cordon-bleu (predicted)	3.646
1387172_a_at	NM_031131	Tgfb2	transforming growth factor, beta 2	3.641
1387625_at	NM_013104	Igfbp6	insulin-like growth factor binding protein 6	3.612
1378355_a_at	NM_001108051	Slc24a4_predicted	solute carrier family 24 (sodium/potassium/calcium exchanger), member 4 (predicted)	3.608
1392590_at	NM_001012032	Arhgap24	Rho GTPase activating protein 24	3.608
1368127_at	NM_017130	Neu2	neuraminidase 2	3.604
1389581_at	NM_001014166	RGD1311155	similar to RIKEN cDNA 9230117N10	3.603
1393129_at	NM_198775	P4ha3	procollagen-proline, 2-oxoglutarate 4-dioxygenase (proline 4-hydroxylase), alpha polypeptide III	3.594
1382908_at	NM_001162411	RGD1560587_predicted	similar to Eph receptor A4 (predicted)	3.591
1383196_at	NM_001126276	Znf579_predicted	zinc finger protein 579 (predicted)	3.59
1394022_at	NM_175582	Id4	inhibitor of DNA binding 4	3.588
1384634_at	---	---	---	3.581
1388791_at	NM_001014102	RGD1309930	similar to 2810022L02Rik protein	3.577
1377369_at	NM_001011954	Cybrd1	cytochrome b reductase 1	3.543
1383258_at	---	RGD1310587	similar to hypothetical protein FLJ14146	3.538
1377390_at	NM_001002802	Bace2	beta-site APP-cleaving enzyme 2	3.536
1376800_at	---	---	Transcribed locus	3.533
1393000_at	---	---	---	3.532
1370391_at	NM_017244	Crabp2	cellular retinoic acid binding protein 2	3.531
1368883_at	NM_030868	Nov	nephroblastoma overexpressed gene	3.506
1388051_at	NM_053755	Slc26a3	solute carrier family 26, member 3	3.494
1387925_at	NM_013079	Asns	asparagine synthetase	3.482
1382294_at	---	---	Transcribed locus	3.464
1373433_at	NM_001134706	LOC680182 /// LOC681284 /// Nsbp1_predicted	nucleosome binding protein 1 (predicted) /// similar to Nucleosome binding protein 1 (Nucleosome binding protein 45) (NBP-45) (GARP45 protein)	3.409
1368000_at	NM_016994	C3	complement component 3	3.403
1390306_at	---	---	Transcribed locus	3.403
1372168_s_at	NM_013104	Igfbp6	insulin-like growth factor binding protein 6	3.399
1392382_at	NM_031131	Tgfb2	Transforming growth factor, beta 2	3.39
1394833_at	---	---	Transcribed locus	3.386
1392943_at	NM_001108016	Oact2	O-acyltransferase (membrane bound) domain containing 2	3.377
1367939_at	NM_012733	Rbp1	retinol binding protein 1, cellular	3.368
1384406_at	XM_001061617 /// XM_002727133	LOC685243	similar to C-C chemokine receptor type 11 (C-C CKR-11) (CC-CKR-11) (CCR-11) (Chemokine receptor-like 1) (CCRL1) (CCX CKR)	3.362
1368021_at	NM_019286	Adh1	alcohol dehydrogenase 1 (class I)	3.341
1370291_at	NM_053650	Pdlim3	PDZ and LIM domain 3	3.332
1378733_at	---	---	Transcribed locus	3.326
1370328_at	NM_138519	Dkk3	dickkopf homolog 3 (Xenopus laevis)	3.325
1393060_at	XM_001078833 /// XM_231125	RGD1305459_predicted	similar to KIAA0605 gene product (predicted)	3.307
1382954_at	---	---	Transcribed locus	3.304
1393351_at	NM_181478	Rdh10	Retinol dehydrogenase 10 (all-trans)	3.284

1367920_at	NM_017192	Edg5	endothelial differentiation, sphingolipid G-protein-coupled receptor, 5	3.277
1371947_at	NM_001008558	Ndn	necdin	3.276
1368128_at	NM_031598	Pla2g2a	phospholipase A2, group IIA (platelets, synovial fluid)	3.275
1383826_at	NM_001107076	Rab40b_predicted	Rab40b, member RAS oncogene family (predicted)	3.268
1377790_at	---	---	Transcribed locus	3.266
1391022_at	NM_001100841	Lamb3	laminin, beta 3	3.247
1370932_at	NM_031322	Lrp4	low density lipoprotein receptor-related protein 4	3.234
1380432_at	NM_001024273	Cmah	cytidine monophospho-N-acetylneuraminic acid hydroxylase	3.234
1388936_at	NM_053392	Cdh11	cadherin 11	3.226
1383021_at	NM_199106	Galnt13	UDP-N-acetyl-alpha-D-galactosamine:polypeptide N-acetylgalactosaminyltransferase 13	3.224
1367992_at	NM_013175	Sgne1	secretory granule neuroendocrine protein 1	3.215
1377868_at	XM_001054048 /// XM_228821	RGD1561019_predicted	similar to hypothetical protein (predicted)	3.209
1388600_at	---	---	CDNA clone IMAGE:7320582	3.178
1389637_at	---	---	Transcribed locus	3.178
1368367_at	NM_054005	Cuzd1	CUB and zona pellucida-like domains 1	3.168
1382054_at	---	---	Transcribed locus	3.161
1395109_at	---	---	Transcribed locus	3.157
1382368_at	NM_001107183	Trove2_predicted	TROVE domain family, member 2 (predicted)	3.155
1370086_at	NM_012559	Fgg	fibrinogen, gamma polypeptide	3.152
1390536_at	---	---	Transcribed locus	3.149
1368399_a_at	NM_031640	Pgcp	plasma glutamate carboxypeptidase	3.148
1367847_at	NM_053611	Nupr1	nuclear protein 1	3.142
1370758_at	NM_198749	Rab15	RAB15, member RAS onocogene family	3.135
1370442_at	NM_173313	Tmsbl1	thymosin beta-like protein 1	3.133
1385506_at	---	---	Transcribed locus	3.133
1392274_at	---	---	Transcribed locus	3.131
1391008_at	---	---	Transcribed locus	3.116
1373156_at	NM_001014274	Armcx2	armadillo repeat containing, X-linked 2	3.104
1372665_at	NM_198738	Psat1	phosphoserine aminotransferase 1	3.102
1382137_at	NM_001106162	Abhd3_predicted	abhydrolase domain containing 3 (predicted)	3.097
1382481_a_at	NM_001107776	Adam33_predicted	a disintegrin and metallopeptidase domain 33 (predicted)	3.097
1367791_at	NM_031645	Ramp1	receptor (calcitonin) activity modifying protein 1	3.069
1389797_at	---	---	Transcribed locus	3.069
1378857_at	XM_001056444 XM_002727646	---	---	3.063
1395821_at	NM_001013191	Cbfb	core binding factor beta	3.061
1389543_at	NM_022257	Masp1	mannan-binding lectin serine peptidase 1	3.047
1374298_at	---	---	Transcribed locus	3.042
1392140_at	---	---	Transcribed locus	3.031
1388320_at	NM_001082549 /// NM_199087	Spint2	serine protease inhibitor, Kunitz type 2	3.03
1383122_at	NM_184051	Prkag2	protein kinase, AMP-activated, gamma 2 non-catalytic subunit	3.026
1383129_at	NM_001085353 /// NM_199408	LOC362065	CG6210-like	3.021
1370623_at	NM_053455	Fgl2	fibrinogen-like 2	3.014
1370508_a_at	NM_031601	Cacna1g	calcium channel, voltage-dependent, T type, alpha 1G subunit	3.01
1370019_at	NM_031834	Sult1a1	sulfotransferase family 1A, phenol-preferring, member 1	3.005
1397830_at	NM_012817	Igfbp5	insulin-like growth factor binding protein 5	2.991
1373373_at	---	---	Transcribed locus	2.982
1398370_at	NM_001111055 NM_001111056 NM_001111057 /// NM_012894	Adarb1	Adenosine deaminase, RNA-specific, B1	2.979
1382631_at	---	---	Transcribed locus	2.976
1384391_at	NM_181478	Rdh10	retinol dehydrogenase 10 (all-trans)	2.964
1377034_at	NM_001031642	Serpinb1a	serine (or cysteine) proteinase inhibitor, clade B, member 1a	2.957
1387122_at	NM_012760	Plagl1	pleiomorphic adenoma gene-like 1	2.957
1374081_at	XM_342506	Casc4_predicted	cancer susceptibility candidate 4 (predicted)	2.956
1374776_at	NM_001109082	RGD1564105_predicted	similar to RIKEN cDNA B130052G07 (predicted)	2.95
1368528_at	NM_134459	Mic2l1	MIC2 like 1	2.945
1372895_at	NM_001014140	RGD1309676	similar to RIKEN cDNA 5730469M10	2.937
1374659_at	NM_001135045 /// NM_001135046	LOC363153 /// RGD1307215	similar to cyclic AMP-regulated phosphoprotein, 21 isoform 2 /// similar to protein phosphatase 1, regulatory (inhibitory) subunit 1C; thymocyte ARPP; DNA segment, Chr 9, Brigham & Womens Genetics 1012 expressed	2.937
1390605_at	---	---	Transcribed locus	2.936

1375845_at	NM_001134425	RGD1562920_predicted	similar to Aig1 protein (predicted)	2.935
1391249_at	NM_001106144	RGD1312005_predicted	similar to DD1 (predicted)	2.906
1395336_at	XM_002730070	RGD1309930	similar to 2810022L02Rik protein	2.889
1370043_at	NM_031753	Alcam	activated leukocyte cell adhesion molecule	2.882
1375999_at	NM_001106144	---	Transcribed locus	2.881
1371232_a_at	XM_001058357 /// XM_215451	Cspg2	chondroitin sulfate proteoglycan 2	2.875
1379571_at	NM_001106482	Pkp4_predicted	plakophilin 4 (predicted)	2.847
1388628_at	NM_001004249	Tmed3	transmembrane emp24 domain containing 3	2.819
1381003_at	NM_001106916	Zfpn1a2_predicted	zinc finger protein, subfamily 1A, 2 (Helios) (predicted)	2.798
1376689_at	NM_001009430	RGD1305457	similar to RIKEN cDNA 1700023M03	2.794
1375908_at	NM_001106818	Eva1_predicted	epithelial V-like antigen 1 (predicted)	2.792
1376734_at	---	---	Transcribed locus	2.782
1388920_at	NM_013107	Bmp6	bone morphogenetic protein 6	2.782
1388054_a_at	XM_215451	Cspg2	chondroitin sulfate proteoglycan 2	2.773
1368920_at	NM_031321	Slit3	slit homolog 3 (Drosophila)	2.769
1373596_at	NM_001029920	RGD1310423	similar to hypothetical protein FLJ31737	2.765
1368130_at	NM_031972	Aldh3a1	aldehyde dehydrogenase family 3, member A1	2.755
1392179_at	---	---	Transcribed locus	2.752
1393335_at	NM_001108254	Egfl6	EGF-like-domain, multiple 6	2.738
1392905_at	XM_002725028 XM_002725029	Gng2	Guanine nucleotide binding protein, gamma 2	2.736
1388298_at	NM_001100885	Myl9_predicted	myosin, light polypeptide 9, regulatory (predicted)	2.726
1383263_at	NM_001106103	Ogn_predicted	osteoglycin (predicted)	2.725
1371689_at	---	---	Transcribed locus	2.724
1378602_at	---	---	Transcribed locus	2.716
1386895_at	NM_053409	Maged1	melanoma antigen, family D, 1	2.71
1368023_at	NM_001109898 /// NM_053431	Qscn6	quiescin Q6	2.709
1389310_at	---	---	Transcribed locus	2.704
1368563_at	NM_024399	Aspa	aspartoacylase	2.703
1368092_at	NM_017181	Fah	fumarylacetoacetate hydrolase	2.697
1378131_at	---	RGD1560736_predicted	similar to solute carrier family 9 (sodium/hydrogen exchanger), isoform 9 (predicted)	2.695
1377934_at	---	---	Transcribed locus	2.689
1377671_at	---	---	Transcribed locus	2.679
1384311_at	XM_001072014 XM_002726382 XM_002726383	---	---	2.678
1388329_at	NM_001004021	Ka13	type I keratin KA13	2.674
1372130_at	XM_001066125 /// XM_232614	Arfgef1_predicted	ADP-ribosylation factor guanine nucleotide-exchange factor 1(brefeldin A-inhibited) (predicted)	2.67
1373676_at	---	---	Transcribed locus	2.656
1383242_a_at	---	---	Transcribed locus	2.651
1397754_at	---	---	Transcribed locus	2.65
1394455_at	---	---	Transcribed locus	2.649
1379529_at	NM_001134706	LOC681284	similar to Nucleosome binding protein 1 (Nucleosome binding protein 45) (NBP-45) (GARP45 protein)	2.644
1383391_a_at	NM_172222	C2	complement component 2	2.642
1379031_at	NM_001106483	Gca_predicted	grancalcin (predicted)	2.633
1389502_at	---	---	---	2.63
1367912_at	NM_021587	Ltbp1	latent transforming growth factor beta binding protein 1	2.623
1390931_at	NM_001106810	Adamts15_predicted	a disintegrin-like and metallopeptidase (reprolysin type) with thrombospondin type 1 motif, 15 (predicted)	2.62
1384322_at	---	---	Transcribed locus	2.619
1387952_a_at	NM_012924	Cd44	CD44 antigen	2.618
1394290_at	---	---	Transcribed locus	2.618
1374248_at	NM_001100758 XM_001076591 XM_343196	Mybpc1	myosin binding protein C, slow type	2.617
1367942_at	NM_019144	Acp5	acid phosphatase 5, tartrate resistant	2.616
1387074_at	NM_053453	Rgs2	regulator of G-protein signaling 2	2.615
1369129_at	NM_019211	Rasgrp1	RAS guanyl releasing protein 1	2.614
1373952_at	NM_184051	Prkag2	protein kinase, AMP-activated, gamma 2 non-catalytic subunit	2.612
1393121_at	NM_001106725	Agr2_predicted	anterior gradient 2 (Xenopus laevis) (predicted)	2.611
1374743_at	XM_002729506	RGD1565362_predicted	similar to channel-interacting PDZ domain protein isoform 1 (predicted)	2.609
1378356_at	NM_001108051	Slc24a4_predicted	solute carrier family 24 (sodium/potassium/calcium exchanger), member 4 (predicted)	2.608
1385239_at	---	---	Transcribed locus	2.605
1369926_at	NM_022525	Gpx3	glutathione peroxidase 3	2.603
1390878_at	XR_006034 /// XR_085761	LOC681309	similar to Thrombospondin-3 precursor	2.603

1383543_at	NM_001113783	Golt1b_predicted	golgi transport 1 homolog B (S. cerevisiae) (predicted)	2.598
1374971_at	---	---	Transcribed locus	2.59
1388802_at	NM_001037365	Bex1	brain expressed X-linked 1	2.582
1370167_at	NM_013082	Sdc2	syndecan 2	2.579
1373659_at	NM_001163002	LOC688257 /// LOC689926	hypothetical protein LOC688257 /// hypothetical protein LOC689926	2.577
1391576_at	---	---	Transcribed locus	2.574
1368105_at	NM_022589	Tspan2	tetraspanin 2	2.571
1393672_at	XM_001070255 /// XM_222716	Hmcn1_predicted	hemicentin 1 (predicted)	2.569
1384063_at	NM_172333	Cthrc1	collagen triple helix repeat containing 1	2.567
1383879_at	XM_001081354 /// XM_002724542	---	---	2.563
1391938_at	NM_001008861	Usp11	ubiquitin specific protease 11	2.558
1367774_at	NM_031509	Gsta3	glutathione S-transferase A3	2.555
1390358_at	NM_175595	Cacna2d3	calcium channel, voltage-dependent, alpha 2/delta 3 subunit	2.552
1387445_at	NM_031573	Phkg1	phosphorylase kinase gamma 1	2.551
1388265_x_at	XM_001058357 XM_215451	Cspg2	chondroitin sulfate proteoglycan 2	2.544
1384150_at	NM_022927	---	Transcribed locus	2.543
1387341_a_at	NM_001025289 NM_001025291	Mbp	myelin basic protein	2.542
1387808_at	NM_031341	Slc7a7	solute carrier family 7 (cationic amino acid transporter, y+ system), member 7	2.536
1395695_at	NM_001100970	Aebp1_predicted	AE binding protein 1 (predicted)	2.535
1374503_at	NM_001107834	Pbx3_predicted	pre B-cell leukemia transcription factor 3 (predicted)	2.532
1383228_at	---	---	---	2.53
1387794_at	NM_031348	Fcna	ficolin A	2.53
1376892_at	NM_001112742 /// NM_032990	Gria3	glutamate receptor, ionotropic, AMPA3 (alpha 3)	2.529
1382189_at	NM_013082	Sdc2	syndecan 2	2.529
1383212_at	---	---	CDNA clone IMAGE:7462850	2.529
1382436_at	NM_001134589	RGD1566265_predicted	similar to RIKEN cDNA 2610002M06 (predicted)	2.526
1372268_at	---	---	Transcribed locus	2.513
1383976_at	---	---	Transcribed locus	2.513
1377097_at	NM_001039085	Cox6b2	cytochrome c oxidase subunit Vlb testes-specific isoform precursor	2.506
1382967_at	NM_181366	Gpr64	G protein-coupled receptor 64	2.5
1389469_at	NM_001107704	Chd1l_predicted	chromodomain helicase DNA binding protein 1-like (predicted)	2.498
1383458_at	---	---	Transcribed locus	2.494
1372557_at	NM_001108842	---	---	2.486
1380356_at	NM_001107260	Slc39a2_predicted	solute carrier family 39 (zinc transporter), member 2 (predicted)	2.469
1376155_at	NM_001134748	RGD1561110_predicted	similar to hypothetical protein 2BE2121 - Chinese hamster (fragment) (predicted)	2.468
1379517_at	---	Rgs6	regulator of G-protein signaling 6	2.466
1376110_at	NM_001012124	Rpp25	ribonuclease P 25 subunit (human)	2.461
1382317_at	XM_001072957 /// XM_232499	---	Transcribed locus	2.46
1372390_at	XM_002725510 /// XM_002728663	---	Transcribed locus	2.459
1398426_at	NM_001109082	RGD1564105_predicted	similar to RIKEN cDNA B130052G07 (predicted)	2.458
1379931_at	---	---	Transcribed locus	2.456
1379238_at	NM_001106865	Ctdspl_predicted	CTD (carboxy-terminal domain, RNA polymerase II, polypeptide A) small phosphatase-like (predicted)	2.45
1382759_at	---	---	Transcribed locus	2.449
1372626_at	NM_001044295	LOC689256	similar to Tumor protein D53 (mD53) (Tumor protein D52-like 1)	2.445
1370166_at	NM_013082	Sdc2	syndecan 2	2.444
1373554_at	---	Spsb1_predicted	splA/ryanodine receptor domain and SOCS box containing 1 (predicted)	2.441
1387907_at	NM_001007235	Itpr1	inositol 1,4,5-triphosphate receptor 1	2.441
1398847_at	NM_053598	Nudt4	nudix (nucleoside diphosphate linked moiety X)-type motif 4	2.44
1395840_at	NM_001008773	Eif1a	eukaryotic translation initiation factor 1A	2.437
1372525_at	NM_001013210	Fkbp14	FK506 binding protein 14	2.436
1382060_at	---	---	Transcribed locus	2.432
1384356_at	NM_001134748	RGD1561110_predicted	similar to hypothetical protein 2BE2121 - Chinese hamster (fragment) (predicted)	2.43
1391212_at	NM_001009675	Tceal1	transcription elongation factor A (SII)-like 1	2.425
1397905_at	---	---	Transcribed locus	2.425
1386936_at	NM_057187	Grifin	galectin-related inter-fiber protein	2.411

			Transcribed locus, strongly similar to NP_112290.2	
	NM_031028		gamma-aminobutyric acid (GABA) B receptor 1 [Rattus	
1375720_at		---	norvegicus]	2.407
1387448_at	NM_019368	Bet1l	blocked early in transport 1 homolog (S. cerevisiae) like	2.407
	XM_001074913 ///			
1371056_at	XM_343402	Neo1	neogenin	2.405
1368419_at	NM_012532	Cp	ceruloplasmin	2.401
	NM_001108164	RGD1304623_pr		
1391021_at		edicted	similar to KIAA1749 protein (predicted)	2.401
1368252_at	NM_057191	Kbtbd10	kelch repeat and BTB (POZ) domain containing 10	2.4
1367909_at	NM_134387	Dcxr	dicarbonyl L-xylulose reductase	2.399
1369526_at	NM_013084	Acadsb	acyl-Coenzyme A dehydrogenase, short/branched chain	2.399
1384059_at	---	---	Transcribed locus	2.397
1399033_at	NM_001013191	Cbfb	core binding factor beta	2.394
1388735_at	---	---	Transcribed locus	2.391
1369409_at	NM_022856	Nab1	Ngfi-A binding protein 1	2.39
1390450_a_at	NM_001106103	Ogn_predicted	osteoglycin (predicted)	2.389
	XR_007329 ///	RGD1563084_pr		
1382660_at	XR_086378	edicted	similar to FLJ20298 protein isoform a (predicted)	2.387
	NM_001108136	RGD1565079_pr		
1379683_at		edicted	Similar to hypothetical protein MGC17839 (predicted)	2.386
1383002_at	---	LOC314964	similar to PHD finger protein 20-like 1 isoform 1	2.384
1382810_at	---	---	Transcribed locus	2.383
	NM_001108051	Slc24a4_predicte	solute carrier family 24 (sodium/potassium/calcium	
1394272_at		d	exchanger), member 4 (predicted)	2.381
1390659_at	---	---	Transcribed locus	2.38
1382934_at	NM_199397	Panx1	Pannexin 1	2.374
	NM_012798		myelin and lymphocyte protein, T-cell differentiation	
1387040_at		Mal	protein	2.372
1367648_at	NM_013122	Igfbp2	insulin-like growth factor binding protein 2	2.368
1377332_at	---	---	Transcribed locus	2.367
1371300_at	NM_198753	Rpl3	ribosomal protein L3	2.362
1390934_at	---	---	Transcribed locus	2.361
	XM_001060972 ///	RGD1305645_pr		
1372646_at	XM_343562	edicted	similar to RIKEN cDNA 1500015O10 (predicted)	2.36
1387197_at	NM_031817	Omd	osteomodulin	2.36
1384932_at	NM_001108617	Pftk1_predicted	PFTAIRE protein kinase 1 (predicted)	2.351
1367811_at	NM_031620	Phgdh	3-phosphoglycerate dehydrogenase	2.35
1370000_at	NM_021663	Nucb2	nucleobindin 2	2.347
1389718_at	---	---	Transcribed locus	2.343
1393120_at	---	---	Transcribed locus	2.343
1392942_at	NM_001108739	---	---	2.338
1367687_a_at	NM_013000	Pam	peptidylglycine alpha-amidating monooxygenase	2.337
1383012_at	NM_001107505	Rhpn2_predicted	rhophilin, Rho GTPase binding protein 2 (predicted)	2.333
1372623_at	---	---	Transcribed locus	2.331
1383469_at	NM_153300	---	Transcribed locus	2.331
1380943_at	NM_001014075	RGD1311648	similar to hypothetical protein FLJ21820	2.329
1388177_at	NM_030993	Ddn	dendrin	2.329
1386968_at	NM_022676	Ppp1r1a	protein phosphatase 1, regulatory (inhibitor) subunit 1A	2.328
1377751_at	---	---	Transcribed locus	2.327
1368321_at	NM_012551	Egr1	early growth response 1	2.322
1372229_at	NM_001106581	Pdk3	pyruvate dehydrogenase kinase, isoenzyme 3	2.322
	NM_001085353 ///			
1374557_at	NM_199408	LOC362065	CG6210-like	2.322
1387376_at	NM_019363	Aox1	aldehyde oxidase 1	2.322
	XM_002725716 ///	LOC679990 ///		
1374969_at	XM_574644	LOC687552	similar to phosphoglucomutase 5	2.319
1379672_at	---	---	Transcribed locus	2.317
1376860_at	NM_022624	Nritp	ion transporter protein	2.315
1394666_at	---	---	---	2.314
1370960_at	NM_012817	Igfbp5	insulin-like growth factor binding protein 5	2.312
1368879_a_at	NM_017327	Gnao	guanine nucleotide binding protein, alpha o	2.31
1389253_at	NM_001025623	Vnn1	vanin 1	2.309
1394596_at	---	---	Transcribed locus	2.309
1380133_at	NM_001012118	Osr2	odd-skipped related 2 (Drosophila)	2.307
1388201_at	NM_013107	Bmp6	bone morphogenetic protein 6	2.305
1394838_at	NM_031582	Aoc3	amine oxidase, copper containing 3	2.296
1383248_at	NM_144739	Fmo5	flavin containing monooxygenase 5	2.295
	XM_001059265 ///			
1384143_at	XM_227472	Cgn_predicted	cingulin (predicted)	2.291
	NM_001166022 ///			
1370216_at	NM_013137	Ddr1	discoidin domain receptor family, member 1	2.287
1382192_at	NM_001106286	Xlkd1_predicted	extracellular link domain-containing 1 (predicted)	2.281
	---		splA/ryanodine receptor domain and SOCS box	
1379611_at		Spsb1_predicted	containing 1 (predicted)	2.277
1395107_at	---	---	Transcribed locus	2.276
1390881_at	NM_175844	Abra	actin-binding Rho activating protein	2.275

1368990_at	NM_012940 XM_001054396 ///	Cyp1b1	cytochrome P450, family 1, subfamily b, polypeptide 1	2.274
1380596_at	XM_226112	---	Transcribed locus	2.273
1385813_at	NM_001024240	RGD1310251	similar to RIKEN cDNA 2010001M09	2.273
1391880_at	--- XM_001064390	---	Transcribed locus	2.271
1396295_at	XM_001068832	LOC685576	hypothetical protein LOC685576	2.271
1376191_at	NM_024390 NM_001007149 NM_001007150	Hpgd	hydroxyprostaglandin dehydrogenase 15 (NAD)	2.27
1370680_at	NM_134466	Stau2	staufen, RNA binding protein, homolog 2 (Drosophila)	2.269
1381487_at	NM_053546	Angpt1	angiopoietin 1	2.263
1382882_x_at	---	---	Non-coding RNA expressed in the brain, repeat sequence, clone 2	2.263
1371633_at	NM_001024870 XM_002726327 ///	Ctnnbl1	beta catenin-like 1	2.262
1393783_at	XR_086230 NM_001100863 XM_001053416 ///	LOC500105	Similar to contactin associated protein-like 2 isoform a	2.262
1374759_at	XM_343087	Galntl1	UDP-N-acetyl-alpha-D-galactosamine:polypeptide N-acetylgalactosaminyltransferase-like 1	2.256
1381906_at	NM_001106421 XR_085894 ///	Tpd52_predicted	tumor protein D52 (predicted)	2.256
1390145_at	XR_086317 XM_001074913 ///	---	Transcribed locus	2.253
1392770_at	XM_343402	Neo1	neogenin	2.251
1382657_at	NM_001108168	Bmp5_predicted	bone morphogenetic protein 5 (predicted)	2.248
1383606_at	NM_001025152 XM_001078764 ///	Mtac2d1 RGD1307524_predicted	membrane targeting (tandem) C2 domain containing 1	2.247
1389007_at	XM_219909		similar to Friedreich ataxia region gene X123 (predicted)	2.247
1377367_at	NM_001033064	Kazald1	Kazal-type serine peptidase inhibitor domain 1	2.246
1382761_at	NM_031080	Pde7a	phosphodiesterase 7A	2.244
1382346_at	---	---	Transcribed locus	2.243
1374065_at	---	---	Transcribed locus	2.24
1389086_at	---	RGD1564043_predicted	Similar to RIKEN cDNA E430021N18 (predicted)	2.239
1393267_at	NM_175765	Psip1	PC4 and SFRS1 interacting protein 1	2.238
1392962_at	---	---	Transcribed locus	2.237
1375894_at	NM_001024266	Lztfl1	leucine zipper transcription factor-like 1	2.232
1386827_at	---	LOC363458	similar to procollagen, type IV, alpha 6	2.229
1377255_at	---	---	---	2.226
1384423_at	XM_002725789	LOC365090	similar to 5-nucleotidase, cytosolic II	2.226
1380387_at	XM_001056575 ///	RGD1559697_predicted	similar to forkhead/winged-helix transcription factor 2 (predicted)	2.224
1386900_at	NM_030835	RAMP4	ribosome associated membrane protein 4	2.223
1380911_at	NM_001108286	RGD1311564_predicted	LOC360590 (predicted)	2.222
1370234_at	NM_019143 NM_001170487 XM_001074493 ///	Fn1	fibronectin 1	2.218
1373321_at	XM_215195	---	Transcribed locus	2.218
1390419_a_at	NM_001004212	Tusc3	tumor suppressor candidate 3	2.218
1373478_at	---	---	Transcribed locus	2.217
1377857_at	---	---	Transcribed locus	2.217
1393172_at	NM_022856	Nab1	Ngfi-A binding protein 1	2.217
1373923_at	NM_181478	Rdh10	Retinol dehydrogenase 10 (all-trans)	2.215
1386889_at	NM_031841	Scd2	stearoyl-Coenzyme A desaturase 2	2.214
1395316_at	NM_001013250	Mageh1	melanoma antigen, family H, 1	2.212
1393613_at	---	RGD1562123_predicted	similar to hypothetical protein (predicted)	2.211
1370875_at	NM_019357	Vil2	villin 2	2.21
1371108_a_at	NM_012504	Atp1a1	ATPase, Na+/K+ transporting, alpha 1 polypeptide	2.205
1367631_at	NM_022266	Ctgf	connective tissue growth factor	2.2
1372282_at	NM_001106411	RGD1307506_predicted	similar to RIKEN cDNA 2310016C16 (predicted)	2.197
1391015_at	NM_001109031	RGD1562251_predicted	similar to DNA segment, Chr 11, ERATO Doi 461, expressed (predicted)	2.196
1398216_at	---	---	Transcribed locus	2.189
1375857_at	XM_001080627 /// XM_220031	RGD1564216_predicted	similar to Myoferlin (Fer-1 like protein 3) (predicted)	2.185
1372048_at	NM_001106607	Podxl2_predicted	podocalyxin-like 2 (predicted)	2.181
1389349_s_at	NM_001004091	Il17re	interleukin 17 receptor E	2.178
1370063_at	NM_080778 NM_134373 ///	Nr2f2	nuclear receptor subfamily 2, group F, member 2	2.175
1370252_at	XM_001071784	Avpi1	arginine vasopressin-induced 1	2.171
1376102_at	NM_001007713	Tmbim1	transmembrane BAX inhibitor motif containing 1	2.17
1396073_at	---	---	Transcribed locus	2.17
1368536_at	NM_057104	Enpp2	ectonucleotide pyrophosphatase/phosphodiesterase 2	2.169

1392776_at	---	---	Transcribed locus	2.169
1389998_at	NM_080778	Nr2f2	Nuclear receptor subfamily 2, group F, member 2	2.168
1390232_at	NM_001025683	RGD1311946	similar to RIKEN cDNA 1810055G02	2.168
1381077_at	---	---	Transcribed locus	2.167
1382746_s_at	---	---	Transcribed locus	2.165
1393944_at	NM_001107403	Zfp521_predicted	zinc finger protein 521 (predicted)	2.164
1378082_at	---	---	Transcribed locus	2.162
1372299_at	NM_001033757 /// NM_001033758 /// NM_182735	Cdkn1c	cyclin-dependent kinase inhibitor 1C (P57)	2.161
1373935_at	NM_001013050	Pold2	polymerase (DNA directed), delta 2, regulatory subunit	2.156
1382422_at	NM_001004087	Pcdh7	Protocadherin 7	2.15
1370228_at	NM_001013110	Srprb /// Tf	transferrin /// signal recognition particle receptor, B subunit	2.148
1379382_at	---	---	Transcribed locus	2.144
1376153_at	---	---	Transcribed locus	2.14
1370180_at	NM_053598	Nudt4	nudix (nucleoside diphosphate linked moiety X)-type motif 4	2.135
1376011_at	---	---	Transcribed locus	2.134
1389179_at	NM_001170467	Cidea_predicted	cell death-inducing DNA fragmentation factor, alpha subunit-like effector A (predicted)	2.133
1390049_at	NM_001033926 /// NM_145669	Fhl1	four and a half LIM domains 1	2.13
1385263_at	XM_001059493 /// XM_574117	RGD1561153_predicted	similar to myosin-VIIb (predicted)	2.128
1382197_at	NM_001106323	Rhod_predicted	ras homolog gene family, member D (predicted)	2.126
1367744_at	NM_080479	Maged2	melanoma antigen, family D, 2	2.122
1392555_at	NM_001108709 NM_001163156	Etv1_predicted	Ets variant gene 1 (predicted)	2.122
1383279_at	NM_199084	Rcbtb2	regulator of chromosome condensation (RCC1) and BTB (POZ) domain containing protein 2	2.117
1368259_at	NM_017043	Ptgs1	prostaglandin-endoperoxide synthase 1	2.116
1389730_at	---	---	Transcribed locus	2.113
1377655_at	NM_130814	Fgf12	Fibroblast growth factor 12	2.111
1378531_at	---	---	Transcribed locus	2.106
1375697_at	NM_001013983	RGD1307736	similar to Hypothetical protein KIAA0152	2.104
1376105_at	NM_001130548	Col14a1_predicted	procollagen, type XIV, alpha 1 (predicted)	2.103
1371060_at	NM_001100637 XM_001064069 /// XM_342183	Trim23	tripartite motif protein 23	2.098
1388662_at	---	---	Transcribed locus	2.098
1393197_at	NM_001107301	Abhd8_predicted	abhydrolase domain containing 8 (predicted)	2.098
1395753_at	NM_012722	Eln	elastin	2.098
1371334_at	NM_001009674	Itm2c	integral membrane protein 2C	2.097
1379754_at	NM_001007149 NM_001007150 /// NM_134466	Stau2	Staufen, RNA binding protein, homolog 2 (Drosophila)	2.096
1395745_at	---	---	Transcribed locus	2.093
1370012_at	NM_031557	Ptgis	prostaglandin I2 (prostacyclin) synthase	2.092
1391194_at	NM_001107415	Sall1_predicted	Sal-like 1 (Drosophila) (predicted)	2.092
1395121_at	---	---	Transcribed locus	2.092
1387886_at	NM_053385	Prelp	proline arginine-rich end leucine-rich repeat protein	2.09
1372744_at	NM_001106482	Pkp4_predicted	plakophilin 4 (predicted)	2.089
1379362_at	---	---	Transcribed locus	2.088
1382059_at	NM_001007690	Fbxo30	F-box protein 30	2.088
1382732_at	NM_001106286	Xlkd1_predicted	extracellular link domain-containing 1 (predicted)	2.088
1377707_at	NM_001106590	Slc35b4_predicted	solute carrier family 35, member B4 (predicted)	2.087
1374954_at	NM_001106610	Hdac11_predicted	histone deacetylase 11 (predicted)	2.086
1397892_at	NM_001008773 XM_001068166 XM_002725199 XM_002728412 /// XM_341448	Eif1a	eukaryotic translation initiation factor 1A	2.083
1379817_at		Purg_predicted	purine-rich element binding protein G (predicted)	2.081
1379868_at	NM_001100976	Pbxip1	pre-B-cell leukemia transcription factor interacting protein 1	2.081
1371950_at	NM_001106945	Pdzd11_predicted	PDZ domain containing 11 (predicted)	2.08
1374518_at	NM_001025018	Tmem77	transmembrane protein 77	2.077
1388713_at	NM_001007682	Thtpa	thiamine triphosphatase	2.076
1372816_at	---	---	Transcribed locus	2.075
1384584_at	---	---	Transcribed locus, moderately similar to NP_007227.1 cytochrome c oxidase subunit I [Rattus norvegicus]	2.073
1368675_at	NM_032084	Chn2	chimerin (chimaerin) 2	2.072
1374726_at	NM_001038615	Fndc1	fibronectin type III domain containing 1	2.065

1385043_at	---	RGD1565362_predicted	similar to channel-interacting PDZ domain protein isoform 1 (predicted)	2.064
1375521_at	NM_001014275	Tceal8	transcription elongation factor A (SII)-like 8	2.062
1382890_at	---	---	Transcribed locus	2.062
1387538_at	NM_022193	Acaca	acetyl-coenzyme A carboxylase alpha	2.062
1389435_at	XM_001078310 /// XM_573600	RGD1560201_predicted	similar to RIKEN cDNA 9130005N14 (predicted)	2.062
1380255_at	---	---	Transcribed locus	2.058
1388111_at	NM_012722	Eln	elastin	2.057
1370817_at	NM_153628	Sec11l3	Sec11-like 3 (S. cerevisiae)	2.054
1372182_at	NM_206847	Pfkp	phosphofructokinase, platelet	2.054
1372256_at	NM_001134933	LOC691657	similar to Cysteine-rich protein 1 (Cysteine-rich intestinal protein) (CRIP)	2.052
1381977_at	XM_002725484	---	---	2.052
1394795_at	---	---	Transcribed locus	2.052
1384617_at	NM_199105	MGC72614	hypothetical LOC310540	2.051
1386879_at	NM_031832	Lgals3	lectin, galactose binding, soluble 3	2.051
1395374_at	---	---	Transcribed locus	2.049
1382217_at	---	---	Transcribed locus	2.047
1391721_at	---	---	CDNA clone IMAGE:7103416	2.045
1395865_at	---	---	---	2.045
1379097_at	NM_001127635	---	---	2.044
1379354_at	NM_001100704	Extl2	exostoses (multiple)-like 2	2.044
1367614_at	NM_012904	Anxa1	annexin A1	2.043
1383673_at	NM_001024789	Nap1l2	nucleosome assembly protein 1-like 2	2.042
1377018_at	NM_001107755	RGD1308745_predicted	Similar to E430002G05Rik protein (predicted)	2.041
1391551_at	---	---	Transcribed locus	2.041
1395355_at	---	---	Transcribed locus	2.041
1387153_at	NM_017062	Ril	reversion induced LIM gene	2.038
1392928_at	NM_001108031	RGD1305721_predicted	similar to RIKEN cDNA 2810055F11 (predicted)	2.038
1391753_at	---	---	Transcribed locus	2.037
1394492_at	NM_001109065	RGD1563482_predicted	similar to hypothetical protein FLJ38663 (predicted)	2.037
1368943_at	NM_020082	Rnase4	ribonuclease, RNase A family 4	2.035
1381482_at	---	---	Transcribed locus	2.034
1376850_a_at	NM_001108660	Ccl27_predicted	chemokine (C-C motif) ligand 27 (predicted)	2.033
1379565_at	NM_001012188	Creb3l2	cAMP responsive element binding protein 3-like 2	2.032
1396237_at	---	---	---	2.03
1376711_at	NM_053457	Cldn11	claudin 11	2.029
1382955_at	XM_001071417 /// XM_218313	Gpr126_predicted	G protein-coupled receptor 126 (predicted)	2.028
1390396_at	NM_001106612	LOC297481	similar to eukaryotic translation initiation factor 4E member 3	2.028
1398538_at	NM_001107301	Abhd8_predicted	abhydrolase domain containing 8 (predicted)	2.028
1388680_at	NM_001030033	C1galt1c1	C1GALT1-specific chaperone 1	2.026
1396119_at	---	---	Transcribed locus	2.025
1370312_at	NM_172067	Spon1	spondin 1	2.024
1382081_at	NM_001108870	Scara3_predicted	scavenger receptor class A, member 3 (predicted)	2.023
1375795_at	---	---	Transcribed locus	2.022
1368051_at	NM_032066	Hsd17b12	hydroxysteroid (17-beta) dehydrogenase 12	2.021
1368323_at	NM_001177321 /// NM_017200	Tfpi	tissue factor pathway inhibitor	2.021
1384169_a_at	NM_001106563	Vav2_predicted	Vav2 oncogene (predicted)	2.021
1372531_at	NM_001100582	Ppfibp2	protein tyrosine phosphatase, receptor-type, F interacting protein, binding protein 2	2.018
1369157_at	NM_017229	Pde3b	phosphodiesterase 3B	2.016
1370807_at	NM_138839	Tmem49	transmembrane protein 49	2.013
1379444_at	---	---	Transcribed locus	2.012
1387439_at	NM_022955	Egfl3	EGF-like-domain, multiple 3	2.011
1398425_at	NM_001024341	MGC109194	similar to hypothetical protein MGC39325-like protein	2.011
1375120_at	NM_175582	Id4	inhibitor of DNA binding 4	2.01
1379826_at	NM_001107957	RGD1560252_predicted	similar to hypothetical protein MGC31967 (predicted)	2.01
1384147_at	NM_001008773	Eif1a	eukaryotic translation initiation factor 1A	2.01
1389788_at	NM_001024975	RGD1307336	similar to hypothetical protein	2.01
1382629_at	NM_001011933	Mlstd2	male sterility domain containing 2	2.008
1374908_at	---	---	Transcribed locus	2.007
1392888_at	NM_001014108	Gpc4	glypican 4	2.007
1386940_at	NM_021989	Timp2	tissue inhibitor of metalloproteinase 2	1.998
1391553_at	---	---	Transcribed locus	1.998
1396086_at	NM_001008334	Tmem97	transmembrane protein 97	1.998
1379971_at	NM_001107772	Zc3h6_predicted	zinc finger CCCH type containing 6 (predicted)	1.997
1389229_at	NM_001007710	Acpl2	acid phosphatase-like 2	1.997
1395343_at	XM_002725800 /// XM_220013	RGD1564625_predicted	similar to transmembrane protein TM9SF3 (predicted)	1.997

1369377_at	NM_013074	Hcrtr2	hypocretin (orexin) receptor 2	1.995
1382482_at	---	---	Transcribed locus	1.995
1372485_at	NM_001007601	Pcbd1	pterin 4 alpha carbinolamine dehydratase/dimerization cofactor of hepatocyte nuclear factor 1 alpha (TCF1) 1	1.994
1386029_at	---	---	---	1.991
1379072_at	XM_001053483 XM_001053550 XM_002727556 XM_002727557	Phka2_mapped	phosphorylase kinase alpha 2	1.988
1386721_at	NM_001107250	Zfp503_predicted	zinc finger protein 503 (predicted)	1.988
1377795_at	---	---	Transcribed locus	1.987
1382118_at	XM_002725510 /// XM_002728663	---	Transcribed locus, strongly similar to NP_001029332.1 hypothetical protein LOC619476 [Rattus norvegicus]	1.987
1393779_x_at	NM_021581	Sc65	synaptonemal complex protein SC65	1.984
1387891_at	NM_053512	Prdx4	peroxiredoxin 4	1.981
1387407_at	NM_133402	Nap1l3	nucleosome assembly protein 1-like 3	1.98
1379902_at	---	---	Transcribed locus	1.979
1397839_at	NM_198749	Rab15	RAB15, member RAS onocogene family	1.979
1387676_at	NM_053947	Mark1	MAP/microtubule affinity-regulating kinase 1	1.978
1372700_at	---	---	Transcribed locus	1.977
1388879_at	XM_002727882 /// XM_344015	RGD1562717_predicted	similar to ABI gene family, member 3 (NESH) binding protein (predicted)	1.977
1397820_at	---	---	Transcribed locus	1.975
1390021_at	NM_001107352	Hist1h2bh	histone cluster 1, H2bh	1.973
1377678_at	---	---	Transcribed locus	1.972
1392747_at	---	---	Transcribed locus	1.972
1393345_at	---	---	Transcribed locus	1.967
1368703_at	NM_053326	Pdlim5	PDZ and LIM domain 5	1.966
1368527_at	NM_017232	Ptgs2	prostaglandin-endoperoxide synthase 2	1.965
1373161_at	NM_001007672	Tmem98	transmembrane protein 98	1.965
1385620_at	NM_001011901	Hsph1	heat shock 105kDa/110kDa protein 1	1.965
1389532_at	XM_001068639 /// XM_225644	Nebl_predicted	Nebulette (predicted)	1.964
1368418_a_at	NM_012532	Cp	ceruloplasmin	1.963
1390645_at	---	---	Transcribed locus	1.963
1389704_at	---	---	Transcribed locus	1.961
1370829_at	NM_172034	Fntb	farnesyltransferase, CAAX box, beta	1.96
1392815_at	NM_001107216	Centd1_predicted	centaurin, delta 1 (predicted)	1.96
1373202_at	NM_053658	Gng3	guanine nucleotide binding protein (G protein), gamma 3	1.958
1390669_at	---	---	Transcribed locus	1.956
1376786_a_at	---	---	Transcribed locus	1.954
1390187_at	---	---	Transcribed locus	1.953
1391184_at	NM_001106877	LOC301121	similar to DNA-binding protein RFX2	1.953
1393219_at	NM_172222	C2	complement component 2	1.952
1380017_at	---	---	Transcribed locus	1.951
1374061_at	NM_001013916	Cd302	CD302 antigen	1.949
1367668_a_at	NM_031841	Scd2	stearoyl-Coenzyme A desaturase 2	1.948
1374728_at	---	---	Transcribed locus	1.947
1372828_at	NM_001031660	Msrb2	methionine sulfoxide reductase B2	1.946
1384399_at	XM_001069855 /// XM_215553	Ankrd50_predicted	ankyrin repeat domain 50 (predicted)	1.943
1376137_at	NM_001106899	Plekhb2_predicted	pleckstrin homology domain containing, family B (evectins) member 2 (predicted)	1.942
1386955_at	NM_053930 /// NM_053931	05-Sep	septin 5	1.941
1388022_a_at	NM_053655	Dnm1l	dynamin 1-like	1.941
1390913_at	---	---	Transcribed locus	1.941
1377246_at	---	LOC685652	similar to keratin 6L	1.937
1382569_at	XM_001068629 /// XM_236503	Paqr9_predicted	progestin and adipoQ receptor family member IX (predicted)	1.937
1378741_at	NM_001014196	RGD1309207	similar to putative phosphatase subunit	1.936
1383213_at	XM_001072957 /// XM_232499	Eps8_predicted	epidermal growth factor receptor pathway substrate 8 (predicted)	1.936
1379431_at	---	---	Transcribed locus	1.935
1381382_at	XM_001065086 /// XM_342169	RGD1564936_predicted	similar to Vacuolar ATP synthase subunit S1 precursor (V-ATPase S1 subunit) (predicted)	1.935
1372764_at	NM_001115046 /// XM_001067744 /// XM_001067805	LOC687565 /// LOC689601	similar to density-regulated protein	1.933
1379556_a_at	NM_001007626	Ggps1	geranylgeranyl diphosphate synthase 1	1.932
1368881_at	NM_019251	Bet1	blocked early in transport 1 homolog (S. cerevisiae)	1.931
1372368_at	---	---	Transcribed locus	1.931
1372926_at	NM_012886	Timp3	Tissue inhibitor of metalloproteinase 3 (Sorsby fundus dystrophy, pseudoinflammatory)	1.93
1377691_at	NM_001025686	Sec22l1	SEC22 vesicle trafficking protein-like 1 (S. cerevisiae)	1.93
1391619_at	NM_207611	Bhlhb9	basic helix-loop-helix domain containing, class B, 9	1.93
1370859_at	NM_001004442	Pdia6	protein disulfide isomerase associated 6	1.927

1389857_at	NM_001127502	Wbp5_predicted	WW domain binding protein 5 (predicted)	1.927
1392416_at	---	---	Transcribed locus	1.927
1386917_at	NM_012744	Pc	Pyruvate carboxylase	1.926
1383901_at	---	---	Transcribed locus	1.925
1395087_at	---	---	Transcribed locus	1.925
1387306_a_at	NM_053633	Egr2	early growth response 2	1.924
1372647_at	XM_002724867	---	---	1.923
1389974_at	---	---	Transcribed locus	1.922
1391439_at	---	---	Transcribed locus, strongly similar to XP_232253.3 PREDICTED: similar to KIAA0819 protein [Rattus norvegicus]	1.921
1370541_at	NM_147210	Nr1d2	nuclear receptor subfamily 1, group D, member 2	1.92
1389095_at	NM_001108317	---	---	1.919
1395940_at	NM_001134744	Agpat5_predicted	1-acylglycerol-3-phosphate O-acyltransferase 5 (lysophosphatidic acid acyltransferase, epsilon) (predicted)	1.919
1383579_at	---	---	Transcribed locus, moderately similar to XP_577744.1 PREDICTED: similar to IKEN cDNA 6720480D16 [Rattus norvegicus]	1.918
1385881_at	NM_001100561	---	Transcribed locus	1.918
1372889_at	---	---	Transcribed locus	1.916
1394517_at	---	---	CDNA clone IMAGE:7103416	1.915
1368156_at	NM_031662	Camkk1	calcium/calmodulin-dependent protein kinase kinase 1, alpha	1.912
1368691_at	NM_001112742 /// NM_032990	Gria3	glutamate receptor, ionotropic, AMPA3 (alpha 3)	1.912
1380699_at	---	---	---	1.912
1373043_at	NM_001109433	LOC683036 /// Sdf2l1_predicted	stromal cell-derived factor 2-like 1 (predicted) /// similar to stromal cell-derived factor 2-like 1	1.911
1383146_at	XR_085753 /// XR_086168	RGD1562629_predicted	similar to neurobeachin (predicted)	1.911
1388743_at	---	---	Transcribed locus	1.911
1379903_at	---	---	Transcribed locus	1.91
1393795_at	NM_001033701	Zfhx1b	zinc finger homeobox 1b	1.91
1394005_s_at	NM_001107895	Surb7_predicted	SRB7 (suppressor of RNA polymerase B) homolog (S. cerevisiae) (predicted)	1.91
1386873_at	NM_017184	Tnni1	troponin I, skeletal, slow 1	1.909
1389580_at	NM_001106478	Smarca3_predicted	SWI/SNF related, matrix associated, actin dependent regulator of chromatin, subfamily a, member 3 (predicted)	1.908
1388728_at	NM_001013174	Laptm4b	lysosomal-associated protein transmembrane 4B	1.905
1380053_at	XM_002725800 /// XM_220013	RGD1564625_predicted	similar to transmembrane protein TM9SF3 (predicted)	1.904
1383912_at	NM_001099647	LOC684848 /// LOC685045	similar to Protein C6orf115	1.904
1389234_at	XM_001066203 /// XM_342759	Vwf	von Willebrand factor	1.904
1395165_at	NM_175765	Psip1	PC4 and SFRS1 interacting protein 1	1.901
1376573_at	NM_001012140	Rab34	RAB34, member of RAS oncogene family	1.898
1395153_at	NM_001107135	Cldn15_predicted	claudin 15 (predicted)	1.898
1372553_at	NM_001007746	MGC94199	similar to RIKEN cDNA 2610301B20; EST AI428449	1.896
1373381_at	NM_001012074	Herc4	hect domain and RLD 4	1.895
1388926_at	---	---	Transcribed locus	1.895
1376799_a_at	NM_001106074	Crlf1_predicted	cytokine receptor-like factor 1 (predicted)	1.893
1377263_at	---	---	---	1.893
1392856_at	XM_001070716 /// XM_577983	RGD1565105_predicted	similar to small EDRK-rich factor 1 (predicted)	1.893
1397929_at	---	---	Transcribed locus	1.893
1374920_at	---	---	Transcribed locus	1.891
1387004_at	NM_031609	Nbl1	neuroblastoma, suppression of tumorigenicity 1	1.891
1374519_at	XM_002726559 XM_002729510	---	---	1.89
1374903_at	NM_001001511	Gcnt2	glucosaminyl (N-acetyl) transferase 2, I-branching enzyme	1.889
1368840_at	NM_134390	Lr8	LR8 protein	1.888
1385738_at	---	---	Transcribed locus	1.888
1392597_at	NM_001108578	RGD1305081_predicted	similar to ionized calcium binding adapter molecule 2 (Iba2) (predicted)	1.887
1367616_at	NM_031545	Nppb	natriuretic peptide precursor type B	1.886
1391513_at	NM_001034926	LOC310946	Similar to hypothetical protein FLJ20331	1.886
1368565_at	NM_019225	Slc1a3	solute carrier family 1 (glial high affinity glutamate transporter), member 3	1.884
1369353_at	NM_021687	Erbb4	v-erb-a erythroblastic leukemia viral oncogene homolog 4 (avian)	1.884
1371691_at	NM_001013427	Rarres2	retinoic acid receptor responder (tazarotene induced) 2	1.883
1374747_at	NM_001108617	Pftk1_predicted	PFTAIRE protein kinase 1 (predicted)	1.883
1388789_at	NM_001108739	---	---	1.882

1374660_at	NM_001106301	---	---	1.881
1384621_at	---	---	---	1.881
1383726_at	NM_001012347	RGD1309360	hypothetical LOC294715	1.879
1377089_a_at	NM_001004090	Tspan5	tetraspanin 5	1.877
1370738_a_at	NM_021666	Trdn	triadin	1.876
1388541_at	---	---	Transcribed locus	1.876
1390336_at	XM_001073261	RGD1307569_predicted	similar to Protein C21orf63 homolog precursor (predicted)	1.876
1369124_at	NM_017254	Htr2a	5-hydroxytryptamine (serotonin) receptor 2A	1.875
1383867_at	NM_001100697 /// XM_001063995 /// XM_226974	---	Transcribed locus	1.875
1388772_at	NM_001106585	Lsm8_predicted	LSM8 homolog, U6 small nuclear RNA associated (S. cerevisiae) (predicted)	1.875
1391476_at	---	---	Transcribed locus	1.874
1373295_at	NM_001011943	Obfc1	oligonucleotide/oligosaccharide-binding fold containing 1	1.873
1374180_at	---	---	Transcribed locus	1.873
1376979_at	---	---	Transcribed locus	1.872
1387942_at	NM_153316	Slc35e4	solute carrier family 35, member E4	1.871
1377059_at	---	---	Transcribed locus	1.87
1382745_at	---	---	Transcribed locus	1.87
1393113_at	NM_001107747	---	---	1.87
1372870_at	NM_001127546	Kdelr3_predicted	KDEL (Lys-Asp-Glu-Leu) endoplasmic reticulum protein retention receptor 3 (predicted)	1.869
1378620_at	---	---	Transcribed locus	1.869
1368124_at	NM_133578	Dusp5	dual specificity phosphatase 5	1.868
1386078_at	NM_001107924	Slc35a1_predicted	solute carrier family 35 (CMP-sialic acid transporter), member 1 (predicted)	1.868
1387219_at	NM_012715	Adm	adrenomedullin	1.868
1379405_at	---	Grlf1_predicted /// LOC686520	glucocorticoid receptor DNA binding factor 1 (predicted) /// similar to Glucocorticoid receptor DNA-binding factor 1 (GAP-associated protein p190)	1.867
1394459_at	XM_001068090 /// XM_228876	RGD1564253_predicted	similar to Protein CXorf17 homolog (predicted)	1.867
1368264_at	NM_057125	Pex6	peroxisomal biogenesis factor 6	1.865
1389089_at	NM_001008885 NM_001164744	RT1-Ke4	RT1 class I, locus Ke4	1.864
1398227_at	---	---	Transcribed locus	1.864
1389741_at	NM_001107117	Lass4_predicted	longevity assurance homolog 4 (S. cerevisiae) (predicted)	1.863
1389020_at	NM_001126300	LOC686539	similar to immunoglobulin superfamily containing leucine-rich repeat	1.862
1369227_at	NM_017067	Chm	choroidermia	1.861
1384707_at	NM_001135855	---	Transcribed locus	1.859
1371935_at	NM_001105953	Tmem9_predicted	transmembrane protein 9 (predicted)	1.858
1373062_at	---	---	Transcribed locus	1.858
1390343_at	NM_001100472	Ccnc	cyclin C	1.858
1389306_at	XM_001058523 XM_216941	---	---	1.857
1367568_a_at	NM_012862	Mgp	matrix Gla protein	1.854
1383434_at	NM_001105857	Pycr1_predicted	pyrroline-5-carboxylate reductase 1 (predicted)	1.853
1389612_at	---	---	Transcribed locus	1.85
1385036_at	NM_001107379	Sncaip_predicted	synuclein, alpha interacting protein (synphilin) (predicted)	1.849
1377681_at	---	---	Transcribed locus	1.848
1387659_at	NM_031776	Gda	guanine deaminase	1.848
1372653_at	NM_001013105	Fkbp11	FK506 binding protein 11	1.847
1369212_s_at	NM_021681 /// NM_172090	Epb4.1l1	erythrocyte protein band 4.1-like 1	1.844
1369269_at	NM_024373	Galnt1	UDP-N-acetyl-alpha-D-galactosamine:polypeptide N-acetylgalactosaminyltransferase 1	1.841
1374953_at	XM_001058924 /// XM_575783	LOC500420	similar to CG12279-PA	1.841
1379584_at	---	---	Transcribed locus	1.841
1369948_at	NM_053401	Ngfrap1	nerve growth factor receptor (TNFRSF16) associated protein 1	1.839
1370251_at	NM_134373	Avpi1	arginine vasopressin-induced 1	1.839
1381775_at	---	---	Transcribed locus	1.839
1374746_at	---	---	Transcribed locus	1.838
1386716_at	---	---	CDNA clone IMAGE:7320582	1.838
1385292_at	NM_021581	Sc65	Synaptonemal complex protein SC65	1.837
1388569_at	NM_177927	Serpinf1	serine (or cysteine) peptidase inhibitor, clade F, member 1	1.837
1371889_at	NM_177421	Slc22a17	solute carrier family 22 (organic cation transporter), member 17	1.835
1372134_at	NM_001106608	Chchd6_predicted	coiled-coil-helix-coiled-coil-helix domain containing 6 (predicted)	1.835

1380808_at	NM_001109668	Tollip_predicted	toll interacting protein (predicted)	1.835
1395512_at	NM_001106074	Crlf1_predicted	cytokine receptor-like factor 1 (predicted)	1.834
1387723_at	NM_017310	Sema3a	sema domain, immunoglobulin domain (Ig), short basic domain, secreted, (semaphorin) 3A	1.831
1369783_a_at	NM_031588	Nrg1	neuregulin 1	1.829
1372401_at	NM_001106655	Nans_predicted	N-acetylneuraminic acid synthase (sialic acid synthase) (predicted)	1.829
1375370_at	---	---	Transcribed locus	1.829
1377662_at	NM_001009474	Pir	pirin	1.829
1377736_at	---	---	Transcribed locus	1.829
1376304_at	---	---	Transcribed locus	1.828
1387910_at	NM_021681 /// NM_172090	Epb4.1l1	erythrocyte protein band 4.1-like 1	1.828
1379093_at	---	---	Transcribed locus	1.826
1389093_at	NM_017198	Pak1	P21 (CDKN1A)-activated kinase 1	1.826
1383837_at	NM_001007801	Yipf3	Yip1 domain family, member 3	1.825
1398387_at	NM_199105	MGC72614	hypothetical LOC310540	1.825
1396614_at	NM_001100700	Sfrp2	secreted frizzled-related protein 2	1.824
1367594_at	NM_017087	Bgn	biglycan	1.823
1369969_at	NM_013063	Parp1	poly (ADP-ribose) polymerase family, member 1	1.823
1387349_at	NM_013028	Shox2	short stature homeobox 2	1.822
1390126_at	XM_002728459	---	---	1.822
1367870_at	NM_032614	Txnl2	thioredoxin-like 2	1.821
1384836_at	NM_001012054	Calml3	calmodulin-like 3	1.821
1397241_at	XM_001073980 /// XM_002729535	RGD1306880_predicted	similar to hypothetical protein MGC47816 (predicted)	1.821
1380688_at	NM_001079884	Galntl4_predicted	UDP-N-acetyl-alpha-D-galactosamine:polypeptide N-acetylgalactosaminyltransferase-like 4 (predicted)	1.819
1383705_at	---	---	CDNA clone IMAGE:7317308	1.819
1379627_at	XM_002725800 /// XM_220013	RGD1564625_predicted	similar to transmembrane protein TM9SF3 (predicted)	1.818
1392557_at	---	---	Transcribed locus	1.818
1391684_at	NM_001108790	Tmem14a_predicted	transmembrane protein 14A (predicted)	1.817
1378105_at	---	---	Transcribed locus	1.816
1369718_at	NM_031120	Ssr3	signal sequence receptor, gamma	1.815
1385553_at	NM_001109525	LOC684506 /// LOC689116	similar to SMP3 mannosyltransferase /// similar to nuclear cap binding protein subunit 2	1.815
1376170_at	NM_001130548	---	---	1.814
1398990_at	---	---	Transcribed locus	1.814
1392629_a_at	NM_001034940	Zcrb1	zinc finger CCHC-type and RNA binding motif 1	1.813
1372721_at	XM_002728992	---	---	1.811
1392171_at	NM_053560	Chi3l1	chitinase 3-like 1	1.811
1367482_at	NM_001126082	RGD1561880_predicted	similar to anaphase promoting complex subunit 11 homolog (predicted)	1.81
1367894_at	NM_022392	Insig1	insulin induced gene 1	1.81
1376991_at	---	---	Transcribed locus	1.809
1378784_at	---	---	Transcribed locus	1.809
1387196_at	NM_022249	Khdrbs3	KH domain containing, RNA binding, signal transduction associated 3	1.809
1392876_at	---	---	Transcribed locus	1.809
1394259_at	NM_001107135	Cldn15_predicted	claudin 15 (predicted)	1.809
1372615_at	NM_031582	Aoc3	amine oxidase, copper containing 3	1.808
1388523_at	NM_001100840	Txndc12	thioredoxin domain containing 12 (endoplasmic reticulum)	1.807
1391146_at	NM_053392	Cdh11	cadherin 11	1.807
1373674_at	NM_001108644	Mfap5_predicted	microfibrillar associated protein 5 (predicted)	1.805
1368982_at	NM_053772	Pkia	protein kinase inhibitor, alpha	1.804
1367705_at	NM_022278	Glrx1	glutaredoxin 1 (thioltransferase)	1.803
1380174_at	---	---	Transcribed locus	1.803
1379108_at	XM_001070777 /// XM_224759	RGD1559968_predicted	Similar to ADP-ribosylation factor guanine nucleotide factor 6 isoform a (predicted)	1.802
1397960_at	NM_001014273	LOC367902	similar to ALEX3 protein	1.802
1398656_at	---	---	---	1.801
1368455_at	NM_133540	Nkg7	natural killer cell group 7 sequence	-1.8
1369235_at	NM_022207	Unc5b	unc-5 homolog B (C. elegans)	-1.8
1371985_a_at	NM_212531	Bat5	HLA-B associated transcript 5	-1.8
1391121_at	NM_001107315	RGD1311793_predicted	similar to DNA segment, Chr 8, ERATO Doi 82, expressed (predicted)	-1.8
1369820_at	NM_053951	Mcf2l	mcf.2 transforming sequence-like	-1.81
1370135_at	NM_131914	Cav2	caveolin 2	-1.81
1371015_at	NM_173096	Mx1	myxovirus (influenza virus) resistance 1	-1.81
1374491_at	NM_198754	Cmtm8	CKLF-like MARVEL transmembrane domain containing 8	-1.81
1378055_at	---	---	Transcribed locus	-1.81
1378109_at	---	---	Transcribed locus	-1.81
1383054_at	NM_001169120	Zfp91	zinc finger protein 91	-1.81
1383240_at	---	Itga6	integrin, alpha 6	-1.81

1391924_at	NM_001044247	LOC361187	Similar to ankyrin repeat and SOCs box-containing protein 5	-1.81
1392398_at	---	---	Transcribed locus	-1.81
1395408_at	NM_001024260	Nostrin	nitric oxide synthase trafficker	-1.81
1369115_at	NM_012492	Adrb2	adrenergic receptor, beta 2	-1.82
1369647_at	NM_012717	Calcrl	calcitonin receptor-like	-1.82
1371078_at	NM_012645	RT1-Aw2	RT1 class Ib, locus Aw2	-1.82
1373427_at	NM_001106641	Rragd_predicted	Ras-related GTP binding D (predicted)	-1.82
1373533_at	---	---	---	-1.82
1373545_at	---	---	Transcribed locus	-1.82
1377497_at	NM_001009681	Oasl1	2'-5' oligoadenylate synthetase-like 1	-1.82
1380210_at	NM_001034849	Gimap1	GTPase, IMAP family member 1	-1.82
1392117_at	---	---	Transcribed locus	-1.82
1393427_s_at	NM_139104	Egfl7	EGF-like domain 7	-1.82
1398732_at	---	LOC688273	hypothetical protein LOC688273	-1.82
1368463_at	NM_053653	Vegfc	vascular endothelial growth factor C	-1.83
1370402_at	NM_139104	Egfl7	EGF-like domain 7	-1.83
1370454_at	NM_031707	Homer1	homer homolog 1 (Drosophila)	-1.83
1371643_at	NM_171992	Ccnd1	Cyclin D1	-1.83
1376746_at	NM_001008893	Ldhd	lactate dehydrogenase D	-1.83
1377719_a_at	---	---	---	-1.83
1379390_at	NM_001031652	St6galnac2	ST6 (alpha-N-acetyl-neuraminyl-2,3-beta-galactosyl-1,3)-N-acetylgalactosaminide alpha-2,6-sialyltransferase 2	-1.83
1384180_at	NM_001024753	Ifit2	interferon-induced protein with tetratricopeptide repeats 2	-1.83
1390281_a_at	NM_001108727	Coq10a_predicted	coenzyme Q10 homolog A (yeast) (predicted)	-1.83
1391617_at	---	---	Transcribed locus	-1.83
1397225_at	---	---	Transcribed locus	-1.83
1398597_at	---	---	Transcribed locus	-1.83
1368227_at	NM_031664	Slc28a2	solute carrier family 28 (sodium-coupled nucleoside transporter), member 2	-1.84
1370081_a_at	NM_001110333 /// NM_001110334 /// NM_001110335 /// NM_001110336 /// NM_031836	Vegfa	vascular endothelial growth factor A	-1.84
1380241_a_at	NM_001106321	Lrp5_predicted	low density lipoprotein receptor-related protein 5 (predicted)	-1.84
1381610_at	---	---	Transcribed locus	-1.84
1383010_at	---	---	Transcribed locus	-1.84
1383199_at	---	---	Transcribed locus	-1.84
1383332_at	---	---	Transcribed locus	-1.84
1386823_at	NM_001030044	LOC498918	iroquois homeobox protein 5	-1.84
1387052_at	NM_031039	Gpt1	glutamic pyruvic transaminase 1, soluble	-1.84
1388211_s_at	NM_031315 /// NM_138907	Cte1 /// Mte1	cytosolic acyl-CoA thioesterase 1 /// mitochondrial acyl-CoA thioesterase 1	-1.84
1389250_at	---	---	Transcribed locus	-1.84
1392795_at	NM_001108430	---	Transcribed locus	-1.84
1394581_at	---	---	Transcribed locus	-1.84
1398661_at	NM_001108938	---	---	-1.84
1371491_at	NM_001105721	Notch1	Notch gene homolog 1 (Drosophila)	-1.85
1371536_at	NM_152790	Carhsp1	calcium regulated heat stable protein 1	-1.85
1372136_at	NM_001169127	---	---	-1.85
1373969_at	NM_001005762	Sorbs3	sorbin and SH3 domain containing 3	-1.85
1374165_at	XM_002724808	RGD1565457_predicted	similar to Rasa4 protein (predicted)	-1.85
1374710_at	---	---	Transcribed locus	-1.85
1376925_at	NM_001025688	Palmd	palmdelphin	-1.85
1379703_at	XM_001072997 /// XM_235398	RGD1311559_predicted	hypothetical LOC315055 (predicted)	-1.85
1389341_at	NM_001107881	Plxnd1_predicted	plexin D1 (predicted)	-1.85
1392073_at	---	---	Transcribed locus	-1.85
1397286_at	---	---	Transcribed locus	-1.85
1398188_at	---	---	Transcribed locus	-1.85
1372561_at	NM_001100669	Smap1l	stromal membrane-associated protein 1-like	-1.86
1378453_at	---	---	---	-1.86
1381556_at	XM_001072319 /// XM_224795	RGD1560014_predicted	similar to hypothetical protein FLJ20035 (predicted)	-1.86
1382835_at	---	---	Transcribed locus	-1.86
1383581_at	NM_001109418	LOC680531	similar to CG3880-PA	-1.86
1384056_at	NM_053429	Fgfr3	Fibroblast growth factor receptor 3	-1.86
1388210_at	NM_138907	Mte1	mitochondrial acyl-CoA thioesterase 1	-1.86
1390531_at	XM_001057758 /// XM_002726306 /// XM_002729259 /// XM_230961	RGD1306056_predicted	similar to Peroxisomal proliferator-activated receptor A interacting complex 285 kDa protein (PPAR-alpha interacting complex protein 285) (predicted)	-1.86

1391503_at	XR_085668 /// XR_086079	Centd3_predicted	centaurin, delta 3 (predicted)	-1.86
1391587_at	---	---	Transcribed locus	-1.86
1392785_at	---	---	Transcribed locus	-1.86
1393558_at	XM_001059353 /// XM_001059408 /// XM_002729169 /// XM_215984	Itga6	integrin, alpha 6	-1.86
1398249_at	NM_053965	Slc25a20	solute carrier family 25 (mitochondrial carnitine/acylcarnitine translocase), member 20	-1.86
1398616_at	NM_001127531	Ap1s2_predicted	adaptor-related protein complex 1, sigma 2 subunit (predicted)	-1.86
1369720_at	NM_053986	Myo1b	myosin Ib	-1.87
1371244_at	NM_001013061	Aprt_predicted	adenine phosphoribosyl transferase (predicted)	-1.87
1372649_at	NM_031607	Hspb7	heat shock 27kD protein family, member 7 (cardiovascular)	-1.87
1373666_at	NM_001047915	Rapgef5	Rap guanine nucleotide exchange factor (GEF) 5	-1.87
1377531_at	---	---	Transcribed locus	-1.87
1378644_at	---	---	Transcribed locus	-1.87
1390403_at	NM_001039002	RGD1304790	similar to CG8312-PA	-1.87
1396660_at	---	---	Transcribed locus	-1.87
1367570_at	NM_031549	Tagln	transgelin	-1.88
1374863_at	NM_001108693	RGD1562168_predicted	similar to retinoid binding protein 7 (predicted)	-1.88
1377720_x_at	---	---	---	-1.88
1388623_at	NM_001011939	Ehd1	EH-domain containing 1	-1.88
1393409_at	---	---	Transcribed locus	-1.88
1397152_at	---	---	Transcribed locus	-1.88
1370814_at	NM_153315	Dhrs4	dehydrogenase/reductase (SDR family) member 4	-1.89
1373617_at	NM_001007721	Emp2	epithelial membrane protein 2	-1.89
1375092_at	---	---	Transcribed locus, moderately similar to XP_995266.1 PREDICTED: similar to Myosin-18B (Myosin XVIIIb) [Mus musculus]	-1.89
1376876_at	---	---	Transcribed locus	-1.89
1377814_at	XM_001057606 /// XM_341638	---	Transcribed locus, strongly similar to XP_341639.2 PREDICTED: similar to Nedd4-binding brain specific protein BEAN [Rattus norvegicus]	-1.89
1389550_at	---	---	Transcribed locus	-1.89
1391669_at	NM_001108095	Ptprb_predicted	protein tyrosine phosphatase, receptor type, B (predicted)	-1.89
1392055_at	---	---	Transcribed locus	-1.89
1367982_at	NM_024484	Alas1	aminolevulinic acid synthase 1	-1.9
1369422_at	NM_138850	Fap	fibroblast activation protein	-1.9
1372144_at	NM_001108004	Dnajb5_predicted	DnaJ (Hsp40) homolog, subfamily B, member 5 (predicted)	-1.9
1372458_at	XM_001072149 /// XM_002724818 /// XM_573394	LOC498178 /// LOC687538 /// LOC689820	similar to SET domain-containing protein	-1.9
1377744_at	---	---	Transcribed locus	-1.9
1379380_at	NM_001106427	Spry1_predicted	sprouty homolog 1 (Drosophila) (predicted)	-1.9
1380083_at	NM_001004100	Klk10	kallikrein 10	-1.9
1383314_at	NM_001109273	RGD1565452_predicted	similar to BC003277 protein (predicted)	-1.9
1383847_at	---	---	Transcribed locus	-1.9
1383995_at	---	---	---	-1.9
1385082_at	---	---	Transcribed locus	-1.9
1388991_at	NM_001134514	RGD1562244_predicted	similar to SEC14 and spectrin domains 1 (predicted)	-1.9
1391433_at	NM_138907	Mte1	mitochondrial acyl-CoA thioesterase 1	-1.9
1393442_at	---	---	Transcribed locus	-1.9
1393639_at	NM_001107657	Myo10_predicted	myosin X (predicted)	-1.9
1368188_at	NM_017233	Hpd	4-hydroxyphenylpyruvic acid dioxygenase	-1.91
1372695_at	---	---	Transcribed locus, strongly similar to XP_997117.1 PREDICTED: similar to fibronectin type III domain containing 5 [Mus musculus]	-1.91
1373166_at	XM_001065445 /// XM_347258	RGD1563309_predicted	similar to diacylglycerol kinase, delta 130kDa isoform 1 (predicted)	-1.91
1376601_at	---	Sema6a_predicted	Sema domain, transmembrane domain (TM), and cytoplasmic domain, (semaphorin) 6A (predicted)	-1.91
1382201_at	NM_199407	Unc5c	unc-5 homolog C (C. elegans)	-1.91
1396618_at	---	---	Transcribed locus	-1.91
1370563_at	NM_138547	LOC191574	3-alpha-hydroxysteroid dehydrogenase	-1.92
1374134_at	NM_001108743	Elk3_predicted	ELK3, member of ETS oncogene family (predicted)	-1.92
1374667_at	---	---	CDNA clone IMAGE:7302289	-1.92
1374862_at	NM_001017376	Phyhip	phytanoyl-CoA hydroxylase interacting protein	-1.92
1383420_at	NM_001037656	LOC502479	similar to lactation elevated 1	-1.92

	XR_085901 ///			
1389663_at	XR_086328	Nbeal2_predicted	neurobeachin-like 2 (predicted)	-1.92
1389712_at	NM_001108506	Ebf3_predicted	early B-cell factor 3 (predicted)	-1.92
1368660_at	NM_021690	Rapgef3	Rap guanine nucleotide exchange factor (GEF) 3	-1.93
1371150_at	NM_171992	Ccnd1	cyclin D1	-1.93
1381904_at	NM_212499	G7c	G7c protein	-1.93
1382202_at	NM_001105931	LOC687661	similar to cut-like 2	-1.93
1383695_at	NM_012685	Vipr1	vasoactive intestinal peptide receptor 1	-1.93
1388175_at	NM_173103	Clcnkb	chloride channel Kb	-1.93
1389255_at	NM_001107407	Cdh5_predicted	Cadherin 5 (predicted)	-1.93
1389604_at	NM_001107778	Hspa12b_predicted	heat shock protein 70kDa 12B (predicted)	-1.93
1389617_at	NM_001108743	Elk3_predicted	ELK3, member of ETS oncogene family (predicted)	-1.93
1393202_a_at	NM_001047888	Igf2bp3	Insulin-like growth factor 2, binding protein 3	-1.93
1393799_at	NM_022207	Unc5b	Unc-5 homolog B (C. elegans)	-1.93
1367679_at	NM_013069	Cd74	CD74 antigen (invariant polypeptide of major histocompatibility complex, class II antigen-associated)	-1.94
1367735_at	NM_012819	Acadl	acetyl-Coenzyme A dehydrogenase, long-chain	-1.94
1367987_at	NM_031097	Rnpep	arginyl aminopeptidase (aminopeptidase B)	-1.94
1369400_a_at	NM_001033964 /// NM_001033965 /// NM_080477	Pfkfb2	6-phosphofructo-2-kinase/fructose-2,6-biphosphatase 2	-1.94
1369716_s_at	NM_012976 /// NM_012977	Lgals5 /// Lgals9	lectin, galactose binding, soluble 5 /// lectin, galactose binding, soluble 9	-1.94
1370082_at	NM_021578	Tgfb1	transforming growth factor, beta 1	-1.94
1375266_at	---	---	Transcribed locus, strongly similar to NP_033959.1 cyclin D2 [Mus musculus]	-1.94
1375896_at	NM_001109307	RGD1559449_predicted	similar to polyploidy associated protein kinase PAPK-A (predicted)	-1.94
1378344_at	---	---	Transcribed locus	-1.94
1388018_at	NM_138879	Sele	selectin, endothelial cell	-1.94
1388848_at	XM_001072750	RGD1308350	similar to hypothetical protein MGC13251	-1.94
1371886_at	NM_001004085	Crat	carnitine acetyltransferase	-1.95
1375498_at	---	---	Transcribed locus	-1.95
1383189_at	---	---	Transcribed locus	-1.95
1388109_at	NM_139110	Gpr116	G protein-coupled receptor 116	-1.95
1388604_at	NM_001159594	LOC679341 /// LOC686019	similar to Calsequestrin-1 precursor (Calsequestrin, skeletal muscle isoform)	-1.95
1391172_at	---	---	Transcribed locus	-1.95
1367897_at	NM_012891	Acadvl	acyl-Coenzyme A dehydrogenase, very long chain	-1.96
1368372_at	NM_012661	Sts	steroid sulfatase	-1.96
1368900_at	NM_031771	Thbd	thrombomodulin	-1.96
1372027_at	---	---	Transcribed locus	-1.96
1372569_at	NM_001107979	---	---	-1.96
1376175_at	NM_001017486	LOC498174	similar to NipSnap2 protein (Glioblastoma amplified sequence)	-1.96
1389757_at	NM_001134537	RGD1310159_predicted	similar to acetyl-coA dehydrogenase -related (111.6 kD) (5G231) (predicted)	-1.96
1368540_at	NM_031807	Tpbg	trophoblast glycoprotein	-1.97
1369983_at	NM_031116	Ccl5	chemokine (C-C motif) ligand 5	-1.97
1372372_at	NM_001008770	RGD1306952	similar to Ab2-225	-1.97
1372385_at	XM_002728821	Dusp8_predicted	Dual specificity phosphatase 8 (predicted)	-1.97
1379613_at	XM_001071334 /// XM_221401	RGD1310490_predicted	similar to hypothetical protein MGC29390 (predicted)	-1.97
1380813_at	---	---	---	-1.97
1382330_at	---	Ddef2_predicted	development and differentiation enhancing factor 2 (predicted)	-1.97
1384115_at	NM_138907	Mte1	Mitochondrial acyl-CoA thioesterase 1	-1.97
1376830_at	NM_001106178	RGD1311132_predicted	similar to RIKEN cDNA E430013E20 gene (predicted)	-1.98
1381133_at	---	---	Transcribed locus	-1.98
1398693_at	NM_001108687	Man1c1_predicted	mannosidase, alpha, class 1C, member 1 (predicted)	-1.98
1368428_at	NM_057155	Xpnpep2	X-prolyl aminopeptidase (aminopeptidase P) 2, membrane-bound	-1.99
1372300_at	---	Dok4_predicted	docking protein 4 (predicted)	-1.99
1388970_at	NM_001106261	Rasip1_predicted	Ras interacting protein 1 (predicted)	-1.99
1373649_at	XM_001077717 /// XM_001079869 /// NM_001170602 /// XM_001067790 ///	LOC687381 /// LOC691853	similar to COX10 homolog, cytochrome c oxidase assembly protein, heme A: farnesyltransferase	-2
1376084_a_at	XM_235691	Espl1_predicted	extra spindle poles like 1 (S. cerevisiae) (predicted)	-2
1379751_at	NM_001106171	Tnrc9_predicted	trinucleotide repeat containing 9 (predicted)	-2
1383618_at	NM_001009369	Mrpl38	mitochondrial ribosomal protein L38	-2
1383914_at	NM_001105210 /// NM_001105211	Mrvi1_predicted	MRV integration site 1 homolog (mouse) (predicted)	-2
1389651_at	NM_031612	Apln	apelin, AGTRL1 ligand	-2

1368008_at	NM_001110137 /// NM_021751	Prom1	prominin 1	-2.01
1371065_at	NM_001004084 /// NM_001101017	LOC688090 /// RT1-Bb	RT1 class II, locus Bb /// similar to RT1 class II histocompatibility antigen, B-1 beta chain precursor (RT1.B-beta(1))	-2.01
1378245_at	NM_001108163	RGD1311958_predicted	similar to 6430514L14Rik protein (predicted)	-2.01
1379501_at	---	---	Transcribed locus	-2.01
1387135_at	NM_020308	Adam15	a disintegrin and metallopeptidase domain 15 (metargidin)	-2.01
1388703_at	NM_001004245	Esam	endothelial cell adhesion molecule	-2.01
1389763_at	---	---	---	-2.01
1393208_at	NM_001106207	Myct1_predicted	myc target 1 (predicted)	-2.01
1393482_at	---	---	Transcribed locus	-2.01
1377385_at	NM_198759	Arhgap27	Rho GTPase activating protein 27	-2.02
1380306_at	---	---	Transcribed locus	-2.02
1380616_at	NM_053914	---	---	-2.02
1389018_at	XM_002726953 /// XM_002729801	---	---	-2.02
1393433_at	NM_001108938	RGD1306592_predicted	similar to Agrin (predicted)	-2.02
1395663_at	NM_001014182	Mall	mal, T-cell differentiation protein-like	-2.02
1368911_at	NM_017099	Kcnj8	potassium inwardly-rectifying channel, subfamily J, member 8	-2.03
1370383_s_at	NM_001008884	RT1-Db1	RT1 class II, locus Db1	-2.03
1381243_at	---	---	Transcribed locus	-2.03
1394367_at	NM_001107760	Dll4_predicted	delta-like 4 (Drosophila) (predicted)	-2.03
1368477_at	NM_012914	Atp2a3	ATPase, Ca++ transporting, ubiquitous	-2.04
1371062_at	XM_001062926 /// XM_214478	Aldh5a1	aldehyde dehydrogenase family 5, subfamily A1	-2.04
1381348_at	---	---	Transcribed locus	-2.04
1385832_s_at	NM_001134992	RGD1560293_predicted	similar to RIKEN cDNA 1200013B08 (predicted)	-2.04
1387039_at	NM_030828	Gpc1	glypican 1	-2.04
1388661_at	NM_001006960	MGC94604	mitochondrial protein, 18 kDa	-2.04
1379359_at	---	---	Transcribed locus	-2.05
1380065_at	XM_346994	---	Transcribed locus	-2.05
1390782_at	NM_001014077	Clec14a	C-type lectin domain family 14, member a	-2.05
1391179_at	---	---	Transcribed locus	-2.05
1373500_at	NM_001008519	Lrpprc	leucine-rich PPR-motif containing	-2.06
1374626_at	NM_001009717	Lrg1	leucine-rich alpha-2-glycoprotein 1	-2.06
1376446_at	NM_001005556	MGC93707	similar to RIKEN cDNA D430028G21	-2.06
1380045_at	NM_145091	Pdp2	Pyruvate dehydrogenase phosphatase isoenzyme 2	-2.06
1385320_at	NM_001014109	LOC317379	similar to Pdz-containing protein	-2.06
1388522_at	NM_001107141	RGD1310383_predicted	similar to T-cell activation protein phosphatase 2C (predicted)	-2.06
1394881_at	NM_001108163	RGD1311958_predicted	similar to 6430514L14Rik protein (predicted)	-2.06
1369944_at	NM_030862	Marcksl1	MARCKS-like 1	-2.07
1375277_at	NM_001143750	LOC499745 /// LOC688240	similar to Notch-regulated ankyrin repeat protein	-2.07
1377840_at	---	RGD1305202_predicted	similar to Protein C20orf160 (predicted)	-2.07
1383554_at	NM_001173349 /// XM_001054034 /// XM_236533	RGD1566282_predicted	similar to RIKEN cDNA D330045A20 (predicted)	-2.07
1389650_at	---	---	Transcribed locus, strongly similar to XP_214980.3 PREDICTED: similar to hypothetical protein DKFZp547K1113 [Rattus norvegicus]	-2.07
1373175_at	NM_001013927	RGD1308734	similar to RIKEN cDNA 1100001H23	-2.08
1383084_at	---	---	Transcribed locus	-2.08
1389332_at	---	---	Transcribed locus	-2.08
1368698_at	NM_012508	Atp2b2	ATPase, Ca++ transporting, plasma membrane 2	-2.09
1369087_at	NM_019306	Flt1	FMS-like tyrosine kinase 1	-2.09
1370810_at	NM_022267	Ccnd2	cyclin D2	-2.09
1374593_at	NM_017171	Prkce	protein kinase C, epsilon	-2.09
1383075_at	NM_171992	Ccnd1	Cyclin D1	-2.09
1384073_at	NM_001025423	Adhfe1	alcohol dehydrogenase, iron containing, 1	-2.09
1368422_at	NM_017149	Meox2	mesenchyme homeobox 2	-2.1
1380460_at	NM_001039024	RGD1311267	similar to RIKEN cDNA 4931426K16 gene	-2.1
1382590_at	NM_001135011	RGD1563347_predicted	similar to RIKEN cDNA 2310015N21 (predicted)	-2.1
1382953_at	---	---	Transcribed locus	-2.1
1395197_at	---	---	Transcribed locus	-2.1
1370905_at	NM_001105759	Dock9	dedicator of cytokinesis 9	-2.11
1372681_at	---	---	---	-2.11
1373288_at	NM_001107547	St5_predicted	suppression of tumorigenicity 5 (predicted)	-2.11

1382255_at	---	---	---	-2.11
1382868_at	NM_001108430	Sema6a_predicted	sema domain, transmembrane domain (TM), and cytoplasmic domain, (semaphorin) 6A (predicted)	-2.11
1374466_at	---	---	Transcribed locus	-2.12
1384415_at	NM_001106045	Sox7_predicted	SRY-box containing gene 7 (predicted)	-2.12
1394569_at	---	---	Transcribed locus	-2.12
1383235_at	XM_001067323	LOC688535	hypothetical protein LOC688535	-2.13
1397760_at	---	---	Transcribed locus	-2.13
1370492_a_at	NM_019306	Flt1	FMS-like tyrosine kinase 1	-2.14
1390426_at	NM_001105721	Notch1	Notch gene homolog 1 (Drosophila)	-2.14
1390601_at	---	---	Transcribed locus	-2.14
1379655_at	---	---	---	-2.15
1383273_a_at	NM_001011945	Pcbp3	poly(rC) binding protein 3	-2.15
1385053_at	---	---	Transcribed locus	-2.15
1386974_at	XM_002729917 /// XM_576401	Phldb1	pleckstrin homology-like domain, family B, member 1	-2.15
1396101_at	NM_031123	Stc1	stanniocalcin 1	-2.15
1371696_at	NM_152242	Gpr56	G protein-coupled receptor 56	-2.16
1375445_at	NM_001108180	Ky_predicted	kyphoscoliosis (predicted)	-2.16
1382138_at	NM_001143750	LOC499745 /// LOC688240	similar to Notch-regulated ankyrin repeat protein	-2.16
1382958_at	NM_013167	Ucp3	uncoupling protein 3 (mitochondrial, proton carrier)	-2.16
1393179_at	---	---	Transcribed locus	-2.16
1368342_at	NM_031544	Ampd3	adenosine monophosphate deaminase 3	-2.17
1372091_at	NM_206950	Mig12	MID1 interacting G12-like protein	-2.17
1373483_at	NM_001108989	Ankrd47_predicted	ankyrin repeat domain 47 (predicted)	-2.17
1384238_at	---	RGD1562969_predicted	similar to Tweety homolog 2 (predicted)	-2.17
1389324_at	NM_053545	Tie1	tyrosine kinase with immunoglobulin-like and EGF-like domains 1	-2.17
1390405_at	---	---	Transcribed locus	-2.17
1393235_at	---	---	Transcribed locus	-2.17
1398062_at	NM_001100669	Smap1l	stromal membrane-associated protein 1-like	-2.17
1389170_at	NM_022260	Casp7	caspase 7	-2.18
1389707_at	---	---	Transcribed locus	-2.18
1390571_at	NM_001025680	Gpr4	G protein-coupled receptor 4	-2.18
1391808_at	---	---	Transcribed locus	-2.18
1370509_at	NM_145091	Pdp2	pyruvate dehydrogenase phosphatase isoenzyme 2	-2.19
1370896_a_at	NM_001170600 /// XM_001053471 /// XM_573030 /// XM_001073458 /// XM_002724492 /// XM_002727708 ///	RGD1564935_predicted	similar to Myh11 protein (predicted)	-2.19
1376197_at	XM_343891	Tcf7_predicted	transcription factor 7, T-cell specific (predicted)	-2.19
1377334_at	NM_001008831	RT1-Ba	RT1 class II, locus Ba	-2.19
1380617_at	NM_001033913 /// NM_145680	Gimap5	GTPase, IMAP family member 5	-2.19
1384651_at	---	---	Transcribed locus, strongly similar to XP_001080814.1 PREDICTED: hypothetical protein [Rattus norvegicus]	-2.19
1367659_s_at	NM_017306	Dci	dodecenoyl-coenzyme A delta isomerase	-2.2
1368407_at	NM_022605	Hpse	heparanase	-2.2
1368976_at	NM_013127	Cd38	CD38 antigen	-2.2
1370449_at	NM_133577	P2ry14	purinergic receptor P2Y, G-protein coupled, 14	-2.2
1370822_at	NM_001008831	RT1-Ba	RT1 class II, locus Ba	-2.2
1373807_at	NM_001110333 /// NM_001110334 /// NM_001110335 /// NM_001110336 /// NM_031836	Vegfa	Vascular endothelial growth factor A	-2.2
1374295_at	NM_001106766	Polrmt_predicted	polymerase (RNA) mitochondrial (DNA directed) (predicted)	-2.2
1376924_a_at	NM_001025688	Palmd	palmdelphin	-2.2
1387027_a_at	NM_012977	Lgals9	lectin, galactose binding, soluble 9	-2.2
1388804_at	---	---	Transcribed locus	-2.2
1389075_at	---	---	Transcribed locus, strongly similar to XP_580018.1 PREDICTED: hypothetical protein XP_580018 [Rattus norvegicus]	-2.2
1369757_at	NM_019312	Itpkb	inositol 1,4,5-trisphosphate 3-kinase B	-2.21
1370913_at	NM_138881	Best5	Best5 protein	-2.21
1374902_at	XM_001068995 /// XM_227396	Iqgap3_predicted	IQ motif containing GTPase activating protein 3 (predicted)	-2.21
1376522_at	---	---	Transcribed locus	-2.21
1368523_at	NM_013219	Cadps	Ca2+-dependent secretion activator	-2.22
1378484_at	NM_001108162	Rasl12_predicted	RAS-like, family 12 (predicted)	-2.22
1381063_at	XM_002727705	---	---	-2.22

1396799_at	---	---	Transcribed locus	-2.22
1398484_at	NM_001134539	RGD1308221_predicted	similar to TBC1 domain family, member 8 (with GRAM domain); vascular Rab-GAP/TBC-containing (predicted)	-2.22
1373245_at	NM_001135009	Col4a1	procollagen, type IV, alpha 1	-2.23
1383059_a_at	NM_001012160	Gkap1	G kinase anchoring protein 1	-2.23
1370071_at	NM_130399	Ada	adenosine deaminase	-2.24
1389388_at	---	---	Transcribed locus	-2.24
1372995_at	NM_001013895	Prkd2	protein kinase D2	-2.25
1375621_at	NM_153298	---	---	-2.25
1377404_at	NM_031123	Stc1	stanniocalcin 1	-2.25
1383943_at	XM_001065965 /// XM_002730026	Dnah7	dynein, axonemal, heavy polypeptide 7	-2.25
1388422_at	NM_001012163	Lims2	LIM and senescent cell antigen like domains 2	-2.25
1390255_at	XM_001058944 /// XM_225889	RGD1565118_predicted	similar to mKIAA0843 protein (predicted)	-2.25
1368473_at	NM_019280	Gja5	gap junction membrane channel protein alpha 5	-2.26
1375934_at	NM_001173349 /// XM_001054034 /// XM_236533	RGD1566282_predicted	similar to RIKEN cDNA D330045A20 (predicted)	-2.26
1378214_at	---	GalNAc4S6ST	N-acetylgalactosamine 4-sulfate 6-O-sulfotransferase	-2.26
1380379_at	XM_001074239 /// XM_002729561 /// XM_575958	RGD1562463_predicted	similar to : F-box protein 44 (predicted)	-2.26
1396435_at	---	---	Transcribed locus	-2.26
1373642_at	XM_001059976 /// XM_002725990	LOC681021	similar to progestin and adipoQ receptor family member VI	-2.27
1377874_at	---	Tbx2_predicted	T-box 2 (predicted)	-2.27
1382183_at	---	---	Transcribed locus	-2.27
1382603_at	---	---	Transcribed locus	-2.27
1388932_at	XM_001060527 /// XM_215963	Lama5	laminin, alpha 5	-2.27
1391570_at	XM_001058944 /// XM_225889	RGD1565118_predicted	similar to mKIAA0843 protein (predicted)	-2.27
1392990_at	NM_001107902	Sox17_predicted	SRY-box containing gene 17 (predicted)	-2.27
1376380_at	---	---	Transcribed locus	-2.28
1387938_at	NM_144762	Baalc	brain and acute leukemia, cytoplasmic	-2.28
1379799_at	---	---	Transcribed locus	-2.29
1388831_at	NM_053811	Slc9a3r2	solute carrier family 9 (sodium/hydrogen exchanger), isoform 3 regulator 2	-2.29
1374355_at	NM_001039454	RGD1561028	similar to MGC47262 protein	-2.3
1392322_at	NM_001024328	Gimap7	GTPase, IMAP family member 7	-2.3
1375951_at	NM_031771	Thbd	thrombomodulin	-2.31
1389054_at	NM_001017500	LOC498368	similar to RIKEN cDNA 0610040J01	-2.31
1389284_at	---	---	Transcribed locus	-2.31
1367999_at	NM_032416	Aldh2	aldehyde dehydrogenase 2	-2.32
1381523_at	---	---	Transcribed locus	-2.32
1383019_at	---	---	Transcribed locus	-2.32
1389244_x_at	NM_022205	Cxcr4	chemokine (C-X-C motif) receptor 4	-2.32
1369957_at	NM_019341	Rgs5	regulator of G-protein signaling 5	-2.33
1384944_at	NM_001108057	---	CDNA clone IMAGE:7384525	-2.33
1393228_at	NM_001014068	Gloxd1	glyoxalase domain containing 1	-2.33
1377462_at	---	---	---	-2.34
1378546_at	---	---	Transcribed locus	-2.34
1379295_at	NM_001135767	LOC688154 /// LOC690825	similar to guanine nucleotide binding protein (G protein), gamma transducing activity polypeptide 2	-2.34
1379748_at	XM_001079914 /// XM_227820	LOC310968	Similar to histocompatibility 28	-2.34
1387976_at	NM_053811	Slc9a3r2	solute carrier family 9 (sodium/hydrogen exchanger), isoform 3 regulator 2	-2.34
1388494_at	XM_001076134 /// XM_225043	Col4a2_predicted	procollagen, type IV, alpha 2 (predicted)	-2.34
1390161_at	NM_001013980	LOC304138	similar to cysteine and tyrosine-rich protein 1	-2.34
1398530_at	NM_022396	Gng11	guanine nucleotide binding protein (G protein), gamma 11	-2.34
1368534_at	NM_024483	Adra1d	adrenergic receptor, alpha 1d	-2.35
1373403_at	NM_001115043	LOC684871	similar to Protein C8orf4 (Thyroid cancer protein 1) (TC-1)	-2.35
1376624_at	---	---	Transcribed locus	-2.35
1384963_at	---	---	---	-2.35
1388694_at	NM_001166403	RT1-149	RT1-149 protein	-2.35
1367702_at	NM_016986	Acadm	acetyl-Coenzyme A dehydrogenase, medium chain	-2.36
1368970_at	NM_053644	Cdh23	cadherin 23 (otocadherin)	-2.36
1370770_s_at	NM_021843 /// NM_021844	Kitl	kit ligand	-2.36
1371525_at	XM_001060536 /// XM_001071999	Slc12a7	solute carrier family 12 (potassium/chloride transporters), member 7	-2.36
1381971_at	NM_001024781	Sox18	SRY-box containing gene 18	-2.36

			Iroquois related homeobox 1 (Drosophila) (predicted) /// similar to Iroquois-class homeodomain protein IRX-1 (Iroquois homeobox protein 1) (Homeodomain protein IRXA1)	
1384312_at	NM_001107331	Irx1_predicted /// LOC501463		-2.36
1389728_at	NM_001107758	Meis2_predicted	Meis1, myeloid ecotropic viral integration site 1 homolog 2 (predicted)	-2.36
1368079_at	NM_053826	Pdk1	pyruvate dehydrogenase kinase, isoenzyme 1	-2.37
1370848_at	NM_138827	Slc2a1	solute carrier family 2 (facilitated glucose transporter), member 1	-2.37
1397851_at	---	---	Transcribed locus	-2.37
1368851_at	NM_012555	Ets1	v-ets erythroblastosis virus E26 oncogene homolog 1 (avian)	-2.38
1370882_at	NM_198740	Hla-dmb	major histocompatibility complex, class II, DM beta	-2.39
1374266_at	XM_001066229 /// XM_225997	Pcdh1_predicted	Protocadherin 1 (cadherin-like 1) (predicted)	-2.39
1378135_at	---	---	Transcribed locus	-2.39
1380546_at	NM_001013932	LOC298250	similar to hypothetical protein FLJ10986	-2.39
1381409_at	---	---	Transcribed locus	-2.39
1391514_at	---	---	Transcribed locus	-2.39
1393691_at	---	LOC688273	hypothetical protein LOC688273	-2.39
1374278_at	NM_001107799	RGD1307696_predicted	similar to dJ881L22.2 (novel protein) (predicted)	-2.4
1393508_at	---	---	Transcribed locus	-2.4
1368013_at	NM_080399 /// XM_002726043	Ddit4l	DNA-damage-inducible transcript 4-like	-2.41
1388949_at	---	---	Transcribed locus	-2.41
1386927_at	NM_012930	Cpt2	carnitine palmitoyltransferase 2	-2.42
1392952_at	NM_001034951	LOC619561	hypothetical protein LOC619561	-2.42
1389198_at	NM_001108579	Sh2d3c_predicted	SH2 domain containing 3C (predicted)	-2.44
1368901_at	NM_031771	Thbd	thrombomodulin	-2.45
1376648_at	NM_001013096	Mycn	v-myc myelocytomatosis viral related oncogene, neuroblastoma derived (avian)	-2.45
1379392_at	NM_001013054	Adprhl1	ADP-ribosylhydrolase like 1	-2.45
1391856_at	NM_001100882	Sema3g	sema domain, immunoglobulin domain (Ig), short basic domain, secreted, (semaphorin) 3G	-2.46
1368300_at	NM_053294	Adora2a	adenosine A2a receptor	-2.47
1368380_at	NM_019156	Vtn	vitronectin	-2.47
1370824_at	NM_145776	Slc38a3	solute carrier family 38, member 3	-2.47
1372549_at	NM_001128155	RGD1561781_predicted	similar to RIKEN cDNA 2600017H02 (predicted)	-2.47
1390253_at	NM_001012112	Ankrd9	ankyrin repeat domain 9	-2.47
1392739_a_at	NM_001014088	RGD1307401	similar to RIKEN cDNA 2310005P05	-2.47
1395734_at	NM_001025688	Palmd	palmdelphin	-2.47
1382712_at	---	---	Transcribed locus	-2.48
1382864_at	NM_001025688	Palmd	palmdelphin	-2.48
1376632_at	NM_001008562	Lmcd1_predicted	LIM and cysteine-rich domains 1 (predicted)	-2.49
1389374_at	NM_001103352	Kifc3	kinesin family member C3	-2.49
1392715_at	NM_176075	Ppargc1b	peroxisome proliferative activated receptor, gamma, coactivator 1 beta	-2.5
1394375_x_at	NM_001108279	RGD1563179_predicted	similar to BAZF (predicted)	-2.5
1370229_at	NM_031967	Ndrg4	N-myc downstream regulated gene 4	-2.51
1372055_at	NM_001135718	RGD1306534_predicted	similar to P-Rex1 (predicted)	-2.51
1376051_at	NM_175757	Cryl1	crystallin, lamda 1	-2.52
1367828_at	NM_022512	Acads	acetyl-Coenzyme A dehydrogenase, short chain	-2.53
1369872_a_at	NM_001033924 /// NM_133550	Fcer2a	Fc receptor, IgE, low affinity II, alpha polypeptide	-2.53
1397343_at	---	---	---	-2.53
1381681_at	---	---	Transcribed locus	-2.54
1382130_at	NM_001169129	Pcdh19_predicted	protocadherin 19 (predicted)	-2.54
1387933_s_at	NM_138848	Podxl	podocalyxin-like	-2.55
1390203_at	---	---	Transcribed locus	-2.55
1373544_at	NM_145672	Cxcl9	chemokine (C-X-C motif) ligand 9	-2.56
1378171_at	---	---	Transcribed locus	-2.56
1391758_at	---	---	---	-2.56
1376371_at	---	---	Transcribed locus	-2.57
1386880_at	NM_130433	Acaa2	acetyl-Coenzyme A acyltransferase 2 (mitochondrial 3-oxoacyl-Coenzyme A thiolase)	-2.57
1388674_at	NM_080782	Cdkn1a	cyclin-dependent kinase inhibitor 1A	-2.57
1388821_at	NM_001108015	RGD1564451_predicted	similar to Tribbles homolog 2 (predicted)	-2.58
1368138_at	NM_017212	Mapt	microtubule-associated protein tau	-2.59
1368174_at	NM_019371	Egln3	EGL nine homolog 3 (C. elegans)	-2.6

1396214_at	NM_021843 /// NM_021844	Kitl	kit ligand	-2.6
1381722_at	NM_001134637	LOC501283	similar to lipid droplet associated protein	-2.61
1393347_at	NM_001033998	Itgal	Integrin alpha L	-2.61
1381804_at	NM_001108279	RGD1563179_predicted	similar to BAZF (predicted)	-2.62
1382995_at	---	---	Transcribed locus	-2.62
1383844_at	NM_001105789	Arhgef15_predicted	Rho guanine nucleotide exchange factor (GEF) 15 (predicted)	-2.62
1390956_at	XR_085883 /// XR_086306	RGD1309798_predicted	Similar to Apolipoprotein L3 (Apolipoprotein L-III) (ApoL-III) (TNF-inducible protein CG12-1) (CG12_1) (predicted)	-2.63
1374159_at	XM_001076120 /// XM_002727139 /// XM_002729977 /// XM_236654	RGD1305208_predicted	Similar to RN49018 (predicted)	-2.65
1382571_at	---	---	Transcribed locus	-2.65
1388856_at	NM_021843 /// NM_021844	Kitl	kit ligand	-2.65
1376633_at	---	---	Transcribed locus	-2.66
1385740_at	NM_001113789 /// NM_001143756	RGD1559981_predicted	similar to leucine rich repeat containing 27 (predicted)	-2.67
1386833_at	NM_001108279	RGD1563179_predicted	similar to BAZF (predicted)	-2.67
1382454_at	NM_145672	Cxcl9	chemokine (C-X-C motif) ligand 9	-2.68
1389548_at	NM_001025423	Adhfe1	alcohol dehydrogenase, iron containing, 1	-2.69
1377286_at	NM_173153	Gimap4	GTPase, IMAP family member 4	-2.7
1384408_at	---	---	Transcribed locus	-2.71
1387134_at	NM_053687	Slfn3	schlafen 3	-2.71
1394711_at	NM_001106921	Prkag3_predicted	protein kinase, AMP-activated, gamma 3 non-catatlytic subunit (predicted)	-2.71
1383811_at	---	---	Transcribed locus	-2.73
1390975_at	---	---	---	-2.75
1375278_at	NM_001108552	Trim2	tripartite motif protein 2	-2.76
1387124_at	NM_012590	Inha	inhibin alpha	-2.76
1389491_at	---	---	Transcribed locus	-2.76
1371824_at	NM_017135	Ak3l1	adenylate kinase 3-like 1	-2.78
1385124_at	NM_001108015	RGD1564451_predicted	similar to Tribbles homolog 2 (predicted)	-2.78
1387224_at	NM_019304	Dgkb	diacylglycerol kinase, beta	-2.8
1372434_at	NM_181088	Cip98	CASK-interacting protein CIP98	-2.81
1374195_at	NM_001107942	Lad1_predicted	ladinin (predicted)	-2.81
1376848_at	---	---	Transcribed locus	-2.81
1385729_at	---	---	Transcribed locus	-2.85
1386685_at	XM_001063390 /// XM_224256	Sacs_predicted	sacsin (predicted)	-2.85
1376831_at	NM_001113781	RGD1308747_predicted	similar to hypothetical protein FLJ10156 (predicted)	-2.86
1377721_at	NM_001077677	RGD1561027_predicted	similar to PACRG (predicted)	-2.86
1389039_at	---	---	Transcribed locus	-2.86
1377084_at	---	---	Transcribed locus	-2.87
1378199_at	XM_001061369 /// XM_343124	Luzp5_predicted	leucine zipper protein 5 (predicted)	-2.87
1369793_a_at	NM_001034009 /// NM_023983	Mcam	melanoma cell adhesion molecule	-2.88
1382773_at	---	---	---	-2.89
1379772_at	NM_031349	Agtrl1	angiotensin receptor-like 1	-2.9
1388732_at	NM_001105950	Slc35f5_predicted	solute carrier family 35, member F5 (predicted)	-2.91
1374546_at	---	---	Transcribed locus	-2.94
1392971_at	---	---	Transcribed locus	-2.95
1382579_at	NM_001106171	Tnrc9_predicted	trinucleotide repeat containing 9 (predicted)	-2.97
1370097_a_at	NM_022205	Cxcr4	chemokine (C-X-C motif) receptor 4	-3
1370419_a_at	NM_053360	Sh3kbp1	SH3-domain kinase binding protein 1	-3
1375420_at	NM_001107749	Tp53i11_predicted	tumor protein p53 inducible protein 11 (predicted)	-3.01
1378094_at	---	---	Transcribed locus	-3.01
1387957_a_at	NM_053360	Sh3kbp1	SH3-domain kinase binding protein 1	-3.01
1379724_at	XM_001064525	LOC685611	similar to pleckstrin homology-like domain, family B, member 2	-3.03
1372158_at	NM_139337	Lrp16	LRP16 protein	-3.04
1389285_at	---	---	Transcribed locus	-3.04
1397133_at	NM_001106202	Tdrd1_predicted	tudor domain containing 1 (predicted)	-3.05
1369928_at	NM_019212	Acta1	actin, alpha 1, skeletal muscle	-3.07
1370522_at	NM_172091 /// NM_172092	Gcgr	glucagon receptor	-3.07

1386212_at	NM_001011908	Spna1	spectrin alpha 1	-3.07
1393559_at	---	---	Transcribed locus	-3.07
1387413_at	NM_053734	Ncf1	neutrophil cytosolic factor 1	-3.09
1388546_at	---	---	---	-3.12
1393454_at	NM_001107279	Pcdh17_predicted	protocadherin 17 (predicted)	-3.12
1388044_at	NM_001033964 /// NM_001033965 /// NM_080477	Pfkfb2	6-phosphofructo-2-kinase/fructose-2,6-biphosphatase 2	-3.22
1374290_at	---	---	Transcribed locus	-3.23
1388462_at	NM_147135	Sbk1	SH3-binding kinase 1	-3.28
1386080_at	XM_001057389 /// XM_342216	Hey1	Hairy/enhancer-of-split related with YRPW motif 1	-3.31
1370372_at	NM_133568	Rasd2	RASD family, member 2	-3.32
1369301_at	NM_031349	Agtrl1	angiotensin receptor-like 1	-3.33
1389092_at	NM_080889	Il2rg	interleukin 2 receptor, gamma (severe combined immunodeficiency)	-3.33
1386832_a_at	NM_001108279	RGD1563179_predicted	similar to BAZF (predicted)	-3.34
1390622_at	---	---	Transcribed locus	-3.34
1397470_at	---	---	Transcribed locus	-3.34
1378292_at	---	---	Transcribed locus	-3.39
1374123_at	---	---	Transcribed locus	-3.42
1370631_at	NM_173097	Reg3g	regenerating islet-derived 3 gamma	-3.47
1374419_at	XM_002727705	---	Transcribed locus	-3.51
1370747_at	NM_012952	Fgf9	fibroblast growth factor 9	-3.55
1393167_at	---	---	Transcribed locus	-3.58
1368137_at	NM_017212	Mapt	microtubule-associated protein tau	-3.6
1368059_at	NM_053955	Crym	crystallin, mu	-3.61
1382303_at	NM_214457	Phactr1	phosphatase and actin regulator 1	-3.62
1395473_at	NM_021858	Gnb3	guanine nucleotide binding protein, beta 3	-3.66
1376770_at	NM_001109310	RGD1559565_predicted	similar to EF hand domain containing 1 (predicted)	-3.67
1384202_at	XM_001076953 /// XM_213790	RGD1566317_predicted	similar to Tescalcin (predicted)	-3.67
1379367_at	NM_001108697	RGD1308251_predicted	similar to RIKEN cDNA 2810405K02 (predicted)	-3.71
1388447_at	NM_001129880	LOC683626	similar to limb-bud and heart	-3.77
1368677_at	NM_012513	Bdnf	brain derived neurotrophic factor	-3.79
1388611_at	NM_001015008	Tcea3	transcription elongation factor A (SII), 3	-3.79
1380127_at	---	---	Transcribed locus	-3.85
1377371_a_at	---	---	Transcribed locus	-3.86
1384392_at	NM_181087	Cyp26b1	cytochrome P450, family 26, subfamily b, polypeptide 1	-3.87
1388583_at	NM_001033882 /// NM_001033883 /// NM_022177	Cxcl12	chemokine (C-X-C motif) ligand 12	-3.87
1384862_at	---	---	Transcribed locus	-3.9
1397393_at	---	---	Transcribed locus	-3.91
1389694_at	NM_001108180	Ky_predicted	kyphoscoliosis (predicted)	-3.96
1368468_at	NM_017286	Cyp11a1	cytochrome P450, family 11, subfamily a, polypeptide 1	-3.97
1372708_at	---	---	---	-4.11
1379833_at	NM_001109189 /// XM_001058675 /// XM_347322	LOC368158 /// RGD1562025_predicted	similar to Nuclear receptor ROR-gamma (Nuclear receptor RZR-gamma) (Thymus orphan receptor) (TOR) /// similar to leucine rich repeat neuronal 6D (predicted)	-4.11
1374698_at	XM_001075627	LOC687508	similar to Cytochrome c oxidase polypeptide VIIa-heart, mitochondrial precursor (Cytochrome c oxidase subunit VIIa-H) (COX VIIa-M)	-4.28
1394251_x_at	NM_001107413	Irx3_predicted	Iroquois related homeobox 3 (Drosophila) (predicted)	-4.28
1387671_at	NM_031115	Sctr	secretin receptor	-4.3
1375052_at	XM_001056441 /// XM_576426	LOC501015	similar to nuclear localized factor 2	-4.55
1380743_at	---	---	Transcribed locus	-4.55
1368387_at	NM_053995	Bdh1	3-hydroxybutyrate dehydrogenase, type 1	-4.58
1391948_at	NM_001108057	Bcl11b_predicted	B-cell leukemia/lymphoma 11B (predicted)	-4.62
1392689_at	NM_001105793	Aloxe3_predicted	arachidonate lipoxygenase 3 (predicted)	-4.63
1387071_a_at	NM_017212	Mapt	microtubule-associated protein tau	-4.85
1389808_at	---	LOC688274	hypothetical protein LOC688274	-5.1
1393023_at	---	---	Transcribed locus	-5.1
1371927_at	NM_001108211	Ankrd23_predicted	ankyrin repeat domain 23 (predicted)	-5.13
1385298_at	NM_001134595	RGD1564851_predicted	similar to putative anion transporter (predicted)	-5.22
1380236_at	XM_001061864 /// XM_002727107	LOC685004	similar to integrin alpha 9	-5.26

	XM_001067254 /// XM_002730131 /// XM_002730132 ///		similar to Intersectin-2 (SH3 domain-containing protein	
1393625_at	XM_233945	LOC313934	1B) (SH3P18) (SH3P18-like WASP-associated protein)	-5.36
1391500_at	---	---	Transcribed locus	-5.65
1392865_at	NM_012952	Fgf9	fibroblast growth factor 9	-5.88
1384247_at	---	---	Transcribed locus	-5.99
1374765_at	---	---	Transcribed locus, moderately similar to NP_036691.2 fibrinogen, gamma polypeptide [Rattus norvegicus]	-6.02
1377946_at	---	---	Transcribed locus	-6.47
1383078_at	NM_001100980	Efnb3	ephrin B3	-6.55
1369608_at	NM_021867	Fgf16	fibroblast growth factor 16	-6.63
1397788_at	---	Rimbp2	RIM binding protein 2	-7.02
1380031_at	---	---	Transcribed locus	-7.04
1368182_at	NM_130739	Acsl6	acyl-CoA synthetase long-chain family member 6	-7.12
1398593_at	NM_001013930	LOC298139	similar to RIKEN cDNA 2310003M01	-7.21
1370773_a_at	NM_001033961 /// NM_020094 /// NM_020095	Kcnip2	Kv channel-interacting protein 2	-7.28
1374148_at	---	---	Transcribed locus, strongly similar to XP_579768.1 PREDICTED: hypothetical protein XP_579768 [Rattus norvegicus]	-7.61
1371904_at	NM_206851	Smyd2	SET and MYND domain containing 2	-7.85
1372848_at	NM_001126280	---	Transcribed locus	-7.94
1369313_at	NM_031677	Fhl2	four and a half LIM domains 2	-8.62
1396949_at	NM_001013930	LOC298139	similar to RIKEN cDNA 2310003M01	-8.91
1395991_at	NM_001100488	Rimbp2	RIM binding protein 2	-8.96
1397534_at	---	---	Transcribed locus, strongly similar to NP_062662.1 cAMP-regulated guanine nucleotide exchange factor II [Mus musculus]	-9.23
1373188_at	NM_001008880	Scn4b	sodium channel, voltage-gated, type IV, beta	-9.51
1386993_at	NM_017240	Myh7	myosin, heavy polypeptide 7, cardiac muscle, beta	-10.67
1390766_at	NM_001024339	Tuba8	tubulin, alpha 8	-11.01
1367928_at	NM_017240	Myh7	myosin, heavy polypeptide 7, cardiac muscle, beta	-11.14
1372383_at	NM_001145469 /// NM_144745	Gpsm1	G-protein signalling modulator 1 (AGS3-like, C. elegans)	-11.43
1379365_at	NM_182952	Cxcl11	chemokine (C-X-C motif) ligand 11	-13.56
1367949_at	NM_017139	Penk1	proenkephalin 1	-13.57
1391072_at	NM_001033924 /// NM_133550	Fcer2a	Fc receptor, IgE, low affinity II, alpha polypeptide	-13.73
1367572_at	NM_012606	Myl3	myosin, light polypeptide 3	-14.78
1393130_at	---	---	Transcribed locus	-15.57
1388293_at	NM_001035252	---	---	-17.08
1392981_at	NM_001107330	Irx4_predicted	Iroquois related homeobox 4 (Drosophila) (predicted)	-18.44
1390776_at	NM_001107413	Irx3_predicted	Iroquois related homeobox 3 (Drosophila) (predicted)	-24.14
1388200_at	NM_001035252	Myl2	myosin, light polypeptide 2, regulatory, cardiac, slow	-32.67
1376884_a_at	XM_001058430 /// XM_213231	Rpl3l_predicted	ribosomal protein L3-like (predicted)	-36.87

Appendix 5. Differentially expressed genes between normal left atrial and left ventricular tissues classified into the Ligand related functional groups

Functional Group/ Probe Set ID	Description	Fold change
Cytokines		
1390112_at	Epidermal growth factor-containing fibulin-like extracellular matrix protein 1	6.19
1369484_at	WNT1 inducible signaling pathway protein 2	4.79
1367852_s_at	Glycoprotein Ib (platelet), beta polypeptide	4.79
1368368_a_at	Liver-specific bHLH-Zip transcription factor 7	4.11
1387625_at	Insulin-like growth factor binding protein 6	3.61
1368883_at	NOV protein	3.51
1372168_s_at	Insulin-like growth factor binding protein 6	3.41
1368128_at	Phospholipase A2, group IIA	3.27
1389543_at	Mannan-binding lectin serine peptidase 1	3.05
1376734_at	NOV protein	2.79
1388920_at	Bone morphogenetic protein 6	2.79
1368920_at	Slit homolog 3 (Drosophila)	2.77
1395695_at	Similar to aortic carboxypeptidase-like protein ACLP	2.53
1388201_at	Bone morphogenetic protein 6	2.31
1370234_at	Fibronectin 1	2.22
1367631_at	Connective tissue growth factor	2.2
1368259_at	Prostaglandin-endoperoxide synthase 1	2.11
1377655_at	Fibroblast growth factor 12	2.11
1372182_at	Phosphofructokinase, platelet	2.06
1376850_a_at	Chemokine (C-C motif) ligand 27 (predicted)	2.03
1387439_at	MEGF6	2.01
1369983_at	Chemokine (C-C motif) ligand 5	1.97
1368527_at	Prostaglandin-endoperoxide synthase 2	1.96
1386955_at	Glycoprotein Ib (platelet), beta polypeptide	1.95
1367894_at	Growth response protein (CL-6)	1.82
1374491_at	Chemokine-like factor super family 8	-1.8
1393427_s_at	Estrogen-regulated protein CBL20, 20.4kD	-1.82
1370402_at	Estrogen-regulated protein CBL20, 20.4kD	-1.83
1368463_at	Vascular endothelial growth factor C	-1.83
1388018_at	Selectin, endothelial cell	-1.95
1387135_at	A disintegrin and metalloproteinase domain (ADAM)15	-2.01
1374626_at	Leucine-rich alpha-2-glycoprotein 1	-2.07
1370770_s_at	Kit ligand	-2.36
1373544_at	Monokine induced by gamma interferon	-2.57
1396214_at	Kit ligand	-2.6
1390956_at	Similar to Apolipoprotein L3 (Apolipoprotein L-III) (ApoL-III) (TNF-inducible protein CG12-1) (CG12_1) (predicted)	-2.62
1388856_at	Kit ligand	-2.66
1382454_at	Monokine induced by gamma interferon	-2.68
1386080_at	Hairy/enhancer-of-split related with YRPW motif 1	-3.32
1388583_at	Chemokine (C-X-C motif) ligand 12	-3.86
1369608_at	Fibroblast growth factor 16	-6.63
1379365_at	Chemokine (C-X-C motif) ligand 11	-13.55

Frizzled receptor ligand		
1382878_at	Secreted frizzled-related protein 1	5.9
1383266_at	Secreted frizzled-related protein 1	4.76
1396614_at	Secreted frizzled-related protein 2	1.83
Growth factor receptor ligand		
1389470_at	B-factor, properdin	9.32
1390112_at	Epidermal growth factor-containing fibulin-like extracellular matrix protein 1	6.19
1369484_at	WNT1 inducible signaling pathway protein 2	4.79
1387625_at	Insulin-like growth factor binding protein 6	3.68
1368883_at	NOV protein	3.51
1372168_s_at	Insulin-like growth factor binding protein 6	3.41
1388920_at	Bone morphogenetic protein 6	2.79
1376734_at	NOV protein	2.79
1388201_at	Bone morphogenetic protein 6	2.31
1367631_at	Connective tissue growth factor	2.2
1377655_at	UI-R-BJ0p-aiq-a-11-0-UI 5', mRNA sequence.	2.11
1395165_at	PC4 and SFRS1 interacting protein 2	1.91
1368463_at	Vascular endothelial growth factor C	-1.83
1388583_at	Chemokine (C-X-C motif) ligand 12	-3.86
1369608_at	Fibroblast growth factor 16	-6.63
Hormone		
1369484_at	WNT1 inducible signaling pathway protein 2	4.79
1387625_at	Insulin-like growth factor binding protein 6	3.61
1368883_at	NOV protein	3.51
1367992_at	Secretory granule neuroendocrine protein 1	3.2
1376734_at	NOV protein	2.79
1372168_s_at	Insulin-like growth factor binding protein 6	2.25
1367631_at	Connective tissue growth factor	2.2
1367894_at	Growth response protein (CL-6)	1.82
1368428_at	X-prolyl aminopeptidase (aminopeptidase P) 2, membrane-bound	-1.99
1367949_at	Preproenkephalin	-13.55
Hormone receptor ligand		
1371400_at	Thyroid hormone responsive protein	38.59
1367564_at	Natriuretic peptide precursor type A	12.88
1387396_at	Hepcidin antimicrobial peptide	11.24
1368367_at	Integral membrane-associated protein 1	3.16
1367616_at	Natriuretic peptide precursor type B	1.89
1387219_at	Adrenomedullin	1.87
1370563_at	3-alpha-hydroxysteroid dehydrogenase	-1.92
1396101_at	Stanniocalcin 1	-2.14
1368468_at	Cytochrome P450, subfamily 11A	-3.97
Notch		
1371491_at	Notch gene homolog 1, (Drosophila)	-1.85
1373483_at	Similar to NG28 (LOC366848), mRNA	-2.17

Appendix 6- Differentially expressed genes between normal left atrial and left ventricular tissues classified into the "receptor" related functional groups.

Functional Group/ Probe set ID	Description	Fold change
Growth factor receptor		
1396152_s_at	Insulin-like growth factor-binding protein 5	4.47
1376425_at	Transforming growth factor, beta 2	3.89
1387172_a_at	Transforming growth factor, beta 2	3.63
1392382_at	Transforming growth factor, beta 2	3.39
1397830_at	Insulin-like growth factor-binding protein 5	2.99
1371232_a_at	Chondroitin sulfate proteoglycan 2 (versican)	2.87
1388054_a_at	Chondroitin sulfate proteoglycan 2 (versican)	2.77
1367912_at	LanC (bacterial lantibiotic synthetase component C)-like 1	2.62
1388265_x_at	Chondroitin sulfate proteoglycan 2 (versican)	2.55
1371056_at	Neogenin	2.41
1367648_at	Insulin-like growth factor binding protein 2	2.36
1370960_at	Insulin-like growth factor-binding protein 5	2.31
1392770_at	Neogenin	2.25
1383213_at	Similar to Eps8 (LOC312812), mRNA	1.93
1369353_at	Receptor tyrosine kinase	1.88
1369948_at	Nerve growth factor receptor associated protein 1	1.84
1369783_a_at	Neuregulin 1	1.83
1370081_a_at	Vascular endothelial growth factor	-1.84
1371491_at	Notch gene homolog 1, (Drosophila)	-1.85
1384056_at	Fibroblast growth factor receptor 3	-1.85
1370082_at	Transforming growth factor, beta 1	-1.93
1368900_at	Thrombomodulin	-1.96
1369087_at	FMS-like tyrosine kinase 1	-2.08
1395197_at	FMS-like tyrosine kinase 1	-2.1
1370492_a_at	FMS-like tyrosine kinase 1	-2.14
1393179_at	FMS-like tyrosine kinase 1	-2.16
1373483_at	Similar to NG28 (LOC366848), mRNA	-2.17
1373807_at	Vascular endothelial growth factor	-2.2
1387124_at	Inhibin alpha	-2.77
1370747_at	Fibroblast growth factor 9	-3.56
1368677_at	Brain derived neurotrophic factor	-3.78
1392865_at	Fibroblast growth factor 9	-5.9
interleukin 1 receptor		
1370747_at	Fibroblast growth factor 9	-3.56
1392865_at	Fibroblast growth factor 9	-5.9
macroglobulin		
1370892_at	Complement component 4a	18.85
1387029_at	Complement component factor h	4.24
1368000_at	Complement component 3	3.41
1393219_at	Complement component 2	1.95
neuropeptide hormone		
1382967_at	G protein-coupled receptor 64	2.5

1369377_at	Hypocretin receptor 2	2.00
1371696_at	G protein-coupled receptor 56	-2.16
PDGF receptor		
1370081_a_at	Vascular endothelial growth factor	-1.84
1369087_at	FMS-like tyrosine kinase 1	-2.08
1395197_at	FMS-like tyrosine kinase 1	-2.1
1370492_a_at	FMS-like tyrosine kinase 1	-2.14
1393179_at	FMS-like tyrosine kinase 1	-2.16
1373807_at	Vascular endothelial growth factor	-2.2
TGFR		
1376425_at	Transforming growth factor, beta 2	3.89
1387172_a_at	Transforming growth factor, beta 2	3.63
1392382_at	Transforming growth factor, beta 2	3.39
1367912_at	LanC (bacterial lantibiotic synthetase component C)-like 1	2.62
1370082_at	Transforming growth factor, beta 1	-1.93
1387124_at	Inhibin alpha	-2.77
VEGF		
1371056_at	Neogenin	2.41
1392770_at	Neogenin	2.25
1369087_at	FMS-like tyrosine kinase 1	2.08
1370081_a_at	Vascular endothelial growth factor	-1.84
1395197_at	FMS-like tyrosine kinase 1	-2.1
1370492_a_at	FMS-like tyrosine kinase 1	-2.14
1393179_at	FMS-like tyrosine kinase 1	-2.16
1373807_at	Vascular endothelial growth factor	-2.2

Appendix 7- Differentially expressed genes between normal left atrial and left ventricular tissues classified into the DNA binding protein functional group

Probe Set ID	Description	Fold change
1368785_a_at	Paired-like homeodomain transcription factor 2	25.99
1377139_at	T-box 5	6.96
1382593_at	Similar to Ets transcription factor (LOC362733), mRNA	5.62
1369067_at	Nuclear receptor subfamily 4, group A, member 3	4.2
1368368_a_at	Liver-specific bHLH-Zip transcription factor 7	4.11
1387365_at	Nuclear receptor subfamily 1, group H, member 3	3.94
1395586_at	Eukaryotic translation elongation factor 1 alpha 1	3.73
1394022_at	Inhibitor of DNA binding 4	3.58
1367847_at	Nuclear protein 1	3.14
1371689_at	Eukaryotic translation elongation factor 1 alpha 1	2.73
1368092_at	Fumarylacetoacetate hydrolase	2.69
1374503_at	Similar to pre B-cell leukemia transcription factor 3 (LOC311876), mRNA	2.53
1389469_at	Similar to chromodomain helicase DNA binding protein 1-like (LOC310707), mRNA	2.5
1383002_at	Similar to PHD finger protein 20-like 1 isoform 1	2.38
1368321_at	Early growth response 1	2.33
1375894_at	Similar to leucine zipper transcription factor-like 1 (LOC316102), mRNA	2.23
1370063_at	Nuclear receptor subfamily 2, group F, member 2	2.17
1389998_at	Nuclear receptor subfamily 2, group F, member 2	2.17
1392555_at	Similar to Ets transcription factor (LOC362733), mRNA	2.13
1391194_at	Sal-like 1	2.08
1375120_at	Inhibitor of DNA binding 4	2.01
1387407_at	Nucleosome assembly protein 1-like 3	1.99
1370541_at	Nuclear receptor subfamily 1, group D, member 2	1.92
1387306_a_at	Early growth response 2	1.92
1389580_at	Similar to transcription factor (LOC295568), mRNA	1.91
1377263_at	Similar to cofactor required for Sp1 transcriptional activation, subunit 9, 33kDa (LOC303074), mRNA	1.89
1369969_at	ADP-ribosyltransferase 1	1.83
1387349_at	Short stature homeobox 2	1.83
1371536_at	Calcium regulated heat stable protein 1	-1.85
1397286_at	Transcription factor 4	-1.85
1368422_at	Mesenchyme homeo box 2	-2.1
1382953_at	T-box 3 (ulnar mammary syndrome)	-2.1
1390426_at	Notch gene homolog 1, (Drosophila)	-2.14
1392990_at	Similar to HMG-box transcription factor (LOC312936), mRNA	-2.27
1381971_at	Similar to Sry-related HMG-box protein (LOC311723), mRNA	-2.36
1368851_at	V-ets erythroblastosis virus E26 oncogene homolog 1 (avian)	-2.38
1376648_at	V-myc myelocytomatosis viral related oncogene, neuroblastoma derived (avian)	-2.45
1386080_at	Hairy/enhancer-of-split related with YRPW motif 1	-3.32

Appendix 8. Filtered signal intensities data of left and right atria 28-day shunt vs. sham biological replicates.

Probe Set ID	RefSeq Transcript ID	Gene Symbol	Gene Title	RA Shunt - Sham Log2 ratio	LA Shunt - Sham Log2 ratio	ANOVA Main effect: Condition; P-value	ANOVA Main effect: Condition;F statistic	FDR Main effect: Condition; Adjusted p-value
1367652_at	NM_012588 /// XM_001053435	Igfbp3	insulin-like growth factor binding protein 3	-1.35	-1.03	1.03024E-07	315.71	0.00320394
1389367_at	XM_001061765 XM_001061820 XM_001069584 /// XM_215570	Schip1	schwannomin interacting protein 1	0.36	0.09	3.19536E-07	236.13	0.003489467
1383161_a_at	---	---	---	0.6	0.54	4.70247E-07	213.72	0.003489467
1371609_at	NM_001004225	RGD1303003	homolog of zebrafish ES1	0.19	0.13	5.81092E-07	202.34	0.003489467
1397468_at	NM_001025697	RGD1305387	similar to RIKEN cDNA 2610207I16	-0.3	-0.43	6.7634E-07	194.54	0.003489467
1387908_at	XM_001077321 /// XM_340809	Rasd1	RAS, dexamethasone-induced 1	-1.17	-1.52	7.53867E-07	189.14	0.003489467
1378074_at	---	---	Transcribed locus	-0.49	-0.99	8.51576E-07	183.25	0.003489467
1370086_at	NM_012559	Fgg	fibrinogen, gamma polypeptide	-0.53	-1.16	1.235E-06	166.35	0.003489467
1386881_at	NM_012588 /// XM_001053435	Igfbp3	insulin-like growth factor binding protein 3	-1.38	-1.07	1.24958E-06	165.84	0.003489467
1368817_at	XM_001055468 XM_001066053	Psme4	proteasome (prosome, macropain) activator subunit 4	0.42	0.27	1.38162E-06	161.55	0.003489467
1372809_at	NM_001106063 XM_001065661 XM_237967	LOC290595	hypothetical gene supported by AF152002	-1.54	-1.71	1.39403E-06	161.17	0.003489467
1382651_at	---	---	Transcribed locus	-0.34	-0.54	1.45792E-06	159.30	0.003489467
1383162_at	---	---	---	0.61	0.61	1.5467E-06	156.86	0.003489467
1373108_at	NM_001012072	Ppp1r3c	protein phosphatase 1, regulatory (inhibitor) subunit 3C	0.26	0.46	1.70416E-06	152.93	0.003489467
1393625_at	XM_001067157 XM_001067202 XM_001067254 /// XM_233945	LOC313934	similar to Intersectin-2 (SH3 domain-containing protein 1B) (SH3P18) (SH3P18-like WASP-associated protein)	0.83	0.42	2.01667E-06	146.33	0.003489467
1377719_a_at	---	---	---	0.56	0.61	2.06254E-06	145.47	0.003489467
1393130_at	---	---	Transcribed locus	1.08	1.3	2.12611E-06	144.31	0.003489467
1373628_at	---	---	Transcribed locus	2.11	1.77	2.32356E-06	140.99	0.003489467
1388821_at	NM_001108015 XM_001068999 /// XM_233982	RGD1564451_predicted	similar to Tribbles homolog 2 (predicted)	0.55	0.3	2.40805E-06	139.67	0.003489467
1372065_at	NM_001012034	Art3	ADP-ribosyltransferase 3	0.26	0.14	2.47287E-06	138.70	0.003489467
1369928_at	NM_019212	Acta1	actin, alpha 1, skeletal muscle	1.59	1.11	2.63643E-06	136.38	0.003489467
1376165_at	XM_001054941 /// XM_342533	Slc24a3	solute carrier family 24 (sodium/potassium/calcium exchanger), member 3	-0.5	-0.81	2.65005E-06	136.20	0.003489467
1367665_at	NM_013220	Ankrd1	ankyrin repeat domain 1 (cardiac muscle)	0.29	0.22	2.69092E-06	135.65	0.003489467
1387805_at	NM_053420	Bnip3	BCL2/adenovirus E1B 19 kDa-interacting protein 3	0.19	0.36	2.69292E-06	135.62	0.003489467
1369484_at	NM_031590	Wisp2	WNT1 inducible signaling pathway protein 2	1.55	0.71	2.92197E-06	132.74	0.003565526
1382137_at	NM_001106162 XM_001072051 /// XM_214618	Abhd3_predicted	abhydrolase domain containing 3 (predicted)	-1.52	-0.67	2.98092E-06	132.04	0.003565526

1383322_at	NM_001002830	Rasl11b	RAS-like family 11 member B	0.87	0.48	3.12385E-06	130.42	0.003598099
1372524_at	---	---	Transcribed locus	-0.6	-0.89	3.47875E-06	126.77	0.003819654
1374765_at	---	---	Transcribed locus, moderately similar to NP_036691.2 fibrinogen, gamma polypeptide [Rattus norvegicus]	1.04	0.45	4.02269E-06	121.99	0.003819654
1390976_at	---	---	Transcribed locus	-0.51	-0.59	4.2185E-06	120.47	0.003819654
1377720_x_at	---	---	---	0.4	0.54	4.34716E-06	119.51	0.003819654
1373964_at	---	---	CDNA clone IMAGE:7326091	0.82	0.52	4.38385E-06	119.25	0.003819654
1387396_at	NM_053469	Hamp	hepcidin antimicrobial peptide	0.17	1.87	4.41986E-06	118.99	0.003819654
1386855_at	---	---	Transcribed locus	-2.31	-1.72	4.4611E-06	118.70	0.003819654
1389612_at	---	---	Transcribed locus	-0.46	-0.56	4.49872E-06	118.43	0.003819654
1382227_at	NM_001106378 XM_001071257 /// XM_215367	Agpat3_predicted	1-acylglycerol-3-phosphate O-acyltransferase 3 (predicted)	-0.41	-0.64	4.70426E-06	117.04	0.003819654
1368515_at	NM_053927	Epb4.1l3	erythrocyte protein band 4.1-like 3	-0.86	-0.95	4.77145E-06	116.60	0.003819654
1383062_at	---	---	Transcribed locus	-0.24	-0.15	4.80513E-06	116.38	0.003819654
1389549_at	---	---	---	0.32	0.24	4.84099E-06	116.15	0.003819654
1393643_at	NM_001108586	Rcn1_predicted	reticulocalbin 1 (predicted)	0.31	0.19	4.9129E-06	115.70	0.003819654
1369186_at	NM_012762	Casp1	caspase 1	0.52	0.32	5.29187E-06	113.44	0.004013947
1398847_at	NM_053598	Nudt4	nudix (nucleoside diphosphate linked moiety X)-type motif 4	-0.55	-0.43	5.56492E-06	111.93	0.004120561
1392996_at	NM_001106276 XM_001061933 /// XM_218858	Cpeb1_predicted	cytoplasmic polyadenylation element binding protein 1 (predicted)	0.55	0.51	6.24324E-06	108.55	0.004444848
1367616_at	NM_031545	Nppb	natriuretic peptide precursor type B	0.42	0.6	6.28873E-06	108.34	0.004444848
1370249_at	NM_012515	Bzrp	benzodiazepine receptor, peripheral	0.29	0.23	6.68102E-06	106.61	0.004536589
1388102_at	NM_138863	Ltb4dh	leukotriene B4 12-hydroxydehydrogenase	0.22	0.35	6.71028E-06	106.48	0.004536589
1388460_at	NM_001013086	Capg	capping protein (actin filament), gelsolin-like	0.63	0.27	7.11508E-06	104.83	0.004633693
1381977_at	---	---	---	-0.39	-0.47	7.16035E-06	104.66	0.004633693
1368028_at	NM_012633	Prph1	peripherin 1	0.67	0.97	7.30091E-06	104.11	0.004633693
1371298_at	---	---	CDNA clone IMAGE:7460165	-0.84	-1.93	7.64756E-06	102.83	0.004756628
1388764_at	NM_001108489 XM_001066654 /// XM_341877	Iqgap1_predicted	IQ motif containing GTPase activating protein 1 (predicted)	0.32	0.24	8.1091E-06	101.23	0.004837201
1377599_at	NM_001012111	Lpin1	lipin 1	-0.68	-0.75	8.17049E-06	101.03	0.004837201
1372979_at	---	---	Transcribed locus	0.57	0.51	8.33981E-06	100.47	0.004837201
1388494_at	XM_001076134 /// XM_225043	Col4a2_predicted	procollagen, type IV, alpha 2 (predicted)	0.91	0.49	8.48896E-06	100.00	0.004837201
1370180_at	NM_053598	Nudt4	nudix (nucleoside diphosphate linked moiety X)-type motif 4	-0.27	-0.26	8.55481E-06	99.79	0.004837201
1370163_at	NM_012615	Odc1	ornithine decarboxylase 1	0.48	0.21	8.93252E-06	98.64	0.004960579
1369389_at	NM_133422	Zfp483	zinc finger protein 483	-0.3	-0.3	9.2641E-06	97.68	0.004965101
1390912_at	XM_001053660 /// XM_001060582	LOC678810 /// LOC685448	hypothetical protein LOC678810 /// hypothetical protein LOC685448	-0.75	-0.51	9.43992E-06	97.19	0.004965101
1372087_at	XM_001071149 /// XM_216665	Harpb64	hypertrophic agonist responsive protein B64	0.43	0.38	9.84111E-06	96.11	0.004965101

1399011_at	NM_001107129 /// XM_001066309 /// XM_222002	Cops6_predicted	COP9 (constitutive photomorphogenic) homolog, subunit 6 (Arabidopsis thaliana) (predicted)	-0.15	-0.15	9.93983E-06	95.85	0.004965101
1376184_at	XM_001069286 /// XM_216965	Lynx1_predicted	Ly6/neurotoxin 1 (predicted)	-0.48	-0.98	9.97141E-06	95.77	0.004965101
1390021_at	NM_001107352 /// XM_001054570 XM_001071676	Hist1h2bh	histone cluster 1, H2bh	0.31	0.29	1.00142E-05	95.66	0.004965101
1379824_at	NM_001108654 XM_001063218 /// XM_342800	Tox_predicted	thymocyte selection-associated HMG box gene (predicted)	-0.41	-0.27	1.00583E-05	95.55	0.004965101
1386911_at	NM_012505	Atp1a2	ATPase, Na+/K+ transporting, alpha 2 polypeptide	-0.45	-0.59	1.11419E-05	92.96	0.005312992
1383219_at	NM_001013942	Rsnl2	restin-like 2	-0.24	-0.32	1.13708E-05	92.45	0.005312992
1368507_at	NM_001004094 /// NM_017280	Psma3 /// Psma3l	proteasome (prosome, macropain) subunit, alpha type 3 /// proteasome subunit alpha type 3-like	0.26	0.16	1.14238E-05	92.33	0.005312992
1373050_at	XM_001071842 /// XM_341215	Tbc1d1_predicted	TBC1 domain family, member 1 (predicted)	0.53	0.18	1.14464E-05	92.28	0.005312992
1388976_at	NM_001106601 XM_001072676 /// XM_216181	RGD1305975_predicted	similar to BolA domain-containing protein like (11.4 kD) (1P25) (predicted)	0.4	0.13	1.2374E-05	90.36	0.005659084
1371336_at	NM_001005876	Hn1	hematological and neurological expressed sequence 1	0.28	0.15	1.29869E-05	89.19	0.005823972
1371566_at	NM_001108769 XM_001075916 /// XM_343414	RGD1311830_predicted	similar to F-box protein FBL2 (predicted)	0.64	0.71	1.32711E-05	88.67	0.005823972
1398429_at	NM_001044242 XM_001079389 /// XM_230327	LOC311254	hypothetical protein LOC311254	0.36	0.25	1.38919E-05	87.58	0.005823972
1368987_at	---	---	---	-0.69	-1.03	1.39336E-05	87.51	0.005823972
1384415_at	NM_001106045 XM_001065660 /// XM_224283	Sox7_predicted	SRY-box containing gene 7 (predicted)	0.46	0.26	1.40428E-05	87.33	0.005823972
1385518_at	NM_001108001 XM_001077893 /// XM_233725	RGD1304931	similar to RIKEN cDNA 2310042D19	-0.31	-0.52	1.41066E-05	87.22	0.005823972
1376282_at	---	---	Transcribed locus	0.6	0.5	1.45105E-05	86.56	0.005823972
1386910_a_at	NM_024148	Apex1	apurinic/apyrimidinic endonuclease 1	0.25	0.15	1.45874E-05	86.43	0.005823972
1393516_at	---	---	Transcribed locus	0.73	1.11	1.46081E-05	86.40	0.005823972
1382143_at	NM_001107287 XM_001078859 /// XM_224535	Farp1_predicted	FERM, RhoGEF (Arhgef) and pleckstrin domain protein 1 (chondrocyte-derived) (predicted)	0.47	0.2	1.4705E-05	86.25	0.005823972
1373661_a_at	NM_022205	Cxcr4	chemokine (C-X-C motif) receptor 4	0.89	0.41	1.47945E-05	86.10	0.005823972
1374017_at	NM_001077675 XM_001080388 /// XM_344967	RGD1562778_predicted	similar to tripartite motif protein 50 (predicted)	0.86	0.1	1.50702E-05	85.68	0.00585835
1372211_at	NM_145673	Mafk	v-maf musculoaponeurotic fibrosarcoma oncogene family, protein K (avian)	0.47	0.04	1.52985E-05	85.33	0.005873688
1369200_at	NM_021576	Nt5e	5' nucleotidase, ecto	0.61	0.4	1.6075E-05	84.19	0.006096534
1384052_at	---	---	Transcribed locus	-0.43	-0.52	1.63006E-05	83.87	0.006107621
1367562_at	NM_012656	Sparc	secreted acidic cysteine rich glycoprotein	0.78	0.31	1.72156E-05	82.64	0.006368357
1370806_at	NM_145084	Retsat	all-trans-13,14-dihydroretinol saturase	-0.85	-1.08	1.74823E-05	82.29	0.006368357
1376799_a_at	NM_001106074 XM_001070792	Crlf1_predicted	cytokine receptor-like factor 1 (predicted)	0.89	0.59	1.76108E-05	82.13	0.006368357

	/// XM_214312							
1376623_at	NM_001009620	MGC105601	similar to hypothetical protein FLJ20898	0.4	0.41	1.93869E-05	80.01	0.006882094
1368260_at	NM_053749	Aurkb	aurora kinase B	-1.16	-1.47	1.94741E-05	79.91	0.006882094
1369631_at	NM_023092 /// XM_001073096 XM_001080717	LOC686250 /// Myo1c	myosin IC /// similar to unconventional myosin Myr2 I heavy chain	0.49	0.3	2.00833E-05	79.25	0.007017637
1372246_at	NM_148892	Ostf1	osteoclast stimulating factor 1	0.31	0.14	2.04692E-05	78.84	0.007068415
1367631_at	NM_022266	Ctgf	connective tissue growth factor	0.98	0.92	2.06832E-05	78.61	0.007068415
1372029_at	XM_001061015 /// XM_236783	LOC316130	similar to mannose-6-phosphate receptor binding protein 1	0.54	0.35	2.17916E-05	77.50	0.007366267
1389545_at	NM_001108941 XM_001056572 /// XM_345195	Tbl1xr1_predicted	transducin (beta)-like 1X-linked receptor 1 (predicted)	0.37	0.15	2.27034E-05	76.64	0.007470973
1388957_at	---	---	CDNA clone IMAGE:7368410	0.47	0.11	2.27734E-05	76.57	0.007470973
1374830_at	---	---	similar to Coiled-coil domain containing protein 3 precursor	0.62	0.62	2.30454E-05	76.32	0.007470973
1381968_at	NM_001105966 XM_001075616 /// XM_213921	Creg_predicted	cellular repressor of E1A-stimulated genes (predicted)	-0.1	-0.25	2.34557E-05	75.96	0.007470973
1374396_at	NM_001011992	Atp6v1c1	ATPase, H+ transporting, V1 subunit C, isoform 1	0.39	0.23	2.36157E-05	75.82	0.007470973
1379392_at	NM_001013054	Adprhl1	ADP-ribosylhydrolase like 1	0.57	0.42	2.37106E-05	75.73	0.007470973
1383279_at	NM_199084	Rcbtb2	regulator of chromosome condensation (RCC1) and BTB (POZ) domain containing protein 2	-0.29	-0.37	2.3783E-05	75.67	0.007470973
1386981_at	NM_012716	Slc16a1	solute carrier family 16 (monocarboxylic acid transporters), member 1	0.72	0.28	2.41314E-05	75.37	0.007504638
1375739_at	NM_139324	Ehd4	EH-domain containing 4	0.29	0.16	0.000024689	74.90	0.007602012
1389533_at	XM_001062865 XM_001073286 XM_001073317 /// XM_232197	Fbln2	fibulin 2	0.8	0.29	2.68046E-05	73.23	0.008062471
1368448_at	NM_021586	Ltbp2	latent transforming growth factor beta binding protein 2	1.2	1.48	2.7142E-05	72.98	0.008062471
1393360_at	---	---	Transcribed locus	0.2	0.21	2.72025E-05	72.94	0.008062471
1379379_at	---	---	Transcribed locus	-0.6	-0.73	2.72214E-05	72.92	0.008062471
1392501_at	---	---	Transcribed locus	-1.44	-0.36	2.76918E-05	72.58	0.008124413
1375415_at	NM_001108976 XM_001056695 /// XM_345581	LOC366468	similar to U7 snRNP-specific Sm-like protein LSM10	0.37	0.22	2.83841E-05	72.09	0.008249687
1385570_at	---	---	---	-0.29	-0.28	2.88276E-05	71.78	0.008301018
1368671_at	NM_022524	Srpx	sushi-repeat-containing protein	-0.17	-0.75	2.95015E-05	71.33	0.008384218
1367846_at	NM_012618	S100a4	S100 calcium-binding protein A4	0.41	0.6	2.96557E-05	71.23	0.008384218
1368253_at	NM_012793	Gamt	guanidinoacetate methyltransferase	-0.52	-0.52	3.05921E-05	70.62	0.008571031
1370097_a_at	NM_022205	Cxcr4	chemokine (C-X-C motif) receptor 4	0.76	0.57	3.10229E-05	70.35	0.008578951
1373232_at	XM_001054194	LOC305771 ///	similar to nidogen 2	0.41	0.29	3.12766E-05	70.19	0.008578951
1390406_at	NM_001106354 XM_001062453 /// XM_215247	Arhgap18_predicted	Rho GTPase activating protein 18 (predicted)	0.37	0.25	3.1448E-05	70.08	0.008578951
1392938_s_at	NM_001108497 XM_001073151 /// XM_341902	RGD1306959_predicted	similar to C11orf17 protein (predicted)	0.91	0.42	3.30092E-05	69.15	0.008811657
1378315_at	---	---	Transcribed locus	-0.38	-0.93	3.30453E-05	69.13	0.008811657

1372067_at	NM_001024800	Txndc1	thioredoxin domain containing 1	0.46	0.23	3.32343E-05	69.02	0.008811657
1371633_at	NM_001024870	Ctnnbl1	beta catenin-like 1	-0.54	-0.42	3.34344E-05	68.91	0.008811657
1396228_at	XM_001059736 /// XM_216388	RGD1308958_predicted	Similar to chromosome 9 open reading frame 5 (predicted)	0.25	0.38	3.41368E-05	68.52	0.008921191
1390881_at	NM_175844	Abra	actin-binding Rho activating protein	-0.32	-0.45	3.47551E-05	68.18	0.009007074
1371643_at	NM_171992	Ccnd1	Cyclin D1	0.9	0.58	3.57994E-05	67.62	0.009201029
1377773_at	---	---	Transcribed locus, weakly similar to NP_766020.1 RIKEN cDNA C030002O17 [Mus musculus]	-0.25	-0.36	3.9112E-05	65.99	0.00997003
1389244_x_at	NM_022205	Cxcr4	chemokine (C-X-C motif) receptor 4	0.68	0.54	3.96638E-05	65.73	0.01002849
1375522_at	NM_148891	Nmt1	N-myristoyltransferase 1	0.34	0.16	4.036E-05	65.41	0.01006581
1374618_at	---	---	Transcribed locus, weakly similar to XP_223161.3 PREDICTED: similar to proto-oncogene AF4 [Rattus norvegicus]	-0.29	-0.36	4.04588E-05	65.37	0.01006581
1387547_a_at	NM_022294	Eltd1	EGF, latrophilin and seven transmembrane domain containing 1	0.5	0.12	4.11493E-05	65.06	0.01015637
1391601_at	XM_001060363 /// XM_222670	Lrrn2_predicted	leucine rich repeat protein 2, neuronal (predicted)	-0.4	-0.3	4.16847E-05	64.83	0.01020751
1398726_at	---	Ascc3l1	Activating signal cointegrator 1 complex subunit 3-like 1	-0.76	-0.9	4.20218E-05	64.69	0.01020964
1388866_at	NM_001109255 XM_001075000 /// XM_575721	RGD1559723_predicted	similar to Sspn protein (predicted)	-0.12	-0.09	4.27054E-05	64.40	0.01029532
1385458_a_at	NM_001108497 /// XM_001073151 /// XM_341902	RGD1306959_predicted	similar to C11orf17 protein (predicted)	1	0.41	4.45236E-05	63.66	0.01040999
1389394_at	---	---	Transcribed locus	0.34	0.21	4.46061E-05	63.62	0.01040999
1372104_at	---	---	Transcribed locus	0.35	0.15	4.46071E-05	63.62	0.01040999
1387189_at	NM_019230	Slc22a3	solute carrier family 22, member 3	-0.78	-0.79	4.48522E-05	63.53	0.01040999
1388728_at	NM_001013174	Laptm4b	lysosomal-associated protein transmembrane 4B	-0.34	-0.21	4.48548E-05	63.52	0.01040999
1383175_a_at	NM_001108497 XM_001073151 /// XM_341902	RGD1306959_predicted	similar to C11orf17 protein (predicted)	1	0.59	4.57001E-05	63.20	0.0105276
1371807_at	XM_001068870 /// XM_216650	RGD1311605_predicted	similar to apoptosis related protein APR-3; p18 protein (predicted)	0.33	0.19	4.62793E-05	62.97	0.01058264
1391852_at	---	---	Transcribed locus	-0.57	-0.58	4.76872E-05	62.45	0.01078003
1388133_at	XM_001077363 /// XM_345860	Csdc2	cold shock domain containing C2, RNA binding	-0.49	-0.65	4.84699E-05	62.17	0.01078003
1367636_at	NM_012756	Igf2r	insulin-like growth factor 2 receptor	0.29	0.1	4.88078E-05	62.05	0.01078003
1385426_at	XM_001076863 /// XM_215707	RGD1305326_	similar to hypothetical protein FLJ20647 (predicted)	0.61	0.14	4.88336E-05	62.04	0.01078003
1374329_at	---	---	Transcribed locus	0.44	0.37	4.88813E-05	62.02	0.01078003
1371809_at	NM_212534	Mrps18b	mitochondrial ribosomal protein S18B	0.34	0.08	4.92223E-05	61.90	0.01078003
1368165_at	NM_017243	Prps1	phosphoribosyl pyrophosphate synthetase 1	-0.16	-0.14	5.0276E-05	61.54	0.01093381
1368097_a_at	NM_053865	Rtn1	reticulon 1	0.37	0.11	5.36548E-05	60.43	0.01158757
1392982_at	---	---	Transcribed locus	-0.18	-0.42	5.56722E-05	59.81	0.01194034

1375708_at	NM_198747	Col27a1	Procollagen, type XXVII, alpha 1	-0.39	-0.07	5.66916E-05	59.51	0.0120757
1389459_at	NM_001107356 XM_001053501 /// XM_225401	RGD1306613_predicted	similar to RIKEN cDNA 1600012F09 (predicted)	0.31	0.18	5.80771E-05	59.11	0.01219046
1371700_at	NM_001034124	Mfap4	microfibrillar-associated protein 4	0.66	0.43	5.82162E-05	59.07	0.01219046
1369407_at	NM_012870	Tnfrsf11b	tumor necrosis factor receptor superfamily, member 11b (osteoprotegerin)	0.86	0.66	5.84063E-05	59.01	0.01219046
1389393_at	XM_001068403 /// XM_341879	RGD1308210	similar to RIKEN cDNA 2210412D01	0.22	0.15	6.03211E-05	58.48	0.01245009
1376895_at	NM_001105749 XM_001062801 /// XM_218851	Il16	interleukin 16	0.3	0.3	6.08091E-05	58.35	0.01245009
1398300_at	NM_012913	Atp1b3	ATPase, Na+/K+ transporting, beta 3 polypeptide	0.31	0.18	6.13472E-05	58.21	0.01245009
1389803_at	---	---	Transcribed locus	-0.19	-0.33	6.15799E-05	58.14	0.01245009
1369670_at	NM_031518 /// XM_001066772	Cd200	Cd200 antigen	0.51	0.36	6.16519E-05	58.12	0.01245009
1369795_at	NM_053981	Kcnj12	potassium inwardly-rectifying channel, subfamily J, member 12	-0.47	-0.95	6.24133E-05	57.92	0.01252252
1370328_at	NM_138519	Dkk3	dickkopf homolog 3 (Xenopus laevis)	0.19	0.2	6.30651E-05	57.76	0.01257218
1386993_at	NM_017240	Myh7	myosin, heavy polypeptide 7, cardiac muscle, beta	1.48	1.44	6.38505E-05	57.56	0.01264327
1391422_at	NM_001013209	Dnajb6	DnaJ (Hsp40) homolog, subfamily B, member 6	0.51	0.03	6.42348E-05	57.46	0.01264327
1397851_at	---	---	Transcribed locus	0.54	0.25	6.74045E-05	56.69	0.01318372
1367957_at	NM_019340	Rgs3	regulator of G-protein signalling 3	0.14	0.36	6.87148E-05	56.38	0.01334837
1371328_at	---	---	---	-0.16	-0.11	7.09611E-05	55.87	0.01334837
1381925_x_at	XM_001066861	LOC497729	hypothetical gene supported by NM_172157	-0.57	0.03	7.12342E-05	55.81	0.01334837
1397634_at	NM_001107613 XM_001078242 /// XM_228027	Anks1_predicted	ankyrin repeat and SAM domain containing 1 (predicted)	-0.33	-0.26	7.16711E-05	55.71	0.01334837
1375303_at	NM_001110490 XM_001059372 /// XM_573863	RGD1564875_predicted	similar to mKIAA0613 protein (predicted)	-0.36	-0.17	7.17324E-05	55.70	0.01334837
1367664_at	NM_013220	Ankrd1	ankyrin repeat domain 1 (cardiac muscle)	0.17	0.28	7.1737E-05	55.70	0.01334837
1371139_at	XM_001057425 XM_001057538 /// XM_343776	Pls3	plastin 3 (T-isoform)	0.43	0.32	7.17612E-05	55.69	0.01334837
1374207_at	XM_001065522 /// XM_344544	Angpt2	angiopoietin 2	0.49	0.85	7.18452E-05	55.68	0.01334837
1389704_at	---	---	Transcribed locus	-0.2	-0.32	7.21093E-05	55.62	0.01334837
1378249_x_at	---	---	---	-0.59	0.09	7.39843E-05	55.22	0.01350398
1398778_at	NM_017278	Psma1	proteasome (prosome, macropain) subunit, alpha type 1	0.22	0.21	7.40831E-05	55.20	0.01350398
1387841_at	NM_022204	Exoc5	exocyst complex component 5	0.33	0.06	7.42526E-05	55.16	0.01350398
1371784_at	NM_213625	Dnajc7	DnaJ (Hsp40) homolog, subfamily C, member 7	0.3	0.13	7.57635E-05	54.85	0.01356842
1391613_at	NM_001107173 XM_001059832 /// XM_222630	Elk4_predicted	ELK4, member of ETS oncogene family (predicted)	0.14	0.11	7.61171E-05	54.78	0.01356842
1389329_at	NM_053862 /// XM_001066972	Lgals8	lectin, galactoside-binding, soluble 8	0.35	0.06	7.62723E-05	54.74	0.01356842
1369249_at	NM_053714 /// XM_001064426	Ank	progressive ankylosis homolog (mouse)	-0.14	-0.4	7.63521E-05	54.73	0.01356842
1370503_s_at	NM_053927	Epb4.1l3	erythrocyte protein band 4.1-like 3	-0.72	-1.05	7.68384E-05	54.63	0.01357726
1369948_at	NM_053401	Ngfrap1	nerve growth factor receptor (TNFRSF16)	-0.21	-0.23	7.79226E-05	54.41	0.01361875

			associated protein 1					
1374635_at	XM_001071577	LOC689663	Hypothetical protein LOC689663	0.38	0.26	7.80277E-05	54.39	0.01361875
1398370_at	NM_001111055 NM_001111056 NM_001111057 /// NM_012894	Adarb1	Adenosine deaminase, RNA-specific, B1	-0.5	-0.26	7.84047E-05	54.32	0.01361875
1382469_at	XM_001068090 /// XM_228876	RGD1564253_predicted	similar to Protein CXorf17 homolog (predicted)	-0.22	-0.25	7.88249E-05	54.24	0.01361875
1377216_at	---	---	Transcribed locus	-0.45	-0.61	7.98288E-05	54.04	0.013716
1383160_at	NM_001108128 XM_001075005 /// XM_235878	Chordc1_predicted	cysteine and histidine-rich domain (CHORD)-containing, zinc-binding protein 1 (predicted)	-0.26	-0.23	8.15107E-05	53.73	0.01392803
1391148_at	---	---	Transcribed locus	-0.12	-0.51	8.26653E-05	53.51	0.01404813
1393974_at	NM_001108837 XM_001081499 /// XM_343970	Meox1_predicted	mesenchyme homeobox 1 (predicted)	1.23	1.42	8.51091E-05	53.07	0.01438483
1383413_at	NM_001106868 XM_001078610 /// XM_217299	Gup1_predicted	Gup1, glycerol uptake/transporter homolog (yeast) (predicted)	-0.37	-0.4	8.72064E-05	52.71	0.01465964
1383472_at	NM_001011975	Aldh1b1	aldehyde dehydrogenase 1 family, member B1	-0.73	-0.91	8.8409E-05	52.50	0.0147374
1379605_at	---	---	Transcribed locus	0.26	0.22	8.86168E-05	52.47	0.0147374
1372276_at	NM_001106378 XM_001071257 /// XM_215367	Agpat3_predicted	1-acylglycerol-3-phosphate O-acyltransferase 3 (predicted)	-0.34	-0.69	9.2277E-05	51.87	0.01526448
1389050_at	XM_001081500 /// XM_573199	RGD1560049_predicted	similar to Dual specificity protein phosphatase 3 (T-DSP11) (predicted)	0.32	0.1	9.33412E-05	51.70	0.01533925
1384542_at	---	---	Transcribed locus, strongly similar to NP_001074393.1 zinc and ring finger 3 [Mus musculus]	-0.76	-0.23	9.41196E-05	51.58	0.01533925
1387345_at	XM_001055468 /XM_001066053	Psme4	proteasome (prosome, macropain) activator subunit 4	0.3	0.2	9.42087E-05	51.56	0.01533925
1388587_at	NM_212505	Ier3	immediate early response 3	0.51	0.35	9.48191E-05	51.47	0.01535822
1369590_a_at	NM_001109986 /// NM_024134	Ddit3	DNA-damage inducible transcript 3	0.31	0.41	9.64046E-05	51.23	0.01546377
1369990_at	NM_001105726 XM_001077901 /// XM_342460	Ptpmt1	protein tyrosine phosphatase, mitochondrial 1	-0.11	-0.15	9.66365E-05	51.19	0.01546377
1373363_at	NM_019217 /// XM_001061557 /// XM_215469	Map1b	microtubule-associated protein 1b	0.41	0.22	9.73595E-05	51.08	0.01546377
1393696_at	NM_001025042	LOC499856	hypothetical protein LOC499856	1.26	1.19	9.74597E-05	51.07	0.01546377
1370575_a_at	NM_022585	Azin1	antizyme inhibitor 1	0.45	0.45	9.86341E-05	50.89	0.0155252
1388348_at	---	---	Transcribed locus	0.32	0.09	9.88453E-05	50.86	0.0155252
1390630_at	---	---	Transcribed locus	-0.28	-0.27	0.000100927	50.56	0.01577245
1380768_at	---	---	Transcribed locus	0.83	0.35	0.000101514	50.48	0.01578489
1370023_at	NM_021654	Gja4	gap junction membrane channel protein alpha 4	0.56	0.57	0.000102732	50.31	0.01589485
1393121_at	NM_001106725 XM_001077035 /// XM_216691	Agr2_predicted	anterior gradient 2 (Xenopus laevis) (predicted)	-0.49	-0.91	0.000105931	49.87	0.01626383
1370229_at	NM_031967	Ndrg4	N-myc downstream regulated gene 4	0.37	0.1	0.000106163	49.84	0.01626383
1385228_x_at	---	---	---	0.38	0.05	0.000107669	49.64	0.01641374
1398378_at	NM_181371	Gstk1	glutathione S-transferase kappa 1	-0.14	-0.26	0.000109741	49.37	0.01660807
1375493_at	---	---	---	-0.39	-0.17	0.00011019	49.31	0.01660807

1371889_at	NM_177421	Slc22a17	solute carrier family 22 (organic cation transporter), member 17	-0.39	-0.38	0.000110919	49.22	0.01660807
1379128_at	NM_001107538 XM_001067343 /// XM_218963	Arhgef17_predicted	Rho guanine nucleotide exchange factor (GEF) 17 (predicted)	-0.19	-0.35	0.00011108	49.20	0.01660807
1398616_at	XM_001068004 /// XM_217618	Ap1s2_predicted	adaptor-related protein complex 1, sigma 2 subunit (predicted)	0.62	0.15	0.000112478	49.02	0.01673657
1391827_at	NM_001107288 XM_001071051 /// XM_224561	Flnb_predicted	filamin, beta (predicted)	0.38	0.23	0.000113628	48.88	0.01677443
1385709_x_at	---	---	Transcribed locus	-0.15	-0.32	0.000113811	48.85	0.01677443
1370012_at	NM_031557	Ptgis	prostaglandin I2 (prostacyclin) synthase	0.54	0.48	0.000115841	48.61	0.01699303
1374547_at	NM_001098782 XM_001080969 /// XM_578157	LOC502663	similar to Small EDRK-rich factor 2 (4F5rel)	0.51	0.3	0.000116852	48.49	0.01706086
1395014_at	---	---	Transcribed locus	0.46	0.49	0.000119223	48.21	0.01732573
1368910_at	NM_019372	Ppm2c	protein phosphatase 2C, magnesium dependent, catalytic subunit	-0.23	-0.16	0.000119845	48.14	0.01733512
1370048_at	NM_053936	Edg2	endothelial differentiation, lysophosphatidic acid G-protein-coupled receptor, 2	-0.28	-0.47	0.000121257	47.98	0.01745819
1370074_at	NM_057196	Baiap2	brain-specific angiogenesis inhibitor 1-associated protein 2	-0.56	-0.36	0.000123912	47.68	0.01768401
1388370_at	NM_001105998 XM_001070498 /// XM_214007	Ccni_predicted	cyclin I (predicted)	-0.18	-0.17	0.000124567	47.61	0.01768401
1399159_a_at	NM_057097	Vamp3	vesicle-associated membrane protein 3	0.16	0.07	0.000125191	47.54	0.01768401
1367836_at	NM_031559	Cpt1a	carnitine palmitoyltransferase 1a, liver	-0.17	-0.58	0.000125445	47.51	0.01768401
1393478_at	---	---	Transcribed locus	-0.17	-0.38	0.000125734	47.48	0.01768401
1375633_at	NM_001002807	Clic1	chloride intracellular channel 1	0.36	0.09	0.000126237	47.42	0.01768401
1370981_at	NM_031765	Rxrg	retinoid X receptor gamma	-0.53	-0.46	0.000128104	47.22	0.01786507
1383130_at	---	---	Transcribed locus	-0.37	-0.23	0.000128986	47.13	0.01790772
1370172_at	NM_017051	Sod2	superoxide dismutase 2, mitochondrial	0.13	0.12	0.000129711	47.06	0.0179283
1393687_at	---	---	Transcribed locus	-0.47	-0.66	0.000130655	46.96	0.01794946
1379511_at	---	---	Transcribed locus	0.45	0.56	0.000131027	46.92	0.01794946
1384112_at	NM_021576	Nt5e	5' nucleotidase, ecto	0.33	0.37	0.000133336	46.68	0.01794946
1376654_at	NM_001107671 XM_001054629 /// XM_227078	RGD1308448_predicted	similar to RIKEN cDNA B130016O10 gene (predicted)	-1.41	-0.41	0.00013378	46.64	0.01794946
1372338_at	XM_001073644 XM_001073681 /XM_001073720	LOC687395	similar to CG9240-PA	-0.44	-0.17	0.000133889	46.63	0.01794946
1398626_s_at	NM_001009268	Actr2	ARP2 actin-related protein 2 homolog (yeast)	0.22	0.13	0.000134194	46.60	0.01794946
1395096_at	---	---	Transcribed locus	-0.99	-1.15	0.000134321	46.58	0.01794946
1389529_at	---	---	Transcribed locus	-0.24	-0.18	0.000134481	46.57	0.01794946
1374043_at	NM_001014011	Gramd3	GRAM domain containing 3	-0.27	-0.19	0.00013552	46.47	0.01795442
1387803_at	NM_022209	Ppp2r2b	protein phosphatase 2 (formerly 2A), regulatory subunit B (PR 52), beta isoform	0.72	0.64	0.000135673	46.45	0.01795442
1391563_at	NM_001109321 XM_001056324 /// XM_577028	RGD1565148_predicted	similar to melanoma associated antigen (mutated) 1-like 1 (predicted)	-0.21	-0.52	0.000137497	46.27	0.0180666
1376785_at	---	---	Transcribed locus	-0.23	-0.41	0.000137682	46.25	0.0180666

1391431_at	---	---	Transcribed locus	-0.42	-0.57	0.00014041	45.99	0.01830923
1371150_at	NM_171992	Ccnd1	cyclin D1	0.75	0.57	0.000140905	45.95	0.01830923
1368853_at	NM_012686	Vsnl1	visinin-like 1	-0.38	-0.41	0.000141585	45.88	0.01830923
1383708_at	NM_001017505	LOC498564	similar to integrin, beta-like 1	0.7	0.35	0.000141886	45.85	0.01830923
1370883_at	NM_001008847	RT1-Da	RT1 class II, locus Da	0.55	0.57	0.000145963	45.48	0.01871736
1394855_at	---	---	Transcribed locus	-0.58	-0.41	0.000146253	45.45	0.01871736
1389300_at	NM_001108918 XM_001079111 /// XM_344957	RGD1563498_predicted	similar to RIKEN cDNA 4930404J24 (predicted)	0.59	0.17	0.000147788	45.32	0.0187529
1387196_at	NM_022249	Khdrbs3	KH domain containing, RNA binding, signal transduction associated 3	-0.18	-0.21	0.0001488	45.23	0.0187529
1387445_at	NM_031573	Phkg1	phosphorylase kinase gamma 1	-0.35	-0.46	0.000149551	45.16	0.0187529
1372294_at	XM_001053103	Perc64	PE responsive protein c64	0.53	0.34	0.000149924	45.13	0.0187529
1374244_at	---	---	---	-0.49	-0.43	0.000149947	45.13	0.0187529
1370268_at	NM_012972	Kcna5	potassium voltage-gated channel, shaker-related subfamily, member 5	-0.92	-0.66	0.000150149	45.11	0.0187529
1368860_at	NM_017180	Phlda1	pleckstrin homology-like domain, family A, member 1	1.17	0.45	0.000152223	44.93	0.01893596
1371531_at	XM_001053139	LOC678880	similar to mammalian retrotransposon derived 8b	-0.39	-0.23	0.000152932	44.87	0.01894838
1368822_at	NM_024369	Fstl1	follistatin-like 1	0.53	0.33	0.000155366	44.67	0.01917355
1387731_at	NM_024376	Gja3	gap junction membrane channel protein alpha 3	-0.12	-0.59	0.000158131	44.44	0.01943764
1374919_at	XM_001078203 /// XM_214035	Recc1	replication factor C 1	-0.09	-0.21	0.000161101	44.20	0.01965876
1372752_at	NM_001013070	Tspan4	tetraspanin 4	0.38	0.4	0.000162667	44.08	0.01965876
1372564_at	NM_001107107 XM_001053903 /// XM_239510	Ets2	v-ets erythroblastosis virus E26 oncogene homolog 2 (avian)	0.47	0.18	0.000163155	44.04	0.01965876
1369065_a_at	NM_001110139 NM_001110823 /// NM_017290 XM_001079470	Atp2a2	ATPase, Ca++ transporting, cardiac muscle, slow twitch 2	-0.07	-0.06	0.000163198	44.03	0.01965876
1398304_at	NM_172035	Fzd2	frizzled homolog 2 (Drosophila)	0.69	0.24	0.000163608	44.00	0.01965876
1375849_at	NM_001107524 XM_001062354 /// XM_218791	Rgma_predicted	RGM domain family, member A (predicted)	-0.34	-0.27	0.000164085	43.96	0.01965876
1367605_at	NM_022511	Pfn1	profilin 1	0.33	0.2	0.000164542	43.93	0.01965876
1389815_at	NM_172045 /// XM_001074638	Ppp1r14b	protein phosphatase 1, regulatory (inhibitor) subunit 14B	0.53	0.17	0.000164987	43.89	0.01965876
1371101_at	NM_080402	Ryk	receptor-like tyrosine kinase	0.33	0.03	0.000166014	43.82	0.01969265
1388483_at	NM_001108982 XM_001079054 /// XM_345674	Cfl2_predicted	cofilin 2, muscle (predicted)	0.23	0.1	0.000166538	43.78	0.01969265
1371382_at	XM_001056685 /// XM_238167	Flna_predicted	filamin, alpha (predicted)	0.32	0.18	0.000169095	43.58	0.01991924
1387777_at	NM_133409	Ilk	integrin linked kinase	0.13	0.25	0.000171222	43.42	0.0200937
1369652_at	NM_012673	Thy1	thymus cell antigen 1, theta	0.63	0.6	0.000175401	43.12	0.02046156
1372468_at	NM_001012164	Cd97	CD97 antigen	0.34	0.16	0.000175673	43.10	0.02046156
1367709_at	NM_017125	Cd63	CD63 antigen	0.12	0.2	0.00017683	43.02	0.0205195
1395233_at	---	---	Transcribed locus	-0.33	-0.45	0.00017868	42.89	0.02065709
1372568_at	XM_001076356 /// XM_236659	Epm2aip1_predicted	EPM2A (laforin) interacting protein 1 (predicted)	-0.16	-0.23	0.000180118	42.79	0.02068151

1388616_at	NM_001009543	MGC72955	similar to RIKEN cDNA 2310042G06	0.37	0.14	0.000180221	42.78	0.02068151
1380210_at	NM_001034849	Gimap1	GTPase, IMAP family member 1	0.47	0.37	0.000181374	42.70	0.02068561
1373075_at	NM_001109061 XM_001061556 /// XM_573350	RGD1560888_predicted	similar to Cell division protein kinase 8 (Protein kinase K35) (predicted)	0.33	0.15	0.000181978	42.66	0.02068561
1372947_at	XM_001057425 XM_001057538 /// XM_343776	Pls3	plastin 3 (T-isoform)	0.44	0.38	0.000182252	42.64	0.02068561
1371527_at	NM_012843	Emp1	epithelial membrane protein 1	0.46	0.43	0.000183629	42.55	0.02076612
1388193_at	XM_001061381 XM_001071073 XM_001071106 /// XM_347168	Hip1	huntingtin interacting protein 1	0.39	0.12	0.00018481	42.47	0.02077108
1370252_at	NM_134373	Avpi1	arginine vasopressin-induced 1	0.25	0.15	0.000185009	42.46	0.02077108
1378819_at	NM_001009643	RGD1310111	similar to RIKEN cDNA 0610012D14	-0.34	-0.05	0.000187534	42.29	0.02097879
1376267_at	---	---	Transcribed locus	0.66	0.19	0.000192611	41.96	0.02146959
1394455_at	---	---	Transcribed locus	-0.3	-0.59	0.000193511	41.90	0.02149283
1398348_at	---	---	Transcribed locus	-0.27	-0.37	0.000194945	41.81	0.02155572
1377366_at	---	---	Transcribed locus	-0.36	-0.16	0.000195925	41.75	0.02155572
1383084_at	---	---	Transcribed locus	0.53	0.41	0.000196398	41.72	0.02155572
1378428_at	---	---	Transcribed locus	0.5	0.39	0.00019685	41.69	0.02155572
1372607_at	NM_001011891	Nubp2	nucleotide binding protein 2	0.34	0.06	0.00019796	41.62	0.02157141
1376577_at	---	---	Transcribed locus	-1.58	-0.31	0.000198977	41.56	0.02157141
1378357_at	---	---	Transcribed locus	-0.1	-0.37	0.000200651	41.46	0.02157141
1375107_at	---	---	---	0.04	0.05	0.000200724	41.46	0.02157141
1394836_at	---	---	Transcribed locus	-0.45	-0.04	0.000201224	41.43	0.02157141
1394000_at	---	---	Transcribed locus, moderately similar to NP_001012779.1 RGM domain family, member B isoform 1 precursor [Homo sapiens]	-0.11	-0.37	0.000201423	41.41	0.02157141
1375138_at	NM_012886 /// XM_001075779	Timp3	tissue inhibitor of metalloproteinase 3 (Sorsby fundus dystrophy, pseudoinflammatory)	0.29	0.3	0.000201848	41.39	0.02157141
1380055_at	NM_001025766	LOC498951	similar to 2010004A03Rik protein	0.79	0.33	0.000203492	41.29	0.02167264
1389302_at	NM_001017446	RGD1310199	similar to RIKEN cDNA D030070L09	0.33	0.13	0.000206481	41.11	0.02172212
1374029_at	---	---	---	0.52	0.48	0.000206523	41.11	0.02172212
1367756_at	NM_053625	Gfm	G elongation factor	0.42	0.01	0.000206575	41.11	0.02172212
1379443_at	NM_001107664	Hps3_predicted	Hermansky-Pudlak syndrome 3 homolog (human) (predicted)	0.27	0.05	0.000207277	41.07	0.02172212
1390356_at	---	---	Transcribed locus	0.15	0.21	0.00020828	41.01	0.02172212
1382745_at	---	---	Transcribed locus	-0.31	-0.19	0.000208612	40.99	0.02172212
1375578_at	---	---	---	-0.36	0.04	0.000209653	40.93	0.02172212
1386929_at	NM_012734	Hk1	hexokinase 1	0.42	0.11	0.000209878	40.92	0.02172212
1389844_at	XM_001066628 /// XM_342763	Fkbp4	FK506 binding protein 4	-0.37	-0.36	0.000210273	40.89	0.02172212
1370882_at	NM_198740	Hla-dmb	major histocompatibility complex, class II, DM beta	0.69	0.75	0.000211014	40.85	0.02172212
1389092_at	NM_080889	Il2rg	interleukin 2 receptor, gamma (severe combined immunodeficiency)	0.65	0.25	0.00021164	40.82	0.02172212

1374698_at	XM_001075606 /// XM_001075627	LOC687508	similar to Cytochrome c oxidase polypeptide VIIa-heart, mitochondrial precursor (Cytochrome c oxidase subunit VIIa-H) (COX VIIa-M)	0.74	0.5	0.000212523	40.77	0.021741
1368470_at	NM_012960	Ggh	gamma-glutamyl hydrolase	-0.27	-0.3	0.00021697	40.52	0.02212314
1371472_at	---	---	Transcribed locus	0.55	0.36	0.000219044	40.41	0.02226159
1392888_at	NM_001014108	Gpc4	glypican 4	0.42	0.49	0.000220093	40.35	0.02229537
1370085_at	NM_013135	Rasa1	RAS p21 protein activator 1	0.36	0.03	0.00022098	40.30	0.02231252
1393281_at	NM_031556 /// NM_133651	Cav1	caveolin, caveolae protein 1	0.2	0.02	0.000223676	40.16	0.02249985
1371690_at	NM_022385	Arl1	ADP-ribosylation factor-like 1	0.17	0.2	0.000224282	40.13	0.02249985
1385285_at	---	---	Transcribed locus	-0.47	-0.68	0.000228429	39.91	0.02284217
1384303_s_at	NM_001033079	Slc6a17	solute carrier family 6 (neurotransmitter transporter), member 17	-0.43	-0.3	0.000229225	39.87	0.02284832
1379770_at	NM_001007750 XM_001079984	Chpt1	choline phosphotransferase 1	-0.17	-0.2	0.000230951	39.78	0.02288819
1390485_at	NM_001106372 XM_001080178 /// XM_215286	March5_predicted	membrane-associated ring finger (C3HC4) 5 (predicted)	0.26	0.1	0.000231423	39.76	0.02288819
1383447_at	NM_001107082 XM_001057770 /// XM_221387	Etv5_predicted	ets variant gene 5 (ets-related molecule) (predicted)	0.86	0.71	0.000231833	39.74	0.02288819
1396237_at	---	---	---	-0.62	-0.61	0.000233435	39.66	0.02291708
1398905_at	NM_001106660 XM_001064435 /// XM_216411	Atp6v1g1_predicted	ATPase, H transporting, lysosomal V1 subunit G1 (predicted)	-0.14	-0.11	0.000233858	39.64	0.02291708
1371536_at	NM_152790	Carhsp1	calcium regulated heat stable protein 1	0.41	0.18	0.000234337	39.61	0.02291708
1383176_at	NM_001108497 XM_001073151 /// XM_341902	RGD1306959_predicted	similar to C11orf17 protein (predicted)	1.09	0.34	0.00023687	39.49	0.02309221
1383407_at	XM_001059303 /// XM_229107	RGD1560293_predicted	similar to RIKEN cDNA 1200013B08 (predicted)	0.22	0.14	0.000240795	39.30	0.02332054
1398759_at	NM_001109912 /// NM_013043 XM_001072618 XM_001072656 /// XM_573819	Tsc22d1	TSC22 domain family, member 1	0.44	0.21	0.000241171	39.28	0.02332054
1371347_at	NM_001025014	Tmem50b	transmembrane protein 50B	-0.16	-0.26	0.000241544	39.26	0.02332054
1388324_at	NM_001082580 /// NM_182668	Nit1	nitrilase 1	0.22	0.27	0.000242962	39.19	0.02332054
1373982_at	NM_001025626 XM_001080965	RGD1306595	similar to hypothetical protein	0.31	-0.01	0.00024366	39.16	0.02332054
1398432_at	XM_001057585 XM_001057687 XM_001057751 /// XM_224620	RGD1559931_predicted	similar to Ankyrin repeat domain protein 28 (predicted)	0.15	0.13	0.000243711	39.16	0.02332054
1391812_at	---	---	Transcribed locus	-0.53	-1.3	0.000247735	38.97	0.02350932
1381388_at	NM_001024882	Ccdc19	coiled-coil domain containing 19	0.37	0.11	0.000249053	38.91	0.02350932
1377761_at	NM_001002819	Gfpt2	glutamine-fructose-6-phosphate transaminase 2	0.46	0.04	0.000249209	38.90	0.02350932
1395844_at	---	---	---	0.41	0.33	0.000249898	38.87	0.02350932
1387791_at	NM_012544	Ace	angiotensin I converting enzyme (peptidyl-dipeptidase A) 1	0.49	0.36	0.000249988	38.86	0.02350932
1379578_at	NM_001105880	Zbtb20_predicted	zinc finger and BTB domain containing 20 (predicted)	-0.24	-0.19	0.00025022	38.85	0.02350932
1380513_at	NM_001013987	RGD1309034	similar to Expressed sequence AW060207	0.57	0.32	0.000251193	38.81	0.02352969

1372560_at	---	---	Transcribed locus	0.27	0.33	0.000253795	38.69	0.02370205
1374778_at	NM_017097	Ctsc	cathepsin C	-0.19	-0.33	0.000256061	38.59	0.02384205
1389809_at	NM_001107807 XM_001054581 /// XM_230899	Tmepai_predicted	transmembrane, prostate androgen induced RNA (predicted)	0.33	0.21	0.000257487	38.53	0.0238828
1370191_at	NM_022585	Azin1	antizyme inhibitor 1	0.26	0.37	0.000258035	38.50	0.0238828
1387079_at	NM_017090	Gucy1a3	guanylate cyclase 1, soluble, alpha 3	-0.28	-0.3	0.000258988	38.46	0.02389988
1387762_s_at	NM_138875 /// XM_001070425	Jund	Jun D proto-oncogene	-0.38	-1.18	0.000260076	38.41	0.0239293
1377655_at	NM_130814	Fgf12	Fibroblast growth factor 12	-0.24	-0.36	0.000261538	38.35	0.02395659
1371572_at	NM_019288	App	amyloid beta (A4) precursor protein	0.24	0.02	0.000262468	38.31	0.02395659
1374711_at	NM_001030030	Cpsf3	cleavage and polyadenylation specificity factor 3	0.38	0.16	0.000262684	38.30	0.02395659
1388697_at	NM_001108923 XM_001058238 /// XM_344971	Inpp5a_predicted	inositol polyphosphate-5-phosphatase A (predicted)	0.28	0.12	0.000263897	38.25	0.02399684
1371639_at	NM_001105932 XM_001079533 /// XM_213780	Vps29_predicted	vacuolar protein sorting 29 (S. pombe) (predicted)	0.05	0.09	0.000268033	38.07	0.02430189
1389351_at	NM_001014269	Lrrfip1	leucine rich repeat (in FLII) interacting protein 1	0.48	0.45	0.00026989	37.99	0.02439913
1374247_at	---	---	---	0.45	0.17	0.000271981	37.91	0.02451691
1372299_at	NM_001033757 NM_001033758 /// NM_182735	Cdkn1c	cyclin-dependent kinase inhibitor 1C (P57)	-0.26	-0.31	0.000273029	37.86	0.02454024
1373781_a_at	NM_001044231 XM_001079264 /// XM_214902	RGD1562305_predicted	similar to suprabasal-specific protein suprabasin (predicted)	1.89	1.16	0.000275537	37.76	0.02462707
1385754_s_at	NM_001037336	Lrrc4	leucine rich repeat containing 4 protein precursor	-0.51	-0.43	0.000275991	37.74	0.02462707
1370912_at	NM_212504	Hspa1b	heat shock 70kD protein 1B (mapped)	-0.07	-0.6	0.000276371	37.73	0.02462707
1367973_at	NM_031530	Ccl2	chemokine (C-C motif) ligand 2	0.93	0.28	0.000280318	37.57	0.02490749
1390250_x_at	XM_001062555	LOC685152	similar to Probable phospholipid-transporting ATPase ID (ATPase class I type 8B member 2)	0.48	0.13	0.000284298	37.41	0.02510344
1390227_at	XM_001053660 /// XM_001060582	LOC678810 /// LOC685448	hypothetical protein LOC678810 /// hypothetical protein LOC685448	-0.63	-0.52	0.000284854	37.39	0.02510344
1395860_at	---	---	Transcribed locus, strongly similar to XP_219944.3 PREDICTED: similar to OTTHUMP00000059175 [Rattus norvegicus]	-0.35	-0.13	0.000284945	37.38	0.02510344
1384136_at	XM_001055606 /// XM_342683	RGD1564287_predicted	similar to mKIAA0704 protein (predicted)	-0.8	-0.59	0.00028624	37.33	0.02514627
1398866_at	NM_139084 /// XM_001068223	Magi3	membrane associated guanylate kinase, WW and PDZ domain containing 3	-0.27	-0.32	0.000292854	37.08	0.02565484
1376749_at	NM_001106103 XM_001054599 XM_001054654 XM_001054725 /// XM_214441	Ogn	osteoglycin (predicted)	0.31	0.64	0.000294172	37.03	0.02568754
1374531_at	---	---	Transcribed locus	0.64	0.62	0.000294879	37.01	0.02568754
1369150_at	NM_053551	Pdk4	pyruvate dehydrogenase kinase, isoenzyme 4	-0.26	-0.74	0.000301509	36.76	0.02619166
1384558_at	NM_001108395 XM_001056849 /// XM_341391	Plac9_predicted	placenta-specific 9 (predicted)	0.47	0.44	0.000303884	36.68	0.02625788
1392869_at	---	---	Transcribed locus	-0.27	-0.42	0.00030396	36.67	0.02625788

1367696_at	NM_030833	Ifitm2	interferon induced transmembrane protein 2 (1-8D)	0.24	0.12	0.000305349	36.62	0.02629205
1395851_at	NM_001108195 XM_001078108 /// XM_236723	Kbtbd5_predicted	kelch repeat and BTB (POZ) domain containing 5 (predicted)	-0.33	-0.4	0.000306046	36.60	0.02629205
1369841_at	NM_021863	Hspa2	heat shock 70kDa protein 2	0.65	0.45	0.000308455	36.51	0.02642605
1384187_at	XM_001068004 /// XM_217618	Ap1s2_predicted	adaptor-related protein complex 1, sigma 2 subunit (predicted)	0.58	0.21	0.000314375	36.31	0.02664182
1386968_at	NM_022676	Ppp1r1a	protein phosphatase 1, regulatory (inhibitor) subunit 1A	-0.33	-0.39	0.00031443	36.30	0.02664182
1398294_at	NM_031005	Actn1	actinin, alpha 1	0.59	0.28	0.000314581	36.30	0.02664182
1396265_at	---	---	Transcribed locus	-0.48	-0.57	0.000315509	36.27	0.02664182
1368064_a_at	NM_012545	Ddc	dopa decarboxylase	-0.27	-0.3	0.00031689	36.22	0.02664182
1371956_at	NM_001101006 XM_001058047 XM_001058171	LOC683077	similar to praja1, RING-H2 motif containing	-0.29	-0.2	0.000317555	36.20	0.02664182
1367960_at	NM_019186	Arl4a	ADP-ribosylation factor-like 4A	-0.27	-0.29	0.000317728	36.19	0.02664182
1378094_at	---	---	Transcribed locus	0.71	0.5	0.000318609	36.16	0.02664182
1388433_at	NM_199498	Krt1-19	keratin complex 1, acidic, gene 19	-0.88	-0.65	0.000318684	36.16	0.02664182
1390614_at	---	---	Transcribed locus	-0.28	-0.33	0.000324491	35.96	0.02692881
1378413_at	---	---	Transcribed locus	-0.47	-0.37	0.000324641	35.96	0.02692881
1371244_at	NM_001013061	Aprt_predicted	adenine phosphoribosyl transferase (predicted)	0.32	0.15	0.000324715	35.96	0.02692881
1380572_at	---	---	Transcribed locus	-0.24	-0.48	0.000328172	35.84	0.02714316
1370642_s_at	NM_031525	Pdgfrb	platelet derived growth factor receptor, beta polypeptide	0.82	0.48	0.000329445	35.80	0.02717617
1368139_s_at	NM_013059	Alpl	alkaline phosphatase, tissue-nonspecific	0.72	0.65	0.00033192	35.72	0.02730791
1395150_at	NM_133603	Kcne2	Potassium voltage-gated channel, Isk-related family, member 2	-0.17	-0.11	0.000334744	35.63	0.02742285
1373937_at	NM_001106870 XM_001078714 /// XM_236739	Fyco1_predicted	FYVE and coiled-coil domain containing 1 (predicted)	-0.13	-0.24	0.000335915	35.59	0.02742285
1392950_at	NM_001106148 XM_001053135 XM_001053210 /// XM_214563	Myot_predicted	myotilin (predicted)	0.32	0.46	0.000336643	35.57	0.02742285
1378374_at	XR_008828	RGD1560137_predicted	similar to expressed sequence AU021034 (predicted)	-0.75	-1	0.000338046	35.53	0.02742285
1385649_at	NM_001108118 XM_001070203 /// XM_235707	Itga5	integrin alpha 5	0.46	0.21	0.000339488	35.48	0.02742285
1372643_at	XM_001053351 /// XM_220117	RGD1563977_predicted	similar to protein 4.1G (predicted)	0.22	0.31	0.000339588	35.48	0.02742285
1379668_at	NM_001108401 XM_001073556 /// XM_341459	RGD1564725_predicted	similar to hypothetical protein B230397C21 (predicted)	-0.08	-0.28	0.000339908	35.47	0.02742285
1368980_at	NM_053758	Plce1	phospholipase C, epsilon 1	0.34	0.16	0.000341503	35.42	0.02742285
1392280_at	NM_198769	Tlr2	toll-like receptor 2	0.4	0.3	0.000341614	35.41	0.02742285
1387172_a_at	NM_031131	Tgfb2	transforming growth factor, beta 2	0.56	0.18	0.000342135	35.40	0.02742285
1388945_at	NM_001025719	RGD1311307	similar to 1300014I06Rik protein	0.04	0.24	0.000346096	35.28	0.02766901
1373894_at	NM_145094	Rab31	RAB31, member RAS oncogene family	0.41	0.32	0.00034749	35.23	0.02770923
1392801_at	XM_001060828	RGD15	similar to novel protein	0.45	0.31	0.000352599	35.08	0.02804467

	/// XM_573856	61145_predicted	(predicted)					
1368041_at	NM_022599	Synj2bp	synaptojanin 2 binding protein	0.3	0.07	0.000359785	34.87	0.02827142
1374839_at	NM_181388	Spg7	spastic paraplegia 7 homolog (human)	0.39	0.26	0.000360163	34.86	0.02827142
1383324_at	XM_001056864 /// XM_342682	Mpp6_predicted	membrane protein, palmitoylated 6 (MAGUK p55 subfamily member 6) (predicted)	0.39	0.18	0.000362589	34.79	0.02827142
1393189_at	XM_001058993 /// XM_343764	Maoa	Monoamine oxidase A	1.1	0.41	0.000365277	34.71	0.02827142
1382076_at	NM_001011944	Slc37a1	solute carrier family 37 (glycerol-3-phosphate transporter), member 1	-0.2	-0.2	0.000365672	34.70	0.02827142
1382721_at	NM_001004273 XM_001081060 XM_001081065	Zfp403	zinc finger protein 403	0.2	0.15	0.000366225	34.68	0.02827142
1383439_at	NM_001108214 XM_001058630 /// XM_244089	Npas2_predicted	neuronal PAS domain protein 2 (predicted)	-0.27	-0.64	0.000366392	34.68	0.02827142
1367663_at	NM_017264	Psme1	proteasome (prosome, macropain) 28 subunit, alpha	-0.28	-0.39	0.000367351	34.65	0.02827142
1375944_at	NM_001107793 XM_001064684 /// XM_230773	Acss2_predicted	acyl-CoA synthetase short-chain family member 2 (predicted)	-0.36	-0.21	0.000368022	34.63	0.02827142
1387905_at	NM_001034032	LOC619393	J domain protein 1	-0.14	-0.32	0.000368487	34.62	0.02827142
1389035_at	NM_001007801	Yipf3	Yip1 domain family, member 3	0.44	0.26	0.000369353	34.59	0.02827142
1380626_at	---	---	Transcribed locus	1.7	0.7	0.000369795	34.58	0.02827142
1388298_at	NM_001100885 XM_001067182 /// XM_215905	Myl9_predicted	myosin, light polypeptide 9, regulatory (predicted)	0.23	0.36	0.000369815	34.58	0.02827142
1392794_at	---	---	Transcribed locus	0.38	0.04	0.000370178	34.57	0.02827142
1388600_at	---	---	CDNA clone IMAGE:7320582	0.34	0.38	0.000370798	34.55	0.02827142
1393592_at	NM_001106392 XM_001061473 /// XM_228219	Hs3st5_predicted	heparan sulfate (glucosamine) 3-O-sulfotransferase 5 (predicted)	-0.42	-0.23	0.000371202	34.54	0.02827142
1387910_at	NM_021681 /// NM_172090	Epb4.1l1	erythrocyte protein band 4.1-like 1	-0.23	-0.38	0.000371717	34.53	0.02827142
1370824_at	NM_145776	Slc38a3	solute carrier family 38, member 3	-0.46	-0.56	0.000371813	34.52	0.02827142
1368059_at	NM_053955	Crym	crystallin, mu	0.9	0.49	0.000375783	34.41	0.02850363
1390148_a_at	NM_001107271 XM_001066329 /// XM_224298	Zfp395_predicted	zinc finger protein 395 (predicted)	-0.3	-0.15	0.000380139	34.29	0.02876385
1372106_at	NM_139324	Ehd4	EH-domain containing 4	0.27	0.2	0.000383887	34.19	0.02897695
1368315_at	NM_053498	Entpd6	ectonucleoside triphosphate diphosphohydrolase 6	-0.25	-0.3	0.00038684	34.11	0.02912915
1372480_at	XM_342840 /// XR_007660	RGD1562123_predicted	similar to hypothetical protein (predicted)	-0.31	-0.21	0.000389643	34.04	0.0291917
1376469_at	---	---	Transcribed locus	-0.34	-0.05	0.000389655	34.04	0.0291917
1395393_at	---	---	Transcribed locus	0.21	0.15	0.000390878	34.01	0.0291917
1379910_at	XM_001072323 /// XM_573497	RGD1561967_predicted	similar to UDP-N-acteylglucosamine pyrophosphorylase 1 homolog (predicted)	0.57	0.22	0.000392684	33.96	0.0291917
1371702_at	NM_001108815 XM_001062155 /// XM_343768	Tm4sf2	transmembrane 4 superfamily member 2	-0.09	-0.32	0.0003932	33.95	0.0291917
1385871_at	NM_001107678 XM_001058645 /// XM_227203	Dhx36_predicted	DEAH (Asp-Glu-Ala-His) box polypeptide 36 (predicted)	0.67	1.16	0.000393303	33.94	0.0291917

1380696_at	---	---	Transcribed locus	-1.14	-1.24	0.000398734	33.80	0.02952436
1391187_at	NM_001106976 XM_001079075 /// XM_220174	Ppl_predicted	periplakin (predicted)	-0.22	-0.89	0.000400723	33.75	0.02960115
1372182_at	NM_206847	Pfkp	phosphofructokinase, platelet	0.42	0.44	0.000403417	33.68	0.02972952
1398455_at	NM_001039037	Zdhhc13	zinc finger, DHHC domain containing 13	0.3	0.16	0.000405833	33.62	0.02983569
1393987_s_at	NM_001112712 NM_001112713 /// NM_031657	Gprk6	G protein-coupled receptor kinase 6	0.29	0.02	0.000406776	33.60	0.02983569
1374454_at	NM_001107810 /// XM_001056609 /// XM_230971	Pcmtd2_predicted	protein-L-isoaspartate (D-aspartate) O-methyltransferase domain containing 2 (predicted)	-0.63	-0.07	0.000408848	33.55	0.02987435
1368544_a_at	NM_053516	Nol3	nucleolar protein 3 (apoptosis repressor with CARD domain)	0.37	0.15	0.000409254	33.54	0.02987435
1368358_a_at	NM_053594	Ptprr	protein tyrosine phosphatase, receptor type, R	0.39	0.3	0.000410185	33.51	0.02987435
1372101_at	NM_138905	Ppap2b	phosphatidic acid phosphatase type 2B	-0.25	-0.16	0.000411522	33.48	0.0298863
1371304_a_at	NM_001100983 /// XM_001070810 /// XM_343144	LOC684520 /// LOC685867 /// LOC685883 /// Myl6_predicted	myosin, light polypeptide 6, alkali, smooth muscle and non-muscle	0.19	0.24	0.000412271	33.46	0.0298863
1384745_at	NM_001107276 XM_001069687 /// XM_224334	Piwil2_predicted	piwi like homolog 2 (Drosophila) (predicted)	-0.37	-0.36	0.000418129	33.32	0.03012176
1373392_at	NM_001024802	Tparl	TPA regulated locus	0.32	0.03	0.000418965	33.30	0.03012176
1390335_at	---	---	Transcribed locus	0.32	0.37	0.00041933	33.29	0.03012176
1388817_at	NM_001025118	LOC310665	hypothetical protein LOC310665	-0.18	-0.18	0.000420322	33.27	0.03012176
1372602_at	NM_001013988	RGD1311800	similar to genethonin 1	-0.15	-0.61	0.000420399	33.27	0.03012176
1398538_at	NM_001107301 XM_001064743 /// XM_224713	Abhd8_predicted	abhydrolase domain containing 8 (predicted)	-0.33	-0.39	0.000421331	33.24	0.03012176
1389475_at	NM_012807	Smo	smoothened homolog (Drosophila)	-0.29	-0.36	0.000424363	33.17	0.03026893
1388908_at	NM_001006966	Peci	peroxisomal delta3, delta2-enoyl-Coenzyme A isomerase	-0.04	-0.26	0.000425485	33.15	0.03027955
1371785_at	NM_181086	Tnfrsf12a	tumor necrosis factor receptor superfamily, member 12a	0.68	0.25	0.000429603	33.05	0.03043866
1374556_at	XM_001079707 /// XM_218704	Smox_predicted	spermine oxidase (predicted)	0.55	0.52	0.000429679	33.05	0.03043866
1391537_at	NM_001108351 XM_001069683 /// XM_341174	RGD1565408_predicted	similar to SERTA domain containing 4 (predicted)	0.5	0.47	0.000433323	32.96	0.0306271
1371432_at	NM_001033683	Vat1	vesicle amine transport protein 1 homolog (T californica)	0.4	0.29	0.000435749	32.91	0.03072868
1374191_at	NM_001030034	Rhbdf1	rhomboid family 1 (Drosophila)	0.31	0.12	0.000443208	32.74	0.03106204
1388714_at	NM_001107304 XM_001070626 /// XM_224727	Ell_predicted	elongation factor RNA polymerase II (predicted)	-0.18	-0.2	0.000443594	32.73	0.03106204
1377422_at	XM_001059230 /// XM_228644	Mtmr1_predicted	Myotubularin related protein 1 (predicted)	0.52	0.34	0.00044414	32.72	0.03106204
1377695_at	XM_001053796 XM_001080149	LOC679629 /// LOC687788	similar to smoothelin, like	-0.15	-0.51	0.000444471	32.71	0.03106204

1399016_at	NM_181081	Myst2	MYST histone acetyltransferase 2	-0.12	-0.16	0.000448265	32.62	0.03125062
1372078_at	NM_001011969	Strap	serine/threonine kinase receptor associated protein	-0.09	-0.24	0.000450303	32.58	0.03125062
1373397_at	NM_138509	Mapre1	microtubule-associated protein, RP/EB family, member 1	0.23	0.07	0.00045065	32.57	0.03125062
1381129_at	---	---	---	0.41	0.06	0.00045141	32.55	0.03125062
1369197_at	NM_023979	Apaf1	apoptotic peptidase activating factor 1	0.4	0.11	0.000452194	32.54	0.03125062
1378140_at	NM_001013433	Arl11	ADP-ribosylation factor-like 11	0.5	0.18	0.000453321	32.51	0.03125902
1379376_at	---	---	Transcribed locus	-0.33	-0.36	0.000456796	32.44	0.03141856
1395893_at	---	---	Transcribed locus	-0.24	-0.06	0.000458045	32.41	0.03141856
1397355_at	---	---	Transcribed locus	-0.76	-0.38	0.000460455	32.36	0.03141856
1368821_at	NM_024369	Fstl1	follistatin-like 1	0.41	0.46	0.000461053	32.35	0.03141856
1389727_at	NM_001108096 /XM_001080952 /// XM_235162	Lrrc10_predicted	leucine-rich repeat-containing 10 (predicted)	0.19	0.1	0.000461594	32.33	0.03141856
1387048_at	NM_053563	Ddx39	DEAD (Asp-Glu-Ala-Asp) box polypeptide 39	0.35	0.17	0.000463325	32.30	0.03141856
1367946_at	NM_017365	Pdlim1	PDZ and LIM domain 1 (elfin)	0.41	0.39	0.000463526	32.29	0.03141856
1392840_at	---	---	Transcribed locus	0.3	0.74	0.000463839	32.29	0.03141856
1392935_at	---	---	Transcribed locus	0.4	0.19	0.000467607	32.21	0.03141856
1371786_at	NM_001025142	Trim35	tripartite motif protein 35	-0.22	-0.25	0.000468639	32.19	0.03141856
1390692_at	XM_001053648 /// XM_233467	Ctps_predicted	cytidine 5'-triphosphate synthase (predicted)	0.38	0.28	0.000469272	32.17	0.03141856
1368829_at	NM_031825	Fbn1	fibrillin 1	0.55	0.13	0.000469581	32.17	0.03141856
1371394_x_at	---	---	---	0.54	0.43	0.000470178	32.15	0.03141856
1367560_at	NM_022402	Arbp	acidic ribosomal phosphoprotein P0	0.1	0.1	0.000470739	32.14	0.03141856
1388337_at	NM_001106031 /// XM_001064625 /// XM_214155	Np	nucleoside phosphorylase	0.18	0.27	0.000471225	32.13	0.03141856
1383782_at	NM_001108702 /// XM_001065741 /// XM_343018	Spast_predicted	spastin (predicted)	0.29	0.16	0.000471799	32.12	0.03141856
1368692_a_at	NM_017127	Chka	choline kinase alpha	0.44	0.44	0.000475957	32.03	0.03159193
1370164_at	NM_130826 /// XM_343032	Hadha	hydroxyacyl-Coenzyme A dehydrogenase/3-ketoacyl-Coenzyme A thiolase/enoyl-Coenzyme A hydratase (trifunctional protein), alpha subunit	-0.1	-0.28	0.000476434	32.02	0.03159193
1394077_at	NM_001007641	Rnd3	Rho family GTPase 3	0.15	0.29	0.000479567	31.96	0.03169519
1391212_at	NM_001009675	Tceal1	transcription elongation factor A (SII)-like 1	-0.48	-0.2	0.000480861	31.93	0.03169519
1386987_at	NM_017020	Il6ra	interleukin 6 receptor, alpha	0.41	0.05	0.000481049	31.93	0.03169519
1376696_at	---	---	Transcribed locus	-0.08	-0.29	0.000484482	31.86	0.03185394
1388988_at	NM_001007664	Abhd14b	abhydrolase domain containing 14b	-0.3	-0.16	0.000487507	31.80	0.03195273
1370112_at	NM_031606	Pten	phosphatase and tensin homolog	0.42	0.17	0.000488451	31.78	0.03195273
1390396_at	NM_001106612 XM_001077522 /// XM_216226	LOC297481	similar to eukaryotic translation initiation factor 4E member 3	-0.13	-0.19	0.000489191	31.77	0.03195273
1373076_at	---	---	Transcribed locus	-0.29	-0.31	0.000490419	31.74	0.03195273
1398598_at	NM_001108208 XM_001054738 /// XM_237042	Dst_predicted	dystonin (predicted)	0.2	0.16	0.000491688	31.72	0.03195273

1376071_at	---	---	Transcribed locus	0.39	0.31	0.00049215	31.71	0.03195273
1397808_at	---	---	Transcribed locus	-0.22	-0.32	0.000494941	31.65	0.03206701
1369086_a_at	NM_017298	Cacna1d	calcium channel, voltage-dependent, L type, alpha 1D subunit	0.26	0.56	0.000498143	31.59	0.03220736
1367866_at	NM_019153	Fbln5	fibulin 5	0.42	0.17	0.000501904	31.52	0.03238324
1392260_at	---	---	---	0.34	0.21	0.000506771	31.43	0.03262957
1384634_at	---	---	---	0.34	0.36	0.000508103	31.40	0.03264772
1372542_at	---	---	Transcribed locus	0.28	0.23	0.000510463	31.36	0.03266713
1368921_a_at	NM_012924	Cd44	CD44 antigen	0.09	0.32	0.000510506	31.36	0.03266713
1390536_at	---	---	Transcribed locus	-0.32	-0.33	0.000513881	31.29	0.03273363
1379169_at	NM_001106873 XM_001059684 /// XM_217310	LOC301113	similar to solute carrier family 25 (mitochondrial carrier; phosphate carrier), member 23	-0.33	-0.37	0.000514672	31.28	0.03273363
1373252_at	XM_001063650 /// XR_005956	LOC300225	similar to formin-like 3 protein	0.22	0.26	0.000516883	31.24	0.03273363
1367584_at	NM_019905	Anxa2	annexin A2	0.46	0.08	0.00051727	31.23	0.03273363
1372897_at	NM_175869	Plod2	procollagen lysine, 2-oxoglutarate 5-dioxygenase 2	0.46	0.39	0.000518729	31.20	0.03273363
1373659_at	XM_001073448 XM_001081719	LOC688257 /// LOC689926	hypothetical protein LOC688257 /// hypothetical protein LOC689926	0.17	0.38	0.000520951	31.16	0.03273363
1388416_at	XM_001056970 /// XM_243524	Lrp1	low density lipoprotein receptor-related protein 1	0.29	0.17	0.000521301	31.15	0.03273363
1388920_at	NM_013107	Bmp6	bone morphogenetic protein 6	0.61	0.51	0.000523096	31.12	0.03273363
1369968_at	NM_017066	Ptn	pleiotrophin	-0.42	-0.37	0.000523134	31.12	0.03273363
1368418_a_at	NM_012532	Cp	ceruloplasmin	0.29	0.4	0.00052557	31.08	0.03273363
1380519_at	NM_001106908 XM_001059953 /// XM_217389	RGD1561425_predicted	similar to RIKEN cDNA 4832428D23 gene (predicted)	-0.59	-0.28	0.00052685	31.05	0.03273363
1378371_at	NM_001106974 XM_001076609 /// XM_220155	Boll_predicted	Bol, boule-like (Drosophila) (predicted)	-0.32	-0.47	0.00052936	31.01	0.03273363
1377879_at	---	---	Transcribed locus	0.24	0.13	0.000530349	30.99	0.03273363
1393249_at	---	---	Transcribed locus	0.33	0.35	0.000530452	30.99	0.03273363
1375698_at	---	---	Transcribed locus	-0.7	-0.58	0.000530712	30.98	0.03273363
1379269_at	NM_181475	Cd2ap	CD2-associated protein	0.22	0.1	0.000530997	30.98	0.03273363
1389741_at	NM_001107117 XM_001065770 /// XM_221796	Lass4_predicted	longevity assurance homolog 4 (S. cerevisiae) (predicted)	-0.2	-0.51	0.00053592	30.89	0.03273363
1371738_at	XM_001078269 /// XM_236774	RGD1308260_predicted	similar to hypothetical protein FLJ10375 (predicted)	0.47	0.22	0.000536325	30.88	0.03273363
1389576_at	NM_001108592 XM_001053334 /// XM_342528	Snrpb2_predicted	U2 small nuclear ribonucleoprotein B (predicted)	0.23	0.07	0.000536687	30.88	0.03273363
1376115_at	---	---	Transcribed locus	-0.09	-0.2	0.000537429	30.86	0.03273363
1378252_at	NM_001105894 XM_001068598 /// XM_221686	Chodl_predicted	chondrolectin (predicted)	0.63	0.26	0.000537647	30.86	0.03273363
1374933_at	NM_001034009 /// NM_023983	Mcam	melanoma cell adhesion molecule	0.63	0.52	0.000538442	30.85	0.03273363
1390788_a_at	XM_001060069	Wdr36_predicted	WD repeat domain 36 (predicted)	0.4	0.45	0.000538888	30.84	0.03273363
1387856_at	NM_019359	Cnn3	calponin 3, acidic	0.28	0.17	0.000539058	30.84	0.03273363

1367661_at	NM_053485	S100a6	S100 calcium binding protein A6 (calcyclin)	0.34	0.21	0.000539295	30.83	0.03273363
1388991_at	XM_001066119 /// XM_230024	RGD1562244_predicted	similar to SEC14 and spectrin domains 1 (predicted)	0.37	0.08	0.000539601	30.83	0.03273363
1396213_at	---	---	---	0.27	0.17	0.000540848	30.80	0.03273363
1388153_at	NM_012820	Acsl1	acyl-CoA synthetase long-chain family member 1	-0.25	-0.39	0.00054193	30.79	0.03273363
1370928_at	NM_001105735 XM_001078236 /// XM_343856	Litaf	LPS-induced TN factor	0.4	0.26	0.00054207	30.78	0.03273363
1368052_at	NM_133526	Tspan8	tetraspanin 8	0.4	0.2	0.000543366	30.76	0.03274264
1398227_at	---	---	Transcribed locus	-0.21	-0.31	0.000544483	30.74	0.03274264
1383263_at	XM_001054725 /// XM_214441	Ogn	osteoglycin (predicted)	0.35	0.5	0.000545377	30.73	0.03274264
1377760_at	NM_001014129	Noc4l	nucleolar complex associated 4 homolog (S. cerevisiae)	-0.15	-0.12	0.000547308	30.69	0.03279524
1383058_at	---	---	Transcribed locus	-0.66	-0.15	0.000551575	30.62	0.03295942
1388963_at	XM_001068638 XM_001068691 /// XM_222785	Astn1	astrotactin 1	0.25	0.18	0.000552747	30.60	0.03295942
1383655_at	NM_001024771	Tnip2	TNFAIP3 interacting protein 2	0.23	0.47	0.000553227	30.59	0.03295942
1386861_at	NM_022674	H2afz	H2A histone family, member Z	-0.11	-0.11	0.000555178	30.56	0.03301241
1367789_at	NM_053580	Slc27a1	solute carrier family 27 (fatty acid transporter), member 1	-0.25	-0.3	0.000556532	30.54	0.03302975
1374262_at	---	---	Transcribed locus	-0.35	-0.32	0.000559784	30.48	0.03303407
1370836_at	NM_145097	Serpina4	serine (or cysteine) proteinase inhibitor, clade A (alpha-1 antiproteinase, antitrypsin), member 4	-0.41	0.07	0.000560085	30.48	0.03303407
1388217_a_at	NM_001033898 /// NM_022535	Calu	calumenin	0.11	0.12	0.000560159	30.47	0.03303407
1382710_at	NM_001003401	Enc1	Ectodermal-neural cortex 1	-0.56	-0.07	0.000561578	30.45	0.03303407
1381434_s_at	XM_001075007	LOC305771 /// ///	similar to nidogen 2	0.43	0.28	0.000562004	30.44	0.03303407
1374273_at	---	---	Transcribed locus	-0.32	-0.3	0.000564026	30.41	0.03303407
1370291_at	NM_053650	Pdlim3	PDZ and LIM domain 3	-0.39	-0.64	0.00056404	30.41	0.03303407
1387331_at	NM_012510	Atp4b	ATPase, H+/K+ exchanging, beta polypeptide	-0.22	-0.22	0.000566665	30.37	0.03312543
1367571_a_at	NM_031511 /// XM_001064965	Igf2	insulin-like growth factor 2	-0.12	-0.82	0.000575803	30.22	0.03359642
1383493_at	---	---	Transcribed locus	-0.62	-0.33	0.000580663	30.14	0.03381655
1398325_at	NM_001005547	Tspan3	tetraspanin 3	-0.12	-0.17	0.000582425	30.11	0.03385578
1372626_at	NM_001044295 XM_001070150	LOC689256	similar to Tumor protein D53 (mD53) (Tumor protein D52-like 1)	-0.27	-0.36	0.000586081	30.05	0.03399829
1371338_at	NM_001008764	Psenen	presenilin enhancer 2 homolog (C. elegans)	-0.29	-0.04	0.000587063	30.04	0.03399829
1389332_at	---	---	Transcribed locus	0.29	0.3	0.000589773	29.99	0.03405999
1388138_at	XM_001066338 /// XM_342172	Thbs4	thrombospondin 4	1.34	2.81	0.000590319	29.99	0.03405999
1389002_at	XM_001053379 XM_001069865	Tln1	talin 1	0.32	0.28	0.000592065	29.96	0.03409744
1372766_at	NM_001107616 XM_001069585 /// XM_228044	Cpne5_predicted	copine V (predicted)	-0.42	-0.03	0.000594322	29.92	0.03411089
1379772_at	NM_031349	Agtrl1	angiotensin receptor-like 1	0.68	0.29	0.000594492	29.92	0.03411089
1373036_at	XR_008037	RGD1561455_predicted	similar to Ras GTPase-activating-like protein IQGAP2 (predicted)	-0.02	-1.1	0.000596146	29.89	0.0341389

1393891_at	NM_001107100 XM_001060711 /// XM_221536	Col8a1_predicted	procollagen, type VIII, alpha 1 (predicted)	1.99	1.58	0.000597606	29.87	0.0341389
1395659_at	XM_001068619	LOC688864	similar to transmembrane protein 61	-0.63	-0.58	0.000598273	29.86	0.0341389
1374822_at	---	---	Transcribed locus	0.51	0.27	0.000599782	29.84	0.03416229
1384036_s_at	---	---	---	0.23	0.42	0.000603098	29.79	0.03428837
1377844_at	NM_001015009	Zadh1	zinc binding alcohol dehydrogenase, domain containing 1	-0.09	-0.16	0.000604862	29.76	0.03432591
1379971_at	NM_001107772 XM_001081128 /// XM_230592	Zc3h6_predicted	zinc finger CCCH type containing 6 (predicted)	-0.47	-0.51	0.000606583	29.73	0.03436087
1375960_at	NM_001010956 NM_001033931	Gmcl1	germ cell-less homolog 1 (Drosophila)	0.39	0.08	0.000608076	29.71	0.03438283
1375921_at	NM_001108586 XM_001073225 /// XM_342481	Rcn1_predicted	Reticulocalbin 1 (predicted)	0.83	0.26	0.000610056	29.68	0.03438945
1392941_at	---	---	Transcribed locus	0.24	0.14	0.000611312	29.66	0.03438945
1380347_at	---	---	Transcribed locus	-0.13	-0.19	0.000611511	29.66	0.03438945
1385138_at	---	---	Transcribed locus	-0.09	-0.26	0.000614283	29.62	0.034483
1388689_at	XM_001059049 XM_001059111	LOC682245	similar to Acylphosphatase, muscle type isozyme (Acylphosphate phosphohydrolase)	-0.7	0.13	0.000616361	29.59	0.03450458
1368570_at	NM_022280	Lrat	lecithin-retinol acyltransferase (phosphatidylcholine-retinol-O-acyltransferase)	0	-0.36	0.000616886	29.58	0.03450458
1369621_s_at	NM_013102 /// XM_001053006 XM_001053007	Fkbp1a	FK506 binding protein 1a	0.21	0.11	0.000620118	29.53	0.03462304
1367874_at	NM_053522	Rhoq	ras homolog gene family, member Q	0.24	0.02	0.000623397	29.48	0.03474376
1384267_at	---	---	Transcribed locus	0.21	0.18	0.000627762	29.42	0.034864
1390696_at	---	---	Transcribed locus	-0.23	-0.06	0.000628026	29.42	0.034864
1379598_at	---	---	Transcribed locus	0.65	0.41	0.000628918	29.40	0.034864
1389020_at	XM_001074652	LOC686539	similar to immunoglobulin superfamily containing leucine-rich repeat	0.92	0.55	0.00063274	29.35	0.03495668
1398487_at	XM_001072172 XM_001072218 XM_001072250 /// XM_222911	Pbx1_predicted	pre-B-cell leukemia transcription factor 1 (predicted)	0.52	-0.01	0.000632837	29.35	0.03495668
1389611_at	NM_013155	Vldlr	very low density lipoprotein receptor	0.47	0.36	0.000637396	29.28	0.03510219
1395696_at	NM_001107356 XM_001053501 /// XM_225401	RGD1306613_predicted	similar to RIKEN cDNA 1600012F09 (predicted)	0.35	0.14	0.000641485	29.22	0.03510219
1373510_at	NM_013090	Vamp1	vesicle-associated membrane protein 1	0.44	0.31	0.000641564	29.22	0.03510219
1385171_s_at	XM_001053796 /XM_001080149	LOC679629 /// LOC687788	similar to smoothelin, like	-0.35	-0.3	0.00064164	29.22	0.03510219
1387599_a_at	NM_017000	Nqo1	NAD(P)H dehydrogenase, quinone 1	0.22	0.25	0.000642806	29.21	0.03510219
1386080_at	XM_001057389 /// XM_342216	Hey1	Hairy/enhancer-of-split related with YRPW motif 1	0.52	0.37	0.000643257	29.20	0.03510219
1387267_at	NM_031073	Ntf3	neurotrophin 3	-0.48	-0.35	0.000643373	29.20	0.03510219
1379808_at	---	---	Transcribed locus	-0.43	-0.41	0.000651841	29.08	0.0354776
1372019_at	NM_001106097 XM_001062474 /// XM_214417	RGD1310128_predicted	similar to DNA segment, Chr 13, Wayne State University 50, expressed (predicted)	0.32	0.02	0.000652535	29.07	0.0354776
1370081_a_at	NM_001110333	Vegfa	vascular endothelial growth factor A	-0.23	-0.06	0.000657404	29.00	0.03567994

1372707_at	XM_001062702 XM_001067160	Rab6a	RAB6A, member RAS oncogene family	0.16	0.11	0.000661358	28.95	0.03583201
1390036_at	NM_198760	Slc16a6	solute carrier family 16 (monocarboxylic acid transporters), member 6	0.48	0.21	0.000663599	28.92	0.03586796
1371575_at	---	---	Clone X5 mRNA sequence	0.19	0.23	0.000665772	28.89	0.03586796
1381886_at	NM_173290 /// XM_001069615	Yy1	YY1 transcription factor	0.61	-0.02	0.000666007	28.89	0.03586796
1386149_at	---	---	---	-0.19	-0.13	0.000666635	28.88	0.03586796
1387753_s_at	NM_139084 /// XM_001068223	Magi3	membrane associated guanylate kinase, WW and PDZ domain containing 3	-0.17	-0.39	0.00067021	28.83	0.03599804
1393000_at	---	---	---	-0.33	-0.37	0.000678146	28.72	0.03635019
1381971_at	NM_001024781	Sox18	SRY-box containing gene 18	0.5	0.42	0.000679104	28.71	0.03635019
1386594_at	---	---	Transcribed locus	-0.82	-0.44	0.000682541	28.67	0.03639403
1373178_at	---	---	Transcribed locus	-0.33	-0.13	0.000683734	28.65	0.03639403
1376888_a_at	NM_001106876	LOC301119	similar to myeloid/lymphoid or mixed lineage-leukemia translocation to 1 homolog	-0.15	-0.29	0.000683975	28.65	0.03639403
1367626_at	NM_012530	Ckm	creatine kinase, muscle	-0.08	-0.18	0.000684604	28.64	0.03639403
1370244_at	NM_013156	Ctsl	cathepsin L	0.17	0.25	0.000686978	28.61	0.03640673
1399137_at	NM_001106476 XM_001078398 /// XM_215717	Metap1_predicted	methionyl aminopeptidase 1 (predicted)	-0.2	-0.28	0.000687185	28.61	0.03640673
1368072_at	NM_019290	Btg3	B-cell translocation gene 3	0.17	0.22	0.000690112	28.57	0.0364357
1381109_at	---	---	Transcribed locus	-0.43	-0.04	0.000690158	28.57	0.0364357
1370154_at	NM_012771	Lyz	lysozyme	0.68	0.56	0.000691246	28.55	0.0364357
1370258_at	NM_134402	Bzw2	basic leucine zipper and W2 domains 2	-0.4	-0.38	0.000696986	28.48	0.03667606
1373140_at	---	---	Transcribed locus	0.18	0.13	0.00069891	28.45	0.03671521
1370828_at	NM_145096 /// XM_001064977	Zdhhc2	zinc finger, DHHC domain containing 2	0.37	0.33	0.000703512	28.40	0.03681798
1392334_at	NM_001008831	RT1-Ba	RT1 class II, locus Ba	-0.58	0.08	0.000704005	28.39	0.03681798
1376916_at	NM_001107460 XM_001065469 /// XM_217825	Zbtb2_predicted	zinc finger and BTB domain containing 2 (predicted)	0.29	0.25	0.00070508	28.38	0.03681798
1387232_at	NM_012827	Bmp4	bone morphogenetic protein 4	0.77	0.84	0.000705602	28.37	0.03681798
1398892_at	NM_173118	Npc2	Niemann Pick type C2	0.27	0.23	0.000706924	28.35	0.03682516
1390133_at	---	---	---	0.36	0.18	0.000708353	28.34	0.03683791
1373838_at	NM_022219	Fut4	fucosyltransferase 4	0.44	0.46	0.000713826	28.27	0.03706055
1367982_at	NM_024484	Alas1	aminolevulinic acid synthase 1	0.26	0.14	0.000716022	28.24	0.03709738
1373102_at	NM_138889	Cdh13	cadherin 13	0.36	0.33	0.000717416	28.22	0.03709738
1371959_at	XM_001062026	Hist2h2aa_predicted	histone cluster 2, H2aa (predicted) /// similar to H2A histone family, member O	0.41	0.06	0.000718114	28.21	0.03709738
1373291_at	XM_001066332 /// XM_341444	Dlc1	deleted in liver cancer 1	-0.11	-0.34	0.000722565	28.16	0.03726543
1371984_at	NM_001110490 XM_001059372 /// XM_573863	RGD1564875_predicted	similar to mKIAA0613 protein (predicted)	-0.31	-0.19	0.000730622	28.06	0.03761858
1370822_at	NM_001008831	RT1-Ba	RT1 class II, locus Ba	0.43	0.35	0.000740897	27.94	0.03801516
1385052_at	---	---	Transcribed locus	0.29	0.24	0.00074174	27.93	0.03801516
1393069_at	NM_001107591 XM_001055342 /// XM_219887	Sfrp5_predicted	secreted frizzled-related sequence protein 5 (predicted)	-0.5	-0.43	0.000741992	27.93	0.03801516

1388656_at	---	---	Transcribed locus	-0.09	-0.29	0.000745527	27.89	0.03811223
1390082_at	XM_001061381 XM_001071073 XM_001071106 /// XM_347168	Hip1	huntingtin interacting protein 1	0.27	0.22	0.000746338	27.88	0.03811223
1397952_at	XM_001068963 /// XM_345202	RGD1561608_predicted	similar to novel protein (predicted)	0.21	0.11	0.000749341	27.84	0.03813404
1387897_at	NM_012809	Cnp1	cyclic nucleotide phosphodiesterase 1	0.46	0.51	0.000750304	27.83	0.03813404
1372935_at	NM_001107155 XM_001080457 /// XM_222278	Tmem119_predicted	transmembrane protein 119 homolog (predicted)	-0.66	-0.6	0.000750443	27.83	0.03813404
1368087_a_at	NM_133545	Ptpn21	protein tyrosine phosphatase, non-receptor type 21	0.34	0	0.000752367	27.81	0.03816944
1373880_at	---	---	Transcribed locus, strongly similar to XP_344704.2 PREDICTED: similar to mKIAA1632 protein [Rattus norvegicus]	-0.15	-0.25	0.000754889	27.78	0.03823499
1389214_at	---	---	---	0.2	-0.01	0.000757148	27.75	0.03828704
1389177_at	NM_001106265 XM_001072627 /// XM_214953	Perp_predicted	PERP, TP53 apoptosis effector (predicted)	-0.56	-0.49	0.000759783	27.72	0.03835792
1371779_at	NM_001108711 XM_001075611 /// XM_343062	Snx6_predicted	sorting nexin 6 (predicted)	0.36	0.01	0.000763206	27.68	0.03846829
1394407_at	---	---	Transcribed locus	0.31	0.12	0.000771302	27.59	0.03881348
1367913_at	NM_130744	Cygb	cytoglobin	0.61	0.28	0.000777377	27.52	0.03905598
1375957_at	---	---	Transcribed locus	0.58	0.28	0.000781647	27.48	0.03920713
1388382_at	NM_001014174	LOC361985	similar to NICE-3	0.08	0.11	0.000788663	27.40	0.03948509
1378400_at	XM_001054191 XM_577043	RGD1560129_predicted	similar to RIKEN cDNA 4632404H22 (predicted)	-0.21	-0.45	0.000790368	27.38	0.03948509
1371746_at	---	---	Transcribed locus	-0.2	-0.06	0.000790997	27.37	0.03948509
1388555_at	NM_001105805 XM_001080157 /// XM_213382	Txnl5_predicted	thioredoxin-like 5 (predicted)	0.13	0.15	0.000795993	27.32	0.03967081
1370419_a_at	NM_053360	Sh3kbp1	SH3-domain kinase binding protein 1	0.28	0.14	0.000798227	27.30	0.03971852
1386890_at	NM_031114	S100a10	S100 calcium binding protein A10 (calpactin)	0.26	0.14	0.000800427	27.27	0.03973618
1388485_at	NM_001013137	Cxcl14	chemokine (C-X-C motif) ligand 14	-0.48	-0.1	0.000801625	27.26	0.03973618
1383135_at	---	---	Transcribed locus	-0.36	-0.73	0.000802743	27.25	0.03973618
1382217_at	---	---	Transcribed locus	-0.29	-0.26	0.000803693	27.24	0.03973618
1371921_at	NM_001007145	Catna1	catenin (cadherin-associated protein), alpha 1	0.11	0.08	0.000808194	27.19	0.03987802
1384268_at	XM_001072068 /// XM_237211	RGD1310683_predicted	similar to hypothetical protein FLJ40432 (predicted)	0.49	0.03	0.000809127	27.18	0.03987802
1372624_at	NM_001108108 XM_001057694 XM_001057761 /// XM_235640	Tmem16f_predicted	transmembrane protein 16F (predicted)	0.3	0.14	0.000812322	27.15	0.03992823
1369418_at	NM_053834	Kcnj9	potassium inwardly-rectifying channel, subfamily J, member 9	-0.24	-0.12	0.000812713	27.14	0.03992823
1376107_at	---	---	Transcribed locus	-0.19	-0.29	0.000814565	27.12	0.0399561
1393169_at	---	---	Transcribed locus	-0.28	-0.19	0.000817363	27.09	0.04003021
1386885_at	NM_022594	Ech1	enoyl coenzyme A hydratase 1, peroxisomal	-0.25	-0.27	0.000824525	27.02	0.04031746
1391669_at	NM_001108095 XM_001078855	Ptprb_predicte	protein tyrosine phosphatase, receptor type,	0.53	0.32	0.000826008	27.00	0.04032657

	/// XM_235156	d	B (predicted)					
1398828_at	NM_013102 ///	Fkbp1a	FK506 binding protein 1a	0.25	0.1	0.00082831	26.98	0.04037557
1373106_at	NM_001036626 XM_001060793	Zfp36l2	zinc finger protein 36, C3H type-like 2	0.27	0.21	0.000831239	26.95	0.04040985
1390716_at	---	---	Transcribed locus	-0.57	-0.61	0.000831612	26.95	0.04040985
1384244_at	NM_001025697	RGD1305387	similar to RIKEN cDNA 2610207I16	-0.24	-0.27	0.000833291	26.93	0.04042826
1384468_at	---	---	Transcribed locus	-0.18	-0.36	0.000835657	26.90	0.04044809
1372848_at	---	---	Transcribed locus	0.98	0.71	0.000836394	26.90	0.04044809
1372142_at	XM_001066031 /// XM_213848	Asna1	arsA arsenite transporter, ATP-binding, homolog 1 (bacterial)	0.4	0.22	0.000837602	26.88	0.04044809
1392258_at	---	---	---	-0.21	-0.14	0.000844731	26.81	0.04065756
1370054_at	NM_131902	Cdkn2c	cyclin-dependent kinase inhibitor 2C (p18, inhibits CDK4)	0.19	0.41	0.000844939	26.81	0.04065756
1387176_at	NM_133591	Rph3al	rabphilin 3A-like (without C2 domains)	-0.34	-0.13	0.000846884	26.79	0.04065756
1388516_at	XM_001076383 /// XM_574528	LOC499235	LRRGT00141	0.39	0.04	0.000847545	26.78	0.04065756
1371547_at	---	---	---	-0.26	-0.19	0.000848476	26.78	0.04065756
1370942_at	NM_031574 ///	Rasa3	RAS p21 protein activator 3	0.3	0.07	0.000850881	26.75	0.04071009
1374168_at	---	---	Transcribed locus	-0.4	-0.5	0.000855182	26.71	0.04075651
1393439_a_at	NM_053714 /// XM_001064426	Ank	progressive ankylosis homolog (mouse)	-0.24	-0.36	0.00085529	26.71	0.04075651
1395119_at	---	---	Transcribed locus	-0.39	-0.56	0.000855783	26.70	0.04075651
1367775_at	NM_012816	Amacr	alpha-methylacyl-CoA racemase	-0.11	-0.14	0.000857139	26.69	0.04075868
1396608_at	---	---	Transcribed locus	-0.31	-0.22	0.000867351	26.59	0.04118128
1390097_at	NM_001012075	Tspyl4	TSPY-like 4	-0.65	-0.44	0.000871865	26.55	0.04128249
1373458_at	XM_001053534	Bex4	brain expressed X-linked 4	-0.61	-0.42	0.000872137	26.54	0.04128249
1383743_at	XM_001070748 /// XM_225336	Lrrc16_predicted	leucine rich repeat containing 16 (predicted)	0.52	0.44	0.000873754	26.53	0.04129617
1368387_at	NM_053995	Bdh1	3-hydroxybutyrate dehydrogenase, type 1	1.05	0.39	0.000877319	26.49	0.0413896
1389157_at	NM_001079700 XM_001076184 /// XM_235488	Cdc42ep1_predicted	CDC42 effector protein (Rho GTPase binding) 1 (predicted)	0.3	0.15	0.000878393	26.48	0.0413896
1396408_at	XM_001081814	LOC688319	similar to RAS-related C3 botulinum substrate 3	-0.43	0	0.000884237	26.43	0.0414798
1390391_at	---	---	Transcribed locus	0.58	0.32	0.000884306	26.43	0.0414798
1371407_at	/// XM_230038	Nckap1	NCK-associated protein 1	0.17	0.1	0.000884672	26.42	0.0414798
1382271_at	NM_001108048 /// XM_001064992 /// XM_234468	Rps6ka5_predicted	ribosomal protein S6 kinase, polypeptide 5 (predicted)	-0.04	-0.47	0.000888655	26.39	0.0414798
1377656_at	NM_001014002	Rbm13	RNA binding motif protein 13	0.18	0.14	0.00089026	26.37	0.0414798
1367574_at	NM_031140	Vim	vimentin	0.33	0.15	0.000892364	26.35	0.0414798
1389189_at	NM_031005	Actn1	actinin, alpha 1	0.49	0.43	0.000893132	26.34	0.0414798
1384515_at	XM_001058425 /// XM_344806	Hey2	hairy/enhancer-of-split related with YRPW motif 2	0.7	0.3	0.000893316	26.34	0.0414798
1388006_at	NM_139041	Muc13	mucin 13, epithelial transmembrane	-0.64	-0.55	0.000893782	26.34	0.0414798
1376015_at	---	---	---	0.02	-0.36	0.000894572	26.33	0.0414798
1373410_at	XM_001056692 /// XM_574821	RGD1563119_predicted	similar to MADS box transcription enhancer factor 2, polypeptide C (myocyte enhancer factor 2C) (predicted)	0.81	0.79	0.000897542	26.30	0.0414798

1392528_at	NM_001037660	Csf2ra	Granulocyte-macrophage colony stimulating receptor alpha	0.4	0.4	0.000897809	26.30	0.0414798
1382995_at	---	---	Transcribed locus	0.56	0.3	0.000898419	26.30	0.0414798
1383853_at	NM_001024767	Dyrk3	dual-specificity tyrosine-(Y)-phosphorylation regulated kinase 3	-0.36	-0.64	0.00089898	26.29	0.0414798
1394598_at	---	---	Transcribed locus	-0.4	0.02	0.000904162	26.24	0.04161447
1373610_at	NM_001107723 /// XM_001075384 /// XM_227663	Sec24d_predicted	SEC24 related gene family, member D (S. cerevisiae) (predicted)	0.26	0.17	0.000904575	26.24	0.04161447
1377032_at	---	---	Transcribed locus, strongly similar to NP_942054.1 Rho GTPase activating protein 15 [Rattus norvegicus]	0.25	0.39	0.000906677	26.22	0.0416309
1372911_at	---	---	Transcribed locus	0.27	0.24	0.00090761	26.21	0.0416309
1379732_at	NM_001025638	Stx11	syntaxin 11	0.38	0.41	0.000914354	26.15	0.04187847
1373806_at	NM_001024866	RGD1311732	similar to hypothetical protein MGC15407	-0.03	-0.33	0.000926499	26.04	0.04237233
1372088_at	NM_001107896 XM_001074157 /// XM_232536	Ppfibp1_predicted	PTPRF interacting protein, binding protein 1 (liprin beta 1) (predicted)	0.41	0.21	0.000940557	25.92	0.04294969
1367977_at	NM_019169	Snca	synuclein, alpha	-0.88	-0.97	0.000941885	25.90	0.04294969
1372476_at	NM_173137	Fads3	fatty acid desaturase 3	0.42	0.31	0.000949764	25.84	0.04319119
1380204_at	---	---	Transcribed locus	-0.49	0.09	0.000950271	25.83	0.04319119
1381880_at	---	---	Transcribed locus	0.64	0.86	0.000951348	25.82	0.04319119
1368810_a_at	NM_001025289	Mbp	myelin basic protein	0.44	0.58	0.000956489	25.78	0.0433613
1388718_at	NM_013044	Tmod1	tropomodulin 1	-0.14	-0.18	0.00096505	25.70	0.04368573
1370415_at	NM_019365	Rassf5	Ras association (RalGDS/AF-6) domain family 5	-0.5	-0.35	0.00097294	25.64	0.04387599
1387504_at	NM_133575	Il1rl2	interleukin 1 receptor-like 2	-0.4	-0.16	0.000973113	25.64	0.04387599
1388705_at	XR_008359	RGD1565037_predicted	similar to selenoprotein SelM (predicted)	0.35	0.23	0.000973922	25.63	0.04387599
1373123_at	XM_001067170 /// XM_225150	RGD1310671_predicted	similar to RIKEN cDNA 4932432N11 gene (predicted)	0.21	0.2	0.000974897	25.62	0.04387599
1370599_a_at	NM_019140	Ptprd	protein tyrosine phosphatase, receptor type, D	-0.23	-0.42	0.000979113	25.59	0.04395878
1392865_at	NM_012952	Fgf9	fibroblast growth factor 9	0.9	0.33	0.000981912	25.56	0.04395878
1390728_at	---	---	---	0.24	0.25	0.000982141	25.56	0.04395878
1381296_at	---	---	Transcribed locus	-0.12	-0.58	0.00098239	25.56	0.04395878
1374480_at	NM_001108030 XM_001080564 /// XM_234275	Daam1_predicted	dishevelled associated activator of morphogenesis 1 (predicted)	0.18	0.09	0.000985997	25.53	0.04399903
1374595_at	NM_001107607 XM_001080123 /// XM_220047	Tnks2_predicted	tankyrase, TRF1-interacting ankyrin-related ADP-ribose polymerase 2 (predicted)	0.22	0.05	0.000986119	25.53	0.04399903
1385532_x_at	NM_001105727 XM_001054724 /// XM_341314	Psmb5	proteasome (prosome, macropain) subunit, beta type 5	-0.19	-0.26	0.000988834	25.51	0.04403627
1394392_at	/// XM_230827	RGD1307696_	similar to dJ881L22.2 (novel protein) (predicted)	-0.5	-0.67	0.000989786	25.50	0.04403627
1381452_at	NM_001109432 XM_001059507	LOC680931	similar to Bone morphogenetic protein 8A precursor (BMP-8A) (Osteogenic protein 2) (OP-2)	0.23	0.27	0.000998479	25.43	0.04435956

Appendix 9. Gene functional classification clustering

Functional Groups	Genes
Functional Group 1	
Enrichment score 1.83	
1378140_at	ADP-RIBOSYLATION FACTOR-LIKE 11
1367960_at	ADP-RIBOSYLATION FACTOR-LIKE 4
1371690_at	ADP-RIBOSYLATION FACTOR-LIKE 1
1367874_at	RAS HOMOLOG GENE FAMILY, MEMBER Q
1372707_at	RAB6A, MEMBER RAS ONCOGENE FAMILY
1387908_at	RAS, DEXAMETHASONE-INDUCED 1
1373894_at	RAB31, MEMBER RAS ONCOGENE FAMILY
1384267_at	RHO GTPASE ACTIVATING PROTEIN 5
1383322_at	RAS-LIKE FAMILY 11 MEMBER B
Functional Group 2	
Enrichment score 1.6	
1398455_at	ZINC FINGER, DHHC DOMAIN CONTAINING 13 (PREDICTED)
1371328_at	AUTOCRINE MOTILITY FACTOR RECEPTOR (PREDICTED)
1377844_at	ZINC BINDING ALCOHOL DEHYDROGENASE, DOMAIN CONTAINING 1
1379971_at	ZINC FINGER CCCH TYPE DOMAIN CONTAINING 6 (PREDICTED)
1390485_at	RING FINGER PROTEIN 153 (PREDICTED)
1379578_at	SIMILAR TO ZBTB20 PROTEIN
1373937_at	FYVE AND COILED-COIL DOMAIN CONTAINING 1 (PREDICTED)
1383160_at	CYSTEINE AND HISTIDINE-RICH DOMAIN (CHORD)-CONTAINING, ZINC-BINDING PROTEIN 1 (PREDICTED)
Functional Group 3	
Enrichment score 1.45	
1386861_at	H2A HISTONE FAMILY, MEMBER Z
1394836_at	H2A HISTONE FAMILY, MEMBER V
1371959_at	HISTONE 2, H2AA
1371959_at	SIMILAR TO HIST2H2AA1 PROTEIN
1390021_at	HISTONE 1, H2BH
1390097_at	TSPY-LIKE 4
1381925_x_at	AT RICH INTERACTIVE DOMAIN 1B (SWI1 LIKE)
1381925_x_at	AT RICH INTERACTIVE DOMAIN 1B (SWI1 LIKE)
Functional Group 4	
Enrichment score 1.17	
1372078_at	SERINE/THREONINE KINASE RECEPTOR ASSOCIATED PROTEIN
1391422_at	DNAJ (HSP40) HOMOLOG, SUBFAMILY B, MEMBER 6
1387905_at	JUN DIMERIZATION PROTEIN 1
1398487_at	PRE-B-CELL LEUKEMIA TRANSCRIPTION FACTOR 1 (PREDICTED)
1385754_s_at	leucine rich repeat containing 4 protein precursor
1398759_at	TRANSFORMING GROWTH FACTOR BETA 1 INDUCED TRANSCRIPT 4
1399016_at	MYST HISTONE ACETYLTRANSFERASE 2
1389351_at	SIMILAR TO FLI-LRR ASSOCIATED PROTEIN-1
1370981_at	RETINOID X RECEPTOR GAMMA
1387762_s_at	JUN D PROTO-ONCOGENE
1370928_at	LPS-INDUCED TN FACTOR
1369389_at	ZINC FINGER PROTEIN 483

1371536_at	CALCIUM REGULATED HEAT STABLE PROTEIN 1
1372299_at	CYCLIN-DEPENDENT KINASE INHIBITOR 1C (P57)
1385228_x_at	DEVELOPMENT AND DIFFERENTIATION ENHANCING
1390728_at	LIM DOMAINS CONTAINING 1
1386080_at	HAIRY/ENHANCER-OF-SPLIT RELATED WITH YRPW MOTIF 1
1393249_at	FRIEND LEUKEMIA INTEGRATION 1
1381886_at	YY1 TRANSCRIPTION FACTOR
1372246_at	OSTEOCLAST STIMULATING FACTOR 1
1367664_at, 1367665_at	ANKYRIN REPEAT DOMAIN 1 (CARDIAC MUSCLE)
1381968_at	CELLULAR REPRESSOR OF E1A-STIMULATED GENES (PREDICTED)
1387196_at	ETOILE, SAM68-LIKE PROTEIN SLM-2
1388133_at	RNA-BINDING PROTEIN PIPPIN
1372564_at	V-ETS ERYTHROBLASTOSIS VIRUS E26 ONCOGENE HOMOLOG 2 (AVIAN) (MAPPED)
1372211_at	V-MAF MUSCULOAPONEUROTIC FIBROSARCOMA ONCOGENE FAMILY, PROTEIN K (AVIAN)
1391212_at	TRANSCRIPTION ELONGATION FACTOR A (SII)-LIKE 1
1389741_at	LONGEVITY ASSURANCE HOMOLOG 4 (S. CEREVISIAE) (PREDICTED)
1370054_at	CYCLIN-DEPENDENT KINASE INHIBITOR 2C (P18, INHIBITS CDK4)
1376888_a_at	SIMILAR TO BTK-PH-DOMAIN BINDING PROTEIN
1395233_at, 1398726_at	WD40 PROTEIN CIAO1
1393360_at	ZINC FINGER PROTEIN 426
1383439_at	NEURONAL PAS DOMAIN PROTEIN 2 (PREDICTED)
1396265_at	SIMILAR TO AB1-133
1380572_at	HAIRY/ENHANCER-OF-SPLIT RELATED WITH YRPW MOTIF-LIKE (PREDICTED)
1384515_at	HAIRY/ENHANCER-OF-SPLIT RELATED WITH YRPW MOTIF 2
1381971_at	SRY-BOX CONTAINING GENE 18
1388714_at	ELONGATION FACTOR RNA POLYMERASE II (PREDICTED)
1373106_at	ZINC FINGER PROTEIN 36, C3H TYPE-LIKE 2
Functional Group 5	
Enrichment score 1.07	
1374698_at	BRCA1 ASSOCIATED PROTEIN 1 (PREDICTED)
1379269_at	CD2-ASSOCIATED PROTEIN
1368507_at	PROTEASOME (PROSOME, MACROPAIN) SUBUNIT, ALPHA TYPE 3
1388656_at	UBIQUITIN-CONJUGATING ENZYME E2D 2
1398778_at	PROTEASOME (PROSOME, MACROPAIN) SUBUNIT, ALPHA TYPE 1
1385532_x_at	PROTEASOME (PROSOME, MACROPAIN) SUBUNIT, BETA TYPE 5
Functional Group 6	
Enrichment score 0.83	
1370268_at	POTASSIUM VOLTAGE-GATED CHANNEL, SHAKER-RELATED SUBFAMILY, MEMBER 5
1393169_at	CALCIUM CHANNEL, VOLTAGE-DEPENDENT, ALPHA 2/DELTA 3 SUBUNIT
1398300_at	ATPASE, NA+/K+ TRANSPORTING, BETA 3 POLYPEPTIDE
1369795_at	POTASSIUM INWARDLY-RECTIFYING CHANNEL, SUBFAMILY J, MEMBER 12
1369086_a_at	CALCIUM CHANNEL, VOLTAGE-DEPENDENT, L TYPE, ALPHA 1D SUBUNIT
1395150_at	POTASSIUM VOLTAGE-GATED CHANNEL, ISK-RELATED FAMILY, MEMBER 2
1369418_at	POTASSIUM INWARDLY-RECTIFYING CHANNEL, SUBFAMILY J, MEMBER 9
Functional Group 7	
Enrichment score 0.61	
1370599_a_at	PROTEIN TYROSINE PHOSPHATASE, RECEPTOR TYPE, D
1368087_a_at	PROTEIN TYROSINE PHOSPHATASE 2E
1391669_at	PROTEIN TYROSINE PHOSPHATASE, RECEPTOR TYPE, B (PREDICTED)

1368358_a_at	PROTEIN TYROSINE PHOSPHATASE, RECEPTOR TYPE, R
1389050_at	SIMILAR TO DUAL SPECIFICITY PROTEIN PHOSPHATASE 3 (T-DSP11)
Functional Group 8	
Enrichment score 0.56	
1368260_at	AURORA KINASE B
1382271_at	RIBOSOMAL PROTEIN S6 KINASE, POLYPEPTIDE 5 (PREDICTED)
1393987_s_at	G PROTEIN-COUPLED RECEPTOR KINASE 6
1387777_at	INTEGRIN LINKED KINASE
1382745_at	SIMILAR TO LYMPHOCYTE ALPHA-KINASE (PREDICTED)
1383853_at	DUAL-SPECIFICITY TYROSINE-(Y)-PHOSPHORYLATION REGULATED KINASE 3
1369150_at	PYRUVATE DEHYDROGENASE KINASE, ISOENZYME 4
1371101_at	RECEPTOR-LIKE TYROSINE KINASE
1387445_at	PHOSPHORYLASE KINASE GAMMA 1
Functional Group 9	
Enrichment score 0.31	
1372088_at	RING FINGER PROTEIN 25
1371956_at	HYPOTHETICAL PROTEIN
1374595_at	TANKYRASE, TRF1-INTERACTING ANKYRIN-RELATED ADP-RIBOSE POLYMERASE 2 (PREDICTED)
1383084_at	SIMILAR TO HYPOTHETICAL PROTEIN FLJ23033
1372065_at	ADP-RIBOSYLTRANSFERASE 3
Functional Group 10	
Enrichment score 0.16	
1388382_at	SIMILAR TO NICE-3
1377760_at	SIMILAR TO HYPOTHETICAL PROTEIN MGC28606
1376623_at	SIMILAR TO HYPOTHETICAL PROTEIN FLJ20898
1372602_at	SIMILAR TO GENETHONIN 1
1388728_at	LYSOSOMAL-ASSOCIATED PROTEIN TRANSMEMBRANE 4B
1380513_at	SIMILAR TO EXPRESSED SEQUENCE AW060207

Appendix 10. GoStat analysis output identifying highly represented Gene Ontology annotations in the atrial abundant gene list obtained from the VO atria vs. ventricles comparison.

Gene Ontology annotation	Best GOs	Gene Symbols	P-Value
endoplasmic reticulum	GO:0005783	SEC22L1; DNAJB9; TMEM98; LEPRE1; TRA1_PREDICTED; PIGX; MAL; HSPA5; CDIPT; FKBP9; TOR3A; LRPAP1; PPIB; RAB2; RAMP4; VKORC1; TMCO1; NUCB2; MINPP1; RGD1305457; SSR2_PREDICTED; SEC11L1; KDELR3_PREDICTED; TLOC1; GGCX; TRAM1; INSIG1; RGD1561254_PREDICTED; SERINC1; PIP5K2C; OLFM1; SEC11L3; PJA2; SEC61A1; DDOST_PREDICTED; ITPR1; TRDN; SYBL1; DDN; FMO3; MGST1; CACNA2D1; ALDH3A2; SCD2; PRKCSH_PREDICTED; CYP1B1; SLN; STAU2; PDIA6; PTGFRN; PSEN2; SRPR; PTGIS; SEP15; SSR1; KDELR1; NCSTN; SEC61B_PREDICTED; SAR1A; RATSG2; P4HB; RPN1; STCH; RGD1311835; KDELC2; DYT1; CALR; YIPF5; MGP; KDELR2; PHTF1	1.55E-16
endoplasmic reticulum part	GO:0044432	FMO3; SEC22L1; ALDH3A2; PRKCSH_PREDICTED; MINPP1; RATSG2; TRA1_PREDICTED; RPN1; RGD1311835; TRAM1; HSPA5; PDIA6; SERINC1; RGD1561254_PREDICTED; CALR; SRPR; DDOST_PREDICTED; PPIB; SEP15; ITPR1; SEC61B_PREDICTED	6.79E-05
membrane	GO:0016020	ST8SIA5; SEC22L1; CD44; ERBB4; ABRA; PIGX; EBPL_PREDICTED; GNB5; SFRP2; GNAO; RGD1309892; PDPN; ATP6AP2; TMEM34; HSPB1; MIC2L1; TMBIM4; CACNA1D; SLC39A8; AOC3; VCAM1; KCNK2; GPC4; RGD1307506_PREDICTED; MGC112790; CAP2; PAM; ANXA6; ICA1; RGD1311946; RGD1561254_PREDICTED; TSPAN6; EPHA1_PREDICTED; WISP2; CTSB; CD302; DDOST_PREDICTED; TM7SF3; RGD1310423; TRPM7; KRT2-8; CACNA2D1; TMED3; EDG2; MSLN; MGC72614; STOM; SLN; PTGFRN; SRPR; SLC35A1_PREDICTED; COPZ1_PREDICTED; KCND3; GOLT1B_PREDICTED; RGD1307736; MAN2A2_PREDICTED; TSPAN3; CDA08; RPN1; SLC22A17; CALR; GORASP2; EPB4.1L3; APH1B; CXADR; JAM3; UPK1B; PKP4_PREDICTED; ENPP1; MBP; RGD1561153_PREDICTED; AKAP7; SFXN1; SCAMP4; GPC3; TMEM55A; PDGFRA; LOC362065; MGAT2; ACP5; PLD3; FRZB; ART3; VKORC1; RGS3; RAB15; NUCB2; MYH10; KRT1-19; SEC11L1; TJP2; SERINC1; GNG3; TRDN; ITPR1; SYBL1; RT1-KE4; PON2; SEC13L1; RND2; FMO3; ALDH3A2; LRP4; PODXL2_PREDICTED; ITGB4; CD164; LPHN1; AGPAT4; KDELR1; NSG1; NCSTN; CPE; TMEM77; P4HB; YIPF1; RGD1562920_PREDICTED; FZD7_PREDICTED; TMEPAI_PREDICTED; LEPROTL1; TMEM14A_PREDICTED; YIPF5; SLC24A3; ERBB2; TGFB1I1; KDELR2; ITM2C; TMEM66; NEO1; TMEM98; LEPRE1; PDGFA; HSPA5; CDIPT; ATP6V1D; SNCAIP_PREDICTED; FNDC1; CD82; PLVAP; PCDH7; FZD2; CD9; IGSF1; KCNJ5; TMEM43; SSR2_PREDICTED; PTP4A2; ALCAM; TLOC1; TRAM1; GNG2; ATP1B4; LBP; SLC39A13; TIMM23; CACNG6; SLCO3A1; SLC30A3; RGD1307343; DDN; QSCN6; FEZ1;	6.79E-05

		SLC39A2_PREDICTED; C1QTNF5; CDH11; COPZ2_PREDICTED; S100A6; IGF1R; GALNT5; ART1_PREDICTED; MAMDC2; PPL_PREDICTED; PSEN2; CSPG2; TM6SF1_PREDICTED; SAR1A; GRIA3; PAQR9_PREDICTED; CYBRD1; RATSG2; GALNTL1; VDP; BACE2; SDC2; SLC24A4_PREDICTED; ABI2; CORIN; HEXA; RGD1305587_PREDICTED; EDG5; LOC299907; TSPAN2; UXS1; TM4SF1_PREDICTED; TPARL; ARF1; SLC3A2; SPINT2; TRA1_PREDICTED; RGD1564216_PREDICTED; KCNJ3; SEC23A_PREDICTED; MAL; ABCB4; PC; LRPAP1; CP; DAF1; TSPAN31; SFRP1; TM4SF2; RAMP4; TMEM97; EXTL2; SDFR1; TMCO1; GPM6A; MOSC2; PROCR; DSC2; ZDHHC13; LAPTM4B; SCAMP1; KDELR3_PREDICTED; GGCX; CLTC; LRRC59; INSIG1; TMEM49; OLFM1; LOC501619; PJA2; SEC11L3; SEC61A1; ACSL4; CTGF; COPG; ARFGAP1; SHMT2; MGST1; SCD2; ARMCX2; PTPRA; APP; CYP1B1; CACNA1G; RHOQ; TM9SF2; SLC29A1; PTGIS; SSR1; RAB13; SEC61B_PREDICTED; FN1; UCP2; TSPAN9_PREDICTED; D1BWG1363E; ATP1A1; CATNA1; RGD1310587; RGD1311835; WFS1; CACNA2D3; OSBPL5; PARP1; VAV2_PREDICTED; KRTCAP2_PREDICTED; PHTF1	
membrane part	GO:0044425	ITM2C; TMEM66; ST8SIA5; SEC22L1; NEO1; CD44; TMEM98; ERBB4; PIGX; EBPL_PREDICTED; GNB5; GNAO; RGD1309892; HSPA5; CDIPT; PDPN; ATP6V1D; ATP6AP2; TMEM34; CD82; PLVAP; MIC2L1; TMBIM4; CACNA1D; SLC39A8; IGSF1; CD9; FZD2; KCNJ5; AOC3; MGC112790; RGD1307506_PREDICTED; GPC4; VCAM1; KCNK2; TMEM43; PAM; SSR2_PREDICTED; ALCAM; TLOC1; TRAM1; ANXA6; GNG2; ICA1; RGD1561254_PREDICTED; RGD1311946; ATP1B4; LBP; TSPAN6; TIMM23; EPHA1_PREDICTED; CACNG6; CTSB; SLCO3A1; CD302; SLC30A3; DDOST_PREDICTED; RGD1307343; TM7SF3; RGD1310423; TRPM7; DDN; KRT2-8; QSCN6; CACNA2D1; TMED3; SLC39A2_PREDICTED; EDG2; MGC72614; STOM; SLN; COPZ2_PREDICTED; IGF1R; PTGFRN; GALNT5; ART1_PREDICTED; PPL_PREDICTED; SLC35A1_PREDICTED; PSEN2; SRPR; COPZ1_PREDICTED; GOLT1B_PREDICTED; KCND3; RGD1307736; GRIA3; PAQR9_PREDICTED; MAN2A2_PREDICTED; CYBRD1; TSPAN3; CDA08; RATSG2; RPN1; GALNTL1; CALR; SLC22A17; BACE2; SDC2; APH1B; EPB4.1L3; CXADR; SLC24A4_PREDICTED; ABI2; CORIN; JAM3; RGD1305587_PREDICTED; EDG5; UPK1B; PKP4_PREDICTED; TSPAN2; UXS1; ENPP1; TM4SF1_PREDICTED; MBP; TPARL; SPINT2; SLC3A2; TRA1_PREDICTED; RGD1564216_PREDICTED; KCNJ3; SCAMP4; SEC23A_PREDICTED; MAL; GPC3; ABCB4; TMEM55A; PDGFRA; LOC362065; ACP5; MGAT2; DAF1; CP; TSPAN31; PLD3; ART3; TM4SF2; RAMP4; TMEM97; EXTL2; SDFR1; TMCO1; VKORC1; GPM6A; MOSC2; PROCR; NUCB2; ZDHHC13; LAPTM4B; DSC2; SCAMP1; SEC11L1; KDELR3_PREDICTED; GGCX; CLTC; LRRC59; INSIG1; TJP2; SERINC1; TMEM49; GNG3; SEC11L3; LOC501619; SEC61A1; ACSL4; ITPR1; TRDN; SYBL1; RT1-KE4; COPG; SEC13L1; ARFGAP1; FMO3; ALDH3A2; SCD2; LRP4; ARMCX2; PTPRA; APP; CACNA1G; PODXL2_PREDICTED; ITGB4; CD164; TM9SF2;	0.00027

		SLC29A1; LPHN1; PTGIS; AGPAT4; KDELR1; SSR1; NSG1; RAB13; NCSTN; SEC61B_PREDICTED; FN1; UCP2; TMEM77; TSPAN9_PREDICTED; YIPF1; D1BWG1363E; CATNA1; ATP1A1; CACNA2D3; WFS1; RGD1311835; RGD1310587; RGD1562920_PREDICTED; FZD7_PREDICTED; TMEPAI_PREDICTED; LEPROTL1; OSBPL5; TMEM14A_PREDICTED; YIPF5; KRTCAP2_PREDICTED; SLC24A3; ERBB2; TGFB1I1; KDELR2; PHTF1	
cellular secretion	GO:0032940	ARFGAP1; SEC22L1; ZWINT; LYN; ARF1; EXOC4; SEC23A_PREDICTED; LPHN1; SNCAIP_PREDICTED; SRPR; YWHAQ; SSR1; KDELR1; CSPG2; RAB2; SAR1A; SNCA; RAB15; MYH10; TRAPPC1; SCAMP1; SSR2_PREDICTED; SEPT5; TLOC1; TRAM1; VDP; OSBPL5; ICA1; BACE2; SEC61A1; YIPF5; LOC498353; KDELR2; SEC13L1	0.00067
secretory pathway	GO:0045045	ARFGAP1; RAB2; SAR1A; SEC22L1; SNCA; ZWINT; ARF1; MYH10; RAB15; TRAPPC1; SCAMP1; EXOC4; SSR2_PREDICTED; TLOC1; SEPT5; TRAM1; VDP; SEC23A_PREDICTED; OSBPL5; ICA1; LPHN1; SNCAIP_PREDICTED; SRPR; YWHAQ; YIPF5; LOC498353; KDELR1; SSR1; CSPG2; SEC13L1; KDELR2	0.00067
protein transport	GO:0015031	ARFGAP1; ARL4A; SEC22L1; TMED3; ARF1; TGFB3; ABRA; TRA1_PREDICTED; EXOC4; SCAMP4; SEC23A_PREDICTED; COPZ2_PREDICTED; MAL; SRPR; YWHAQ; COPZ1_PREDICTED; KDELR1; SSR1; RAB13; CSPG2; ARL1; SEC61B_PREDICTED; RGD1307736; RAB2; RGD1566265_PREDICTED; RGD1311490_PREDICTED; RAMP4; AKAP5; SAR1A; RAB15; ARL5A; SGNE1; RATSG2; SCAMP1; RGD1311835; SSR2_PREDICTED; TLOC1; KDELR3_PREDICTED; TRAM1; VDP; CLTC; RAB40B_PREDICTED; CALR; TIMM23; SEC61A1; YIPF5; SYBL1; COPG; SEC13L1; KDELR2	0.000678
extracellular region part	GO:0044421	COL14A1_PREDICTED; TPARL; DNAJB9; PRSS23; PRDX4; SPINT2; TGFB3; BGN; RGD1308472_PREDICTED; SOD3; TRA1_PREDICTED; SLIT3; FMOD; PDGFA; ARMET_PREDICTED; SMOC1; GPC3; LAMB3; PDPN; CGREF1; HAMP; ACP5; CHI3L1; PPIB; SPG20; LRPAP1; CP; DAF1; MFAP5_PREDICTED; SFRP1; FRZB; ADM; ART3; MIC2L1; FGL2; TMEM97; EXTL2; GGH; SLC39A8; FZD2; MOSC2; NUCB2; TGFB2; FUT8; AOC3; RARRES2; AGA; C1QTNF7_PREDICTED; GPC4; VCAM1; PPIC; DKK3; ACP6; SGNE1; PAM; RECK_PREDICTED; SSR2_PREDICTED; KDELR3_PREDICTED; CLU; ADAMTS1; HTRA1; RGD1311946; ALDH1B1; LBP; OLFM1; WISP2; DDOST_PREDICTED; CTGF; RT1-KE4; CTHRC1; KRT2-8; GPX3; CRLF1_PREDICTED; AEBP1_PREDICTED; FMO3; CACNA2D1; CNTF; SDF4; LRP4; PRKCSH_PREDICTED; GPX7_PREDICTED; C1QTNF5; CYP1B1; PON3; COL12A1; MSLN; ITGB4; DNAJC3; CD164; TM9SF2; IGF1R; PTGFRN; SLC35A1_PREDICTED; PTGIS; THBS4; XBP1; KDELR1; CSPG2; FN1; CPE; EFEMP1; IGFBP2; RGD1311155; P4HB; STCH; LTBP1; CACNA2D3; FZD7_PREDICTED; ELN; FBLN1_PREDICTED; TIMP1; CALR; DYT1; SLC22A17; BACE2; MGP; C3; VNN1; PDE7A; IGFBP6; KRTCAP2_PREDICTED; CTSL	0.000678
Co-translational protein targeting to membrane	GO:0006613	TRAM1; SRPR; SSR1; CSPG2; SSR2_PREDICTED; TLOC1	0.000841

Appendix 11. Differentially expressed gene list generated by two-way ANOVA (p< 0.001) analysis for the interaction Tissue x Condition effect obtained by comparing the following four groups: LA shunt, LA sham, LV shunt and LV sham.

Probe Set ID	Gene Name	Gene Symbol	ANOVA Atria Shunt; Sample mean	ANOVA Atria Sham; Sample mean	ANOVA LV Shunt; Sample mean	ANOVA LV Sham; Sample mean	ANOVA Interaction: Tissue x Condition; P-value	ANOVA Interaction: Tissue x Condition; F statistic
1383219_at	restin-like 2	Rsnl2	7.53	7.91	7.94	8.07	0.000001	159.13
1379482_at	transmembrane 6 superfamily member 1 (predicted)	Tm6sf1_predicted	6.30	6.59	6.61	6.47	0.000075	54.95
1397726_at	JNK/SAPK-inhibitory kinase	JIK	4.42	4.23	4.43	4.74	0.000089	52.43
1368216_at	RAB28, member RAS oncogene family	Rab28	9.99	10.22	9.77	9.88	0.000103	50.25
1392912_at	calcyclin binding protein	Cacybp	7.89	8.08	7.62	7.50	0.000115	48.75
1374447_at	ubiquitin specific peptidase 9, X chromosome (predicted)	Usp9x_predicted	8.36	8.20	8.15	8.31	0.000116	48.56
1372809_at	hypothetical gene supported by AF152002	LOC290595	5.25	6.94	3.59	3.71	0.000123	47.83
1367676_at	high mobility group box 2	Hmgb2	6.94	6.95	7.33	6.98	0.000144	45.68
1379376_at	Transcribed locus	---	7.15	7.51	7.10	6.97	0.000150	45.13
1388163_at	solute carrier family 25 (mitochondrial carrier; adenine nucleotide translocator), member 5	Slc25a5	11.26	11.15	11.29	11.35	0.000155	44.72
1370086_at	fibrinogen, gamma polypeptide	Fgg	3.67	4.64	3.29	3.26	0.000178	42.96
1374622_at	Transcribed locus	---	4.46	5.00	4.43	4.16	0.000188	42.25
1393625_at	similar to Intersectin-2	LOC313934	6.55	6.08	9.09	9.24	0.000197	41.71
1398659_at	similar to crossveinless 2 CG15671-PA	LOC501231	2.43	2.39	2.38	2.43	0.000224	40.14
1384017_at	leucine-rich repeat kinase 1 (predicted)	Lrrk1_predicted	6.85	7.03	6.15	5.89	0.000226	40.03
1391197_at	---	---	4.07	3.84	4.15	4.24	0.000269	38.02
1374374_x_at	similar to KIAA1960 protein (predicted)	RGD1308066_predicted	2.84	2.70	2.87	3.14	0.000297	36.94
1388802_at	brain expressed X-linked 1	Bex1	6.54	6.79	5.38	4.56	0.000318	36.19
1367957_at	regulator of G-protein signalling 3	Rgs3	7.48	7.03	7.01	6.86	0.000360	34.86
1370515_x_at	synaptotagmin VII	Syt7	4.75	4.60	4.86	5.09	0.000390	34.02
1369066_at	MAP-kinase activating death domain	Madd	3.52	3.40	3.49	3.75	0.000414	33.41
1395851_at	kelch repeat and BTB (POZ) domain containing 5 (predicted)	Kbtbd5_predicted	6.79	7.26	6.51	6.10	0.000422	33.23
1378074_at	Transcribed locus	---	7.63	8.55	8.99	9.41	0.000438	32.85
1369335_at	KPL2 protein	Kpl2	2.73	2.62	2.66	2.79	0.000441	32.79
1370281_at	fatty acid binding protein 5, epidermal	Fabp5	9.58	9.98	9.37	9.31	0.000457	32.44
1372469_at	similar to Ephrin type-B receptor 4 precursor (Tyrosine-protein kinase receptor MDK-2) (Developmental kinase 2)	LOC686310	6.89	7.04	7.26	7.17	0.000468	32.20

	(Tyrosine kinase MYK-1)							
1367846_at	S100 calcium-binding protein A4	S100a4	8.07	7.47	7.21	7.31	0.000474	32.08
1376184_at	Ly6/neurotoxin 1 (predicted)	Lynx1_predicted	6.35	7.30	7.68	7.99	0.000534	30.92
1392529_at	sprouty homolog 4 (Drosophila) (predicted)	Spry4_predicted	6.52	6.22	6.44	6.59	0.000542	30.79
1387908_at	RAS, dexamethasone-induced 1	Rasd1	5.29	7.23	4.39	4.75	0.000574	30.25
1368982_at	protein kinase inhibitor, alpha	Pkia	8.11	8.07	7.98	8.28	0.000615	29.60
1371702_at	transmembrane 4 superfamily member 2	Tm4sf2	8.87	9.21	8.40	8.36	0.000624	29.48
1371075_at	myosin, heavy polypeptide 13, skeletal muscle	Myh13	4.73	4.67	4.64	5.09	0.000633	29.34
1387898_at	heat shock protein, alpha-crystallin-related, B6	Hspb6	11.79	12.03	12.72	12.67	0.000644	29.19
1372774_at	Coenzyme Q6 homolog (yeast)	Coq6	7.13	7.31	6.82	6.69	0.000661	28.96
1368987_at	---	---	4.43	5.36	4.14	3.98	0.000672	28.80
1381569_at	---	---	4.88	4.85	4.84	5.22	0.000675	28.77
1372720_at	BTB (POZ) domain containing 1	Btbd1	10.67	10.83	10.66	10.68	0.000700	28.44
1378862_at	---	---	4.29	4.13	4.26	4.45	0.000781	27.48
1387322_at	sema domain, transmembrane domain (TM), and cytoplasmic domain, (semaphorin) 6B	Sema6b	4.47	4.27	4.53	4.72	0.000799	27.29
1389951_at	Transcribed locus	---	3.80	3.70	3.74	3.84	0.000823	27.04
1370936_at	dimethylglycine dehydrogenase precursor	Dmgdh	2.60	2.55	2.60	2.86	0.000837	26.89
1387808_at	solute carrier family 7 (cationic amino acid transporter, y+ system), member 7	Slc7a7	5.32	5.88	4.67	4.20	0.000854	26.72
1389554_at	Transcribed locus	---	8.26	8.54	6.32	6.03	0.000868	26.58
1382221_at	Transcribed locus	---	4.70	4.57	4.14	4.60	0.000874	26.52
1368505_at	regulator of G-protein signaling 4	Rgs4	7.11	7.26	7.60	7.41	0.000875	26.52
1397839_at	RAB15, member RAS onocogene family	Rab15	5.51	6.08	5.03	4.90	0.000900	26.28
1384645_at	similar to hypothetical protein DKFZp313N0621 (predicted)	RGD1560717_predicted	4.47	4.41	4.51	4.79	0.000923	26.07
1379220_at	Transcribed locus, moderately similar to XP_001479561.1	---	4.52	4.69	4.66	4.39	0.000924	26.06
1370408_at	putative small membrane protein NID67	Nid67	7.12	6.99	7.49	7.71	0.000925	26.06
1367557_s_at	glyceraldehyde-3-phosphate dehydrogenase	Gapdh	13.17	13.22	13.25	13.18	0.000959	25.76
1381372_at	Centrosomal protein 76	Cep76	3.30	3.18	3.30	3.57	0.000967	25.69